Charged Polymers and Hydrogels as Antimicrobial Materials for Prevention of Infections

A Thesis Submitted for the Degree of

Doctor of Philosophy

By

Jiaul Hoque

New Chemistry Unit

Jawaharlal Nehru Centre for Advanced Scientific Research

(A Deemed University)

Bangalore - 560064 (INDIA)

January-2017

Dedicated to my Parents and Haldar's Group at JNCASR

Declaration

I hereby declare that the matter embodied in the thesis entitled "**Charged Polymers and Hydrogels as Antimicrobial Materials for Prevention of Infections**" is the result of the investigations carried out by me at the New Chemistry Unit, Jawaharlal Nehru Centre for Advanced Scientific Research, Bangalore, India under the supervision of **Prof. Jayanta Haldar** and that it has not been submitted elsewhere for the award of any degree or diploma.

In keeping with the general practice in reporting the scientific observations, due acknowledgement has been made whenever the work described is based on the findings of other investigators. Any omission that might have occurred due to oversight or error in judgement is regretted.

_____

Mr. Jiaul Hoque

(PhD Student)

Certificate

I hereby certify that the matter embodied in this thesis entitled "**Charged Polymers and Hydrogels as Antimicrobial Materials for Prevention of Infections**" has been carried out by **Mr. Jiaul Hoque** at the New Chemistry Unit, Jawaharlal Nehru Centre for Advanced Scientific Research, Bangalore, India under my supervision and that it has not been submitted elsewhere for the award of any degree or diploma.

_____

Prof. Jayanta Haldar

(Research Supervisor)

Acknowledgments

Firstly, I thank my research supervisor, Prof. Jayanta Haldar for guidance, encouragement and the freedom that he offered to work in and explore new things. Specially, I thank him for his suggestions pertaining to my work and his way of tackling various problems which has helped me immensely including my presentation skills. It is from him I learnt to ask the basic and fundamental questions in science. He was instrumental in making me complete as a researcher and I thank him for all that he has done for me.

I came across a wonderful scientist at JNCASR, Prof. C.N.R. Rao F.R.S and I thank him for excellent facilities to carry out world-class research. I really admire him for his talks on the history of science and scientists and it's from him I heard the true meaning of science: observation.

I would like to thank all my course coordinators, Prof. Jayanta Haldar (JNCASR), Prof. Subi. J. George (JNCASR), Prof. Hemalatha Balaram (JNCASR), Prof T. Govindaraju (JNCASR) Prof. Ranjani Viswanatha (JNCASR) Prof. Sebastian C. Peter (JNCASR) and Prof. Tapas K. Maji (JNCASR).

I fail in my duty if I do not express my gratitude to all my collaborators for their excellent cooperation and discussions. I thank Dr. B.R. Shome and Dr. P. Krishnamoorthy ICAR-NIVEDI, Bangalore; Prof. Kaustuv Sanyal and Mr. Vikas Yadav from MBGU, JNCASR, for all their help during this thesis.

I shall never forget the support, encouragement and contribution of my lab members, Venky, Diwakar, Chandradhish, Padma, Goutham, Mohini, Paramita, Swagatam, Sreyan, Brinta, Kathakali, Dr. Sandip, Dr. Vijay. I also thank all the short-term students Pratik, Nivin, Spandhana, Utsarga and Shanola for their help in synthesis of some compounds.

I acknowledge technical staff Dr. R. G. Prakash (Animal house in-charge), Kannan (TEM), Jagdish (XPS) Vasu (UV/PL/IR/TGA/AES), Mahesh (NMR), Sivakumar (ATR-FT-IR/HR-MS) and Selvi (FE-SEM). I am especially thankful to Dr. R. G. Prakash (Animal house in-charge) for helping with animal studies.

I thank my friends Dr. Subham, Dr. Sunita, Surya, Abhijeet, Shubhojit, Nabadyuti, Dr. Pralok, Dr. Ankit, Dr. Arpan, Anand, Vikas, Dr. Suman, Deboshree, Pramoda, Satya, Dr.

Mohit, Rajashekhar, Yugandhar, Dr. Prakash, Dr. Anindita, Dr. Ramana, Dr. Suresh, Soumya, Sohini, Samyantak, Nivedita, Papri, Samarth, Krishnendu, Shreya, Niloy, Manaswee, Satyajit and Rajib for making my stay in JNCASR pleasant and enjoyable. I specially thank Dr. Subham Bhtattacharjee who has suggested me to join Jayanta's lab at JNCASR.

I would like to express my sincere thanks to all the academic, administrative, security, library, complab and health center staff of JNCASR for making our campus life smooth and easy.

I owe everything to my parents who have always encouraged me to do whatever I want in life and I am indebted to them for being there for me.

Preface

The ability of bacteria to grow on different surfaces is a huge concern in hospitals and households due to the increased risk of microbial infections. The thesis, divided into nine chapters, deals with the design and development of various cationic antimicrobial polymers and hydrogels as antimicrobial materials for the prevention of infections on both abiotic and biotic surfaces.

Chapter 1 introduces the role of surfaces in spreading microbial infections and describes the different strategies to create antimicrobial coatings for prevention of infections.

Chapter 2A describes a new methodology to functionalize a synthetic polymer, polyethyleneimine, with cationic and hydrophobic moieties to develop water-insoluble and organo-soluble antimicrobial paints. The polymers when coated onto surfaces killed both bacteria and fungi upon contact and were shown to retain activity when mixed with medically relevant polymer such as poly-lactic acid and with commercial paints. Various spectroscopic and microscopic studies suggested that microbial membrane stability was compromised upon interaction with the polymer. Microbes (bacteria) in multiples passages were unable to develop resistance against the polymer. Although these polymers can be potentially used to paint walls or hospital equipment, their non-biodegradability hinders their use inside the body. **Chapter 2B** addresses this unmet need and describes a unique synthetic approach to introduce cleavable groups such as amide or esters into the side alkyl chains of the cationic PEI based polymers. These side chain degradable polymers were shown to hydrolyze both chemically and enzymatically into water-soluble, non-toxic zwitterionic polymers. The polymers also showed potent antimicrobial and antibiofilm efficacy against both bacteria and fungi when coated onto surfaces. The possible hydrolysed products were shown to be non-toxic both *in-vitro* and *in-vivo*. Medical grade catheter when coated with the polymer showed 4.2 log reduction of MRSA burden in a murine model of subcutaneous infection.

Chapter 3A is aimed in developing biodegradable antimicrobial coatings based on water-insoluble and organo-soluble polymers from naturally occurring polymer chitin. This novel approach introduced quaternary ammonium group with different alky chains into C-6 position of chitin thus resulting in organo-soluble polymers with degradable backbone. The polymeric coating inactivated both bacteria and fungi and inhibited microbial colonization onto surfaces. The polymers were shown to be degradable both *in-vitro* and *in-vivo* (in rat

subcutaneously). In a mice model of MRSA infection, polymer coated medical grade catheter showed 3.2 log reduction of bacterial burden in comparison to uncoated catheter. **Chapter 3B** deals with *in-situ* development of silver polymeric nanocomposites using the cationic chitin derivatives developed in Chapter 3A. The composites were shown to act on microbes by both release and contact based mechanism. Further, when coated onto surfaces, the composites showed enhanced activity, killed microbes rapidly and inactivated pathogens for an extended period of time. The composite coated surfaces could also inhibit microbial (both bacterial and fungal) colonization on them. Composite coated medical grade catheter reduced MRSA count (4.8 log on the catheter surface and 5.1 log in the surrounding tissue) in comparison to uncoated catheter in a murine model.

In **Chapter 4A** development of broad spectrum cationic small molecular biocides for topical infection has been described. The molecules were designed by optimizing hydrophobic/hydrophilic balance and by spatial positioning of hydrophobicity. Importantly, unlike antibiotics, bacteria find it difficult to develop resistance against these membrane-active molecules. The molecules with more confined and less pendent hydrophobicity were selectively active towards bacteria and capable of eradicating established bacterial biofilms. In MRSA model of skin infection, one of the potent molecules reduced bacterial burden by 5.2 logs in comparison to untreated skin. **Chapter 4B** describes the development of an antibacterial hydrogel capable of delivering the most potent small molecular biocide developed in Chapter 4A over time. Biocide loaded hydrogels were shown to have potent antibacterial activity without causing toxicity to mammalian cells. Further, the gels showed negligible skin toxicity in various animal models (e.g., rat, guinea pig and rabbit). They were also shown to annihilate established bacterial biofilms both *in-vitro* and *in-vivo* in murine model of MRSA skin infection (bacterial burden was reduced by 4.8 logs).

Infection at wound sites due to surgery or accident represents a major threat as it delays healing and in severe cases, leads to sepsis. Injectable bioadhesive materials are often used non-invasively to close wounds. However, such injectable bioadhesives materials rarely come with both antibacterial, hemostatic and wound healing properties. **Chapter 5A** presents the development of an injectable hydrogel with innate bioadhesive, antibacterial, hemostatic and wound healing capabilities. An antibacterial polymer was first developed from naturally occurring polymer chitosan and subsequently used to prepare the gel with a bioadhesive polymer, polydextran aldehyde. The polymers formed gel within a few seconds upon mixing. The gel was shown to have strong adhesive and antibacterial activities. Further, it was shown to prevent sepsis, cease bleeding and promote healing at the wound sites *in-vivo*. Infection

into sites of no or lesser vascularity is a huge threat since antibiotics cannot reach these places. **Chapter 5B** deals with the development of an injectable hydrogel for local and controlled delivery of antibiotics. Vancomycin, one of the most potent antibiotics, was loaded into a injectable hydrogel developed in Chapter 5A both covalently and non-covalently. The gel was found to release the antibiotic for more than a month and shown to have excellent antibacterial activity. The activity of the gel was further validated in a mice model and a reduction of 5.2 logs MRSA burden was observed compared to non-treated mice. In addition to these, it showed excellent hemostatic and wound healing properties.

Table of Contents

Chapter 2A: Non-Degradable Polyethylenimine-based Quaternary Hydrophobic Polymers as Antimicrobial Paint

Chapter 2B: Charge-Switchable Polyethylenimine-based Antimicrobial Paint with Hydrolysable Amide or Ester Groups in Side Chains of Polymers

Chapter 3A: Biodegradable and Biocompatible Chitin-based Cationic Hydrophobic Polymers as Antimicrobial Paint

Chapter 3B: Dual Action Quaternary Chitin-Silver Nanocomposites as Antimicrobial Paint that Kill Microbes and Inhibit Biofilms on Catheter

Chapter 4A: Membrane-Active Cationic Small Molecules with Multiple Non-Peptidic Amide groups as Potent Antibacterial and Antibiofilm Agents

Chapter 4B: Dextran-Based Antibacterial Hydrogels for Extended Release of Cationic Small Molecular Biocide and Eradication of Topical Biofilms

Chapter 5A: An Injectable Bioadhesive and Hemostatic Hydrogel with Innate Wound Healing and Antibacterial Properties

Chapter 5B: Vancomycin-loaded Injectable Bioadhesive Hydrogels that Deliver Antibiotic Locally and Kill Bacteria Efficiently

Chapter 1

An Introduction to Antimicrobial Polymers and Hydrogels for Prevention of Infections

1.1 Infectious diseases: A global threat to human life

Infectious diseases are a serious threat public health and a significant burden on global economies.[1] Infectious diseases led to more human deaths than any other disease and are responsible for more than 25% of all fatalities world-wide (about 8.2 million of the total 28.3 million deaths).[2] In India the situation is even poorer as the burden of infectious diseases in India is among the highest in the world.[3] These diseases are caused mainly by the microorganisms such as bacteria, viruses, fungi, parasites, etc. Among all these causative organisms, bacterial infectious diseases contribute almost 54.3% to overall global infectious disease burden (6.6 million deaths).[2] Bacteria are responsible for causing various diseases like respiratory infections, chronic diseases (such as gastric ulcers and gastric cancer), tuberculosis, diarrhoea, sepsis, pneumonia, endocarditis, skin and soft tissue infections, etc. In addition to bacterial infections, fungi are also identified as major pathogens in human especially in bloodstream infections (6.3% of overall infectious diseases are caused by fungi).[2] Superficial infections of the skin are the most common fungal diseases in humans and affect ~25% (or ~1.7 billion) of the general population worldwide.[4] Of particular concern is the high rate of mortality associated with invasive fungal infections (e.g., candidiasis, aspergillosis, meningitis, etc.) which often exceeds 50% despite the availability of several antifungal drugs.[2,4]

1.2 Modes of spreading of infections: Community- and hospital-acquired infections

There are many ways via which the infectious diseases spread: person-to-person spread (e.g., sexual transmission, needle injection, fomites or contaminated surfaces, etc.), common vehicle spread (food-borne, water-borne, fecal-oral blood products, etc.), zoonoses (animal bites e.g., rabies virus or hepatitis from primates, airborne) and vector borne: mosquitoes, flies, etc.).[5-7] However among all these modes, it is the contaminated surface or fomite which is responsible for more than 50% of all microbial infections.[8] Microbe contaminated surfaces may act as reservoirs of microbes which could in turn lead to the spread of infection upon being touched by a healthy individual. Common objects from community such as door knobs, linen, public telephones, children toys etc. are touched by infected people, pathogenic microorganism are deposited onto surfaces. Moreover, coughing, sneezing, breathing or even talking generate aerosolized droplets of moisture containing bacteria which upon disposition onto objects lead to surface contamination. When these contaminated surfaces are touched by

healthy individuals, microbial infections can be transmitted.[9-12] Infections caused by contaminated objects from community are called as community acquired infections (CAIs).

Infectious microbes (e.g. bacteria, fungi, etc.) can be traced to several sources in hospitals including the ambient atmosphere of the operating room, surgical equipment, clothing worn by medical professionals, resident bacteria on the patient's skin, and bacteria already in the body.[13-15] In addition, increase in the usage of biomaterials and medical devices such as catheters, cardiac pacemakers, hip implants, and contact lenses, etc. can cause serious implant-associated infections resulting from the implant contaminations.[16] Although sterilization and the use of aseptic techniques greatly reduces the levels of bacteria found in hospital settings, pathogenic microorganisms are still found at the site of approximately 90% of all implants. Infections caused by contaminated objects from hospital are known as hospital-acquired infections (HAIs) or nosocomial infections and it is estimated that almost 60% of all nosocomial infections are related to medical device and implants.[17] Device-related infection may result in substantial clinical complications, including death, as well as economic consequences such as increased healthcare costs generated by prolonged hospital stays or revision surgery. Many different sources contribute to the HAIs starting from surgical site infections (SSIs), urinary tract infections (UTIs), blood stream infections, pneumoniae, etc. and cost a heavy financial burden in addition to patient's sufferings (Figure 1.1). In the United States alone, recent estimates of direct costs for healthcare-associated infections were estimated to range from US$28 billion to $45 billion in 1 year.[18]

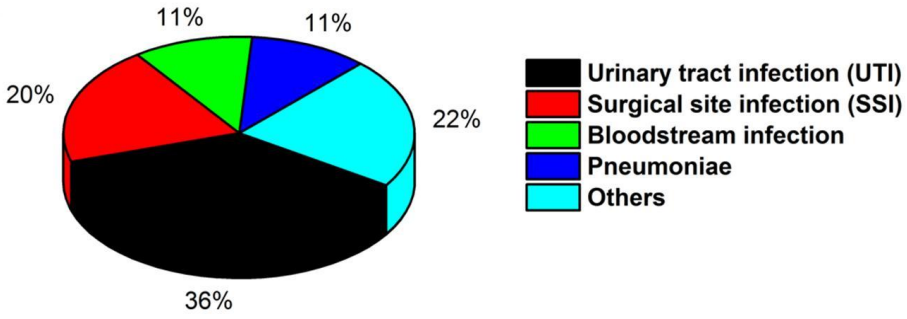

Figure 1.1: Sites of the most common nosocomial infections.

1.3 Microorganisms causing CAIs and HAIs

The Gram-positive bacteria *Staphylococcus aureus* is responsible for most of the HAIs and CAIs.[19] Other Gram-positive bacteria such as *Enterococcus* spp. and *Streptococcus* spp. and Gram-negative bacteria such as *Klebsiella* spp., *Escherichia* spp., *Enterobacter* spp.,

Pseudomonas spp., *Acenetobacter* spp. are also responsible for hospital associated infections. Among these microorganisms, staphylococci, particularly *Staphylococcus epidermidis* and other coagulase-negative staphylococci, *Staphylococcus aureus*, *Enterococcus* spp. account for the majority of infections in both of temporarily inserted and of permanently implanted biomedical devices. Among the various pathogenic fungi, *Candida* spp. are the most common cause of bloodstream infection in hospitalized patients.[4] The other fungal spp. that cause serious infections are *Cryptococcus* spp. (e.g., *Cryptococcus neoformans* that causes meningitis).

1.4 Surface contamination and microbial biofilms

Contamination of surfaces involves via the adhesion of microbial (e.g., bacterial) cells on the surfaces. The basic stages of bacterial adhesion are generally described by a two-stage binding model: an initial, rapid, and reversible interaction between the bacterial cell surface and the material surface, followed by a second irreversible stage that includes specific and nonspecific interactions between so-called adhesion proteins expressed on the pathogen surface (fimbriae or pilli) and binding molecules on the material surface (Figure 1.2).[20] Several quantifiable material surface features have been proposed to directly impact stage I bacterial adhesion.[20,21] These factors include material surface roughness, charge, degree of hydrophobicity, Lewis acid-base character, and hydrogen bonding capacity, etc. However, across the range of studies reported, some of these factors appear to enhance adhesion consistently. For example, increased surface roughness is proposed to increase bacterial adhesion due to the higher available surface area.[21] However, other studies which have observed a potential influence of surface roughness do not quantify these effects to a degree of statistical significance and have not identified a threshold roughness metric below which adhesion is mitigated.[22] Likewise, some studies have shown surface charge and/or hydrophobicity as critical to stage I adhesion efficiency, given the conditions that these surface properties modulate long- and mid-range forces and the capacity of bacteria to access the material surface in aqueous environments.[23] However, other studies with similar or different bacterial species find no correlation with hydrophobicity and suggest that the Lewis acid-base character (capacity for charge transfer between bacterial cells and material surface functional groups) as the key determinant.[24] A strong correlation between the mechanical stiffness of a material surface and the adhesion of bacteria has also been demonstrated.[25]

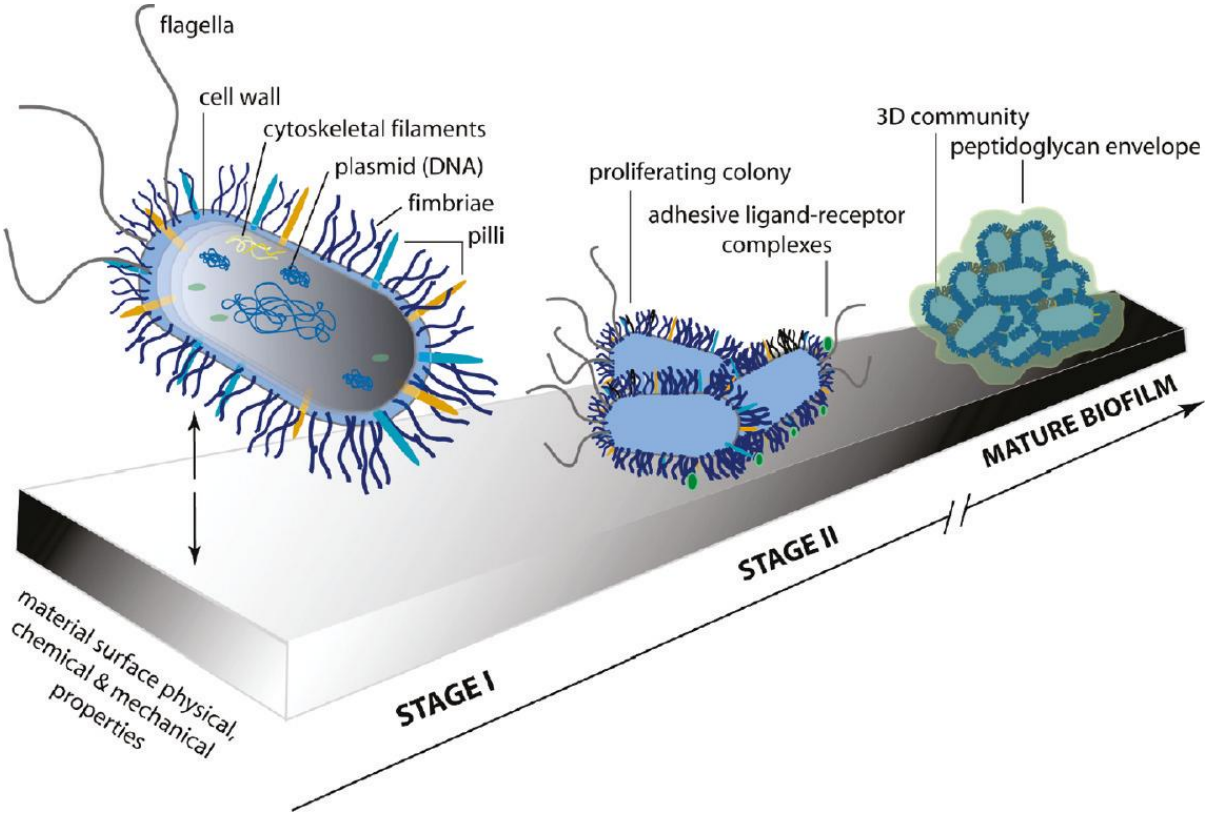

Figure 1.2: Schematic of prokaryotic, prototypical bacterial cell structure and the two-stage bacterial adhesion model that precedes organization of a mature biofilm (Figure was taken from reference 20 with the permission from American Chemical Society).

Infectious biofilms can be divided into surface-related (abiotic, e.g., implant's surface and biotic surfaces e.g., human skin) and tissue-associated or mucus-embedded cellular aggregates.[26] Most, if not all, medically important microorganisms can grow in biofilms, including bacteria (Gram-positive and Gram-negative; aerobic and anaerobic) and fungi (both moulds and yeast).[26] It has now been recognized that biofilms can potentially form on any foreign object inserted into the human body, such as implants or catheters, as well as in any place in the human body, such as in the lungs of patients with cystic fibrosis, or in chronic wounds that have an impaired blood supply. During biofilm formation, microbes secrete an exopolysaccharide layer that retains nutrients and protects the microorganisms from the immune response. With the protective polysaccharide coating and sequestered nutrients, microorganism in biofilms exhibit extreme resistance to antibiotics. In some cases, it has been found that killing bacteria in a biofilm requires roughly 1000 times the antibiotic dose necessary to achieve the same results in a suspension of cells. It has been found that nearly 99% of bacteria on earth live in biofilms and are associated with nearly 80% of all bacterial infections in humans.[26,27] Clearly, to prevent infections one needs to inhibit microbial colonization and subsequent biofilm formation onto surfaces possibly by interfering with

either stage I or stage II. More importantly, it would be idyllic to kill the microorganism immediately upon their adhesion onto surfaces thereby eliminating the chances of re-infecting the surface. If by chance the microbes are able to form biofilms on surface, the surfaces must be able to eradicate the established biofilms possibly by disrupting the protective exopolymeric layer as well as killing the embedded microbial cells.

1.5. Strategies to prevent infections: antimicrobial surface

The tremendous resistance of microbial biofilms to conventional antibiotic therapy and exceptionally high infecting ability of biofilms have prompted a great deal of research on developing antimicrobial surfaces and coatings that resist bacterial colonization.[28,29] Despite the potentially intimidating complexity of bacterial populations and of materials surface characteristics, there has been significant progress in the development of three general strategies to limit microbial colonization onto material surfaces: adhesion resistance (non-fouling strategy), biocide releasing (release-based strategy) and contact killing (contact-based strategy) (Figure 1.3).[20]

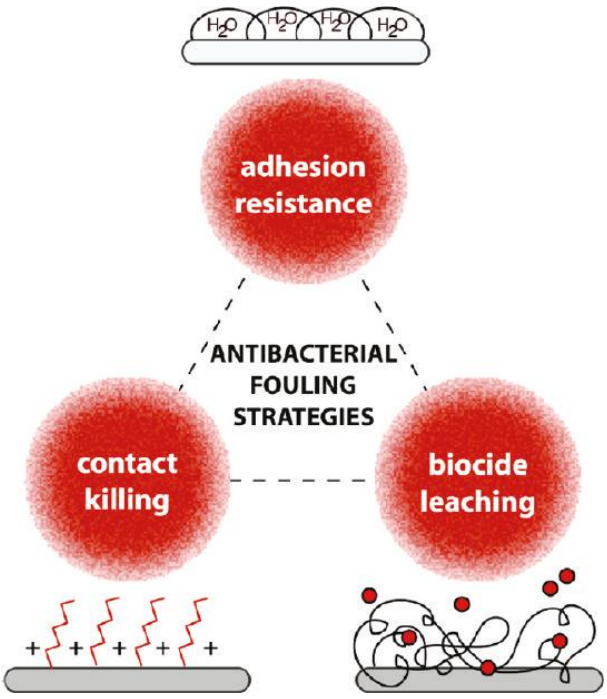

Figure 1.3: Three chief strategies for antibacterial surface design (Figure was taken from reference 20 with the permission from American Chemical Society).

1.5.1 Antifouling surface (adhesion resistance surface)

Antifouling fouling surface focuses on inhibiting microbial adhesion or reducing the capacity of microbes to achieve stage I and/or stage II adhesion. Such 'low-fouling' coatings also reduce the ability of planktonic microbes to adhere, thereby interfering with the earliest stages of biofilm formation (Figure 1.4A).[30]

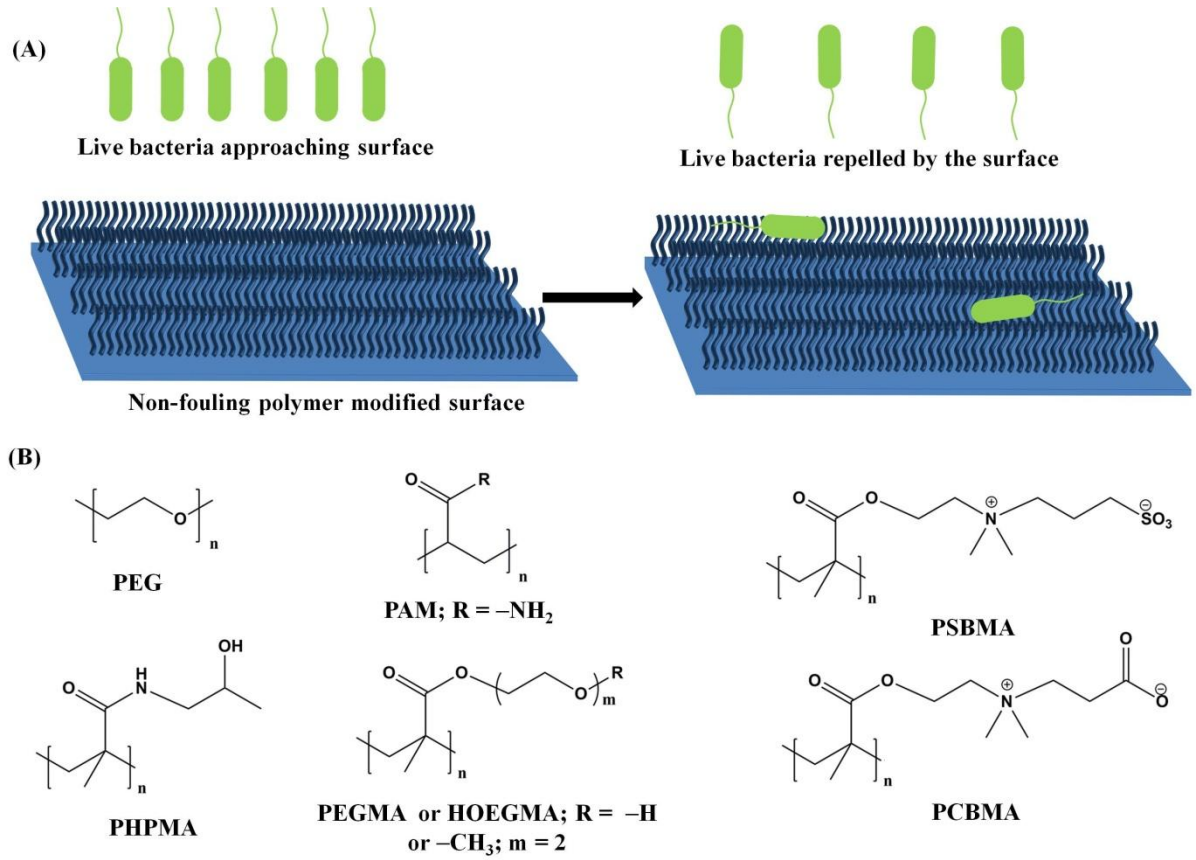

Figure 1.4: Mode of action of antifouling surface and various adhesion resistant materials. (A) Schematic representation of an antifouling polymer modified surface repelling bacteria. (B) Structures of some adhesion resistant polymers used in developing antifouling surface.

Different materials with microbial repelling properties have been successfully applied onto surfaces to yield antifouling coatings. One well established method for preventing microbial adhesion to surfaces is to coat them with a layer of poly(ethylene glycol), or PEG. It involves deposition of a self-assembled monolayer on a substrate (usually a gold surface), followed by fictionalization of the SAM to contain the required PEG functionality (Figure 1.4B).[31] Antifouling surface has also been developed by catecholic initiator from metal surfaces via surface-initiated polymerization of methyl methacrylate macromonomers with oligo(ethylene glycol) (OEG).[30] PEG polymeric surfaces are antifouling because of mainly

the hydrophilic interaction with the microbial cell, which does not favour microbial attachment to the surface. PEG, and modified PEG surfaces have been shown to inhibit the adhesion of microbes by up to a 3 log reduction.[8] The major drawback of this technology is that the deposition of PEG requires multiple synthetic steps and can only be done to a surface during manufacture.

Diamond-like carbon (DLC) films comprised of metastable, amorphous carbon with significant sp^3 character, containing small quantities of hydrogen hence known as amorphous hydrogenated carbon, was shown to possess microbe repelling properties. DLC, being biocompatible, has been used in surface coating for biomedical devices such as stents or replacement joints.[32] Reduction in microbial adhesion of more than 10^6 CFU/cm^2 was shown to be achieved by such coatings.[33] However, like other antifouling materials, poor antimicrobial activity of DLC and extensive chemical method (such as chemical vapor deposition) to coat the surfaces limit its application in antimicrobial coatings.

Water droplet contact angle is a measure of surface energy (i.e. hydrophilicity or hydrophobicity) thus can be used as an indicator of how easy it is for a microbe to colonize a surface. For self-cleaning surfaces, either an exceptionally hydrophilic (less than 10˚) or a highly hydrophobic (>140˚) surface is required.[8] Intermediate contact angles of 30-100˚ do not have easy clean features and are significantly easier for microbes to stick to, and conceivably form a biofilm. Hydrophobic materials (130˚ contact angle) were shown to significantly reduce microbial adhesion to a sample submerged in a microbial suspension.[34] The major drawback of the hydrophobic easy clean materials is that whilst preventing microbial contamination in the area treated, it does not address the problem of pathogenic microbes which are incident upon the surface. It merely moves them elsewhere and therefore does not offer fully effective solution of microbial contamination.

Recently polymers with zwitterionic head groups such as poly(phosphorylcholine), poly (sulfobetaine) and poly(carboxybetaine) polymers have been shown to inhibit bacterial adhesion and biofilm formation on surfaces (Figure 1.4B).[35,36] It is postulated that the zwitterionic head can associate a large amount of water making the material heavily hydrophilic. This leads to reversible interactions between the incident microbes and the surface-discouraging adhesion of microbial cells. These zwitterionic surfaces was shown to be promising for coating medical devices such as catheters, because of their biomimetic nature which firstly provides biocompatibility by reducing attachment of human cells to the device and secondly offers protection against bacterial biofilm formation. However, these

types of surfaces, like the easy clean technologies discussed earlier, still do not fully address the problem of microbial contamination as they have no antimicrobial functionality.

1.5.2 Release-based coating (biocide releasing)

The release based approach is focused on biocide leaching, in which antimicrobial compounds are released and diffused over time from a material surface, inducing death either of nearby (but nonadhered) bacteria or of adhered bacteria (Figure 1.5A).[17] A variety of active antimicrobials such as antibiotics, metal salts or nanoparticle, bioactive species (e.g., phage virus), etc. has been impregnated onto surfaces to develop biocide-releasing antimicrobial surfaces.[8]

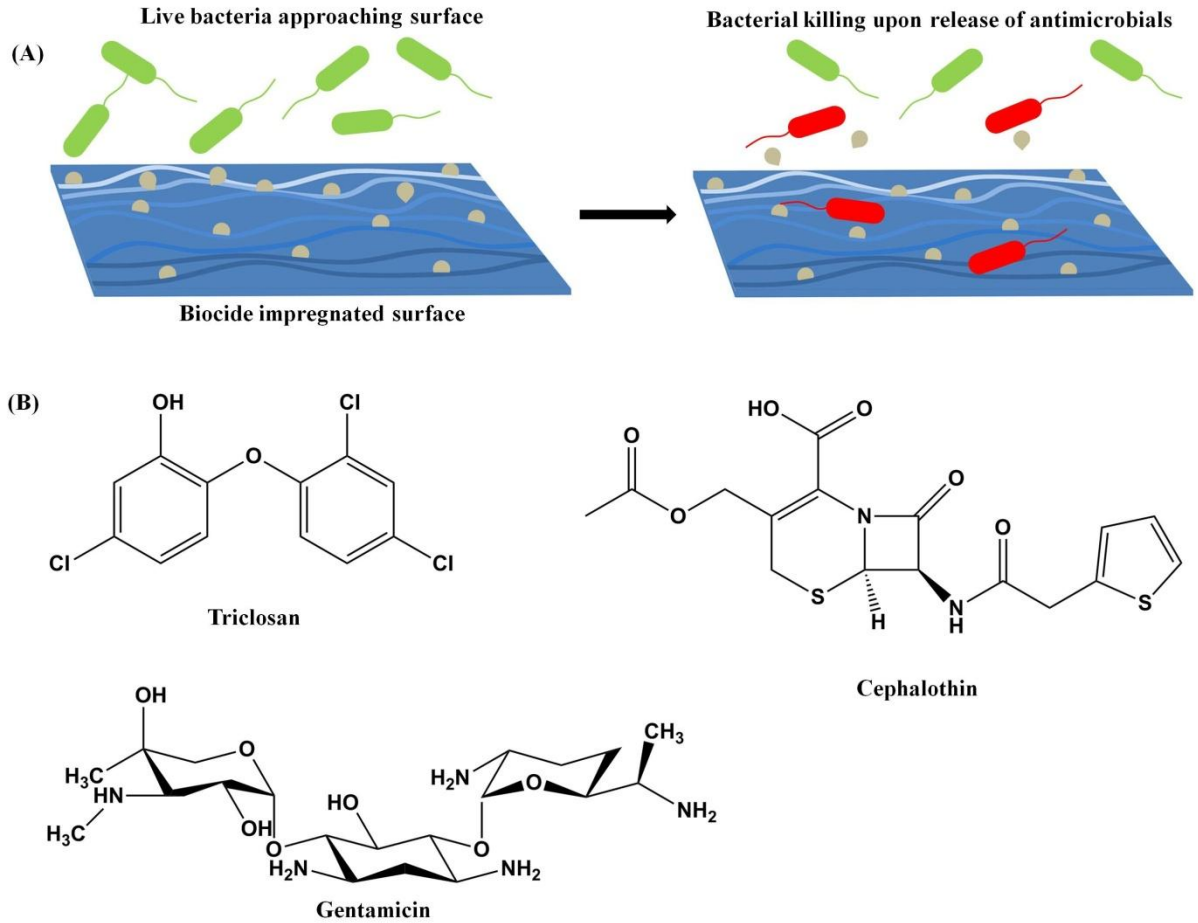

Figure 1.5: Release-based antimicrobial surface. (A) Schematic representation of a release-based antimicrobial coating wherein the active antimicrobial kills microbes upon release. (B) Structures of various antibiotics used in developing release-active surface.

One of the most heavily marketed and most widespread products for suppressing microbial growth is Microban. Microban incorporates Triclosan (5-chloro-2-(2,4-

dichlorophenoxy)- phenol), a broad spectrum phenolic antimicrobial, into a surface (Figure 1.5B). The antibiotic then leaches from the surface to perform the antimicrobial function. Triclosan is found in many products such as hand wash soaps, toothpastes as well as on touch surfaces and items like chopping boards and cling film, etc. Microban has been shown to suppress bacterial growth within the domestic, especially kitchen, environments also; though it is not widely used within hospitals.[8] Other antibiotics such cephalothin, gentamicin, etc. have also been utilized in developing release-active surfaces.[8] However, there has been significant concern about possible development of antibiotic resistance. Furthermore Triclosan can, under the action of UV light, produce dioxins, which are extremely hazardous to humans.

Silver has long been known to be an antimicrobial and the metal ions (Ag^+) have a significant antimicrobial activity against a variety of microorganism and have found uses in a number of commercial applications.[37,38] These include the silver sulfadiazine creams, successfully applied topically to burns patients. This cream consists of 1% silver sulfadiazine and 0.2% chlorhexidine digluconate and is effective as a result of the synergistic action of these antimicrobials. Silver has also been successfully used in wound dressings and as an additive in catheters and other medical devices.[39] When it comes to available commercial coating products; AgION Technology's AgION™ and AcryMed's SilvaGard™ are two of the most well known products. Both of these silver-containing products rely on the diffusion of Ag^+ ions from the substrate material and their subsequent action on adherent microbes as antimicrobials. It is believed that the effectiveness of Ag^+ as an antimicrobial is due to its ability to bind with thiol (–SH) groups on proteins and enzymes of microbes thereby inactivating them. Despite the initial effectiveness of these existing antimicrobial coatings, they have one major drawback-they are non-permanent, relying on diffusible antimicrobials to which microbes can develop resistance. Another possible drawback of silver based antimicrobials is the possibility of Ag^+ cytotoxicity towards mammalian cells.

Like silver, copper has long been considered to be a hygienic material.[40] It has been known since the 1980s that copper, along with other heavy metals such as cadmium and lead, is toxic to microbes. The antimicrobial activities of copper and some of its alloys have been assessed. A number of microbes of clinical importance, including methicillin-resistant *S. aureus, E. coli, C. difficile,* etc. have been shown to be inactivated by the copper containing surfaces.[40,41] Despite its excellent antimicrobial response however, copper may not be a suitable because of its instability in ambient conditions. Further, cytotoxicity towards

mammalian cells and unwanted release could further reduce its application in biomedical arena.

Another important way of developing release-active surfaces is by immobilizing bacteriophage viruses that infect prokaryotic cells.[42] Phages usually target individual species of bacteria, bind to their surface, inject their genetic material and replicate within the bacterial host. If the replication of the phage is a ‘‘lytic’’ process, the eventual result is the lysis of the host cell, and the release of more phages. The replication process is self propagating until there is no more host organism available. Developments of a phage containing wound dressing, hydrogel-coated silicone catheter, etc. with lytic bacteriophages have been well documented.[43,44] It was shown that phage-modified catheter surface reduced biofilm formation significantly. A phage-modified surface is certainly an interesting antimicrobial approach, in particular because organisms resistant to antibiotics do not show resistance towards phages. Equally, it only needs one phage to infect a host cell for a cascade in phage production thus is a very efficient way of disinfecting a surface without significantly deactivating the surface.[45] There are, however, a number of potential problems exist. The first is the inherent specificity of the phage for individual bacterial species. One other area of concern is that of phage resistance-bacteria can become resistant to a phage through mutations.

1.5.3 Contact killing

The contact-killing approach is focused on killing microbes upon contact, which seeks to biochemically induce death (e.g., via cell lysis) of microbes that have adhered stably to a surface (Figure 1.6A).[46] This is generally achieved via conjugation of an active antimicrobial (e.g., antibiotics, antimicrobial peptide, quaternary ammonium compounds, etc.) with the surface (Figure 1.6B).[46-50] However, because of the pathogen specific activity and resistance development, antibiotic based coatings are severely limited. Antimicrobial peptide (AMP) based coatings, on the other hand, suffer from high production cost of AMPs, low stability under *in-vivo* conditions and high toxicity towards mammalian cells. Antimicrobial surface coatings based on quaternary ammonium compounds (QACs) having high antimicrobial efficacy and the ability to withstand microbial resistance development were therefore largely reported.[51]

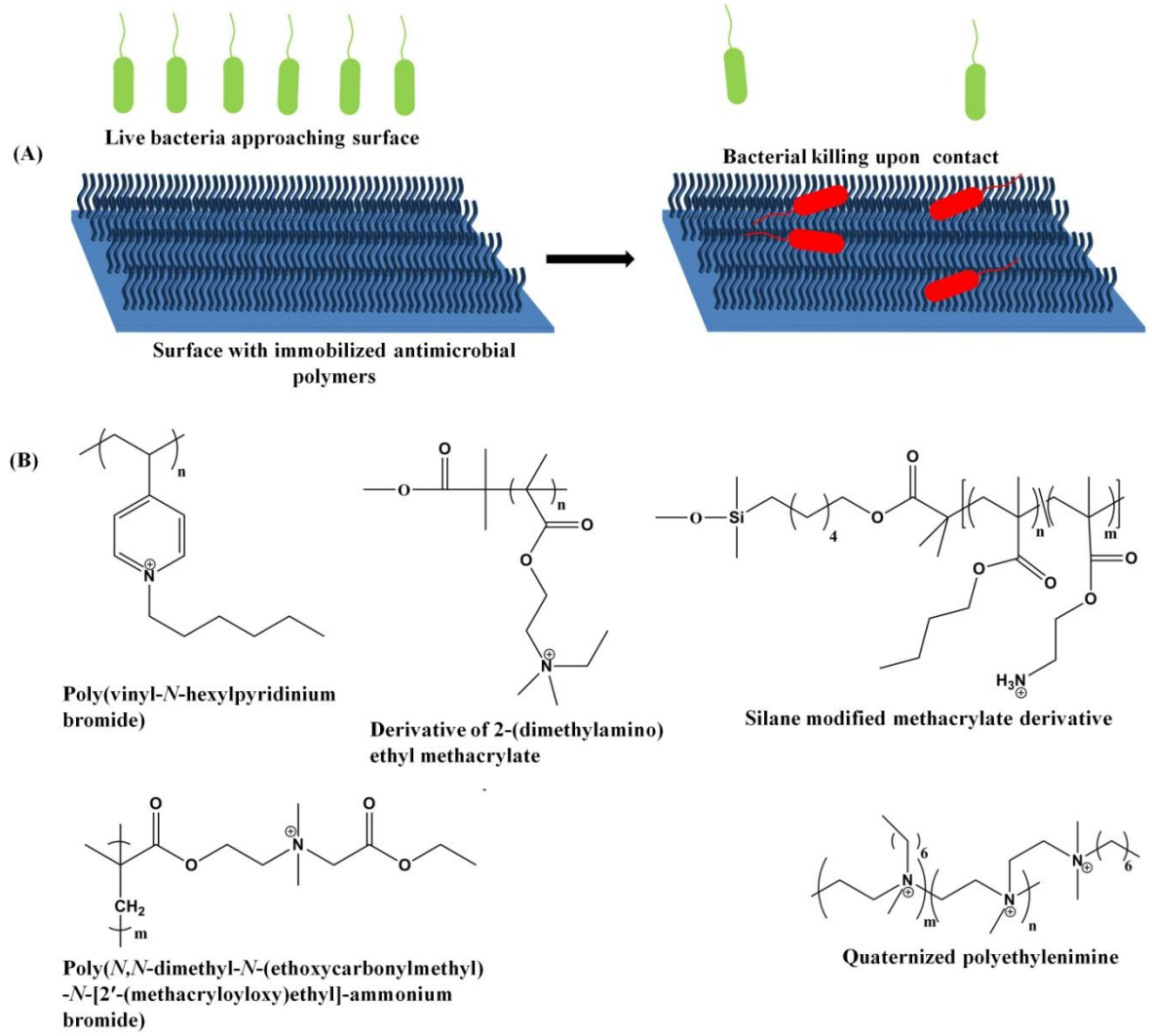

Figure 1.6: Contact-based antimicrobial surface. (A) Schematic representation of a contact-based antimicrobial coating wherein the active antimicrobial immobilized covalently kills microbes upon contact. (B) Structures of various quaternary polymers used in developing contact-active surface.

Surfaces with cations deposited upon them were shown to kill microbes upon contact in the early 1970s.[47] Recently surfaces treated with hydrophobic polycations were demonstrated to kill microbes in a similar manner upon contact with the modified surface possibly by causing physical damage to the microbe's cell envelope.[52] The basic premise of these materials is to target microbes by taking into account of two most important features of the microbial cell envelope which are hydrophobic and negatively charged. By developing a coating consisting of hydrophobic polymer chains, interaction with the microbe cell envelope is favored. However, the polymer chains will not tend to stand erect from the surface to interact with an incident microbe without some form of repulsive interaction between them. To this end, a positively charged moiety is required which would keep the hydrophobic

chains separated and erect from the surface, and also electrostatically attract microbes, due to the net negative charge on their surface. In effect, the hydrophobically modified cationic materials attract a microbe towards the modified surface, resulting in the puncturing of the microbial cell envelope, and subsequent death of the cell. The following sections deals with various charged polymers and hydrogels and their applications as antimicrobial coatings in preventing (biotic and abiotic) surface associated infections.

1.6 Charged polymers and hydrogels as antimicrobial coatings

The first examples of non-leaching surfaces capable of killing microorganisms on contact were described in the early 1970s.[47] Researchers from Dow Corning Corporation found that 3-(trimethoxysilyl)-propyldimethylalkyl ammonium chlorides with alkyl chain lengths varying from 6 to 22 carbons have high activity against algae in solution. However, when such compounds, e.g., 3-(trimethoxysilyl)-propyldimethyloctadecyl ammonium chloride (Si-QAC), were immobilized on surface. The modified surfaces were shown to be algicidal, bactericidal and fungicidal. In the early 1980's, a high throughput approach was demonstrated where solids upon chemisorption of organic or inorganic cations killed different microorganisms.[47] Remarkably, cations that had no antimicrobial activity in solution were capable of forming antimicrobial surfaces. Substance which formed a cation other than a proton was found to actively kill microorganisms. Non-cationic or acidic materials were generally shown to be inactive. More recent efforts focus on the development of new strategies for the immobilization of conventional antimicrobial agents (e.g. antimicrobial polymers, hydrogels, etc.) as described below.

1.6.1 Covalently immobilized non-leaching polycationic chains

1.6.1.1 Non-natural polycations

A significant number of non-natural polycationic compounds with antimicrobial properties have been developed and were used in developing antimicrobial surfaces upon covalent immobilization onto surfaces (Figure 1.6B).[53-55] The polymeric chains with an optimal balance of charge and hydrophobicity resisted hydrophobic inter chain aggregation via electrostatic repulsion and were able to penetrate microbial cell membranes effectively. To illustrate, surfaces containing immobilized long-chain alkylated cationic polyvinylpyridines (PVP) and alkylated cationic polyethylenimines have been reported to be lethal to microbes.[53] For example, glass slides or biomedical non-bactericidal polymers upon covalent modification with poly(vinyl-*N*-hexylpyridinium bromide) was found to kill 90 to 99% of

Gram-positive and Gram-negative bacteria. Further, the length of the alkyl chains was found to have significant effect on antimicrobial efficacy of the immobilized polymers and was shown optimum hydrophobicity (Figure 1.7).[53] Remarkably, these coatings do not promote microbial resistance. Unfortunately less is known about their cytotoxicity and biocompatibility i.e., their biological behaviour when implanted *in-vivo*. However, very recently, the biocompatibility and *in-vivo* activity of alkylated cationic polyethylenimines based coatings have been described wherein the coatings were shown to be compatible towards cornea or bone tissue *in-vivo* and shown to be active in both cornea and bone infections model.[5657]

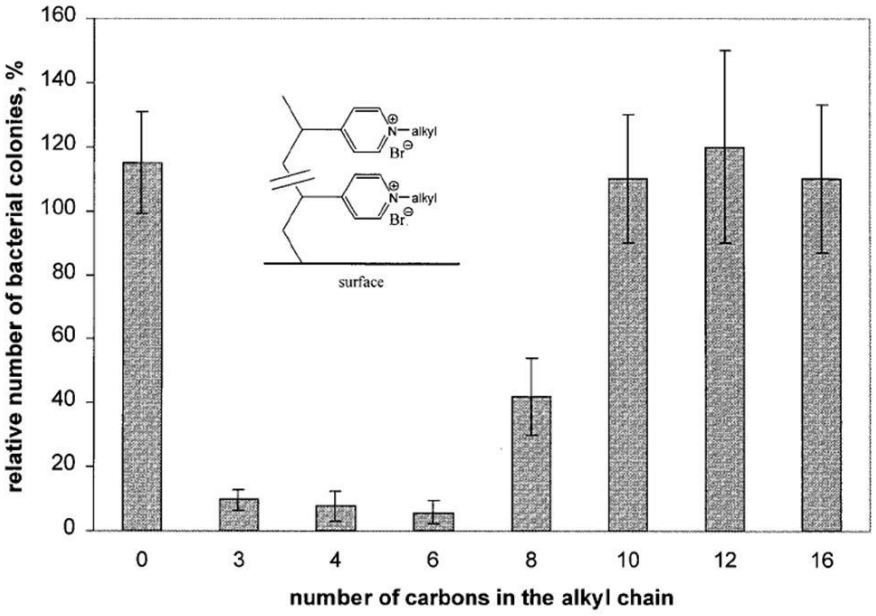

Figure 1.7: The percentage of bacterial (*S. aureus*) colonies grown on the surfaces of glass slides modified with PVP that was *N*-alkylated with different linear alkyl bromides relative to the number of colonies grown on a commercial NH_2-glass slide (used as a standard). The bacterial cells were sprayed from an aqueous suspension (10^6 cells per ml) onto the surfaces (Figure was taken from the reference 53 with permission from Proceedings of the National Academy of Sciences, USA).

Another approach to render medical device surfaces antimicrobial involves the silanization with quaternary ammonium-containing silane agents (Figure 1.6B). For example, the modification of micro-fibrillated cellulose with alkoxysilane octadecyldimethyl-(3-trimethoxysilylpropyl)-ammonium chloride rendered the material highly microbiocidal.[58] In another example, hydrolytically stable polymer, *N*-alkylmethoxysilane pyridinium based coating on glass surfaces was shown to be lethal against various bacteria tested.[55] However, the success rate of obtaining high quality silane coatings is not particularly high. The problem

lies in exceptional sensitivity of the silane coating chemistry to experimental conditions, such as the solvent, humidity, the concentration of the trace amount of water in the solvent, surface cleaning, temperature, etc. Competitive reactions can easily lead to polymer and aggregate formation due to cross linking in the solution phase before being immobilized onto surface. As a result, the quality of the silane coating varies greatly from lab to lab and from person to person. The precise antimicrobial mechanism of cationic polymers immobilized onto surfaces remains ambiguous. However, it is thought that the mechanism of action involves penetration of the long cationic polymer into the cell membrane leading to cell membrane disruption.[52] Another proposed mechanism of action involves ion exchange between the positive charges on the surface and structurally critical mobile cations within the membrane.[23] The loss of these structural cations results in the loss of membrane integrity. Further investigation is required to unravel the mechanism behind the antimicrobial properties of polycationic chains.

1.6.1.2 Natural polycations

Among the various natural biopolymers, chitosan has been mostly used in developing antimicrobial surface. Being a polycationic polymer, chitosan can be an alternative to the non-natural polycationic polymers described above as antimicrobial agents for biomedical devices. Chitosan, a derivative of naturally occurring chitin and composed of β-(1-4)-linked 2-amino-2-deoxy-D-glucopyranose and 2-acetamido-2-deoxy-D-glucopyranose units, is inherently antimicrobial, non-toxic and biodegradable which make this polymer an suitable candidate for use in biomedical device coating.[59] Several biomedical devices containing chitosan including wound dressings and devices for artery closure have been approved by the Food and Drug Administration (FDA). The immobilization of chitosan to confer antimicrobial and cell adhesive properties to orthopaedic and craniofacial implant devices has also been described.[60] Notably, surfaces coated with chitosan have been shown to resist biofilm formation by both bacteria and yeast.[61] Though found to be effective, insolubility in organic or aqueous solvents and poor antimicrobial activity of chitosan limit its applications as broad spectrum and effective antimicrobial coatings. Moreover, the antimicrobial activity of chitosan is mostly pH dependent which can further reduce its efficacy. For example, chitosan has been shown to be inactive in contact with bile fluids (pH above 7.0) possibly due to the deprotonation of amine groups in the polymer.

1.6.2 Physically adsorbed non-leaching polycationic chains

In general, the immobilization of polycationic chains described in the previous section requires different chemical strategies for different surfaces which might be an obstacle for the scaling-up of the coating process. Further, it requires several chemical steps that might affect the physical properties of biomedical devices and ultimately their biological performance. An alternative approach has been described recently in which antimicrobial surfaces were fabricated by a simple dip-coating or a "painting" methodology.[62,63] Instead of covalently immobilizing the polycations to a surface, the polymer was physically immobilized by noncovalent hydrophobic interactions. To illustrate, polymeric coatings of water-insoluble and organo-soluble *N,N*-dodecylmethyl-polyethyleneimine on glass surfaces has been described by simple 'painting' of the polymer from their organic solvents (Figure 1.8).[63] The coating was able to eliminate influenza virus as well as *E. coli* and *S. aureus* with 100% efficiency. Broadly applicable coating method based on emulsion polymerization using water-insoluble antimicrobial emulsifiers has also been developed. In this case, a water-insoluble diblock copolymer, PS-b-P4VMP, which consists of a hydrophobic (polystyrene, PS) and an antimicrobial hydrophilic (poly(4-vinyl-N-methylpyridinium iodide), P4VMP) block, was used as an emulsifier in the aqueous emulsion polymerization of mixtures of styrene and butyl acrylate.[64] Coatings prepared from stable aqueous suspensions of these polymers were shown to act as contact-active antimicrobial surfaces against *S. aureus*. More recently, a non-covalent coating based on cellulose-graft-poly(2-ethyl-1,3-oxazoline) terminated with an antimicrobial *N,N*-dimethyldodecylammonium (DDA) which killed microbial cells on contact has been developed.[65]

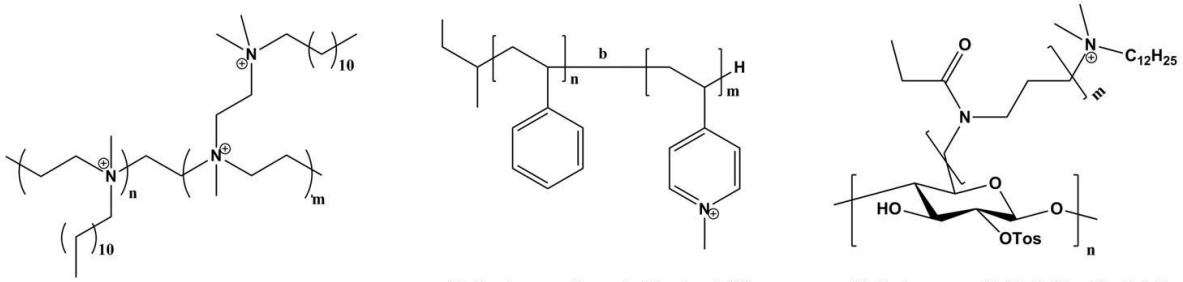

N,N-dodecylmethyl-polyethyleneimine

Polystyrene-b-poly(4-vinyl-*N*-methylpyridinium iodide

Cellulose-graft-Poly(2-ethyl-1,3-oxazoline) Terminated with *N,N*-dimethyldodecyl ammonium

Figure 1.8: Structures of various cationic polymers used in developing antimicrobial paint non-covalently.

The microbicidal mechanism of these paintings is thought to be the same as the one described for the covalent immobilization of polycationic polymers. It requires the physical contact of the microorganism with the painting. In addition, bactericidal effect has also been observed to be related to the molecular composition and organization in the top 2-3 nm of the surface and increases with increasing hydrophilicity and pyridinium concentration of the surface. It should be mentioned that antimicrobial paint using two different antimicrobial materials have been developed and were shown to be highly efficacious in removing microbial infection.[66-68] For example, silver bromide-poly(4-vinylpyridine)-*co*-poly(4-vinyl-*N*-hexylpyridinium bromide) (AgBr/NPVP) nanocomposites were prepared via on-site precipitation of AgBr nanoparticles from poly(4-vinyl-*N*-hexylpyridinium bromide) polymer which yielded dual action antimicrobial coating materials.[66] The polymeric nanocomposites were shown to act via both release-active as well as contact-active mode of action thereby displaying long lasting activity and enhanced biofilm inhibition ability.

1.6.3. Antimicrobial hydrogel for prevention of infection

Hydrogels are a class of materials formed from natural or synthetic polymers that exhibit three-dimensional (3D) networks with high to ultra-high degree of water content. Hydrogels have been used in many biomedical applications, including drug and protein delivery, tissue engineering, cell culture, antimicrobial coatings and wound dressing. Importantly, due to their high water content, gels provide a moist, heavily hydrated environment to the wound area thus facilitating cellular immunological activity essential to the wound healing process. However, this same hydrated environment can also facilitate microbial infection. Thus, gels capable of imparting antimicrobial action are desirable. Many antimicrobial hydrogel have been developed by imparting various antimicrobial agents (e.g, quaternary ammonium groups, antibiotics, metal nanoparticles, etc.) directly or indirectly into the hydrogel matrix made up of either natural or synthetic polymers.

1.6.3.1. Natural polymeric hydrogels

Naturally occurring polymers because of their inherent biocompatibility and biodegradability have been utilised extensively to develop antimicrobial hydrogels.[69] To illustrate, soft positive charge containing polyelectrolyte complex hydrogel system based on chitosan-γ-poly(glutamic acid) was shown to possess antimicrobial activities against bacteria, and at the same time demonstrated effectiveness in promoting 3T3 fibroblasts cell proliferation. The hydrogels were also evaluated and proved useful for wound-healing capabilities.[70]

Permanently positive charge containing and broad spectrum antimicrobial hydrogel based on dimethylalkylammonium chitosan (with various degrees of quaternization)-graft-poly(ethylene glycol) methacrylate (qC-g-EM) and poly(ethylene glycol) diacrylate has been developed (Figure 1.9).[69,71]

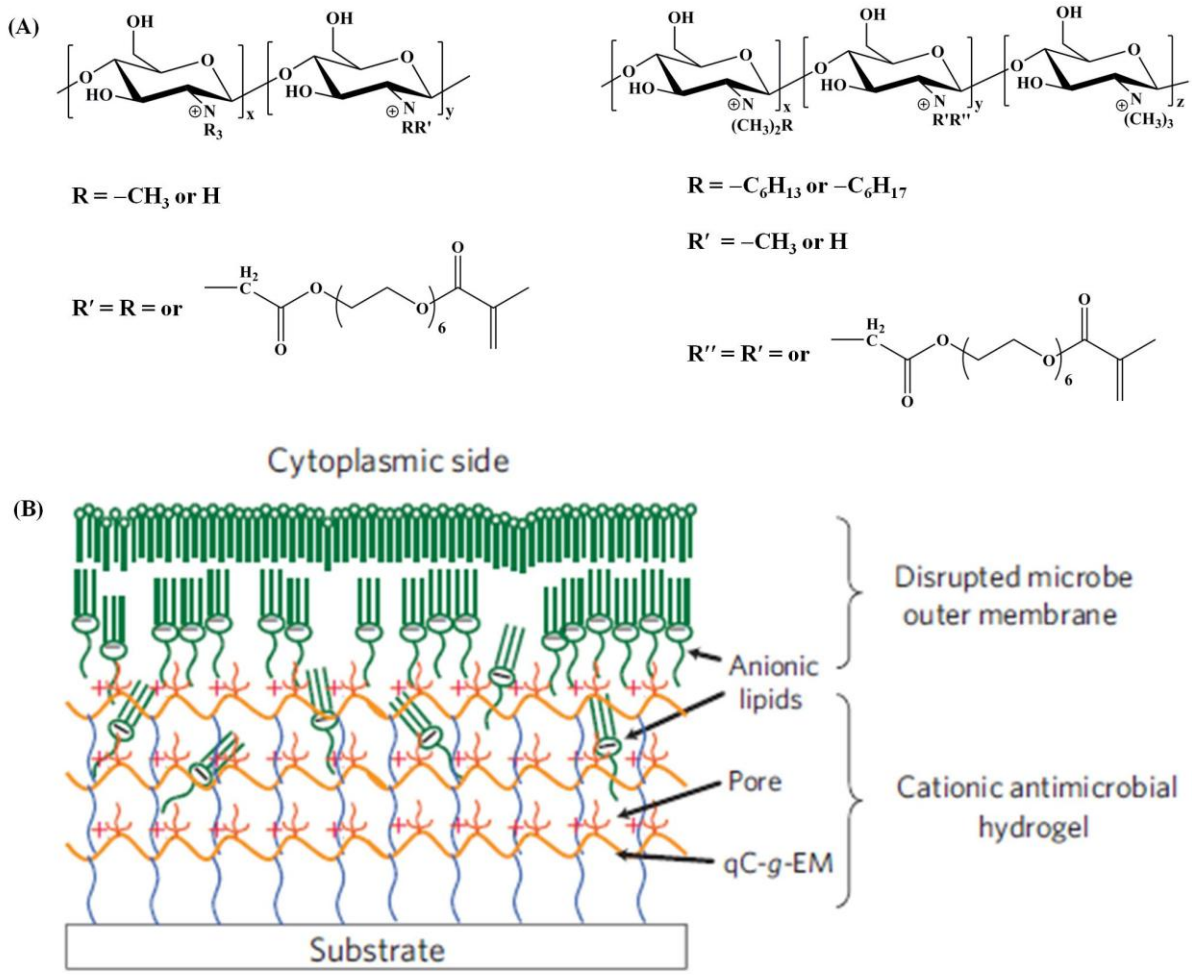

Figure 1.9: (A) Synthesis of modified chitosan-based antimicrobial polymers. (B) Schematic diagram of the 'anion sponge' model showing parts of the negatively-charged bacterial membrane being 'suctioned' into the pores of the hydrogel (Figure was reproduced from the reference 69 with the permission from Elsevier).

Chitosan because of its biocompatible and intrinsic antimicrobial activity was used as precursor polymer. Furthermore, quaternization and fictionalization was shown to enhance the polymer's solubility in water and activity against pathogenic microbes. The cationic nanoporous hydrogels obtained via UV polymerization of dimethylalkylammonium chitosan-graft-poly(ethylene glycol) methacrylate have been successfully immobilized onto contact lenses and were shown to be biocompatible. The mechanism of the gel is thought be a membrane-active action: the anionic bacterial cell wall/membrane would first interact with

the cationic hydrogel surface at several fixed points via electrostatic attraction, followed by insertion of the hydrophobic segments of the hydrogel into the hydrophobic regions of the lipid membrane, thereby inducing leakage of cell contents and subsequent lysis. Synthesis and antimicrobial activity of chitosan hydrogels which were cross-linked with various concentrations of oxalyl bis-4-(2,5-dioxo-2H-pyrrol-1(5H)-yl)benzamide.[72] Although natural polymeric hydrogels have seen significant success in antimicrobial activity, batch-to-batch variation in molecular weights of natural polymers may compromise reproducibility and affect physical properties. Immunogenecity is often reported with the use of natural polymers, which is caused by impurities in natural polymers.

1.6.3.2. Synthetic polymeric hydrogels

Synthetic cationic polymers have emerged as important antimicrobial alternatives to antibiotics.[73,74] These materials can be synthesized in a variety of ways and can be composed of either biodegradable or non-biodegradable polymer backbones. A plethora of antimicrobial synthetic cationic polymers have been reported such as poly(acrylate) and poly(norbornene) systems, poly(ethyleneimine)s (PEIs), poly(arylamide)s, poly-β-lactams, poly-α-amino acids and polycarbonates (Figure 1.10).[69,73]

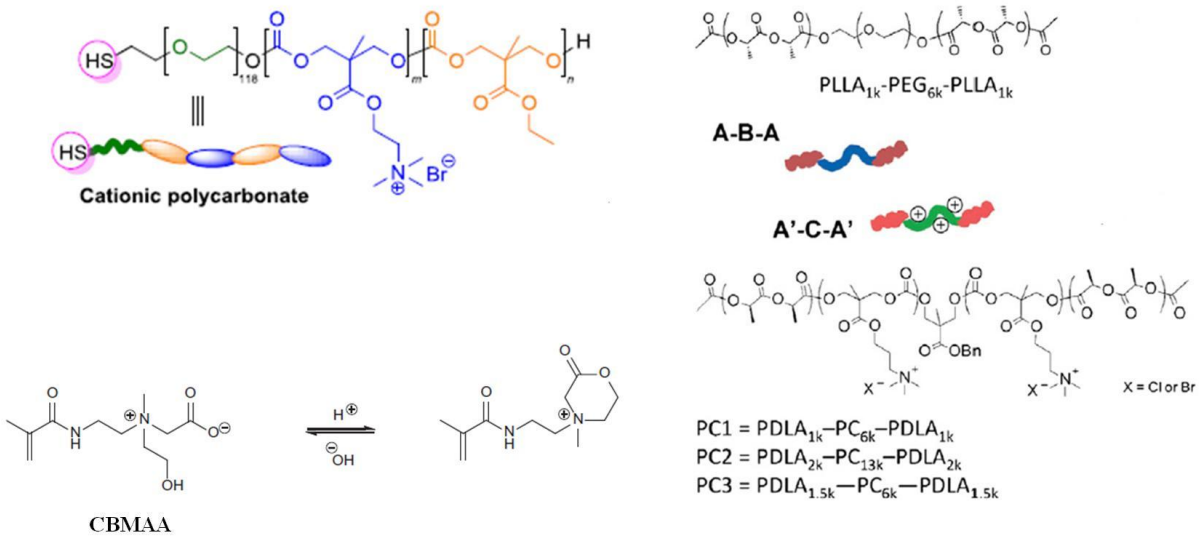

Figure 1.10: Structures of various synthetic antimicrobial polymers used in developing antimicrobial hydrogel (Figure was reproduced from the reference 69 with the permission from Elsevier).

In spite of this, there have only been a few attempts to develop hydrogel from synthetic cationic polymers in which the gel would be intrinsically antimicrobial. For example,

antimicrobial and antifouling hydrogels were developed *in-situ* from cationic polycarbonate and four-arm poly(ethylene glycol) (PEG) via Michael addition and shown to display strong antimicrobial properties.[75] These gels were also successfully coated onto catheter and shown to be active against pathogen. In another example, the synthesis of physically cross-linked broad-spectrum antimicrobial hydrogels derived from the stereocomplexation of biodegradable polymers PLLA-PEG-PLLA (PLLA = poly(L-lactide)) and polycationic PDLA-CPC-PDLA (PDLA = poly(D-lactide), CPC = cationic polycarbonate) was described.[76] Notably, these gels were not antimicrobial but also found to destroy established microbial biofilms. Dual action antimicrobial and antifouling hydrogels were also prepared by UV-photopolymerization in the presence of carboxybetaine dimethacrylate (cross-linker), 2-hydroxy-2-methylpropiophenone (initiator).[77] Here, a cationic six-membered *N*,*N*-dimethyl-2-morpholinone (CB-ring; antimicrobial) was used wherein the ring due proton abstraction switched to a zwitterionic carboxy betaine (CB-OH; antifouling) moiety. An impressive killing efficiency was demonstrated for the cationic hydrogel while the zwitterionic gel upon deprotonation showed non-fouling activities. In addition, acrylate/methacrylate, poly(allylamine) polymer based systems have been modified into antimicrobial hydrogels by simple cross-linking.[78,79] However, synthetic complexities, high production cost along with multiple synthetic steps are some of the limitations of synthetic polymer based hydrogels.

1.6.3.3. Peptide-based hydrogels

In addition to the polymer-based hydrogel systems described above, several notable peptide-based antimicrobial hydrogels have also been reported. For example, β-hairpin hydrogel scaffold based on the self-assembling 20-residue peptide MAX1 (2 wt%) was developed whereby the hydrogel was shown to possess intrinsic broad-spectrum antibacterial activity.[80] This is possibly a result of the polycationic, lysine-rich hydrogel surface having the ability to disrupt negatively-charged bacterial cell membranes via electrostatic interactions. Notably, the hydrogel was also shown permit mammalian cell adhesion and proliferation while simultaneously inhibiting bacterial growth.

An injectable β-hairpin hydrogel based on the 20-residue peptide MARG1 was also developed which was shown to be capable of killing MRSA on contact.[81] Activity towards MRSA was thought to be from arginine residues in addition to lysine, which possibly brings about specific interactions with the bacteria. Modified epsilon-poly-L-lysine (EPL), an antimicrobial peptide produced by *Streptomyces albulus*, with methacrylamide moieties, were

cross-linked with PEG diacrylate to form biocompatible antibacterial hydrogels.[82] EPL was selected for its edibility, non-toxicity, biodegradability, and low production costs. The resulting hydrogel materials were found to exhibit excellent activity against a number of clinically relevant bacteria and fungi. Furthermore, the hydrogels could be immobilized onto plastic surfaces via UV-generated surface radicals cross-linked to free acrylates/methacrylates, making them excellent candidates for use as antimicrobial coatings for medical devices and implants.

1.6.4. Hydrogel releasing active agents

Though antimicrobial hydrogel systems were shown to have incredible efficacy in destroying multi drug-resistant microbes and breaking down biofilms upon contact, the interactions between the antimicrobial polymers and microbial cell membranes are non-specific, and in most cases the hydrogels also result in mammalian cell death above certain concentrations. In addition, many applications (avascular, e.g., cartilage tissue or less vascular, e.g., bone tissue infections where antibiotics cannot reach effectively) still require the incorporation of antibiotics in combination with hydrogels to fight bacterial infections without compromising human cell viability. Penicillins and cephalosporins are the most widely used antibiotics followed by fluoroquinolones.[69] However, their overuse and misuse have led to an increasing number of resistant pathogens. Thus a combination of synthetic antimicrobial polymers and antibiotics could potentially evade problems of drug resistance by virtue of the polymer's membrane-lytic mechanism while mitigating polymer toxicity since the co-usage of antibiotics allows for a smaller amount of polymer to be used.

To illustrate, combined PVA/chitosan hydrogels together with minocycline, a broad-spectrum antibiotic, was described with improved wound healing activity due to both minocycline and the antifungal effect of chitosan.[83] In spite of the advantages of utilizing antimicrobial hydrogels for the delivery of antibiotics, in most of the studies, hydrogels themselves do not possess any antimicrobial activity. Several other polysaccharides have been used for the delivery of therapeutics due to their biocompatibility and biodegradability. For example, dextran-based hydrogels containing the broad-spectrum antifungal drug amphotericin B was shown to kill *C. albicans* efficiently without causing hemolysis.[84] Recently, there have been substantial advances towards the use of silver ions and silver nanoparticles (AgNPs) in hydrogels for wound treatment. The antimicrobial activity of silver and other metal salts has been attributed to the metal cation causing cell membrane disruption

and subsequent lysis. Potential applications for metal containing hydrogels include the use of silver-impregnated gels for medical devices, coatings, water purification, and contact lenses.

1.6.5. Injectable bioadhesive hydrogel

Injectable bioadhesives hydrogels containing a group of liquid or semiliquid compounds are applied to a tissue incision for the purpose of closing wounds, adhering to soft tissues and hemostasis.[85] They comprise natural substances and/or synthetic chemicals, typically in the form of monomers, pre-polymers, or non cross-linked polymers. When delivered to a tissue at the surgical site components undergo polymerization or cross-linking reaction among themselves as well as react to the components of extracellular matrix (ECM) leading to an insoluble adhesive matrix. However, infection at the incision sites (e.g., surgical site infections, SSI) can often lead to many complexities such as prolonged wound healing, wound dehiscence, abscess formation and, in severe cases, sepsis. SSIs thus represent a significant clinical burden in patients that are typically readmitted, often into intensive care units. Thus an ideal adhesive hydrogel should rapidly solidify in the physiological condition to minimize bleeding and demonstrate strong tissue bonding, tissue healing and activity in controlling infections at the site applications.

However commonly used adhesive gels generally lack antibacterial properties and demands extensive antibiotics usage to prevent or control infections. For example, the fibrin-based adhesive containing fibrinogen and thrombin does not have any antibacterial activity. Further, these materials are prone to cause immunogenic reaction because of the usage of natural proteins. Biocompatible bioadhesive materials were therefore developed either from natural or synthetic polymers and antibacterial activity have been imparted by using additional antimicrobials or by making polymeric components inherently antimicrobial. Many antibacterial injectable hydrogels been described by encapsulating various antibacterial agents such as antibiotics, metal nanoparticles, etc. into the matrix and were shown to kill microorganism upon releasing the active materials.[85] However, the materials lack permanent antibacterial activity and might suffer from uncontrolled and unwanted release of the antibacterial agents. Injectable hydrogel with inherent antibacterial activity have also been developed. To illustrate, an antimicrobial chitosan-dextran (CD) hydrogel was found to be active against a variety of microorganism.[86] Syringe-injectable bioadhesive hydrogels with inherent antibacterial properties prepared from mixing polydextran aldehyde and branched polyethylenimine was also described.[87] These adhesives killed both Gram-negative and Gram-positive bacteria, while sparing human erythrocytes. The cationic adhesive was also

effective in a cecal ligation and puncture model, preventing sepsis and significantly improving survival.

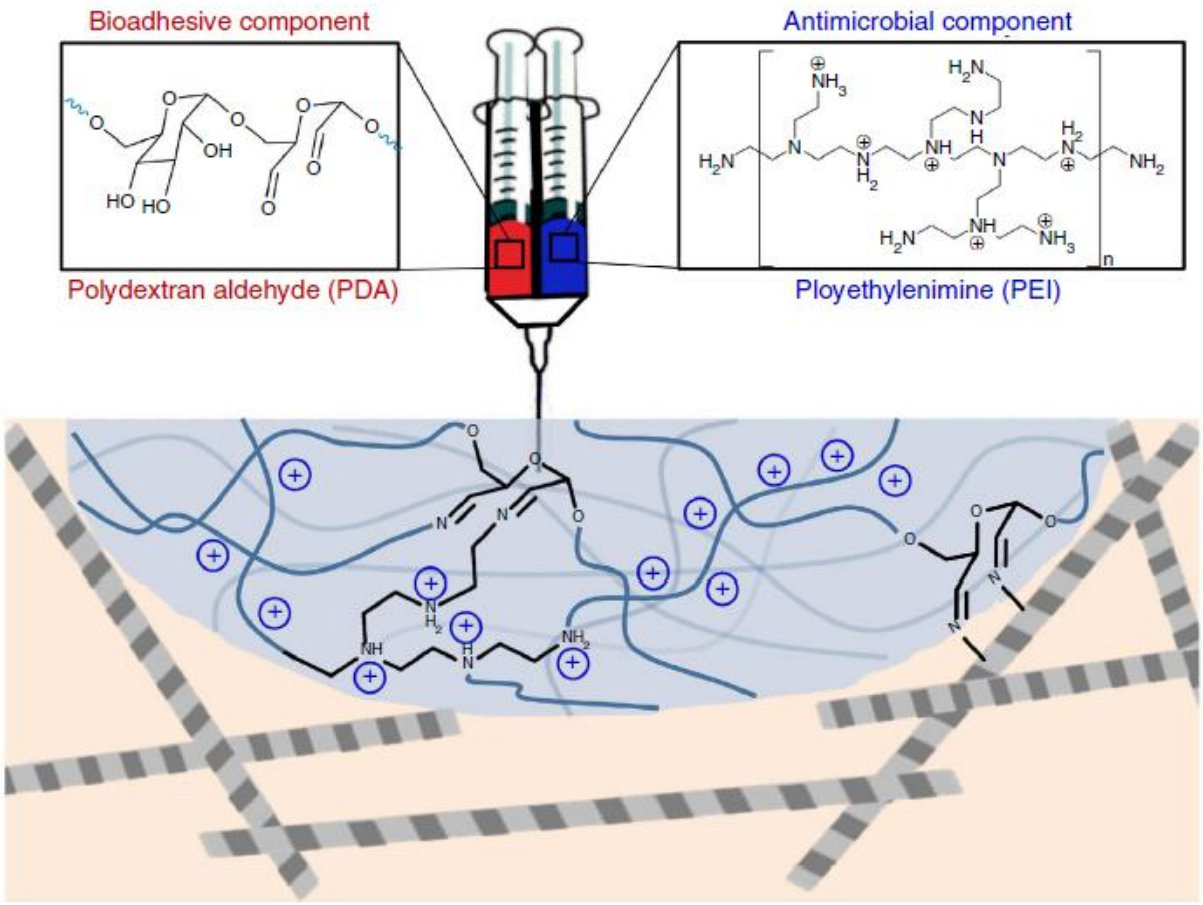

Figure 1.11: Design of injectable bioadhesive hydrogels with inherent antibacterial activity. The precursor components such as bioadhesive PDA and an antibacterial PEI, define the material's bioadhesive and antibacterial properties, respectively (Figure was taken from the reference 87 with the permission from Nature Publishing Group).

1.7. Unmet challenges in antimicrobial coatings and prevention of infections

Antimicrobial coatings developed by impregnating antibiotics, metal nanoparticles or various other biocides for the abiotic surfaces such as medical devices and implants are limited due to cumulative toxicity, increased development of microbial resistance and unwanted release of biocides. In contrast, contact-active antibacterial coatings developed by immobilizing antibacterial agents, e.g., antibacterial polymers, do not leach out from the surface and are less likely to allow bacterial resistance development. However, covalent immobilization of antibacterial polymers on surfaces is limited due to several synthetic steps, using of harsh reagents and elevated temperatures. Non-covalent modification of surfaces, on the other hand, is simple, facile and easy to apply. Despite evidences of antimicrobial activity of

polymers coated non-covalently, there are no clear-cut reports on the structure-activity relationship of the quaternary polymers used for antimicrobial coatings for the prevention of infection. It is therefore necessary to understand the structure-activity relationship and mechanism of action of the polymers at the molecular level. Also, microbial resistance, one of the major threats at present time, is yet to be understood against the water-insoluble and organo-soluble antimicrobial polymers. Further, the antimicrobial activity of cationic polymers has been mostly investigated against bacteria although the fungal infections remain as a key hazard to human health. When associated with the bacterial infections, fungal proliferation has been shown to induce an increased frequency or severity of diseases.[38,39] Hence it is meaningful to develop polymers with both antibacterial and antifungal activity and study their structure-activity relationship for the future development of broad spectrum multifunctional coating materials.

Further, to be suitable for use in biomedical devices and implants, the antimicrobial polymers should be degradable and biocompatible. Unfortunately, commonly used polymers are mostly non-degradable and often lack biocompatibility. The long-term exposure of non-degradable coatings might results in unpredictable cytotoxicity and can create hindrance in implant-tissue integration for many indwelling devices applications. Ideally, an antibacterial coating should kill bacteria and prevent microbial colonization on medical devices or implants for desired period of time and disappear after its intended use. Thus developing biodegradable antimicrobial coatings and determining their biocompatibility and biodegradability require comprehensive investigation. The lack of *in-vivo* activity also limits the usage of the currently developed antimicrobial coating materials. It is therefore necessary to understand and evaluate the *in-vivo* activity of the materials along with their biofilm inhibition properties.

Biomedical devices that are used in less vascular tissue (e.g., bone infection due to bone fixture devices) or in avascular tissue (e.g., cartilage infections due to joint replacement devices) often suffer from many complications. Microbial contamination of these devices can lead to severe infections which are difficult to treat because of the limited penetration of antibiotics. It requires revision surgeries which further bring about new infections along with the suffering of patients and enhanced cost. Antimicrobial device coatings which act by both release- and contact-active mechanisms thus removing bacteria both from the device surface and surrounding tissue will be more suitable for such applications. Moreover, coating with dual mechanism of action should be developed *in-situ* to overcome the synthetic complexity mainly associated with the dual action antimicrobial coatings. Further, the materials would be

easily applicable onto device surfaces non-covalently for easy fabrication. It is therefore desirable to develop antimicrobial coatings with both release- and contact-active mechanisms especially from a highly active and biodegradable antimicrobial polymer and a release-active antimicrobial which act relatively more selectively towards microbes and capable of withstanding microbial resistance development.

Biodegradable antimicrobial polymer- or peptide-loaded gels are more attractive than gels encapsulated with antibiotics or metal nanoparticles as antibiotics easily develop drug resistance and it is relatively more difficult to mitigate toxicity of metal nanoparticles due to their nondegradability. Particularly, when hydrogels are used to simultaneously co-deliver antimicrobial polymers/peptides and conventional antimicrobial agents, a strong synergistic effect can be achieved. This co-delivery approach significantly mitigates antimicrobial polymer/ peptide-associated toxicity toward human tissue and normal human flora by allowing for smaller amounts of polymer/peptide to be used. The polymer/peptide in turn enhances the potency of the conventional antimicrobial agents, and together, they can reduce the incidence of drug resistance. For future clinical applications, it is important to test hydrogels against clinically-isolated microbes, especially multidrug-resistant strains, and evaluate the in vitro and in vivo biocompatibility of hydrogels and encapsulated cargo. With rational design, synthetic polymer chemistry, and comprehensive in vitro and in vivo evaluation, hydrogel systems having broad-spectrum antimicrobial activity against multidrug-resistant microbes, high selectivity and negligible toxicity, would find great potential in the prevention and treatment of infections.

Superficial infections associated with the topical biotic surfaces such as human skin represent a continuous threat because of the regular and harsh exposure of such surfaces towards open environments. Topical ointments and gels that are applied to treat such infections generally use antibiotics or antimicrobial peptides as antimicrobial component. However, these agents are increasingly becoming ineffective in treating the superficial infections. While the usage of antibiotic is largely limited by the resistance development in microbes, use of antimicrobial peptides or lipopeptides, though being highly effective, are limited due to their high cost of production and synthetic complexicity. To overcome these challenges, significant progress has been made in developing antimicrobial gels suitable for topical applications. These materials generally include either metal or metal oxide nanoparticles as antimicrobial components which act on microbes by releasing active ions or include a cationic polymer with quaternary ammonium groups which act on microbes upon contact. While the toxicity and microbial resistance development still remain the major issues

for the inorganic nanoparticle containing gels, antimicrobial activity of cationic hydrogels depends on cross-linking degree, hydrophobicity, and charge density. Moreover, these gels are generally are incapable of eradicating bacterial biofilms. For treating superficial infections, a highly active yet non-toxic antimicrobial compounds capable of eradicating established microbial biofilms (e.g., membrane-active cationic small molecules in simple synthetic methodology thus overcoming the synthetic challenges associated with AMPs) can be developed. These molecules can subsequently be loaded into a biocompatible hydrogel wherein the compounds upon gradual release from the gel will kill microorganism and annihilate biofilm without resistance development.

To seal the leakage and cease the bleeding from the damaged tissue at the wound site, bioadhesives antimicrobial hydrogels capable of fixing themselves with the tissue are used as non-invasive sealants. These materials offer numerous advantages over traditional wound management techniques not only by controlling bleeding but also by acting as void fillers thereby facilitating a faster wound healing. However, infections at the wound site due to surgical contamination or diffusion of skin microbes can be severely life threatening and can cause whole body infection known as sepsis. Given the capacities of bioadhesive materials, more investigations are expected to focus on improving upon existing adhesives and developing new antimicrobial sealants. Challenges of making ideal tissue adhesives, which can be utilized in various clinical applications, are multi-fold. Strong adhesion, safety and biocompatibility, ease of accessibility and use in clinical environment, and last but not least the high antimicrobial efficacy are among the challenges to be addressed. Considering their promising performances, new tissue adhesives with enhanced antimicrobial activity and higher wound healing capacity might be the solution to many of those challenges. In addition, inherently active tissue adhesives than can deliver antibiotics locally in a controlled manner can be more effective as these material will not only act synergistically but also be effective in reducing infection in avascular or less vascular tissue level by delivering antibiotics at the target site more efficiently.

1.8. Scope of the thesis

Microbial contamination on both biotic and abiotic surfaces is the major cause of deadly community-acquired and hospital-acquired (nosocomial) infections. Thus there is an ever-growing demand to develop antimicrobial surfaces which can effectively prevent microbial colonization on the desired surface without causing mammalian cell toxicity. In addition,

growing microbial resistance with diminishing antibiotic pipeline urges the need for antimicrobial coating materials that can withstand microbial resistance development. Current methods of developing antimicrobial surfaces involve usages of either various release-active antimicrobials such as antibiotics, inorganic nanoparticles, etc. which are limited due to resistant development in microbes and toxicity or covalent immobilization of cationic antimicrobial polymers which require several chemical synthetic strategies with multiple number of synthetic steps thus limiting their practical feasibility. It is therefore necessary to develop coating materials which can be applied onto surfaces non-covalently via simple one-step painting method. Lack of proper structure-activity relationship of the coatings further requires detailed investigation of the cationic antimicrobial polymers at the molecular level. Also, to be suitable in biomedical device coatings, biocompatible and/or biodegradable coating materials that can be applied onto surfaces non-covalently are required which after their use would disappear. Also, by combining two different coating strategies (such as release and contact active methods) there is still a chance to improve the antimicrobial efficacy and long lasting activity of the materials. In addition, to be suitable for biotic surface associated infections (e.g., superficial or dip tissue level), coating materials with high antimicrobial activity and biocompatibility are required to overcome the poor efficacy under *in-vivo* conditions and biocompatibility of the currently used topical and bioadhesive antimicrobials. Because of their high biocompatibility and capacity in delivering antimicrobials into the target sites, hydrogels with potent yet non-toxic antimicrobial agents are to be developed. This thesis therefore aims at the design and development of various cationic antimicrobial polymers and hydrogels as antimicrobial materials to combat infections on both abiotic and biotic surfaces.

Chapter 2A describes the preparation of novel antimicrobial coating materials based on polyethylenimine (PEI) and study their structure-activity relationship and the mechanism of action at the molecular level. Synthesis of colorless water-insoluble and organo-soluble PEI derivatives by *Eschweiler-Clarke methylation* of PEIs and subsequent quaternization of *N*-methyl PEIs with alkyl bromides was reported for the first time. The method allowed the synthesis of cationic PEIs with known structure and high reproducibility. Further, structure-activity relationships of the cationic PEI derivatives were studied by preparing a library of polymers with different molecular weights, molecular architecture and varying hydrophilic/hydrophobic balance. Linear polymers with octadecyl chain were found to be more active than the branched polymers. The polymers, when painted onto surfaces, inactivate both airborne and waterborne bacteria completely including drug-resistant bacteria and pathogenic

fungi. These polymeric materials showed excellent compatibility with other polymers and commercial paint thus could be useful for the development of self-defensive "microbicidal paint". The cationic polymers were shown to inactivate both bacteria and fungi by disrupting the membrane integrity and were shown to stall development of microbial resistance. Further, the polymers showed negligible hemolytic activity towards human erythrocytes. Thus the cationic polymeric materials developed in this chapter could potentially be used as ″microbicidal paint″ in hospital walls, floors, surgical equipments, etc.

However, the non-biodegradability of the alkylated cationic PEIs hinders their use inside the body. **Chapter 2B** addresses this unmet need and describes a unique approach to introduce cleavable groups such as amide or esters into the side alkyl chains of the cationic PEI based polymers. Introduction of cleavable groups such as amide or ester between the positive charge and hydrophobic alkyl chain of cationic PEI polymers led to the synthesis of side-chain degradable polymers. The length of side chains of these polymers was much closer to the octadecyl chain (a hexadecyl chain along with the amide or ester group) which allowed synthesizing water-insoluble and organo-soluble yet antimicrobial polymers with cleavable groups. The polymers also showed potent antimicrobial and antibiofilm efficacy against both bacteria and fungi when coated onto surfaces. Medical grade catheters were shown to be effective in reducing bacterial count and inhibiting biofilm formation in-vivo upon coating with these polymers. Notably, the hydrolysed polymers were shown to exceptionally biocompatible under both in-vitro and in-vivo conditions. The method of developing cationic PEI derivatives with amide and ester groups in the alkyl chain thus provided side-chain degradable coatings materials. However, as the PEI is non-degradable in nature the polymers (backbone) were not fully biodegradable.

Chapter 3A is thus aimed in developing biodegradable antimicrobial coatings from a naturally occurring polymer chitin which backbone is degradable in the presence of enzymes (lysozyme and chitinase). This novel approach introduced quaternary ammonium group with different alky chains into C-6 position of chitin thus resulting in organo-soluble cationic chitin polymers. The effect of degree of quaternization (DQ) and length of hydrophobic alkyl chain on the material's solubility and antimicrobial activity were systematically evaluated. The polycationic materials were able to kill both drug-sensitive and drug-resistant bacteria including multi drug-resistant (MDR) clinical isolates and shown to inhibit biofilm formation upon coating onto various surfaces. Not only against bacteria, the polymers showed excellent efficacy against various human pathogenic fungi and were also shown to be effective in inhibiting fungal biofilm

formation on the coated surface. Notably, the polymers were non-toxic towards mammalian cells and susceptible towards hydrolytic enzymes under both *in vitro* and *in vivo* upon subcutaneous implantation in mice. Upon painting these polymers, medical grade polyurethane catheter was shown to be effective in reducing bacterial burden and inhibiting biofilm formation *in vivo*. The polymeric coatings developed so far inactivate microbes only upon contact (contact-active killing).

Chapter 3B describes the successful development of biocompatible and dual action antimicrobial polymer-silver nanocomposites via *in-situ* reduction of silver ions using the quaternary chitin derivatives. As the quaternary chitin polymers contain terminal aldehyde groups (came from the naturally occurring chitin) reduction silver ions to metallic silver occurred *in-situ*. In addition, the polymers with its electron donating atoms such as nitrogen or oxygen acted as potent capping agent to the silver nanoparticle and therefore can lead to polymer-silver nanocomposites. The organo-soluble nanocomposites when coated onto surfaces were shown to be highly active against both Gram-positive and Gram-negative bacteria including various human pathogenic fungi. Importantly, the composites were found to kill both bacteria and fungi at a much faster rate than the polymer alone and showed remarkably long-lasting activity. Further, the composites inhibited both bacterial and fungal biofilm formation on the coated surfaces even after repeated challenges. Negligible toxicity towards mammalian cells was observed both *in-vitro* and *in-vivo*. The composites upon coating to a medical grade catheter showed excellent efficacy in reducing microbial burden both on the catheter and in the surrounding tissues in a mice model of subcutaneous infection. Further coated catheter was also shown to be effective in inhibiting bacterial biofilm formation under *in-vivo* conditions.

Chapter 4A describes development of cationic small molecular biocides featuring two positive charges, multiple non-peptide amide groups placed in different places of the molecules and variable hydrophobic/hydrophilic character which mimics the action of natural microbicidal peptides yet stable under plasma conditions and non-toxic towards mammalian cells. The molecules synthesized via facile inexpensive methodology not only displayed good antibacterial activity against wild-type bacteria but also showed activity against various drug-resistant bacteria. The biocides were also shown to eradicate established biofilms. Mechanistic studies revealed that the cationic molecules inactivated bacteria by disrupting the membrane integrity and were shown to hinder the propensity of bacterial resistance development. Negligible toxicity against human erythrocytes and human embryo kidney cells were observed for the most active molecules. Further the molecules showed high 50% lethal doses *in-vivo* and no skin toxicity upon application on skin. Notably, the optimised molecule was shown to reduce bacterial burden

and eradicate preformed bacterial biofilm in a murine model of superficial skin infection. Development of new classes of non-toxic small molecules with high antibacterial and antibiofilm activities thus could lead to the new generation of therapeutics which would find applications in various healthcare especially topical treatments.

Chapter 4B describes development of antibacterial and antibiofilm hydrogels capable of eradicating established topical bacterial biofilms without causing substantial skin toxicity. The hydrogels were prepared using dextran methacrylate (Dex-MA), a highly biocompatible and photopolymerizable polymer, and the optimised cationic biocide developed in chapter 4A via direct loading of the biocide with desired and controlled amounts. The biocide impregnated gels displayed strong antibacterial activity against both drug-sensitive and drug-resistant bacteria. The gels were shown to release the biocide for an extended period of time and killed bacteria by releasing the biocide into the surroundings. Moreover, the gels not only eradicated established bacterial biofilms *in-vitro* but also shown to be highly efficacious in clearing established bacterial biofilm in superficial skin infection in mice model. Notably, excellent skin compatibility was observed for all the hydrogel formulations in different animal models (high lethal dose in rat model, no skin sensitization in guinea pig model and negligible skin irritation in rabbit model). The biocompatible antibiofilm gels developed in this chapter might hold great promise to be used in removing bacterial biofilms and treating topical infections.

Infection at wound sites due to surgery or accident represents a major threat as it delays healing and in severe cases, leads to sepsis. Injectable bioadhesive materials are often used non-invasively to close wounds. However, such injectable bioadhesives materials rarely come with both antibacterial, hemostatic and wound healing properties. **Chapter 5A** describes the development of a biocompatible injectable hydrogel with inherent bioadhesive, antibacterial, wound healing and hemostatic capabilities suitable in wound sealing and wound infection treatment at the tissue level. The two component injectable hydrogels were prepared *in-situ* from an antibacterial *N*-(2-hydroxypropyl)-3-trimethylammonium chitosan chloride (HTCC) and bioadhesive polydextran aldehyde (PDA). The components upon mixing reacted with other via imine bond formation leading to hydrogelation and also reacted with the amine groups of extracellular matrix (ECM) when present thus providing the bioadhesive properties. The gels were shown to be active against both Gram-positive and Gram-negative bacteria. Mechanistic studies revealed that the gels killed bacteria upon contact by disrupting the membrane integrity of pathogen. Importantly, the gels were shown to be efficacious in preventing sepsis in a cecum ligation and puncture (CLP) model in mice. The gels were also shown to be effective in facilitating wound healing in rats and ceasing bleeding from a damaged liver in mice. Notably,

the gel showed negligible toxicity towards human red blood cells and no inflammation to the surrounding tissue upon subcutaneous implantation in mice thereby proving it as a safe and effective antibacterial sealant.

Infections in relatively less vascular tissues (e.g., bone tissue infections), in avascular tissues (e.g., cartilage tissue infections) or in necrotic tissues (e.g., surgical site infections, SSI) are very challenging because of the limited penetration of antibiotics into the target tissues. **Chapter 5B** deals with the development of a dual action antibacterial injectable hydrogel for controlled release of antibiotics and delivering the drug locally to treat such infections. The syringe deliverable bioadhesive hydrogel was prepared by mixing the buffer solution of PDA containing antibiotic vancomycin and aqueous solution of the antibacterial polymer HTCC developed in Chapter 5A. The antibiotic was loaded via primarily covalent (imine) bond formed between the aldehyde group of PDA and amine group of vancomycin. The gel was shown to release the antibiotic over an extended period of time at different pH. Importantly, antibiotic loaded gels showed much higher activity than the gel alone against bacteria for an extended period of time. The gels were also shown to be impressively active under *in-vivo* conditions. Further, when bacteria were injected at a distal site far from the gel, the vancomycin loaded gel was shown to eradicate infection completely *in-vivo*. No toxicity towards human red blood cells (hRBC) and to the surrounding tissue was observed under *in-vivo* conditions. The dual action injectable bioadhesive gel prepared in this chapter therefore might hold promise in combating infections at less vascular or avascular tissue level.

BIBLIOGRAPHY

1. Morens, D. M.; Folkers, G. K.; Fauci, A. S. Emerging infections: a perpetual challenge. *Lancet Infect. Dis.* **2008,** *8*, 710-719.
2. Morens, D. M.; Folkers, G. K.; Fauci, A. S. The challenge of emerging and re-emerging infectious diseases. *Nature* **2004,** *430*, 242-249.
3. Ganguly, N. K.; Arora, N. K.; Chandy, S. J.; Fairoze, M. N.; Gill, J. P. S.; Gupta, U.; Hossain, S.; Joglekar, S.; Joshi, P. C.; Kakkar, M.; Kotwani, A.; Rattan, A.; Sudarshan, H.; Thomas, K.; Wattal, C.; Easton, A.; Laxminarayan, R.; Resistance, G. A. Rationalizing antibiotic use to limit antibiotic resistance in India. *Indian J. Med. Res.* **2011,** *134*, 281-294.
4. Brown, G. D.; Denning, D. W.; Gow, N. A.; Levitz, S. M.; Netea, M. G.; White, T. C. Hidden killers: human fungal infections. *Sci. Transl. Med.* **2012,** *4*, 165rv13.
5. Sanborn, W. R. The relation of surface contamination to the transmission of disease. *Am. J. Public Health Nations Health* **1963,** *53*, 1278-1283.
6. Ayliffe, G. A. The progressive intercontinental spread of methicillin-resistant Staphylococcus aureus. *Clin. Infect. Dis.* **1997,** *24 Suppl. 1*, S74-S79.
7. Dancer, S. J. Importance of the environment in meticillin-resistant Staphylococcus aureus acquisition: the case for hospital cleaning. *Lancet Infect. Dis.* **2008,** *8*, 101-113.
8. Page, K.; Wilson, M.; Parkin, I. P. Antimicrobial surfaces and their potential in reducing the role of the inanimate environment in the incidence of hospital-acquired infections. *J. Mater. Chem.* **2009,** *19*, 3819-3831.
9. Oie, S.; Hosokawa, I.; Kamiya, A. Contamination of room door handles by methicillin-sensitive/methicillin-resistant Staphylococcus aureus. *J. Hosp. Infect.* **2002,** *51*, 140-143.
10. Dietze, B.; Rath, A.; Wendt, C.; Martiny, H. Survival of MRSA on sterile goods packaging. *J. Hosp. Infect.* **2001,** *49*, 255-261.
11. Banerjee, D.; Fraise, A.; Chana, K. Writing pens are an unlikely vector of cross-infection with methicillin resistant Staphylococcus aureus (MRSA). *J. Hosp. Infect.* **1999,** *43*, 73-75.
12. Bures, S.; Fishbain, J. T.; Uyehara, C. F. T.; Parker, J. M.; Berg, B. W. Computer keyboards and faucet handles as reservoirs of nosocomial pathogens in the intensive care unit. *Am. J. Infect. Control* **2000,** *28*, 465-471.
13. Talon, D. The role of the hospital environment in the epidemiology of multi-resistant bacteria. *J. Hosp. Infect.* **1999,** *43*, 13-17.
14. Hota, B. Contamination, disinfection, and cross-colonization: are hospital surfaces reservoirs for nosocomial infection? *Clin. Infect. Dis.* **2004,** *39*, 1182-1189.
15. Neely, A. N.; Maley, M. P. Survival of enterococci and staphylococci on hospital fabrics and plastic. *J. Clin. Microbiol.* **2000,** *38*, 724-726.
16. Darouiche, R. O. Treatment of infections associated with surgical implants. *N. Engl. J. Med.* **2004,** *350*, 1422-1429.
17. Hetrick, E. M.; Schoenfisch, M. H. Reducing implant-related infections: active release strategies. *Chem. Soc. Rev.* **2006,** *35*, 780-789.
18. Salwiczek, M.; Qu, Y.; Gardiner, J.; Strugnell, R. A.; Lithgow, T.; McLean, K. M.; Thissen, H. Emerging rules for effective antimicrobial coatings. *Trends Biotechnol.* **2014,** *32*, 82-90.
19. Boyce, J. M.; Potter-Bynoe, G.; Chenevert, C.; King, T. Environmental contamination due to methicillin-resistant Staphylococcus aureus: possible infection control implications. *Infect. Control Hosp. Epidemiol.* **1997,** *18*, 622-627.
20. Lichter, J. A.; Van Vliet, K. J.; Rubner, M. F. Design of antibacterial surfaces and interfaces: polyelectrolyte multilayers as a multifunctional platform. *Macromolecules* **2009,** *42*, 8573-8586.

21. Tang, H. Y.; Wang, A. F.; Liang, X. M.; Cao, T.; Salley, S. O.; McAllister, J. P.; Ng, K. Y. S. Effect of surface proteins on Staphylococcus epidermidis adhesion and colonization on silicone. *Colloids Surf., B* **2006,** *51*, 16-24.
22. Cao, T.; Tang, H.; Liang, X.; Wang, A.; Auner, G. W.; Salley, S. O.; Ng, K. Y. Nanoscale investigation on E. coli adhesion to modified silicone surfaces. *Methods Mol. Biol.* **2011,** *736*, 379-388.
23. Murata, H.; Koepsel, R. R.; Matyjaszewski, K.; Russell, A. J. Permanent, non-leaching antibacterial surfaces - 2: how high density cationic surfaces kill bacterial cells. *Biomaterials* **2007,** *28*, 4870-4879.
24. Wang, A.; Cao, T.; Tang, H.; Liang, X.; Black, C.; Salley, S. O.; McAllister, J. P.; Auner, G. W.; Ng, K. Y. Immobilization of polysaccharides on a fluorinated silicon surface. *Colloids Surf., B* **2006,** *47*, 57-63.
25. Lichter, J. A.; Thompson, M. T.; Delga-Dillo, M.; Nishikawa, T.; Rubner, M. F.; Van Vliet, K. J. Substrata mechanical stiffness can regulate adhesion of viable bacteria (vol 9, pg 1571, 2008). *Biomacromolecules* **2008,** *9*, 2967-2967.
26. Bjarnsholt, T.; Ciofu, O.; Molin, S.; Givskov, M.; Hoiby, N. Applying insights from biofilm biology to drug development - can a new approach be developed? *Nat. Rev. Drug Discov.* **2013,** *12*, 791-808.
27. Costerton, J. W.; Stewart, P. S.; Greenberg, E. P. Bacterial biofilms: a common cause of persistent infections. *Science* **1999,** *284*, 1318-1322.
28. Lewis, K.; Klibanov, A. M., Surpassing nature: rational design of sterile-surface materials. *Trends Biotechnol.* **2005,** *23*, 343-348.
29. Campoccia, D.; Montanaro, L.; Arciola, C. R. A review of the biomaterials technologies for infection-resistant surfaces. *Biomaterials* **2013,** *34*, 8533-8554.
30. Banerjee, I.; Pangule, R. C.; Kane, R. S. Antifouling coatings: recent developments in the design of surfaces that prevent fouling by proteins, bacteria, and marine organisms. *Adv. Mater.* **2011,** *23*, 690-718.
31. Ostuni, E.; Chapman, R. G.; Liang, M. N.; Meluleni, G.; Pier, G.; Ingber, D. E.; Whitesides, G. M. Self-assembled monolayers that resist the adsorption of proteins and the adhesion of bacterial and mammalian cells. *Langmuir* **2001,** *17*, 6336-6343.
32. Hauert, R. A review of modified DLC coatings for biological applications. *Diamond Relat. Mater.* **2003,** *12*, 583-589.
33. Liu, C.; Zhao, Q.; Liu, Y.; Wang, S.; Abel, E. W. Reduction of bacterial adhesion on modified DLC coatings. *Colloids Surf., B* **2008,** *61*, 182-187.
34. Parkin, I. P.; Palgrave, R. G. Self-cleaning coatings. *J. Mater. Chem.* **2005,** *15*, 1689-1695.
35. Cheng, G.; Zhang, Z.; Chen, S. F.; Bryers, J. D.; Jiang, S. Y. Inhibition of bacterial adhesion and biofilm formation on zwitterionic surfaces. *Biomaterials* **2007,** *28*, 4192-4199.
36. Hirota, K.; Murakami, K.; Nemoto, K.; Miyake, Y. Coating of a surface with 2-methacryloyloxyethyl phosphorylcholine (MPC) co-polymer significantly reduces retention of human pathogenic microorganisms. *FEMS Microbiol. Lett.* **2005,** *248*, 37-45.
37. Atiyeh, B. S.; Costagliola, M.; Hayek, S. N.; Dibo, S. A. Effect of silver on burn wound infection control and healing: review of the literature. *Burns* **2007,** *33*, 139-148.
38. Kumar, A.; Vemula, P. K.; Ajayan, P. M.; John, G. Silver-nanoparticle-embedded antimicrobial paints based on vegetable oil. *Nat. Mater.* **2008,** *7*, 236-241.
39. Noyce, J. O.; Michels, H.; Keevil, C. W. Potential use of copper surfaces to reduce survival of epidemic meticillin-resistant Staphylococcus aureus in the healthcare environment. *J. Hosp. Infect.* **2006,** *63*, 289-297.
40. Weaver, L.; Michels, H. T.; Keevil, C. W. Survival of Clostridium difficile on copper and steel: futuristic options for hospital hygiene. *J. Hosp. Infect.* **2008,** *68*, 145-151.

41. Noyce, J. O.; Michels, H.; Keevil, C. W., Inactivation of influenza A virus on copper versus stainless steel surfaces. *Appl. Environ. Microbiol.* **2007,** *73*, 2748-2750.
42. Sulakvelidze, A.; Alavidze, Z.; Morris, J. G. Bacteriophage therapy. *Antimicrob. Agents Chemother.* **2001,** *45*, 649-659.
43. Markoishvili, K.; Tsitlanadze, G.; Katsarava, R.; Morris, J. G.; Sulakvelidze, A. A novel sustained-release matrix based on biodegradable poly(ester amide)s and impregnated with bacteriophages and an antibiotic shows promise in management of infected venous stasis ulcers and other poorly healing wounds. *Int. J. Dermatol.* **2002,** *41*, 453-458.
44. Curtin, J. J.; Donlan, R. M., Using bacteriophages to reduce formation of catheter-associated biofilms by Staphylococcus epidermidis. *Antimicrob. Agents Chemother.* **2006,** *50*, 1268-1275.
45. Pearson, H. A.; Sahukhal, G. S.; Elasri, M. O.; Urban, M. W. Phage-bacterium war on polymeric surfaces: can surface-anchored bacteriophages eliminate microbial infections? *Biomacromolecules* **2013,** *14*, 1257-1261.
46. Klibanov, A. M. Permanently microbicidal materials coatings. *J. Mater. Chem.* **2007,** *17*, 2479-2482.
47. Ferreira, L.; Zumbuehl, A. Non-leaching surfaces capable of killing microorganisms on contact. *J.Mater. Chem.* **2009,** *19*, 7796-7806.
48. Wach, J. Y.; Bonazzi, S.; Gademann, K. Antimicrobial surfaces through natural product hybrids. *Angew. Chem. Int. Ed.* **2008,** *47*, 7123-7126.
49. Pritchard, E. M.; Valentin, T.; Panilaitis, B.; Omenetto, F.; Kaplan, D. L. Antibiotic-releasing silk biomaterials for infection prevention and treatment. *Adv. Funct. Mater.* **2013,** *23*, 854-861.
50. Cado, G.; Aslam, R.; Seon, L.; Garnier, T.; Fabre, R.; Parat, A.; Chassepot, A.; Voegel, J. C.; Senger, B.; Schneider, F.; Frere, Y.; Jierry, L.; Schaaf, P.; Kerdjoudj, H.; Metz-Boutigue, M. H.; Boulmedais, F. Self-defensive biomaterial coating against bacteria and yeasts: polysaccharide multilayer film with embedded antimicrobial peptide. *Adv. Funct. Mater.* **2013,** *23*, 4801-4809.
51. Milovic, N. M.; Wang, J.; Lewis, K.; Klibanov, A. M., Immobilized N-alkylated polyethylenimine avidly kills bacteria by rupturing cell membranes with no resistance developed. *Biotechnol. Bioeng.* **2005,** *90*, 715-722.
52. Lin, J.; Qiu, S. Y.; Lewis, K.; Klibanov, A. M., Mechanism of bactericidal and fungicidal activities of textiles covalently modified with alkylated polyethylenimine. *Biotechnol. Bioeng.* **2003,** *83*, 168-172.
53. Tiller, J. C.; Liao, C. J.; Lewis, K.; Klibanov, A. M. Designing surfaces that kill bacteria on contact. *Proc. Natl. Acad. Sci. USA* **2001,** *98*, 5981-5985.
54. Han, H.; Wu, J. F.; Avery, C. W.; Mizutani, M.; Jiang, X. M.; Kamigaito, M.; Chen, Z.; Xi, C. W.; Kuroda, K. Immobilization of amphiphilic polycations by catechol functionality for antimicrobial coatings. *Langmuir* **2011,** *27*, 4010-4019.
55. Sambhy, V.; Peterson, B. R.; Sen, A. Multifunctional silane polymers for persistent surface derivatization and their antimicrobial properties. *Langmuir* **2008,** *24*, 7549-7558.
56. Behlau, I.; Mukherjee, K.; Todani, A.; Tisdale, A. S.; Cade, F.; Wang, L.; Leonard, E. M.; Zakka, F. R.; Gilmore, M. S.; Jakobiec, F. A.; Dohlman, C. H.; Klibanov, A. M. Biocompatibility and biofilm inhibition of N,N-hexyl,methyl-polyethylenimine bonded to Boston Keratoprosthesis materials. *Biomaterials* **2011,** *32*, 8783-8796.
57. Schaer, T. P.; Stewart, S.; Hsu, B. B.; Klibanov, A. M. Hydrophobic polycationic coatings that inhibit biofilms and support bone healing during infection. *Biomaterials* **2012,** *33*, 1245-1254.

58. Andresen, M.; Stenstad, P.; Moretro, T.; Langsrud, S.; Syverud, K.; Johansson, L. S.; Stenius, P. Nonleaching antimicrobial films prepared from surface-modified microfibrillated cellulose. *Biomacromolecules* **2007,** *8*, 2149-2155.
59. Bumgardner, J. D.; Wiser, R.; Gerard, P. D.; Bergin, P.; Chestnutt, B.; Marini, M.; Ramsey, V.; Elder, S. H.; Gilbert, J. A. Chitosan: potential use as a bioactive coating for orthopaedic and craniofacial/dental implants. *J. Biomater. Sci. Polym. Ed.* **2003,** *14*, 423-438.
60. Greene, A. H.; Bumgardner, J. D.; Yang, Y.; Moseley, J.; Haggard, W. O. Chitosan-coated stainless steel screws for fixation in contaminated fractures. *Clin. Orthop. Relat. Res.* **2008,** *466*, 1699-1704.
61. Carlson, R. P.; Taffs, R.; Davison, W. M.; Stewart, P. S. Anti-biofilm properties of chitosan-coated surfaces. *J. Biomater. Sci. Poly. Ed.* **2008,** *19*, 1035-1046.
62. Park, D.; Wang, J.; Klibanov, A. M. One-step, painting-like coating procedures to make surfaces highly and permanently bactericidal. *Biotechnol. Prog.* **2006,** *22*, 584-589.
63. Haldar, J.; An, D. Q.; de Cienfuegos, L. A.; Chen, J. Z.; Klibanov, A. M. Polymeric coatings that inactivate both influenza virus and pathogenic bacteria. *Proc. Natl. Acad. Sci. USA* **2006,** *103*, 17667-17671.
64. Fuchs, A. D.; Tiller, J. C. Contact-active antimicrobial coatings derived from aqueous suspensions. *Angew. Chem. Int. Ed. Engl.* **2006,** *45*, 6759-6762.
65. Bieser, A. M.; Thomann, Y.; Tiller, J. C. Contact-active antimicrobial and potentially self-polishing coatings based on cellulose. *Macromol. Biosci.* **2011,** *11*, 111-121.
66. Sambhy, V.; MacBride, M. M.; Peterson, B. R.; Sen, A. Silver bromide nanoparticle/polymer composites: Dual action tunable antimicrobial materials. *J. Am. Chem. Soc.* **2006,** *128*, 9798-9808.
67. Wong, S. Y.; Moskowitz, J. S.; Veselinovic, J.; Rosario, R. A.; Timachova, K.; Blaisse, M. R.; Fuller, R. C.; Klibanov, A. M.; Hammond, P. T. Dual functional polyelectrolyte multilayer coatings for implants: permanent microbicidal base with controlled release of therapeutic agents. *J. Am. Chem. Soc.* **2010,** *132*, 17840-17848.
68. Min, J. H.; Choi, K. Y.; Dreaden, E. C.; Padera, R. F.; Braatz, R. D.; Spector, M.; Hammond, P. T. Designer dual therapy nanolayered implant coatings eradicate biofilms and accelerate bone tissue repair. *ACS Nano* **2016,** *10*, 4441-4450.
69. Ng, V. W. L.; Chan, J. M. W.; Sardon, H.; Ono, R. J.; Garcia, J. M.; Yang, Y. Y.; Hedrick, J. L. Antimicrobial hydrogels: A new weapon in the arsenal against multidrug-resistant infections. *Adv. Drug Deliv. Rev.* **2014,** *78*, 46-62.
70. Tsao, C. T.; Chang, C. H.; Lin, Y. Y.; Wu, M. F.; Wang, J. L.; Young, T. H.; Han, J. L.; Hsieh, K. H. Evaluation of chitosan/gamma-poly(glutamic acid) polyelectrolyte complex for wound dressing materials. *Carbohydr. Polym.* **2011,** *84*, 812-819.
71. Li, P.; Poon, Y. F.; Li, W. F.; Zhu, H. Y.; Yeap, S. H.; Cao, Y.; Qi, X. B.; Zhou, C. C.; Lamrani, M.; Beuerman, R. W.; Kang, E. T.; Mu, Y. G.; Li, C. M.; Chang, M. W.; Leong, S. S. J.; Chan-Park, M. B. A polycationic antimicrobial and biocompatible hydrogel with microbe membrane suctioning ability. *Nat. Mater.* **2011,** *10*, 149-156.
72. Mohamed, N. A.; Fahmy, M. M. Synthesis and antimicrobial activity of some novel cross-linked chitosan hydrogels. *Int. J. Mol. Sci.* **2012,** *13*, 11194-11209.
73. Samal, S. K.; Dash, M.; Van Vlierberghe, S.; Kaplan, D. L.; Chiellini, E.; van Blitterswijk, C.; Moroni, L.; Dubruel, P. Cationic polymers and their therapeutic potential. *Chem. Soc. Rev.* **2012,** *41*, 7147-7194.
74. Kuroda, K.; DeGrado, W. F. Amphiphilic polymethacrylate derivatives as antimicrobial agents. *J. Am. Chem. Soc.* **2005,** *127*, 4128-4129.
75. Liu, S. Q.; Yang, C.; Huang, Y.; Ding, X.; Li, Y.; Fan, W. M.; Hedrick, J. L.; Yang, Y. Y. Antimicrobial and antifouling hydrogels formed in situ from polycarbonate and poly(ethylene glycol) via Michael addition. *Adv. Mater.* **2012,** *24*, 6484-6489.

76. Li, Y.; Fukushima, K.; Coady, D. J.; Engler, A. C.; Liu, S.; Huang, Y.; Cho, J. S.; Guo, Y.; Miller, L. S.; Tan, J. P.; Ee, P. L.; Fan, W.; Yang, Y. Y.; Hedrick, J. L. Broad-spectrum antimicrobial and biofilm-disrupting hydrogels: stereocomplex-driven supramolecular assemblies. *Angew. Chem. Int. Ed. Engl.* **2013,** *52*, 674-678.
77. Cao, B.; Tang, Q.; Li, L. L.; Humble, J.; Wu, H. Y.; Liu, L. Y.; Cheng, G. Switchable antimicrobial and antifouling hydrogels with enhanced mechanical properties. *Adv. Healthc. Mater.* **2013,** *2*, 1096-1102.
78. Bertal, K.; Shepherd, J.; Douglas, C. W. I.; Madsen, J.; Morse, A.; Edmondson, S.; Armes, S. P.; Lewis, A.; MacNeil, S. Antimicrobial activity of novel biocompatible wound dressings based on triblock copolymer hydrogels. *J. Mater. Sci.* **2009,** *44*, 6233-6246.
79. Andrews, M. A.; Figuly, G. D.; Chapman, J. S.; Hunt, T. W.; Glunt, C. D.; Rivenbark, J. A.; Chenault, H. K. Antimicrobial hydrogels formed by crosslinking polyallylamine with aldaric acid derivatives. *J. Appl. Polym. Sci.* **2011,** *119*, 3244-3252.
80. Salick, D. A.; Pochan, D. J.; Schneider, J. P. Design of an Injectable beta-Hairpin Peptide Hydrogel That Kills Methicillin-Resistant Staphylococcus aureus. *Adv. Mater.* **2009,** *21*, 4120-4123.
81. Salick, D. A.; Kretsinger, J. K.; Pochan, D. J.; Schneider, J. P. Inherent antibacterial activity of a peptide-based beta-hairpin hydrogel. *J. Am. Chem. Soc.* **2007,** *129*, 14793-14799.
82. Zhou, C.; Li, P.; Qi, X.; Sharif, A. R.; Poon, Y. F.; Cao, Y.; Chang, M. W.; Leong, S. S.; Chan-Park, M. B. A photopolymerized antimicrobial hydrogel coating derived from epsilon-poly-L-lysine. *Biomaterials* **2011,** *32*, 2704-2712.
83. Sung, J. H.; Hwang, M. R.; Kim, J. O.; Lee, J. H.; Il Kim, Y.; Kim, J. H.; Chang, S. W.; Jin, S. G.; Kim, J. A.; Lyoo, W. S.; Han, S. S.; Ku, S. K.; Yong, C. S.; Choi, H. G. Gel characterisation and in vivo evaluation of minocycline-loaded wound dressing with enhanced wound healing using polyvinyl alcohol and chitosan. *Int. J. Pharm.* **2010,** *392*, 232-240.
84. Zumbuehl, A.; Ferreira, L.; Kuhn, D.; Astashkina, A.; Long, L.; Yeo, Y.; Iaconis, T.; Ghannoum, M.; Fink, G. R.; Langer, R.; Kohane, D. S. Antifungal hydrogels. *Proc. Natl. Acad. Sci. USA* **2007,** *104*, 12994-12998.
85. Mehdizadeh, M.; Yang, J. Design strategies and applications of tissue bioadhesives. *Macromol. Biosci.* **2013,** *13*, 271-288.
86. Aziz, M. A.; Cabral, J. D.; Brooks, H. J. L.; Moratti, S. C.; Hanton, L. R. Antimicrobial properties of a chitosan dextran-based hydrogel for surgical use. *Antimicrob. Agents Chemother.* **2012,** *56*, 280-287.
87. Giano, M. C.; Ibrahim, Z.; Medina, S. H.; Sarhane, K. A.; Christensen, J. M.; Yamada, Y.; Brandacher, G.; Schneider, J. P. Injectable bioadhesive hydrogels with innate antibacterial properties. *Nat. Commun.* **2014,** *5*, 4095.

Chapter 2A

Non-Degradable Polyethylenimine-based Quaternary Hydrophobic Polymers as Antimicrobial Paint

Abstract

Chapter 2A *describes the synthesis of water-insoluble and organo-soluble quaternary polyethylenimine derivatives via a new synthetic methodology aimed at developing highly effective antimicrobial paint materials, and demonstrates their structure-activity relationship (SAR) by varying molecular architecture, molecular weight and length of the alkyl chain against various bacteria and fungi. Simple brush, dip or spin coating were employed to coat the polymers on different surfaces such as glass, polystyrene, silicon, etc. The coated surfaces were shown to completely inactivate (~5 log reductions) human pathogenic bacteria including drug-resistant strains such as methicillin-resistant Staphylococcus aureus (MRSA), vancomycin-resistant enterococci (VRE) and beta lactam-resistant Klebsiella pneumoniae (K. pneumoniae) and fungi such as Candida spp. and Cryptococcus spp. upon contact. Notably, linear polymers were more active and found to have higher killing rate than the branched polymers as expressed by minimum inhibitory amount (MIA) of the polymers required per unit area. The polymer coated surfaces also exhibited significant activity in various complex mammalian fluids such as serum, plasma and blood and showed negligible hemolysis at an amount much higher than MIA. The polymers also showed excellent compatibility with other medically relevant polymers (polylactic acid, PLA) and commercial paint. Surfaces coated with the cationic hydrophobic coatings were shown to disrupt the lipid membrane of both bacteria and fungi thereby displaying membrane-active mode of action. Further, microbe (bacteria) found difficult to develop resistance against these membrane-active polymers in sharp contrast to conventional antibiotics and lipopeptides. This approach of developing cationic organo-soluble and non-degradable polymers thus leads to coating materials that can be used to create permanent antimicrobial paint in domestic and hospital areas.*

Publication based on this work

1. Hoque, J. *et al.* Broad spectrum antibacterial and antifungal polymeric paint materials: synthesis, structure-activity relationship and membrane-active mode of action. *ACS Appl. Mater. Interfaces* **2015**, *7*, 1804.

2A.1 Introduction

Cationic antimicrobials are well known for the development of self-sterilizing surfaces and used for a number of applications such as at hospital surfaces, surgical equipments, protective clothes in hospitals, medical implants, wound dressings, food packaging materials, and everyday consumer products.[1-4] Among the various positively charged antimicrobials, cationic polymers with quaternary ammonium groups show great promise in the field of antimicrobial coatings. In order to achieve this, a number of polycations possessing antimicrobial properties such as *N*-alkylated poly (4-vinyl pyridine), quaternized polyethylenimine, quaternary derivatives of acrylic acid, poly(ester-carbonate), cellulose, etc., were applied covalently or non-covalently onto the surfaces.[5-7] However, covalent modification requires different chemical modification strategies for different surfaces. The harsh reaction conditions required for such modifications may alter the surface properties of the biomaterials/common objects such as mechanical properties, transparency, etc. Further, involvement of multiple synthetic steps in this method limits its practical usage.[8] To overcome these difficulties, water insoluble and organo-soluble cationic antimicrobial polymers have been developed, and the solutions of these polymers in various suitable organic solvents are coated onto surfaces in the form of paint.[9,10] The non-covalent strategy to create "microbicidal paint" is thus facile, straightforward and easy to apply.

Despite evidences of antimicrobial activity, there are no clear-cut reports on the structure-activity relationship of the non-covalently coated polymers. It is therefore necessary to understand the structure-activity relationship at the molecular level in order to develop exactly known and future antimicrobial coating materials. Also, microbial resistance, one of the major threats at present time, is yet to be understood against the water-insoluble and organo-soluble antimicrobial polymers. Further, the antimicrobial activity of cationic polymers has been mostly investigated against bacteria although the fungal infections remain as a key hazard to human health. Moreover when associated with the bacterial infections, fungal proliferation has been shown to induce an increased frequency or severity of diseases.[11,12] Hence it is meaningful to develop polymers with both antibacterial and antifungal activity and study their structure-activity relationship for the future development of broad spectrum multifunctional coating materials.

In this chapter, novel antimicrobial coating materials were therefore developed from a commercially available polymer polyethylenimine (PEI) and detailed structure-activity relationship along with the membrane-active mode of action was demonstrated. The cationic

water-insoluble and organo-soluble polymers were synthesized by a new two-step synthetic methodology (*Eschweiler-Clarke methylation* of PEIs and subsequent quaternization of *N*-methyl PEIs with alkyl bromides). The antimicrobial activities of the polymer-coated surfaces were evaluated against various human pathogenic bacteria and fungi, including drug resistant strains. Structure-activity relationship was studied by varying the molecular architecture (branched vs linear), molecular weight (750, 25 and 2 kDa branched PEI and 217, 87 and 22 kDa linear PEIs) of the PEIs and also by varying the length of hydrophobic alkyl chain in quaternary PEIs. The effectiveness of these polymers as antimicrobial coating was also evaluated along with the conventional polymers and commercial paint. Hemocompatibility of the polymeric coating was evaluated with human red blood cells (hRBC). Bacterial propensity to develop resistance against these polymers was studied against both Gram-positive and Gram-negative bacteria by the challenging the polymer coatings repeatedly.

2A.2 Results and discussion

2A.2.1 Synthesis and characterization of cationic PEI derivatives

A new synthetic methodology has been introduced to prepare water insoluble and organo-soluble polymers from polyethylenimines (PEIs) using *Eschweiler-Clarke* methylation and subsequent quaternization (Scheme 2A.1 and 2A.2).

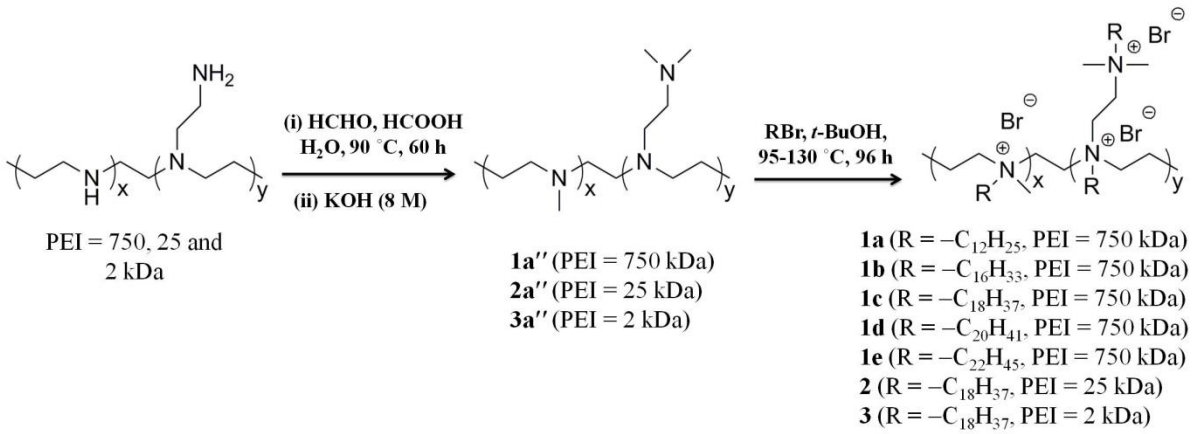

Scheme 2A.1: Synthesis of water-insoluble and organo-soluble branched cationic PEI derivatives.

Branched PEIs (M_w = 750, 25 and 2 kDa) were first converted into *N*-methyl PEIs (**1a′′**, **2a′′** and **3a′′**) where all the primary and secondary amino groups were fully converted to the tertiary amines using excess formic acid and formaldehyde. The reaction was carried out at

90 ˚C for 60 h. The structures of the resultant polymers (*N*-methyl PEIs) were confirmed by a combination of ^{1}H-NMR and FT-IR spectroscopy.

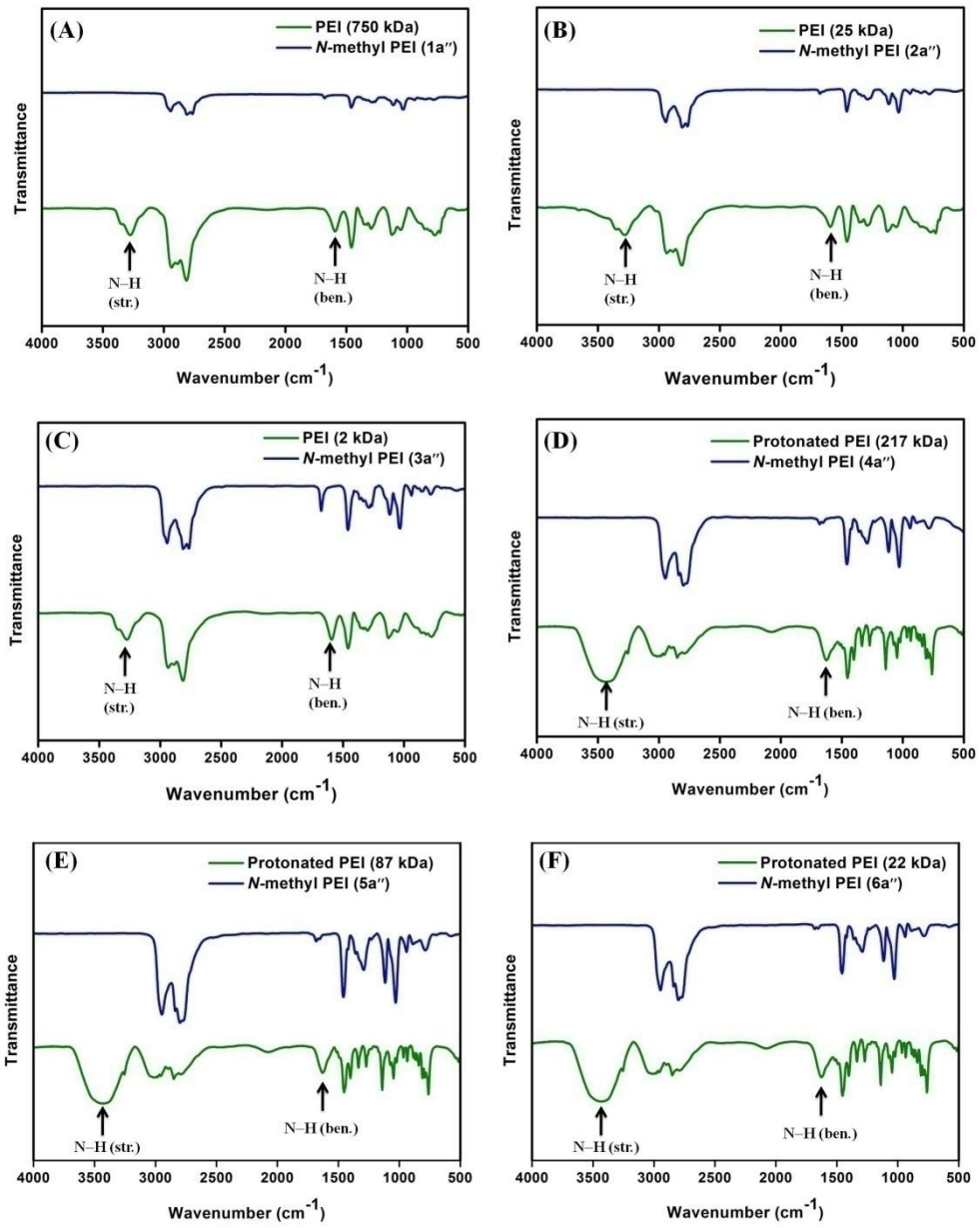

Figure 2A.1: FT-IR spectra of *N*-methyl PEI derivatives. (A-C) Branched *N*-methyl PEIs obtained from PEI of molecular weight 750, 25 and 2 kDa respectively. (D-F) Linear *N*-methyl PEIs obtained from PEI of molecular weight 217, 87 and 22 kDa respectively.

The proton spectra showed that the polymers had a peak at 2.2 ppm corresponding to –N(*CH*$_3$)– group in addition to the peaks from 2.3-2.6 ppm for the –N(*CH*$_2$*CH*$_2$)– groups. However, complete methylation was confirmed from FT-IR spectra. The IR spectra of all the branched *N*-methylated PEIs showed complete disappearance of the peaks at 3282 cm^{-1} and

1600 cm^{-1} corresponding to the N–H bond stretching and bending respectively, which were observed in the parent PEIs (Figure 2A.1A-C).

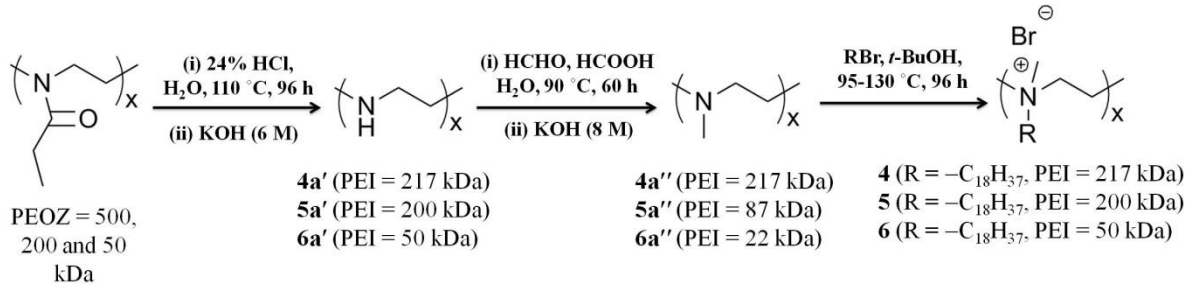

Scheme 2A.2: Synthesis of water insoluble and organo-soluble linear cationic PEI derivatives.

To prepare linear *N*-methyl PEIs, first commercially available poly(2-ethyl-2-oxazoline) (PEOZs) (500, 200 and 50 kDa) were deprotected by hydrochloric acid and then deprotonated with aqueous KOH to obtain linear PEIs (**4a′**, **5a′** and **6a′**; M_w = 217, 87 and 22 kDa respectively). Finally, linear *N*-methyl PEIs (**4a″**, **5a″** and **6a″**) were obtained from linear PEIs following the same procedure as described for the branched *N*-methyl PEIs (Scheme 2A.2) Like the branched polymers, linear *N*-methyl PEIs also showed complete disappearance of the N–H bond stretching and bending peaks at 3280 cm^{-1} and 1600 cm^{-1} respectively (2A.1D-F).

As the antimicrobial activity and solubility of cationic polymers are known to depend not only on charge density but also on degree of hydrophobicity, the polycationic PEI derivatives must possess optimum hydrophilic/hydrophobic balance to ensure high activity as well as water insolubility. Thus various quaternary PEI derivatives with varying alkyl chain length were prepared (Scheme 2A.1 and 2A.2). Further, to obtain polymers of different architectures and molecular weights, all the branched and linear *N*-methyl PEIs were fully quaternized by reacting with alkyl bromides at 95-130 ˚C for 96 h (this allowed precise control of hydrophobic/hydrophilic balance). Quaternization of the tertiary amine groups of *N*-methyl PEIs was confirmed via ^{1}H-NMR and also verified by elemental analyses. Notably, the proton NMR spectra of all the cationic PEI derivatives showed no peaks at 2.2-2.6 ppm which correspond to the peaks for –N(CH_3)– and –N(CH_2CH_2)– groups in *N*-methyl PEIs (Figure 2A.2). The structure of the polymers was also confirmed by means of elemental analysis. By this method it was possible to determine structures of all the cationic PEI derivatives at the molecular level. All the final cationic hydrophobic polymers were found to

be almost colorless and thermally stable. Thermal stability of all the derivatives was measured by thermogravimetric analysis and was found to be stable even above 200 ˚C.

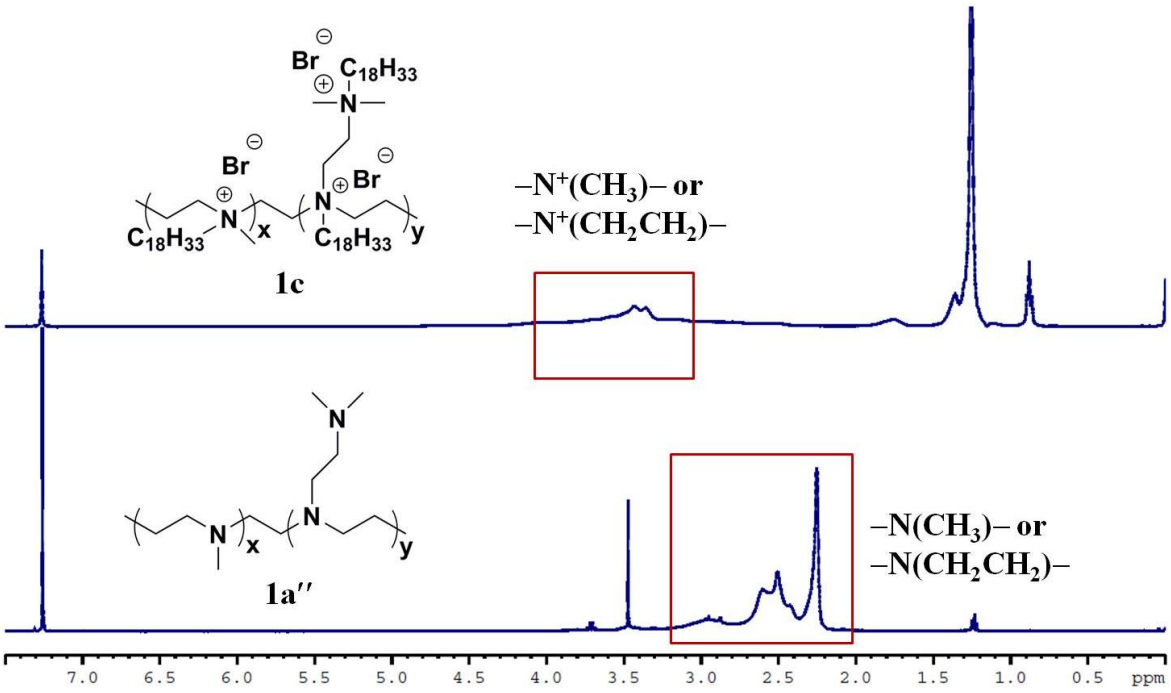

Figure 2A.2: ^{1}H-NMR spectra of PEI derivatives. (A) ^{1}H-NMR spectrum of *N*-methyl PEI (**1a′′**); (B) ^{1}H-NMR spectrum of quaternized PEI (**1c**) obtained from *N*-methyl PEI (**1a′′**) and octadecyl bromide.

Since the goal was to develop of water-insoluble and organo-soluble polymers which can be simply be coated onto surfaces non-covalently, the solubility of all the polymers was checked in water as well as in various organic solvents. The hydrophobic polycations **1a** (bearing $-C_{12}H_{25}$ alkyl chain and branched PEI of M_w = 750 kDa) and **1b** (bearing $-C_{16}H_{33}$ alkyl chain and branched PEI of M_w = 750 kDa) were found to be partially soluble in water whereas all other derivatives **1c** (bearing $-C_{18}H_{37}$ alkyl chain and branched PEI of M_w = 750 kDa), **1d** (bearing $-C_{20}H_{41}$ alkyl chain and branched PEI of M_w = 750 kDa), **1e** (bearing $-C_{22}H_{45}$ alkyl chain and branched PEI of M_w = 750 kDa), **2** (bearing $-C_{18}H_{37}$ alkyl chain and branched PEI of M_w = 25 kDa), **3** (bearing $-C_{18}H_{37}$ alkyl chain and branched PEI of M_w = 2 kDa), **4** (bearing $-C_{18}H_{37}$ alkyl chain and linear PEI of M_w = 217 kDa), **5** (bearing $-C_{18}H_{37}$ alkyl chain and linear PEI of M_w = 87 kDa) and **6** (bearing $-C_{18}H_{37}$ alkyl chain and linear PEI of M_w = 22 kDa) were found to be completely insoluble in water. On the other hand, the polymers were found to be soluble in chloroform, dichloromethane, *n*-butanol, *N*,*N*-dimethyl

formamide (DMF) and dimethyl sulfoxide (DMSO). The polycations were soluble in chloroform up to the highest tested concentration 200 mg/mL. Since the polymers **1a** and **1b** were partially soluble in water, no further experiments were performed with these polymers.

2A.2.2 Antibacterial activity

2A.2.2.1 Activity by spray method

In order to evaluate the ability of these polymers to serve as antibacterial paint, glass slides were coated with solutions of the polymers in chloroform by brush coating/drop-casting/spin coating. This method of painting the polymers onto surface non-covalently allowed simple, straightforward and facile coating. Further to mimic the scenario of natural deposition of bacteria onto surfaces, bacteria were sprayed onto the polymer coated glass surfaces along with the non-coated glass surface (control).[13] Bacterial growth was seen on non-coated glass surface as indicated by the presence of colonies, whereas no colony (at least 5-log reductions with respect to control) was observed on polymer-coated surfaces (Figure 2A.3). In order to evaluate the role of hydrophobicity and hence the hydrophobic/hydrophilic balance, surfaces coated with polycations (100% DQ with PEI of M_w = 750 kDa) of varying long chain (**1c** bearing $-C_{18}H_{37}$, **1d** bearing $-C_{20}H_{41}$ and **1e** bearing $-C_{22}H_{45}$) were assayed for antibacterial activity. These polymers with different hydrophobic/hydrophilic balance showed different activities. Polymer **1c** coated surface showed 100% activity at 0.4 μg/mm^2 against *S. aureus* and at 12.5 μg/mm^2 against *E. coli* respectively whereas polymers **1d** and **1e** showed 100% activity at 0.6 μg/mm^2 and 1.2 μg/mm^2 against *S. aureus* and did not show any activity till 12.5 μg/mm^2 against *E. coli*. Thus polymer **1c** with $-C_{18}H_{37}$ long chain was found to be most effective.

In order to evaluate the effect of molecular architecture and molecular weight of the polymers on antibacterial activity, bacteria were sprayed onto the glass surfaces coated with branched and linear polymers of different molecular weights having same $-C_{18}H_{37}$ alkyl chain (**1c**, **2**, **3**, **4**, **5** and **6**). It was observed that linear polymers were more active than the branched ones (e.g., surfaces coated with branched polymer **1c** exhibited 100% activity (5-log reductions) against *S. aureus* at 0.4 μg/mm^2 and against *E. coli* at 12.5 μg/mm^2 whereas surfaces coated with linear polymer **6** exhibited 100% activity against *S. aureus* at 0.2 μg/mm^2 and against *E. coli* at 6.25 μg/mm^2 respectively (Figure 2A.3A-F). It was also observed that among the branched polymers, **1c** with highest molecular weight (PEI of 750 kDa) and among the linear polymers, **6** with lowest molecular weight (PEI of 22 kDa) were

the most active (Figure 2A.3A-F). These results clearly showed that different molecular architecture and molecular weight have different impact on the antibacterial activity of the polymers when coated onto the surface.

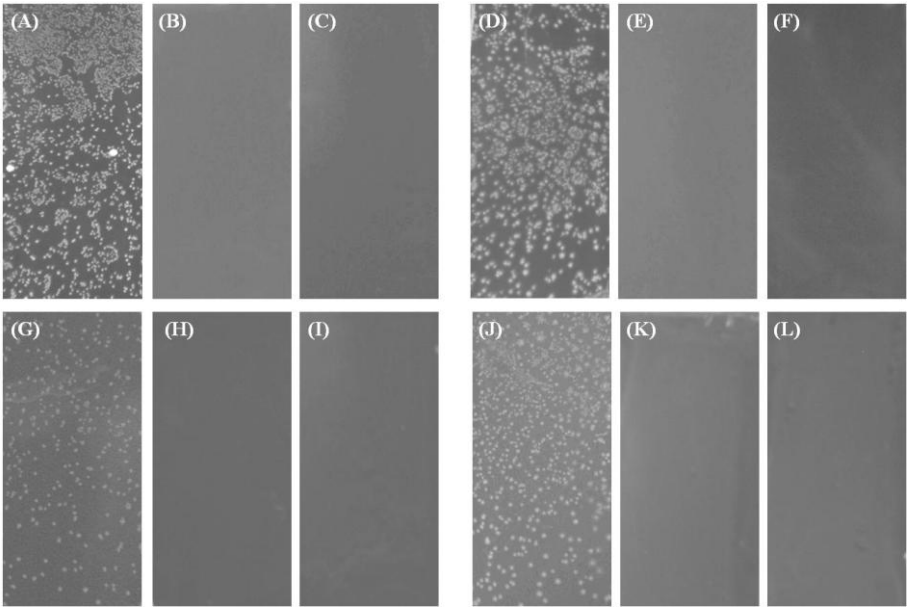

Figure 2A.3: Antibacterial activity of polymer coated glass surface. Photographs of microscopic glass slides: (A) and (D) non-coated glass slides (controls); (B) and (E) slides coated with **1c** (0.4 μg/mm^2 and 12.5 μg/mm^2); (C) and (F) slides coated with **6** (0.2 μg/mm^2 and 6.25 μg/mm^2); (G) and (J) slides coated with PLA (2.55 μg/mm^2); (H) and (K) slides coated with **1c** along with PLA (0.4 μg/mm^2 + 2.55 μg/mm^2 PLA and 12.5 μg/mm^2 + 2.55 μg/mm^2 PLA); (I) and (L) slides coated with **6** along with PLA (0.2 μg/mm^2 + 2.55 μg/mm^2 PLA and 6.25 μg/mm^2 + 2.55 μg/mm^2 PLA). Slides A-C and G-I for *S. aureus* and slides D-F and J-L for *E. coli* respectively. Each white dot corresponds to a bacterial colony grown from a single surviving bacterial cell.

Further, in order to find the utility of these polycations to be used as antimicrobial coating materials in house-hold and biomedical applications, the polymers were coated along with medically relevant polymer PLA and commercial paint, and the surfaces were similarly assayed for antibacterial activity. Surfaces coated with branched polymer **1c** along with PLA (2.55 μg/mm^2) exhibited 100% activity against *S. aureus* at 0.4 μg/mm^2 and against *E. coli* at 12.5 μg/mm^2 whereas surfaces coated with linear polymer **6** along with PLA (2.55 μg/mm^2) exhibited 100% activity against *S. aureus* at 0.2 μg/mm^2 and against *E. coli* at 6.25 μg/mm^2 respectively (Figure 2A.3G-L). Notably, when polymers **1c** and **6** were brush-coated onto glass surface along with the commercial paint solution (10 wt% and 5 wt%; w/v) for **1c** and **6** respectively), both branched and linear polymers showed 100% antibacterial activity even after loading with commercial paint against both *S. aureus* and *E. coli* (Figure 2A.4). Further,

1c and **6**, when coated onto the glass surface along with PLA, retained antibacterial activity against both *S. aureus* and *E. coli*. These results thus indicated that these polymers could potentially be used to develop self-defensive biomaterials and paint.

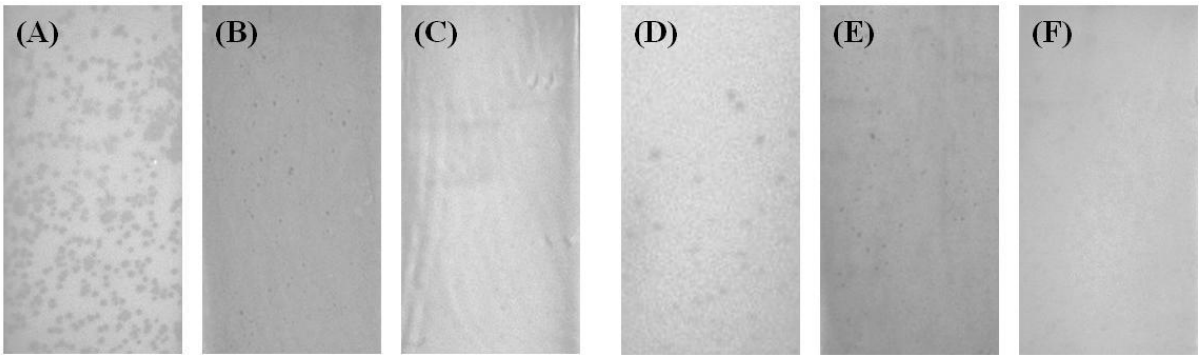

Figure 2A.4: Photographs of microscopic glass slides showing antibacterial activity of polymers coated with commercial paint: (A) and (D) non-coated glass slides (controls); (B) and (E) slides coated with **1c** along with paint (10 wt% and 5 wt% loading respectively); (C) and (F) slides coated with **6** (5 wt% and 2.5 wt% loading respectively). Aqueous suspensions of *S. aureus* (slides A-C) and *E. coli* (slides D-F) respectively were sprayed onto the slides, followed by drying in air for 2 min, covering with solid growth agar, and incubating at 37 °C for 48 h. Each dot corresponds to a bacterial colony grown from a single surviving bacterial cell.

2A.2.2.2 Activity against water-borne bacteria (Minimum inhibitory amount)

To simulate the natural conditions of water-borne bacteria and to establish the efficacy of polymer coatings against these bacteria, antibacterial efficacy of the polymers was also evaluated with bacterial suspensions.[14] The polymer coated surfaces were found to inhibit both *S. aureus* and *E. coli* and the minimum inhibitory amounts (MIAs) per unit area of polymer coated surfaces were determined by measuring the optical density (OD) at 600 nm and also by inspecting visual turbidity (the minimum amount of polymer coated onto surface at which no visible bacterial growth observed) (Table 2A.1). As observed in case of the spray method, polymer with $-C_{18}H_{37}$ alkyl chain (**1c**) was found to be most active among the polymers obtained from PEI of 750 kDa with varying chain length (**1c**, **1d** and **1e**) (Figure 2A.5A). When polymers with different molecular architecture and weights having same $-C_{18}H_{37}$ alkyl chain were evaluated against both Gram-positive and Gram-negative bacteria, linear polymers were found to be more active than the branched ones. The MIAs for the branched polymers **1c**, **2** and **3** were 0.98 μg/mm^2, 0.98 μg/mm^2 and 1.95 μg/mm^2 respectively whereas MIAs for the linear polymers **4**, **5** and **6** were 0.24 μg/mm^2 each against *S. aureus*. The MIAs for **1c**, **2** and **3** were 15.6 μg/mm^2, 31 μg/mm^2 and 31 μg/mm^2 whereas

for **4**, **5** and **6** were 7.8 μg/mm^2, 3.9 μg/mm^2 and 3.9 μg/mm^2 against *E. coli* respectively (Table 2A.1). However, all the polymers were more active towards Gram-positive *S. aureus* than the Gram-negative *E. coli*. This might be due to the high hydrophobic character of these polymers conferred by higher alkyl chain length which causes polymer aggregation, which in turn causes poor interactions with the cell surface of the Gram-negative bacteria composed of an additional outer lipid membrane made up of lipopolysaccharides.[15] Further, these polymers were also found to be active against *P. aeruginosa*, a bacterium which forms biofilm onto surface most frequently and is difficult to treat (Table 2A.1).

Table 2A.1 Antibacterial and hemolytic activities of polymer coated surfaces

	MIA (μg/mm^2)						
	Drug sensitive bacteria			Drug resistant bacteria			HA_{50}
Polymers	*S. aureus*	*E. coli*	*P. aeruginosa*	MRSA	VRE	*K. pneumoniae*	(μg/mm^2)
1c	0.98	15.6	3.9	0.98	0.98	15.6	>31
2	0.98	31	7.8	0.98	0.98	31	>31
3	1.95	31	7.8	0.98	0.98	>31	>31
4	0.24	7.8	1.95	0.24	0.24	7.8	>31
5	0.24	3.9	1.95	0.24	0.24	7.8	>31
6	0.24	3.9	1.95	0.24	0.24	7.8	>23

MRSA = Methicillin-resistant *S. aureus* (ATCC 33591); VRE = vancomycin-resistant *Enterococcus faecium* (ATCC 51559); *K. pneumoniae* = beta lactam-resistant *K. pneumoniae* (ATCC 700603); HA_{50} = amount of the polymer (μg/mm^2) coated in well at which 50% hemolysis occurs.

When tested against drug-resistant bacteria, these polymers were found to inhibit MRSA, VRE and beta lactam-resistant *K. pneumoniae* (Table 2A.1) thus showing their broad spectrum antibacterial activity. The MIA values of the most potent polymer **6** were found to be 0.24 μg/mm^2 against MRSA and VRE and 7.8 μg/mm^2 against *K. pneumoniae*. Next, to find out whether these polymers are bacteriostatic or bactericidal, aliquots from the wells that appeared to have less or no turbidity were plated on agar plate and minimum bactericidal amount (MBA, μg/mm^2) were determined where no colony was observed. These polymers showed bactericidal effect against both Gram-positive and Gram-negative bacteria including drug-resistant ones. For example, the MBA of the most potent polymer **6** were found to be 0.24 μg/mm^2 against *S. aureus* and 7.8 μg/mm^2 against *E. coli* respectively.

2A.2.2.3 Bactericidal kinetics

To establish how fast these polymers kill bacteria upon contact and also to understand the effect of molecular architecture on killing rate, the rate of action were investigated towards both *S. aureus* and *E. coli* using branched polymer **1c** and linear polymer **6** at the respective MIAs and 6 × MIAs. Linear polymer **6** killed *S. aureus* (~5 log reduction) at 30 min at 6 × MIA whereas branched polymer **1c** killed *S. aureus* (~5 log reduction) at 90 min at 6 × MIA (Figure 2A.5B). Polymer **6**, on the other hand, killed *E. coli* (~5 log reduction) at 60 min at 6 × MIA whereas **1c** killed *E. coli* (~5 log reduction) at 240 min at 6 × MIA (Figure 2A.5C). These results thus indicate that the cationic hydrophobic polymer coatings have remarkably high killing rates against both the bacteria making them suitable for efficient antimicrobial coating. Further, linear polymer has higher killing rate than branched polymer against both Gram-positive and Gram-negative bacteria.

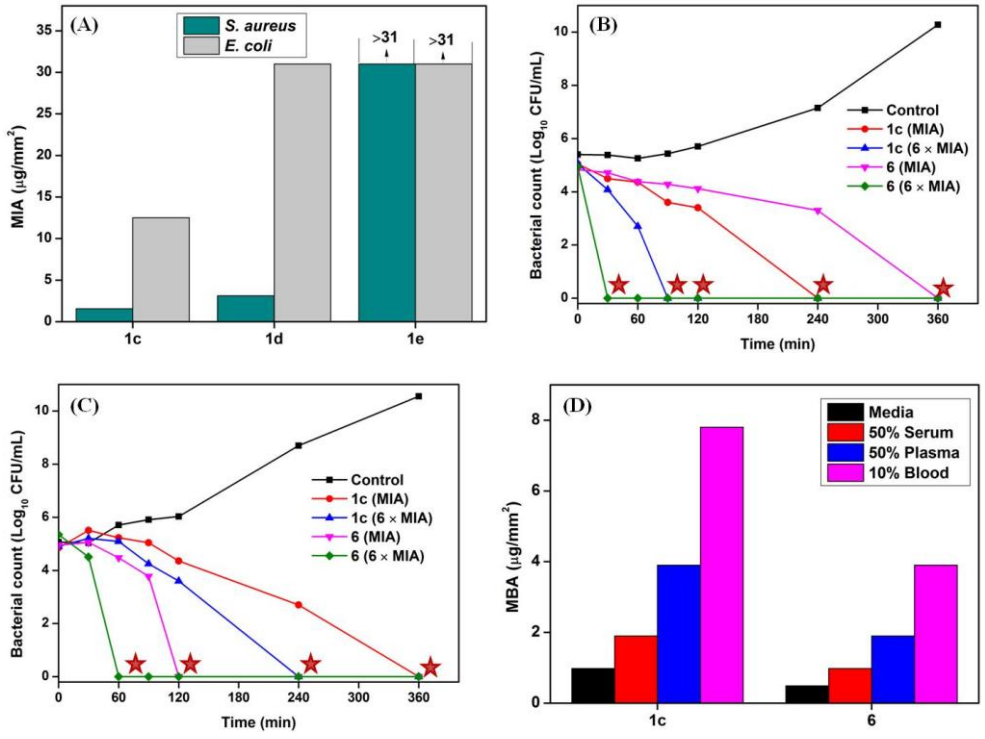

Figure 2A.5: Antibacterial activities of cationic polymers. (A) Minimum inhibitory amounts of **1c**, **1d** and **1e** toward *S. aureus* and *E. coli*. Antibacterial kinetics of the PEI derivatives (**1c** and **6)** at two different amounts: MIA and 6 × MIA towards *S. aureus* (B) and *E. coli* (C) respectively. Stars represent < 50 CFU/mL. (D) Minimum bactericidal amount (μg/mm^2) of PEI derivatives (**1c** and **6**) against methicillin-resistant *S. aureus* (MRSA) after exposure to various mammalian fluid systems.

2A.2.2.4 Activity in complex mammalian fluids

A serious concern of the health industry is the infections caused due to contamination of surfaces of medical implants and devices, which upon implantation come in direct contact with body fluids.[16] Hence, the antibacterial activity of the polymers in various mammalian fluids (50% serum, 50% plasma and 10% blood) was investigated against MRSA, a Gram-positive drug resistant bacterium that causes many infections in humans undergoing implant surgery. Both **1c** and **6** were found to be active in 50% serum, 50% plasma and 10% blood. The MBA values of **1c** and **6** were 0.98 $\mu g/mm^2$ and 0.49 $\mu g/mm^2$ in 50% serum; 1.95 $\mu g/mm^2$ and 0.98 $\mu g/mm^2$ in 50% plasma and 7.8 $\mu g/mm^2$ and 1.95 $\mu g/mm^2$ in 10% blood respectively (Figure 2A.5D). The above results thus suggest that these polymers could possibly be used *in-vivo* as antimicrobial coatings in various medical implants and devices.

2A.2.3 Membrane-active mode of action

To establish the mode of antibacterial action, disruption of cytoplasmic membrane potential was performed with the polymer coated surfaces against both *S. aureus* and *E. coli* using potential sensitive dye diSC_3(5) by fluorescence spectroscopy. The dye was first added to bacterial cells and as the dye accumulated in the membranes, the fluorescence intensity decreased because of self-quenching.[17] Upon addition to the coated surfaces and subsequent disruption of the membrane potential, an increase in fluorescence intensity was observed due to diSC3(5) being displaced into the solution. All the polymers coated surfaces except **1d** and **1e** were found to depolarize the membrane potential of both bacteria (Figure 2A.6A and B). Interestingly, surfaces coated with linear polymers (**4-6**) were found to be more active in depolarizing the membrane potential compared the surfaces coated with branched polymers (**1c**, **2-3**). Further, polymer **6**, which is most active among all the polymers, showed maximum membrane dissipation effect. Also, surfaces coated with polymers **1d** and **1e** having $-C_{20}H_{41}$ and $-C_{22}H_{45}$ alkyl chain respectively were unable to dissipate the membrane potential thus proving to be ineffective against bacteria as also reflected from their high MIA values.

Mechanism of antibacterial activity of the polycation coated surfaces against *S. aureus* and *E .coli* was further established by fluorescence microscopy.[18] Fluorescence microscopy images showed high cell viability in case of the control samples by displaying green fluorescence of SYTO 9 which labels only the live bacteria (Figure 2A.6C and E for *S. aureus* and *E. coli* respectively). However, cells treated with the polymer coated surface

showed complete membrane permeabilization seen by red fluorescence of propidium iodide (PI) (Figure 2A.6D and F for *S. aureus* and *E. coli* respectively). Since PI is membrane impermeable and penetrates only when the bacterial membrane is compromised, the microscopy technique thus indicated that the cationic polymer interacted and subsequently disrupted the membrane integrity of the bacteria.

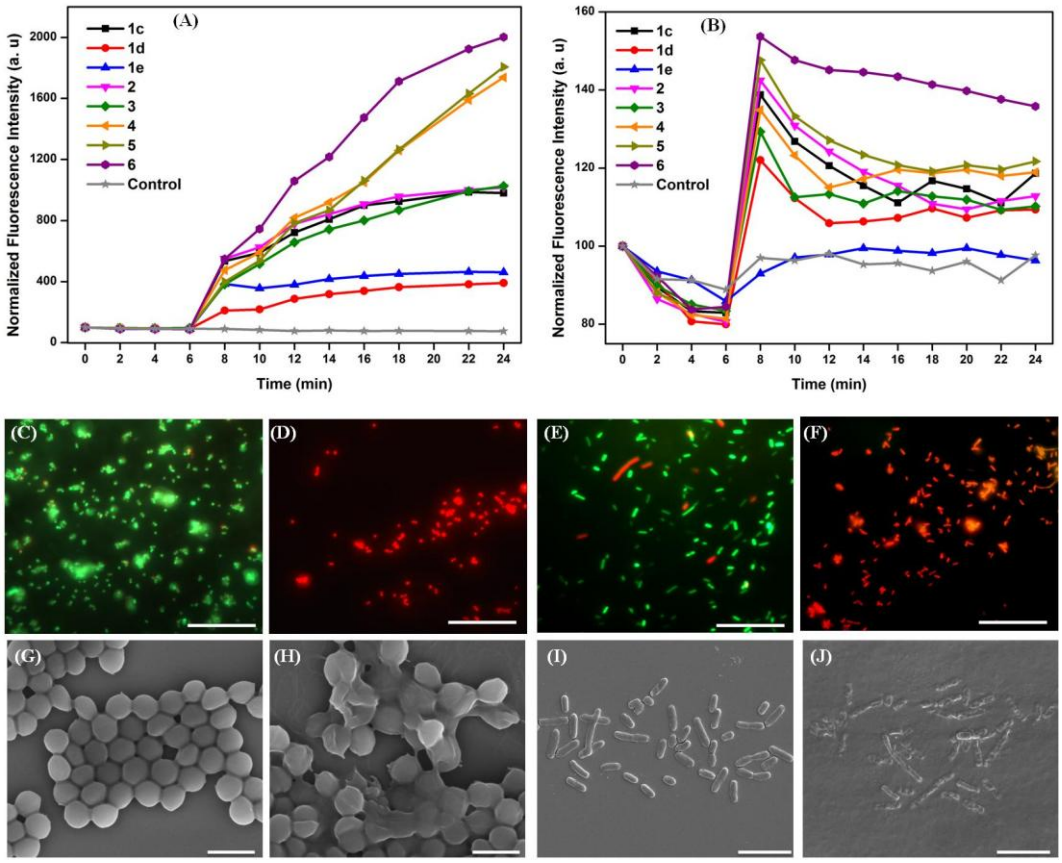

Figure 2A.6: Mechanistic investigation of antibacterial activity of polymer coatings. Membrane depolarization for *S. aureus* (A) and *E. coli* (B) respectively. Fluorescence microscopy images of bacteria untreated (C: *S. aureus*; E: *E. coli*) and treated with the surface coated with **6** (D: *S. aureus*; F: *E. coli*) after staining with SYTO 9 and PI. Each image is a result of superposition of an image taken for the green fluorescent dye (SYTO 9) and red fluorescent dye (PI) using the appropriate filters. Scale bar is 20 μm. Scanning electron microscopy images of *S. aureus* (G and H) and *E. coli* (I and J) cells after a 2 h exposure to the uncoated surfaces (G and I), surfaces coated with the polymer **6** (H and J). Scale bar 1 μM for G and H and 5 μM for I and J.

In order to have better insight into the mechanism of action of the polymer coated surfaces, scanning electron microscopy (SEM) was also used to visually characterize the morphology of bacteria upon contact with polymer coated surfaces. The micrographs presented for non-coated wells (control) showed that bacteria retained well-defined morphology and surface smoothness characteristic of unperturbed cells (Figure 2A.6G and I

for *S. aureus* and *E. coli* respectively). In contrast, once treated with polymer (**6**) coated surface, bacteria exhibited morphological deformations (Figure 2A.6H and J for *S. aureus* and *E. coli* respectively). The appearance of irregularly shaped bacteria indicated a loss of structural integrity, thereby suggesting a specific and undermining interaction of hydrophobic polycations with the negatively charged bacterial cell membrane.[8] Since the polymers are water insoluble and coated onto surfaces, it is best expected that when painted onto surfaces, the polymers killed bacteria on contact due to rupturing of bacterial cell membranes by erect fragments of the polymer chains.

2A.2.4 Antifungal activity

2A.2.4.1 Minimum inhibitory amount

The antimicrobial activity of cationic polymers has been mostly investigated against bacteria although the fungal infections remain as a key hazard to human health. Furthermore, fungal proliferation has been shown to induce an increased frequency or severity of diseases upon association with the bacterial infections.[19] Hence it is meaningful to develop polymers with both antibacterial and antifungal activity and study their structure-activity relationship for the future development of broad spectrum multifunctional coating materials. In order to find the utility of the cationic polymers developed herein to be used as antifungal coating materials, the antifungal efficacy of all the branched and linear polymers were evaluated against different pathogenic *Candida* spp. (*C. albicans* SC5314, *C. dubliniensis* CD36, *C. tropicalis* MYA3404) and *Cryptococcus* spp. (*C. neoformans var. grubii* (serotype A) H99, *C. gattii* (serotype B) WM276 and *C. neoformans var. neoformans* (serotype D) JEC21). First, the role of hydrophobicity and hence the hydrophobic/hydrophilic balance of the polycations (100% DQ with PEI of M_w = 750 kDa) with varying long chain (**1c** bearing $-C_{18}H_{37}$, **1d** bearing $-C_{20}H_{41}$ and **1e** bearing $-C_{22}H_{45}$) were established. Like bacteria, the polymers with different hydrophobic/hydrophilic balance showed different activity against fungi as well (Figure 2A.7A). Polymer **1c** coated surface showed 100% activity at 0.98 μg/mm^2 against *Cryptococcus neoformans ser A* and at 3.8 μg/mm^2 against *C. dubliensis* respectively whereas polymers **1d** and **1e** showed 100% activity at 0.98 μg/mm^2 and 1.25 μg/mm^2 against *Cryptococcus neoformans ser A* and did not show any activity till 31 μg/mm^2 against *C. dubliensis* respectively (Table 2A.2 and Figure 2A.7A). Thus like bacteria, polymer **1c** with $-C_{18}H_{37}$ long chain was found to be most effective against fungi. The polymer coated surfaces were found to inhibit completely all the human pathogenic fungi species tested

(Table 2A.2). Linear polymers were found to be more active compared to branched polymers (e.g., MIA values of linear polymers **4**, **5** and **6** are 0.63 μg/mm^2 for each polymer whereas the same for **1c, 2** and **3** are 3.75 μg/mm^2, 5 μg/mm^2 and 10 μg/mm^2 against *C. tropicalis*). Among the branched polymers, the polymer **1c**, with the highest molecular weight and among all the linear polymers, polymer **6** with the lowest molecular weight showed maximum activity (Table 2A.2). However, among all the polymers, polymer **6** was found to be most active against all the fungi tested similar to the results obtained against bacteria. The MIA values for polymer **6** were 0.63-2.5 μg/mm^2 against *Candida* spp. and 0.13-0.25 μg/mm^2 against *Cryptococcus* spp.

Table 2A.2 Antifungal activity of polymer coated surfaces

Polymers	MIA (μg/mm^2)					
	Candida spp.			*Cryptococcus spp.*		
	C. albicans	*C. dubliniensis*	*C. tropicalis*	*C. neoformans Ser A*	*C. neoformans Ser B*	*C. neoformans Ser D*
1c	10	3.8	3.8	0.98	0.98	0.49
2	>31	>31	5.0	0.98	0.98	0.98
3	>31	>31	10	0.98	0.98	1.95
4	10	1.25	0.63	0.49	0.48	0.49
5	10	0.63	0.63	0.25	0.25	0.49
6	2.5	0.63	0.63	0.13	0.25	0.13

C. albicans = Candida albicans; *C. dubliniensis = Candida dubliniensis*; *C. tropicalis = Candida tropicalis*; *C. neoformans Ser A = Cryptococcus neoformans Ser A*; *C. neoformans Ser B = Cryptococcus neoformans Ser B*; *C. neoformans Ser D = Cryptococcus neoformans Ser D*

The cationic hydrophobic polymers were not only fungistatic but also fungicidal. For example, the minimum fungicidal amount (MFA) of the most potent polymer **6** was found to be 0.49 μg/mm^2 and 0.25 μg/mm^2 against *C. tropicalis* and *C. neoformans* Ser D respectively. However, it is noteworthy that both branched and linear polymers were found to be less active against *C. albicans* as evident from their high MIA or MFA values (Table 2A.2).

2A.2.4.2 Fungicidal kinetics

To understand the effect of molecular architecture on fungal killing rate and to establish how fast these polymers kill fungi upon contact, the rate of action was investigated against *C. dubliniensis* using surfaces coated with both branched polymer **1c** and linear polymer **6**.

Surface coated with polymer **1c** killed *C. dubliniensis* within 4-6 hours at 8 × MIA whereas surfaces coated with polymer **6** killed *C. dubliniensis* in 6-8 hours at 8 × MIA (Figure 2A.7B). Even at their respective MIA values, polymers **1c**- and **6**-coated surfaces killed the fungal cells at 8 hours. Therefore, it was observed that both branched and linear polymers have similar antifungal kinetics.

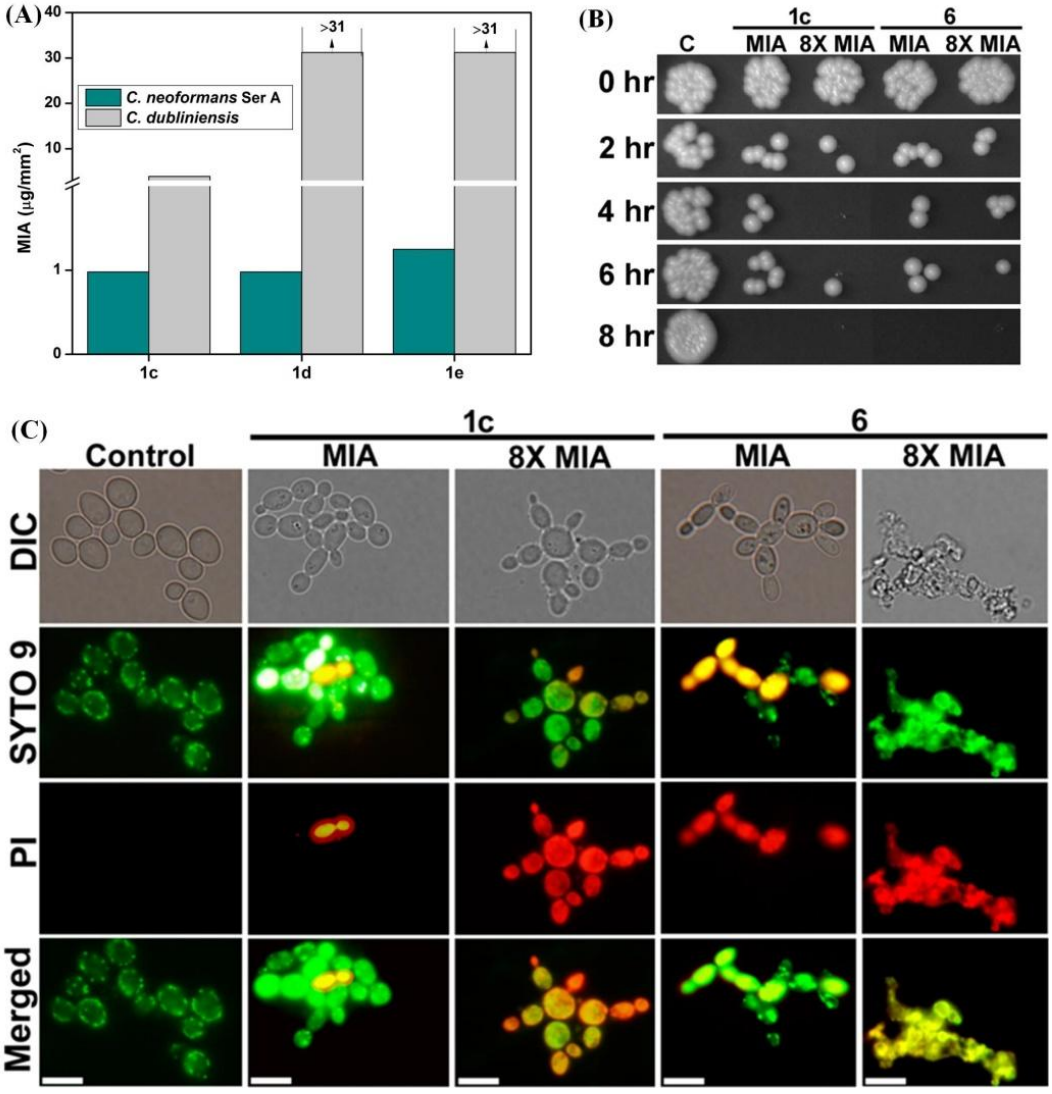

Figure 2A.7: Antifungal activities of cationic polymers. (A) MIA values of **1c**, **1d** and **1e** against *Cryptococcus neoformans* ser A and *Candida dubliniensis*. (B) Antifungal kinetics of polymers **1c** and **6** coated surfaces at different amounts (MIA and 8 × MIA) against *C. dubliniensis*: representative cross section of the YPD agar plate showing the growth of fungal colonies at different times. (C) Mechanistic investigation of antifungal activity of polymer coatings. Fluorescence microscopy images of *C. dubliniensis* after staining with SYTO 9 and PI exposed to the uncoated surfaces (control), surfaces coated with the polymers **1c** and **6** at MIA and 8 × MIA respectively. Scale bar 5 μm.

2A.2.5 Membrane-active mode of antifungal action

It was observed that the cationic polymers interact with the cellular membrane of bacteria and thereby disrupts the membrane integrity causing cell death. To know whether these hydrophobic polycations interact with and damage the cell membrane of fungi, LIVE/DEAD assay was performed with the fungal cell using SYTO 9 and PI dyes by fluorescence microscopy.[20] *C. dubliniensis* was used as a model fungus and treated with both branched and linear polymer **1c** and **6** coated surfaces. The microscopy images showed the presence of viable cells in case of control samples (plain surface) as observed by green fluorescence (Figure 2A.7C). The cells treated with the polymer-coated surfaces on the other hand showed red color fluorescence of PI thus indicating the compromised cell membrane (Figure 2A.7C). These results indicate that the cationic polymers interact with the fungal cell membrane and disrupt the integrity of the membrane presumably leading to cell death.

2A.2.6 Hemocompatibility

To be used in community and healthcare settings, compatibility of the polymeric coatings should be addressed. Antimicrobial coatings thus should selectively kill only pathogenic microorganism over the other non-pathogenic cells such as mammalian cells. The compatibility of the polymer coatings were therefore evaluated against human red blood cells (hRBCs). Interestingly, it was found that these polymers are non-hemolytic even upto 6.25 $\mu g/mm^2$. Only 25-35% hemolysis was observed at 31 $\mu g/mm^2$. Interestingly, the two most active polymers, **1c** and **6**, showed negligible hemolysis upto 6.25 $\mu g/mm^2$ which is 10-200 times more than their MIA values (Table 2A.1). These results portrayed the non-hemolytic nature of these materials and enhanced their claim to be used as antimicrobial coatings in various bio-medical and self-defensive biomaterial applications.

2A.2.7 Propensity of bacterial resistance development

Due to the increasing growth of drug resistance in microorganism, the potential emergence of bacterial resistance against these polymers was assessed by serial exposure of bacteria to the polymer-coated surfaces.[21] Both Gram-positive and Gram-negative bacteria were exposed to serial passages of branched polymer **1c** and linear polymer **6** and the change in MIA values were monitored over a period of 20 passages. After 20 serial passages, the MIAs of polymers **1c** and **6** remained same whereas norfloxacin, a nucleic acid targeting antibiotic, showed 850-fold increase in minimum inhibitory concentration (MIC) against sensitive *S. aureus* and

colistin, a lipid II targeting lipopeptide, showed 250 fold increase-in MIC against sensitive *E. coli* respectively (Figure 2A.8). These membrane-active polycations were thus able to stall the development of bacterial resistance and these studies demonstrated that these polymers could be used to create permanent microbicidal paint.

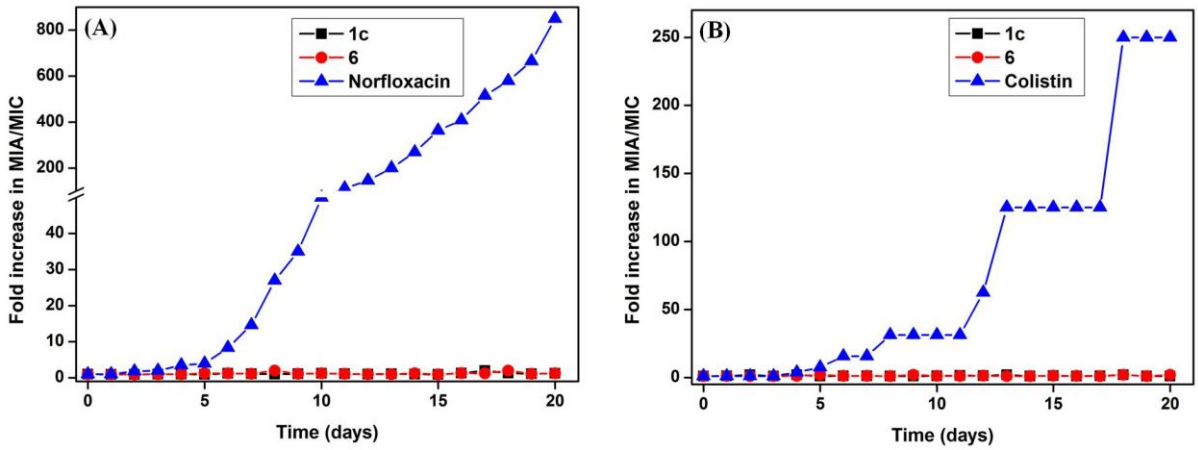

Figure 2A.8: Development of bacterial resistance against: (A) *S. aureus* with polymers (**1c** and **6**) and ciprofloxacin; (B) *E. coli* with polymers (**1c** and **6**) and colistin.

2A.2.8 Leaching test

By ^{1}H-NMR study, it was found that the polycations **1a** and **1b** were partially soluble in water whereas all other polymers (**1c-1e**, **2-6**) were insoluble. However, to confirm further that these polymers kill bacteria on contact and not by leaching, zone of inhibition test was performed with polymer coated filter papers. Filter papers (0.5 cm diameter) coated with polymers were placed onto an agar plate where ~200 µL of 10^{9} CFU/mL of bacteria (*S. aureus* and *E. coli*) were spread by spread-plate method. Polymers **1a** and **1b** showed zone of inhibition against both *S. aureus* and *E. coli* thus confirming that these polymers are partially soluble in water and therefore leaches from the coated surface. On the other hand, no zone of inhibition was found for **1c-1e** and **2-6** thus suggesting that these polymers remained onto the coated surface and kill microorganism on contact (Figure 2A.9). In order to prove further another experiment was performed by taking the two most active polymers (**1c** and **6**). If **1c** and **6** are soluble/partially soluble in water, enough of the polymer would be leached into the overlaid agar gels upon incubation. Further, the polymers would then leach out of gel slabs into the covered bacterial cells and kill bacteria upon placing these pre-incubated agar slabs onto non-coated glass surfaces sprayed with bacteria. However, the leaching test controls showed essentially as many colonies as the control slide (sprayed with bacterial suspension

and covered with fresh agar gel). So it can be concluded that the leaching of the polymers from the coated surface is negligible in terms of their bactericidal activity.

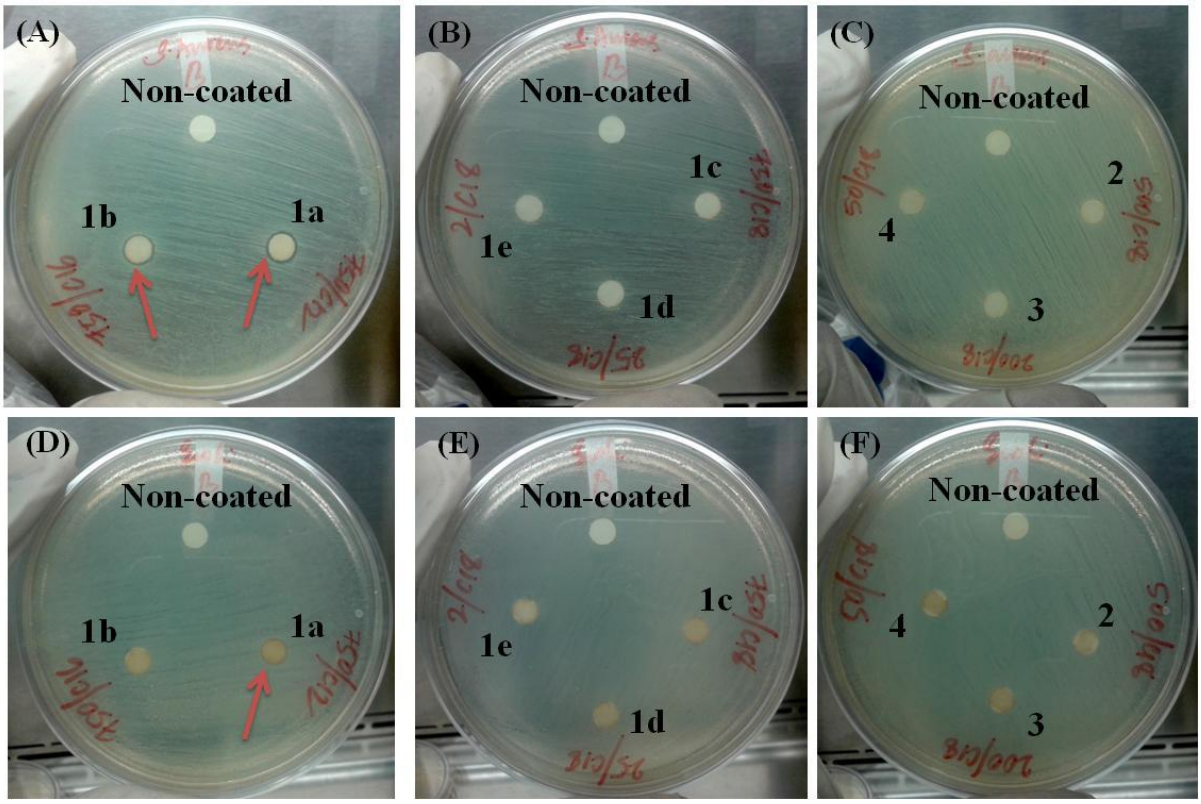

Figure 2A.9: Leaching test: zone of inhibition of cationic PEI derivatives against both Gram-positive bacterium *S. aureus* (A-C) and Gram-negative bacterium *E. coli* (D-F).

2A.3 Conclusion

In conclusion a simple method of developing water-insoluble and organo-soluble polymeric materials was demonstrated. The polymers, when painted onto surfaces, inactivated both airborne and waterborne bacteria completely, including drug-resistant ones and also various pathogenic fungi. The coated surfaces were found to be active in many complex mammalian fluids making them suitable for *in-vivo* applications. These polymeric materials showed excellent compatibility with other polymers and commercial paint thus could be useful for the development of self-defensive biomaterial and "microbicidal paint". Structure-activity relationship studies indicated that the linear polymers are more active and have faster killing rate than the branched ones and an optimum alkyl chain length hence an optimum hydrophobic/hydrophilic balance is required for maximum activity of the water insoluble polymers. The cationic polymers were shown to inactivate bacteria and fungi by disrupting

the membrane integrity, which stalled the development of microbial resistance. Further, the polymers showed negligible hemolytic activity at concentrations much higher than the MIAs and are thus hemocompatible. Thus the cationic polymeric materials developed herein could potentially be used as ″microbicidal paint″ for a wide variety of biomedical and house-hold applications.

2A.4 Experimental section

2A.4.1 Chemicals and instrumentation

Branched PEIs (M_w values of 750, 25, and 2 kDa), poly(2-ethyl-2-oxazoline) (*M*w values of 500, 200, and 50 kDa), 1-bromododecane, 1-bromohexadecane, 1-bromooctadecane, 1-bromoeicosane and 1-bromodocosane were purchased from Sigma-Aldrich while formic acid (90% vol/vol), formaldehyde (37-40% vol/vol), potassium hydroxide (KOH), dichloromethane, chloroform, acetone, methanol, ethanol, *n*-butanol, *tert*-butanol, *N,N*-dimethylformamide (DMF), dimethyl sulfoxide (DMSO), tetrahydrofuran (THF) (all ACS grade) were purchased from SD-FINE, India. Bacterial and fungal growth media and agar were supplied by HIMEDIA, India. Propidium iodide (PI) and SYTO 9 dyes were purchased from Sigma-Aldrich and Invitrogen respectively. Bacterial strains, *S. aureus* (MTCC 737), *E. coli* (MTCC 447) were obtained from MTCC (Chandigarh, India). *P. aeruginosa* (ATCC 424), vancomycin-resistant enterococci (VRE) (ATCC 51559), beta lactam-resistant *K. pneumoniae* (ATCC 700603), methicillin-resistant *S. aureus* (MRSA) (ATCC 33591) were obtained from ATCC (Rockville, MD). The fungal strains used in this study are *C. albicans* (SC5314), *C. dubliniensis* (CD36), *C. tropicalis* (MYA3404), *C. neoformans var. grubii* (serotype A) (H99), *C. gattii* (serotype B) (WM276) and *C. neoformans var. neoformans* (serotype D) (JEC21). ^{1}H-NMR (400 MHz) and ^{13}C-NMR (100 MHz) spectra were recorded on a Bruker AMX-400 instrument. FT-IR spectra of the solid compounds were recorded on Bruker IFS66 V/s spectrometer using KBr pellets. IR spectra of all the liquid compounds were recorded on the same instrument using NaCl crystal. Elemental analysis was performed in a Thermo Finnigan FLASH EA 1112 CHNS analyzer. A WS5000 spin coater, Techno India, India was used to prepare polymer coatings. Leica DM2500 fluorescent microscope was used for bacterial imaging whereas Olympus microscope (Model BX51) and Olympus DP71 camera were used for the fungal imaging. Scanning electron microscope images were obtained using Quanta 3D FEG, FEI field emission scanning electron microscopy.

Thermogravimetric analyses were performed on a TGA 850C Mettler, Toledo thermogravimetric analyzer.

2A.4.2 Synthesis of hydrophobic cationic polymers

2A.4.2.1 Branched *N*-methyl-PEIs (1a′′, 2a′′ and 3a′′)

50% aqueous solution of PEIs *(PEIs of 750, 25 and 2 kDa; 1a′, 2a′ and 3a′)* (10 g, 0.12 mol/repeating unit) was transferred to a round bottom flask to which 90% formic acid (24.5 mL, 0.48 mol) was added followed by 37% formaldehyde (29.3 mL, 0.36 mol) and 20 mL of water (Scheme 1A). The reaction mixture was stirred at 90 °C for 60 h. After cooling down to room temperature, the pH of the reaction mixture was adjusted to 11 using 8 M KOH solution. The deprotonated *N*-methylated PEI was extracted several times by chloroform and the entire organic solution was subjected to repeated water wash. Chloroform was then removed to yield yellow viscous product with 100% degree of methylation.

1a′′: FT-IR ($\overline{\nu}$): 2945 and 2782 cm^{-1} (C–H str), 1460 cm^{-1} (C–H bend), 1030 cm^{-1} (C–N str); ^{1}H NMR (400 MHz, $CDCl_3$, δ): 2.253 (s, 3H, –N(CH_3)–), 2.424-2.603 (m, 4H, –N(CH_2CH_2)–).

2a′′: FT-IR ($\overline{\nu}$): 2944 and 2782 cm^{-1} (C–H str), 1461 cm^{-1} (C–H bend), 1050 cm^{-1} (C–N str); ^{1}H NMR (400 MHz, $CDCl_3$, δ): 2.244 (s, 3H, –N(CH_3)–), 2.409-2.601 (m, 4H, –N(CH_2CH_2)–).

3a′′: FT-IR ($\overline{\nu}$): 2954 and 2792 cm^{-1} (C–H str), 1463 cm^{-1} (C–H bend), 1033 cm^{-1} (C–N str); ^{1}H NMR (400 MHz, $CDCl_3$, δ): 2.237 (s, 3H, –N(CH_3)–), 2.395-2.590 (m, 4H, –N(CH_2CH_2)–).

2A.4.2.2 Branched *N*-alkyl *N*-methyl PEIs (1a-1e, 2, 3)

Branched *N*-methylated-PEIs (1 g, 17.5 mmol/repeating units) were dissolved in 75 mL *tert*-butanol in a screw-top pressure tube and 1-bromoalkanes (70 mmol) were added to it (Scheme 1A). The reaction mixture was heated at 95 °C (for 1-bromododecane), 105 °C (for 1-bromohexadecane), 120 ˚C (for 1-bromooctadecane), 125 °C (for 1-bromoeicosane) and 130 °C (for 1-bromodocosane) for 96 h. After the reaction, the solvent was removed to its one tenth of the initial volume. Then excess of acetone (200 mL) was added to the reaction mixture and the precipitate was filtered off. The precipitate was dissolved in $CHCl_3$ and acetone was added to re-precipitate the product for further purification. Finally, excess solvent was decanted off and the precipitate was dried using high vacuum pump to yield colorless branched *N*-alkyl *N*-methyl PEI polymers (**1a-1e**, **2** and **3**).

1a: ^{1}H-NMR (400 MHz, $CDCl_3$, δ): 0.852 (t, 3H, terminal $-CH_3$), 1.228-1.348 (br m, 18H, $-(CH_2)_9$), 1.823 (q, 2H, $-CH_2-CH_2N^+(CH_2)_2(CH_3)-$), 3.272-4.047 (m, 9H, $-(CH_2)_2N^+(CH_2)(CH_3)-$). Elemental analysis: Calculated C: 58.81; H: 10.53; N: 4.57; Found C: 58.20; H: 10.55; N: 4.51.

1b: ^{1}H-NMR (400 MHz, $CDCl_3$, δ): 0.858 (t, 3H, terminal $-CH_3$), 1.234-1.351 (br m, 26H, $-(CH_2)_{13}$), 1.766 (q, 2H, $-CH_2-CH_2N^+(CH_2)_2(CH_3)-$), 3.081-4.063 (m, 9H, $-(CH_2)_2N^+(CH_2)(CH_3)-$). Elemental analysis: Calculated C: 62.96; H: 11.12; N: 3.86; Found C: 62.89; H: 11.07; N: 3.79.

1c: ^{1}H-NMR (400 MHz, $CDCl_3$, δ): 0.876 (t, 3H, terminal $-CH_3$), 1.202-1.358 (br m, 30H, $-(CH_2)_{15}$), 1.761 (q, 2H, $-CH_2-CH_2N^+(CH_2)_2(CH_3)-$), 3.270-4.109 (m, 9H, $-(CH_2)_2N^+(CH_2)(CH_3)-$). Elemental analysis: Calculated C: 64.59; H: 11.36; N: 3.59; Found C: 64.50; H: 11.22; N: 3.51.

1d: ^{1}H-NMR (400 MHz, $CDCl_3$, δ): 0.877 (t, 3H, terminal $-CH_3$), 1.254-1.367 (br m, 37H, $-(CH_2)_{17}$), 1.805 (m, 2H, $-CH_2-CH_2N^+(CH_2)_2(CH_3)-$), 3.214-4.239 (m, 9H, $-(CH_2)_2N^+(CH_2)(CH_3)-$). Elemental analysis: Calculated C: 66.002; H: 11.56; N: 3.35; Found C: 65.89; H: 11.30; N: 3.30.

1e: ^{1}H-NMR (400 MHz, $CDCl_3$, δ): 0.880 (t, 3H, terminal $-CH_3$), 1.226-1.367 (br m, 38H, $-(CH_2)_{19}$), 1.767 (m, 2H, $-CH_2-CH_2N^+(CH_2)_2(CH_3)-$), 3.179-4.059 (m, 9H, $-(CH_2)_2N^+(CH_2)(CH_3)-$). Elemental analysis: Calculated C: 67.24; H: 11.73; N: 3.14; Found C: 67.18; H: 11.51; N: 3.09.

2: ^{1}H-NMR (400 MHz, $CDCl_3$, δ): 0.874 (t, 3H, terminal $-CH_3$), 1.251-1.350 (br m, 30H, $-(CH_2)_{15}$), 1.766 (m, 2H, $-CH_2-CH_2N^+(CH_2)_2(CH_3)-$), 3.240-4.010 (m, 9H, $-(CH_2)_2N^+(CH_2)(CH_3)-$). Elemental analysis: Calculated C: 64.59; H: 11.36; N: 3.59; Found C: 64.48; H: 11.20; N: 3.50.

3: ^{1}H-NMR (400 MHz, $CDCl_3$, δ): 0.870 (t, 3H, terminal $-CH_3$), 1.212-1.348 (br m, 30H, $-(CH_2)_{15}$), 1.751 (m, 2H, $-CH_2-CH_2N^+(CH_2)_2(CH_3)-$), 3.161-3.949 (m, 9H, $-(CH_2)_2N^+(CH_2)(CH_3)-$). Elemental analysis: Calculated C: 64.59; H: 11.36; N: 3.59; Found C: 64.47; H: 11.12; N: 3.47.

2A.4.2.3 Deacetylated linear PEIs (4a′, 5a′ and 6a′)

Fully deacylated linear PEIs were prepared by the acid-catalyzed hydrolyses of the commercial PEOZs (500, 200 and 50 kDa).[40] Typically, 10.0 g of the PEOZs was added to 400 mL of 24% (wt/vol) HCl, followed by refluxing for 96 h. The POEZ crystals dissolved completely in 2 h, but, 3 h later, a white precipitate appeared. The precipitate in each case was isolated by filtration and then air-dried. The resultant white powders were confirmed to be pure PEI hydrochlorides by a combination of NMR and elemental analysis. Protonated linear PEIs were then deprotonated using aqueous KOH solution. Briefly, 10 g of protonated linear PEIs were dissolved in distilled water (50 mL) and 6 M KOH was added till the pH of

the solution became ~11. Deprotonated PEIs as white precipitates were filtered, and washed repeatedly with distilled water till it became neutral (pH~7). Separately, 217, 87 and 22 kDa linear PEIs without *N*-acyl groups were obtained from commercial PEOZs of 500, 200 and 50 kDa.

4a′: ^{1}H NMR (400 MHz, D_2O, δ): 3.149 (s, –N(CH_2CH_2)–).

5a′: ^{1}H NMR (400 MHz, D_2O, δ): 2.903 (s, –N(CH_2CH_2)–).

6a′: ^{1}H NMR (400 MHz, D_2O, δ): 2.894 (s, –N(CH_2CH_2)–).

2A.4.2.4 Linear *N*-methyl PEIs (4a′′, 5a′′ and 6a′′)

Linear *N*-methyl PEIs were prepared from linear PEIs following procedure similar to the synthesis of branched *N*-methyl PEIs.

4a′′: FT-IR ($\overline{\nu}$): 2951 and 2794 cm^{-1} (C–H str), 1454 cm^{-1} (C–H bend), 1018 cm^{-1} (C–N str); ^{1}H NMR (400 MHz, $CDCl_3$, δ): 2.252 (s, 3H, –N(CH_3)–), 2.505 (s, 4H, –N(CH_2CH_2)–).

5a′′: FT-IR ($\overline{\nu}$): 2944 and 2780 cm^{-1} (C–H str), 1461 cm^{-1} (C–H bend), 1033 cm^{-1} (C–N str); ^{1}H NMR (400 MHz, $CDCl_3$, δ): 2.245 (s, 3H, –N(CH_3)–), 2.495 (s, 4H, –N(CH_2CH_2)–).

6a′′: FT-IR ($\overline{\nu}$): 2944 and 2794 cm^{-1} (C–H str), 1454 cm^{-1} (C–H bend), 1028 cm^{-1} (C–N str); ^{1}H NMR (400 MHz, $CDCl_3$, δ): 2.242 (s, 3H, –N(CH_3)–), 2.491 (s, 4H, –N(CH_2CH_2)–).

2A.4.2.5 Linear N-alkyl N-methyl PEIs (4, 5 and 6)

Linear *N*-alkyl *N*-methyl PEIs were prepared from linear *N*-methyl PEIs following procedure similar to the synthesis branched *N*-alkyl *N*-methyl PEIs (**4**, **5** and **6**).

4: ^{1}H NMR (400 MHz, $CDCl_3$, δ): 0.865 (t, 3H, terminal –CH_3), 1.257-1.359 (br m, 30H, –$(CH_2)_{15}$), 1.744 (m, 2H, –CH_2–$CH_2N^+(CH_2)_2(CH_3)$–), 3.175-3.879 (m, 9H, –$(CH_2)_2N^+(CH_2)(CH_3)$–). Elemental analysis: Calculated C: 64.59; H: 11.36; N: 3.59; Found C: 64.53; H: 11.29; N: 3.44.

5: ^{1}H NMR (400 MHz, $CDCl_3$, δ): 0.896 (t, 3H, terminal –CH_3), 1.212-1.364 (br m, 30H, –$(CH_2)_{15}$), 1.764 (m, 2H, –CH_2–$CH_2N^+(CH_2)_2(CH_3)$–), 3.170-4.109 (m, 9H, –$(CH_2)_2N^+(CH_2)(CH_3)$–). Elemental analysis: Calculated C: 64.59; H: 11.36; N: 3.59; Found C: 64.39; H: 11.16; N: 3.49.

6: ^{1}H NMR (400 MHz, $CDCl_3$, δ): 0.880 (t, 3H, terminal –CH_3), 1.192-1.358 (br m, 30H, –$(CH_2)_{15}$), 1.748 (m, 2H, –CH_2–$CH_2N^+(CH_2)_2(CH_3)$–), 3.179-4.012 (m, 9H, –$(CH_2)_2N^+(CH_2)(CH_3)$–). Elemental analysis: Calculated C: 64.59; H: 11.36; N: 3.59; Found C: 64.48; H: 11.19; N: 3.49.

2A.4.3 Solubility of *N*-alkyl *N*-methyl PEIs

A small portion (10 mg) of all the PEI derivatives were added in 1 ml of various organic solvents (chloroform, dichloromethane, methanol, ethanol, *n*-butanol, *N*,*N*-dimthylformamide, dimethyl sulfoxide, tetrahydrofuran) and vortexed for about 10-15 min and observed visually to check the solubility. The solubility limit was also determined visually after vortexing for 10-15 min of different amounts (10, 20, 50, and 100 mg) of the PEIs derivatives in 1 ml of solvent. However, to test water solubility, 10 mg of the PEIs derivatives in 1 ml of water was vortexed for 10-15 min and kept for 12 h. The aqueous part was decanted and subjected to freeze drying. ^{1}HNMR spectra were recorded with the freeze dried sample in $CDCl_3$.

2A.4.4 Preparation of the film

PEI derivatives were first dissolved/suspended in *n*-butanol (50 mg/ml) and the solutions were serially diluted (2-fold serial dilution). Solutions of different concentrations (20 μl) were added into wells of a 96-well plate. The solution was first air-dried and finally dried in vacuum oven at 50° C to prepare a film onto the flat-bottom surface of wells of 96-well plate. Each concentration was applied in triplicate for all the polymers for antimicrobial activity studies. In order to make films on surfaces such as microscopic glass slide as microbicidal coating, solution of PEI derivatives (in $CHCl_3$, 350 μl) were coated using a spin coater. Antimicrobial coating of these derivatives were prepared along with the medically relevant polymers such polylactic acid (PLA) using spin coater from the solutions (350 μl) of PEI derivatives (of different concentrations) and PLA (10 mg/mL) in chloroform. In order to prepare microbicidal paint, different amount of PEI derivatives were brush coated along with the commercial paint solution (100 mg/mL and 50 mg/mL of PEI derivatives **1c** and **6** respectively in paint solution).

2A.4.5 Antibacterial activity

2A.4.5.1 Determination of antibacterial activity by spray method (air-borne bacteria)

Bacteria were grown for 6 h in suitable nutrient media at 37 °C under constant shaking. The 6 h grown bacteria (1 mL) was centrifuged down at a speed of 12000 rpm for 1 min. The bacterial pellet was then washed twice with 1X PBS (pH-7.4). Final concentration of the bacterial solution was then adjusted to 10^7 CFU/mL for *S. aureus* and 10^6 CFU/mL for *E. coli* and the volume was made to 10 mL. The bacterial solution was then sprayed onto the

polymers coated glass slides (2.5 cm × 5.5 cm) at a spray rate of approximately 10 mL/min. The sprayed slides were then carefully transferred into a petridish and dried in air for about 2 min. A slab of nutrient agar was then placed onto the glass slide and the pertidish was sealed and kept at 37 °C till visible colonies developed.[41] The coated and non-coated slides were imaged using a Cell Biosciences Gel Documentation instrument. Images were captured under white light and processed using Alpha-imager software. A similar experiment was performed with (PLA/Paint + **1c**) and (PLA/Paint + **6**) coated glass slides, i.e., the glass slides were coated with the polymers **1c** and **6** along with the PLA and paint individually and antibacterial efficacy of the coated slides were evaluated similarly.

2A.4.5.2 Determination of antibacterial activity (water-borne bacteria)

To determine the antibacterial activity of the polymers, 200 μL of 10^5 CFU/mL of bacteria were added to the polymers coated wells of 96-well plate following the coating procedure as described above. Two controls were made: in one control no solvent was added to the wells (blank wells) containing equal volume of bacteria (10^5 CFU/mL) and the other one where initially coating solvent was added and then dried. The plates were then were incubated at 37°C for 24 h. The visual turbidity was recorded before and after incubation to determine the minimum inhibitory amount, MIA (μg/mm^2 present in the well).

2A.4.5.3 Antibacterial kinetics

96-Well plate was coated with the polymers **1c** and **6** at two different concentrations: MIA and 6 × MIA for both *S. aureus* and *E. coli* respectively following the coating procedure as described above. Bacterial suspension (200 μL) containing approximately 4.9×10^5 CFU/mL *S. aureus* in nutrient broth and 5.1×10^5 CFU/mL *E. coli* in Luria-Bertani (LB) broth were added, and the plates were incubated at 37 °C under constant shaking. The initial time of addition of the bacteria to the wells was taken as zero, and 10 μL aliquots were withdrawn from each of the wells at definite time intervals. These aliquots were then added to 90 μL of 0.9% saline. These solutions were further diluted by a factor of 2, and 20 μL of the final solutions was plated on nutrient or LB agar plates immediately. The plates were incubated at 37 °C for 24 h, and bacterial colonies were counted. A plot of colony forming unit (CFU) in logarithmic scale versus time (Log_{10} CFU/mL *vs* min) was then plotted to determine the bactericidal kinetics.

2A.4.5.4 Antibacterial activity in mammalian systems

Blood (sodium heparin as anticoagulant) was donated by a healthy human donor. Plasma was isolated by centrifugation of the blood at 3500 rpm for 5 min. Serum was obtained by using SST^{TM} II Advance tube (BD vacutainer) (Ref 367956) containing human blood and then centrifuging at 3500 rpm for 5 min. Methicillin resistant *S. aureus* (MRSA) was grown at nutrient media for 6 h (~ 10^9 CFU/mL). Finally, MRSA was diluted in minimum essential medium (MEM) and mixed with all three mammalian systems individually to obtain 10^5 CFU/mL in 50% serum, 50% plasma, and 10% blood. 200 μL of 50% serum, 50% plasma, and 10% blood containing 10^5 CFU/mL of MRSA were added to the wells of 96-well plate coated with the polymers (**1c** and **6**). Likewise the MIA experiment, two controls were made: in one control no solvent was added to the wells (blank wells) and the other one is solvent-dried well. The plates were then placed in an incubator at 37 ˚C for 24 h. After incubation, aliquots from the each well (20 μL) were plated on nutrient agar plates. The plates were then incubated at 37 °C for 24 h, and colonies were observed.

2A.4.6 Mechanism of antibacterial action

2A.4.6.1 Cytoplasmic membrane depolarization assay

The 96-well plates were coated following the similar coating procedure as mentioned previously to give polymer concentration of 1.56 μg/mm^2 for *S. aureus* and 15.6 μg/mm^2 for *E. coli*. Midlog phase bacterial cells (*S. aureus* and *E. coli*) were harvested, washed with 5 mM HEPES and 5 mM glucose and resuspended in 5 mM glucose, 5 mM HEPES buffer and 100 mM KCl solution in 1:1:1 ratio (10^8 CFU/mL).[42] Measurements were made in black 96-well plate containing 200 μL of bacterial suspension and 2 μM diSC$_3$(5) (3,3′-dipropylthiadicarbocyanine iodide). The fluorescence of the dye was allowed to quench for 20 min for *S. aureus* and 40 min for *E. coli* and 0.2 mM EDTA was used in case of *E. coli* to allow dye uptake through the outer membrane. Bacterial suspension was then placed in polymer coated 96-well plate (black plate, clear bottom with lid) and fluorescence intensity was measured at every 2 minutes interval for 25 min at excitation wavelength of 622 nm (slit width: 10 nm) and emission wavelength of 670 nm (slit width: 20 nm).

2A.4.6.2 Fluorescence microscopy

Bacterial suspension (200 μL, 10^9 CFU/mL and 10^8 CFU/mL for *S. aureus* and *E. coli* respectively) were added to the well of 96 well plate coated with polymer **6** (at 6 × MIA). A

control was made similarly in non-coated wells. The 96-well plate was placed in incubator at 37 °C under constant shaking for 4 h. After the incubation, the bacterial suspension was harvested and washed with PBS twice and finally resuspended in 100 µL PBS. Then, 10 µL of the bacterial suspension was combined with 20 µL of a fluorescent probe mixture containing 3.0 µM green fluorescent nucleic acid stain SYTO 9 (Invitrogen, USA) and 15.0 µM red fluorescent nucleic acid stain propidium iodide (PI) (Sigma Aldrich ,USA) (1:1 v/v). The mixture was incubated in dark for 15 min and a 5 µL aliquot was placed on a glass slide, which was then covered by a cover slip, sealed and examined under fluorescence microscope. Excitation was done for SYTO 9 at 488 nm and at 543 nm for PI respectively. Emission was collected using a band pass filter for SYTO 9 at 500-550 nm and a long pass filter for PI at 590-800 nm. In all cases, a ×100 objective was used with immersion oil, giving a total magnification of ×1000. Images were captured with a Leica DM 2500 fluorescence microscope.

2A.4.6.3 Scanning electron microscopy

Bacterial suspension (200 µL, 10^8 CFU/mL for both *S. aureus* and *E. coli* respectively) in suitable nutrient media were added to the wells of 96-well plate coated with polymer **6** (6 × MIA). Bacteria were incubated at 37°C for 2 h. After incubation, the bacterial suspension from the wells was transferred to 1 mL eppendrof tube and centrifuged. The bacterial pellet was resuspended in 30% ethanol and subsequently dehydrated with 50%, 70%, 90%, and 100% ethanol. Finally, the bacteria were resuspended in 70% ethanol and 5 µL of the bacterial suspension in ethanol was drop casted onto silicon wafer and dried. The samples were sputter coated with gold prior to imaging using Quanta 3D FEG, FEI field emission scanning electron microscopy.

2A.4.7 Antifungal activity

2A.4.7.1 Minimum inhibitory amount (MIA)

The yeast cultures were grown overnight in 5 mL YPD (1% Yeast extract, 2% Peptone and 2% Dextrose). The growth was measured by optical density (OD_{600}) and cells were diluted in fresh media to get a concentration of 10^5 cells/mL. After the dilution, 200 µL of the fungal cell suspension (equal to 2 x 10^4 cells) was added into the polymers coated wells of 96-well plate. The plates were incubated at 30 °C for 20 hours with shaking (180 rpm) to allow sufficient growth of the fungal cells. The growth of the fungi was measured at OD_{600} using

YPD wells as blank. The OD_{600} values were analyzed by calculating mean and standard deviation and further plotting the graph. The amount present in the well ($\mu g/mm^2$) where the OD of the test well matched with that of blank well was taken as MIA. To account for the optical density contributed by the polymer coating on the wells, only media (200 μL) was added in the coated wells and used as blank for the respective concentrations.

2A.4.7.2 Minimum fungicidal amount (MFA)

To discriminate between the fungistatic and fungicidal effect of the polymers, aliquots from the wells that appeared to have less or no turbidity were plated on agar plates. For this, 3 μL of the culture from each well was taken after the MIA experiment, and spotted on to the YPD agar plate. The YPD plates were then incubated for 24 hours at 30 °C to allow the growth of the live cells. The amount of the polymers present in the well ($\mu g/mm^2$) for which no colony was observed on agar plate was taken as the minimum fungicidal amount (MFA) for each fungus.

2A.4.7.3 Kinetics of antifungal activity

To determine the rate of fungal killing by the polymers coated surfaces, a time course experiment was performed and the antifungal activity of the most active polymers from branched and linear groups (**1c** and **6**) was determined. For this, the cells were grown and added (10^5 cells/mL) into the polymers coated wells of 96 well plate coated at two different concentrations (MIA and 8 × MIA) as described above. At every 2 hours interval, 3 μL of cells were spotted on YPD plate starting at 0 hour till 12 hours. The plates were then incubated at 30 °C for next 24 hours and growth was assayed to determine the time required to kill the fungus.

2A.4.8 Mechanism of antifungal action

In order to have insights into the mechanism of antifungal activity by the polymer coatings, a fluorescence based LIVE/DEAD assay was performed. *C. dubliniensis* cells were grown as described previously in polymers coated 96-well plates for 12 hours at different concentrations of a branched polymer **1c** and a linear polymer **6** (MIA or 8 × MIA). The cells were then collected from all wells and pelleted. Following, the cells were washed with 1 mL of autoclaved water and finally resuspended in 100 μL of Milli-Q water. The live and dead cells were stained by adding 1 μL of propidium iodide (PI) and 1 μL of SYTO 9 (3.0 μM

SYTO 9 and 15.0 μM PI). The mixture was then kept for incubation at room temperature for 30 minutes in dark. The cells were then observed under microscope for the fluorescence signal. Bright field imaging was done for DIC images, SYTO 9 fluorescence was monitored using the green emission filter and PI fluorescence was determined in the red emission filter. The images were captured in Olympus microscope (Model BX51) using Olympus DP71 camera. The images were further processed using Image Pro-Plus software, Image J and Adobe Photoshop.

2A.4.9 Resistance development study

MIA values of polymers (**1c** and **6**) were determined against both *S. aureus* and *E. coli* following procedure as described previously. After the initial MIA experiment, serial passaging was initiated by harvesting bacterial cells grown at the sub-MIA of the polymers (at [MIA]/2) and was subjected to another MIA assay. After 24 h incubation period, cells grown in the sub-MIA of the polymers (at [MIA]/2) from the previous passage were once again harvested and assayed for the MIA.[43] The process was repeated for 20 passages. Norfloxacin and colistin were chosen for *S. aureus* and for *E. coli* respectively as the controls. In case of norfloxacin and colistin, the initial MIC values were also determined against respective bacteria and the process was repeated for 20 passages following similar procedure as above. The fold increase in MIA/MIC values of the polymers and the controls was plotted against the number of passages.

2A.4.10 Hemolytic assay

Human red blood cells (hRBC) were isolated from freshly drawn, heparinized human blood and resuspended to 5 vol% in phosphate buffered saline (PBS) (pH 7.4). Then, 200 μL of hRBC suspension (5 vol% in PBS) was added to the wells of 96-well plate coated with polymers. Two controls were made, one non-coated well dried after using only solvent and another non-coated well with the solution of Triton X-100 (1 vol %). The plates were then incubated for 1 h at 37°C and were then centrifuged at 3500 rpm for 5 min. Following centrifugation, 100 μL of the supernatant from each well was transferred to a fresh 96-well plate, and absorbance at 540 nm was measured. Percentage of hemolysis was determined as $(A - A_0)/(A_{total} - A_0) \times 100$, where A is the absorbance of the test well (wells coated with polymers), A_0 the absorbance of the wells with negative controls (wells without any polymer

coating), and A_{total} the absorbance of the well with 100% hemolysis (wells with Triton X-100, 1 vol%), all at 540 nm.

2A.4.11 Leaching test

2A.4.11.1 Leaching test 1 (Zone of inhibition)

Whatman filter paper (Whatman, cat. no. 1440125) was cut into a circular pieces (0.5 cm diameter) and each piece was dipped into the solutions of the polymers in chloroform (10 mg/mL for *S. aureus* and 100 mg/mL for *E. coli*) to coat the paper. Bacteria (*S. aureus* and *E. coli*, 10^9 CFU/mL) were spread onto the agar plate by spread plate method using sterile non-toxic cotton swab and allowed to dry for 2-3 min. The coated filter papers were then placed on the agar plates and incubated at 37 °C for 24 h. After incubation, the zone of inhibition was examined to determine the leaching nature of the coating (not-suitable for permanent non-covalent coating). A non-coated filter paper (dipped into only chloroform) was used as control experiment.

2A.4.11.2 Leaching test 2

In order to prove further that the coated polymers kill bacteria on contact and not by leaching, the following experiment was also performed by taking the two most active polymers (**1c** and **6**). **1c** and **6**-coated glass slides not sprayed with a bacterial suspension were overlaid with the growth agar gel slabs, placed in a Petri dish, sealed, and incubated at 37 °C for 18 h. Consequently, the polymers coated onto glass slides were allowed to leach into the gel slabs. Then the bacterial (*S. aureus*) suspension was sprayed onto non-coated glass slides, followed by overlaying with the agar gel slabs that had been previously exposed to the **1c**- and **6**-coated slides and a subsequent incubation at 37 °C for 24 h. A similar experiment was performed with a non-coated glass slide sprayed with a bacterial suspension where a fresh agar gel slab was placed onto it (as control). The amount of the polymers **1c** and **6** used for coating was 0.4 and 0.2 $\mu g/mm^2$ respectively.

2A.4.12 Thermogravimetric analysis

Thermogravimetric analyses were performed on a TGA 850C Mettler, Toledo thermogravimetric analyzer. Samples (5-10 mg) of the PEI derivatives were used for each experiment. The measurement was done from 30 to 500 °C at a constant heating rate H_R of 10 °C/min under nitrogen atmosphere (40 mL/min).

BIBLIOGRAPHY

1. Schaer, T. P.; Stewart, S.; Hsu, B. B.; Klibanov, A. M. Hydrophobic polycationic coatings that inhibit biofilms and support bone healing during infection. *Biomaterials* **2012**, *33*, 1245-1254.
2. Li, Y.; Kumar, K. N.; Dabkowski, J. M.; Corrigan, M.; Scott, R. W.; Nusslein, K.; Tew, G. N. New bactericidal surgical suture coating. *Langmuir* **2012**, *28*, 12134-12139.
3. Yang, W. J.; Cai, T.; Neoh, K. G.; Kang, E. T.; Dickinson, G. H.; Teo, S. L.; Rittschof, D. Biomimetic anchors for antifouling and antibacterial polymer brushes on stainless steel. *Langmuir* **2011**, *27*, 7065-7076.
4. Fernandez-Saiz, P.; Lagaron, J. M.; Ocio, M. J. Optimization of the film-forming and storage conditions of chitosan as an antimicrobial agent. *J. Agric. Food Chem.* **2009**, *57*, 3298-3307.
5. Wong, S. Y.; Li, Q.; Veselinovic, J.; Kim, B. S.; Klibanov, A. M.; Hammond, P. T. Bactericidal and virucidal ultrathin films assembled layer by layer from polycationic N-alkylated polyethylenimines and polyanions. *Biomaterials* **2010**, *31*, 4079-4087.
6. Wong, S. Y.; Han, L.; Timachova, K.; Veselinovic, J.; Hyder, M. N.; Ortiz, C.; Klibanov, A. M.; Hammond, P. T. Drastically Lowered Protein Adsorption on Microbicidal Hydrophobic/Hydrophilic Polyelectrolyte Multilayers. *Biomacromolecules* **2012**, *13*, 719-726.
7. Waschinski, C. J.; Zimmermann, J.; Salz, U.; Hutzler, R.; Sadowski, G.; Tiller, J. C. Design of contact-active antimicrobial acrylate-based materials using biocidal macromers. *Adv. Mater.* **2008**, *20*, 104-108.
8. Mukherjee, K.; Rivera, J. J.; Klibanov, A. M. Practical aspects of hydrophobic polycationic bactericidal "paints". *Appl. Biochem. Biotechnol.* **2008**, *151*, 61-70.
9. Haldar, J.; An, D. Q.; de Cienfuegos, L. A.; Chen, J. Z.; Klibanov, A. M. Polymeric coatings that inactivate both influenza virus and pathogenic bacteria. *Proc. Natl. Acad. Sci. USA* **2006**, *103*, 17667-17671.
10. Park, D.; Wang, J.; Klibanov, A. M. One-step, painting-like coating procedures to make surfaces highly and permanently bactericidal. *Biotechnol. Prog.* **2006**, *22*, 584-589.
11. Carlson, E. Effect of strain of Staphylococcus aureus on synergism with Candida albicans resulting in mouse mortality and morbidity. *Infect. Immun.* **1983**, *42*, 285-92.
12. Shirtliff, M. E.; Peters, B. M.; Jabra-Rizk, M. A. Cross-kingdom interactions: Candida albicans and bacteria. *FEMS Microbiol. Lett.* **2009**, *299*, 1-8.
13. Haldar, J.; Weight, A. K.; Klibanov, A. M. Preparation, application and testing of permanent antibacterial and antiviral coatings. *Nat. Protoc.* **2007**, *2*, 2412-7.
14. Lee, S. B.; Koepsel, R. R.; Morley, S. W.; Matyjaszewski, K.; Sun, Y.; Russell, A. J. Permanent, nonleaching antibacterial surfaces. 1. Synthesis by atom transfer radical polymerization. *Biomacromolecules* **2004**, *5*, 877-882.
15. Chen, C. Z. S.; Beck-Tan, N. C.; Dhurjati, P.; van Dyk, T. K.; LaRossa, R. A.; Cooper, S. L. Quaternary ammonium functionalized poly(propylene imine) dendrimers as effective antimicrobials: Structure-activity studies. *Biomacromolecules* **2000**, *1*, 473-480.
16. Darouiche, R. O. Current concepts - treatment of infections associated with surgical implants. *N. Engl. J. Med.* **2004**, *350*, 1422-1429.
17. Uppu, D. S. S. M.; Samaddar, S.; Ghosh, C.; Paramanandham, K.; Shome, B. R.; Haldar, J. Amide side chain amphiphilic polymers disrupt surface established bacterial bio-films and protect mice from chronic Acinetobacter baumannii infection. *Biomaterials* **2016**, *74*, 131-143.

18. Lin, J.; Qiu, S. Y.; Lewis, K.; Klibanov, A. M. Mechanism of bactericidal and fungicidal activities of textiles covalently modified with alkylated polyethylenimine. *Biotechnol. Bioeng.* **2003**, *83*, 168-172.
19. Harriott, M. M.; Noverr, M. C. Candida albicans and Staphylococcus aureus form polymicrobial biofilms: effects on antimicrobial resistance. *Antimicrob. Agents Chemother.* **2009**, *53*, 3914-3922.
20. Ravikumar, T.; Murata, H.; Koepsel, R. R.; Russell, A. J. Surface-active antifungal polyquaternary amine. *Biomacromolecules* **2006**, *7*, 2762-2769.
21.Yarlagadda, V.; Akkapeddi, P.; Manjunath, G. B.; Haldar, J. Membrane active vancomycin analogues: a strategy to combat bacterial resistance. *J. Med. Chem.* **2014**, *57*, 4558-4568.

Chapter 2B

Charge-Switchable Polyethylenimine-based Antimicrobial Paint with Hydrolysable Amide or Ester Groups in Side Chains of Polymers

Abstract

Chapter 2B *describes development of a charge-switchable antimicrobial coating for biomedical devices or implants based on water-insoluble and organo-soluble cationic polyethylenimine derivatives that contain degradable amide or ester groups in the side alkyl chain. The side-chain degradable polymers were synthesized from polyethylenimine (PEI) via Eschweiler-Clarke methylation followed by quaterisation with amide/ester containing alkyl bromides. The polymers, coated non-covalently onto surfaces from their organic solution, were shown to inactivate both bacteria and fungi upon contact (5-log reduction). Also, polymer coated surfaces were shown to effectively inhibit microbial (bacterial and fungal) biofilm formation. Importantly, these polymers were hydrolyzed in the presence of acid and enzymes which led to switching charge from active and non-toxic cationic polymers to inactive and highly biocompatible zwitterionic polymers. Partly zwitterionic polymers, products of partially hydrolyzed cationic polymers, were shown to have improved biocompatibility with relatively lesser changes in their antibacterial activity compared to the respective cationic polymers. Notably, fully hydrolyzed zwitterionic polymer showed remarkable biocompatibility towards mammalian cells (the minimum inhibitory concentration (MIC) and 50% hemolytic concentration (HC_{50}) of cationic polymers were 39-625 and >5000 μg/mL, the corresponding zwitterionic polymers showed MIC and HC_{50} of >10000 and >40000 μg/mL respectively). Further, the fully zwitterionic polymer was shown to be completely non-lethal upon intra-peritonea (i.p.) administration in mice (LD_{50}>175 mg/kg). Moreover when tested, cationic polymer-coated catheter showed ~99.99% methicillin-resistant S. aureus (MRSA) reduction and inhibited biofilm formation in a mice model of subcutaneous infection. Current antimicrobial coatings to prevent microbial colonization on medical devices and implants are mostly based on non-degradable polymers which often lack biocompatibility and can lead to unpredictable toxicity. Thus the side chain degradable antimicrobial polymers might hold promise as safe and effective antimicrobial coatings to prevent implant-associated infections.*

Publication based on this work

1. Hoque, J. *et al.* Charge switchable polymeric coatings: tuning antimicrobial and cytotoxic activities of side chain degradable polyethylenimine derivatives. Manuscript submitted.

2B.1 Introduction

Usage of medical devices and implants such as catheters, contact lenses, cardiac pacemakers, hip implants, etc. to restore the function of damaged or diseased organ tissue involves challenges, in particular, implant-associated infections resulting from the microbial contamination and subsequent formation of biofilms.[1,2] Coating of the device surfaces with an antimicrobial agent has been shown to be a promising approach to thwart the microbial infections.[3,4] However, antimicrobial coatings developed by impregnating biocides such as antibiotics, metal nanoparticles, etc. often suffer from unwanted release of the biocides, cumulative toxicity and higher propensity of microbial resistance development.[5,6] On the other hand, antimicrobial coatings developed by immobilizing antibacterial agents (e.g., antimicrobial polymers) are generally non-degradable and toxic.[7,8] The long-term exposure of non-degradable coatings might results in unpredictable cytotoxicity and hinders implant-tissue integration for many indwelling devices applications. Moreover, for combating infections effectively the coatings are simultaneously required to inactivate microbes and inhibit biofilm formation.[9,10] To be suitable for biomedical applications, an antimicrobial coating should kill microbes and prevent their colonization on medical devices or implants for required period of time and, where applicable, then transformed into an inactive non-toxic form.

Chapter 2B herein deals with the design and development of a charge-switchable antimicrobial coating based on water-insoluble and organo-soluble cationic polyethylenimine derivatives bearing hydrolysable amide or ester groups in the side alkyl chain, which upon hydrolysis in presence of acid or enzymes, transforms into highly non-toxic zwitterionic polymers. Antibacterial coatings that switch charge from cationic to zwitterionic have been developed where the modified surfaces were shown to be efficacious in killing and/or removing bacteria.[11,12] However, the immobilization of charge-switchable moiety involves highly costly and practically challenging covalent modification and subsequent polymerization of the moiety onto surface.[13] It is therefore highly desirable to develop cost-effective antimicrobial coatings that can be applied directly non-covalently onto surfaces where the coatings should prevent microbial colonization without causing substantial toxicity towards mammalian cells and gradually hydrolyses from an active cationic form to a non-toxic zwitterionic form.

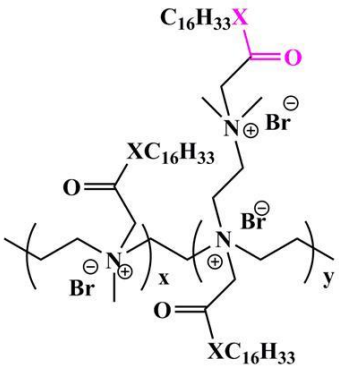

1a (PEI = 750 kDa, X = –NH)
1b (PEI = 25 kDa, X = –NH)
1c (PEI = 2 kDa, X = –NH)
2a (PEI = 750 kDa, X = –O)
2b (PEI = 25 kDa, X = –O)
2c (PEI = 2 kDa, X = –O)

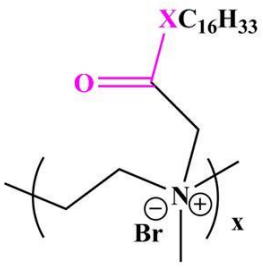

3a (PEI = 217 kDa, X = –NH)
3b (PEI = 87 kDa, X = –NH)
3c (PEI = 22 kDa, X = –NH)
4a (PEI = 217 kDa, X = –O)
4b (PEI = 87 kDa, X = –O)
4c (PEI = 22 kDa, X = –O)

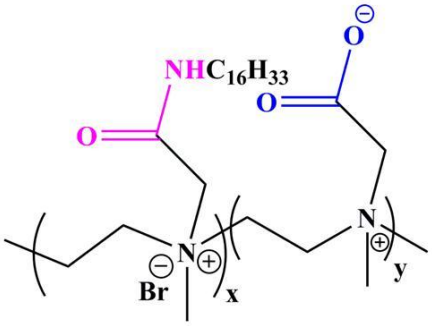

5a (22% zwitterionic)
5b (48% zwitterionic)
5c (78% zwitterionic)

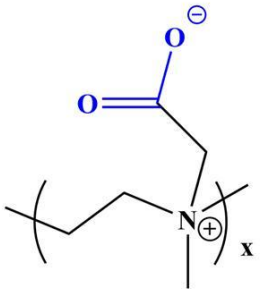

5d (100% zwitterionic)

Figure 2B.1: Structures of amide or ester containing side-chain degradable antimicrobial polymers and various partially or completely hydrolyzed products.

In chapter 2A, polyethylenimines based water-insoluble and organo-soluble cationic polymers bearing octadecyl chains have been developed and were used as effective antimicrobial coatings. However, these polymers are non-degradable in nature and are mainly suitable for hospital walls, floors, operating equipments, etc. as permanent antimicrobial coatings. Introduction of cleavable groups such as amide or ester (known to hydrolyze in the presence of acids and enzymes such amidases or esterases[14,15]) between the positive charge and hydrophobic alkyl chain of cationic PEI polymers can provide side-chain degradable polymers. These polymers, upon hydrolysis via the cleavable groups can lead to the formation of zwitterionic polymers which are generally highly biocompatible. In this chapter quaternary polyethylenimines derivatives bearing cleavable amide or ester groups in the side hexadecyl chains were therefore developed and have been successfully used as charge-switchable antimicrobial coatings (Figure 2B.1). The length of side chains of these polymers

was much closer to the octadecyl chain (a hexadecyl chain along with the amide or ester group) which allowed synthesizing water-insoluble and organo-soluble yet antimicrobial polymers with cleavable groups.

The polymers when coated onto surfaces were shown to be effective in killing both bacteria and fungi. Further, the surfaces were also shown to be efficacious in inhibiting formation of both bacterial and fungal biofilm. Interestingly, they were shown to gradually degrade in the presence of acid and enzymes. Moreover, polymers with amide and ester groups were shown to hydrolyze at different rates which allowed tuning the rate of degradation of side-chain degradable polymers. Further, partly zwitterionic polymers (Figure 2B.1), products of partial hydrolysis, were shown to be active towards microbes and non-toxic towards mammalian cells. Importantly, fully zwitterionic polymers (Figure 2B.1), product of complete hydrolysis of PEI derivatives, were shown to be exceptionally non-toxic towards mammalian cells both *in-vitro* and *in-vivo*. Notably, medical grade catheters when coated with these polymers were shown to reduce methicillin-resistant *Staphylococcus aureus* (MRSA) burden by >99.99% and inhibit formation of biofilm in animal model.

2B.2 Results and discussion

2B.2.1 Synthesis of polymers

2B.2.1.1 Synthesis of cationic PEI derivatives

The side-chain degradable polymers were synthesized by quaternizing *N*-methyl PEI with *N*-hexadecyl-2-bromoethanamide or *N*-hexadecyl-2-bromoethanoate. *N*-Hexadecyl-2-bromoethanamide and *N*-hexadecyl-2-bromoethanoate were obtained by reacting 1-aminohexadecane and 1-hexadecanol with bromoacetyl bromide in the presence of aqueous K_2CO_3 (Scheme 2B.1).

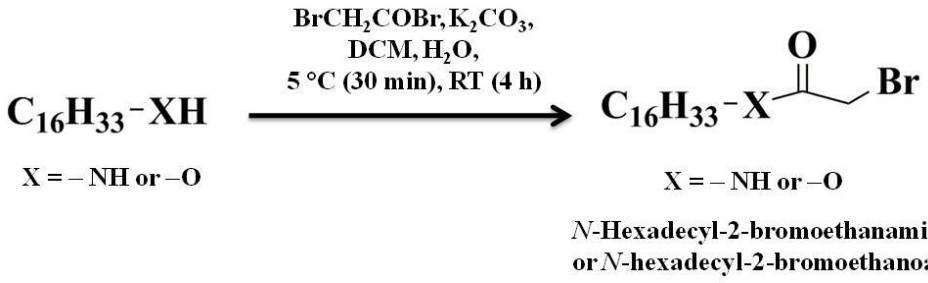

Scheme 2B.1: Synthesis of *N*-hexadecyl-2-bromoethanamide and *N*-hexadecyl-2-bromoethanoate.

The reaction was carried out at 5 ˚C for 30 min (initial addition time of highly reactive bromoacetyl bromide) and then at room temperature for about 4 h to give quantitative yield. *N*-Methyl PEIs of different molecular weights were obtained via Eschweiler-Clarke methylation of both branched and linear PEIs (750, 25 and 2 kDa branched PEIs and 217, 87 and 22 kDa linear PEIs) following the same protocol as described in the Section 2A.4.2 in Chapter 2A. Finally, all the tertiary amine groups of both branched and linear *N*-methyl PEIs were quaternized with *N*-hexadecyl-2-bromoethanamide or *N*-hexadecyl-2-bromoethanoate which yielded water-insoluble and organo-soluble quaternary polymers with amide or ester groups in the side alkyl chain (Scheme 2B.2 and 3). Thus a total of twelve polymers (**1a-1c**, **2a-2c**, **3a-3c** and **4a-4c**) were synthesized.

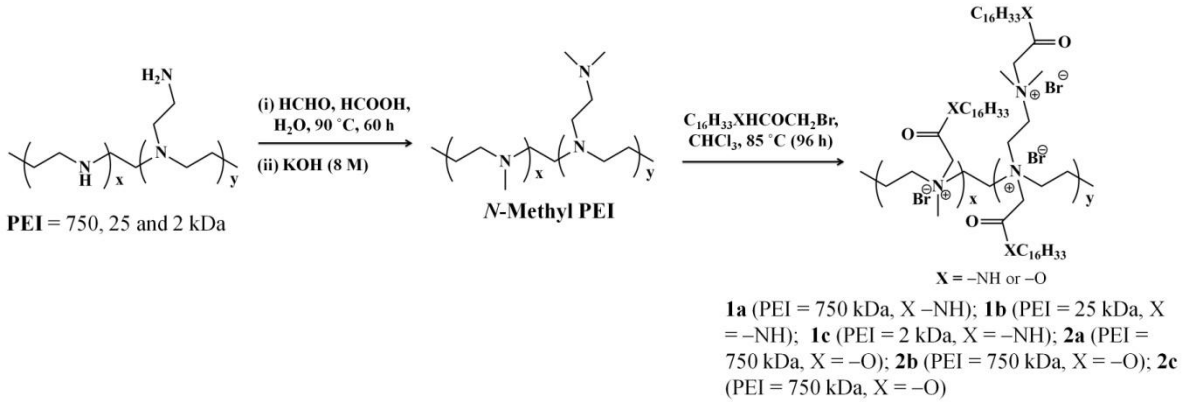

Scheme 2B.2: Synthesis of side-chain degradable cationic branched PEI derivatives.

Polymers **1a-1c** were obtained from branched PEIs of 750, 25 and 2 kDa and contained amide bearing hexadecyl chain; polymers **2a-2c** were obtained from branched PEIs of 750, 25 and 2 kDa and contained ester bearing hexadecyl chain; polymers **3a-3c** were obtained from linear PEIs of 217, 87 and 22 kDa and contained amide bearing hexadecyl chain whereas polymers **4a-4c** were obtained from linear PEIs of 217, 87 and 22 kDa and contained ester bearing hexadecyl chain respectively. Introduction of amide and ester functionality was confirmed from FT-IR as the spectra showed the presence of amide and ester groups in the cationic PEI derivatives (at 1680 cm^{-1} and 1555 cm^{-1} corresponding to amide I and amide II stretching frequencies for **1a-1c** and **3a-3c**, and at 1739 cm^{-1} corresponding to ester carbonyl stretching frequency for **2a-2c** and **4a-4c** respectively). However, the complete quaternization of the tertiary amine groups of *N*-methyl PEIs was confirmed via ^{1}H-NMR as the spectra revealed the complete disappearance of the tertiary methyl and methylene protons at 2.2-2.5 ppm and showed the presence of quaternary methyl and methylene protons at 3.2-4.7 ppm. Since the goal was to develop of water-insoluble and

organo-soluble antimicrobial polymers which can be easily be coated onto surfaces non-covalently, the solubility of all the polymers was checked in water as well as in various organic solvents. Notably, all other polymers were found to be insoluble in water. On the other hand, the polymers were soluble in chloroform, dichloromethane, *n*-butanol, dimethyl sulfoxide (DMSO), etc. However, it should be mentioned that the branched polymers were found to be more soluble in organic solvents than the linear polymers. The polycations were soluble in chloroform up to the highest tested concentration 200 mg/mL.

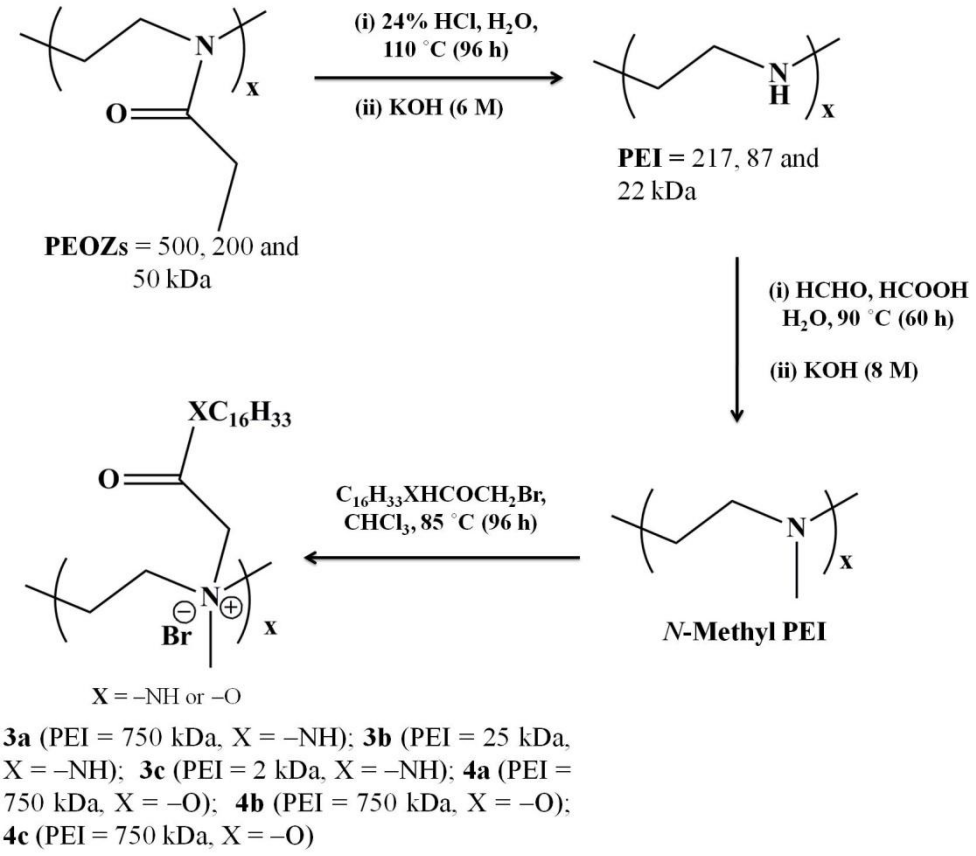

Scheme 2B.3: Synthesis of side-chain degradable cationic linear PEI derivatives.

2B.2.1.2 Synthesis of zwitterionic PEI derivatives

The gradual hydrolysis of the quaternary PEI derivatives would yield partially zwitterionic polymers and complete hydrolysis will lead to the formation of fully zwitterionic polymers. In order to understand the effect of hydrolysis on the biological activity profile, various partially (22%, 48%, 78%) and fully zwitterionic polymers were synthesized. Synthesis of partially zwitterionic polymers (**5a-5c**) were performed by introducing an easily removable *tert*-butyl ester group into the *N*-methyl PEI (PEI of 22 kDa) by reacting it with *tert*-butyl bromoacetate with 22%, 48% and 78% degrees of quaternization (Scheme 2B.4).

Introduction of ester group was confirmed from FT-IR as the spectra showed the presence of ester groups at 1739 cm^{-1} corresponding to ester carbonyl stretching frequency in all the cationic PEI derivatives containing *tert*-butyl bromoacetate (**5a′-5c′**). The degree of quaternization was calculated by ^{1}H-NMR from the ratio of *tert*-butyl moiety (1.519 ppm) to the quaternized (3.4-3.6 ppm) and non-quaternized methylene moiety (2.3-2.5 ppm).

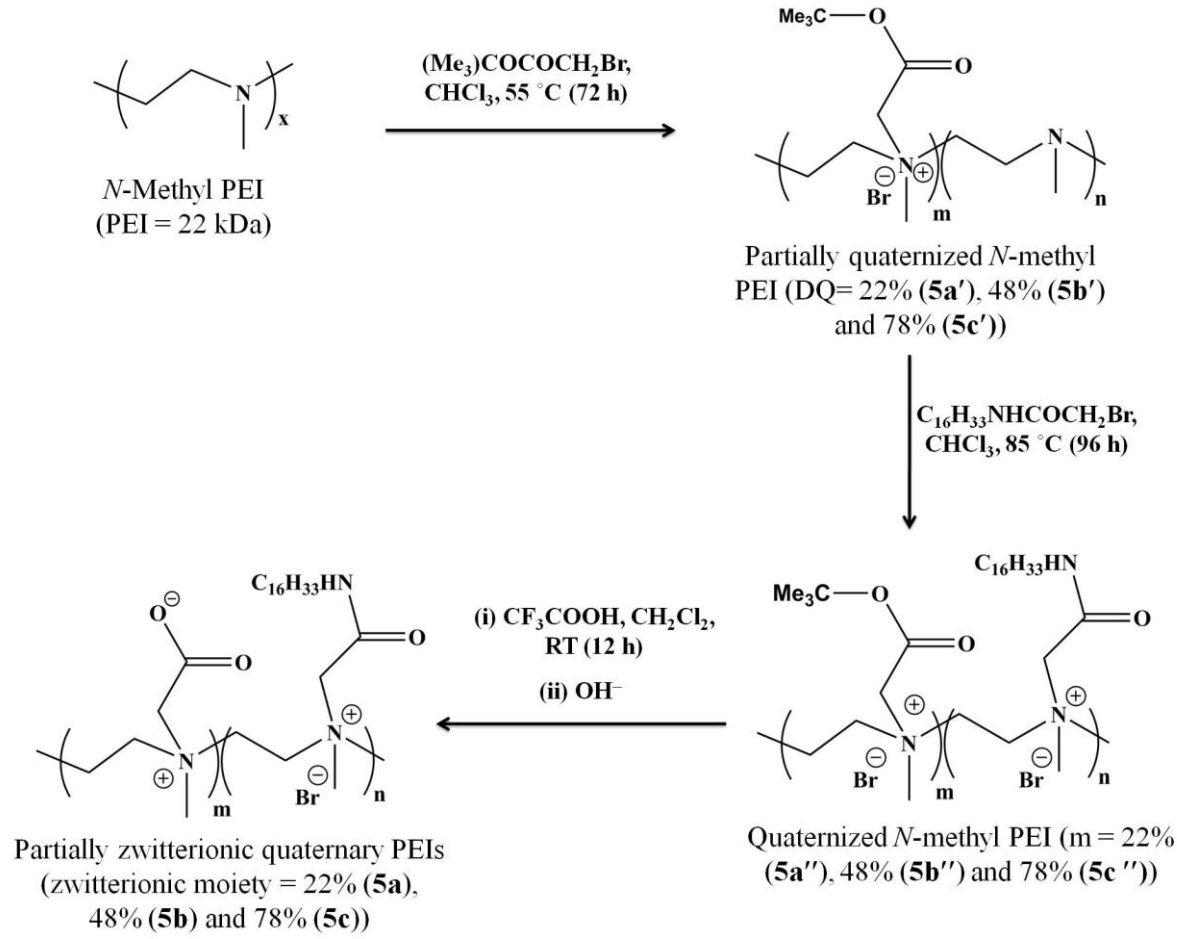

Scheme 2B.4: Synthesis of partially zwitterionic PEI derivatives.

Then the remaining tertiary amine groups of **5a′-5c′** were completely quaternized with *N*-hexadecyl-2-bromoethanamide to obtain **5a′′-5c′′** (Scheme 2B.4). The polymers were characterized by FT-IR and ^{1}H-NMR spectroscopy. FT-IR spectra showed the presence of amide and ester groups in at 1739 cm^{-1}, 1680 cm^{-1} and 1555 cm^{-1} corresponding to ester carbonyl, amide carbonyl, and amide N–H stretching frequencies respectively. The complete quaternization of the remaining tertiary amine groups of **5a′-5c′** was confirmed via ^{1}H-NMR as the spectra showed disappearance of the tertiary methyl and methylene protons (at 2.2-2.5 ppm). Finally, *tert*-butyl ester groups were fully hydrolyzed in the presence of trifluoroacetic

acid and protons of carboxylic acid groups were exchanged with an ion exchange resin to obtain the partially zwitterionic PEI derivatives (**5a-5c**). IR spectra of **5a-5c** showed a new peak at 1640 cm^{-1} corresponding to the stretching frequency of carbonyl group of carboxylate moiety in addition to the amide groups (no peak was observed at 1739 cm^{-1} which further confirmed the removal of *tert*-butyl group).

Synthesis of fully zwitterionic PEI derivative (**5d**) was performed following the same method. In this case, *N*-methyl PEI (PEI of 22 kDa) was fully quaternized with only *tert*-butyl bromoacetate to obtain polymer **5d′** (Scheme 2B.5). Finally, all the ester groups were completely hydrolyzed by trifluoroacetic acid and then subsequently treated with a hydroxyl ion exchange resin as before to obtain the fully zwitterionic polymer (**5d**). The polymer showed peak at 1640 cm^{-1} corresponding to the stretching frequency of carbonyl group of carboxylate moiety (no peak corresponding to the stretching frequency of carbonyl group of ester at 1739 cm^{-1} was observed). Notably, zwitterionic polymers (both partially and fully zwitterionic) were found to be soluble in water. While the polymers with low zwitterionic moiety (22%) were less soluble, all other zwitterionic polymers were found to be highly soluble in water. The above facts thus indicated that the amide or ester containing cationic PEI derivatives will slowly be removed from the coated surface upon hydrolysis.

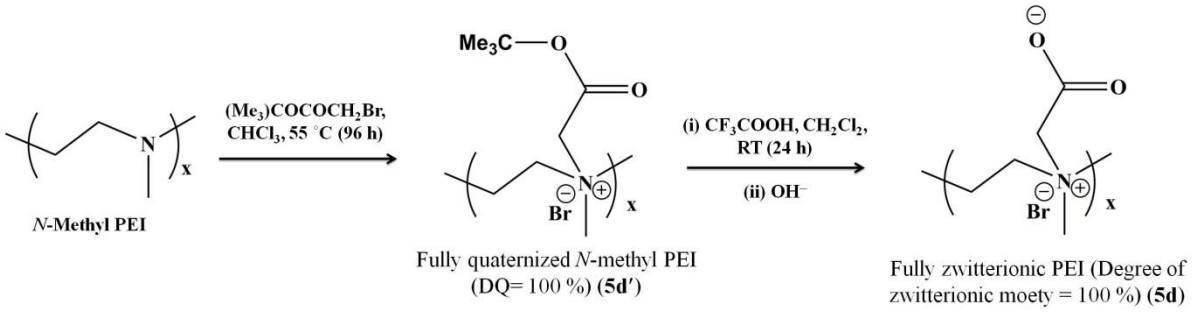

Scheme 2B.4: Synthesis of fully zwitterionic PEI derivatives.

2B.2.2 Antibacterial activity

2B.2.2.1 Activity by spray method

To evaluate the ability of the side-chain degradable PEI derivatives as antibacterial paint, glass slides were coated from organic solutions of the polymers (in chloroform) by brush coating/drop-casting/spin coating. Bacteria were then sprayed onto the polymer coated as well as non-coated glass surfaces as described in the previous chapter. While numerous colonies of bacteria were observed on the non-coated glass surfaces, no colony (~5-log reductions with respect to control) was observed on polymer-coated surfaces (Figure 2A.2).

As observed in the case of non-degradable quaternary PEI derivatives (section 2A.2.2 in Chapter 2A), linear polymers (with both amide and ester groups) were more active than the branched polymers. Further, ester containing polymers were found to be more active than the amide bearing polymers against both *S. aureus* and *E. coli*. For example, polymer **3c** (obtained from PEI of 22 kDa and contains amide bearing hexadecyl chain) coated surface showed 100% activity at 0.4 μg/mm^2 against *S. aureus* and at 6.25 μg/mm^2 against *E. coli* whereas polymer **4c** showed 100% activity at 0.2 μg/mm^2 against *S. aureus* and 3.12 μg/mm^2 against *E. coli* respectively. The above results thus suggested that these polymers could potentially be used as antibacterial coatings on various surfaces.

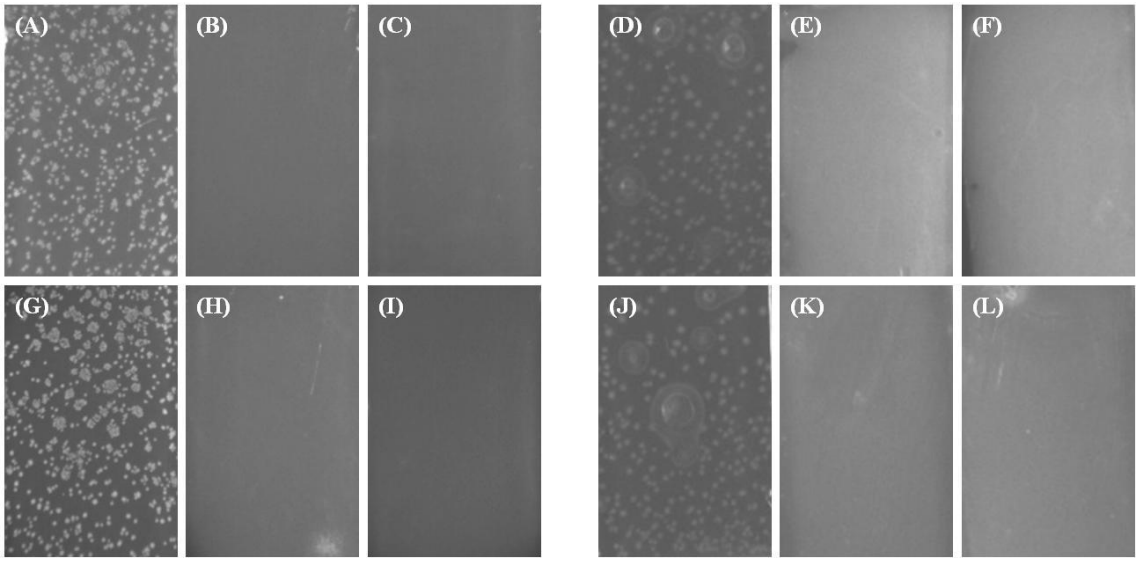

Figure 2B.2: Antibacterial activity of polymer coated glass surface. Photographs of microscopic glass slides: (A) and (D) non-coated glass slides (controls); (B) and (E) slides coated with **3c** (0.4 μg/mm^2 and 6.25 μg/mm^2); (C) and (F) slides coated with **4c** (0.2 μg/mm^2 and 3.12 μg/mm^2); (G) and (J) slides coated with PLA (2.55 μg/mm^2); (H) and (K) slides coated with **3c** along with PLA (0.4 μg/mm^2 + 2.55 μg/mm^2 PLA and 6.25 μg/mm^2 + 2.55 μg/mm^2 PLA); (I) and (L) slides coated with **4c** along with PLA (0.2 μg/mm^2 + 2.55 μg/mm^2 PLA and 3.12 μg/mm^2 + 2.55 μg/mm^2 PLA). Slides A-C and G-I for *S. aureus* and slides D-F and J-L for *E. coli* respectively. Each white dot corresponds to a bacterial colony grown from a single surviving bacterial cell.

Antibacterial activity of the polymers was also evaluated along with a medically relevant polymer PLA, and the coated glass surfaces were similarly assayed for by spraying bacteria. Notably, both the polymers retained their activity even after coating along with PLA. For example, surfaces coated with **3c** along with PLA (2.55 μg/mm^2) exhibited 100% activity at 0.4 μg/mm^2 against *S. aureus* and 6.25 μg/mm^2 against *E. coli* whereas surfaces coated with **4c** along with PLA (2.55 μg/mm^2) exhibited 100% activity at 0.2 μg/mm^2 against

S. aureus and at 3.12 μg/mm^2 against *E. coli* respectively (Figure 2B.2G-L). The above results therefore indicated that these polymers could potentially be used to develop self-defensive biomaterials.

2B.2.2.2 Activity against water-borne bacteria (Minimum inhibitory amount)

The antibacterial activity of the quaternary PEI derivatives was evaluated against both Gram-positive and Gram-negative bacteria using bacterial suspension.[16] First the polymers were coated into the wells of a 96-well plate and then bacterial suspensions (~10^5 CFU/mL, 200 μL) in suitable media were added to the polymer-coated wells and incubated for 24 h at 37 ˚C. Antibacterial activity of all the polymers was represented as minimum inhibitory amount (MIA, μg/mm^2).

Table 2B.1: Antibacterial activity of cationic PEI derivatives

Polymer	MIA (μg/mm^2)						HA_{50} (μg/mm^2)
	Drug-sensitive bacteria			Drug-resistant bacteria			
	S. aureus	*E. coli*	*P. aeruginosa*	MRSA	VRE	*K. pneumoniae*	
1a	0.48	31.2	>31.2	0.48	0.48	>31.2	>31.2
1b	0.98	31.2	>31.2	0.48	0.48	>31.2	>31.2
1c	0.98	31.2	>31.2	0.48	0.48	>31.2	>31.2
2a	0.48	3.9	7.8	0.48	0.24	31.2	>31.2
2b	0.24	3.9	15.6	0.48	0.24	15.6	>31.2
2c	0.24	3.9	15.6	0.48	0.24	15.6	>31.2
3a	0.24	7.8	15.6	0.48	0.24	15.6	>31.2
3b	0.24	7.8	15.6	0.48	0.24	15.6	>31.2
3c	0.24	7.8	15.6	0.48	0.24	31.2	>31.2
4a	0.24	3.9	15.6	0.24	0.24	15.6	>31.2
4b	0.24	3.9	15.6	0.24	0.24	15.6	>31.2
4c	0.24	3.9	7.8	0.24	0.24	7.8	>31.2

MRSA = Methicillin-resistant *S. aureus* (ATCC 33591); VRE = vancomycin-resistant *Enterococcus faecium* (ATCC 51559); *K. pneumoniae* = beta lactam-resistant *K. pneumoniae* (ATCC 700603); HA_{50} = amount of the polymer (μg/mm^2) coated in well at which 50% hemolysis occurs

All the polymers were found to inhibit the growth of both *S. aureus* and *E. coli* as observed by visual turbidity. For example, MIA values of **1a-1c**, **2a-2c**, **3a-3c** and **4a-4c** were 0.48-0.98 μg/mm^2, 0.24-0.48 μg/mm^2, 0.24 μg/mm^2 and 0.24 μg/mm^2 against *S. aureus* and 31.2 μg/mm^2, 3.9 μg/mm^2, 7.8 μg/mm^2 and 3.9 μg/mm^2 against *E. coli* respectively. Like the spray method, linear polymers were found to be slightly more active than the branched polymers (Table 2B.1). In summary, polymers **3c** and **4c** (obtained from PEI of 22 kDa and

contains amide and ester bearing hexadecyl chain respectively) were found to be the most active polymers. The MIA values of **3c** and **4c** were 0.24 μg/mm^2 each against *S. aureus* and 7.8 μg/mm^2 and 3.9 μg/mm^2 against *E. coli* respectively (Table 2B.1). The polymers also found to be active against difficult-to-treat Gram-negative bacterium *P. aeruginosa*. MIA values of **3c** and **4c** were 15.6 μg/mm^2 and 7.8 μg/mm^2 against *P. aeruginosa* (Table 2B.1). When tested against drug-resistant bacteria, these polymers were found to inhibit the growth of methicilin-resistant *S. aureus* (MRSA), vancomycin-resistant *E. faecium* (VRE) and beta-lactam-resistant *Klebsiela pneumoniae* respectively. The MIA values of polymers **3c** and **4c** were 0.48 μg/mm^2 and 0.24 μg/mm^2 against MRSA, 0.24 μg/mm^2 each against VRE and 31.2 μg/mm^2 and 7.8 μg/mm^2 against *Klebsiela pneumonaie* respectively (Table 2B.1).

2B.2.2.3 Bactericidal kinetics

To establish how fast these polymers kill bacteria upon contact and also to understand the effect of isosteric substitution (amide and ester) on killing rate, the rate of action were investigated towards both *S. aureus* and *E. coli* using polymer **3c** and **4c** at their respective MIA and 6 × MIA values. Both polymer **3c** and **4c** were found to kill *S. aureus* (~5 log reduction) at 30 min at 6 × MIA and at 60 min at MIA. On the other hand, **3c** and **4c** were found to kill *E. coli* (~5 log reduction) at 240 min at 6 × MIA. Notably, **3c** was found to be bacteristatic at MIA whereas **4c** was found to kill *E. coli* (~5 log reduction) at 240 min even at MIA which is its minimum bactericidal amount. These results thus indicate that the cationic hydrophobic polymer coatings have remarkably high killing rates against both the bacteria making them suitable for efficient antimicrobial coating. Further isosteric substitution was found to have negligible effect on killing kinetics.[17]

2B.2.2.4 Membrane-active mode of antibacterial action

The mode of action of the cationic PEI derivatives was examined by confocal laser scanning microscopy (CLSM) via live and dead assay using SYTO 9 and propidium iodide (PI) respectively.[18] SYTO 9, a membrane-permeable green fluorescent dye, is known to bind with the nucleic acid of bacteria and stain with green fluorescence. PI, on the other hand, is a membrane impermeable red fluorescent dye and cannot stain live bacteria. The microscopy images of non-treated samples showed green fluorescence for both *S. aureus* and *E. coli* thereby indicated the cell viability in control samples (Figure 2B.3A and D). The cell treated with one of the most active polymer (**3c**) at its MIAs which were also its minimum

bactericidal amounts (MBAs) for the respective bacteria, showed appearance red fluorescence thereby indicated the loss of membrane integrity (Figure 2B.3B and E). Notably, images of the cells treated with the **3c** at its 6 × MBAs showed complete red fluorescence of PI thereby suggested membrane disruption for both *S. aureus* and *E. coli* (Figure 2B.3C and F).

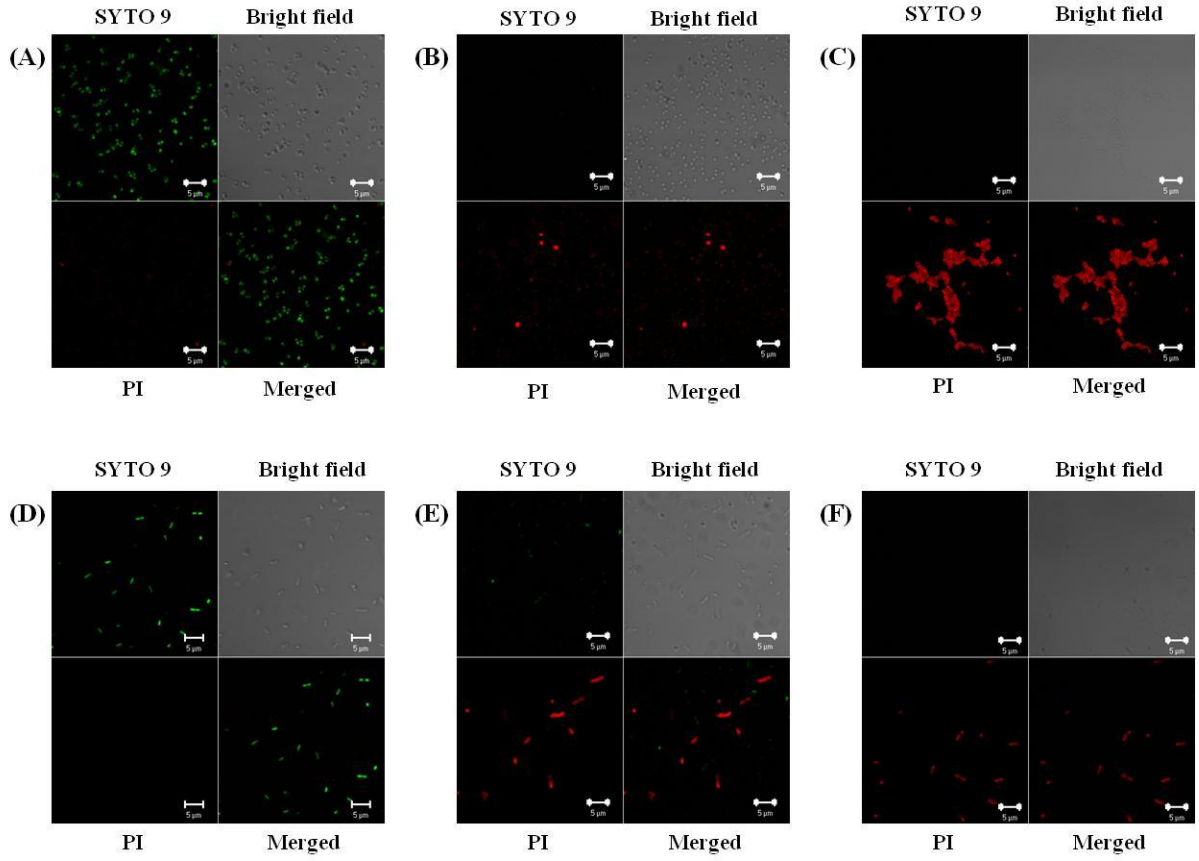

Figure 2B.3: Modes of antibacterial action. CLSM images of bacterial cells: untreated (A) *S. aureus* and (D) *E. coli*; cells treated with the surface coated with **3c** at MIAs (B) *S. aureus* (E) *E. coli*; cells treated with the surface coated with **3c** at 6 × MIAs (C) *S. aureus* and (E) *E. coli* respectively, all after staining with SYTO 9 and PI.

2B.2.3 Bacterial biofilm inhibition

It is estimated that almost 80% of the infections in human occurs due to the biofilm formation.[2] Bacterial contamination onto surfaces and subsequent colonization can result in surface-associated communities known as biofilms.[4] Biofilms are protected by extracellular polymeric substances (EPS) and pose a significant barrier to host immune systems and antibiotics because of the impermeable and defensive EPS.[19] Thus inhibiting bacterial biofilm formation would indirectly or directly help in preventing infections. The antibiofilm property of the cationic PEI derivatives was evaluated by coating the polymers onto glass surface and

determining efficacy of the polymers in inhibiting bacterial biofilm formation. Glass cover slips, coated with the most active polymer **3c** at two different amounts (MIA and 6 × MIA), were challenged against both *S. aureus* and *E. coli* respectively under static conditions for 24 h and 72 h respectively. The cover slips were then imaged by confocal laser scanning microscopy (CLSM) via a green fluorescent dye SYTO 9 staining. The non-coated cover slips showed huge bacterial growth with an effective thickness of 13-18 μm thus indicating thick and matured biofilm formation for both *S. aureus* and *E. coli* respectively (Figure 2B.4A and D). In contrast, the polymer coated glass surface at respective MIA values showed relatively fewer bacteria with less cluster and growth against both *S. aureus* and *E. coli* (Figure 2B.4B and E). Interestingly, polymer-coated surfaces showed fewer bacteria with an effective thickness of 2-4 μm thereby indicating the presence of only mono-layered bacteria at respective 6 × MIA values against both *S. aureus* and *E. coli* respectively (Figure 2B.4C and F). The above results thus indicated that the cationic PEI derivative upon coating onto surfaces is capable of preventing bacterial colonization onto the surface.

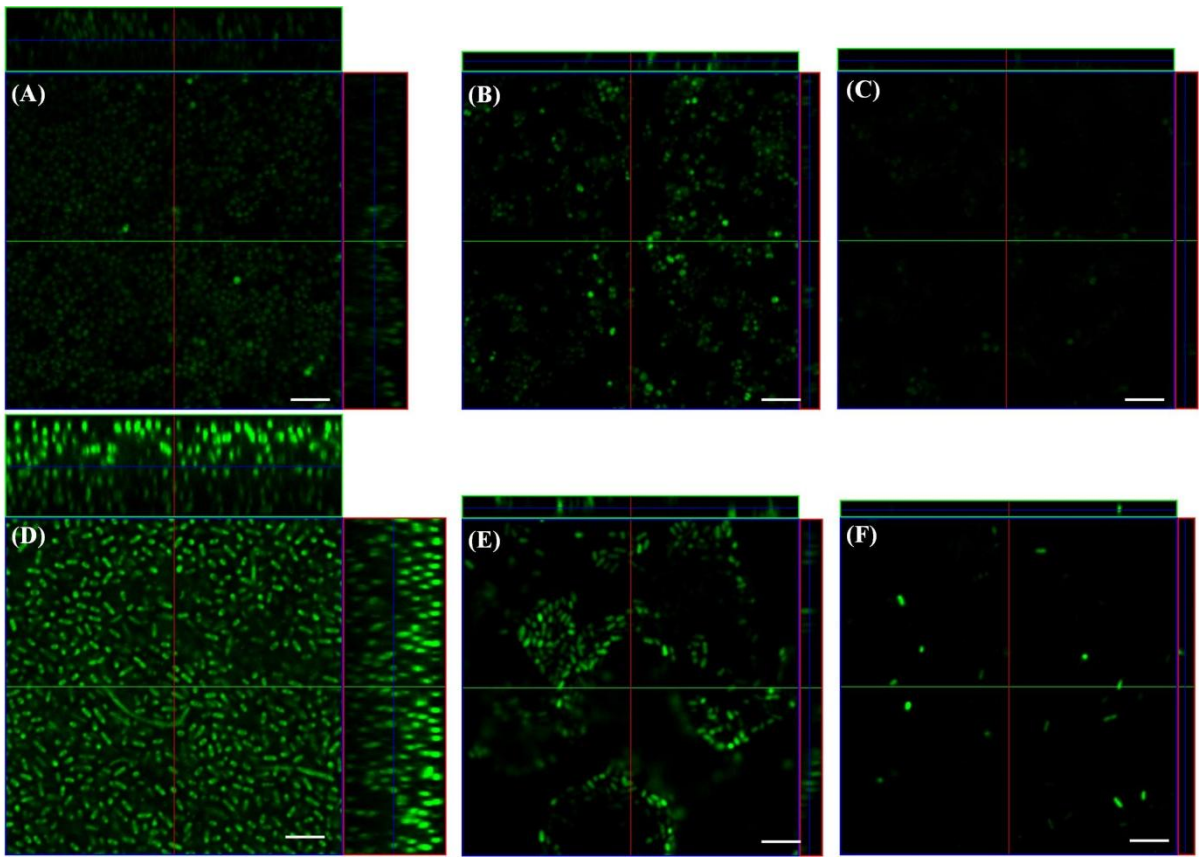

Figure 2B.4: Antibiofilm activity of the polymeric coating. Confocal laser scanning microscopy images of (A and D) non-coated cover glass; (B and E) cover glass coated with 0.06 μg/mm^2 and 3.9 μg/mm^2 and (C and F) with 0.36 μg/mm^2 and 23.4 μg/mm^2 respectively. A-C for *S. aureus* and D-F for *E. coli* respectively. Scale bar 5 μm.

Further, when the bacterial counts were determined in the biofilms, (8±1.2) log reduction of *S. aureus* and (7±0.8) log reduction of *E. coli* were observed for the polymer coated surface at 6 × MIA compared to noncoated surface (the control surfaces showed 12.8 log CFU/mL of *S. aureus* and 10.5 log CFU/mL of *E. coli* respectively).

2B.2.4 Antifungal activity

2B.2.4.1 Minimum inhibitory amount

Antifungal efficacy of all the polymers was evaluated against various pathogenic *Candida* spp. (*C. albicans*, *C. dubliniensis*, *C. tropicalis*) and *Cryptococcus* spp. (*C. neoformans var. grubii* (serotype A), *C. neoformans var. gattii* (serotype B) and *C. neoformans var. neoformans* (serotype D)). Like bacteria, the side-chain degradable polymers showed activity against all the fungi tested (Table 2B.2). Among all the polymers, **3c** and **4c** were found to be most active. MIA values of **3c** and **4c** were 3.9 μg/mm^2 each against *C. albicans*, 3.9 and 0.49 μg/mm^2 against *C. dubliensis*, 0.98 and 0.19 μg/mm^2 against the *C. tropicalis*, 0.24 and 0.03 μg/mm^2 against *C. noeformans* ser A, 0.49 and 0.06 μg/mm^2 against *C. noeformans* ser B and *C. noeformans* ser D respectively (Table 2B.2).

Table 2B.2: Antifungal activities of polymers

Polymer	MIA (μg/mm^2)					
	C. albicans	*C. dubliniensis*	*C. tropicalis*	*C. neoformans* Ser A	*C. neoformans* Ser B	*C. neoformans* Ser D
1a	31.2	15.6	15.6	0.49	1.95	0.98
1b	31.2	15.6	15.6	0.98	1.95	3.9
1c	31.2	3.9	3.9	0.24	1.95	3.9
2a	1.95	0.49	0.98	0.12	0.49	0.24
2b	1.95	0.98	0.98	0.12	0.98	0.49
2c	1.95	0.98	0.98	0.12	0.98	0.49
3a	7.8	3.9	3.9	0.12	0.49	0.24
3b	3.9	1.95	1.95	0.24	0.49	0.24
3c	3.9	3.9	0.98	0.24	0.49	0.49
4a	3.9	0.98	0.49	0.06	0.12	0.12
4b	3.9	0.49	0.19	0.03	0.12	0.06
4c	3.9	0.49	0.19	0.06	0.06	0.06

C. albicans = Candida albicans; *C. dubliniensis = Candida dubliniensis*; *C. tropicalis = Candida tropicalis*; *C. neoformans Ser A = Cryptococcus neoformans Ser A*; *C. neoformans Ser B = Cryptococcus neoformans Ser B*; *C. neoformans Ser D = Cryptococcus neoformans Ser D*

Thus the side-chain degradable polymers like their non-degradable counterparts in Chapter 2A were found to be more active towards Cryptococcus spp. than the Candida spp. Further,

the amide and ester containing polymers were found to be slightly more active than the PEI polymers without any amide or ester groups (Chapter 2A). This could be possibly due to additional hydrogen bonding interaction with the cell membrane of the pathogens other than possible electrostatic and van der Walls interactions. The polymers were also found to be fungicidal. For example, the minimum fungicidal amount (MFA) of the most potent polymer **4c** was found to be 0.49 μg/mm^2 and 0.06 μg/mm^2 against *C. dubliensis* and *C. neoformans* Ser A respectively.

2B.2.4.2 Fungicidal kinetics

To establish how fast these polymers killed fungi upon contact, the rate of funficidal action was investigated against *C. dubliensis* using surfaces coated with polymer **3c** and **4c**. The coated surface killed *C. dubliensis* within 4-8 hours at 8 × MIA. It should be mentioned that amide containing polymer (**3c**) showed relatively higher killing kinetics than the corresponding ester containing polymer (**4c**). This could be possibly due to the higher hydrogen bonding donating as well as accepting abilities of the amide functionality than the only hydrogen bonding accepting ability of the ester containing polymer.[17] However at MIA, the polymers were found to be fungistatic (Figure 2B.5A and B).

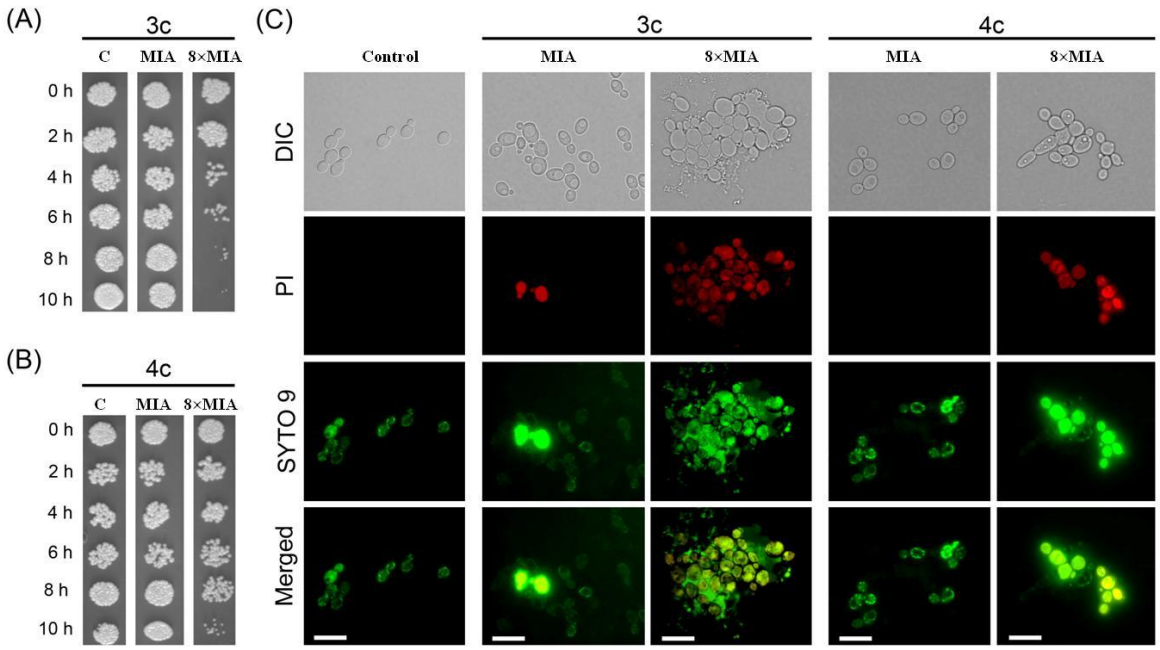

Figure 2B.5: Antifungal activities of side-chain degradable cationic PEI derivatives. (A and B) Antifungal kinetics of polymers **3c** and **4c** coated surfaces at different amounts (MIA and 8 × MIA) against *C. dubliensis*. Mechanistic investigation of antifungal activity of polymer

coatings. (C) Fluorescence microscopy images of *C. dubliensis* after staining with SYTO 9 and PI. Scale bar 20 μm.

2B.2.4.3 Mechanism of antifungal action

To examine whether these hydrophobic polycations interact with the cell membrane of fungi thereby leading to membrane disruption, LIVE/DEAD assay was performed with the fungal cell (*C. dubliensis*) using green fluorescent SYTO 9 and red fluorescent PI dyes via fluorescence microscopy.[20] The fungal cells were treated with the polymer coated surfaces at two different amounts (MIA and 6 × MIA) of two most active polymers (**3c** and **4c**) for about 6 h and then imaged after staining with the dyes. The microscopy images showed the presence of viable cells in the case of control samples (plain surface) as observed by green fluorescence (Figure 2B.5C). The cells treated with the polymer-coated surfaces, on the other hand, showed red color fluorescence of PI thus indicating the compromised cell membrane (Figure 2B.5C) at both the amounts. The appearance of red fluorescence indicated that the fungal cell membrane was compromised upon treatment with the cationic hydrophobic polymers thereby allowing the cell membrane impermeable dye PI to enter inside the cell. The above facts thus indicated that the cationic polymers interact with the fungal cell membrane and disrupt the integrity of the membrane presumably leading to cell death.

2B.2.5 Fungal biofilm inhibition

Fungal biofilms, like bacterial biofilms, are difficult to treat and allow rapid resistance development against various antifungal drugs.[21,22] Further, fungal biofilms can allow the formation of bacterial colonies on their surface and lead to enhanced microbial resistance development against antibiotics.[22] Thus not only the antifungal activity against plankotonic fungi but also antibiofilm activity of the cationic PEI derivatives needs to addressed. Herein, the antibiofilm properties of the most active polymers **3c** and **4c** were evaluated by coating the polymers onto the wells of 6-well plate and determining their efficacy in inhibiting fungal biofilm formation via fluorescence microscopy.[47] The wells were coated with different amounts (MIA, 2 × MIA) and then were incubated with *C. dubliensis* for about 48 h under stationary conditions. The wells were then imaged. While the non-coated wells showed huge fungal growth with cell cluster indicative of biofilm formation (Figure 2B.6A), the polymers were shown to inhibit biofilm formation at effectively 2 × MIA (Figure 2B.6B and C). Further, both the polymers were shown to be almost equally active in inhibiting biofilm

formation. The above results therefore suggested that these polymers might be used as antibiofilm coatings as well.

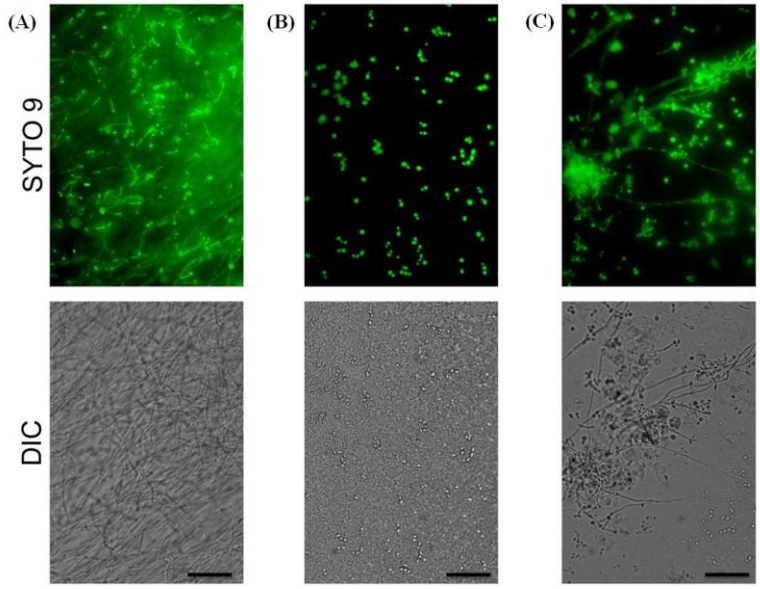

Figure 2B.6: Antibiofilm activity of PEI derivatives. (A) Non-coated glass surfaces; (B and C) glass surfaces coated with polymer **3c** and **4c** at 2 × MIA respectively. Scale bar 40 μm.

2B.2.6 Toxicity of the cationic PEI derivatives

2B.2.6.1 *In-vitro* toxicity

Toxicity of the antimicrobial polymer-modified biomaterial surfaces is a major concern for the application in healthcare settings. Toxicity of the PEI derivatives coated surfaces was therefore evaluated with human erythrocytes and was expressed as HA_{50} (the amount of the coated polymer that caused 50% hemolysis).[20] The polymers were found to be non-hemolytic upto 3.9 μg/mm^2. Only 17-25% hemolysis was observed even at 31.2 μg/mm^2 of polymer coating. The 50% hemolytic amount (HA_{50}) for all the polymers was therefore more than 31.2 μg/mm^2. Notably, **3c** and **4c**, the two most active polymers caused negligible hemolysis up to 15.6 and 7.8 μg/mm^2 which were significantly higher than to their MIA values (Table 2B.1). The above results thus indicated the polymers are selectively active toward bacteria.

2B.2.6.2 *In-vivo* toxicity

To be suitable for application in biomedical devices and implants, the polymers should be compatible towards mammalian cells under *in-vivo* conditions. Thus the compatibility of the polymeric coating was further assessed by coating the polymer onto medical grade polyurethane catheter and then implanting the coated catheter in mice subcutaneously. After

4 days, mice were sacrificed and the tissue surrounding the catheter was collected, fixed in formalin for about 24 h. Finally, the inflammatory responses were then recorded by haematoxylin and eosin staining. The non-coated catheter was shown to have no inflammation as indicated by normal epidermis and dermis layer with usual architecture (Figure 2B.7A and B). Interestingly, tissue samples surrounding the catheters coated with ~4 μg/mm^2 and 8 μg/mm^2 of **3c** and **4c** also showed negligible inflammation as indicated by normal skin epidermis and dermis layer with regular adipose tissue with few inflammatory cells (Figure 2B.7C-F)

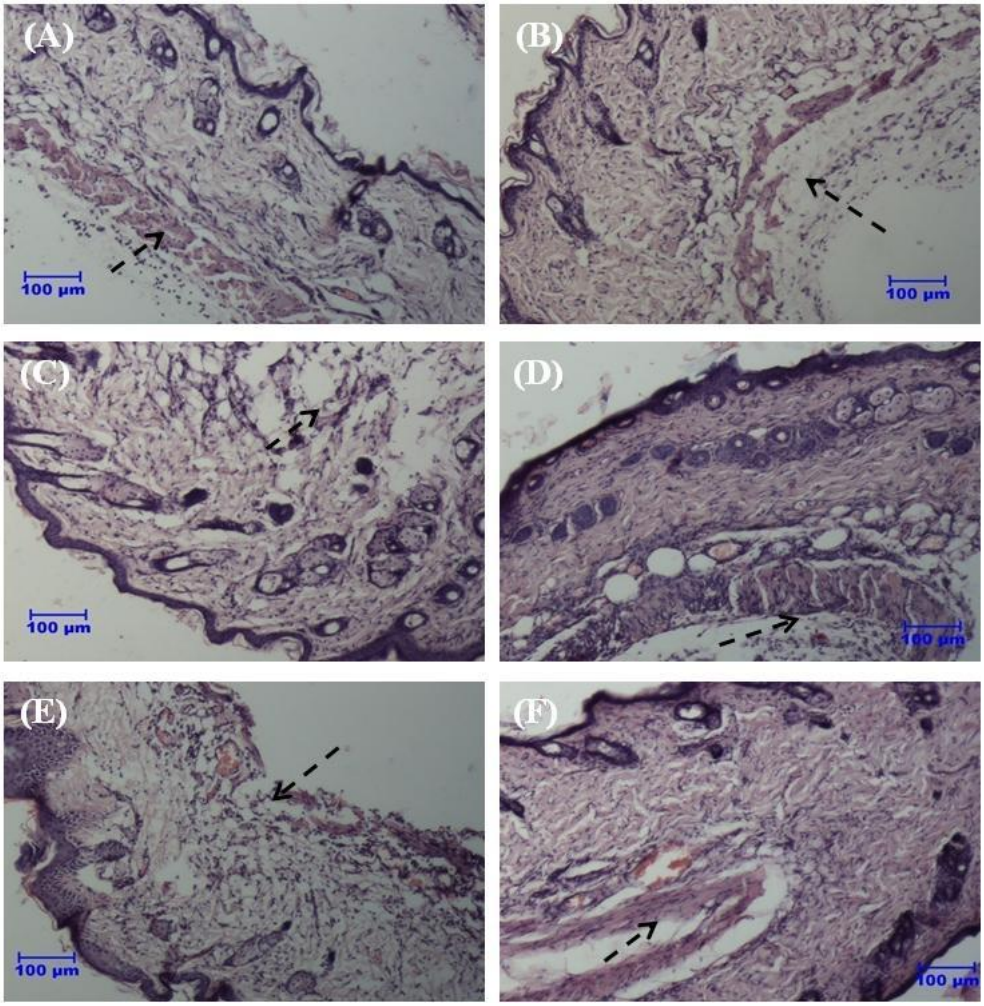

Figure 2B.7: *In -vivo* biocompatibility of the polymers. Mice skin and subcutaneous tissue histopathology: (A) tissue showing normal architecture of epidermis, dermis and subcutaneous tissues surrounding the non-coated catheter (arrow) of normal healthy mice; (B) tissue showing normal skin epidermis and dermis layer with normal adipose tissue surrounding the non-catheter in subcutaneous tissues (arrow); (C and D) showing normal appearance of skin with thin layer of epidermis, hair follicles, sweat glands with few infiltration of inflammatory cells in the dermis layer (arrow) for catheter coated with **3c** at 4 and 8 μg/mm^2; (C and D) showing epidermis and dermis layer with infiltration of few inflammatory cells (arrow) for catheter coated with **4c** at 4 and 8 μg/mm^2 respectively.

2B.2.7 Hydrolysis and bioactivity of hydrolyzed polymers

2B.2.7.1 Chemical and enzymatic hydrolysis

Common disinfectants that are used to combat infections are becoming more and more useless as the disinfectants cause development of resistance in microbes and toxic effects towards mammalian cells. Further, non-degradable antimicrobials can create hindrance in tissue-implant integration and unwanted immune responses from host. One potentially effective strategy to reduce infection and to avoid aforementioned problems would thus be, where appropriate, to use degradable materials.[23] Thus the degradability of the cationic PEI derivatives along with the effect of amide and ester functionality on rate degradation was established under both acidic and enzymatic conditions (infection sites are generally acidic in nature and various proteolytic or esterases enzymes are available in the infections site either from the host or from the pathogen). Two of the most active amide and ester containing polymers (**3c** and **4c**) were therefore treated with 0.2 M HCl to study the degradation under acidic conditions. Also, the amide containing polymer **3c** was treated with enzyme trypsin and ester containing polymer **4c** was treated with lipase to study the degradation under enzymatic conditions. The study was performed by taking the polymer suspension in the above mentioned solutions and determining the % of one of the hydrolyzed products 1-aminohexadecane or 1-hexadecanol in the hydrolysis mixture via ^{1}H-NMR (1-aminohexadecane showed peaks at 1.55 ppm corresponding to β–CH_2 protons whereas 1-hexadecanol showed a unique peak at 3.33 ppm corresponding to α–CH_2 protons). Also IR spectra of the hydrolysed products mixture showed the presence of carboxylic acid group at 3409 cm^{-1} for the acid form whereas 1627 cm^{-1} for the acid salt form.

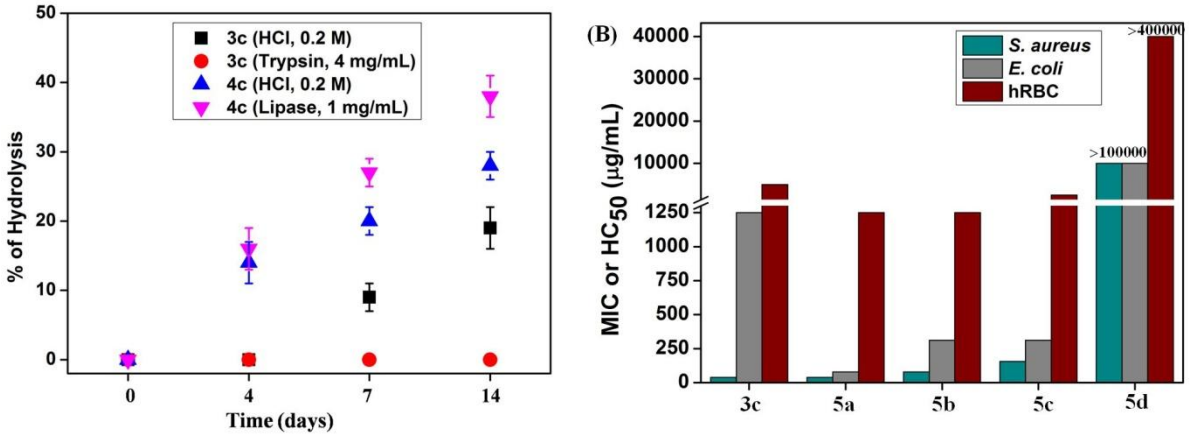

Figure 2B.8: Hydrolysis of PEI derivatives. (A) Degree of hydrolysis of the both the amide and ester bearing polymers at different conditions. (B) Antibacterial and hemolytic activities of the partially and fully zwitterionic PEI derivatives.

Interestingly under acidic conditions, both amide and ester containing polymers hydrolyzed significantly and the extent of hydrolysis was found to vary greatly depending on the hydrolysis time and nature of hydrolysing groups (Figure 2B.8A). For example, the degree of hydrolysis for the amide containing polymer (**3c**) was 19±3% whereas the same for the ester containing polymer (**4c**) was found to be 28±2% under acidic condition. Moreover as expected, the rate of degradation of the ester containing polymer was found to be much higher than that of the amide containing polymer (Figure 2B.8A). On the other hand, while the ester containing polymer **4c** showed remarkable degree of hydrolysis in the presence of lipases, amide containing polymer **3c** failed to show any considerable amount of degradation in the presence of enzyme trypsin. For example, the degree of hydrolysis for polymer **4c** was found to be 38±3% in the presence of lipase and also showed gradual degradation with time. Moreover, the rate of hydrolysis was much faster for the polymer **4c** under enzymatic condition (Figure 2B.8A). On the contrary, the amide containing polymer (**3c**) showed negligible hydrolysis in the presence of trypsin. The above results suggested that by selective choice of cleavable groups, the rate of degradation as well time required for the degradation could be tuned. Since the proteolytic enzymes are generally more selective towards their substrates, it should be mentioned that amide bearing polymers could be susceptible towards other proteolytic enzymes especially microbial amidases. However, together the above results suggested that by introducing hydrolysable functionality in the side chain of water-insoluble and organo-soluble PEI derivatives and by varying the nature of side chain functionality, it is possible to obtain side-chain degradable polymers with tunable rate of degradation.

2B.2.7.2 Biological activity of the hydrolyzed polymers

Hydrolysis of the cationic PEI derivatives will lead to formation of various partially hydrolyzed polymers followed by the formation of fully zwitterionic polymers. To understand how the antibacterial and hemolytic activities vary due to hydrolysis, biological activity of various partially and fully zwitterionic polymers was evaluated against both bacteria and hRBC. Since the zwitterionic polymers were found to be partially or completely soluble in water, activities of these polymers were represented in terms of minimum inhibitory concentration or hemolytic concentration (HC_{50}, at which 50% hemolysis occurs). Further, to compare the activity of these polymers with the corresponding cationic PEI derivative, biological activities of the cationic PEI derivative was converted to MIC (μg/mL) and HC_{50} (μg/mL) from MIA (μg/mm^2) and HA_{50} (μg/mm^2) (The conversion was done by

assuming the minimum inhibitory amount or hemolytic amount present in 200 μL of broth or PBS that were used to determine the antibacterial or hemolytic activities).

Notably, the polymers with partially zwitterionic moiety were found to have slightly higher antibacterial and hemolytic activities. For example, MIC and HC_{50} values of polymer **5a** (with ~22% zwitterionic charge) were 39 μg/mL against *S. aureus,* 78 μg/mL against *E. coli* and 1250 μg/mL against hRBC (Figure 2B.8B). (MIC and HC_{50} values of the corresponding cationic polymer **3c** were 39 μg/mL against *S. aureus,* 1250 μg/mL against *E. coli* and >5000 μg/mL against hRBC). It should be mentioned that the polymers with partially zwitterionic charge were partly soluble in water in contrast to polymer **3c** which is completely insoluble in water. As a result polymer **5a** could engage its antibacterial and hemolytic activities in solution differently than being immobilized onto surface. Notably, upon increasing the zwitterionic charge, both the activity and toxicity were found to decrease. For example, polymers **5b** and **5c** (with 47% and 79% zwitterionic charge) showed MIC values of 39 μg/mL and 78 μg/mL against *S. aureus* and 156 μg/mL and 312 μg/mL against *E. coli* respectively whereas HC_{50} values were found to be 1250 μg/mL and 5000 μg/mL (Figure 2B.8B). Interestingly, polymer with 100% zwitterionic charge (**5d**) displayed no activity till 10000 μg/mL against both the bacteria and showed negligible hemolysis till 40000 μg/mL (Figure 2B.8C). Notably, the zwitterionic polymer (**5d**) was shown to be completely non-lethal upon intra-peritoneal administration in mice (LD_{50}>175 mg/kg). Thus by switching the charge of the side chain hydrolysable PEI polymers from cationic to zwitterionic, it was possible to obtain highly non-toxic polymers. It should be mentioned that the cationic PEI derivatives upon hydrolysis would become water soluble and therefore would be removed from site of application. Further, as the most active cationic PEI derivatives (**3c** and **4c**) were from the linear PEI of molecular weight 22 kDa, complete hydrolysis of these polymer will lead to zwitterionic polymer of molecular weight less than 50 kDa and are therefore expected to be cleared from body through renal filtration.

2B.2.8 *In-vivo* activity

To be used in device applications, the polymeric coatings should display activity under *in-vivo* conditions.[24] Further, the polymer should also be able to inhibit bacterial biofilm formation in more complex *in-vivo* situation. Herein the antibacterial and antibiofilm efficacies of the two most active side-chain degradable polymers were assessed by coating the medical grade polymer-coated catheters (polyurethane, 5 Fr, 12 mm) and then implanting

the catheter subcutaneously in mice. To mimic the microbial contamination, the catheter was contaminated with methicillin-resistant *S. aureus* (MRSA) infection-one of the most leading biofilm forming bacteria in healthcare and clinical settings. Catheter pieces were infected with an average load of ~1.1-2.3 × 10^8 CFU of MRSA at the time of insertion in mice (a quantity much greater than that would be encountered in a clinical setting). After 96 h the control catheter showed 8.1 log CFU/catheter bacteria thereby indicated the prevalence and growth of MRSA. Notably, 2.2 and 3.4 log CFU reduction of MRSA was observed in the case of **3c**-coated catheter at 4 μg/mm^2 and 8 μg/mm^2 of polymer coating respectively (Figure 2B.9A). On the other hand, 1.9 and 3.2 log CFU reduction of MRSA was observed in the case of **4c**-coated catheter at 4 μg/mm^2 and 8 μg/mm^2 of polymer coating respectively (Figure 2B.9A). The above facts thus indicated that both amide and ester containing polymers were capable of reducing the MRSA contamination. Further, both the polymers showed almost similar activity (amide containing polymer was found to be slightly more active than the ester containing polymer). Further, an amount-dependent activity was observed for the polymeric coatings (Figure 2B.9A).

To evaluate the efficacy of the polymeric coatings in preventing the infection in the surrounding tissues, mice skin tissue was collected and enumerated for cell counting after homogenization. Interestingly, tissue surrounding the catheters coated with 4 μg/mm^2 and 8 μg/mm^2 of **3c** showed MRSA reduction of 2.1 and 3.9 log CFU compared to tissue for non-coated catheter (Figure 2B.9B). On the other hand, tissue surrounding the catheters coated with 4 μg/mm^2 and 8 μg/mm^2 of **4c** showed reduction of 2.7 and 3.4 log CFU of MRSA compared to tissue for non-coated catheter (Figure 2B.9B). The above facts therefore indicated that the polymers were also capable of inhibiting bacterial infection into the surrounding tissue.

To evaluate the potential of the polymeric coating in inhibiting bacterial biofilm formation, the MRSA contaminated catheters were imaged using SEM after sacrificing the mice and harvesting the catheter. While the non-coated catheter showed large amount of bacteria in several layers along with the mice tissue indicative of biofilm formation (Figure 2B.9C), **3c**-coated catheter (at 8.0 μg/mm^2) revealed only a fewer amount of bacteria with no cell clusters indicative of no bacterial colonization onto catheter surface (Figure 2B.9D). The above results thus portrayed the efficacy of the polymer coatings in killing bacteria and inhibiting biofilm inhibition under *in vivo* conditions.

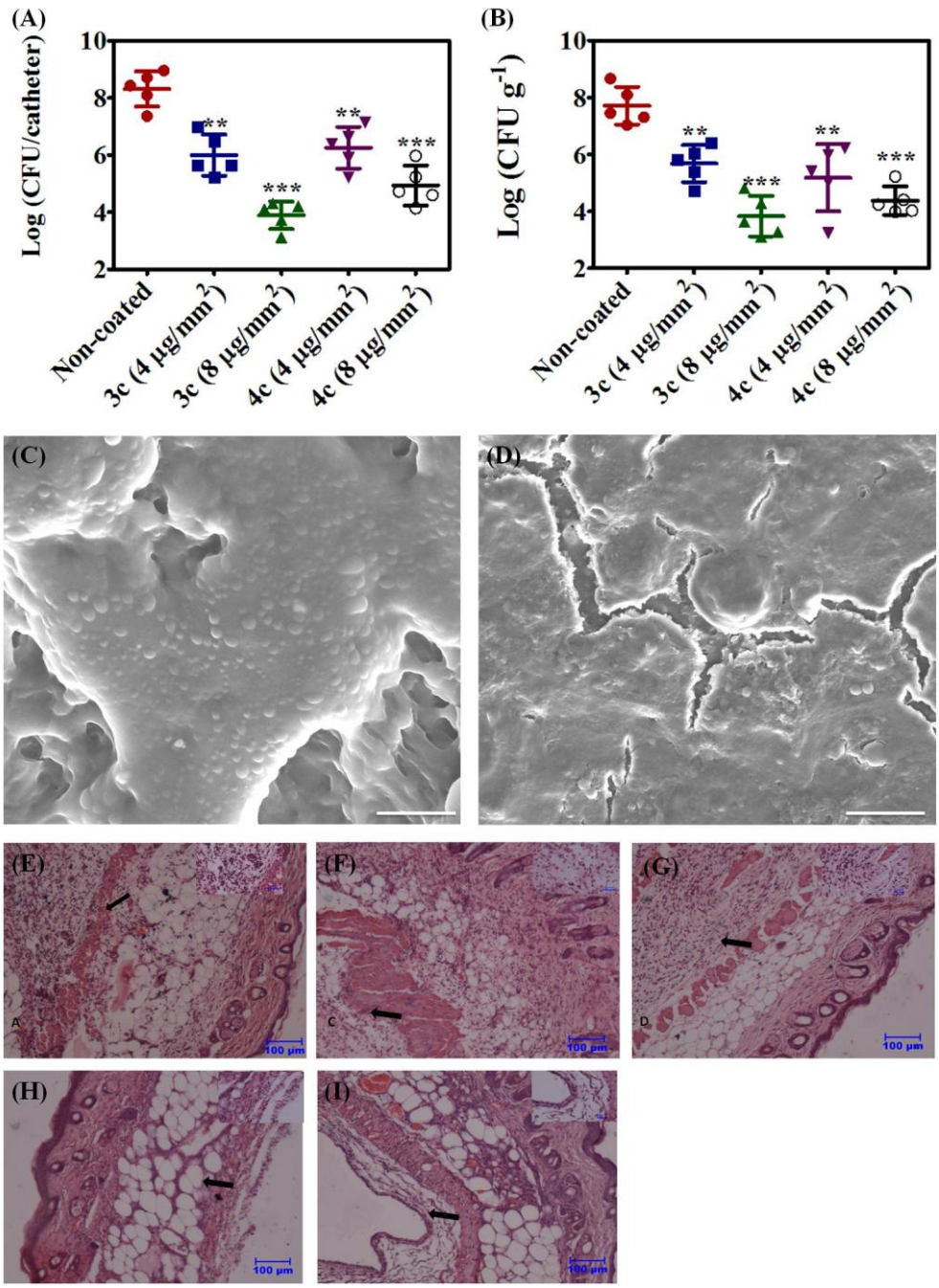

Figure 2B.9: *In-vivo* antibacterial activity of the cationic PEI derivatives. Effect of polymer-coated catheters on MRSA inoculated at the time of insertion: (A) bacterial count after harvesting catheter from mice; (B) bacterial count from the catheter surrounding tissue samples; p values (*) are <0.005, <0.0001, <0.005 and <0.0001 for **3c** (4 μg/mm^2), **3c** (8 μg/mm^2), **4c** (4 μg/mm^2) and **4c** (8 μg/mm^2) respectively. Field emission scanning electron microscopy (FESEM) images of (C) non-coated catheter and (D) **3c**-coated catheter. Scale bar 5 μm. Mice skin and subcutaneous tissue histopathology: (E) tissue surrounding MRSA infected non-coated catheter; tissue surrounding MRSA-infected catheter coated with (F) 4 μg/mm^2 of polymer **3c**; (G) 8 μg/mm^2 of polymer **3c**, (H) 4 μg/mm^2 of polymer **4c**; (I) 8 μg/mm^2 of polymer **4c**. Cells were stained with haematoxylin and eosin staining agents. Insets are the high resolution images.

To examine the extent of infection in the surrounding tissue, histolopathological responses were studied to evaluate the inflammatory responses due to MRSA contamination in the skin and subcutaneous tissue level. As expected, severe infiltration of inflammatory cells mainly neutrophils and mononuclear cells in the subcutaneous tissues with congestion of blood vessels were observed for non-coated catheters infected with MRSA (Figure 2B.9E). In contrast, tissue surrounding the catheter coated with ~4.0 μg/mm^2 of polymer **3c** showed moderate infiltration of inflammatory cells mainly with neutrophils and damage to skin dermis layer thereby indicating low reduction of MRSA at the tissue level (Figure 2B.9F). However, tissue surrounding the catheter coated with ~8.0 μg/mm^2 of polymer **3c** showed negligible infiltration of inflammatory cells and no damage to skin dermis layer thereby indicating significant reduction of MRSA at the tissue level (Figure 2B.9G). Similar results were observed for the catheters coated with the polymer 4c (Figure 2B.9H and I). The above results therefore portrayed the potential of the polymers in inhibiting the bacterial colonization onto surfaces.

2B.2.9 Propensity of bacterial resistance development

The ability in hindering development of bacterial resistance by the side-chain degradable cationic polymers was assessed by serial exposure of bacteria to the polymer-coated surfaces like the previous non-degradable polymers. Both amide and ester containing polymers (**3c** and **4c**) were challenged against Gram-positive *S. aureus* and Gram-negative *E. coli*. After 14 serial passages, the MIAs of polymers **3c** and **4c** remained almost same (only 2-4 fold increase) whereas nofloxacin, a nucleic acid targeting Gram-positive antibiotic, showed 269 fold increase in MIC against sensitive *S. aureus* and colistin, a lipid II targeting Gram-negative lipopeptide, showed 125 fold increase in MIC against sensitive *E. coli* respectively. These membrane-active polymers were thus able to stall the development of bacterial resistance.

2B.3. Conclusion

In summary, a simple method of developing side-chain hydrolyzable polyethylenimine derivatives was developed and demonstrated their use as bactericidal paint. The polymers were shown to kill both bacteria and fungi and inhibit formation of their biofilm on the coated surface. The polymers were also found to be non-hemolytic towards human erythrocytes under in-vitro conditions and cause minimal to negligible inflammation at the tissue level

upon subcutaneous implantation. Further, side chains of the polymers were found to degrade in the presence of acid and hydrolytic enzymes. The rate of hydrolsis as well as degree of hydrolysis was dependant on the nature of degradation. Ester containing polymers were degradable under both acidic and enzymatic conditions than the amide containing polymer. Importantly, both antibacterial and hemolytic activities were found to decrease with the increase in percentage of zwitterionic moiety. Further, fully zwitterionic polymer was shown to be completely non-toxic both *in-vitro* and *in-vivo* thereby indicated that switching charge from cationic to zwitterionic improved biocompatibility. Notably, the coated surface showed almost >99.99% bacterial reductions and displayed excellent efficacy in inhibiting bacterial biofilm formation *in-vivo*. Thus the side-chain hydrolyzable PEI derivatives developed herein could be used as safe and effective ″bactericidal paint″ in a wide variety of biomedical applications.

2B.4. Experimental section

2B.4.1 Materials and instrumentation

1-Hexadecanol, 1-aminohexadecane, bromoacetyl bromide, branched polyethylenimine (Mol wt 750, 25 and 2 kDa), poly(2-ethyl-2-oxazoline) (PEOZ) (Mol wt 500, 200 and 50 kDa) were purchased from Sigma-Aldrich and used as received. Phosphorous pentaoxide (P_2O_5), potassium carbonate (K_2CO_3), anhydrous sodium sulphate (Na_2SO_4), potassium hydroxide (KOH), dichloromethane (DCM), chloroform, acetone and anhydrous diethylether were purchased from Spectrochem, India and were of analytical grade. DCM and chloroform were dried over P_2O_5 and stored over molecular sieves (4 Å). An attenuated total reflectance Fourier transform infrared (ATR FT-IR) spectrometer was used to record IR spectra using diamond as ATR crystal. Bruker AMX-400 (400 MHz for ^{1}H NMR and 100 MHz for ^{13}C NMR) spectrometer was used to record nuclear magnetic resonance (NMR) spectra in deuterated solvents. Tecan infinite pro series M200 microplate reader was used to record optical density (OD) and fluorescence intensity. *Staphylococcus aureus* and *Escherichia coli* (MTCC 737and 443) were purchased from MTCC (Chandigarh, India). Methicillin-resistant *Staphylococcus aureus* (MRSA) (ATCC 33591) was obtained from ATCC (Rockville, MD, USA). Growth media and agar for bacteria culture were provided by HIMEDIA, India. Studies on human subject, e.g., human red blood cells (hRBC) were conducted following the guidelines provided by Institutional Bio-Safety Committee (IBSC) at Jawaharlal Nehru Centre for Advanced Scientific Research (JNCASR). Studies on animals were conducted

according to the protocols provided by the Institutional Animal Ethics Committee (IAEC) at the Jawaharlal Nehru Centre for Advanced Scientific Research (JNCASR).

2B.4.2 Synthesis of cationic polymers

2B.4.2.1 *N*-hexadecyl-2-bromoethanoate and *N*-hexadecyl-2-bromoethanamide

1-Aminoalkanes (60 mmol) was dissolved in DCM (100 mL) and a solution of K_2CO_3 (12.4 g, 90 mmol) in water (100 mL) was added to it. The binary mixture was then cooled to 5 °C in a cold incubator connected to a chiller. Bromoacetyl bromide (18.2 g, 90 mmol) was dissolved in DCM (75 mL) and was added to the mixture drop wise for about 30 min. After the completion of addition, the reaction mixture was stirred at room temperature for about 4 h. After the reaction, organic layer was separated using a separating funnel and the aqueous layer was subjected to repeated wash with DCM (2 × 50 mL). All the organic solutions were combined and washed with water repeatedly (3 × 100 mL). The final organic layer was then passed through anhydrous Na_2SO_4. The DCM layer was collected and the solvent was evaporated to obtain colourless liquids/solids with 100 % yield. The products were characterized by FT-IR, ^{1}H-NMR and ^{13}C-NMR spectroscopy.

***N*-hexadecyl-2-bromoethanamide:** FT-IR ($\bar{\nu}$): 3250 cm^{-1} (amide N–H str.), 2927 cm^{-1} (–CH_2-assym. str.), 2849 (–CH_2– sym. str.), 1679 cm^{-1} (Amide I, C=O str.), 1562 cm^{-1} (Amide II, N–H ben.), 1468 cm^{-1} (–CH_2– scissor); ^{1}H-NMR: (400 MHz, $CDCl_3$): δ 0.878 (t, terminal –CH_3, 3H), 1.300 (m, –$(CH_2)_{13}$–, 26H), 1.547 (q, –$CH_2(CH_2)_{13}$–, 2H), 3.279 (t, –CONHCH_2–, 2H), 3.883 (s, –COCH_2Br, 2H), 6.575 (br s, amide –NHCO, 2H); ^{13}C NMR (100 MHz, $CDCl_3$): δ 14.193, 22.769, 26.903, 29.334, 29.413, 29.578, 29.636, 29.718, 29.818, 32.095, 40.413, 165.567.

***N*-hexadecyl-2-bromoethanoate:** FT-IR ($\bar{\nu}$): 2930 cm^{-1} (–CH_2-assym. str.), 2850 (–CH_2– sym. str.), 1743 cm^{-1} (C=O str. of ester), 1468 cm^{-1} (–CH_2– scissor); ^{1}H-NMR: (400 MHz, $CDCl_3$): δ 0.879 (t, terminal –CH_3, 3H), 1.300 (m, –$(CH_2)_{13}$–, 26H), 1.547 (q, –$CH_2(CH_2)_{13}$–, 2H), 3.479 (t, –COOCH_2–, 2H), 3.883 (s, –COCH_2Br, 2H), ^{13}C NMR (100 MHz, $CDCl_3$): δ 14.193, 22.769, 26.903, 29.334, 29.413, 29.578, 29.636, 29.718, 29.818, 32.095, 40.413, 177.566.

2B.4.2.2 Synthesis of *N*-Methyl-PEIs

Branched and linear *N*-methyl-PEIs were synthesized following the same protocol as described in the section 2A.4.2 in Chapter 2A.

2B.4.2.3 Synthesis of side-chain hydrolyzable cationic PEI derivatives

N-Methyl-PEIs were reacted with *N*-hexadecyl-1-bromoethanoate or *N*-hexadecyl-1-bromoethanamide to obtain the quaternary PEI derivatives (**1a-1c**, **2a-2c, 3a-3c** and **4a-4c**). Branched *N*-methylated-PEIs (1 g, 17.5 mmol/repeating units) were dissolved in 75 mL dry chloroform in a screw-top pressure tube and *N*-hexadecyl-1-bromoethanoate or *N*-hexadecyl-1-bromoethanamide (35 mmol) were added to it. The reaction mixture was heated at 85 °C *N*-*N*-hexadecyl-1-bromoethanamide and 55 °C *N*-hexadecyl-1-bromoethanoate for about 96 h. After the reaction, the solvent was removed to its one tenth of the initial volume. Then excess of acetone (200 mL) was added to the reaction mixture and the precipitate was filtered off. The precipitate was dissolved in $CHCl_3$ and acetone was added to re-precipitate the product for further purification. Finally, excess solvent was decanted off and the precipitate was dried using high vacuum pump to yield colorless side-chain degradable PEI polymers (**1a-1c**, **2a-2c, 3a-3c** and **4a-4c**).

1a: FT-IR ($\bar{\nu}$): 3200-3450 cm^{-1} (amide N–H str.), 2930 cm^{-1} (–CH_2– assym. str.), 2860 cm^{-1} (–CH_2– sym. str.), 1680 cm^{-1} (amide I, C=O str.), 1555 cm^{-1} (amide II, N–H ben.), 1470 cm^{-1} (–CH_2– scissor); ^{1}H-NMR (400 MHz, $CDCl_3$): δ 0.857 (t, terminal –*CH_3*, 3H), 1.232 (–CH_3*$(CH_2)_{13}$*CH_2–, 26H), 1.512 ($CH_3(CH_2)_{13}$*CH_2*CH_2–, 2H), 3.188 (–(*CH_3*)$N^+(CH_2CH_2)_2(CH_2CONH)$–, 3H), 3.483-3.586 (–$(CH_3)N^+$(*$CH_2CH_2$*)$_2(CH_2CONH)$–, 4H), 3.844 (–$CH_2CONH$*$CH_2$*$CH_2$–, 2H), 4.476 (–$(CH_3)N^+(CH_2CH_2)_2$(*$CH_2$*$CONH)$–, 2H), 8.318 (–$CH_2CO$*$NH$*$CH_2CH_2$–, 1H); ^{13}C NMR (CP-MAS, 100 MHz): δ 14.75, 24.44, 30.52, 32.87, 40.32, 46.57, 52.92, 57.14, 66.49, 163.69; Elemental analysis: C 60.12, H 10.33, N 6.68 (calculated); C 60.03, H 10.53, N 6.57 (found).

1b: FT-IR ($\bar{\nu}$): 3200-3450 cm^{-1} (amide N–H str.), 2932 cm^{-1} (–CH_2– assym. str.), 2865 cm^{-1} (–CH_2– sym. str.), 1678 cm^{-1} (amide I, C=O str.), 1553 cm^{-1} (amide II, N–H ben.), 1468 cm^{-1} (–CH_2– scissor); ^{1}H-NMR (400 MHz, $CDCl_3$): δ 0.865 (t, terminal –*CH_3*, 3H), 1.238 (–CH_3*$(CH_2)_{13}$*CH_2–, 26H), 1.526 ($CH_3(CH_2)_{13}$*CH_2*CH_2–, 2H), 3.202 (–(*CH_3*)$N^+(CH_2CH_2)_2(CH_2CONH)$–, 3H), 3.497-3.602 (–$(CH_3)N^+$(*$CH_2CH_2$*)$_2(CH_2CONH)$–, 4H), 3.877-3.994 (–$CH_2CONH$*$CH_2$*$CH_2$–, 2H), 4.503 (–$(CH_3)N^+(CH_2CH_2)_2$(*$CH_2$*$CONH)$–, 2H), 8.331 (–$CH_2CO$*$NH$*$CH_2CH_2$–, 1H); ^{13}C NMR (CP-MAS, 100 MHz): δ 14.70, 24.34, 30.52, 32.78, 40.30, 46.54, 52.92, 57.24, 66.42, 163.59; Elemental analysis: C 60.12, H 10.33, N 6.68 (calculated); C 60.01, H 10.57, N 6.60 (found).

1c: FT-IR ($\bar{\nu}$): 3200-3450 cm^{-1} (amide N–H str.), 2927 cm^{-1} (–CH_2– assym. str.), 2857 cm^{-1} (–CH_2– sym. str.), 1676 cm^{-1} (amide I, C=O str.), 1550 cm^{-1} (amide II, N–H ben.), 1469 cm^{-1} (–CH_2– scissor); ^{1}H-NMR (400 MHz, $CDCl_3$): δ 0.868 (t, terminal –*CH_3*, 3H), 1.244 (–CH_3*$(CH_2)_{13}$*CH_2–, 26H), 1.534 ($CH_3(CH_2)_{13}$*CH_2*CH_2–, 2H), 3.214 (–(*CH_3*)$N^+(CH_2CH_2)_2(CH_2CONH)$–, 3H), 3.504 - 3.602 (–$(CH_3)N^+$(*$CH_2CH_2$*)$_2(CH_2CONH)$–, 4H), 3.877-4.095 (–$CH_2CONH$*$CH_2$*$CH_2$–, 2H), 4.518-4.719 (–$(CH_3)N^+(CH_2CH_2)_2$(*$CH_2$*$CONH)$–, 2H), 8.318 (–$CH_2CO$*$NH$*$CH_2CH_2$–, 1H); ^{13}C NMR (CP-MAS, 100 MHz): δ 14.65, 23.49, 30.42, 32.77, 40.39, 46.67, 51.22, 57.04, 66.45, 163.49; Elemental analysis: C 60.12, H 10.33, N 6.68 (calculated); C 60.05, H 10.48, N 6.53 (found).

2a: FT-IR ($\overline{\nu}$): 2920 cm^{-1} (–CH_2– assym. str.), 2860 cm^{-1} (–CH_2– sym. str.), 1750 cm^{-1} (–C=O str.), 1470 cm^{-1} (–CH_2– scissor); ^{1}H-NMR (400 MHz, $CDCl_3$): δ 0.855 (t, terminal –*CH_3*, 3H), 1.234 (–CH_3*$(CH_2)_{13}$*CH_2–, 26H), 1.655 ($CH_3(CH_2)_{13}$*CH_2*CH_2–, 2H), 3.584-3.618 (–(*CH_3*)$N^+(CH_2CH_2)_2(CH_2COOCH_2)$–, 3H), 4.177 (–$(CH_3)N^+$(*$CH_2CH_2$*)$_2(CH_2COOCH_2)$– and (–$CH_2COO$*$CH_2$*$CH_2$–, 6H), 4.704 (–$(CH_3)N^+(CH_2CH_2)_2$(*$CH_2$*$COOCH_2$)–, 2H),; ^{13}C NMR (CP-MAS, 100 MHz): δ 14.89, 24.55, 27.25, 27.82, 32.86, 46.26, 46.86, 47.51, 52.40, 53.04, 53.82, 60.07, 61.83, 66.37, 165.17; Elemental analysis: C 59.98, H 10.07, N 3.33 (calculated); C 59.71, H 10.21, N 3.17 (found).

2b: FT-IR ($\overline{\nu}$): 2923 cm^{-1} (–CH_2– assym. str.), 2858 cm^{-1} (–CH_2– sym. str.), 1750 cm^{-1} (–C=O str.), 1472 cm^{-1} (–CH_2– scissor); ^{1}H-NMR (400 MHz, $CDCl_3$): δ 0.851 (t, terminal –*CH_3*, 3H), 1.230 (–CH_3*$(CH_2)_{13}$*CH_2–, 26H), 1.647 ($CH_3(CH_2)_{13}$*CH_2*CH_2–, 2H), 3.579-3.663 (–(*CH_3*)$N^+(CH_2CH_2)_2(CH_2COOCH_2)$–, 3H), 4.166 (–$(CH_3)N^+$(*$CH_2CH_2$*)$_2(CH_2COOCH_2)$– and (–$CH_2COO$*$CH_2$*$CH_2$–, 6H), 4.698 (–$(CH_3)N^+(CH_2CH_2)_2$(*$CH_2$*$COOCH_2$)–, 2H),; ^{13}C NMR (CP-MAS, 100 MHz): δ 14.9, 24.52, 27.18, 30.66, 32.84,34.22, 35.74, 46.98, 52.53, 53.58, 54.36, 62.05, 66.19, 165.32; Elemental analysis: C 59.98, H 10.07, N 3.33 (calculated); C 59.85, H 10.16, N 3.20 (found).

2c: FT-IR ($\overline{\nu}$): 2918 cm^{-1} (–CH_2– assym. str.), 2855 cm^{-1} (–CH_2– sym. str.), 1747 cm^{-1} (–C=O str.), 1467 cm^{-1} (–CH_2– scissor); ^{1}H-NMR (400 MHz, $CDCl_3$): δ 0.830 (t, terminal –*CH_3*, 3H), 1.209 (–CH_3*$(CH_2)_{13}$*CH_2–, 26H), 1.623 ($CH_3(CH_2)_{13}$*CH_2*CH_2–, 2H), 3.564-3.605 (–(*CH_3*)$N^+(CH_2CH_2)_2(CH_2COOCH_2)$–,3H), 3.654-4.143 (–$(CH_3)N^+$(*$CH_2CH_2$*)$_2(CH_2COOCH_2)$– and (–$CH_2COO$*$CH_2$*$CH_2$–, 6H), 4.699 (–$(CH_3)N^+(CH_2CH_2)_2$(*$CH_2$*$COOCH_2$)–, 2H),; ^{13}C NMR (CP-MAS, 100 MHz): δ 14.89, 24.55, 27.25, 27.82, 32.86, 46.26, 46.86, 47.51, 52.40, 53.04, 53.82, 60.07, 61.83, 66.37, 165.17; Elemental analysis: C 59.98, H 10.07, N 3.33 (calculated); C 59.72, H 10.31, N 3.15 (found).

3a: FT-IR ($\overline{\nu}$): 3200-3450 cm^{-1} (amide N–H str.), 2925 cm^{-1} (–CH_2– assym. str.), 2867 cm^{-1} (–CH_2– sym. str.), 1677 cm^{-1} (amide I, C=O str.), 1550 cm^{-1} (amide II, N–H ben.), 1467 cm^{-1} (–CH_2– scissor); ^{1}H-NMR (400 MHz, $CDCl_3$): δ 0.879 (t, terminal –*CH_3*, 3H), 1.256 (–CH_3*$(CH_2)_{13}$*CH_2–, 26H), 1.546 ($CH_3(CH_2)_{13}$*CH_2*CH_2–, 2H), 3.228 (–(*CH_3*)$N^+(CH_2CH_2)_2(CH_2CONH)$–, 3H), 3.882-3.963 (–$(CH_3)N^+$(*$CH_2CH_2$*)$_2(CH_2CONH)$–, 4H), 4.563 (–$CH_2CONH$*$CH_2$*$CH_2$–, 2H), 5.004 (–$(CH_3)N^+(CH_2CH_2)_2$(*$CH_2$*$CONH$)–, 2H), 8.312 (–$CH_2CO$*$NH$*$CH_2CH_2$–, 1H); ^{13}C NMR (CP-MAS, 100 MHz): δ 14.71, 24.50, 30.53, 32.80, 40.42, 46.63, 52.85, 57.17, 66.49, 163.65; Elemental analysis: C 60.12, H 10.33, N 6.68 (calculated); C 59.94, H 10.41, N 6.59 (found).

3b: FT-IR ($\overline{\nu}$): 3200-3450 cm^{-1} (amide N–H str.), 2927 cm^{-1} (–CH_2– assym. str.), 2857 cm^{-1} (–CH_2– sym. str.), 1675 cm^{-1} (amide I, C=O str.), 1560 cm^{-1} (amide II, N–H ben.), 1474 cm^{-1} (–CH_2– scissor); ^{1}H-NMR (400 MHz, $CDCl_3$): δ 0.880 (t, terminal –*CH_3*, 3H), 1.256 (–CH_3*$(CH_2)_{13}$*CH_2–, 26H), 1.549 ($CH_3(CH_2)_{13}$*CH_2*CH_2–, 2H), 3.231 (–(*CH_3*)$N^+(CH_2CH_2)_2(CH_2CONH)$–, 3H), 3.976 (–$(CH_3)N^+$(*$CH_2CH_2$*)$_2(CH_2CONH)$–, 4H), 4.361-4.579 (–$CH_2CONH$*$CH_2$*$CH_2$–, 2H), 5.028 (–$(CH_3)N^+(CH_2CH_2)_2$(*$CH_2$*$CONH$)–, 2H), 8.307 (–$CH_2CO$*$NH$*$CH_2CH_2$–, 1H); ^{13}C NMR (CP-MAS, 100 MHz): δ 14.66, 24.46, 30.60, 32.81, 40.35, 46.60, 52.82, 57.21, 66.33, 163.65; Elemental analysis: C 60.12, H 10.33, N 6.68 (calculated); C 60.01, H 10.38, N 6.50 (found).

3c: FT-IR ($\overline{\nu}$): 3200-3450 cm^{-1} (amide N–H str.), 2940 cm^{-1} (–CH_2– assym. str.), 2853 cm^{-1} (–CH_2– sym. str.), 1671 cm^{-1} (amide I, C=O str.), 1551 cm^{-1} (amide II, N–H ben.), 1460

cm^{-1} (–CH_2– scissor); ^{1}H-NMR (400 MHz, $CDCl_3$): δ 0.880 (t, terminal –*CH_3*, 3H), 1.284 (–CH_3*$(CH_2)_{13}$*CH_2–, 26H), 1.551 ($CH_3(CH_2)_{13}$*CH_2*CH_2–, 2H), 3.229 (–(*CH_3*)$N^+(CH_2CH_2)_2(CH_2CONH)$–, 3H), 3.835-3.976 (–$(CH_3)N^+$(*$CH_2CH_2$*)$_2(CH_2CONH)$–, 4H), 4.600 (–$CH_2CONH$*$CH_2$*$CH_2$–, 2H), 5.025-5.046 (–$(CH_3)N^+(CH_2CH_2)_2$(*$CH_2$*$CONH)$–, 2H), 8.329 (–$CH_2CO$*$NH$*$CH_2CH_2$–, 1H); ^{13}C NMR (CP-MAS, 100 MHz): δ 14.89, 24.51, 32.90, 40.60, 46.35, 53.13, 56.54, 56.83, 66.39, 164.77; Elemental analysis: C 60.12, H 10.33, N 6.68 (calculated); C 59.81, H 10.52, N 6.63 (found).

4a: FT-IR ($\overline{\nu}$): 2920 cm^{-1} (–CH_2– assym. str.), 2863 cm^{-1} (–CH_2– sym. str.), 1750 cm^{-1} (–C=O str.), 1460 cm^{-1} (–CH_2– scissor); ^{1}H-NMR (400 MHz, $CDCl_3$): δ 0.880 (t, terminal –*CH_3*, 3H), 1.259 (–CH_3*$(CH_2)_{13}$*CH_2–, 26H), 1.696-1.773 ($CH_3(CH_2)_{13}$*CH_2*CH_2–, 2H), 3.954-4.114 (–(*CH_3*)$N^+(CH_2CH_2)_2(CH_2COOCH_2)$– and (–$(CH_3)N^+$(*$CH_2CH_2$*)$_2(CH_2COOCH_2)$–, 7H), 4.689-4.888 ((–$(CH_3)N^+(CH_2CH_2)_2$(*$CH_2$*$COOCH_2)$– and –$CH_2COO$*$CH_2$*$CH_2$–, 4H); ^{13}C NMR (CP-MAS, 100 MHz): δ 14.90, 24.63, 29.37, 32.87, 34.33, 40.61, 46.89, 47.51,52.89, 57.07, 65.95, 162.86; Elemental analysis: C 59.98, H 10.07, N 3.33 (calculated); C 59.67, H 10.51, N 3.09 (found).

4b: FT-IR ($\overline{\nu}$): 2920 cm^{-1} (–CH_2– assym. str.), 2863 cm^{-1} (–CH_2– sym. str.), 1750 cm^{-1} (–C=O str.), 1460 cm^{-1} (–CH_2– scissor); ^{1}H-NMR (400 MHz, $CDCl_3$): δ 0.878 (t, terminal –*CH_3*, 3H), 1.255 (–CH_3*$(CH_2)_{13}$*CH_2–, 26H), 1.678-1.689 ($CH_3(CH_2)_{13}$*CH_2*CH_2–, 2H), 3.828-4.221 (–(*CH_3*)$N^+(CH_2CH_2)_2(CH_2COOCH_2)$– and (–$(CH_3)N^+$(*$CH_2CH_2$*)$_2(CH_2COOCH_2)$–, 7H), 4.676-4.870 ((–$(CH_3)N^+(CH_2CH_2)_2$(*$CH_2$*$COOCH_2)$– and –$CH_2COO$*$CH_2$*$CH_2$–, 4H); ^{13}C NMR (CP-MAS, 100 MHz): δ 14.90, 24.69, 29.35, 32.87, 34.33, 40.61, 46.89, 47.41,52.89, 57.07, 65.93, 163.86; Elemental analysis: C 59.98, H 10.07, N 3.33 (calculated); C 59.61, H 10.36, N 3.14 (found).

4c: FT-IR ($\overline{\nu}$): 2910 cm^{-1} (–CH_2– assym. str.), 2863 cm^{-1} (–CH_2– sym. str.), 1750 cm^{-1} (–C=O str.), 1456 cm^{-1} (–CH_2– scissor); ^{1}H-NMR (400 MHz, $CDCl_3$): δ 0.877 (t, terminal –*CH_3*, 3H), 1.255 (–CH_3*$(CH_2)_{13}$*CH_2–, 26H), 1.690 ($CH_3(CH_2)_{13}$*CH_2*CH_2–, 2H), 3.827-4.224 (–(*CH_3*)$N^+(CH_2CH_2)_2(CH_2COOCH_2)$– and (–$(CH_3)N^+$(*$CH_2CH_2$*)$_2(CH_2COOCH_2)$–, 7H), 4.752-4.869 ((–$(CH_3)N^+(CH_2CH_2)_2$(*$CH_2$*$COOCH_2)$– and –$CH_2COO$*$CH_2$*$CH_2$–, 4H); ^{13}C NMR (CP-MAS, 100 MHz): δ 14.90, 24.52, 27.18, 30.66, 32.84, 34.22, 35.74, 46.98. 52.53, 54.36.62.05,66.19 165.32; Elemental analysis: C 59.98, H 10.07, N 3.33 (calculated); C 59.72, H 10.22, N 3.11 (found).

2B.4.2.4 Synthesis of partially zwitterionic PEI derivative

N-Methyl-PEIs (1 g, 17.5 mmol/repeating units) were dissolved in dry chloroform (75 mL) in a screw-top pressure tube and *tert*-butyl bromoacetate was added to it. The reaction mixture was heated at 55 °C for 72 h. After the reaction, the volume of the reaction mixture was reduced. Then excess of anhydrous acetone or diethylether (~200 mL) was added to the reaction mixture to precipitate the product. The precipitate was filtered off using a sintered glass funnel and then dissolved in $CHCl_3$ to re-precipitate the product again using excess acetone for further purification. Finally, the solvent was decanted off and high vacuum pump was used to dry the precipitate to obtain partially cationic PEI polymers (**5a′**, **5b′** and **5c′**).

Then **5a′**, **5b′** and **5c′**polymers were re-dissolved in chloroform (60 mL) and *N*-hexadecyl-1-bromoethanamide (3 equivalent with respect to remaining tertiary amine groups) was added. The mixture was stirred in oil bath for about 96 h and then precipitated similarly as mentioned above to obtain **5a′′**, **5b′′** and **5c′′**. Finally, these polymers were dissolved in dichloromethane (50 mL) and trifluoroacetic acid (4% v/v) was added and stirred for about 24 h at room temperature. After the reaction the product was precipitated with acetone. The precipitate was then dissolved in water and the solution was stirred with an amberlite ion-exchange resin (IRA 400, hydroxide containing) for 4 h at room temperature. The resin was discarded and filtrate was freeze dried to obtain the partially zwitterionic PEI derivatives (**5a**, **5b** and **5c**).

5a′: FT-IR ($\overline{\nu}$): 2915 cm^{-1} (–CH_2– assym. str.), 2860 cm^{-1} (–CH_2– sym. str.), 1745 cm^{-1} (–C=O str.), 1465 cm^{-1} (–CH_2– scissor); ^{1}H-NMR (400 MHz, $CDCl_3$): δ 1.521 (s, C*(CH₃)₃*OCO–, 9H), 2.363-2.484 (–N(*CH₂CH₂*)N–, 4H), 3.018-3.387 (–*CH₃*)N^+(CH_2CH_2)$_2$–, 3H), 3.428-3.597 – (CH_3)N^+(*CH₂CH₂)₂*–, 4H), 4.220-4.354 (–CH_3)N^+(CH_2CH_2)$_2$*CH₂*COO–, 2H).

5b′: FT-IR ($\overline{\nu}$): 2910 cm^{-1} (–CH_2– assym. str.), 2863 cm^{-1} (–CH_2– sym. str.), 1743 cm^{-1} (–C=O str.), 1467 cm^{-1} (–CH_2– scissor); ^{1}H-NMR (400 MHz, $CDCl_3$): δ 1.508 (s, C*(CH₃)₃*OCO–, 9H), 2.350-2.479 (–N(*CH₂CH₂*)N–, 4H), 3.028-3.382 (–*CH₃*)N^+(CH_2CH_2)$_2$–, 3H), 3.428-3.597 – (CH_3)N^+(*CH₂CH₂)₂*–, 4H), 4.220-4.354 (–CH_3)N^+(CH_2CH_2)$_2$*CH₂*COO–, 2H).

5c′: FT-IR ($\overline{\nu}$): 2918 cm^{-1} (–CH_2– assym. str.), 2864 cm^{-1} (–CH_2– sym. str.), 1742 cm^{-1} (–C=O str.), 1465 cm^{-1} (–CH_2– scissor); ^{1}H-NMR (400 MHz, $CDCl_3$): δ 1.498 (s, C*(CH₃)₃*OCO–, 9H), 2.298-2.491 (–N(*CH₂CH₂*)N–, 4H), 3.118-3.401 (–*CH₃*)N^+(CH_2CH_2)$_2$–, 3H), 3.398-3.607 – (CH_3)N^+(*CH₂CH₂)₂*–, 4H), 4.228-4.361 (–CH_3)N^+(CH_2CH_2)$_2$*CH₂*COO–).

5a′′: FT-IR ($\overline{\nu}$): 3200-3450 cm^{-1} (amide N–H str.), 2940 cm^{-1} (–CH_2– assym. str.), 2853 cm^{-1} (–CH_2– sym. str.), 1737 cm^{-1} (–C=O str.), 1671 cm^{-1} (amide I, C=O str.), 1551 cm^{-1} (amide II, N–H ben.), 1460 cm^{-1} (–CH_2– scissor); ^{1}H-NMR (400 MHz, $CDCl_3$): δ 0.880 (t, terminal –*CH₃*, 3H), 1.284 (–CH_3*(CH₂)₁₃*CH_2–, 26H), 1.456 (s, C*(CH₃)₃*OCO–), 1.551 ($CH_3(CH_2)_{13}$*CH₂*CH_2–, 2H), 3.229 (–(*CH₃*)N^+(CH_2CH_2)$_2$(CH_2CONH)–, 3H), 3.835-3.976 (–(CH_3)N^+(*CH₂CH₂*)$_2$(CH_2CONH)–, 4H), 4.600 (–CH_2CONH*CH₂*CH_2–, 2H), 5.025-5.046 (–(CH_3)N^+(CH_2CH_2)$_2$(*CH₂*CONH)–, 2H), 8.329 (–CH_2CO*NH*CH_2CH_2–, 1H).

5b′′: FT-IR ($\overline{\nu}$): 3200-3450 cm^{-1} (amide N–H str.), 2942 cm^{-1} (–CH_2– assym. str.), 2850 cm^{-1} (–CH_2– sym. str.), 1735 cm^{-1} (–C=O str.), 1671 cm^{-1} (amide I, C=O str.), 1555 cm^{-1} (amide II, N–H ben.), 1460 cm^{-1} (–CH_2– scissor); ^{1}H-NMR (400 MHz, $CDCl_3$): δ 0.878 (t, terminal –*CH₃*, 3H), 1.282 (–CH_3*(CH₂)₁₃*CH_2–, 26H), 1.466 (s, C*(CH₃)₃*OCO–, 9H), 1.549 ($CH_3(CH_2)_{13}$*CH₂*CH_2–, 2H), 3.2231 (–(*CH₃*)N^+(CH_2CH_2)$_2$(CH_2CONH)–, 3H), 3.825-3.941 (–(CH_3)N^+(*CH₂CH₂*)$_2$(CH_2CONH)–, 4H), 4.580 (–CH_2CONH*CH₂*CH_2–, 2H), 5.012-5.236 (–(CH_3)N^+(CH_2CH_2)$_2$(*CH₂*CONH)–, 2H), 8.320 (–CH_2CO*NH*CH_2CH_2–, 1H).

5c″: FT-IR ($\overline{\nu}$): 3200-3450 cm^{-1} (amide N–H str.), 2940 cm^{-1} (–CH_2– assym. str.), 2855 cm^{-1} (–CH_2– sym. str.), 1740 cm^{-1} (–C=O str.), 1672 cm^{-1} (amide I, C=O str.), 1550 cm^{-1} (amide II, N–H ben.), 1462 cm^{-1} (–CH_2– scissor); ^{1}H-NMR (400 MHz, $CDCl_3$): δ 0.882 (t, terminal –*CH*$_3$, 3H), 1.284 (–CH_3*(CH$_2$)$_{13}$*CH_2–, 26H), 1.459 (s, C*(CH$_3$)$_3$*OCO–), 1.548 ($CH_3(CH_2)_{13}$*CH$_2$*CH_2–, 2H), 3.199 (–*CH*$_3$)N^+($CH_2CH_2)_2$(CH_2CONH)–, 3H), 3.795-3.896 (–$(CH_3)N^+$(*CH$_2$CH$_2$*)$_2$(CH_2CONH)–, 4H), 4.620 (–CH_2CONH*CH$_2$*CH_2–, 2H), 5.185-5.396 (–$(CH_3)N^+$($CH_2CH_2)_2$(*CH$_2$*CONH)–, 2H), 8.298 (–CH_2CO*NH*CH_2CH_2–, 1H).

5a: FT-IR ($\overline{\nu}$): 3200-3450 cm^{-1} (amide N–H str.), 2942 cm^{-1} (–CH_2– assym. str.), 2855 cm^{-1} (–CH_2– sym. str.), 1670 cm^{-1} (amide I, C=O str.), 1639 cm^{-1} (ester –C=O str.), 1555 cm^{-1} (amide II, N–H ben.), 1460 cm^{-1} (–CH_2– scissor); ^{1}H-NMR (400 MHz, $CDCl_3$): δ 0.881 (t, terminal –*CH*$_3$, 3H), 1.284 (–CH_3*(CH$_2$)$_{13}$*CH_2–, 26H), 1.551 ($CH_3(CH_2)_{13}$*CH$_2$*CH_2–, 2H), 3.230 (–*CH*$_3$)N^+($CH_2CH_2)_2$(CH_2CONH)–, 3H), 3.845-3.876 (–$(CH_3)N^+$($CH_2CH_2)_2$(*CH$_2$*COO)– and $(CH_3)N^+$(*CH$_2$CH$_2$*)$_2$(CH_2CONH)–, 6H), 4.588 (–CH_2CONH*CH$_2$*CH_2–, 2H), 5.185-5.146 (–$(CH_3)N^+$($CH_2CH_2)_2$(*CH$_2$*CONH)–, 2H), 8.309 (–CH_2CO*NH*CH_2CH_2–, 1H).

5b: FT-IR ($\overline{\nu}$): 3200-3450 cm^{-1} (amide N–H str.), 2940 cm^{-1} (–CH_2– assym. str.), 2853 cm^{-1} (–CH_2– sym. str.), 1671 cm^{-1} (amide I, C=O str.), 1637 cm^{-1} (ester –C=O str.), 1551 cm^{-1} (amide II, N–H ben.), 1460 cm^{-1} (–CH_2– scissor); ^{1}H-NMR (400 MHz, $CDCl_3$): δ 0.880 (t, terminal –*CH*$_3$, 3H), 1.284 (–CH_3*(CH$_2$)$_{13}$*CH_2–, 26H), 1.551 ($CH_3(CH_2)_{13}$*CH$_2$*CH_2–, 2H), 3.229 (–*CH*$_3$)N^+($CH_2CH_2)_2$(CH_2CONH)–, 3H), 3.835-3.976 (–$(CH_3)N^+$($CH_2CH_2)_2$(*CH$_2$*COO)– and $(CH_3)N^+$(*CH$_2$CH$_2$*)$_2$(CH_2CONH)–, 6H), 4.600 (–CH_2CONH*CH$_2$*CH_2–, 2H), 5.025-5.046 (–$(CH_3)N^+$($CH_2CH_2)_2$(*CH$_2$*CONH)–, 2H), 8.329 (–CH_2CO*NH*CH_2CH_2–, 1H).

5c: FT-IR ($\overline{\nu}$): 3200-3450 cm^{-1} (amide N–H str.), 2945 cm^{-1} (–CH_2– assym. str.), 2855 cm^{-1} (–CH_2– sym. str.), 1670 cm^{-1} (amide I, C=O str.), 1635 cm^{-1} (ester –C=O str.), 1554 cm^{-1} (amide II, N–H ben.), 1462 cm^{-1} (–CH_2– scissor); ^{1}H-NMR (400 MHz, $CDCl_3$): δ 0.884 (t, terminal –*CH*$_3$, 3H), 1.289 (–CH_3*(CH$_2$)$_{13}$*CH_2–, 26H), 1.548 ($CH_3(CH_2)_{13}$*CH$_2$*CH_2–, 2H), 3.232 (–*CH*$_3$)N^+($CH_2CH_2)_2$(CH_2CONH)–, 3H), 3.795-3.989 (–$(CH_3)N^+$($CH_2CH_2)_2$(*CH$_2$*COO)– and $(CH_3)N^+$(*CH$_2$CH$_2$*)$_2$(CH_2CONH)–, 6H), 4.619 (–CH_2CONH*CH$_2$*CH_2–, 2H), 5.187-5.141 (–$(CH_3)N^+$($CH_2CH_2)_2$(*CH$_2$*CONH)–, 2H), 8.304 (–CH_2CO*NH*CH_2CH_2–, 1H).

2B.4.2.5 Synthesis of fully zwitterionic PEI derivatives

N-Methyl-PEIs (1 g, 17.5 mmol/repeating units) were dissolved in dry chloroform (75 mL) in a screw-top pressure tube and *tert*-butyl bromoacetate (70 mmol) was added to it. The reaction mixture was heated at 55 °C for 96 h. After the reaction, the volume of the reaction mixture was reduced. Then excess of anhydrous acetone or diethylether (~200 mL) was added to the reaction mixture to precipitate the product. The precipitate was filtered off using a sintered glass funnel and then dissolved in $CHCl_3$ to re-precipitate the product again using excess acetone for further purification to obtain fully quaternized PEI polymer (**5d′**). Then, the polymer was dissolved in dichloromethane (50 mL) and trifluoroacetic acid (4% v/v) was

added and stirred for about 24 h at room temperature. After the reaction the product was precipitated with acetone. The precipitate was then dissolved in water and the solution was stirred with an amberlite ion-exchange resin (IRA 400, hydroxide containing) for 4 h at room temperature. The resin was discarded and filtrate was freeze dried to obtain the partially zwitterionic PEI derivatives (**5d**).

5d′: FT-IR ($\overline{v}$): 2940 cm^{-1} (–CH_2– assym. str.), 2853 cm^{-1} (–CH_2– sym. str.), 1737 cm^{-1} (–C=O str.), 1460 cm^{-1} (–CH_2– scissor); ^{1}H-NMR (400 MHz, $CDCl_3$): δ 1.456 (s, C*(CH₃)₃*OCO–, 9H), 3.229 (–(*CH₃*)N^+(CH_2CH_2)–, 3H), 3.835-3.976 (–(CH_3)N^+(*CH₂CH₂*)–, 4H), 4.600 (–CH_2COO–, 2H).

5d: FT-IR ($\overline{v}$): 2948 cm^{-1} (–CH_2– assym. str.), 2850 cm^{-1} (–CH_2– sym. str.), 1642 cm^{-1} (–C=O str.), 1465 cm^{-1} (–CH_2– scissor); ^{1}H-NMR (400 MHz, $CDCl_3$): δ 3.239 (–(*CH₃*)N^+(CH_2CH_2)–, 3H), 3.835-3.976 (–(CH_3)N^+(*CH₂CH₂*)–, 4H), 4.600 (–CH_2COO–, 2H).

2B.4.3 Solubility test

Solubility of the polymers was evaluated following same protocol as described in the section 2A.4.3 in Chapter 2A.

2B.4.4 Preparation of the film

Coating of different surfaces by the polymers was performed following same protocol as described in the section 2A.4.4 in Chapter 2A.

2B.4.5 Antimicrobial activity

2B.4.5.1 Determination of antibacterial activity by spray method (air-borne bacteria)

Antibacterial activity of the polymer coated surfaces was evaluated following same protocol as described in the section 2A.4.5.1 in Chapter 2A.

2B.4.5.2 Determination of antibacterial activity (water-borne bacteria)

Antibacterial activity of the polymer coated surfaces was evaluated following same protocol as described in the section 2A.4.5.2 in Chapter 2A

2B.4.5.3 Antibacterial kinetics

96-Well plate was coated with the polymers **3c** and **4c** at two different amounts: MIA and 6 × MIA for both *S. aureus* and *E. coli* respectively following the coating procedure as described above. Bacterial suspension (200 μL) containing approximately 5.1×10^5 CFU/mL *S. aureus*

in nutrient broth and 5.5×10^5 CFU/mL *E. coli* in Luria-Bertani (LB) broth were added, and the plates were incubated at 37 °C under constant shaking. The initial time of addition of the bacteria to the wells was taken as zero, and 3 μL aliquots were withdrawn from each of the wells at definite time intervals. These aliquots were then spot plated immediately on suitable agar plates. The plates were incubated at 37 ˚C for 24 h, and bacterial colonies were monitored. The plates were then imaged to visualize the killing efficiency at different time interval.

2B.4.5.4 Mechanism of antibacterial action

Bacterial suspension (200 μL, 10^9 CFU/mL and 10^8 CFU/mL for *S. aureus* and *E. coli* respectively) were added to the well of 96 well plate coated with polymer **6** (at 6 × MIA). A control was made similarly in non-coated wells. The 96-well plate was placed in incubator at 37 °C under constant shaking for 4 h. After the treatment, bacteria were collected in an eppendorf tube, centrifuged and resuspended in PBS. The suspension (5 μL) was then combined with a mixture containing 3.0 μM green fluorescent dye SYTO 9 and 15.0 μM red fluorescent dye PI (Sigma-Aldrich, USA). The mixture was incubated in the dark for 15 min. Finally, aliquot (5 μL) was placed on a glass slide, covered with a cover slip, sealed, and examined under a confocal laser scanning microscope (Zeiss 510 Meta Confocal Microscope). Excitation wavelength for SYTO 9 was 450-490 nm and for PI was 515-560 nm. Emission wavelength was for SYTO 9 at 500-550 nm and for PI at 590-800 nm and was collected using a band-pass filter.

2B.4.6 Bacterial biofilm inhibition assay

First, the glass cover slips (18 mm) were coated with various amounts of the polymers and were placed into the wells of a 6-well plate. Midlog phase culture of *S. aureus* and *E. coli* (~10^9 CFU/mL) were suspended to ~10^5 CFU/mL into suitable media (nutrient media supplemented with 1% glucose and NaCl for *S. aureus* and M9 media supplemented with 0.02% casamino acid and 0.5% glycerol for *E. coli* respectively). Then, 2 mL of the bacterial suspensions were added to the wells containing the polymer coated cover slips and allowed to incubate at 37 ˚C under stationary conditions. A similar experiment was performed by placing 2 mL of respective bacterial suspensions to the wells containing the uncoated cover slips as control experiment. After 24 h, the cover slips were removed carefully and washed once with PBS. Finally cover glasses were placed on a glass slide and SYTO 9 solution (15

μL, 3 μM) was added to the cover glass and was covered by another coverslip. The cover glasses were air-sealed and then incubated in dark for 15 min. Both treated and non-treated cover slips were then imaged using a confocal laser scanning microscope (Zeiss 510 Meta confocal microscope). In another set of experiments, after the incubation, 100 μL of trypsin-EDTA solution was added to the biofilm to dissolve. Cell suspension of biofilms was then assessed by plating serial 10-fold dilutions on suitable agar plates. After 24 h of incubation, bacterial colonies were counted, and cell viability was expressed as log10(CFU/mL) along with the control.

2B.4.7 Antifungal assay

2B.4.7.1 Minimum inhibitory amount (MIA)

Antifungal activity of the polymer coated surfaces was evaluated following same protocol as described in the section 2A.4.7.1 in Chapter 2A.

2B.4.7.2 Minimum fungicidal amount (MFA)

Minimum fungicidal amount of the polymer coated surfaces was evaluated following same protocol as described in the section 2A.4.7.2 in Chapter 2A.

2B.4.7.3 Kinetics of antifungal activity

Kinetics of Antifungal activity of the polymer coated surfaces was evaluated following same protocol as described in the section 2A.4.7.3 in Chapter 2A.

2B.4.8 Mechanism of antifungal action

Mechanism of antifungal action of the polymer coated surfaces was evaluated following same protocol as described in the section 2A.4.8 in Chapter 2A.

2B.4.9 Fungal biofilm inhibition assay

The antibiofilm activity of the polymeric coatings was evaluated by coating the cationic PEI derivatives onto the wells of 6-well plate. Two different amounts were used to coat the surfaces: MIA and 6 × MIA of polymers **3c** and **4c** respectively. Then fungal suspension (2 mL, ~10^5 CFU/mL) was then added to the wells and plates were kept at 30 ˚C under stationary conditions for about 48 h. After the incubation, the plates were directly used to

visualize the growth of fungi and their biofilm formation under fluorescence microscope ny staining the wells with SYTO 9.

2B.4.10 Hydrolysis study

Hydrolysis study of the side-chain degradable polymers was performed by taking the polymers (**3c** and **4c**) suspension (5 mg/mL) in acid (HCl, 0.2 M) and in enzymes (4 mg/mL of trypsin for **3c** and 1 mg/mL of lipase for **4c**). Then the suspensions were kept under constant shaking at 37 ˚C. After different time interval, the suspensions were directly freeze-dried. To the freeze-dried sample in the case of enzymes treated polymers, chloroform and methanol mixture (9:1) was added and the filtrate was collected. Finally, the freeze dried samples were used to record IR and NMR spectra. The presence of hydrolyzed functional groups was confirmed by IR spectroscopy and the extent of hydrolysis was confirmed via 1h-NMR spectroscopy.

2B.4.11 Biocompatibility of polymers

2B.4.11.1 Hemolytic activity of cationic PEI derivatives

Hemolytic assay of the polymeric coating was evaluated following same protocol as described in the section 2A.4.10 in Chapter 2A.

2B.4.11.2 Hemolytic activity of zwitterionic PEI derivatives

Human red blood cells (hRBC) were isolated from freshly drawn, heparinised human blood and resuspended to 5 vol% in phosphate buffered saline (PBS) (pH 7.4). Then, 200 μL of hRBC suspension (5 vol% in PBS) was added to the wells of 96-well plate coated with polymers. Two controls were made, one non-coated well dried after using only solvent and another non-coated well with the solution of Triton X-100 (1 vol %). The plates were then incubated for 1 h at 37°C and were then centrifuged at 3500 rpm for 5 min. Following centrifugation, 100 μL of the supernatant from each well was transferred to a fresh 96-well plate, and absorbance at 540 nm was measured. Percentage of hemolysis was determined as $(A - A_0)/(A_{total} - A_0) \times 100$, where A is the absorbance of the test well (wells coated with polymers), A_0 the absorbance of the wells with negative controls (wells without any polymer coating), and A_{total} the absorbance of the well with 100% hemolysis (wells with Triton X-100, 1 vol%), all at 540 nm.

2B.4.11.3 *In-vivo* toxicity of cationic PEI derivatives

Male BALB/c (6-8 weeks old, 18-22 g) were used for the experiment. Polymers (**3c** and **4c**) coated catheters (~4.0 μg/mm^2 and 8.0 μg/mm^2) were sterilized by UV-irradiation before implantation. Mice were anesthetized with ketamine (40 mg/kg) and xylazine (2 mg/kg of xylazine). The hair at the back of each mouse was clipped and then shaved aseptically. A midline incision was then made in the skin above the mid-thoracic spine and a subcutaneous (s.c.) pouch was created by blunt dissection extending interiorly in each mouse. Catheters were then placed in the s.c. pockets of mice. The incisions were closed with 3.0 vicryl sutures. After 96 h, mice were killed by isoflurane and the coated catheters along with the surrounding tissues were removed aseptically and placed in formalin. The tissues were washed in running tap water for about 1 h and were dehydrated by successive treatment with 70%, 90% and 100% ethanol, each for 1 h. The samples were then cleaned with xylene twice for 1 h and were then kept in melted paraffin at 56 ˚C thrice for paraffin embedding. A semi-automatic microtome was used to prepare longitudinal and transverse sections (5 mm) were prepared and placed on glass slide covered with Meyer's egg albumin. The sections were dried at 40 ˚C for 2 h. Fixed sections were dipped successively in 100%, 90%, 70% and 50% ethanol; each for 1 h and then in water to carry out the rehydration. Haematoxylin and eosin (H & E) staining agent was then used to stain the sections. Finally, the sections were covered with DPX (SRL, India) mounting medium along with the cover glasses and observed under light microscope (Nikon, Japan).

2B.4.11.4 *In-vivo* toxicity of fully zwitterionic PEI derivative

The numbers of animals per groups, dosage of polymers etc. were used according to the Organisation for Economic Cooperation and Development (OECD) Guidelines for the Testing of Chemicals (OECD 425). BALB/c mice (female, 6-8 weeks, 18-21 g) were used for the systemic toxicity studies. Mice were divided into control and test groups with 5 mice per group. Various doses (5.5, 17.5, 55 and 175 mg/kg) of the test polymer, HTCC, were used as per the OECD guidelines. Solution (200 μL) of small molecular biocide in sterilized saline was injected into each mouse (5 mice per group) via intra-peritoneal (i.p.) and subcutaneous (s.c.) routes of administration. All the mice were monitored for the next 14 days after the administration of the polymer. During the observation period of 14 days, onset abnormality was monitored for all the tested amounts. Saline (200 μL) was used as control. For the acute dermal toxicity studies, fur of the mice was shaved 24 h before the experiment. To the shaved

region, the biocide solution (40 μL) of different concentration was applied. Adverse effect on the skin of mice was monitored along with mortality rate for 14 days post treatment.

2B.4.12 *In-vivo* activity of cationic PEI derivatives

All catheters were 5-French polyurethane catheters and were cut into pieces (12 mm length, average weight ~25 mg). The catheter pieces were heat sealed on both ends and were coated as mentioned previously with different amounts (~2.5 μg/mm^2, 5.0 μg/mm^2 and 7.5 μg/mm^2). All animals were treated in accordance with protocols approved by the Institutional Animal Ethics Committee (IAEC) at the Jawaharlal Nehru Centre for Advanced Scientific Research (JNCASR). In each group, a total of five mice weighing 18-22 g (6-8 weeks old) were used. Mice were anesthetized with ketamine-xylazine (40 mg/kg of ketamine and 2 mg/kg of xylazine). The hair at back of each mouse was clipped and then shaved aseptically. An incision was produced in the dorsal midline, and subcutaneous (s.c.) pouches were made by blunt dissection. Coated catheters were inoculated with ~6.9 × 10^7 CFU/mL methicilin-resistant *S. aureus* (MRSA) and incubated without shaking at 37 ˚C for 60 min to allow the adherence of the pathogens. The bacteria contaminated catheters were then placed in the s.c. pockets of mice. The pouches and incisions were closed with 3.0 vicryl sutures and mice were allowed to have access of food and water. After 96 h, mice were killed by isoflurane and the coated catheters were removed aseptically and placed in eppendrof tube containing 1 mL of nutrient broth. Then the solution containing catheter was sonicated for 5 min in a water bath sonicator (550 W, 37,000 Hz; S 60H Elmasonic sonicator). The broth was serially diluted and surface plated on nutrient agar plate to determine the number of bacteria. A similar experiment was performed by taking non-coated catheter as control. For SEM imaging, the catheter samples after removing from mice was placed in formalin for 24 h and then dehydrated with subsequent treatment of 30, 50, 70, 90 and 100% of ethanol. Finally the catheter pieces were imaged by FESEM after gold sputtering. For histopathological studies tissue surrounding the gel was collected, fixed in 10% formalin and analyzed similarly as described in the previous section.

2B.4.13 Resistance development study

Resistance development assay of the polymeric coating was evaluated following same protocol as described in the section 2A.4.9 in Chapter 2A.

BIBLIOGRAPHY

1. Busscher, H. J.; van der Mei, H. C.; Subbiahdoss, G.; Jutte, P. C.; van den Dungen, J. J.; Zaat, S. A.; Schultz, M. J.; Grainger, D. W. Biomaterial-associated infection: locating the finish line in the race for the surface. *Sci. Transl. Med.* **2012,** *4*, 153rv10.
2. Arciola, C. R.; Campoccia, D.; Speziale, P.; Montanaro, L.; Costerton, J. W. Biofilm formation in Staphylococcus implant infections. A review of molecular mechanisms and implications for biofilm-resistant materials. *Biomaterials* **2012,** *33*, 5967-5982.
3. Salwiczek, M.; Qu, Y.; Gardiner, J.; Strugnell, R. A.; Lithgow, T.; McLean, K. M.; Thissen, H. Emerging rules for effective antimicrobial coatings. *Trends Biotechnol.* **2014,** *32*, 82-90.
4. Darouiche, R. O. Current concepts - treatment of infections associated with surgical implants. *N. Engl. J. Med.* **2004,** *350*, 1422-1429.
5. Hetrick, E. M.; Schoenfisch, M. H. Reducing implant-related infections: active release strategies. *Chem. Soc. Rev.* **2006,** *35*, 780-789.
6. Kumar, A.; Vemula, P. K.; Ajayan, P. M.; John, G. Silver-nanoparticle-embedded antimicrobial paints based on vegetable oil. *Nat. Mater.* **2008,** *7*, 236-241.
7. Wong, S. Y.; Moskowitz, J. S.; Veselinovic, J.; Rosario, R. A.; Timachova, K.; Blaisse, M. R.; Fuller, R. C.; Klibanov, A. M.; Hammond, P. T. Dual functional polyelectrolyte multilayer coatings for implants: permanent microbicidal base with controlled release of therapeutic agents. *J. Am. Chem. Soc.* **2010,** *132*, 17840-17848.
8. Han, H.; Wu, J. F.; Avery, C. W.; Mizutani, M.; Jiang, X. M.; Kamigaito, M.; Chen, Z.; Xi, C. W.; Kuroda, K. Immobilization of amphiphilic polycations by catechol functionality for antimicrobial coatings. *Langmuir* **2011,** *27*, 4010-4019.
9. Campoccia, D.; Montanaro, L.; Arciola, C. R. A review of the biomaterials technologies for infection-resistant surfaces. *Biomaterials* **2013,** *34*, 8533-8554.
10.Campoccia, D.; Montanaro, L.; Arciola, C. R. A review of the clinical implications of anti-infective biomaterials and infection-resistant surfaces. *Biomaterials* **2013,** *34*, 8018-8029.
11.Cheng, G.; Xite, H.; Zhang, Z.; Chen, S. F.; Jiang, S. Y. A switchable biocompatible polymer surface with self-sterilizing and nonfouling capabilities. *Angew. Chem. Int. Ed.* **2008,** *47*, 8831-8834.
12. Cao, Z. Q.; Mi, L.; Mendiola, J.; Ella-Menye, J. R.; Zhang, L.; Xue, H.; Jiang, S. Y. Reversibly switching the function of a surface between attacking and defending against bacteria. *Angew. Chem. Int. Ed.* **2012,** *51*, 2602-2605.
13. Cao, Z. Q.; Brault, N.; Xue, H.; Keefe, A.; Jiang, S. Y. Manipulating sticky and non-sticky properties in a single material. *Angew. Chem. Int. Ed.* **2011,** *50*, 6102-6104.
14. Tehrani-Bagha, A.; Holmberg, K. Cleavable surfactants. *Curr. Opin. Colloid Interface Sci.* **2007,** *12*, 81-91.
15. Hellberg, P. E.; Bergstrom, K.; Holmberg, K. Cleavable surfactants. *J. Surfactants. Deterg.* **2000,** *3*, 81-91.
16. Sambhy, V.; MacBride, M. M.; Peterson, B. R.; Sen, A. Silver bromide nanoparticle/polymer composites: dual action tunable antimicrobial materials. *J. Am. Chem. Soc.* **2006,** *128*, 9798-9808.
17. Uppu, D. S. S. M.; Konai, M. M.; Baul, U.; Singh, P.; Siersma, T. K.; Samaddar, S.; Vemparala, S.; Hamoen, L. W.; Narayana, C.; Haldar, J. Isosteric substitution in cationic-amphiphilic polymers reveals an important role for hydrogen bonding in bacterial membrane interactions. *Chem. Sci.* **2016,** *7* (7), 4613-4623.
18. Chen, L.; Zhu, Y.; Yang, D. L.; Zou, R. F.; Wu, J. C.; Tian, H. Synthesis and antibacterial activities of antibacterial peptides with a spiropyran fluorescence probe. *Sci. Rep.* **2014,** *4*.

19. Davies, D., Understanding biofilm resistance to antibacterial agents. *Nat. Rev. Drug Discov.* **2003,** *2* (2), 114-122.
20. Uppu, D. S.; Samaddar, S.; Ghosh, C.; Paramanandham, K.; Shome, B. R.; Haldar, J. Amide side chain amphiphilic polymers disrupt surface established bacterial bio-films and protect mice from chronic Acinetobacter baumannii infection. *Biomaterials* **2016,** *74*, 131-143.
21. Harriott, M. M.; Noverr, M. C. Candida albicans and Staphylococcus aureus form polymicrobial biofilms: effects on antimicrobial resistance. *Antimicrob. Agents Chemother.* **2009,** *53*, 3914-3922.
22. Shirtliff, M. E.; Peters, B. M.; Jabra-Rizk, M. A. Cross-kingdom interactions: Candida albicans and bacteria. *FEMS Microbiol. Lett.* **2009,** *299*, 1-8.
23. Daghighi, S.; Sjollema, J.; van der Mei, H. C.; Busscher, H. J.; Rochford, E. T. Infection resistance of degradable versus non-degradable biomaterials: an assessment of the potential mechanisms. *Biomaterials* **2013,** *34*, 8013-8017.
24. Chen, R.; Willcox, M. D.; Ho, K. K.; Smyth, D.; Kumar, N. Antimicrobial peptide melimine coating for titanium and its in vivo antibacterial activity in rodent subcutaneous infection models. *Biomaterials* **2016,** *85*, 142-151.

Chapter 3A

Biodegradable and Biocompatible Chitin-based Cationic Hydrophobic Polymers as Antimicrobial Paint

Abstract

Chapter 3A *describes the development of highly antimicrobial water-insoluble and organo-soluble quaternary chitin derivatives aimed at obtaining biodegradable antimicrobial coatings to overcome toxicity associated with the coating materials. The polycationic paint was found to inactivate various pathogenic bacteria including multi drug-resistant methicillin-resistant Staphylococcus aureus (MRSA), vancomycin-resistant Enterococcus faecium (VRE) and beta lactam-resistant Klebsiella pneumoniae and fungi such as Candida spp. and Cryptococcus spp (~5 log reduction). The polymers killed both bacteria and fungi by disrupting the cell membrane causing death upon contact. Surfaces coated with the polymers inhibited formation of biofilms against both bacteria and fungi. Importantly, coated surfaces displayed negligible toxicity against human erythrocytes and showed minimal to negligible inflammation upon implantation in mice. Notably, the polymers were shown to be degradable in the presence of lysozyme. Further, subcutaneous implantation of polymer discs in rats led to 15-20% degradation in 4 weeks. In a murine model of subcutaneous infection, polymer-coated medical grade catheter reduced MRSA burden by 3.7 log compared to non-coated catheter with less inflammation in the surrounding tissue. Further, no biofilm development was observed on the coated catheters under in-vivo conditions. The biodegradable polycationic materials thus developed herein represent novel class of safe and effective coating agents for the prevention of device-related infections.*

Publications based on this work

1. Hoque, J. *et al.* A biodegradable polycationic paint that kills bacteria *in vitro* and *in vivo. ACS Appl. Mater. Interfaces* **2016**, *8,* 29298.

2. Hoque, J. *et al.* Broad-spectrum polycationic paint kills multi-drug-resistant bacteria and pathogenic fungi and inhibits biofilm formation: an *in vitro* and *in vivo* evaluation. Manuscript under submission.

3A.1 Introduction

In Chapter 2B, charge-switchable antimicrobial coatings to prevent infections in biomedical device and implants were developed wherein the polymers (quaternary polyethylenimine) were shown to degrade via the hydrolysable side alkyl chain bearing amide or ester groups. Further, the hydrolyzed zwitterionic polymers were shown to be highly biocompatible towards mammalian cells. However, the polymers degrade only via the hydrolysis of the side chains and are not fully degradable as the backbone is synthetic in nature. Thus, where applicable, an antimicrobial coating should kill microbes and prevent colonization on medical devices or implants for desired period of time and then disappear after its intended usage without causing significant toxicity towards mammalian cells during or after its use.[1,2] To this end, antimicrobial polymeric coating with biodegradable backbone would be suitable. Naturally occurring polymers because of their high biocompatibility and biodegradability are considered as potential candidates.[3-5] Herein, chapter 3A deals with the development of biodegradable and biocompatible antimicrobial polymers from naturally occurring polymer chitin and demonstrates their use as non-covalent antimicrobial coatings.

Chitin, the second most abundant polymer in nature, is used as wound dressings, artificial skin, preservatives in cosmetics, antithrombic and hemostatic materials, contact lenses, sutures and materials to support bone growth in orthopedic applications, etc.[6,7] In addition, it is inherently antimicrobial and susceptible towards human enzymes lysozymes thus making it completely biodegradable in human body.[8,9] However, insolubility of chitin in almost all the common organic solvents limits its practical use. Further, the antibacterial activity of pristine chitin is very low. Direct usage of chitin as antimicrobial paint is thus limited due to its processability and lack of antibacterial activity.[10,11] It was envisioned that by introducing cationic charge and hydrophobicity into chitin and by balancing the charge/hydrophobic ratio, water insoluble and organo-soluble polymers with degradable backbone and enhanced antimicrobial activity could be developed. Moreover, as microbial (e.g. bacterial) cell membrane is mostly negatively charged due to the presence of anionic phospholipids, introduction of positive charges and hydrophobicity would render cationic chitin derivatives antimicrobial.

This chapter thus described the design and synthesis of organo-soluble quaternary chitin polymers and demonstrated their use as biodegradable microbicidal paint. The effect of degree of quaternization (DQ) and length of hydrophobic alkyl chain on the material's solubility and antimicrobial activity were systematically evaluated. The polycationic

materials were able to kill both drug-sensitive and drug-resistant bacteria including multi drug-resistant (MDR) clinical isolates and shown to inhibit biofilm formation upon coating onto various surfaces. Not only against bacteria, the polymers showed excellent efficacy against various human pathogenic fungi and were shown to be effective in inhibiting fungal biofilm formation on the coated surface. Notably, the polymers were non-toxic towards mammalian cells and susceptible towards hydrolytic enzymes under both *in vitro* and *in vivo* upon subcutaneous implantation in mice. Upon painting these polymers, medical grade polyurethane catheter was shown to be effective in reducing bacterial burden and inhibiting biofilm formation *in vivo* in murine model against MRSA.

3A.2 Results and discussion

3A.2.1 Synthesis of cationic chitin derivatives

The water insoluble and organo-soluble quaternary chitin derivatives were synthesized by tosylation of chitin (degree of acetylation, DA ~75%) and subsequent quaternization of the tosylchitin (Scheme 3A.1). Chitin was first selectively tosylated at the C-6 position of the sugar unit by reacting with tosylchloride (20 equivalents per sugar unit) at low temperature (8 $^{\circ}$C).[12] Reaction at low temperature allowed the regioselective tosylation only at the primary hydroxyl group of the sugar unit of chitin. Three different tosylchitins were prepared as Tsch 1, Tsch 2, and Tsch 3 (obtained after 24 h, 48 h and 72 h of tosylation). As the degree of acetylation of chitin was ~75%, the remaining 25% free amine groups may interfere in the subsequent quaternization reactions of tosyl-chitin with *N*,*N*-dimethylalkylamines (e.g., via cross linking of polymer chains) (Scheme 3A.1). The tosylchitins were therefore reacted with acetic anhydride to protect the free amino group. Since the *N*-acetylation led to some *O*-acetylation, tosylchitin was further treated with methanolic KOH to remove the unwanted *O*-acetylation. It should be mentioned that during KOH treatment some detosylation also happened. The final *N*-acetylated tosylchitins were characterized by FT IR, ^{1}H NMR and elemental analysis (Supporting Information). The degree of substitution (DS) by tosyl group was calculated by sulfur to nitrogen (S/N) ratio. The tosylchitins were then finally reacted with *N*,*N*-dimethylalkylamines to synthesize various quaternized chitin derivatives (Scheme 1). Nine different quaternary polymers were prepared: **1a-1c**, **2a-2c** and **3a-3c** by reacting Tsch 1 (DS ~39%), Tsch 2 (DS ~48%) and Tsch 3 (DS ~55%) with *N*,*N*-dimethyl dodecylamine, *N*,*N*-dimethyl tetradecylamine, and *N*,*N*-dimethyl hexadecylamine

respectively at 120 ˚C for 72 h (Scheme 3A.1). The quaternary polymers were characterized by FT-IR, ^{1}H-NMR, and elemental analysis.

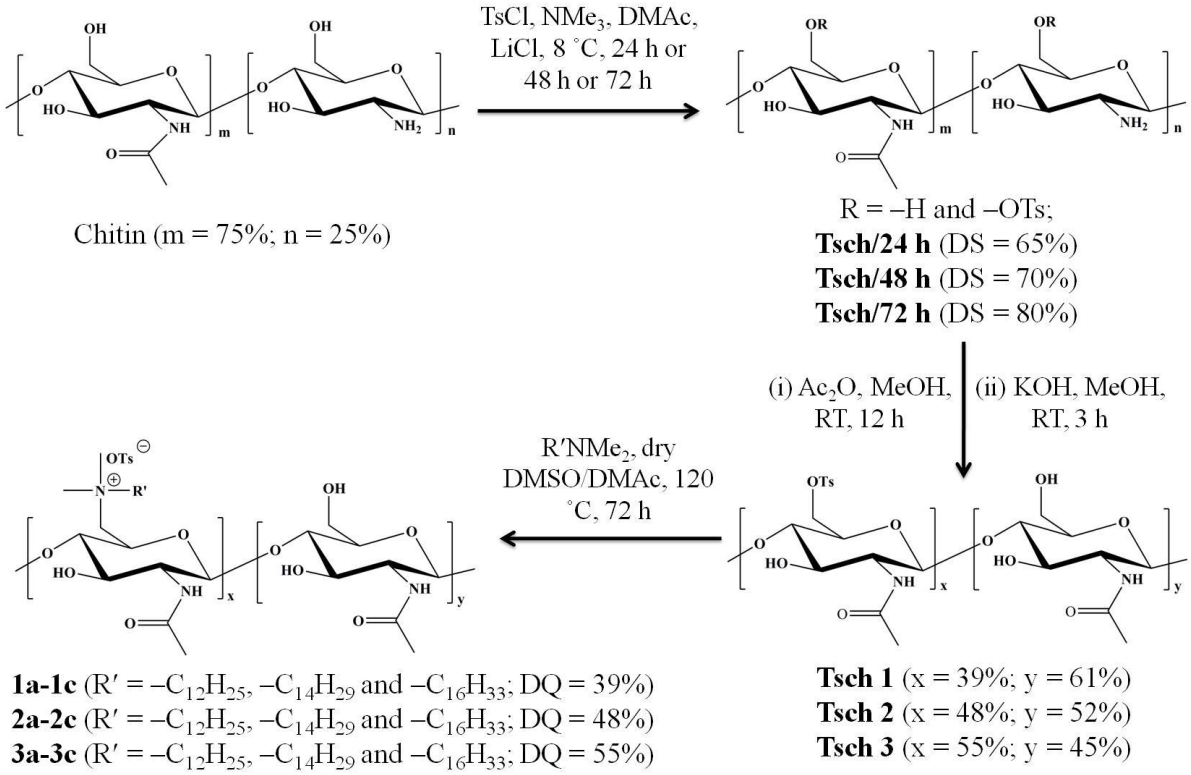

Scheme 3A.1: Synthesis of quaternary hydrophobic chitin polymers. DS = degree of substitution; DQ = degree of quaternization.

The quaternization of tosylchitins with *N,N*-dimethylalkylamines was confirmed from ^{1}H-NMR as the NMR spectra clearly revealed the presence of only two doublet aromatic peaks at δ ~7.1 and ~7.5 ppm corresponding to protons of benzene ring in tosylate anion of quaternized chitin derivatives. By this method, for the first time, it was possible to synthesize completely water-insoluble quaternary chitin derivatives. The molecular weights of the organo-soluble polymers were determined by gel permeation chromatography (GPC) using pullulan as standard. The range of weight-average molecular weight (M_w) of the polymers was found to be 1.05×10^5 to 2.17×10^5 Da depending on the degree of quaternization and length of the alkyl chain (Table 3A.1). The M_w of the polymers was found to increase with increase in both alkyl chain length as well increase in DQ (polydispersity index, PDI = 1.25-1.64). Solubility in water was tested by suspending the polymers in water, centrifuging the insoluble polymers after vigorous mixing followed by freeze drying the supernatant and recording NMR with the dried samples. If no detectable signals were observed in the NMR

spectra of the freeze dried samples the polymers were considered as water insoluble (within the detection limits of NMR). All the polymers except **1a** (**1b-1c**, **2a-2c**, and **3a-3c**) were found to be insoluble in water. The polymer **1a** (with $-C_{12}H_{25}$ long chain and 39% of degree of quaternization, DQ) was found to be slightly soluble in water (no further experiment was therefore performed with **1a**). However, all the polymers were found to be highly soluble in various organic solvents such as methanol, DMF, DMSO, etc.

Table 3A.1 Molecular weights of the polymers

Chitin derivatives	M_n	M_w	PDI
1a	64000	105000	1.64
1b	91000	139000	1.52
1c	100000	148000	1.48
2a	82000	128000	1.56
2b	124000	173000	1.39
2c	139000	183000	1.31
3a	126000	158000	1.25
3b	148000	214000	1.45
3c	159000	217000	1.36

M_n = Number-average molecular weight; M_w = weight-average molecular weight; PDI = polydispersity index; M_n and M_w are presented in Da.

3A.2.2 Antibacterial activity

3A.2.2.1 Activity by spray method

To establish the simplicity of the coating procedure, polystyrene plates, glass slides or cover glasses were coated using the solution of polymers in methanol by simple brush-or dip- or spin-coating or drop-casting. To simulate the natural deposition of airborne bacteria onto surface, a suspension of the human pathogenic bacteria in PBS buffer (pH 7.4) was sprayed onto non-coated (control) and the polymer-coated glass surfaces similarly as described in previous chapters. The slides were incubated at 37 ˚C for 24 h along with suitable agar to allow the bacterial growth. As expected, non-coated glass surface showed the presence of bacterial colonies thereby indicated the bacterial growth. However, less or no bacterial colony was observed on polymer-coated surfaces depending on the amount painted onto surface. For example, surfaces coated with **2c** (having $-C_{16}H_{33}$ long chain and DQ of 48%) showed (55 ± 5)%, (85 ± 7)%, and 100% reduction of viable *S. aureus* at 0.04 μg/mm^2, 0.08 μg/mm^2 and 0.15 μg/mm^2 with respect to non-coated glass surface. Similarly **2c** coated surface showed (15 ± 9)%, (45 ± 6)%, (75 ± 5)% and 100% reduction of viable *E. coli* at 0.15 μg/mm^2, 0.3 μg/mm^2, 0.6 μg/mm^2 and 1.2 μg/mm^2 (Figure 3A.1).

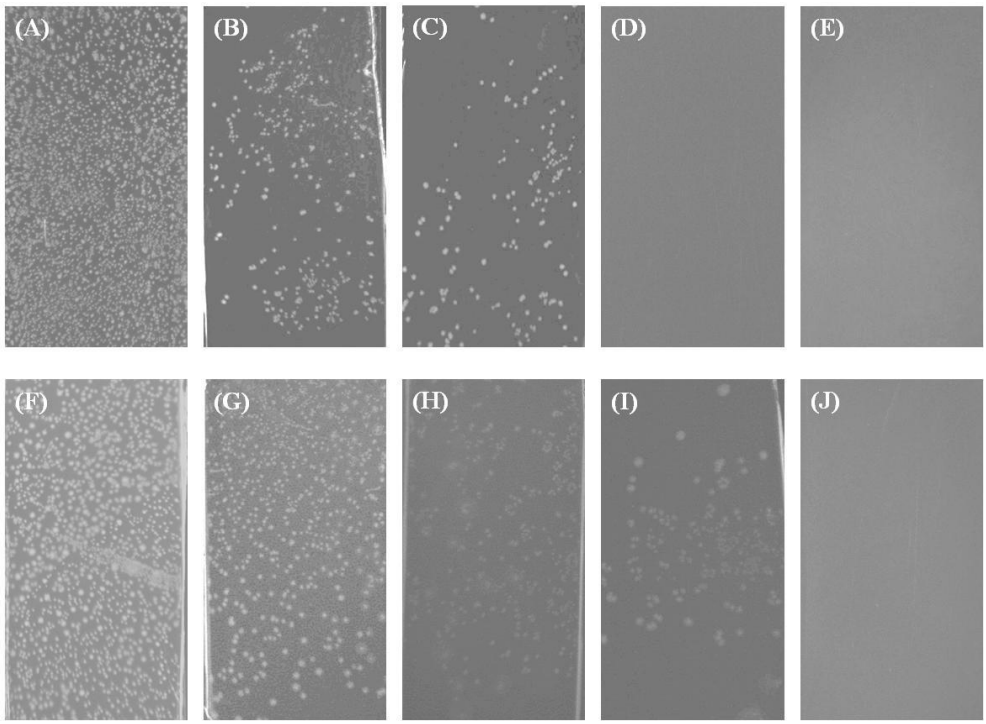

Figure 3A.1: Antibacterial activity of chitin derivatives. Photographs of microscopic glass slides: (A and F) non-coated glass slides (controls); (B and G) coated slides with 0.04 and 0.15 μg/mm^2 of **2c**; (C and H) coated slides with and 0.08 and 0.3 μg/mm^2 of **2c**; (D and I) coated slides with and 0.15 and 0.6 μg/mm^2 of **2c**; (E and J) coated slides with 0.3 and 1.2 μg/mm^2 of **2c**. Slides A-E for *S. aureus* and F-J for *E. coli* respectively. Each white dot corresponds to a bacterial colony grown from a single surviving bacterial cell.

Notably, polymer **1b** and **1c**-coated surfaces showed complete reduction of viable bacterial (100% activity) at 0.6 μg/mm^2 and 0.3 μg/mm^2 against *S. aureus* and, at 2.6 μg/mm^2 and 1.5 μg/mm^2 against *E. coli* respectively. Polymers **2a**, **2b** and **2c**-coated surfaces, on the other hand, exhibited 100% activity at 1.2 μg/mm^2, 0.6 μg/mm^2 and 0.15 μg/mm^2 against *S. aureus* and at 2.4 μg/mm^2, 2.4 μg/mm^2 and 1.2 μg/mm^2 against *E. coli* respectively. Polymers **3a**, **3b** and **3c** coated surfaces though showed 100% activity at 1.2 μg/mm^2, 0.6 μg/mm^2 and 0.3 μg/mm^2 against *S. aureus* but found to be inactive against *E. coli* till 12 μg/mm^2. Among all the polymers, **1c** and **2c** were found to be the two most active ones against both the bacteria (Figure 3A.2A-F). The high antibacterial activity of these polymers against both Gram-positive and Gram-negative bacteria thus demonstrated that these polymers could be potentially used as bactericidal paint in healthcare settings. Interestingly, polymer **2c** when coated onto the glass surface along with medically relevant polymer such as polylactic acid (PLA) showed antibacterial activity. It is noteworthy that the chitin polymers

even after loading with PLA were found to be equally active (e.g., 100% activity was observed for 0.15 μg/mm^2 of **2c** along with 2.5 μg/mm^2 of PLA against *S. aureus* and 1.2 μg/mm^2 of **2c** along with 2.5 μg/mm^2 of PLA against *E. coli* respectively) (Figure 3A.2G-L). These findings thus furnished that these chitin polymers could be used to develop self-defensive biomaterials.

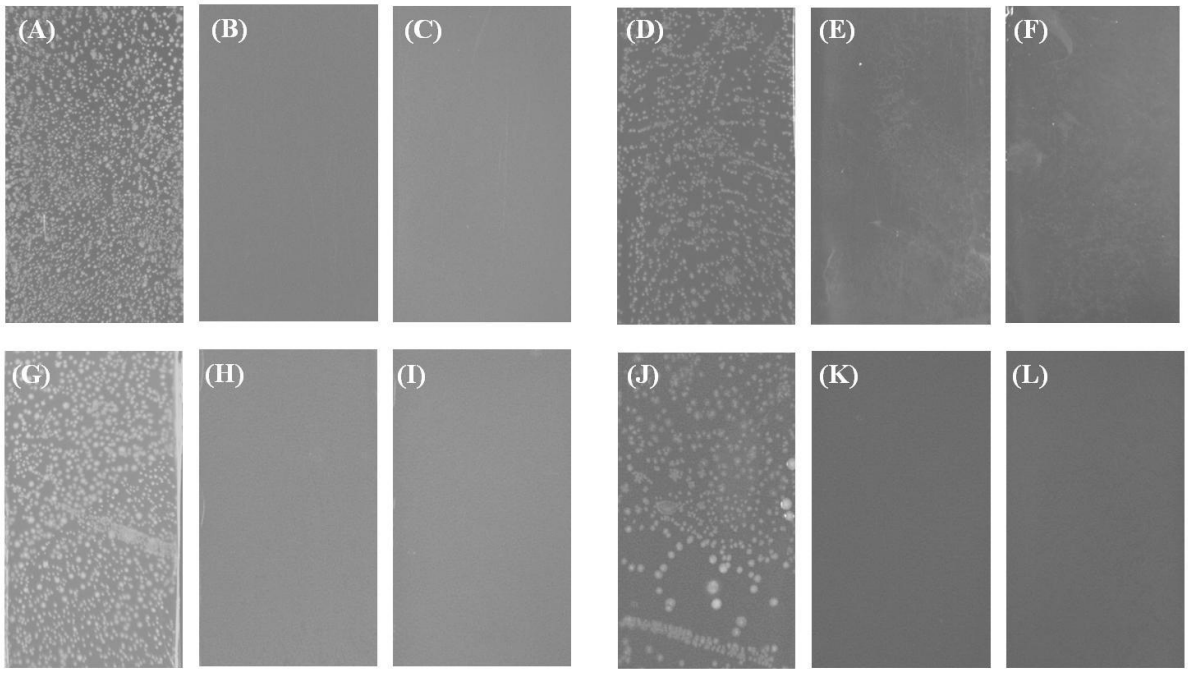

Figure 3A.2: Antibacterial activity of polymer coated surfaces. Photographs of microscopic glass slides after spraying bacteria and incubating for 24 h; (A) and (D): non-coated glass slides (controls); (B) and (E): slides coated with **1c** (0.3 and 1.5 μg/mm^2); (C) and (F): slides coated with **2c** (0.15 and 1.2 μg/mm^2); (G) and (J): slides coated with PLA (2.5 μg/mm^2); middle panel of (H) and (K): slides coated with (0.3 μg/mm^2 **1c** + 2.5 μg/mm^2 PLA) and (1.5 μg/mm^2 **1c** + 2.5 μg/mm^2 PLA); right panel of (I) and (L): slides coated with (0.15 μg/mm^2 **2c** + 2.5 μg/mm^2 PLA) and (1.2 μg/mm^2 **2c** + 2.5 μg/mm^2 PLA).

3A.2.2.2 Activity against water-borne bacteria (Minimum inhibitory amount)

After preparing the polymeric film in the polystyrene well plate, antibacterial efficacy of the coatings was determined by adding bacterial suspensions in nutrient broth. The activity, expressed as minimum inhibitory amount (MIA), i.e., the minimum amount required to inhibit the growth of bacteria, was represented similarly as mentioned in the previous chapters. The cationic polymers were found to inhibit the growth of both Gram-positive *S. aureus* and Gram-negative *E. coli* completely as observed by visual turbidity (Table 3A.2). The polymers showed different activity depending on the length of alkyl chain and the degree of quaternization (DQ). Among all the polymers, **1c** (with $-C_{16}H_{33}$ long chain and DQ of

39%) and **2c** (with $-C_{16}H_{33}$ long chain and DQ of 48%) were found to be most active polymers. MIA values of **1c** and **2c** were 0.12 μg/mm^2 and 0.06 μg/mm^2 against *S. aureus* and 3.9 μg/mm^2 each against *E. coli* (Table 3A.2). Interestingly, activity for the polymers with DQ 39% and 48% was found to increase with increase in alkyl chain length against Gram-positive *S. aureus* and remained almost unchanged against Gram-negative *E. coli* upon increasing chain length (Table 3A.2).

Table 3A.2 Antibacterial and hemolytic activities of polymer coated surfaces

Polymers	MIA (μg/mm^2)						HA_{50} (μg/mm^2)
	Wild type bacteria			Drug resistant bacteria			
	S. aureus	*E. coli*	*P. aeruginosa*	MRSA	VRE	*K. pneumoniae*	
1b	0.12	7.8	7.8	0.62	0.24	7.8	> 31.2
1c	0.12	3.9	15.6	0.32	0.12	7.8	> 31.2
2a	0.48	7.8	31.2	0.78	0.48	31.2	> 31.2
2b	0.24	3.9	15.6	0.39	0.24	15.6	> 31.2
2c	0.06	3.9	7.8	0.06	0.06	15.6	> 31.2
3a	0.24	15.6	31.2	0.32	0.24	> 31.2	> 31.2
3b	0.24	15.6	> 31.2	0.32	0.24	> 31.2	> 31.2
3c	0.12	31.2	> 31.2	0.24	0.32	> 31.2	> 31.2

MRSA = Methicillin-resistant *S. aureus* (ATCC 33591); VRE = vancomycin-resistant *E. faecium* (ATCC 51559); *K. pneumoniae* = beta-lactam-resistant *K. pneumoniae* (ATCC 700603)

For example, MIA values of **2a**, **2b**, and **2c** having $-C_{12}H_{25}$, $-C_{14}H_{29}$ and $-C_{16}H_{39}$ long chain and DQ of 48% were 0.48 μg/mm^2, 0.24 μg/mm^2 and 0.06 μg/mm^2 against *S. aureus* whereas MIA values of **2a**, **2b**, and **2c** were 7.8 μg/mm^2, 3.9 μg/mm^2 and 3.9 μg/mm^2 against *E. coli*. Antibacterial activity of the polymers with 55% DQ (**3a**, **3b** and **3c** having $-C_{12}H_{25}$, $-C_{14}H_{29}$ and $-C_{16}H_{39}$ long chain) was found to increase with increase in chain length against *S. aureus* (MIA values **3a**, **3b** and **3c** against *S. aureus* were 0.24 μg/mm^2, 0.24 μg/mm^2 and 0.12 μg/mm^2 respectively). However, the activity of **3a**, **3b** and **3c** was found to decrease with the increase in chain length against *E. coli* (MIA values **3a**, **3b** and **3c** were 15.6 μg/mm^2, 15.6 μg/mm^2 and 31.2 μg/mm^2 against *E. coli*) (Table 3A.2). The polymers also showed activity against *P. aeruginosa*, an opportunistic bacterium known to cause many nosocomial infections. The most active polymer **2c** showed and MIA of 7.8 μg/mm^2 against *P. aeruginosa*. Not only against drug-sensitive bacteria, surfaces coated with the polymers showed activity against various drug-resistant bacteria such as methicillin-resistant *S. aureus* (MRSA), vancomycin-resistant *E. faecium* (VRE), and beta-lactam-resistant *K. pneumoniae*

thus indicated the broad spectrum antibacterial nature. The two most potent polymers **1c** and **2c** showed MIA values of 0.32 μg/mm^2 and 0.06 μg/mm^2 against MRSA, 0.12 μg/mm^2 and 0.06 μg/mm^2 against VRE and 7.8 μg/mm^2 and 15.6 μg/mm^2 against beta-lactam resistant *K. pneumoniae* respectively (Table 3A.2). To establish how fast these polymers kill bacteria upon contact, the rate of action were investigated towards both *S. aureus* and *E. coli* using one of the most active polymers **2c** at MIA and 6 × MIA. Polymer **2c** killed *S. aureus* and *E. coli* (~5 log reduction) at 120 min and 240 min at 6 × MIA. These results thus indicate that the cationic hydrophobic polymer coatings have remarkably high killing rates against both the bacteria making them suitable for efficient antimicrobial coating.

The relatively lesser activity of the polymers with higher DQ or higher alkyl chain length (e.g., **3a**, **3b** and **3c)** against Gram-negative bacteria might be due to polymer aggregation because of highly hydrophobic nature of these polymers conferred by higher number of alkyl chains, which in turn is a consequence of higher degree of quaternization. This causes poor interactions with the cell surface of the Gram-negative bacteria, which possess an outer lipid membrane composed of lipopolysaccharides.[21] The above fact was supported by contact angle measurements as polymer with higher degree of quaternization (**3c,** $-C_{16}H_{33}$ long chain and DQ ~ 55%) showed static contact angle (θ_{avg}) of (112 ± 4)˚ whereas polymer with lower degree of quaternization (**2c**, $-C_{16}H_{33}$ long chain and DQ ~ 48%) showed θ_{avg} of (85 ± 2)˚ indicating that polymers with higher degree of quaternization are more hydrophobic.

Antibacterial activity of the chitin derivatives was also evaluated against various multi-drug resistant (MDR) clinical isolates. All the isolates were highly resistant to common antibiotics such as ampicillin, kanamycin, meropenem, ciprofloxacin, erythromycin, tetracycline, doxycycline and minocycline (MIC values of most of the antibiotics were >250 μg/mL) and were sensitive to only tigecycline and colistin (MIC = 0.5-1.0 μg/mL). The polymers were found to be highly active against the Gram-positive clinical strains and moderately active against the Gram-negative strains (Table 3A.3). One of the most active polymers, **2c** displayed MIA values of 0.06 μg/mm^2 each against two of the tested clinical isolates of MRSA. The polymer also showed activity against Gram-negative clinical isolates. However, unlike the Gram-positive bacteria, the most active polymer **2c** did not display good activity against Gram-negative strains. Interestingly, polymer **1b** (with $-C_{12}H_{25}$ alkyl chain and 39% DQ) showed activity against Gram-negative bacteria (MIA values of **1b** were 3.9, 2.0, 3.9 and 7.8 μg/mm^2 against multi-drug-resistant *E. coli*, *A. baumannii*, *P. aeruginosa* and

K. pneumoniae respectively. The above results thus emphasize the broad-spectrum nature of the cationic chitosan derivatives and show their potency as antibacterial agents.

Table 3A.3 Antibacterial activities of polymers against clinical isolates

Polymers	MIA ($\mu g/mm^2$)					
	MRSA R3889	MRSA R3889	*E. coli* R3597	*A. baumannii* R674	*P. aeruginosa* R590	*K. pneumoniae* R3421
1b	0.06	0.12	3.9	2.0	3.9	7.8
1c	0.06	0.06	>7.8	>7.8	>7.8	>7.8
2a	0.48	0.48	>7.8	7.8	7.8	>7.8
2b	0.24	0.24	>7.8	3.9	3.9	>7.8
2c	0.06	0.06	7.8	3.9	>7.8	>7.8
3a	2.0	3.9	>7.8	>7.8	>7.8	>7.8
3b	0.24	0.24	>7.8	>7.8	>7.8	>7.8
3c	0.12	0.12	>7.8	>7.8	>7.8	>7.8

MRSA = Methicillin-resistant *S. aureus*; 51559); *E. coli* = *Escherichia coli*; *K. pneumoniae* = *Klebsiela pneumoniae*; *A. baumannii* = *Acinetobacter baumannii*; *P. aeruginosa* = *Pseudomonas aeruginosa*

3A.2.3 Membrane-active mode of action

The membrane-active mode of action of the surface-immobilized cationic chitin polymers were studied against both *S. aureus* and *E. coli*. Sustaining membrane potential is an essential criterion for the bacteria to survive. The dissipation of the membrane potential was studied using a potential sensitive dye $DiSC_3(5)$ (3,3′-dipropylthiadicarbocyanine iodide).[13] All the polymers were found to depolarize the membrane potential of both the bacteria (Figure 3A.3A and B). The extent of depolarization was found to depend on degree of quaternization (DQ) and length of alkyl chain. Comparing the membrane depolarization ability of polymers containing the same alkyl chain length ($-C_{16}H_{33}$) but varying DQ (**1c**, **2c** and **3c**), it was observed that the polymer with 48% DQ (**2c)** was the most efficient. In case of polymers with same DQ but varying alkyl chain length (**2a**, **2b** and **2c**), **2c** (with $-C_{16}H_{33}$ alkyl chain) was the most effective in depolarizing the *S. aureus* cell membrane (Figure 3A.3A). On performing a similar study against *E. coli*, with the polymers of constant chain length but variable DQ (**1b**, **2b** and **3b**), **1b** (DQ = 39%) was most efficient. Polymers with same DQ and varying the alkyl chain length (**2a**, **2b** and **2c**), on the other hand, **2a** ($-C_{12}H_{25}$) was most effective in depolarizing the membrane potential of *E. coli* (Figure 3A.3B**)**. However, polymers with higher DQ (**3a-3c**) were found to be less effective in dissipating membrane potential of both the bacteria. The above results were in agreement with the antibacterial

efficacy displayed by these polymers. To further substantiate the mode of action of these polymers, leakage of intracellular K^+ ion was studied using potassium ion sensitive dye, PBFI-AM against both *S. aureus* and *E. coli* respectively.[14] All the polymers were found to cause leakage of intracellular K+ ion from both the bacteria and a similar structure activity relationship was observed in case of K^+ ion leakage as observed for membrane depolarization (Figure 3A.3C and D).

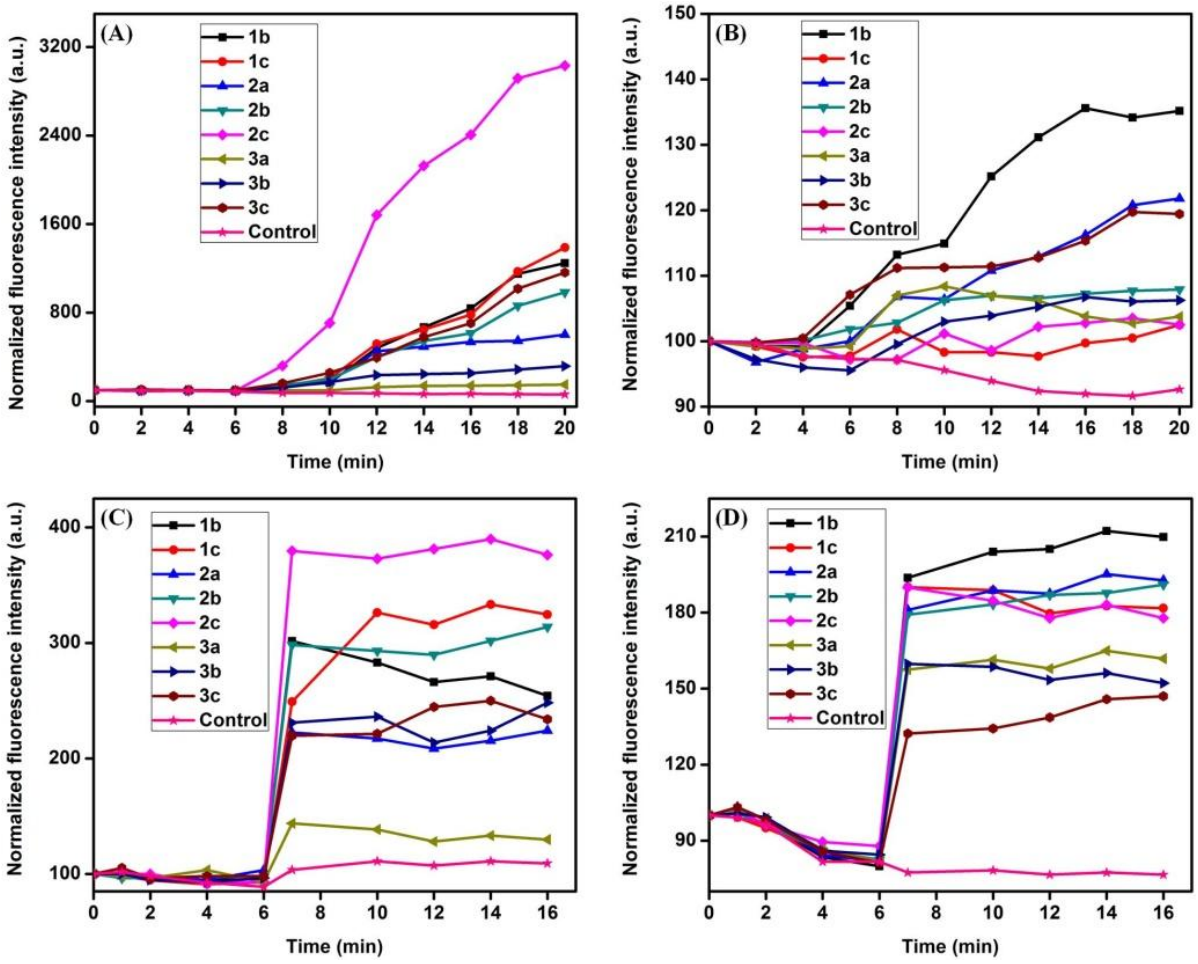

Figure 3A.3: Mechanism of antibacterial action. (A and B) Cytoplasmic membrane depolarization ability of polymers against *S. aureus* and *E. coli*; (C and D) intracellular K^+ ion leakage ability of polymers against *S. aureus* and *E. coli* respectively.

The mode of action of was further examined by fluorescence microscopy via live and dead assay using SYTO 9 and propidium iodide (PI) respectively.[15] The fluorescence microscopy images of non-treated samples showed green fluorescence for both *S. aureus* and *E. coli* thereby indicated the cell viability in control samples (Figure 3A.4A and C). However, images of the cells treated with the **2c**-coated surface showed red fluorescence of PI thereby indicated membrane disruption for both *S. aureus* and *E. coli* (Figure 3A.4B and D). To

visualize the morphological changes in the treated bacteria, scanning electron microscopy (SEM) was used to image both **2c**-treated and non-treated bacteria.[16] The SEM images of the untreated bacteria showed smooth and well-defined surface characteristic of unperturbed bacteria against both *S. aureus* and *E. coli* respectively (Figure 3A.4E and G). On the other hand, treated bacteria showed rough and deformed cell surface thereby indicated perturbation of the cell surface for both *S. aureus* and *E. coli* respectively (Figure 3A.4F and H).

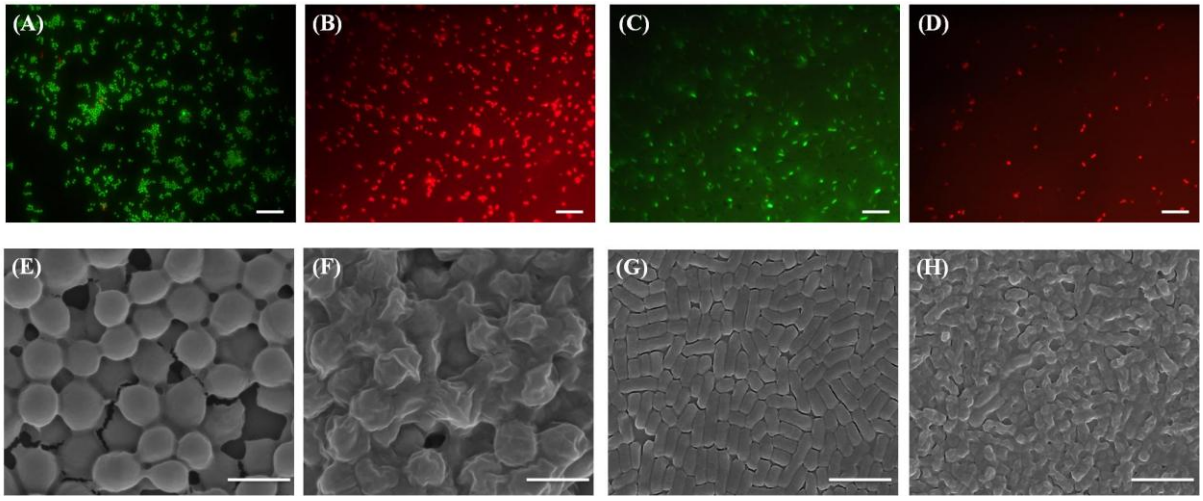

Figure 3A.4: Mechanism of antibacterial action. Fluorescence microscope images of *S. aureus* (A and B) and *E. coli* (C and D) cells after a 4 h exposure to the uncoated surfaces (A and C) and surfaces coated with the **2c** (B and D). Live (green) and dead (red) cells were stained with staining agents SYTO 9 and propidium iodide (PI) respectively. Scale bar 20 μm. Scanning electron microscope images of *S. aureus* (E and F) and *E. coli* (G and H) cells after a 2 h exposure to the uncoated surfaces (E and G), surfaces coated with the polymer **2c** (F and H). Scale bar 1 μm for (E and F) and 3 μm for (F and H) respectively.

3A.2.4 Biofilm inhibition ability

The antibiofilm properties of one the most active polymers (**2c**) was evaluated by coating the polymers onto glass surface and determining efficacy of the polymer in inhibiting bacterial biofilm formation under stationary conditions.[17] Glass cover slips coated with **2c** at two different amounts (MIA and 6 × MIA) were challenged under stationary conditions for 24 h against *S. aureus* and 72 h against *E. coli* respectively. The cover slips were then imaged by confocal laser scanning microscopy (CLSM) after 24 h for *S. aureus* and 72 h for *E. coli* respectively. The non-coated cover slips showed huge bacterial growth with an effective thickness of 16-20 μm thus indicating thick and matured biofilm formation for both *S. aureus* and *E. coli* respectively (Figure 3A.5A and D).

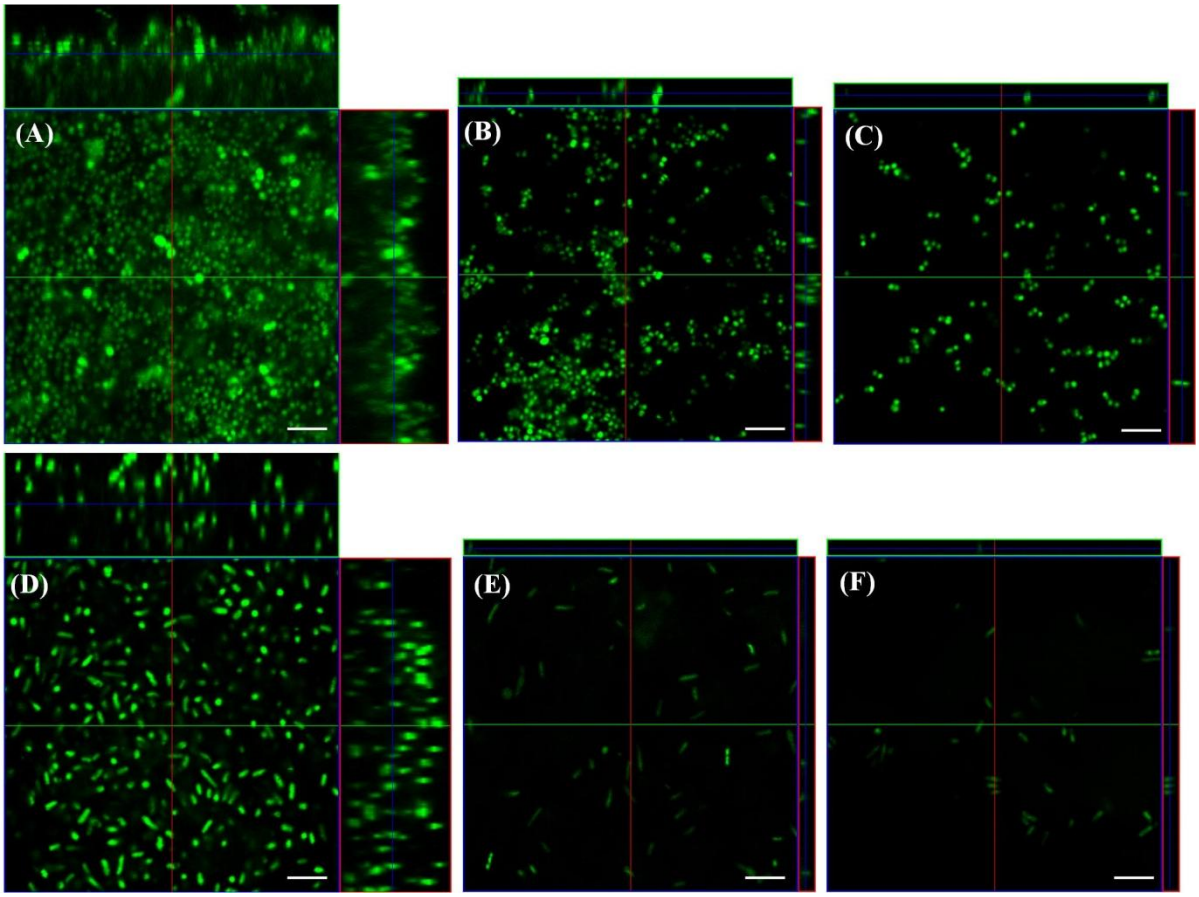

Figure 3A.5: Antibiofilm activity of the polymeric coating. Confocal laser scanning microscopy images of (A and D) non-coated cover glass; (B and E) cover glass coated with 0.06 μg/mm^2 and 3.9 μg/mm^2 and (C and F) with 0.36 μg/mm^2 and 23.4 μg/mm^2 respectively. A-C for *S. aureus* and D-F for *E. coli* respectively. Scale bar 5 μm.

Interestingly, polymer-coated surfaces showed fewer bacteria with an effective thickness of 2-4 μm thereby indicating the presence of only mono-layered bacteria at 6 × MIA values against both *S. aureus* and *E. coli* respectively (Figure 3A.5C and F). Further, when the bacterial counts were determined in the biofilms, (9±0.7) log reduction of *S. aureus* and (8±0.6) log reduction of *E. coli* were observed for the polymer coated surface at 6 × MIA compared to noncoated surface (the control surfaces showed 13.2 log CFU/mL of *S. aureus* and 11.6 log CFU/mL of *E. coli* respectively).

Not only against drug sensitive but the polymer showed excellent efficacy in inhibiting biofilm formation against multi drug-resistant clinical isolates. When tested under similar conditions, the polymer coated glass surfaces inhibited formation of biofilm for the clinical isolates of both MRSA and E. coli. While the non-coated cover slips showed huge bacterial biofilm with the effective thickness of 15-20 μm indicative of highly dense and matured biofilm formation for both MRSA and *E. coli* clinical isolates (Figure 3A.6A and D),

2c coated glass surfaces inhibited biofilm formation at its MIA values (Figure 3A.6B and E). The coated surfaces showed high efficacy in inhibiting biofilm formation at 6 × MIA as only few bacteria were observed for both the strain on the surface with no biofilm (Figure 3A.6C and F). The above results thus indicated that the cationic chitin polymer prevents bacterial colonization onto the surface.

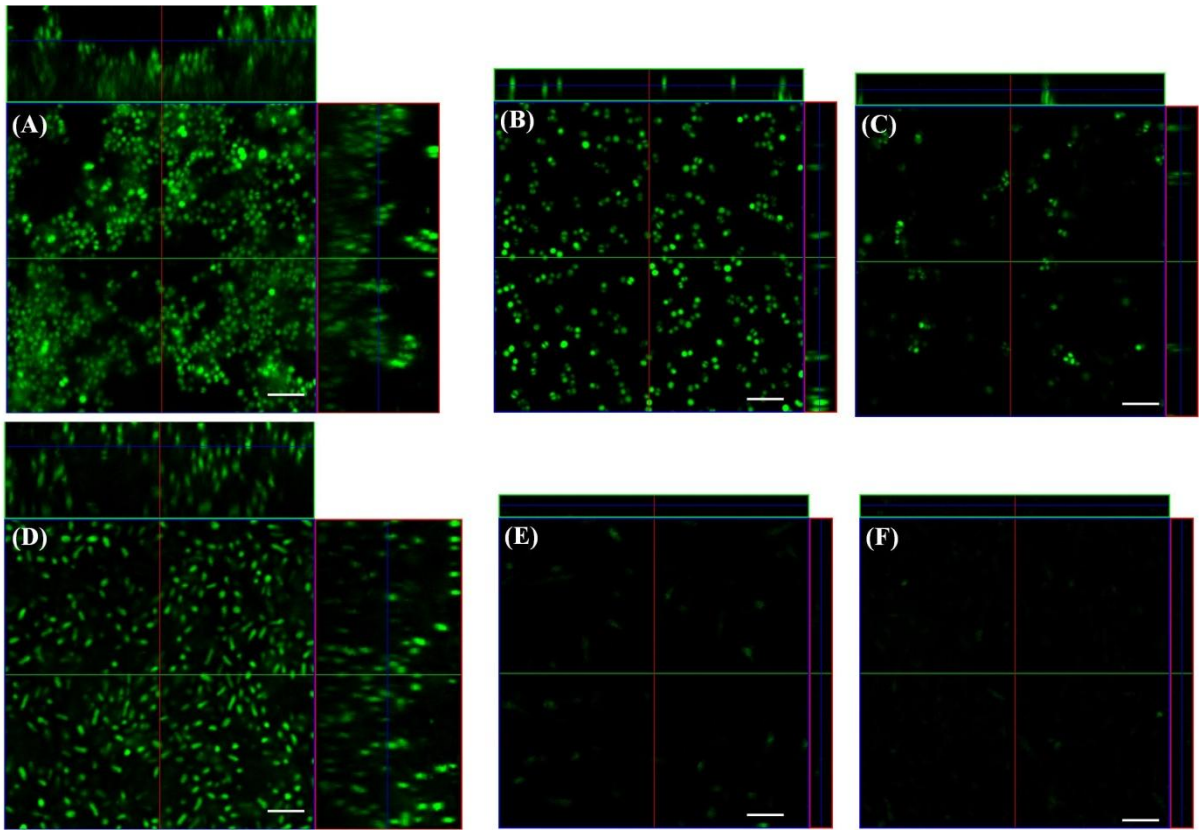

Figure 3A.6: Biofilm inhibition ability of the polymeric coating. Confocal laser scanning microscopy images of (A and D) non-coated cover glass; (B and E) cover glass coated with 0.12 μg/mm^2 and 3.9 μg/mm^2 and (C and F) with 0.48 μg/mm^2 and 23.4 μg/mm^2 respectively. A-C is for MRSA clinical isolate and D-F for *E. coli* clinical isolate respectively. Scale bar 5 μm.

3A.2.5 Antifungal activity

3A.2.5.1 Minimum inhibitory amount

Antifungal efficacy of all the polymers were evaluated against different pathogenic *Candida* spp. (*C. albicans*, *C. dubliniensis*, *C. tropicalis*) and *Cryptococcus* spp. (*C. neoformans var. grubii* (serotype A), *C. gattii* (serotype B) and *C. neoformans var. neoformans* (serotype D)). Like bacteria, the polymers with different hydrophobic/hydrophilic balance showed different activity against fungi (Table 3A.4). Among all the polymers, **1c** (with $-C_{16}H_{33}$ long chain and DQ of 39%) and **2c** (with $-C_{16}H_{33}$ long chain and DQ of 48%) were found to be most active

polymers. MIA values of **1c** and **2c** were 0.06-1.0 μg/mm^2 and 0.12-2.01 μg/mm^2 against the fungal species tested (Table 3A.4). Importantly, activity for the polymers with DQ 39% and 48% was found to increase with increase in alkyl chain length against *Cryptococcus* spp and found to remain almost unchanged against *Candida* spp.

Table 3A.4 Antibacterial activities of polymers against pathogenic fungi

Polymers	MIA (μg/mm^2)					
	C. albicans	*C. dubliniensis*	*C. tropicalis*	*C. neoformans Ser A*	*C. neoformans Ser B*	*C. neoformans Ser D*
1b	1.0	1.0	0.12	1.0	0.24	0.48
1c	2.0	0.48	0.12	0.12	0.12	0.24
2a	1.0	0.48	0.24	2.0	0.48	0.48
2b	1.0	1.0	0.48	1.0	0.24	0.48
2c	1.0	1.0	0.24	0.48	0.12	0.06
3a	>7.8	7.8	2.0	7.8	7.8	1.0
3b	7.8	3.9	0.2	2.0	0.48	0.24
3c	>7.8	2.0	0.2	0.24	0.24	0.24

C. albicans = Candida albicans; *C. dubliniensis = Candida dubliniensis*; *C. tropicalis = Candida tropicalis*; *C. neoformans Ser A = Cryptococcus neoformans Ser A*; *C. neoformans Ser B = Cryptococcus neoformans Ser B*; *C. neoformans Ser D = Cryptococcus neoformans Ser D*

For example, MIA values of **2a**, **2b**, and **2c** having $-C_{12}H_{25}$, $-C_{14}H_{29}$ and $-C_{16}H_{39}$ long chain and DQ of 48% were 2.0 μg/mm^2, 1.0 μg/mm^2 and 0.12 μg/mm^2 against *C. neoformans Ser A* whereas MIA values of the polymers were 1.0 μg/mm^2, 1.0 μg/mm^2 and 2.0 μg/mm^2 against *Candida albicans* respectively. Antifungal activity of the polymers with 55% DQ (**3a**, **3b** and **3c** having $-C_{12}H_{25}$, $-C_{14}H_{29}$ and $-C_{16}H_{39}$ long chain) was found to increase with increase in chain length against *Cryptococcus* spp., *C. dubliniensis* and *C. tropicalis* (MIA values **3a**, **3b** and **3c** against *C. neoformans Ser A* were 7.8 μg/mm^2, 2.0 μg/mm^2 and 0.2 μg/mm^2 respectively). However, the activity of these highly hydrophobic polymers (**3a**, **3b** and **3c**) was found to be very low against *C. albicans* (Table 3A.4). Interestingly, polymers **1c** and **2c** showed remarkable antifungal activity against *C. albicans*. For example, MIA values of **1c** and **2c** were 1.0 μg/mm^2 and 2.0 μg/mm^2 against *Candida albicans*. The above facts therefore indicated these polymers could be used as potent antifungal materials. The high antifungal activity of the chitin derivatives against all the fungal species tested could be due to a likely interaction with the fungal cell membrane which also contains chitin as one of its structural components. The polymers were not only fungistatic but also fungicidal. For example, the

minimum fungicidal amount (MFA) of the most potent polymer **2c** was found to be 1.0 μg/mm^2 and 0.48 μg/mm^2 against *C. albicans* and *C. neoformans* Ser A respectively.

3A.2.5.2 Fungicidal rate kinetics

To establish how fast these polymers kill fungi upon contact, the rate of action was investigated against *C. albicans* using surfaces coated with polymer **2c**. The coated surface killed *C. albicans* within 4-6 hours at 8 × MIA. Even at MIA, the polymer killed the fungal cells at 6-8 hours (Figure 3A.7A).

3A.2.5.3 Membrane-active modes of action

To see whether these hydrophobic polycations interact with and damage the cell membrane of fungi, LIVE/DEAD assay was performed with the fungal cell using SYTO 9 and PI dyes by fluorescence microscopy in a similar way as described for bacteria previously. *C. albicans* was used a model fungus and treated with one of the most active polymers **2c**. The microscopy images showed the presence of viable cells in case of control samples (plain surface) as observed by green fluorescence (Figure 3A.7B). The cells treated with the polymer-coated surfaces on the other hand showed red color fluorescence of PI thus indicating the compromised cell membrane (Figure 3A.7C). These results indicate that the cationic polymers interact with the fungal cell membrane and disrupt the integrity of the membrane presumably leading to cell death.

3A.2.5.4 Biofilm inhibition ability

The antibiofilm properties of one of the most active polymers **2c** was evaluated by coating the polymers onto the wells of 6-well plate and determining efficacy of the polymer in inhibiting fungal biofilm formation under stationary conditions. Wells coated with **2c** at two different amounts (MIA and 2 × MIA) were challenged against *C. albicans*, one of the most common pathogenic fungi that often forms biofilm on virtually any surface. The wells were then imaged by CLSM after 48 h. The non-coated wells showed huge fungal growth indicative of biofilm formation (Figure 3A.7D). In contrast, the polymer at MIA inhibited biofilm formation significantly (Figure 3A.7E). Interestingly, polymer-coated surfaces showed almost no biofilm formation by *C. albicans* thereby indicated high efficacy in inhibiting fungal biofilms (Figure 3A.7F). The above facts indicated that these cationic chitin derivatives are extremely potent in inhibiting microbial biofilm formations.

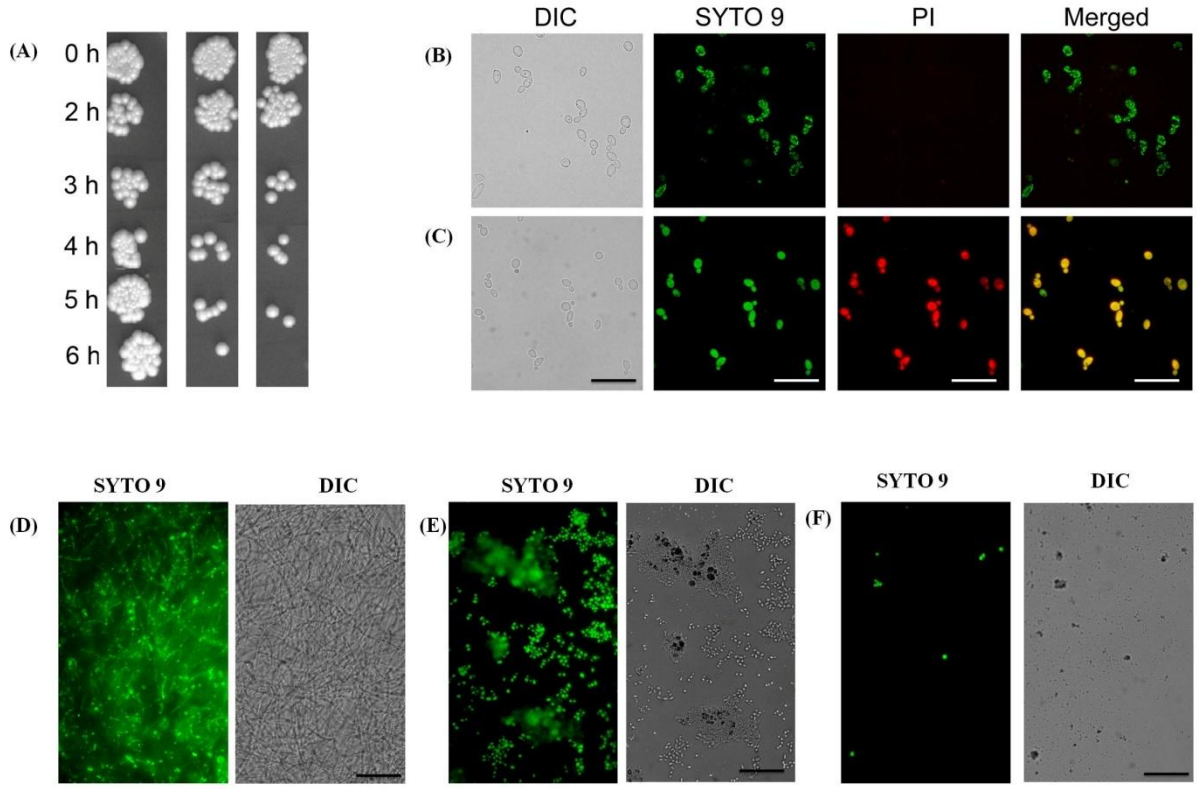

Figure 3A.7: Antifungal activities of chitin derivatives. (A) Antifungal kinetics of polymers 2**c** coated surfaces at different amounts (MIA and 8 × MIA) against *C. albicans*: representative cross section of the YPD agar plate showing the growth of fungal colonies at different times. Mechanistic investigation of antifungal activity of polymer coatings. Fluorescence microscopy images of *C. albicans* after staining with SYTO 9 and PI exposed to (B) uncoated surfaces (control) and (C) surfaces coated with **2c**. Scale bar 20 μm. Antibiofilm activity of chitin derivative coated surface: (D) Non-coated surface; (E and F) 2c-coated surfaces at MIA and 2 × MIA respectively. Scale bar 40 μm.

3A.2.6 Biodegradation

3A.2.6.1 *In-vitro* biodegradation

To establish the degradability of the cationic chitin derivatives, a thin film of the polymers was prepared onto cover slip and treated with the lysozyme over a period of time.[18] Finally the rate of degradation was calculated by the loss of weight from the films after different time interval. All the tested polymers (**1b**, **1c** and **2c**) were found to degrade in the presence of lysozyme under *in vitro*. The length of the alkyl chain (tetradecyl in **1b** *vs* hexadecyl in **1c**) or the extent of DQ (39% in **1c** *vs* 48% in **2c**) found to have minimal effect on the rate or degree of hydrolysis at the experimental conditions (Figure 3A.8A). All the polymers showed 10-14% degradation under the experimental conditions. Notably, the rate of degradation of the

cationic chitin derivatives was found to be slow than chitin possibly due to the chemical modification at the repeating unit.[19]

3A.2.6.2 *In-vivo* biodegradation

To further confirm the nature of biodegradation of chitin polymers, polymer disks were implanted subcutaneously in rat's body.

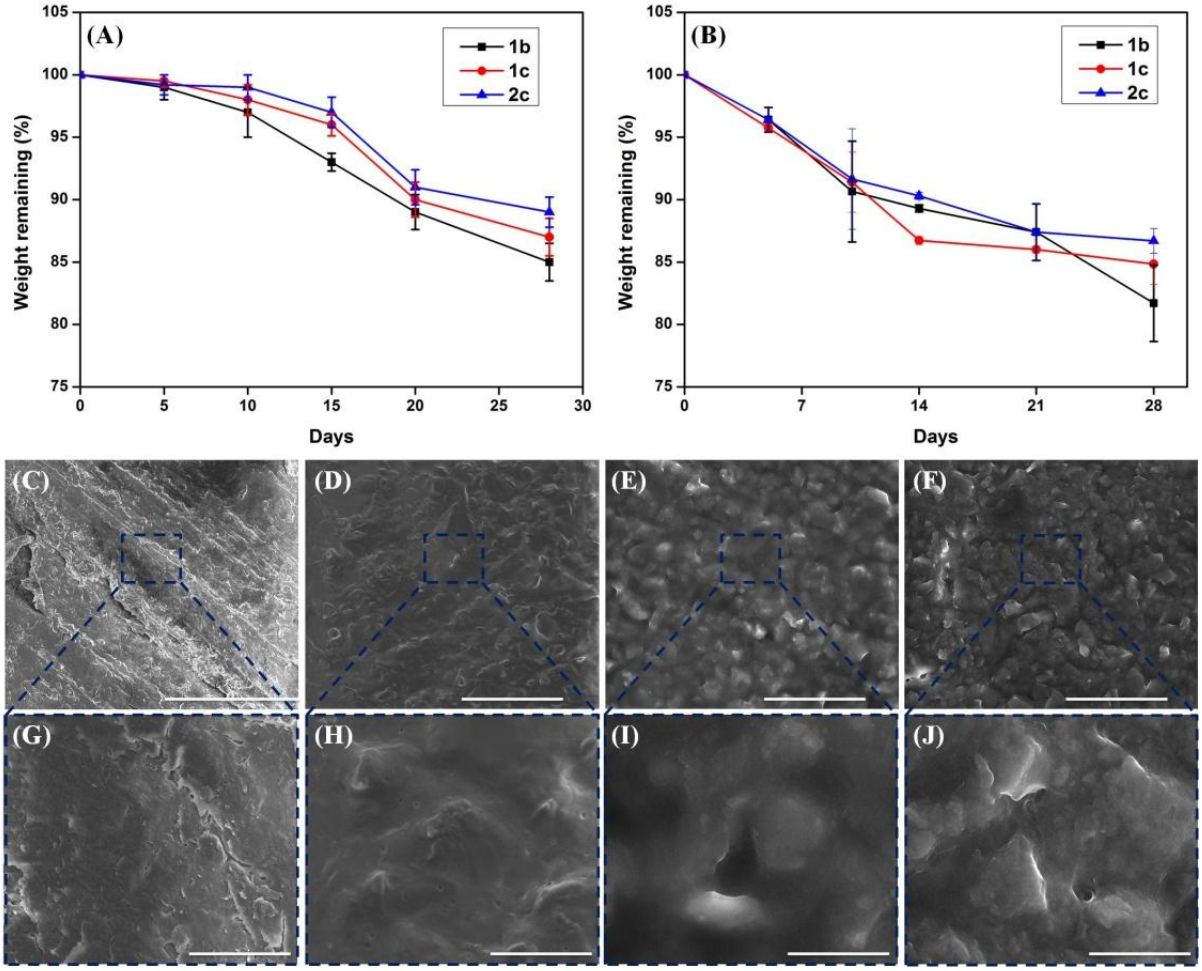

Figure 3A.8: Biodegradation of polymers. (A) *In-vitro* degradation in the presence of lysozyme by weight-loss method; (B) *in-vivo* degradation upon subcutaneous implantation of disc of polymer in rat by weight-loss method. Scanning electron microscopy images of disc of polymer **2c**: (C and G) surface of the untreated disc; (D and H) surface of the disc after 14 days; (E and I) surface of the disc after 21 days and (F and J) surface of the disc after 28 days. (C-F) Represents low resolution images and (G-J) high resolution images respectively.

The rate of degradation was then studied after harvesting the disk from the rat's body after different time period and measuring the loss of weight. All the tested polymers with different DQ and alkyl chain length were found to degrade under in-vivo conditions as well. Polymer **1b** showed ~20% degradation as compared ~16% and ~15% degradation of **1c** and **2c** after 4

weeks of implantation (Figure 3A.8B). Overall, the rate of degradation of the polymers was slightly higher *in-vivo* than *in-vitro*. The polymer discs were also imaged by scanning electron microscopy to visualize the morphological changes of the surfaces of discs due to degradation. The treated discs showed porous structures with holes as compared to the non-treated polymer disc after day 14, 21 and 28 (Figure 3A.8C-F). Further, it was observed that with time both the number of pores and pore size increased thereby indicating the gradual degradation of the polymer under *in vivo* conditions (Figure 3A.8G-J).

3A.2.7 Biocompatibility

3A.2.7.1 *In-vitro* toxicity

Hemocompatibility of the polymer coated surfaces was determined with human erythrocytes and was expressed as HA_{50} (the amount of the coated polymer that caused 50% hemolysis). The polymers were found to be almost non-hemolytic upto 7.8 $\mu g/mm^2$. Only 20-30% hemolysis was observed even at 31.2 $\mu g/mm^2$ of polymer paint (Figure 3A.9A). Notably, **1c** and **2c**, the two most active polymers caused 5.8% hemolysis up to 12.5 $\mu g/mm^2$ which was much higher compared to their MIA values (Table 3A.2). These results thus indicated the polymers are selectively active toward bacteria. To visualize the effect, both treated and non-treated hRBC were also imaged microscopy (Figure 3A.9B). The images show RBCs taken from polymer coated surface as well as from the non-coated surface. The blood cells displayed characteristic healthy and round morphology, indicating that the polymer-coated surfaces are non-hemolytic. In contrast, when the highly toxic detergent triton-X (0.5%, v/v) was added, full hemolysis was observed as no hRBC was seen under the microscope.

3A.2.7.2 *In-vivo* toxicity

The compatibility of the polymeric paint was further assessed under *in-vivo* conditions by coating medical grade catheter and implanting the coated catheter subcutaneously in mice.[20] After 4 days, mice were euthanized and tissue surrounding the catheter were collected, fixed in formalin and then analyzed. The tissue surrounding the catheter was imaged by haematoxylin and eosin staining and inflammatory responses were seen. Tissue samples surrounding the catheters coated with 2.5 $\mu g/mm^2$, 5.0 $\mu g/mm^2$ and 7.5 $\mu g/mm^2$ of polymer showed minimal to mild inflammation after 4 days of implantation (like tissue surrounding the non-coated catheters (Figure 3A.9C-F).

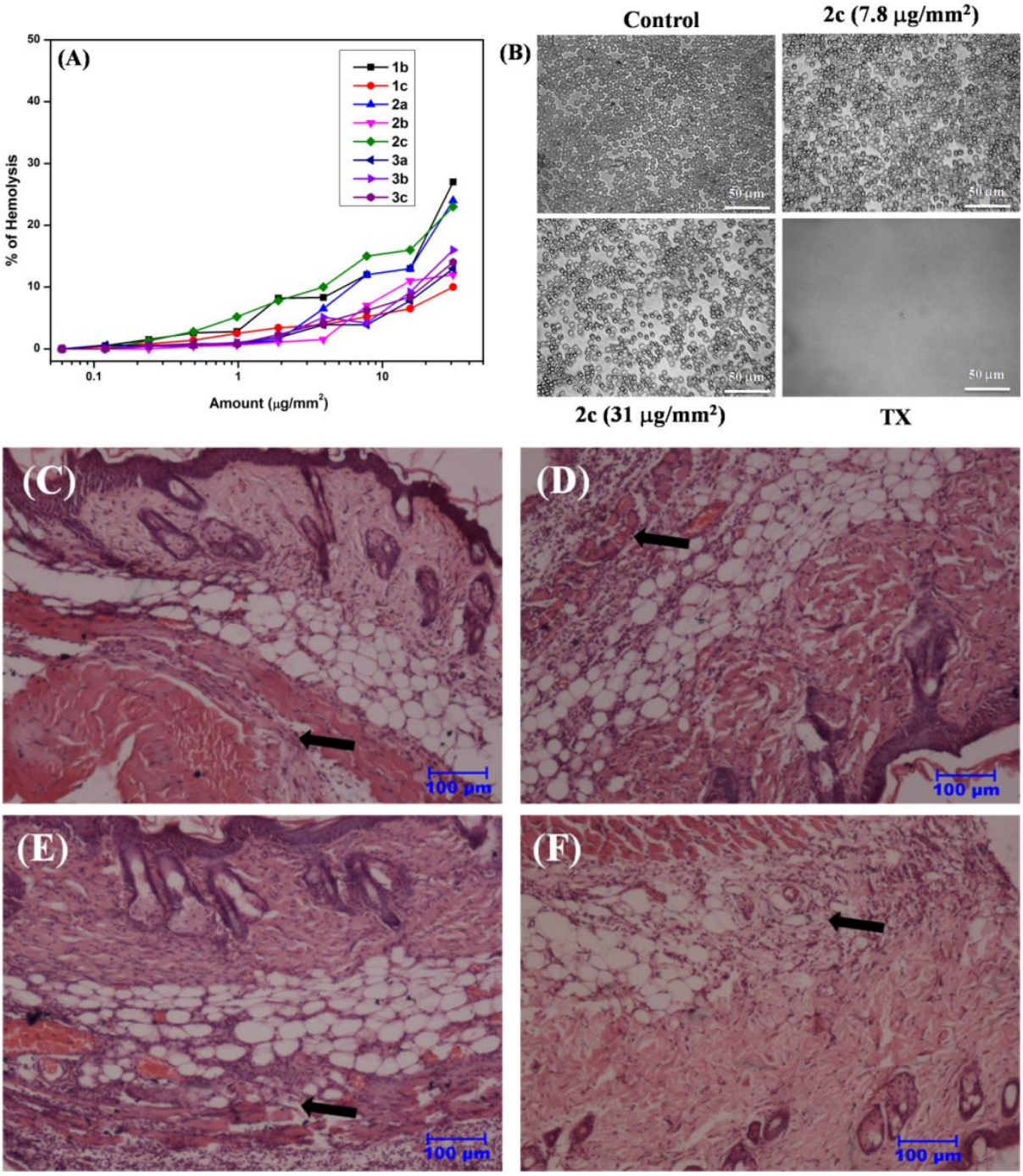

Figure 3A.9: *In-vitro* and *in-vivo* biocompatibility of the polymers. (A) % of Hemolysis of polymers as a function of the amount of polymer-coating; (B) phase-contrast images of erythrocytes taken from the polymer-coated surfaces or from the control TCTP surface with and without TX (Triton-X). Mice skin and subcutaneous tissue histopathology: (C) tissue showing normal architecture of epidermis, dermis and subcutaneous tissues surrounding the non-coated catheter (arrow); (D) tissue showing normal skin epidermis and dermis layer with normal adipose tissue surrounding the catheter in subcutaneous tissues (arrow) surrounding the catheter coated with 2.5 μg/mm^2 of **2c**; (E) tissue showing normal dermis layer of skin with sweat and sebaceous gland along with mild infiltration of inflammatory cells (arrow) surrounding the catheter coated with 5.0 μg/mm^2 of **2c**; (F) tissue showing only few infiltrations of inflammatory cells with neutrophils (arrow) with intact epidermis and dermis layer surrounding the catheter coated with 7.5 μg/mm^2 of **2c**.

3A.2.8 *In-vivo* activity and biofilm inhibition

While many polymers display potent *in vitro* antibiofilm efficacy, lack of activity under more complex *in vivo* conditions has been one of the major drawbacks for the antibacterial polymers. Herein *in vivo* antibacterial and antibiofilm efficacies of the polymers were assessed by implanting medical grade polymer-coated catheters (polyurethane, 5 Fr, 12 mm) subcutaneously in mice against methicillin-resistant *S. aureus* (MRSA) infection-one of the most leading biofilm forming bacteria in healthcare and clinical settings. Catheter samples were given bacterial load of ~1.7×10^7 CFU of MRSA at the time of implantation in mice (a quantity greater than that would be encountered in clinical settings). After 96 h, the control samples showed bacterial burden of 7.4 log CFU/catheter thereby showed the prevalence and growth of MRSA. On the other hand, the coated catheter samples showed reduction in bacterial count depending on the amount of the polymer coated. Catheter coated with ~2.5 μg/mm^2 of the polymer showed 1.2 log reduction in bacterial count ($p = 0.0232$) whereas coated-catheter with 5.0 μg/mm^2 of polymer showed a reduction of 2.5 log CFU of MRSA ($p = 0.013$). However, catheter coated with 7.5 μg/mm^2 of polymer showed 3.7 log CFU of MRSA reduction with significant p value ($p < 0.0001$) (Figure 3A.10A). To see bacterial prevalence in the surrounding tissue of the contaminated catheter, tissue samples surrounding catheter were also collected and analysed for cell counting. It was observed that the tissue samples surrounding to 2.5 μg/mm^2 coated catheter displayed only 1.7 log reduction compared to control. However, the tissue samples surrounding to 5.0 μg/mm^2 and 7.5 μg/mm^2 **2c**-coated catheters showed significant bacterial reduction compared to control (2.7 log and 3.5 log of bacterial reduction (p values are 0.0001 and <0.0001) (Figure 3A.10B). Finally, to evaluate the potential of the polymer coating in inhibiting bacterial biofilm formation, we visualized the implanted catheter using SEM. Uncoated catheter displayed large amount of bacteria in multiple layers thus indicated a thick biofilm formation (Figure 3A.10C). In contrast, polymer coated catheter (at 7.5 μg/mm^2) revealed a fewer amount of bacteria with no cell clusters thus indicating no biofilm formation onto the surface (Figure 3A.10D). The above results thus portrayed the efficacy of the polymer coatings in killing bacteria and inhibiting biofilm inhibition under *in vivo* conditions.

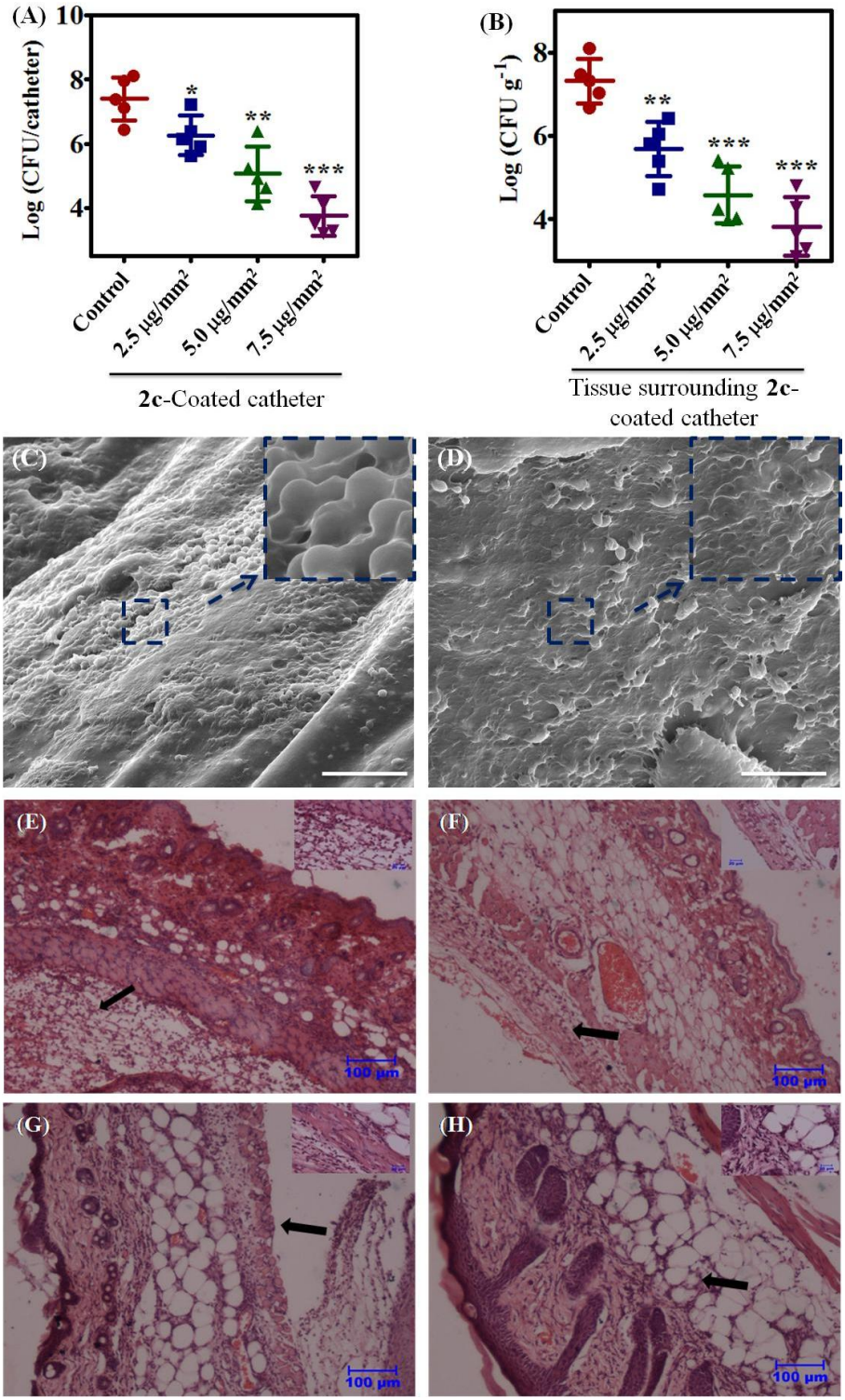

Figure 3A.10: *In-vivo* antibacterial activity of polymer-coated catheters. Effect of polymer-coated catheters on MRSA inoculated at the time of catheter insertion: (A) bacterial count after harvesting catheter from mice; (B) bacterial count from the catheter surrounding tissue samples; p value (*) is <0.0001 for **2c** at 7.5 μg/mm^2. Field emission scanning electron microscopy (FESEM) images of (C) non-coated catheter and (D) **2c**-coated catheter (inset showing the high resolution microscopy images). Mice skin and subcutaneous tissue histopathology: (E) tissue surrounding MRSA infected non-coated catheter; tissue surrounding MRSA-infected catheter coated with (F) 2.5 μg/mm^2 of polymer **2c**; (G) coated

with 5.0 μg/mm^2 of polymer 2c and (H) coated with 7.5 μg/mm^2 of polymer **2c**. Cells were stained with haematoxylin and eosin staining agents. Insets are the high resolution images.

Histology was performed to evaluate the inflammatory responses towards MRSA in the skin and subcutaneous tissue level surrounding both coated and non-coated catheters. Non-coated catheters infected with MRSA showed severe infiltration of inflammatory cells mainly neutrophils and mononuclear cells in the subcutaneous tissues with congestion of blood vessels (inset) surrounding the catheter and severe damage to dermis layer of skin (Figure 3A.10E). In contrast, tissue surrounding catheter coated with ~2.5 μg/mm^2 of polymer showed moderate infiltration of inflammatory cells (arrow) mainly with neutrophils (inset) and moderate damage to skin dermis layer thereby indicating slight reduction of MRSA count (Figure 3A.10F). However, tissues nearby to catheter coated with ~5.0 μg/mm^2 and ~7.5 μg/mm^2 of **2c** showed normal epidermis layer of skin with sweat and sebaceous gland along with mild-to-negligible infiltration of inflammatory cells (arrow) with neutrophils and mononuclear cells (inset) (Figure 3A.10G and H). The above results thus portrayed the potential of the polymers in inhibiting the bacterial colonization onto surfaces.

3A.2.9 Propensity of bacterial resistance development

Propensity of microbial (e.g., bacterial) resistance development against these polymers was assessed by serial exposure of bacteria to the polymer-coated surfaces. The most active chitin derivative (**2c**) was challenged with the bacteria grown at the sub-MIA level of the polymer for Gram-positive *S. aureus* and Gram-negative *E. coli*. After 14 serial passages, the MIAs of polymer remained almost same (only 2-3 fold increase) whereas norfloxacin, a nucleic acid targeting Gram-positive antibiotic, showed 269 fold increase in MIC against sensitive *S. aureus* and colistin, a lipid II targeting Gram-negative lipopeptide, showed 125 fold increase in MIC against sensitive *E. coli* respectively. These membrane-active polymers were thus able to stall the development of bacterial resistance and therefore could be suitable for use in clinical settings.

3A.3. Conclusion

A simple method of developing biodegradable antimicrobial paint based on water-insoluble and organo-soluble cationic hydrophobic chitin polymers was developed. Surfaces coated with polymers were shown to kill both drug-sensitive and drug-resistant bacteria including multi drug-resistant clinical isolates. The polymers showed excellent compatibility with other

polymers suitable for developing self-defensive biomaterials. The hydrophobically modified polymers were shown to inactivate both bacteria and fungi by disrupting their cell membrane-integrity. Importantly, surfaces coated with the polymers inhibited various pathogenic bacterial and fungal biofilm formations on them. The polymers were shown to be non-hemolytic towards human erythrocytes and minimal inflammation towards surrounding tissue *in-vivo* in mice. Catheter coated with polymer not only reduced MRSA burden but also displayed excellent efficiency in inhibiting bacterial biofilm formation under *in vivo* conditions in mice. Moreover, both *in vitro* and *in vivo* studies showed that the polymers were slowly degradable in the presence of enzymes. Thus the biocompatible and biodegradable coatings developed herein bears potential to be used as antibacterial paint to prevent device-associated infections.

3A.4 Experimental Section

3A.4.1 Materials and instrumentation

Chitin with a degree of acetylation ~75% and potassium hydroxide (KOH) were purchased from SD Fine, India. *N,N*-dimethyldodecylamine was purchased from Across Organics, Belgium. Lithium chloride (LiCl), potassium bromide (KBr), triethylamine (NEt_3), acetic anhydride (Ac_2O), p-toluene sulfonylchloride (TsCl), *N,N*-dimethyltetradecylamine, *N,N*-dimethylhexadecylamine and anhydrous *N,N* dimethylacetamide (DMAc) were obtained from Sigma-Aldrich, USA. Anhydrous dimethyl sulfoxide (DMSO), anhydrous diethylether (Et_2O) and all other solvents were purchased from Spectrochem, India and were of analytical grade. Methanol was dried with calcium hydride and stored over 4Å molecular sieves. Triethylamine was dried with KOH and stored over KOH. Bacterial strains *S. aureus* (MTCC 737), *E. coli* (MTCC 443) and *P. aeruginosa* (MTCC 424) were purchased from MTCC (Chandigarh, India). Vancomycin-resistant *E. faecium* (VRE) (ATCC 51559), methicilin-resistant *S. aureus* (MRSA) (ATCC 33591) *β*-lactam-resistant *K. pneumoniae* (ATCC 700603) were obtained from ATCC (Rockvillei, Md). All the clinical isolates were obtained from National Institute of Mental Health and Neuro Sciences (NIMHANS), India. The fungal strains are *Candida albicans* (SC5314), *Candida dubliniensis* (CD36), *Candida tropicalis* (MYA3404), *Cryptococcus neoformans var. grubii* (serotype A) (H99), *Cryptococcus gattii* (serotype B) (WM276) and *Cryptococcus neoformans var. neoformans* (serotype D) (JEC21). Nuclear magnetic resonance spectra (^{1}H-NMR) were recorded on a Bruker AMX-400 instrument (400 MHz) in deuterated solvents. Infra red spectra of the polymers were recorded

on a Bruker IFS66 V/s spectrometer using potassium bromide pellets. Thermo Finnigan FLASH EA 1112 CHNS analyzer was used to perform elemental analysis of the polymers. Molecular weights of the polymers were recorded by Gel permeation chromatography (GPC) on a Shimadzu-LC 20AD instrument. Polymer coatings and paints were made by a WS5000 spin coater, Techno India, India. Optical density (OD) values were measured by a TECAN (Infinite series, M200) Plate Reader. Eppendorf 5810R centrifuge was used for bacterial centrifugation. Bacterial imaging was performed using a Leica DM2500 fluorescent microscope. A Zeiss 510 Meta confocal laser scanning microscope was used for confocal microscopy imaging.

3A.4.2 Synthesis of polymers

3A.4.2.1 Synthesis of tosyl-chitin

Chitin (2.0 g, equivalent to ~10 mmol of pyranose unit) and lithium chloride (LiCl, 5.2 g) dried at 80 ˚C overnight and at 130 ˚C for 4 h respectively and then were taken in a three-necked round bottom flask fitted with rubber septa. The flask was purged with oxygen-free nitrogen, and anhydrous *N,N*-dimethylacetamide (DMAc) (104 mL) was added. The mixture was then stirred at room temperature until all the solids were dissolved. To the resultant solution was added dry NEt_3 (28.8 mL, 208 mmol) and the flask was transferred to a cold reaction chamber at 8 ˚C. A solution of tosyl chloride (38.12 g, 200 mmol) in DMAc (48 mL) was added to the reaction mixture and the reaction was allowed to proceed for either 24 h or 48 h or 72 h at the same temperature. At the end, the reaction mixture was filtered to remove the insoluble solid and to the filtrate, excess acetone was added to obtain tosylchitin as yellowish white color precipitate. The precipitate was filtered and washed successively with methanol (100 mL × 4), water (100 mL × 4), and acetone (100 mL × 4).

Tosylchitin powder (2.5 g) was acetylated by acetic anhydride (1000 μL or 925 μL or 860 μL for tosylchitins obtained after 24 h or 48 h or 72 h of tosylation respectively) in dry methanol (50 mL) overnight. Acetylated tosylchitin (2.0 g) was then treated with methanolic potassium hydroxide (45 mL or 50 mL or 55 mL, 0.1 N KOH for tosylchitins obtained after 24 h or 48 h or 72 h of tosylation respectively) for 3 h at room temperature to give *N*-acetylated tosyl-chitin. The *N*-acetylated tosyl-chitins were characterized by ^{1}H NMR and elemental analysis. The degree of tosylation (DS) was calculated as the ratio of sulfur by nitrogen obtained in elemental analysis (DS = S/N × 100%) (1). The tosylchitins obtained after acetylation and subsequent base treatment is referred as tosylchitin (Tsch). The

tosylchitins obtained after 24 h, 48 h and 72 h were referred as Tsch 1, Tsch 2 and Tsch 3 respectively.

Tsch 1: FT-IR ($\overline{\nu}$): 3400 cm^{-1} (OH str.), 1660 cm^{-1} (Amide I, C=O str.), 1600 cm^{-1} (phenylene), 1550 cm^{-1} (Amide II, C=O str.), 1175 cm^{-1} (SO_2), and 815 cm^{-1} (phenylene); ^{1}H-NMR (400 MHz, DMSO-d_6, δ): 1.873 (s, –NHCO*CH*$_3$), 2.287 (s, –O_2S–C_6H_4–*CH*$_3$), 3.864-4.863 (m, Cell–*H*), 7.111 (d, SO_3–C_6H_4–CH_3, *m*-H), 7.478 (d, SO_3–C_6H_4–CH_3, *o*-H), 7.797 (broad, –NHCO*CH*$_3$); Anal. calcd: C 48.98, H 5.82, N 5.29, S: 4.84; found: C 48.32, H 5.84, N 5.32, S 4.81.

Tsch 2: FT-IR ($\overline{\nu}$): 3400 cm^{-1} (OH str.), 1665 cm^{-1} (Amide I, C=O str.), 1600 cm^{-1} (phenylene), 1555 cm^{-1} (Amide II, C=O str.), 1175 cm^{-1} (SO_2), and 815 cm^{-1} (phenylene); ^{1}H-NMR (400 MHz, DMSO-d_6, δ): 1.896 (s, –NHCO*CH*$_3$), 2.285 (s, –O_2S–C_6H_4–*CH*$_3$), 3.730-4.860 (m, Cell–*H*), 7.112 (d, SO_3–C_6H_4–CH_3, *m*-H), 7.478 (d, SO_3–C_6H_4–CH_3, *o*-H), 7.796 (broad, –NHCO*CH*$_3$); Anal. calcd: C 49.28, H 5.71, N 5.0, S 5.71; found: C 48.74, H 5.96, N 5.1, S 5.70.

Tsch 3: FT-IR ($\overline{\nu}$): 3450 cm^{-1} (OH str.), 1660 cm^{-1} (Amide I, C=O str.), 1600 cm^{-1} (phenylene), 1550 cm^{-1} (Amide II, C=O str.), 1175 cm^{-1} (SO_2), and 815 cm^{-1} (phenylene); ^{1}H-NMR (400 MHz, DMSO-d_6, δ): 1.907 (s, –NHCO*CH*$_3$), 2.287 (s, –O_2S–C_6H_4–*CH*$_3$), 3.859-4.861 (m, Cell–*H*), 7.112 (d, SO_3–C_6H_4–CH_3, *m*-H), 7.477 (d, SO_3–C_6H_4–CH_3, *o*-H), 7.796 (broad, –NHCO*CH*$_3$); Anal. calcd: C 49.56, H 5.62, N 4.74, S 6.5; found: C 49.31, H 5.87, N 4.81, S 6.15.

3A.4.2.2 Synthesis of quaternized chitin polymers

Tosylchitins (1.0 g) with different degrees of tosylation were first dissolved in anhydrous *N*,*N*-dimethyl acetamide (DMAc) (30 mL) in sealed screw-top pressure tube. To the reaction mixture was added *N*,*N*-dimethylalkylamines (10 equivalent per tosylated sugar unit) and the reaction was allowed to proceed at 120 ˚C for 72 h. After the reaction, diethyl ether was added in excess (150 mL) to precipitate the quaternized chitin derivatives. The precipitate was filtered through a sintered glass funnel and was washed repeatedly with diethyl ether to obtain pure quaternary chitin derivatives with 100% degree of quaternization (with respect to tosyl groups for each tosylchitin). Finally the precipitates were dried in vacuum oven to give colorless/faint yellowish products with 70-80% yield. The quaternary chitin derivatives were characterized by FT-IR, ^{1}H-NMR and elemental analysis.

1a: FT-IR ($\overline{\nu}$): 3415 cm^{-1} (OH str.), 2925 cm^{-1} (–CH_2– assym. Str.), 2850 cm^{-1} (–CH_2– sym. Str.), 1680 cm^{-1} (Amide I, C=O str.), 1630 cm^{-1} (phenylene), 1560 cm^{-1} (Amide II, NH ben.), 1470 cm^{-1} (–CH_2– scissor), 1380 cm^{-1} (SO_2, asymmetric), 1170 cm^{-1} (SO_2, symmetric); ^{1}H-NMR: (400 MHz, DMSO-d_6, δ): 0.856 (t, –*CH*$_3$(CH_2)$_{11}$–N^+(CH_3)$_2$–, 3H), 1.241 (m, –CH_3*(CH*$_2$*)*$_9$$CH_2CH_2$–$N^+$($CH_3$)$_2$–, 18H), 1.655 (m,

–$CH_3(CH_2)_9CH_2CH_2–N^+(CH_3)_2$–, 2H), 1.907 (s, –NHCO$CH_3$), 2.288 (s, $SO_3–C_6H_4–CH_3$), 3.063-4.855 (m, Cell–*H* and –$CH_3(CH_2)_9CH_2CH_2–N^+(CH_3)_2$–), 7.113 (d, $SO_3–C_6H_4–CH_3$, *m*-H), 7.483 (d, $SO_3–C_6H_4–CH_3$, *o*-H); Anal. Calcd: C 56.11, H 7.94, N 5.60, S 3.66; found: C 55.81, H 7.98, N 5.42, S 3.50.

1b: FT-IR ($\overline{v}$): 3415 cm^{-1} (OH str.), 2930 cm^{-1} (–CH_2– assym. Str.), 2855 cm^{-1} (–CH_2– sym. Str.), 1680 cm^{-1} (Amide I, C=O str.), 1630 cm^{-1} (phenylene), 1560 cm^{-1} (Amide II, NH ben.), 1470 cm^{-1} (–CH_2– scissor), 1380 cm^{-1} (SO_2, asymmetric), 1170 cm^{-1} (SO_2, symmetric); ^{1}H-NMR: (400 MHz, DMSO-d_6, δ): 0.855 (t, –$CH_3(CH_2)_{13}–N^+(CH_3)_2$–, 3H), 1.241 (m, –$CH_3(CH_2)_{11}CH_2CH_2–N^+(CH_3)_2$–, 22H), 1.677 (m, –$CH_3(CH_2)_{11}CH_2CH_2–N^+(CH_3)_2$–, 2H), 1.907 (s, –NHCO$CH_3$), 2.287 (s, $SO_3–C_6H_4–CH_3$), 3.054-4.830 (m, Cell–*H* and –$CH_3(CH_2)_{11}CH_2CH_2–N^+(CH_3)_2$–), 7.108 (d, $SO_3–C_6H_4–CH_3$, *m*-H), 7.479 (d, $SO_3–C_6H_4–CH_3$, *o*-H); Anal. Calcd: C 57.17, H 8.14, N 5.43, S 3.55; found: C: 56.90, H: 8.29, N: 5.26, S: 3.50.

1c: FT-IR ($\overline{v}$): 3420 cm^{-1} (OH str.), 2920 cm^{-1} (–CH_2– assym. Str.), 2850 cm^{-1} (–CH_2– sym. Str.), 1675 cm^{-1} (Amide I, C=O str.), 1630 cm^{-1} (phenylene), 1565 cm^{-1} (Amide II, NH ben.), 1470 cm^{-1} (–CH_2– scissor), 1375 cm^{-1} (SO_2, asymmetric), 1165 cm^{-1} (SO_2, symmetric); ^{1}H-NMR: (400 MHz, DMSO-d_6, δ): 0.846 (t, –$CH_3(CH_2)_{15}–N^+(CH_3)_2$–, 3H), 1.238 (m, –$CH_3(CH_2)_{13}CH_2CH_2–N^+(CH_3)_2$–, 26H), 1.658 (m, –$CH_3(CH_2)_{13}CH_2CH_2–N^+(CH_3)_2$–, 2H), 1.883 (s, –NHCO$CH_3$), 2.287 (s, $SO_3–C_6H_4–CH_3$), 2.992-4.849 (m, Cell–*H* and –$CH_3(CH_2)_{13}CH_2CH_2–N^+(CH_3)_2$–), 7.110 (d, $SO_3–C_6H_4–CH_3$, *m*-H), 7.481 (d, $SO_3–C_6H_4–CH_3$, *o*-H); Anal. Calcd: C 58.03, H 8.32, N 5.27, S 3.44; found: C 57.90, H 8.54, N 5.16, S 3.28.

2a: FT-IR ($\overline{v}$): 3415 cm^{-1} (OH str.), 2925 cm^{-1} (–CH_2– assym. Str.), 2850 cm^{-1} (–CH_2– sym. Str.), 1680 cm^{-1} (Amide I, C=O str.), 1630 cm^{-1} (phenylene), 1560 cm^{-1} (Amide II, NH ben.), 1470 cm^{-1} (–CH_2– scissor), 1380 cm^{-1} (SO_2, asymmetric), 1170 cm^{-1} (SO_2, symmetric); ^{1}H-NMR: (400 MHz, DMSO-d_6, δ): 0.852 (t, –$CH_3(CH_2)_{11}–N^+(CH_3)_2$–, 3H), 1.235 (m, –$CH_3(CH_2)_9CH_2CH_2–N^+(CH_3)_2$–, 18H), 1.662 (m, –$CH_3(CH_2)_9CH_2CH_2–N^+(CH_3)_2$–, 2H), 1.906 (s, –NHCO$CH_3$), 2.281 (s, $SO_3–C_6H_4–CH_3$), 3.023-4.838 (m, Cell–*H* and –$CH_3(CH_2)_9CH_2CH_2–N^+(CH_3)_2$–), 7.115 (d, $SO_3–C_6H_4–CH_3$, *m*-H), 7.487 (d, $SO_3–C_6H_4–CH_3$, *o*-H); Anal. Calcd: C 57.44, H 8.15, N 5.43, S 4.14; found: C 57.01, H 8.28, N 5.31, S 4.01.

2b: FT-IR ($\overline{v}$): 3410 cm^{-1} (OH str.), 2950 cm^{-1} (–CH_2– assym. Str.), 2850 cm^{-1} (–CH_2– sym. Str.), 1675 cm^{-1} (Amide I, C=O str.), 1630 cm^{-1} (phenylene), 1560 cm^{-1} (Amide II, NH ben.), 1470 cm^{-1} (–CH_2– scissor), 1378 cm^{-1} (SO_2, asymmetric), 1168 cm^{-1} (SO_2, symmetric); ^{1}H-NMR: (400 MHz, DMSO-d_6, δ): 0.885 (t, –$CH_3(CH_2)_{13}–N^+(CH_3)_2$–, 3H), 1.237 (m, –$CH_3(CH_2)_{11}CH_2CH_2–N^+(CH_3)_2$–, 22H), 1.651 (m, –$CH_3(CH_2)_{11}CH_2CH_2–N^+(CH_3)_2$–, 2H), 1.882 (s, –NHCO$CH_3$), 2.290 (s, $SO_3–C_6H_4–CH_3$), 3.027-4.859 (m, Cell–*H* and –$CH_3(CH_2)_{11}CH_2CH_2–N^+(CH_3)_2$–), 7.121 (d, $SO_3–C_6H_4–CH_3$, *m*-H), 7.494 (d, $SO_3–C_6H_4–CH_3$, *o*-H); Anal. Calcd: C 58.43, H 8.36, N 5.24, S 3.99; found: C 58.20, H 8.45; N 5.19, S 3.85.

2c: FT-IR ($\overline{v}$): 3418 cm^{-1} (OH str.), 2928 cm^{-1} (–CH_2– assym. Str.), 2858 cm^{-1} (–CH_2– sym. Str.), 1678 cm^{-1} (Amide I, C=O str.), 1632 cm^{-1} (phenylene), 1562 cm^{-1} (Amide II, NH ben.), 1465 cm^{-1} (–CH_2– scissor), 1377 cm^{-1} (SO_2, asymmetric), 1167 cm^{-1} (SO_2,

symmetric); ^{1}H-NMR: (400 MHz, DMSO-d_6, δ): 0.855 (t, $-CH_3(CH_2)_{15}-N^+(CH_3)_2-$, 3H), 1.239 (m, $-CH_3(CH_2)_{13}CH_2CH_2-N^+(CH_3)_2-$, 26H), 1.658 (m, $-CH_3(CH_2)_{13}CH_2CH_2-N^+(CH_3)_2-$, 2H), 1.956 (s, $-NHCOCH_3$), 2.287 (s, $SO_3-C_6H_4-CH_3$), 3.026-4.861 (m, Cell–*H* and $-CH_3(CH_2)_{13}CH_2CH_2-N^+(CH_3)_2-$), 7.108 (d, $SO_3-C_6H_4-CH_3$, *m*-H), 7.479 (d, $SO_3-C_6H_4-CH_3$, *o*-H); Anal. Calcd: C 59.35, H 8.56, N 5.06, S 3.86; found: C 58.95, H 8.68, N 4.98, S 3.79.

3a: FT-IR ($\overline{\nu}$): 3424 cm^{-1} (OH str.), 2922 cm^{-1} (–CH_2– assym. Str.), 2852 cm^{-1} (–CH_2– sym. Str.), 1684 cm^{-1} (Amide I, C=O str.), 1630 cm^{-1} (phenylene), 1560 cm^{-1} (Amide II, NH ben.), 1470 cm^{-1} (–CH_2– scissor), 1382 cm^{-1} (SO_2, asymmetric), 1170 cm^{-1} (SO_2, symmetric); ^{1}H-NMR: (400 MHz, DMSO-d_6, δ): 0.850 (t, $-CH_3(CH_2)_{11}-N^+(CH_3)_2-$, 3H), 1.234 (m, $-CH_3(CH_2)_9CH_2CH_2-N^+(CH_3)_2-$, 18H), 1.656 (m, $-CH_3(CH_2)_9CH_2CH_2-N^+(CH_3)_2-$, 2H), 1.882 (s, $-NHCOCH_3$), 2.285 (s, $SO_3-C_6H_4-CH_3$), 2.941-4.840 (m, Cell–*H* and $-CH_3(CH_2)_9CH_2CH_2-N^+(CH_3)_2-$), 7.113 (d, $SO_3-C_6H_4-CH_3$, *m*-H), 7.486 (d, $SO_3-C_6H_4-CH_3$, *o*-H); Anal. Calcd: C 58.41, H 8.32, N 5.29, S 4.54; found: C 58.32, H 8.48, N 5.18, S 4.50.

3b: FT-IR ($\overline{\nu}$): 3419 cm^{-1} (OH str.), 2925 cm^{-1} (–CH_2– assym. Str.), 2851 cm^{-1} (–CH_2– sym. Str.), 1676 cm^{-1} (Amide I, C=O str.), 1630 cm^{-1} (phenylene), 1558 cm^{-1} (Amide II, NH ben.), 1476 cm^{-1} (–CH_2– scissor), 1380 cm^{-1} (SO_2, asymmetric), 1174 cm^{-1} (SO_2, symmetric); ^{1}H-NMR: (400 MHz, DMSO-d_6, δ): 0.838 (t, $-CH_3(CH_2)_{13}-N^+(CH_3)_2-$, 3H), 1.238 (m, $-CH_3(CH_2)_{11}CH_2CH_2-N^+(CH_3)_2-$, 22H), 1.657 (m, $-CH_3(CH_2)_{11}CH_2CH_2-N^+(CH_3)_2-$, 2H), 1.883 (s, $-NHCOCH_3$), 2.287 (s, $SO_3-C_6H_4-CH_3$), 2.944-4.849 (m, Cell–*H* and $-CH_3(CH_2)_{11}CH_2CH_2-N^+(CH_3)_2-$), 7.111 (d, $SO_3-C_6H_4-CH_3$, *m*-H), 7.480 (d, $SO_3-C_6H_4-CH_3$, *o*-H); Anal. Calcd: C 59.45, H 8.55, N 5.09, S 4.36; found: C 59.36, H 8.60, N 4.98, S 4.29.

3c: FT-IR ($\overline{\nu}$): 3415 cm^{-1} (OH str.), 2928 cm^{-1} (–CH_2– assym. Str.), 2850 cm^{-1} (–CH_2– sym. Str.), 1676 cm^{-1} (Amide I, C=O str.), 1635 cm^{-1} (phenylene), 1562 cm^{-1} (Amide II, NH ben.), 1465 cm^{-1} (–CH_2– scissor), 1375 cm^{-1} (SO_2, asymmetric), 1164 cm^{-1} (SO_2, symmetric); ^{1}H-NMR: (400 MHz, DMSO-d_6, δ): 0.851 (t, $-CH_3(CH_2)_{15}-N^+(CH_3)_2-$, 3H), 1.234 (m, $-CH_3(CH_2)_{13}CH_2CH_2-N^+(CH_3)_2-$, 26H), 1.653 (m, $-CH_3(CH_2)_{13}CH_2CH_2-N^+(CH_3)_2-$, 2H), 1.886 (s, $-NHCOCH_3$), 2.285 (s, $SO_3-C_6H_4-CH_3$), 3.023-4.844 (m, Cell–*H* and $-CH_3(CH_2)_{13}CH_2CH_2-N^+(CH_3)_2-$), 7.116 (d, $SO_3-C_6H_4-CH_3$, *m*-H), 7.489 (d, $SO_3-C_6H_4-CH_3$, *o*-H); Anal. Calcd: C 60.42, H 8.75, N 4.90, S 4.20; found: C 60.38, H 8.80, N 4.82, S 4.15.

3A.4.3 Gel permeation chromatography

The products were further characterized by gel permeation chromatography (GPC). Molecular weights and polydispersities were determined on a Shimadzu-LC 20AD instrument with refractive index detector using a phenogel 5µ 10E5A column (300 × 7.8 mm-Part No. 00H-0446-K0). GPC samples were run in *N*,*N*-dimethylacetamide solvent as mobile phase (flow rate of 1 mL/min). Seven different molecular weight pullulan standards obtained from Sigma-Aldrich (USA-catalogue 96351) were used for calibration in GPC. The range of

pullulan standards was from 10 to 805 kDa (10, 21.7, 48, 113, 200, 366 and 805 kDa). The molecular weights reported are relative to these standards.

3A.4.4 Solubility of the chitin derivatives

The solubility of the polymers in organic and aqueous solvents was studied following similar protocol as described in section of 2A.4.3 in Chapter 2A.

3A.4.5 Preparation and characterization of the paint

3A.4.5.1 Preparation of paint

The polymers were coated onto different surfaces following similar protocol as described in section of 2A.4.4 in Chapter 2A.

3A.4.5.2 Static contact angle measurement

The water contact angle measurements were performed by using the static sessile drop method with a contact angle goniometer. The images of water droplets (of size of 2 µl of deionized water) on the polymer coated surfaces were recorded using a camera attached to the contact angle goniometer. Contact angles were obtained by analyzing the images of the water droplets. A minimum of five measurements in five different spots were recorded for each sample, and the values reported are the average of these measurements.

3A.4.6 Determination of antibacterial activity by spray method (air-borne bacteria)

The same protocol was followed using all the polymeric coatings as described in the section 2A.4.5.1 in Chapter 2A.

3A.4.7 Antibacterial activity against water-borne bacteria (MIA)

The same protocol was followed using all the polymeric coatings as described in the section 2A.4.5.2 in Chapter 2A.

3A.4.8 Mechanism of antibacterial action

3A.4.8.1 Membrane depolarization assay

The same protocol was followed using all the polymeric coatings as described in the section 2A.4.6 in Chapter 2A. The polymer coating used in this experiment was 1.25 µg/mm^2 for *S. aureus* and 12.5 µg/mm^2 for *E. coli* respectively.

3A.4.8.2 Intracellular K^+ ion leakage assay

Midlog phase bacteria (*S. aureus* and *E. coli*) were washed and resuspended in a 1:1 mixture of HEPES (10 mM) and glucose solution (0.5% wt/vol) in a similar way as described in the membrane depolarization assay (5). The suspension (150 µL, 10^8 CFU/mL) was added to the non-coated wells of 96-well plate (black plate, clear bottom with lid). Then 50 µL of potassium ion sensitive dye PBFI-AM (4 µM) was added to the bacterial suspension. Fluorescence intensity of the dye was recorded for about 6 min to obtain a stable baseline. Then the dye containing bacterial suspension was added to the wells of another black plate coated with polymers. The fluorescence intensity of PBFI-AM was then recorded for about 20 min at every 2 minutes interval using plate reader with excitation wavelength of 346 nm (slit width: 10 nm) and emission wavelength of 505 nm (slit width: 20 nm). The polymer coating used in this experiment was 1.25 µg/mm^2 for *S. aureus* and 12.5 µg/mm^2 for *E. coli* respectively.

3A.4.8.3 Live and dead assay

The same protocol was followed using all the polymeric coatings as described in the section 2A.4.6.2 in Chapter 2A.

3A.4.8.4 Scanning electron microscopy

The same protocol was followed using all the polymeric coatings as described in the section 2A.4.6.3 in Chapter 2A.

3A.4.9 Bacterial biofilm inhibition assay

Bacterial biofilm inhibition assay was performed by coating the most active polymer (**2c**) onto cover glass at MIA and 6 × MIA following the protocol as described in the section 2B.4.6 in Chapter 2B.

3A.4.10 Antifungal assay

3A.4.10.1 Minimum inhibitory amount (MIA)

Minimum inhibitory amount of the polymer coated surfaces was evaluated following same protocol as described in the section 2A.4.7.1 in Chapter 2A.

3A.4.10.2 Minimum fungicidal amount (MFA)

Minimum fungicidal amount of the polymer coated surfaces was evaluated following same protocol as described in the section 2A.4.7.2 in Chapter 2A.

3A.4.10.3 Kinetics of antifungal activity

Kinetics of Antifungal activity of the polymer coated surfaces was evaluated following same protocol as described in the section 2A.4.7.3 in Chapter 2A.

3A.4.11 Mechanism of antifungal action

Mechanism of antifungal action of the polymer coated surfaces was evaluated following same protocol as described in the section 2A.4.8 in Chapter 2A.

3A.4.12 Fungal biofilm inhibition assay

Fungal biofilm inhibition assay was performed by coating the most active polymer (**2c**) onto cover glass at MIA and 2 × MIA following the protocol as described in the section 2B.4.9 in Chapter 2B.

3A.4.13 Biodegradation

3A.4.13.1 *In-vitro* biodegradation

Microscopic cover slip (18 mm) were coated with the known amount of polymers **1b**, **1c** and **2c** following the coating procedure as described previously. The cover slips were placed in a 6-well plate (the weight of uncoated and the polymer-coated cover slips were recorded to calculate the coating amount). Phosphate buffer saline (PBS, pH = 7.2) was used for this study and the enzyme was chicken egg lysozyme (≥ 40,000 units/mg protein). Lysozyme was dissolved in the PBS to give an enzyme concentration of 4 mg/mL and then was added (4 mL) to the wells of 6-well plate containing coated cover slips. As control experiment, another polymer coated cover slip was placed in enzyme-free buffer-solution. The samples were incubated in a shaker incubator at 37 ˚C for 28 days under constant agitation. The cover slips were then removed at different time intervals from the plates, washed with Millipore water and dried in a vacuum oven till its weight remained unchanged. The weights of the dried cover slips were recorded and the extent of hydrolysis was calculated as % of the weight loss of the film after lysozyme treatment.

3A.4.13.2 *In-vivo* degradation

In vivo degradation was performed with Wistar rats following the protocols approved by the Institutional Animal Ethics Committee (IAEC) in Jawaharlal Nehru Centre for Advanced Scientific Research. In each group, a total of five male wistar rats weighing 250-350 g were used. The rats were anesthetized with ketamine (100 mg/kg) and xylazine (5 mg/kg) intra-peritoneally. The backs of the rats were shaved aseptically. A midline incision was then made in the skin above the mid-thoracic spine and a subcutaneous (s.c.) pouch was created by blunt dissection extending in each rat interiorly. Polymer discs (11 mm of diameter) of the polymers (**1b**, **1c** and **2c**) of known weight (40-60 mg) were made by a hydraulic press. Next the discs were sterilized by UV irradiation, soaked in sterile PBS for about 1 h (pH 7.4) prior to implantation and inserted into the s.c. pouch of rat. The incision was then closed with silk suture (6.0). After definite time intervals, the rats were killed and the polymer disc samples were harvested. The samples were then rinsed with Millipore water and dried to a constant weight at 60 ˚C in a vacuum oven. Finally the weight of the dried disc samples was recorded. The extent of *in vivo* degradation was expressed as the percentage of the weight loss of after implantation. Further, to visualize the surface morphology of the disc, discs were gold coated and imaged by Quanta 3D FEG FEI scanning electron microscope.

3A.4.14 Biocompatibility

3A.4.14.1 Hemolytic activity

Hemolytic assay of the polymeric coating was evaluated following same protocol as described in the section 2A.4.10 in Chapter 2A.

3A.4.14.2 *In-vivo* toxicity

In-vivo toxicity of the cationic chitin derivatives were evaluated by coating the most active polymers (**2c**) onto medical grade catheter following the same protocol as described in the section 2B.4.11.3 in chapter 2B.

3A.4.15 *In-vivo* activity

In-vivo activity of the cationic chitin derivatives were evaluated by coating the most active polymers (**2c**) onto medical grade catheter following the same protocol as described in the section 2B.4.12 in chapter 2B.

3A.4.16 Resistance development study

Resistance development assay of the polymeric coating (**2c**) was evaluated following same protocol as described in the section 2A.4.9 in Chapter 2A.

BIBLIOGRAPHY

1. Daghighi, S.; Sjollema, J.; van der Mei, H. C.; Busscher, H. J.; Rochford, E. T. Infection resistance of degradable versus non-degradable biomaterials: an assessment of the potential mechanisms. *Biomaterials* **2013,** *34*, 8013-8017.
2. Hsu, B. B.; Park, M. H.; Hagerman, S. R.; Hammond, P. T. Multimonth controlled small molecule release from biodegradable thin films. *Proc. Natl. Acad. Sci. U S A* **2014,** *111*, 12175-12180.
3. Hayashi, T. Biodegradable polymers for biomedical uses. *Prog. Polym. Sci.* **1994,** *19*, 663-702.
4. Li, Y. L.; Maciel, D.; Rodrigues, J.; Shi, X. Y.; Tomas, H. Biodegradable polymer nanogels for drug/nucleic acid delivery. *Chem. Rev.* **2015,** *115*, 8564-8608.
5. Tharanathan, R. N., Biodegradable films and composite coatings: past, present and future. *Trends Food Sci. Technol.* **2003,** *14*, 71-78.
6. Kumar, M. N. V. R.; Muzzarelli, R. A. A.; Muzzarelli, C.; Sashiwa, H.; Domb, A. J. Chitosan chemistry and pharmaceutical perspectives. *Chem. Rev.* **2004,** *104*, 6017-6084.
7. Kumar, M. N. V. R. A review of chitin and chitosan applications. *React. Funct. Polym.* **2000,** *46*, 1-27.
8. Tomihata, K.; Ikada, Y. In vitro and in vivo degradation of films of chitin and its deacetylated derivatives. *Biomaterials* **1997,** *18*, 567-575.
9. Krajewska, B.; Wydro, P.; Janczyk, A. Probing the modes of antibacterial activity of chitosan. Effects of pH and molecular weight on chitosan interactions with membrane lipids in Langmuir films. *Biomacromolecules* **2011,** *2*, 4144-4152.
10. Rabea, E. I.; Badawy, M. E. T.; Stevens, C. V.; Smagghe, G.; Steurbaut, W. Chitosan as antimicrobial agent: applications and mode of action. *Biomacromolecules* **2003,** *4*, 1457-1465.
11. Sahariah, P.; Benediktssdottir, B. E.; Hjalmarsdottir, M. A.; Sigurjonsson, O. E.; Sorensen, K. K.; Thygesen, M. B.; Jensen, K. J.; Masson, M. Impact of chain length on antibacterial activity and hemocompatibility of quaternary N-alkyl and N,N-dialkyl chitosan derivatives. *Biomacromolecules* **2015,** *16*, 1449-1460.
12. Zou, Y. Q.; Khor, E. Preparation of c-6 substituted chitin derivatives under homogeneous conditions. *Biomacromolecules* **2005,** *6*, 80-87.
13. Yarlagadda, V.; Samaddar, S.; Paramanandham, K.; Shome, B. R.; Haldar, J. Membrane disruption and enhanced inhibition of cell-wall biosynthesis: A synergistic approach to tackle vancomycin-resistant bacteria. *Angew. Chem. Int. Ed.* **2015,** *54*, 13644-13649.
14. Konai, M. M.; Ghosh, C.; Yarlagadda, V.; Samaddar, S.; Haldar, J. Membrane active phenylalanine conjugated lipophilic norspermidine derivatives with selective antibacterial activity. *J. Med. Chem.* **2014,** *57*, 9409-9423.
15. Wang, Y.; Corbitt, T. S.; Jett, S. D.; Tang, Y. L.; Schanze, K. S.; Chi, E. Y.; Whitten, D. G. Direct visualization of bactericidal action of cationic conjugated polyelectrolytes and oligomers. *Langmuir* **2012,** *28*, 65-70.
16. Hartmann, M.; Berditsch, M.; Hawecker, J.; Ardakani, M. F.; Gerthsen, D.; Ulrich, A. S. Damage of the bacterial cell envelope by antimicrobial peptides Gramicidin S and PGLa as revealed by transmission and scanning electron microscopy. *Antimicrob. Agents Chemother.* **2010,** *54*, 3132-3142.
17. Gao, G. Z.; Lange, D.; Hilpert, K.; Kindrachuk, J.; Zou, Y. Q.; Cheng, J. T. J.; Kazemzadeh-Narbat, M.; Yu, K.; Wang, R. Z.; Straus, S. K.; Brooks, D. E.; Chew, B. H.; Hancock, R. E. W.; Kizhakkedathu, J. N. The biocompatibility and biofilm resistance of

implant coatings based on hydrophilic polymer brushes conjugated with antimicrobial peptides. *Biomaterials* **2011,** *32*, 3899-3909.
18. Bieser, A. M.; Tiller, J. C. Mechanistic considerations on contact-active antimicrobial surfaces with controlled functional group densities. *Macromol. Biosci.* **2011,** *11*, 526-534.
19. Tomihata, K.; Ikada, Y., In vitro and in vivo degradation of films of chitin and its deacetylated derivatives. *Biomaterials* **1997,** *18*, 567-575.
20. Sherertz, R. J.; Forman, D. M.; Solomon, D. D. Efficacy of dicloxacillin-coated polyurethane catheters in preventing subcutaneous Staphylococcus aureus infection in mice. *Antimicrob. Agents Chemother.* **1989,** *33*, 1174-1178.

Chapter 3B

Dual Action Quaternary Chitin-Silver Nanocomposites as Antimicrobial Paint that Kill Microbes and Inhibit Biofilms on Catheter

Abstract

Chapter 3B *reports in-situ development of highly effective dual action polymer-silver nanocomposites from quaternary chitin derivatives and a silver salt. The cationic antimicrobial polymers, water-insoluble and organo-soluble derivatives of naturally occurring polymer chitin, acted as both reducing and stabilizing agents to silver para toulenesulfonate (AgPTS) thereby provided a highly stable polymer-silver nanocomposites. The polymeric nanocomposites upon coating onto surfaces non-covalently via simple brush/spin/dip coating completely inactivated both Gram-positive and Gram-negative bacteria including the drug-resistant pathogens such as methicillin-resistant Staphylococcus aureus (MRSA), vancomycin-resistant Enterococcus faecium (VRE) and beta lactam-resistant Klebsiella pneumoniae (Minimum inhibitory amount, MIA 0.06-1.9 $\mu g/mm^2$). The nanocomposites were also shown to be highly effective against various human pathogenic fungi such as such as Candida spp. and Cryptococcus spp. (MIA 0.06-1.0 $\mu g/mm^2$). Importantly, the composites killed both bacteria and fungi at much lower amount than the individual components and were found to have rapid killing rates (30-60 min for bacteria and 2-3 h for fungi). The nanocomposite coated surfaces showed remarkably long-lasting activity over a period of 14 days as tested and did not allow microbial (bacterial) resistant development even till 14 passages. Further, the composites when coated onto surfaces were shown to be effective in inhibiting both bacterial and fungal biofilm formation even after repeated challenges of the same surface. Notably, negligible in-vitro toxicity towards human erythrocytes and minimal inflammation to the tissue in-vivo was observed for the composites. Also, the composites showed excellent efficacy in reducing bacterial burden (4.9 log CFU reduction at 8.0 $\mu g/mm^2$ of coating) both on the catheter and in the surrounding tissues (5.8 log CFU reduction) when a composite-coated catheter was infected with MRSA and implanted in mice subcutaneously. Further the coated catheter was also shown to be effective in inhibiting MRSA biofilm formation in-vivo. The one-pot synthesis of the polymeric nanocomposites from a biocompatible antimicrobial polymer thus could be used as safe and effective antimicrobial coatings in various biomedical devices and implants.*

Publication based on this work

1. Hoque, J. *et al.* *In-situ* synthesis of dual action polymer-silver nanocomposites that effectively kill microbes and inhibit biofilm formation. Manuscript submitted.

3B.1 Introduction

Microbial infection at the site of implanted medical devices such as orthopaedic implants, catheter, etc. presents a serious ongoing problem in the biomedical arena.[1-3] Infections due to the device implantation in the less vascular tissue (e.g., bone infection due to bone fixture devices) or in avascular tissue (e.g., cartilage infections due to joint replacement devices) are particularly more challenging because of the limited penetration of antibiotics which makes it very difficult to treat infections in those tissues.[4-6] The situation is even more complicated upon bacterial biofilm formation on the device surfaces which is known to be resistant against both host defence systems and common antibiotic therapy.[7] For example, infection associated with prosthetic joints, in particular osteomyelitis is by far the most common reason for complications which often require multiple revision surgeries and in extreme cases removal of the implants (74.3%).[8,9] Though revision surgery (e.g., revision arthroplasty) have been shown to remove/reduce infections, it can often lead to various other complications such as re-infections of the implants due to surgical procedure or from the surrounding microbes hidden at the tissue level along with the increased cost, pain and suffering of the patients undergoing surgeries.[10] It is therefore necessary to develop antimicrobial coatings which not only prevent infections on the medical devices but also eliminates difficult-to-treat bacteria at the surrounding tissue level.

Dual action antimicrobial polymeric nanocomposites, composed of metal nanoparticles dispersed inside an antimicrobial polymeric matrix thus inactivating microbes upon contact and by releasing active ingredients, offer great potential and several advantages over the existing individual systems.[11-14] These materials will not only kill pathogen on contact but also will be able to inactivate microorganisms by releasing active antimicrobials into the surroundings thus removing infections at the neighboring tissue level of a implants. Further, the antimicrobial components present in the nanocomposites can act simultaneously leading to an enhanced antimicrobial activity. Moreover, the nanomaterials can release the active antimicrobials over an extended period of time thereby can provide long-lasting antibacterial activity particularly required to combat device related infections especially in less vascular or avascular tissue level.

Among various nanoparticles, silver nanoparticles are of special interest because of their broad-spectrum antimicrobial activity toward different pathogens, e.g., bacteria, fungi, viruses, etc.[15,16] It has been shown that Ag^+ ion, the active component of the silver-based antimicrobials, deactivate surface proteins, intracellular enzymes, DNA, etc. Silver-

containing materials have been widely used by the biomedical industry in catheters, dental material, medical devices and implants, and wound dressings.[17-19] However, most of the techniques used to incorporate silver into polymeric matrices involve synthesis of complex silver compounds, mixing *ex-situ* synthesized silver particles with the polymers, or complicated physical techniques such as sputtering and plasma deposition.[20-24] These methods are generally costly, time-consuming and add complexity to the fabrication process. In addition, the polymers in the nanocomposites are generally non-active or poorly active against microbes and are toxic towards mammalian cells. Thus the composites mainly depend on the amount of nanoparticles present in the systems for their antimicrobial activity and can cause significant toxicity to mammalian cells. It is therefore desirable to develop dual action polymer-silver nanocomposites in a simple method wherein the composites can be coated onto surfaces non-covalently as paint and will be able to kill microbes rapidly and more effectively via both contact- and release-active mechanism without causing toxicity to mammalian cells.

In chapter 3A, water-insoluble and organo-soluble quaternary *N,N*-dimethylalkyl ammonium chitin polymers capable of inactivating microbes (bacteria and fungi) and inhibiting biofilm formation were developed. Further, the polymers were shown to be biocompatible and biodegradable in both *in-vitro* and *in-vivo*. However, though highly effective against Gram-positive bacteria, antimicrobial efficacy of the polymers was found to be very low against Gram-negative bacteria. Further, *in-vivo* antimicrobial efficacy of the polymers was found to be poor when infected with higher number bacteria. Moreover, the coated surfaces require direct microbial contact with the polymer to achieve antimicrobial activity (the polymers are water-insoluble thus cannot diffuse from the coated surface and cannot kill the surrounding microorganism efficiently). Interestingly, the chitin polymer would still have its terminal aldehyde groups (no chemical modification was performed here while preparing the quaternary chitin derivatives) and therefore are expected to be able to reduce silver ions to metallic silver *in-situ*.[25] In addition, the polymers with its electron donating atoms such as nitrogen or oxygen can act as potent capping agent to the silver nanoparticle and therefore can lead to stable and active polymer-silver nanocomposites.

Herein chapter 3B describes the successful development of biocompatible and dual action antimicrobial polymer-silver nanocomposites via *in-situ* reduction of silver ions using the quaternary chitin derivatives. The organo-soluble nanocomposites allowed non-covalent immobilization of the materials directly onto surfaces as paint and were shown to be highly active against both Gram-positive and Gram-negative bacteria including various human

pathogenic fungi. Importantly, the composites were found to kill both bacteria and fungi at a much faster rate than the polymer alone and showed long-lasting durable activity. Further, the composites inhibited both bacterial and fungal biofilm formation on the coated surfaces even after repeated challenges. Negligible toxicity towards mammalian cells was observed both *in-vitro* and *in-vivo*. The composites upon coating to a medical grade catheter showed excellent efficacy in reducing microbial burden both on the catheter and in the surrounding tissues in a mice model of subcutaneous infection. Further coated catheter was also shown to be effective in inhibiting MRSA biofilm formation in mice model.

3B.2 Results and discussion

3B.2.1 Synthesis and characterization of the nanocomposites

The *in-situ* synthesis of the silver-polymer nanocomposites was depicted in Scheme 3B.1. The nanocomposites consist of one of the most active quaternary chitin derivatives (**2c**, having $-C_{16}H_{33}$ long chain with 48% degree of quaternization) from chapter 3A and *in-situ* generated silver nanoparticle stabilized by the same polymer. The nanocomposites were prepared by adding the dimethyl sulfoxide (DMSO) solution of silver paratoluene sulfonate (AgPTS) to an equal volume of methanolic solution of the polymer and keeping the mixture at room temperature for the required period of time under dark condition (Figure 3B.1A). Two different composites were prepared by varying the amount of the silver salt (AgPTS) while keeping the polymer amount constant (**2c**:AgPTS = 1:1 and 1:0.5, w/w). The formation of silver nanoparticle was indicated by the appearance of yellow followed by brownish colour with time (Figure 3B.1A). The color changes as observed may be attributed to the surface plasmon resonance (SPR) of the *in-situ* generated silver nanoparticles (AgNP). However, no color change was observed for methanolic solution of polymer containing equal volume of DMSO and DMSO solution of AgPTS containing equal volume of methanol under similar conditions. The above facts therefore suggested that the polymer is responsible for the reduction of silver ions. The rate of formation as well as the overall time required for the complete reduction of the silver salt was monitored by observing surface plasmon of silver nanoparticle via UV-visible absorption spectroscopy. Polymer-capped silver nanoparticle had an SPR band at ~415 nm and detectable amount of the Ag nanoparticle was observed after 12 h in the absorption spectra for both the composites (Figure 3B.1B and C). The formation of nanoparticle was found to be time dependent and almost 5-7 days were required for the reduction of the silver ions (the complete reduction of all the silver ions required 10-11 days

for both the compositions). However, composite with lower silver salt/polymer ratio was found to get reduced at a relatively higher rate than the composite with higher silver salt/polymer ratio (Figure 3B.1B and C). Finally, solid **2c**-AgNP nanocomposites were obtained by precipitation from the nanocomposite solutions upon addition of acetone. The solid composites could be easily re-dissolved in methanol, ethanol, DMSO, etc. to give back the clear solutions.

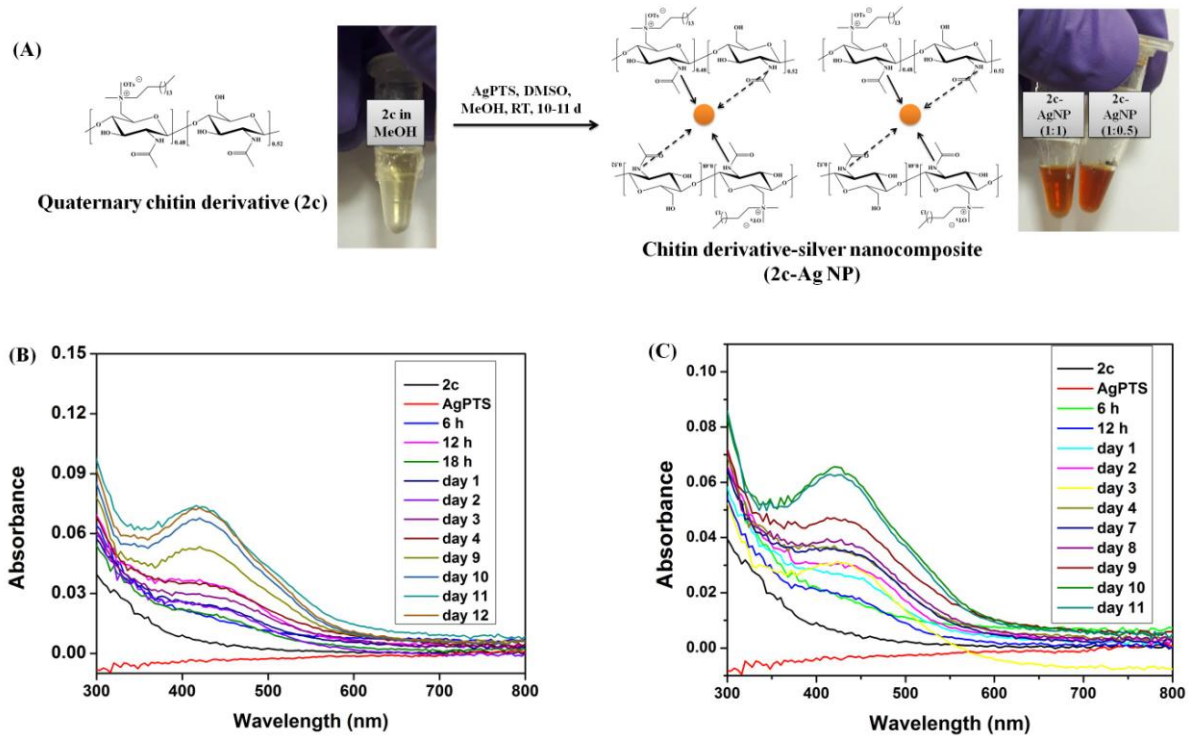

Figure 3B.1: Preparation of polymer-silver nanocomposites. (A) Schematic representation of synthesis of **2c**-AgNP nanocomposites. The nanoparticles shown in orange circle are shown to be stabilized by the capping effect of the polymer. Eppendorf tubes showing the polymer and polymer nanocomposites before and after the silver nanoparticle formation. UV-visible absorption spectra of the *in-situ* generated silver nanoparticle at different time interval. (B and C) surface plasmon absorbance for the 1:1 **2c**:AgNP and 1:0.5 **2c**:AgNP mixture.

The formation of Ag nanoparticles was further confirmed by the transmission electron microscopy (TEM) as the TEM images clearly indicate the presence of spherical nanoparticles of 5-25 nm in 1:1 composites and 5-20 nm in 1:0.5 composites (Figure 3B.2A and 3A). Further, uniform distribution of nanoparticles was observed for both the composites which suggested that reduction is taking place in the vicinity of the polymeric chains. As the formation of the nanoparticle takes place very close to polymer chains, the growing nanoparticles are stabilized as well as prevented from aggregation by the capping effects of

the coordinating nitrogen or oxygen atoms of the polymers. Also steric isolation by the polymeric chain in stabilization of the silver nanoparticles cannot be ignored.

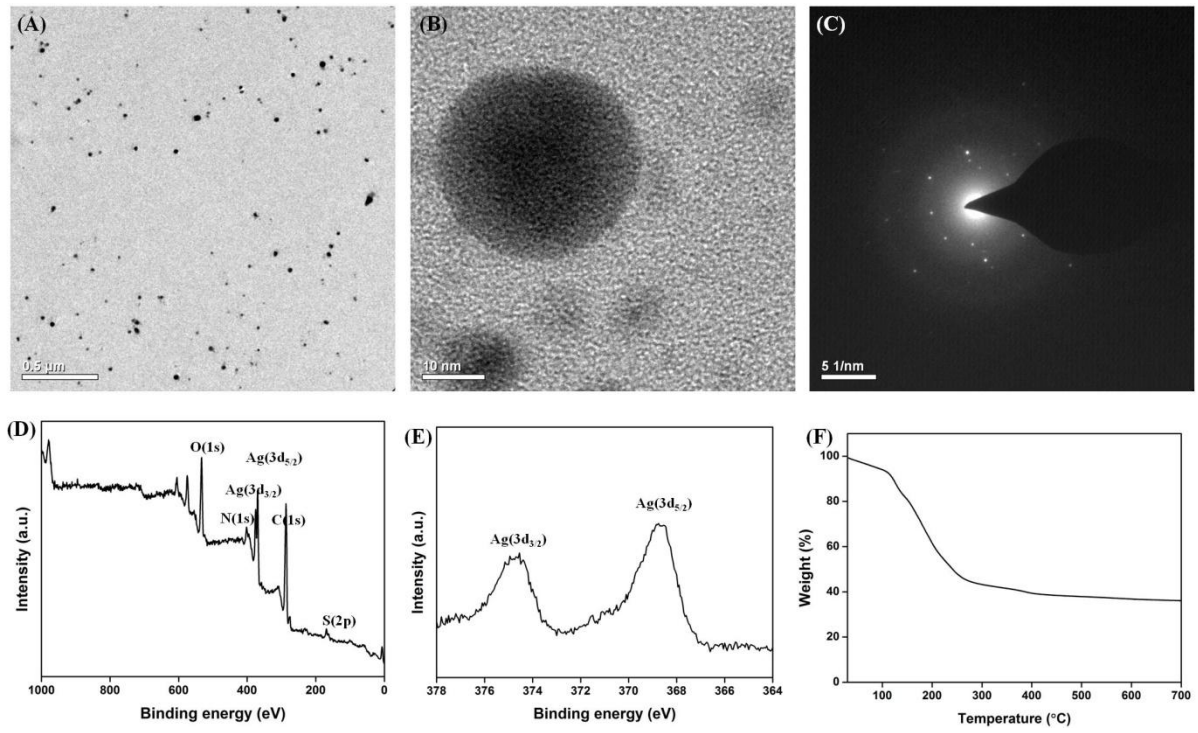

Figure 3B.2: Characterization of 1:1 **2c**-AgNP composite. (A) TEM image of the nanocomposites showing uniform distribution of the silver nanoparticle. (B) HRTEM image of the nanoparticles showing lattice fringes. (C) Relevant selected area diffraction (SAED) pattern of the nanocomposites. X-ray photoelectron spectra of the nanocomposites: (D) survey scan and (E) relevant high resolution silver scan. (F) Thermogravimetric analysis curve showing % wt loss due to heating.

However, no significant effect on the size distribution of the nanoparticles was observed when the amount of the precursor silver salt was varied while keeping the polymer amount constant (1:1 and 1:0.5 **2c**:AgPTS). Nonetheless, it should be mentioned that 1:0.5 composite was found to have more particles of somewhat lesser size (average size 5-10 nm) as compared to 1:1 composite (average size 10-20 nm) probably due to higher capping and stabilizing effect from the polymer (Figure 3B.2A and 3A). The high resolution TEM images showed the appearance lattice fringes characteristic of metal nanoparticles (Figure 3B.2B and 3B). The crystalline nature of the nanoparticles was confirmed by selected area electron diffraction (SAED) pattern as the spectra revealed the presence of sharp spots with diffused rings (Figure 3B.2C and 3C). The chemical identity of the composites was established by energy dispersive X-ray spectroscopy (EDX). EDX spectra were recorded during TEM

imaging wherein the electron beam was focused on an approximately 0.1 μm × 0.1 μm particle-rich region. The EDX spectra of both the composites clearly indicated the presence of silver in the composites along with the other characteristic elements such as carbon, nitrogen and sulfur. However, the EDX did not conclusively prove that whether the peak for silver is from the silver ion or from the reduced silver. In order to establish the oxidation state of the silver and to prove that all the silver ions got reduced by the polymer, x-ray photoelectron spectroscopy (XPS) was employed.

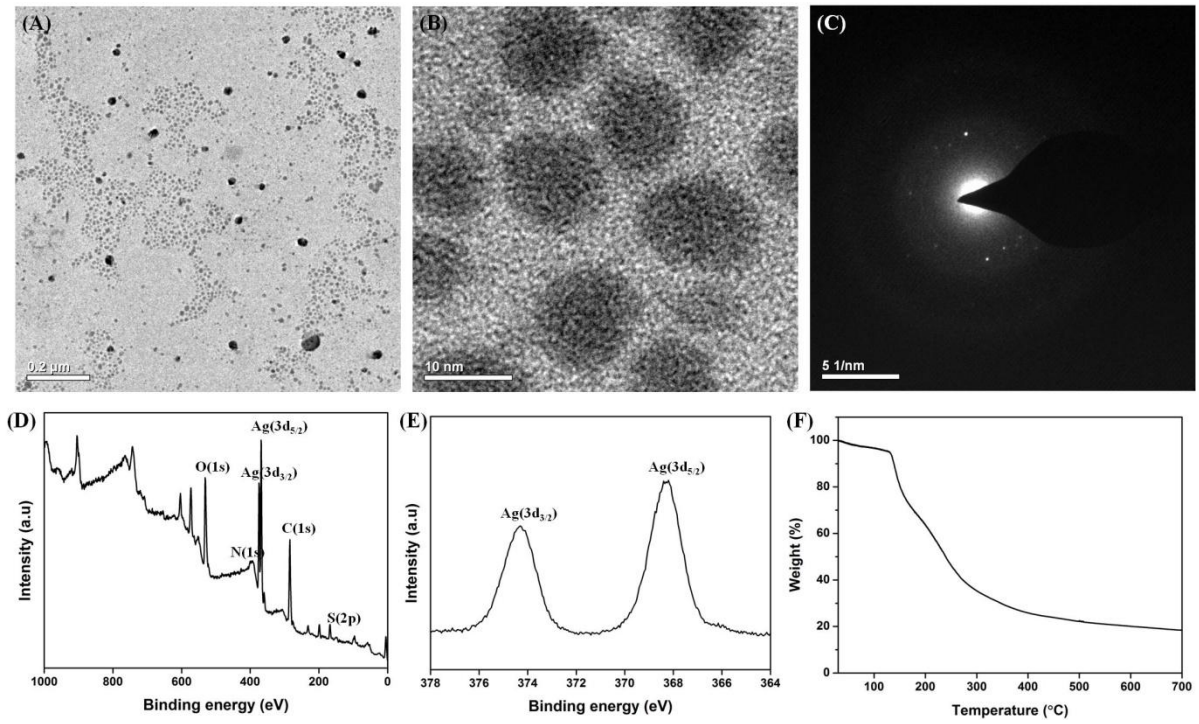

Figure 3B.3: Characterization of 1:0.5 **2c**-AgNP composite. (A) TEM image of the nanocomposites showing uniform distribution of the silver nanoparticle. (B) HRTEM image of the nanoparticles showing lattice fringes. (C) Relevant selected area diffraction (SAED) pattern of the nanocomposites. X-ray photoelectron spectra of the nanocomposites: (D) survey scan and (E) relevant high resolution silver scan. (F) Thermogravimetric analysis curve showing % wt loss due to heating.

XPS spectra of the silver in the Ag 3d ($3d_{5/2}$ and $3d_{3/2}$) regions are very sensitive to its chemical environment and provide important information in discriminating silver ions and metallic silver. XPS spectra for both the composites was recorded by making a thin film on silicon wafers and the survey scan as well as Ag $3d_{3/2}$ and $3d_{5/2}$ spectra of **2c**-AgNP composite films were analysed (Figure 3B.2 and 3). The survey scan showed the presence of carbon, nitrogen, oxygen, sulfur and silver atoms for both 1:1 and 1:0.5 composites thereby

establishing the chemical composition of the polymer-silver nanocomposites (Figure 3B.2D and 3D). XPS spectra of the above product showed a C 1s peak with binding energy at 286.4 eV, characteristic of carbon bonded to oxygen in chitin macromolecules. Moreover, the Ag 3d spectra showed peaks at 368.2 and 374.2 eV assigned to Ag $3d_{5/2}$ and Ag $3d_{3/2}$ peaks, respectively, matching with binding energy value of silver in zero oxidation state (Figure 3B.2E and 3E). The above facts indicated that the silver is present in zero oxidation and the nanocomposites contained only the metallic nanosilver.

To quantify the amount of silver (wt%) present in the composites, thermogravimetric analyses (TGA) of both 1:1 and 1:0.5 **2c**-AgNP composites were performed using a heating rate of 5 ˚C/min under argon flow. The curves showed two stages of weight loss for the composites (Figure 3B.2F and 3F). A very slight weight loss in the first stage between 60-140 ˚C indicated the loss of adsorbed moisture. However, the second stage of weight loss which occurred between 180-400 ˚C indicated the degradation of the polymer **2c** mtarix, leaving only the silver residue. The amount of residue left by pure **2c** as char was negligible (1.7%). The weight percentage of AgNP in 1:1 and 1:0.5 composites were found to be 38.1 ± 0.4% and 18.9 ± 0.3% (experimental value) respectively (Figure 3B.2F and 3F). The complete reduction of the silver salts by the polymer would provide 38.7% and 19.3% of silver (calculated value) in 1:1 and 1:0.5 composites respectively. Notably, the above results were in good agreement with the theoretically calculated values thus suggested that all the silver salt was reduced by the polymers (as found by the XPS earlier). The slightly lower silver content in the composites than the theoretical values could be due to loss of some silver during precipitation or washing steps and the presence of slightly moisture content in the composites.

The fact that the polymer almost retained its structural integrity in the nanocomposites was confirmed via FT-IR spectrum as the spectra for both the composites clearly revealed the presence of all the functional groups like the precursor polymer (Figure 3B.4). The IR absorption peaks at 3200-3600 cm^{-1} indicated the stretching frequencies of O–H and N–H from the chitin derivative **2c**. Peaks at 2918 cm^{-1} and 2857 cm^{-1} showed the peaks for C–H stretching (of methylene and methyl groups). Importantly, the C=O and N–H stretching frequencies from the amide groups were observed at 1661 cm^{-1} and 1541 cm^{-1} for both the composites. To identify the possible interactions between the silver nanoparticles and chitin derivatives, a change in the relative intensity ratio I_{1661}/I_{1541} was calculated. It is expected that

the attachment of silver to nitrogen atoms in the polymer-silver nanocomposites would reduce the vibrational intensity of the N–H bonds because of the increase in the molecular weight of the complex which would become heavier after Ag binding.

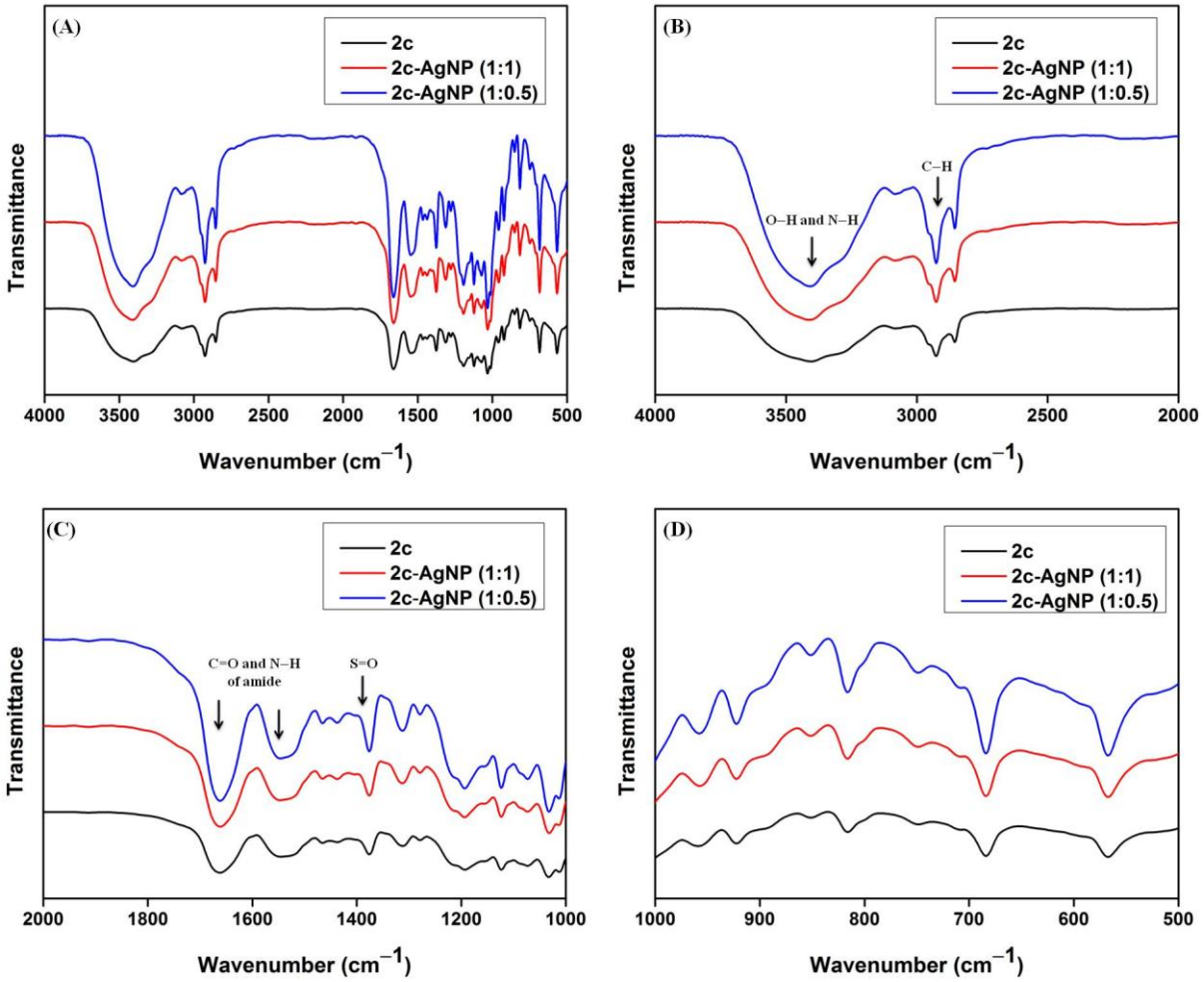

Figure 3B.4: FT-IR spectra of polymer-silver nanocomposites. (A) Full spectra of **2c**, 1:1 and 1:0.5 **2c**-AgNP composites; (B) expanded spectra from 4000 to 2000 cm^{-1} of **2c**, 1:1 and 1:0.5 **2c**-AgNP composites; (C) expanded spectra from 2000 to 1000 cm^{-1} of **2c**, 1:1 and 1:0.5 **2c**-AgNP composites; (D) expanded spectra from 1000 to 500 cm^{-1} of **2c**, 1:1 and 1:0.5 **2c**-AgNP composites.

Interestingly, I_{1661}/I_{1541} ratio for the polymer alone was found to decrease from 1.6 to 1.4 for 1:0.5 composite and 1.3 for 1:1 composite respectively. The above facts thus suggested that the silver could be coordinated with the nitrogen atoms of the polymer leading to stabilization of the silver nanoparticles. Interestingly, when tested for the stability of the silver nanoparticle present in the composites (stability was checked directly from the reaction mixture without precipitation), the particles were found to be highly stable till the tested 6-8

weeks. Thus, by this method polymer-silver nanocomposies were prepared via a simple one-pot reaction without any external reducing and stabilizing agents.

The solid polymer nanocomposites were dissolved in methanol at different amount. The methanolic solution was then coated onto various surfaces such as polystyrene, glass, silicon, polyurethane, etc. via brush-or dip- or spin-coating or drop-casting. Upon drying the composites yielded good film onto the coated surfaces. For having a stable and proper film on surfaces (e.g., catheter), the composites were dissolved in methanol-DMSO or only DMSO and then coated.

3B.2.2 *In-vitro* antibacterial activity

3B.2.2.1 Activity by spray method

Antibacterial activity was determined by spraying the pathogen onto coated glass surfaces as described in the previous chapters. The surfaces were then incubated at 37 ˚C for 24 h along with suitable agar. As expected, the non-coated glass surface showed numerous bacterial colonies thereby indicated the bacterial growth on the plain surface which does not have any antibacterial activity (Figure 3B.5A and E). However, less or no bacterial colonies were observed on nanocomposite-coated surfaces depending on the amount present. Interestingly, the nanocomposites showed remarkably higher activity than the polymer alone against both Gram-positive *S. aureus* and Gram-negative *E. coli*. For example, surfaces coated with 1:1 and 1:0.5 **2c**-AgNP composites showed 100% reduction (~5 log) of viable *S. aureus* at 0.04 $\mu g/mm^2$ each (61.9% polymer with 38.1% AgNP for 1:1 composite and 81.1% polymer with 18.9% AgNP for 1:0.5 composite) while the polymer **2c** coated surfaces showed 100% reduction at 0.15 $\mu g/mm^2$ (Figure 3B.5B-D). Similarly surfaces coated with 1:1 and 1:0.5 **2c**-AgNP composites showed 100% reduction (~5 log) of viable *E. coli* at 0.02 $\mu g/mm^2$ and 0.04 $\mu g/mm^2$ respectively while **2c** coated surface showed 100% reduction at 0.6 $\mu g/mm^2$ (Figure 3B.5F-H). The above results therefore indicated that these nanocomposites were highly efficient in killing bacteria upon contact. Further, the composites were found to be more active against *E. coli* than *S. aureus*. The above results also showed that 1:1 composite is more active than the 1:0.5 composite. Clearly the high antibacterial activity of these nanocomposites against both Gram-positive and Gram-negative bacteria suggested that these materials could be used as potent bactericidal paint.

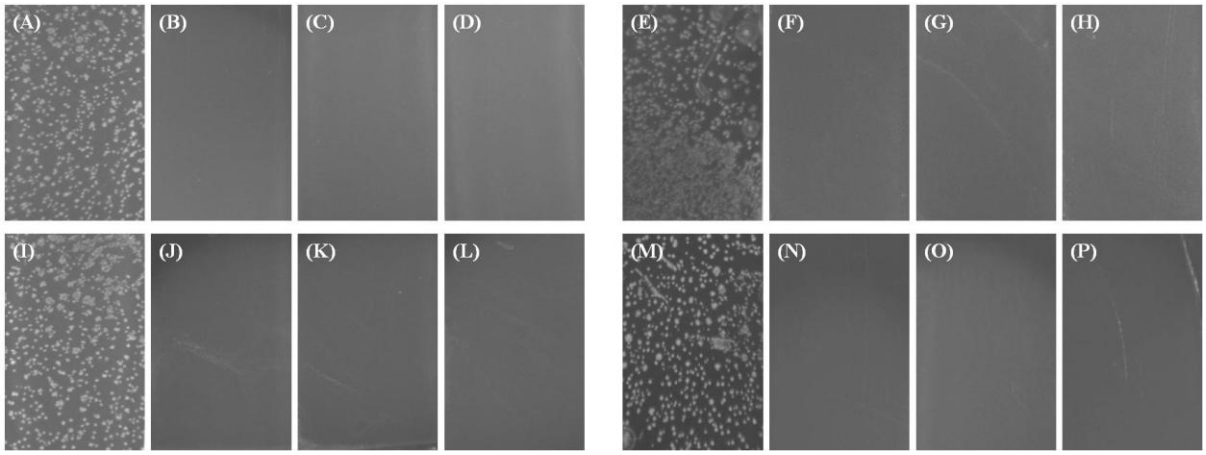

Figure 3B.5: Antibacterial activity of polymer coated surfaces. Photographs of microscopic glass slides after spraying bacteria and incubating for 24 h; (A) and (E): non-coated glass slides (controls); (B) and (F): slides coated with **2c** (0.15 and 0.6 μg/mm^2); (C) and (G): slides coated with 1:1 **2c**-AgNP composite (0.04 and 0.02 μg/mm^2); (D) and (H): slides coated with 1:0.5 **2c**-AgNP composite (0.04 and 0.04 μg/mm^2); (I) and (M): slides coated with PLA (2.5 μg/mm^2); (J) and (N): slides coated with (0.15 μg/mm^2 **2c** + 2.5 μg/mm^2 PLA) and (0.6 μg/mm^2 **1c** + 2.5 μg/mm^2 PLA); (K) and (O): slides coated with (0.04 μg/mm^2 1:1 **2c**-AgNP composite + 2.5 μg/mm^2 PLA) and (0.02 μg/mm^2 1:1 **2c**-AgNP composite + 2.5 μg/mm^2 PLA); (L) and (P): slides coated with (0.04 μg/mm^2 1:0.5 **2c**-AgNP composite + 2.5 μg/mm^2 PLA) and (0.04 μg/mm^2 1:0.5 **2c**-AgNP composite + 2.5 μg/mm^2 PLA).

Notably, the nanocomposites when coated onto the glass surface along with medically relevant polymer such as polylactic acid (PLA) also killed bacteria (~5 log CFU) completely upon spraying. For example surfaces, coated with PLA (2.5 μg/mm^2) and the **2c**-AgNP composites, showed 100% reduction (~5 log) of viable *S. aureus* at 0.04 μg/mm^2 of coating for both the 1:1 and 1:0.5 composites. On the other hand surfaces, coated with PLA (2.5 μg/mm^2) and **2c**, showed 100% reduction at 0.15 μg/mm^2 of the polymer coating (Figure 3B.5I-L). Similar activity was for the *E. coli* also. For example, surfaces coated with PLA (2.5 μg/mm^2) and the **2c**-AgNP composites showed 100% reduction (~5 log CFU) of viable *E. coli* at 0.02 μg/mm^2 for 1:1 composite and at 0.04 μg/mm^2 for 1:0.5 composite respectively. On the other hand, surfaces coated with PLA (2.5 μg/mm^2) and the polymer **2c** showed 100% reduction at 0.6 μg/mm^2 of the polymer coating (Figure 3B.5M-P). The above results therefore showed that the composites retained their activity even after coating along with PLA. These findings thus furnished that the composites could be potentially used to develop self-defensive biomaterials.

3B.2.2.2 Activity against water-borne bacteria (Minimum inhibitory amount)

Antibacterial efficacy of the nanocomposites against water-borne bacteria was determined by coating polystyrene well plate followed by addition of bacterial suspensions in suitable broth. The plates (containing 200 μL of ~10^5 CFU/mL bacteria) were incubated at 37 ˚C for about 24 h and then visual turbidity was observed. The efficacy was expressed as minimum inhibitory amount (MIA), i.e., the minimum amount required to inhibit the growth of bacteria required/unit surface area as defined in chapter 2A. Like the spray method, the nanocomposites showed superior activity against bacteria over the polymer alone (Figure 3B.6). To illustrate, MIA values of the polymer **2c** were 0.06 μg/mm^2 and 3.9 μg/mm^2 against *S. aureus* and *E. coli* respectively. On the other hand, MIA values of the **2c**-AgNP nanocomposites were found to be 0.06 μg/mm^2 each for both 1:1 and 1:0.5 composites (0.04 μg/mm^2 of **2c** with 0.02 μg/mm^2 of AgNP for 1:1 composite and 0.05 μg/mm^2 of **2c** with 0.01 μg/mm^2 of AgNP for 1:0.5 composite) against *S. aureus* and, 0.24 μg/mm^2 for the 1:1 composite (0.13 μg/mm^2 of **2c** with 0.09 μg/mm^2 of AgNP) and 0.48 μg/mm^2 for 1:0.5 composite (0.3 μg/mm^2 of **2c** with 0.18 μg/mm^2 of AgNP) against *E. coli* respectively (Figure 3B.6A and B). The composites also showed high activity against *P. aeruginosa*, an opportunistic Gram-negative bacterium known to cause many nosocomial infections. While the MIA value of polymer **2c** was found to be 7.8 μg/mm^2 against *P. aeruginosa*, 1:1 and 1:0.5 composites showed MIA values of 0.48 μg/mm^2 (0.3 μg/mm^2 of **2c** with 0.18 μg/mm^2 of AgNP) and 0.98 μg/mm^2 (0.61 μg/mm^2 of **2c** with 0.37 μg/mm^2 of AgNP) respectively against the same pathogen (Figure 3B.6C). Not only against drug-sensitive bacteria, surfaces coated with the composites showed activity against various drug-resistant bacteria such as methicillin-resistant *S. aureus* (MRSA), vancomycin-resistant *E. faecium* (VRE), and beta-lactam-resistant *K. pneumoniae*. To illustrate, MIA values of the polymer **2c** were 0.06 μg/mm^2 each against drug-resistant MRSA and VRE. On the other hand, MIA values of 1:1 and 1:0.5 composites were found to be 0.06 μg/mm^2 each (0.04 μg/mm^2 **2c** with 0.02 μg/mm^2 AgNP for 1:1 composite and 0.05 μg/mm^2 **2c** with 0.01 μg/mm^2 AgNP for 1:0.5 composite) against MRSA and VRE (Figure 3B.6D and E). Against drug-resistant Gram-negative *K. pneumoniae*, while MIA value of polymer **2c** was 15.6 μg/mm^2, MIA values of 1:1 and 1:0.5 composites were found to be 1.9 μg/mm^2 (1.2 μg/mm^2 of **2c** with 0.7 μg/mm^2 of AgNP) and 3.9 μg/mm^2 (2.4 μg/mm^2 of **2c** with 1.5 μg/mm^2 of AgNP) respectively against the same bacteria (Figure 3B.6F).

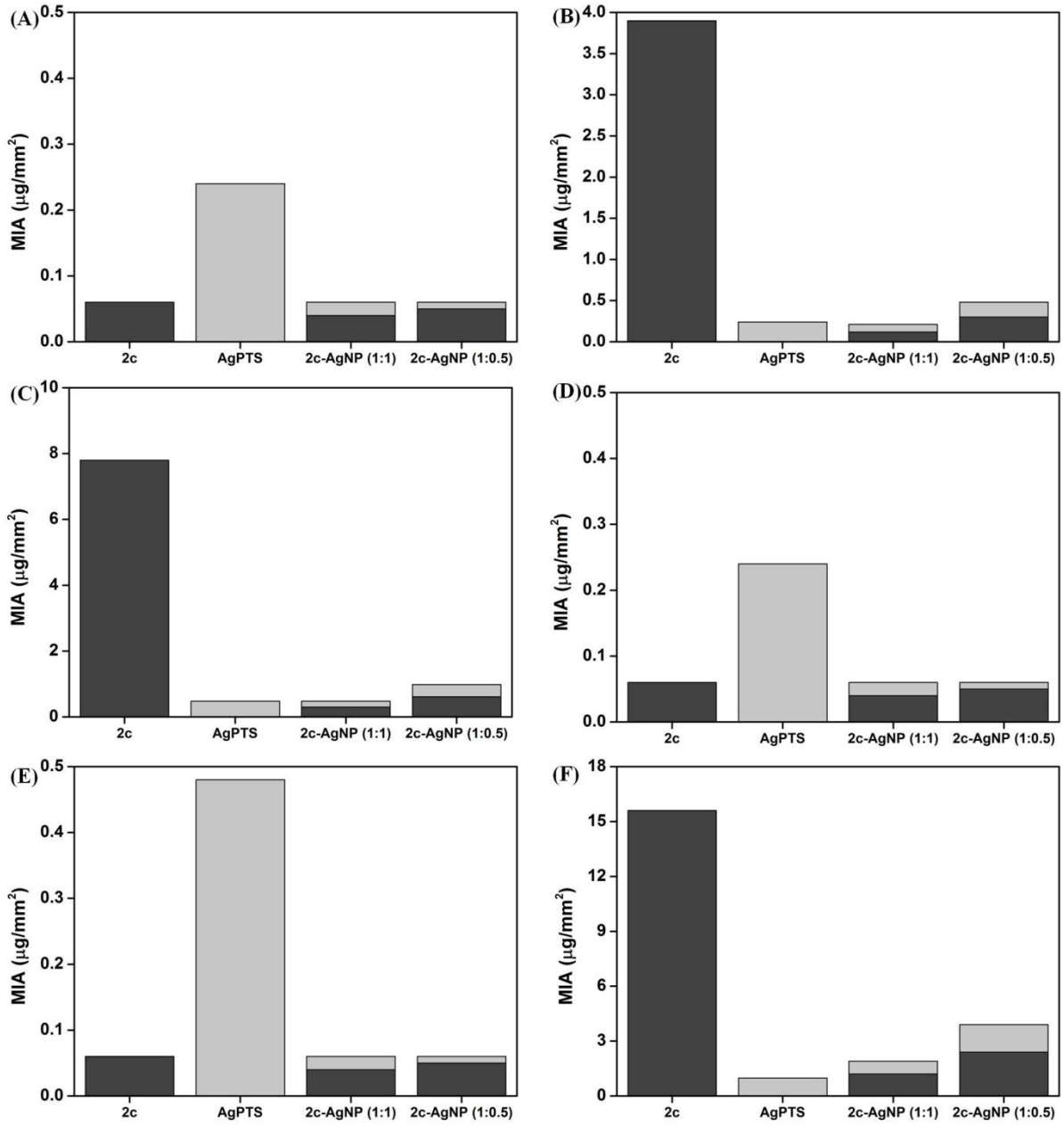

Figure 3B.6: Antibacterial activity (MIA) of composite coated surfaces after adding bacterial suspension and incubating for 24 h: (A) *S. aureus*; (B) *E. coli*; (C) *P. aeruginosa*; (D) MRSA; (E) VRE and (F) beta lactam-resistant *K. pneumoniae*.

The above results therefore indicated that polymer-nanocomposites are more active against bacteria than the polymer alone. Further, the composites showed reasonably higher activity against Gram-negative bacteria than the polymer. One of the limitations with the hydrophobically modified cationic chitin derivatives was that the polymers were found to be less active against Gram-negative bacteria. By developing polymer-silver nanocomposites, it was therefore possible to obtain antimicrobial coating materials which are equally active against both Gram-positive and Gram-negative bacteria. Interestingly though not significantly

enough, both the composites showed MIA values lesser than the AgPTS alone (MIA values of AgPTS were 0.24 μg/mm^2 and 0.24 μg/mm^2 against *S. aureus* and *E. coli*). However, it should be mentioned that while AgPTS film can release all its silver ions into the solution immediately, only a fraction of silver ions will be released into the solution after 24 h by the polymer-silver nancomposites to have activity. Overall, 1:1 composite was more active than the 1:0.5 composite. Not only inhibition, the composites showed complete killing of the bacteria upon treatment with the coated surface. For example, the minimum bactericidal amounts (expressed as MBA, μg/mm^2) were found to be 0.06 μg/mm^2, 0.39 μg/mm^2, 0.98 μg/mm^2, 0.24 μg/mm^2, 0.24 μg/mm^2 and 1.9 μg/mm^2 against *S. aureus*, *E. coli*, *P. aeruginosa*, MRSA, VRE and *K. pneumoniae* respectively.

3B.2.2.3 Bactericidal kinetics

To establish how fast the composites kill bacteria upon contact, the rate of action was investigated towards both *S. aureus* and *E. coli* using the more active 1:1 composite along with **2c** and AgPTS at their respective MIA and 6 × MIA values.

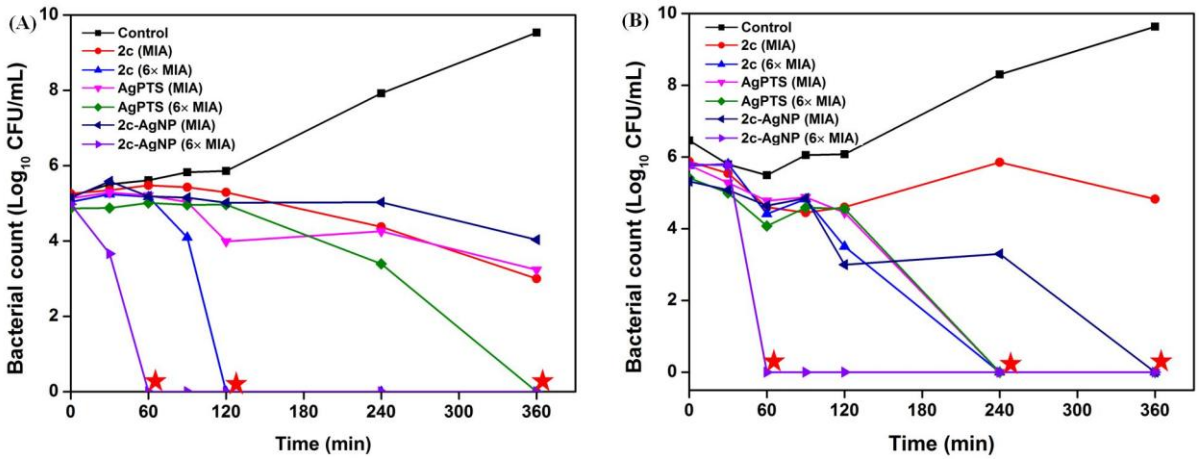

Figure 3B.7: Kinetics of antibacterial action. Rate of killing for the composite (1:1), polymer **2c** and AgPTS, all at two different amounts: MIA and 6 × MIA towards *S. aureus* (A) and *E. coli* (B) respectively. Stars represent < 50 CFU/mL.

While polymer **2c** was found to kill *S. aureus* (~5 log reduction) at 120 min at 6 × MIA, 1:1 composite was found to kill the same bacteria at only 60 min at 6 × MIA. Notably, AgPTS was found to kill *S. aureus* at 360 min at 6 × MIA (Figure 3B.7A). On the other hand, while **2c** killed *E. coli* (~5 log reduction) at 240 min at 6 × MIA, 1:1 composite was found to kill the same bacteria at only 60 min at 6 × MIA. Notably, AgPTS was found to kill *E. coli* at 240

min at 6 × MIA (Figure 3B.7B). These results thus indicate that the composite coatings have remarkably higher killing rates against both the bacteria making them suitable for efficient antimicrobial coating.

3B.2.2.4 Membrane-active mode of action

The mode of action of the nanocomposites was examined by confocal laser scanning microscopy (CLSM) via live and dead assay using SYTO 9 and propidium iodide (PI) respectively following protocols described earlier in the previous chapters.

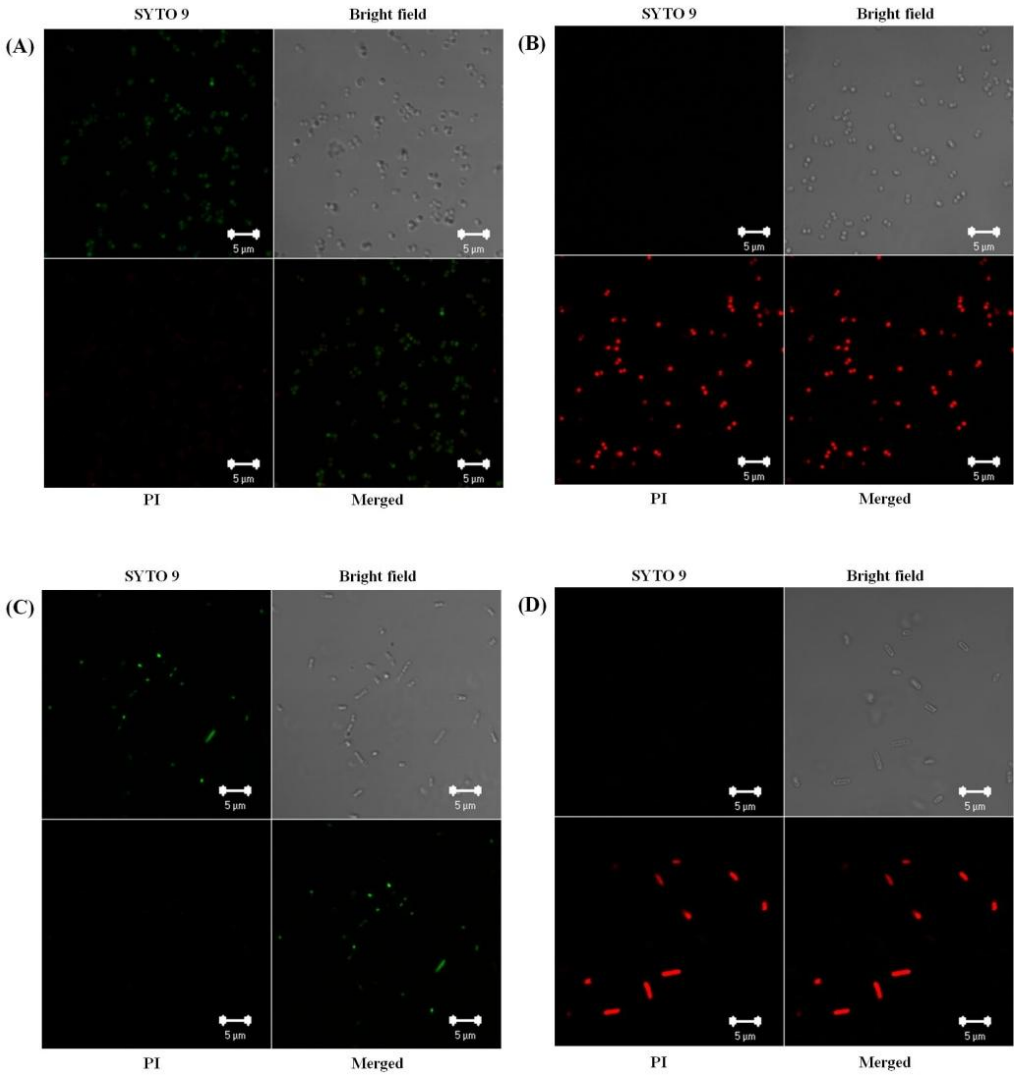

Figure 3B.8: Membrane-active mode of antibacterial action. CLSM images of bacterial cells: untreated (A) *S. aureus* and (B) *E. coli*; cells treated with the surface coated with 1:1 composite against (C) *S. aureus* (D) *E. coli* respectively, all after staining with SYTO 9 and PI.

The polystyrene well plates were coated with the polymer nanocomposites at 6 × MIA and then bacteria were treated with the surface for about 4 h. The confocal microscopy images of non-treated samples showed green fluorescence for both *S. aureus* and *E. coli* thereby indicated the cell viability in control samples (Figure 3B.8A and C). The cell treated with 1:1 nanocomposite at its 6 × MIAs, showed appearance red fluorescence thereby indicated the loss of membrane integrity for both *S. aureus* and *E. coli* (Figure 3B.8B and D).

3B.2.3 Bacterial biofilm inhibition

The antibiofilm activity of the nanocomposites was therefore evaluated by coating the composite (1:1) onto glass surface at its 6 × MIA against MRSA and *P. aeruginosa*, two of the most frequently biofilm forming bacteria and often causes nosocomial infections via biofilm formation.[26] Further, antibiofilm efficacy of the composite was compared to that of the polymer **2c** by challenging the same surface repeatedly. Coated glass cover slips were challenged against both MRSA and *P. aeruginosa* under stationary conditions at 37 ˚C. The glass surfaces were then imaged by confocal laser scanning microscopy (CLSM) after 24 h. The non-coated cover slips showed huge bacterial growth with an effective thickness of 12-16 μm thus indicating thick and matured biofilm formation for both MRSA and *P. aeruginosa* respectively (Figure 3B.9A and Figure 3B.10A). In contrast, both the polymer and the nancomposite coated surfaces showed only monolayered bacteria with an effective thickness of 2-3 μm after 24 h against both MRSA and *P. aeruginosa* (Figure 3B.9B-C and Figure 3B.10B-C) thereby signifies that both polymer and nancomposite were capable of inhibiting the biofilm formation till 24 h. However, when the same surfaces were challenged again for another 24 h and 48 h against both MRSA and *P. aeruginosa*, the control surfaces further showed thickening of the biofilm layer (Figure 3B.9D and G for MRSA and Figure 3B.10D and G for *P. aeruginosa* respectively). Notably, the polymer-coated surfaces showed cluster of bacteria with an effective thickness of 4-8 μm thereby indicating that the polymer was failing to inhibit biofilm formation (Figure 3B.9E and H for MRSA and Figure 3B.10E and H for *P. aeruginosa* respectively). On the contrary, nancomposite coated surfaces showed only few bacteria with an effective thickness of 2-3 μm even after 48 h and 72 h against both MRSA and *P. aeruginosa* (Figure 3B.9F and I for MRSA and Figure 3B.10F and I for *P. aeruginosa* respectively). The above results thereby signified the efficacy of the nancomposite in inhibiting biofilm formation for longer duration.

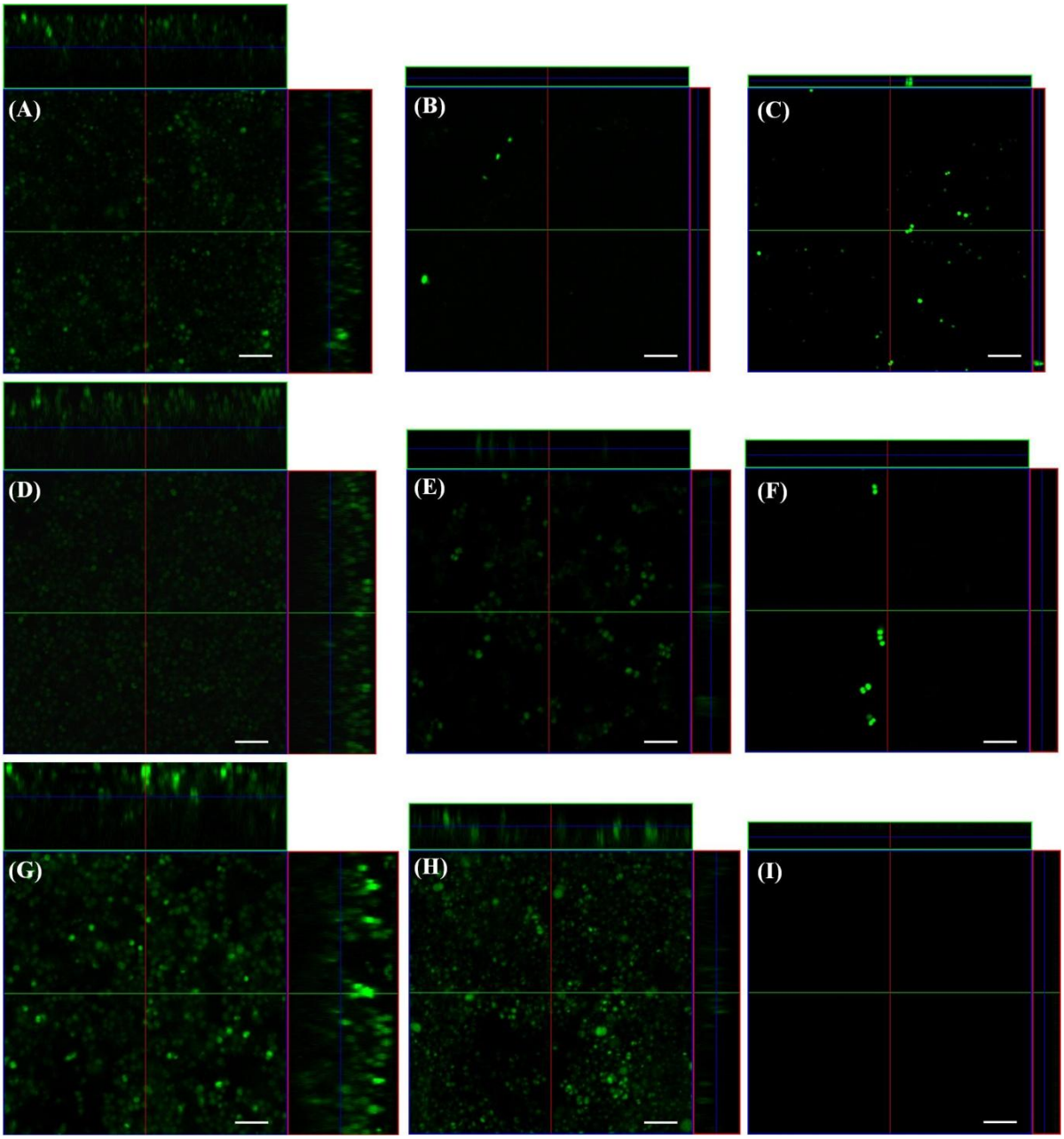

Figure 3B.9: Biofilm inhibition ability of the nanocomposite against MRSA. Confocal laser scanning microscopy images of non-coated, **2c**-and nanocomposite-coated cover glass surfaces. (A-C): Surfaces for non-coated, **2c**-and nanocomposite-coated cover glasses after 24 h; (D-F): Surfaces for non-coated, **2c**-and nanocomposite-coated cover glasses after 48 h and (G-I): Surfaces for non-coated, **2c**-and nanocomposite-coated cover glasses after 72 h of treatment against MRSA. Scale bar 5 μm.

Further, when the bacterial counts were determined in the biofilms, (12±1.4) log reduction of *S. aureus* after 72 h and (10±0.9) log reduction of *E. coli* after 120 h were observed for the polymer coated surface at 6 × MIA compared to noncoated surface (the control surfaces showed 14.8 log CFU/mL of *S. aureus* and 12.2 log CFU/mL of *E. coli* respectively).

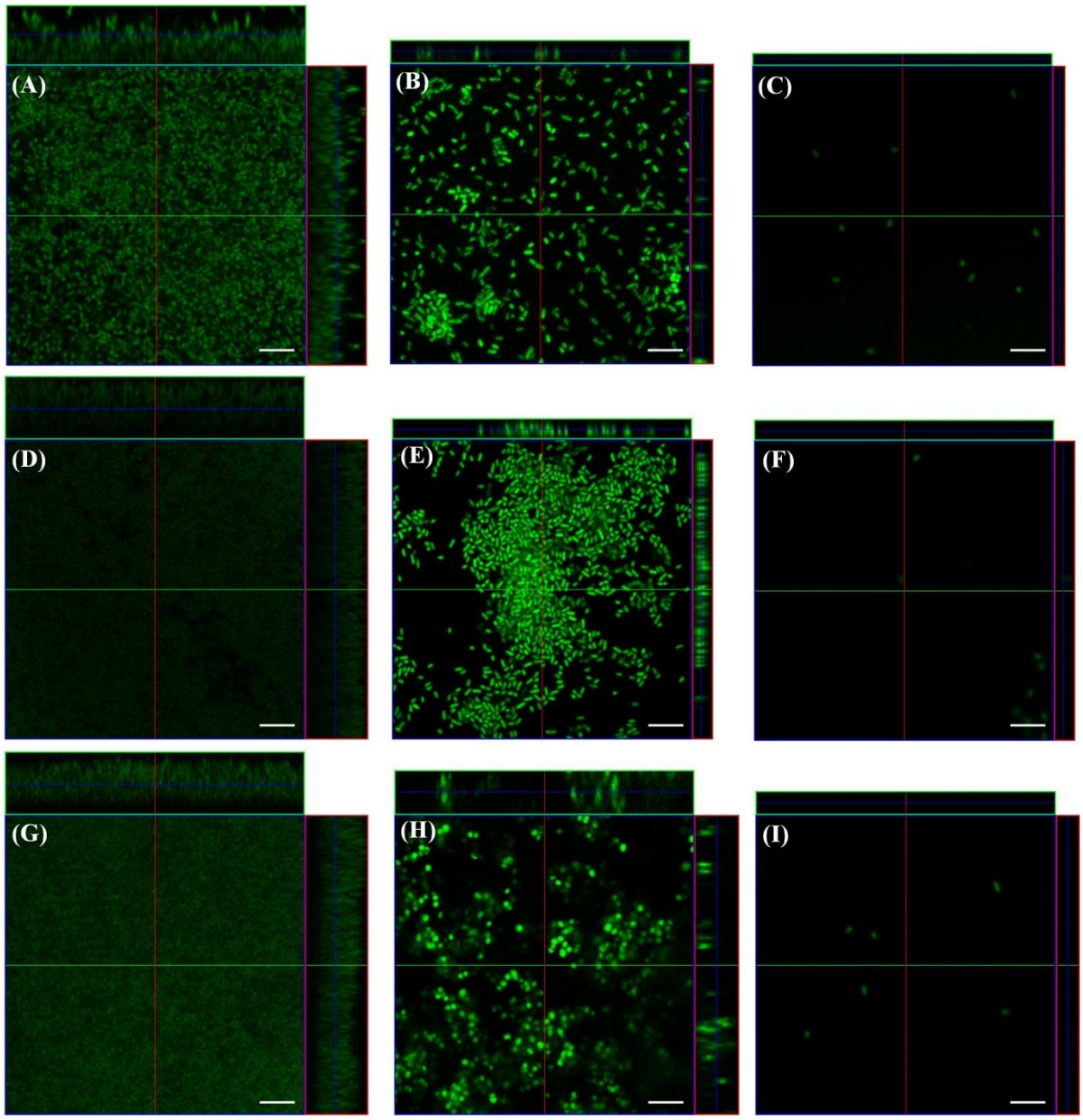

Figure 3B.10: Biofilm inhibition ability of the nanocomposite against *P. aeruginosa*. Confocal laser scanning microscopy images of non-coated, **2c**-and nanocomposite-coated cover glass surfaces. (A-C): Surfaces for non-coated, **2c**-and nanocomposite-coated cover glasses after 24 h; (D-F): Surfaces for non-coated, **2c**-and nanocomposite-coated cover glasses after 48 h and (G-I): Surfaces for non-coated, **2c**-and nanocomposite-coated cover glasses after 72 h of treatment against *P. aeruginosa*. Scale bar 5 μm.

3B.2.4 Antifungal activity

3B.2.4.1 Minimum inhibitory amount

Antifungal efficacy of both the composites was evaluated against different *Candida* spp. (*C. albicans*, *C. dubliniensis*, *C. tropicalis*) and *Cryptococcus* spp. (*C. neoformans var. grubii*

(serotype A), *C. neoformans var. gattii* (serotype B) and *C. neoformans var. neoformans* (serotype D)) and expressed as minimum inhibitory amount (MIA)/unit surface area as defined in chapter 2A. Like bacteria, the nanocomposites showed superior activity over the polymer alone against the fungal species tested (Figure 3B.11). For example, while the MIA value of polymer **2c** was found to be 1.0 μg/mm^2 against *Candida albicans*, 1:1 and 1:0.5 **2c**-AgNP composites showed MIA values of 1.0 μg/mm^2 (0.62 μg/mm^2 of **2c** with 0.38 μg/mm^2 of AgNP) and 2 μg/mm^2 (1.6 μg/mm^2 of **2c** with 0.38 μg/mm^2 of AgNP) respectively against the same fungi (Figure 3B.11A). Thus only 1:1 composite was showed better activity against *C. albicans* over the polymer whereas 1:0.5 did not show any improvement in activity. However, the composites were found to be more active against other *Candida* spp. For example, while the MIA value of **2c** was 1.0 μg/mm^2 against *C. dubliensis*, 1:1 and 1:0.5 composites showed MIA values of 0.48 μg/mm^2 each (0.3 μg/mm^2 **2c** with 0.18 μg/mm^2 AgNP for 1:1 composite and 0.39 μg/mm^2 **2c** with 0.09 μg/mm^2 AgNP for 1:0.5 composite) against the same fungi (Figure 3B.11B). Against *C. tropicalis*, another *Candida* spp., **2c** showed MIA value of 0.24 μg/mm^2 whereas 1:1 and 1:0.5 composites showed MIA values of 0.12 μg/mm^2 each (0.08 μg/mm^2 **2c** with 0.04 μg/mm^2 AgNP for 1:1 composite and 0.1 μg/mm^2 **2c** with 0.02 μg/mm^2 AgNP for 1:0.5 composite) against the same fungi (Figure 3B.11C). Notably, the nanocomposites showed very high activity against *Cryptococcus* spp. as well. While the MIA values of **2c** were found to be 0.48 and 0.12 μg/mm^2 against *C. neoformans ser A* and *C. neoformans ser B* respectively, 1:1 and 1:0.5 composites showed MIA values of 0.12 μg/mm^2 each (0.08 μg/mm^2 **2c** with 0.04 μg/mm^2 AgNP for 1:1 composite and 0.1 μg/mm^2 **2c** with 0.02 μg/mm^2 AgNP for 1:0.5 composite) against both the species (Figure 3B.11D and E). Against *C. neoformans ser D*, another *Cryptococcus* spp., **2c** showed MIA value of 0.06 μg/mm^2 whereas 1:1 and 1:0.5 **2c**-AgNP composites also showed MIA values of 0.06 μg/mm^2 each (0.04 μg/mm^2 **2c** with 0.02 μg/mm^2 AgNP for 1:1 composite and 0.05 μg/mm^2 **2c** with 0.01 μg/mm^2 AgNP) against the same species (Figure 3B.11F).

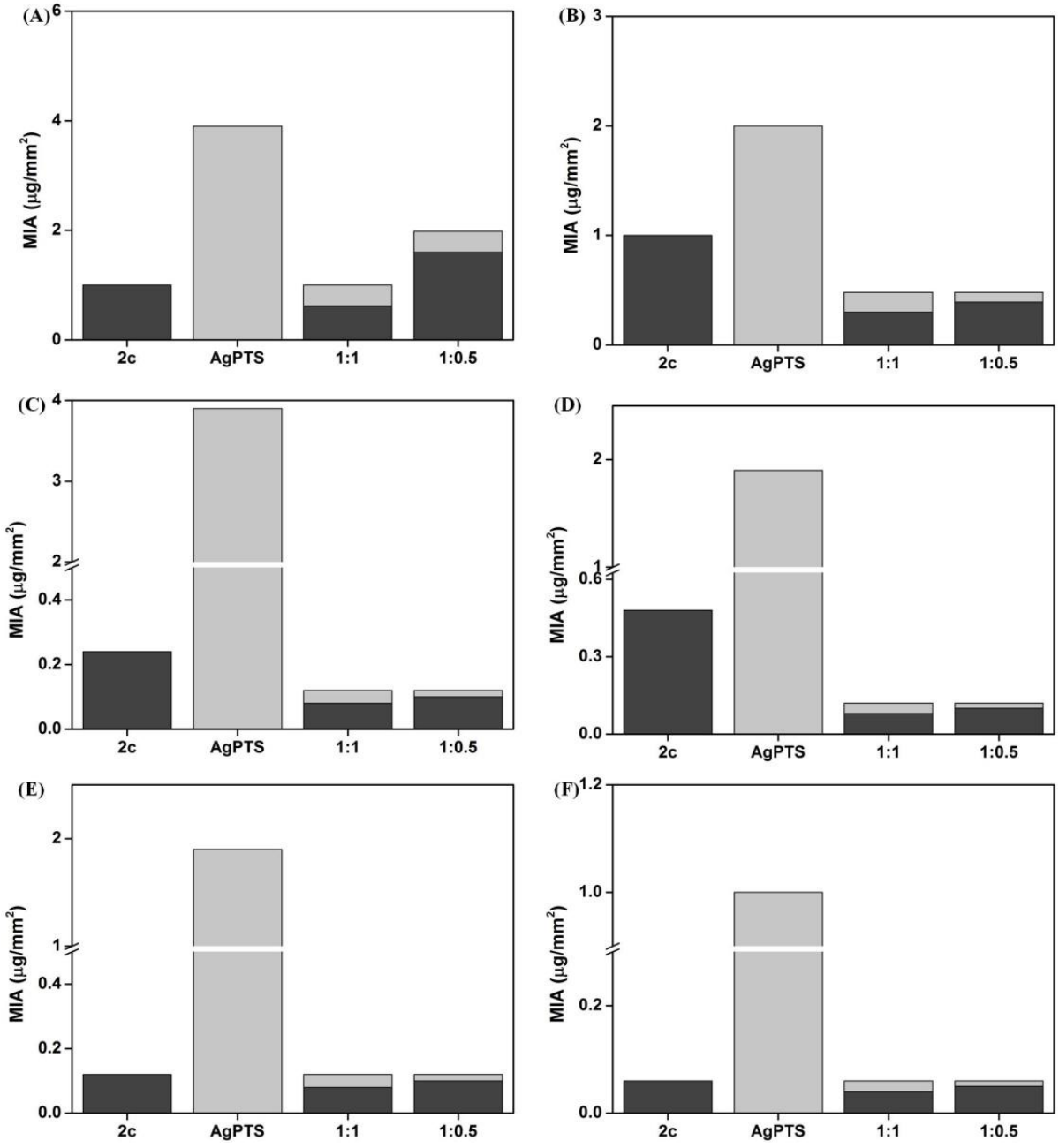

Figure 3B.11: Antifungal activity of composite coated surfaces after adding bacterial suspension and incubating for 24 h: (A) *C. albicans*; (B) *C. dubliensis*; (C) *C. tropicalis*; (D) *C. neformans* ser A; (E) *C. neformans* ser B and (F) *C. neformans* ser D.

The above results therefore indicated that polymer-nanocomposites especially 1:1 are more active against fungi than the polymer. However, as mentioned earlier that the nanocomposite films might release only a fraction of the silver ion into the suspension leading to relatively less activity unlike the spray method wherein the pathogen are in direct contact with both antimicrobial polymer and silver. The composites were also shown to be fungicidal as well. The minimum fungicidal amounts (MFA) of the more active 1:1 composite were found to be

3.9 μg/mm^2 against *C. albicans*, 2.0 μg/mm^2 against *C. dubliensis*, 0.24 μg/mm^2 against *C. tropicalis*, 0.48 μg/mm^2 against *C. neoformans ser A*, 0.06 μg/mm^2 each against *C. neoformans ser B* and *C. neoformans ser D* respectively. The above results therefore indicated that in most of the cases minimum inhibitory amount is the minimum fungicidal amount for the composite.

3B.2.4.2 Fungicidal kinetics

To establish how fast the composites killed fungi, the rate of fungicidal action was investigated against *C. albicans* using surfaces coated with the composite (1:1).

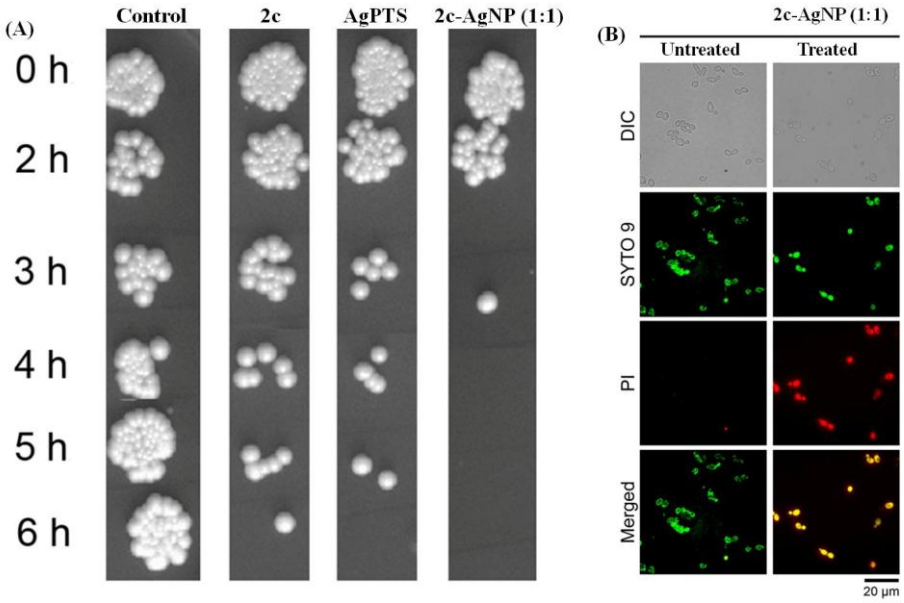

Figure 3B.12: Antifungal activities of the composites. (A) Antifungal kinetics of polymers 2**c** coated surfaces at different amounts (MIA and 8 × MIA) against *C. albicans*: representative cross section of the YPD agar plate showing the growth of fungal colonies at different times. Mechanistic investigation of antifungal activity of polymer coatings. Fluorescence microscopy images of *C. albicans* after staining with SYTO 9 and PI exposed to uncoated surfaces (control) and nanocomposite (1:1) coated surfaces.

The rate of killing was also compared with the polymer and AgPTS at the respective 8 × MIA values by treating the coated surfaces with ~10^5 CFU/mL cells. While the polymer and AgPTS coated surfaces killed fungi within 6 h, the composite coated surface killed *C. albicans* only within 3 (Figure 3B.12A). The above results therefore suggested that the composite acted at a much faster rate than the polymer alone.

3B.2.4.3 Membrane-active mode of antifungal action

As the nanocomposites contain cationic polymer which was shown to be membrane active, the composites are also expected to show membrane-active mode of action leading cell death. To examine the mode of action of the composites, LIVE/DEAD assay was performed with the fungal cell (*C. albicans*) using green fluorescent SYTO 9 and red fluorescent PI dyes via confocal laser scanning microscopy (CLSM). Untreated fungi showed the presence of viable cells in the case of control samples (non-coated surface) as observed by the green fluorescence of SYTO 9 (Figure 3B.13B). Cells treated with the composites-coated surfaces, on the other hand, showed red fluorescence of PI thus indicated the compromised cell membrane (Figure 3B.13B).

3B.2.5 Fungal biofilm inhibition

The antibiofilm properties of the nanocomposites were evaluated by coating the more active composite (1:1 **2c**-AgNP) onto the wells of a 6-well plate and determining the ability in inhibiting fungal biofilm formation via fluorescence microscopy. The wells were coated (at MIA of *C. albicans*) and then incubated for about 48 h under stationary conditions. After the treatment, the supernatant from the wells was carefully removed, washed with PBS and then stained with SYTO 9.

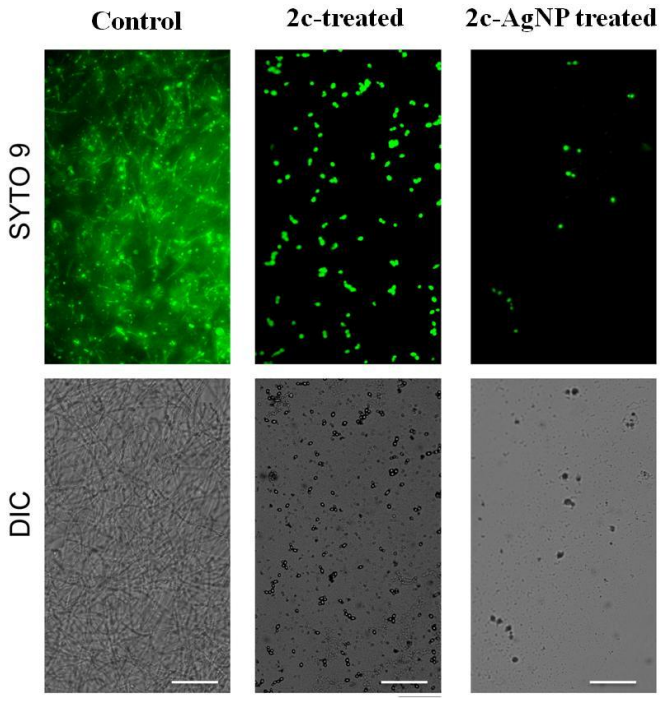

Figure 3B.13: Antibiofilm activity of the polymer-silver nanocomposite (1:1) coated surface. Scale bar 40 μm.

The bottom of the wells was directly imaged via fluorescence microscopy. While the non-coated wells showed huge fungal growth with filamentous structure indicative of biofilm formation (Figure 3B.13), the composite-coated surface was shown to have only few fungal cells without any filamentous structure. The above results thus suggested that the composite was capable of preventing fungal biofilm formation upon coating onto surface. In contrast though the polymer coated surface showed biofilm inhibition, the surface showed higher cell density at the respective MIA (Figure 3B.13). The above results therefore suggested that the composite was more active in inhibiting fungal biofilm and thus might be used as antibiofilm coatings.

3B.2.6 Silver ion release study (Zone of inhibition)

The composites were previously shown to be active upon contact onto the coated surface wherein both components of the composites were shown to act on contact. To prove that the silver nanocomposites kill microorganism also by releasing the silver ion to the surroundings, Kirby Bauer testing of zone of inhibition was performed.[13] Circular Whatman filter paper was dip coated with only polymer (**2c**), only AgPTS and with both 1:1 and 1:0.5 2c-AgNP composites. The coated papers were then kept on agar plate containing bacterial suspension (freshly grown bacteria were sprayed onto the plate and the plates were covered by the bacterial solution). If the antimicrobial component(s) leach out from the coated paper, a clear zone of inhibition is expected due to bacterial death in the respective zone. Notably, the polymer coated paper did not show any inhibition zone against both *S. aureus* and *E. coli* thereby indicated that it can kill pathogen only upon contact (Figure 3B.14A and B). However, both AgPTS and polymer-AgNP coated papers showed significant zone of inhibition. The observed inhibition zone is a result of the leaching of active biocidal species Ag^+ ion from the AgPTS or embedded Ag nanoparticles present in the composite into the surrounding aqueous medium. Importantly, nanocomposites showed significantly lower zone of inhibition compared to AgPTS. This could be due to the hydrophobically modified chitin derivative which reduces the leaching of Ag^+ ion from surface by reducing the contact area of the surrounding aqueous media and the gradual dissolution of silver into Ag^+ ion in sharpt contrast to already Ag^+ ion of AgPTS. However, the above study also suggested that the nanocomposites kill pathogen not only upon contact but also by releasing Ag^+ ion into the surroundings.

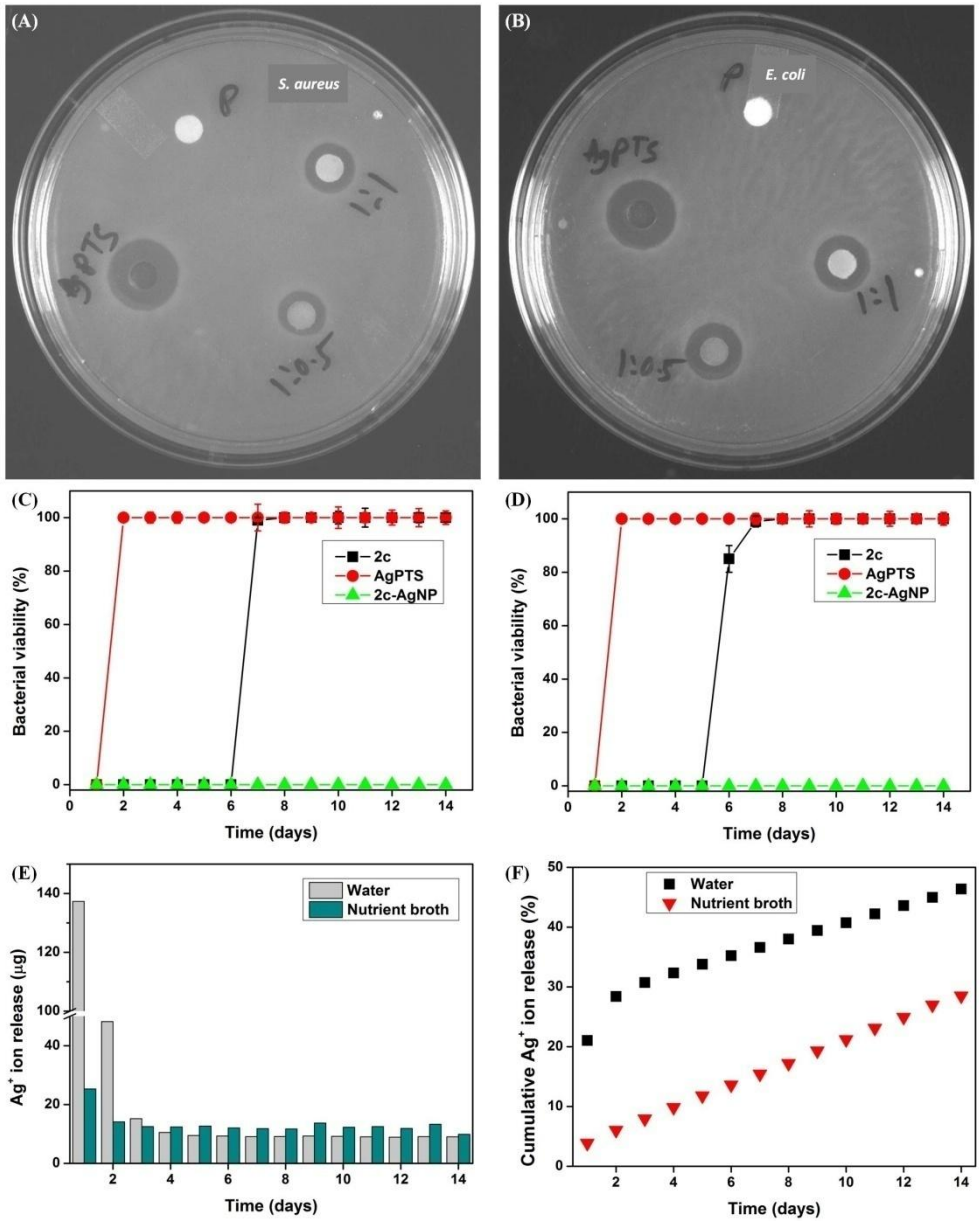

Figure 3B.14: Bacterial lawn growth inhibition, long lasting antibacterial activity and release kinetics of the nanocomposites. (A) Representative agar plate showing the zone of inhibition in an (A) *S. aureus* lawn and (B) *E. coli* lawn produced by diffusion of the antimicrobials. Long lasting antibacterial activity of the polymer **2c**, AgPTS and nanocomposite (1:1) coated surfaces challenged repeatedly for 14 days against (C) *S. aureus* and (D) *E. coli* respectively. Release kinetics of silver ion from the composite film. (E) Silver ion release from the composite coated surface in each day; (F) cumulative silver ion release from the composite coated surface.

3B.2.7 Long lasting activity and silver ion release kinetics

To be useful in biomedical devices and implants (e.g., orthopaedic implants) the coating should show activity over an extended period of time for the complete eradication of pathogen.[13] Antimicrobial polymer-nanocomposites are expected to display long lasting activity because of their dual action (both release and contact active mechanism) and higher

efficacy. The antibacterial activities of the composites were therefore tested over an extended period of time. Polymer (**2c**) alone, AgPTS alone and the 1:1 and 1:0.5 **2c**-AgNP composites were coated onto glass cover slips (18 mm diameter) and then incubated daily with freshly grown bacteria (3.9 μg/mm^2 of coating against *S. aureus* and 7.8 μg/mm^2 of coating against *E. coli* for all the materials). At the end of each incubation cycle (approximately 24 h), the broth was inspected for bacterial growth (by visual turbidity). A quantity of 20 μL of the medium was also plated on suitable agar plates and incubated to visualize bacterial colonies. This was performed to distinguish between the bactericidal and bacteriostatic effect in cases where the broth was still clear. At the end of each daily cycle, the old medium was discarded and fresh broth containing bacterial suspension was added to the coated cover slips. The method allowed testing the ability of the composites to generate sufficient amounts of bioavailable Ag^+ ions each day without getting depleted. Bioavailable silver released each day would therefore be removed with the old broth, and the ability of the composite to generate more active species would be tested. Further, the method would unambiguously allow testing the repeatability of the coatings.

Notably, the composite was shown to inhibit bacterial growth completely till 14 days as tested against both *S. aureus* and *E. coli* (Figure 3B. 14C and D). In contrast, AgPTS was shown to be effective inhibiting bacterial growth only for the first inoculation. The above facts therefore suggested that the composite sustained a sufficient concentration of bioavailable Ag+ ions in the medium for days along with its contact active mode of action to kill both *S. aureus* and *E. coli*. On the other hand, only the polymer coated surfaces was shown to inhibit *S. aureus* growth for 6 days and *E. coli* growth for 5 days Figure 3B. 14C and D. The reason for this short duration of polymer can be explained as follows. The cationic polymers kill bacteria by disrupting the membrane integrity upon contact. Also, the polymers are known to have bacteria-adsorbing effects (capture of negatively charged bacteria by cationic polymer). Once the polymer kills/captures bacteria, the cell membrane remnants/cell debris presumably remain tightly adsorbed on the polymer-coated surface thus preventing further antibacterial action. In contrast, composite continues to release Ag+ ions into the medium even after the surface is completely covered by dead bacteria also possibly by removing dead bacteria upon its release and hence allowing further contact with the antibacterial polymer, thereby showing long-lasting activity.

To prove that the composite coated surfaces released Ag^+ ion over an extended period of time, release kinetics was performed by atomic emission spectroscopy (AES) by

measuring the amount of the Ag^+ ion into released media. Glass cover slips (12 mm diameter) were coated with 1:1 nanocomposite thus containing certain amount of silver. Then the cover slips were dipped into 0.5 mL of water or nutrient broth and were incubated under constant shaking. After 24 h of incubation, the released media were collected and equal volume of fresh media (water and broth) was added. The cycle was repeated for about 14 days. Finally the amount of silver ion was quantified via AES. Rapid release of Ag^+ ion was observed from in first two days the polymer-silver nanocomposite (containing 653 μg of AgNP) in water (137 μg in day 1 and 47 μg in day 2). Interestingly, the release of Ag^+ ion was found to be much lower in the case of nutrient media (25 μg in day 1 and 14 μg in day 2). However, from day 3, the composite released almost similar amount of Ag^+ ion in both water and nutrient broth (Figure 3B. 14E). After day 14, the composite was shown to release 46% and 29% of the total silver content in water and nutrient broth respectively under the experimental conditions (Figure 3B.14F). Clearly the nanocomposite was able to release the silver ion over an extended period of time thus leading to long lasting (and higher biofilm inhibition) activity.

3B.2.8 Toxicity of the nanocomposites

3B.2.8.1 *In-vitro* toxicity (Hemolytic activity)

Hemocompatibility of the nanocomposite-coated surfaces was evaluated with human red blood cells (hRBC) and expressed as HA_{50} (the amount of the coated polymer that caused 50% hemolysis). The composites were found to be almost non-hemolytic upto 3.9 $\mu g/mm^2$. Only 5-6% hemolysis occurred at 7.8 $\mu g/mm^2$ of the composites coating which is much higher than their MIA values (Figure 3B.15A). These results thus indicated the polymers are selectively active toward bacteria over human erythrocytes. To visualize the effect of composite coating on the morphology of the erythrocytes, both treated and non-treated hRBC were also imaged microscopy. The microscopy images showed that RBCs taken from the composite coated surface as well as from the non-coated surface have characteristic healthy and round morphology, indicating that the composites are indeed non-hemolytic. In contrast, when the highly toxic detergent Triton-X (TX, 0.5%, v/v) was added, full hemolysis was observed as no blood cells were seen under the microscope (Figure 3B.15B).

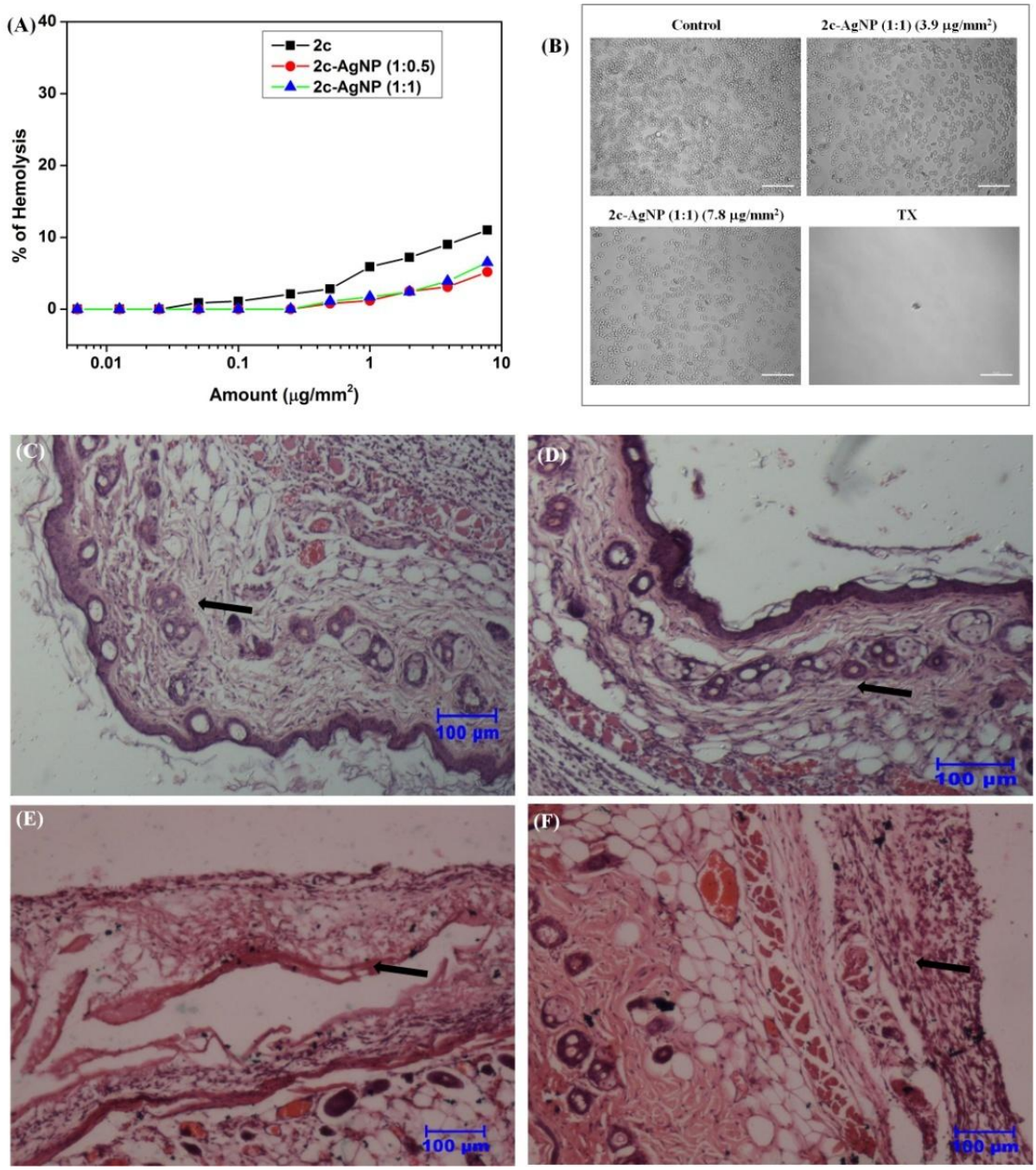

Figure 3B.15: *In-vitro* and *in-vivo* biocompatibility of the 1:1 **2c**-AgNP composite. (A) % of Hemolysis of polymers as a function of the amount of polymer-coating; (B) phase-contrast images of hRBC taken from the coated-coated surfaces or from the non-coated surface with and without TX (Triton-X). Mice skin and subcutaneous tissue histopathology: (C) tissue surrounding the non-coated catheter showing normal architecture of epidermis, dermis and subcutaneous tissues (arrow); (D) tissue surrounding the composite catheter (~2 μg/mm^2) showing normal skin epidermis and dermis layer with normal adipose tissue (arrow); (E) tissue surrounding the composite catheter (4 μg/mm^2) showing normal dermis layer of skin with sweat and sebaceous gland (arrow); (F) tissue surrounding the composite catheter (8 μg/mm^2) showing only few infiltrations of inflammatory cells with neutrophils (arrow) with intact epidermis and dermis layer.

3B.2.8.2 *In-vivo* toxicity

The compatibility of the nanocomposite coated surfaces was further evaluated under *in-vivo* conditions upon subcutaneous implantation of composite coated catheter in mice.[27] Mice skin tissue surrounding the catheter was collected after 4 days, fixed with formalin and then imaged by haematoxylin and eosin staining. Tissue samples surrounding the catheters coated with 2 μg/mm^2, 4 μg/mm^2 and 8 μg/mm^2 of the composite showed negligible to mild inflammation after 4 days of implantation (like tissue surrounding the non-coated catheters (Figure 3B.15C-F). This showed that not only the polymer but also gradual release of silver did not cause any significant toxicity to the surrounding tissue.

3B.2.9 *In-vivo* activity and biofilm inhibition

Antibacterial and antibiofilm properties of the composites were evaluated by implanting composite-coated catheters (polyurethane, 5 Fr, 12 mm) subcutaneously in mice after infecting the catheter with MRSA. Catheter samples were given bacterial load of ~1.1×10^8 CFU of MRSA at the time of implantation.[28] After 96 h the mice were sacrificed, catheters were harvested and analyzed for cell counting. Notably, the control catheters showed bacterial burden of 8.6 log CFU thereby indicated the prevalence and growth of MRSA. However, all the coated catheters showed significantly lesser amount of bacteria. Polymer **2c** coated catheters (~8 μg/mm^2) showed 2.4 log reductions in MRSA count. However, the nanocomposite coated catheters showed remarkable reduction in MRSA count depending on the amount coated. For example, 1:1 composite coated-catheter with 4.0 μg/mm^2 and 8.0 μg/mm^2 coating showed a reduction of 3.7 and 4.9 log CFU of MRSA respectively (Figure 3B.16A). Clearly the nanocomposite coated surfaces showed much superior activity than the polymer alone at the same amount of coating. Further, the composite showed better activity even when coated lesser amount than the polymer alone. The above results therefore indicated that the composite are highly active under *in-vivo* conditions.

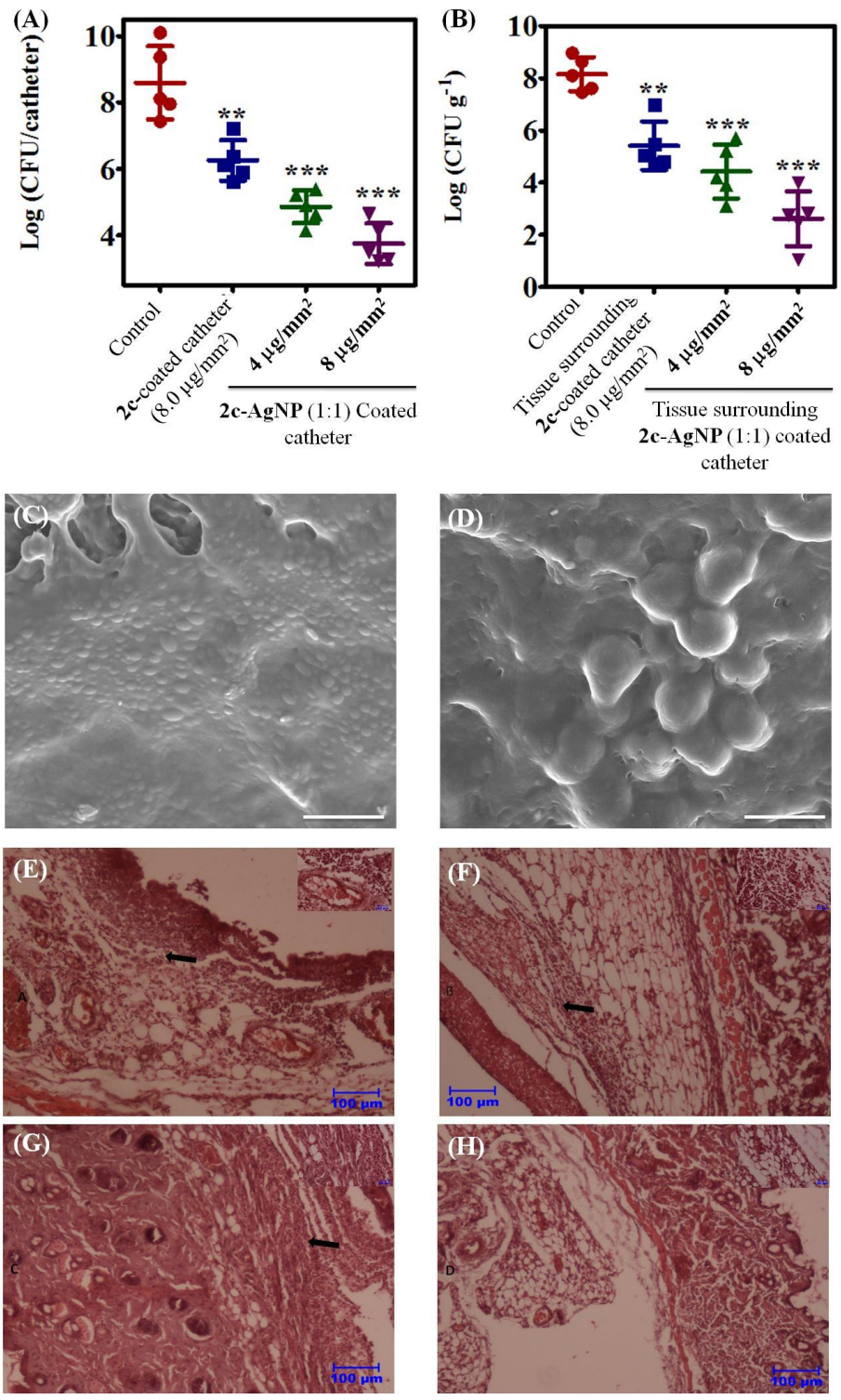

Figure 3B.16: *In-vivo* antibacterial activity of polymer-nanocomposite coated catheters. (A) Bacterial count after harvesting coated and non-coated catheters from mice; (B) bacterial count from tissue samples surrounding the catheters; p value (*) is <0.0001 for the composite at 8.0 µg/mm^2. Field emission scanning electron microscopy (FESEM) images of (C) non-coated catheter and (D) nanocomposite-coated catheter. Mice skin and subcutaneous tissue histopathology: (E) tissue surrounding MRSA infected non-coated catheter; tissue surrounding MRSA-infected catheter coated with (F) 8.0 µg/mm^2 of polymer **2c**; (G) 4.0

μg/mm^2 of composite and (H) 8.0 μg/mm^2 of composite. Cells were stained with haematoxylin and eosin staining agents. Insets are the high resolution images.

As the polymer nanocomposite can release silver ions in the surrounding tissue thereby might reduce the bacterial count at the tissue level more effectively than the polymer. To see bacterial prevalence in the surrounding tissue, tissue samples were also collected and analysed for cell counting. It was observed that the tissue surrounding to 8.0 μg/mm^2 polymer-coated catheter displayed only 2.8 log reduction of MRSA compared to tissue surrounding to non-coated infected catheter. However, the tissue samples surrounding to 4.0 μg/mm^2 and 8.0 μg/mm^2 nanocomposite-coated catheters showed significant bacterial reduction of MRSA (3.8 log and 5.8 log reduction) (Figure 3B.16B). The superior activity of the nanocomposite thus suggested that these materials could be potentially used in various biomedical devices specially used in less vascular or avascular body parts. The antibiofilm efficacy of the nanocomposite coating was also evaluated by observing the catheter surface via scanning electron microscopy (SEM). Uncoated catheter was shown to display large amount of bacteria in multiple layers along with the mice skin tissue indicated a thick biofilm formation (Figure 3B.16C). In contrast, nanocomposit coated catheter (at 8.0 μg/mm^2) showed a fewer amount of bacteria with no clusters thereby indicated no biofilm formation onto the surface (Figure 3B.16D). The above results thus portrayed the efficacy of the nanocomposite in killing bacteria and inhibiting biofilm inhibition under *in-vivo* conditions.

Histopathological analysis of the surrounding tissue was also performed to evaluate the inflammatory responses. Tissue surrounding non-coated catheter (infected with MRSA) showed severe infiltration of inflammatory cells mainly neutrophils and mononuclear cells in the subcutaneous tissues (arrow) with congestion of blood vessels (inset) surrounding the catheter and severe damage to dermis layer of skin (Figure 3B.16E). In contrast, tissue surrounding catheter coated with ~8.0 μg/mm^2 of polymer alone showed moderate infiltration of inflammatory cells (arrow) mainly with neutrophils (inset) and moderate damage to skin dermis layer indicative of slight reduction of MRSA at the tissue level (Figure 3B.16F). However, tissues nearby to catheter coated with ~4.0 and 8.0 μg/mm^2 of nanocomposite showed normal epidermis layer of skin with sweat and sebaceous gland along with mild-to-negligible infiltration of inflammatory cells with neutrophils and mononuclear cells (Figure 3B.16G and H). The above results thus further confirmed that the nanocomposite reduced bacterial count not only on the catheter surface but in the surrounding tissue.

3B.2.10 Propensity of bacterial resistance development

Because of the membrane-active mode of action, the nanocomposites are also expected to withstand bacterial resistance development. The ability of the composites in hindering emergence of resistance development was assessed by serial exposure of bacteria to the composite coated surfaces. The coated surfaces were challenged against both *S. aureus* and *E. coli* repeatedly. Notably, the MIA values of both the composites were found to be unchanged (only 2-4 fold increase) whereas nofloxacin, a nucleic acid targeting Gram-positive antibiotic, showed 267 fold increase in MIC against sensitive *S. aureus* and colistin, a lipid II targeting Gram-negative lipopeptide, showed 124 fold increase in MIC against sensitive *E. coli* respectively after 14 serial passages (Figure 3B.17). These membrane-active composites thus can withstand the development of bacterial resistance.

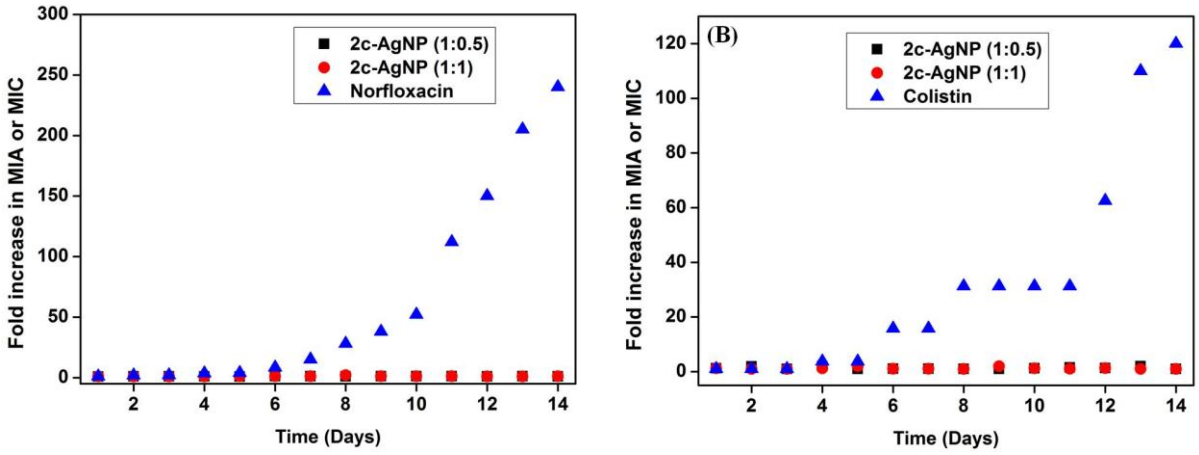

Figure 3B.17: Development of bacterial resistance against: (A) *S. aureus* with **2c**-AgNP composites (1:1 and 1:0.5) and ciprofloxacin; (B) *E. coli* with composites (1:1 and 1:0.5) and colistin.

3B.3 Conclusion

In conclusion, highly effective dual action polymer-silver nanocomposites were developed of *in-situ* from a quaternary chitin derivative and a silver salt. The polymer acted as both reducing and stabilizing agents to silver nanoparticles thereby provided highly stable polymer-silver nanocomposites. The nanocomposites upon coating onto surfaces non-covalently were shown to inactivate both Gram-positive and Gram-negative bacteria including the drug-resistant pathogens completely. The nanocomposites were also shown to be highly effective against various human pathogenic fungi such as such as *Candida* spp. and *Cryptococcus* spp. Rapid bactericidal and fungicidal activity was observed for the composites compared to individual components. Further, the composites were shown to be effective in

inhibiting both bacterial and fungal biofilm formation in contrast to polymer. The composite coated surfaces were shown to have long-lasting activity against microbes. Notably, the composites showed negligible toxicity towards human erythrocytes *in-vitro* and minimal inflammation at the tissue level *in-vivo*. Also, the composites showed excellent efficacy in reducing bacterial burden both on the catheter and in the surrounding tissues in a mice model of subcutaneous MRSA infection. The composite coated catheter was also shown to be effective in inhibiting MRSA biofilm formation under *in-vivo* conditions. The polymeric nanocomposites obtained from a biocompatible antimicrobial polymer via one-pot synthesis thus portrayed that these materials could be used as safe and effective antimicrobial coatings in biomedical devices and implants.

3B.4 Experimental section

3B.4.1 Materials and instrumentation

Chitin with a degree of acetylation ~75% and potassium hydroxide (KOH) were purchased from SD Fine, India. Lithium chloride (LiCl), potassium bromide (KBr), triethylamine (NEt_3), acetic anhydride (Ac_2O), p-toluene sulfonylchloride (TsCl), silver *para*-tolunesulfonate (AgPTS), *N,N*-dimethylhexadecylamine and anhydrous *N,N* dimethylacetamide (DMAc) were obtained from Sigma-Aldrich, USA. Anhydrous dimethyl sulfoxide (DMSO), anhydrous diethylether (Et_2O) and all other solvents were purchased from Spectrochem, India and were of analytical grade. Methanol was dried with calcium hydride and stored over 4 Å molecular sieves. Triethylamine was dried with KOH and stored over KOH. Bacterial strains *S. aureus* (MTCC 737), *E. coli* (MTCC 443) and *P. aeruginosa* (MTCC 424) were purchased from MTCC (Chandigarh, India). Vancomycin-resistant *E. faecium* (VRE) (ATCC 51559), methicilin-resistant *S. aureus* (MRSA) (ATCC 33591) *β*-lactam-resistant *K. pneumoniae* (ATCC 700603) were obtained from ATCC (Rockvillei, Md). . The fungal strains are *Candida albicans* (SC5314), *Candida dubliniensis* (CD36), *Candida tropicalis* (MYA3404), *Cryptococcus neoformans var. grubii* (serotype A) (H99), *Cryptococcus gattii* (serotype B) (WM276) and *Cryptococcus neoformans var. neoformans* (serotype D) (JEC21). Nuclear magnetic resonance spectra (^{1}H NMR) were recorded on a Bruker AMX-400 instrument (400 MHz) in deuterated solvents. Infra red spectra of the polymers were recorded on a Bruker IFS66 V/s spectrometer using potassium bromide pellets. Thermo Finnigan FLASH EA 1112 CHNS analyzer was used to perform elemental analysis of the polymers. Scanning electron microscope images were obtained using Quanta 3D FEG, FEI field emission scanning electron microscopy. Thermogravimetric analyses were

performed on a TGA 850C Mettler, Toledo thermogravimetric analyzer. UV-Visible spectra were taken by Perkin Elmer Lambda 900 UV/Vis/NIR spectrometer. TEM was performed on a Technai F30 UHR version electron microscope, using a field emission gun (FEG) operating at an accelerating voltage of 200 kV. Atomic emission spectroscopy was performed in Perkin Elmar Optima 7000 DV instrument with inductively coupled plasma set up. Polymer coatings and paints were made by a WS5000 spin coater, Techno India, India. Optical density (OD) values were measured by a TECAN (Infinite series, M200) Plate Reader. Eppendorf 5810R centrifuge was used for bacterial centrifugation. Bacterial imaging was performed using a Leica DM2500 fluorescent microscope. A Zeiss 510 Meta confocal laser scanning microscope was used for confocal microscopy imaging.

3B.4.2 Synthesis of polymer

The synthesis of the quaternary chitin derivative (**2c**) was performed following same protocol as described in section of 3A.4.2 in Chapter 3A.

3B.4.3 Preparation and characterization of nanocomposites

3B.4.3.1 Preparation of nanocomposites

To prepare the Ag-containing composites, **2c** (0.1 g) was dissolved in 1 mL of dry methanol. The required amount of AgPTS (0.1 g or 0.05 g) was dissolved in 1 mL anhydrous dimethyl sulfoxide. Both the polymer and the AgPTS solutions were then mixed vigorously and kept in dark place at room temperature for about 10-11 days. Finally, the polymeric composite was precipitated in acetone and dried under vacuum for 24 h to yield a brownish solid.

3B.4.3.2 Characterization of nanocomposites

To monitor the growth of the silver nanoparticle, the reaction mixture (methanol-DMSO containing the composites) was directly used for UV-visible absorption spectroscopy. After definite time interval, 20 μL of the composite solution was taken in UV cuvette and then absorption was recorded everyday for next 12 days. Also, the solution was kept for 2 months to check the stability of the nanoparticle. For TEM imaging, solid composites were redissolved in methanol and then drop casted on TEM grid. Also, the composite solutions were directly drop-casted on the grid and then TEM images were recorded to see the difference in sized due to precipitation. For X-ray photoelectron spectroscopy (XPS) measurements, the solutions were directly drop casted on silicon wafers, dried and then used

for XPS. Thermogravimetric analyses were performed by taking the solid samples (5-10 mg) and the measurements were done from 30 to 700 ˚C for both the composites at a constant heating rate of 5 ˚C/min under argon atmosphere (40 mL/min).

3B.4.4 Preparation of surface coating

The solid composites were dissolved in methanol or DMSO at required amounts and then were coated onto different surfaces following same protocol as described in section of 2A.4.4 in Chapter 2A.

3B.4.5 Antimicrobial activity

3B.4.5.1 Determination of antibacterial activity by spray method (air-borne bacteria)

Antibacterial activity of the nanocomposite coated surfaces (glass slides, 2.5 cm × 5.5 cm) was evaluated following same protocol as described in the section 2A.4.5.1 in Chapter 2A.

3B.4.5.2 Determination of antibacterial activity (water-borne bacteria)

Antibacterial activity of the nanocomposite coated surfaces (wells of polystyrene tissue culture plate) was evaluated following same protocol as described in the section 2A.4.5.2 in Chapter 2A.

3B.4.5.3 Antibacterial kinetics

Antibacterial kinetics of the nanocomposite coated surfaces (wells of polystyrene tissue culture plate) was evaluated following same protocol as described in the section 2A.4.5.3 in Chapter 2A.

3B.4.5.4 Mechanism of antibacterial action

Membrane-active mode of action of the nanocomposite coated surfaces (wells of polystyrene tissue culture plate) against *S. aureus* and *E. coli* was evaluated following same protocol as described in the section 2B.4.5.4 in Chapter 2B.

3B.4.6 Bacterial biofilm inhibition assay

Biofilm inhibition abilities of the nanocomposite coated surfaces (cover slips with 18 mm of diameter) against MRSA and *P. aeruginosa* were evaluated following same protocol as described in the section 2B.4.6 in Chapter 2B.

3B.4.7 Antifungal assay

3B.4.7.1 Minimum inhibitory amount (MIA)

Antibacterial activity of the nanocomposite coated surfaces (wells of polystyrene tissue culture plate) was evaluated following same protocol as described in the section 2A.4.7.1 in Chapter 2A

3B.4.7.2 Minimum fungicidal amount (MFA)

Antibacterial activity of the nanocomposite coated surfaces (wells of polystyrene tissue culture plate) was evaluated following same protocol as described in the section 2A.4.7.2 in Chapter 2A.

3B.4.7.3 Kinetics of antifungal activity

Antibacterial activity of the nanocomposite coated surfaces (wells of polystyrene tissue culture plate) was evaluated following same protocol as described in the section 2A.4.7.3 in Chapter 2A.

3B.4.8 Mechanism of antifungal action

Antibacterial activity of the nanocomposite coated surfaces (wells of polystyrene tissue culture plate) was evaluated following same protocol as described in the section 2A.4.8 in Chapter 2A.

3B.4.9 Fungal biofilm inhibition assay

Biofilm inhibition ability of the nanocomposite coated surfaces (wells of polystyrene tissue culture plate) against fungi was evaluated following same protocol as described in the section 2B.4.9 in Chapter 2B.

3B.4.10 Zone of inhibition study

Whatman filter paper (Whatman, cat no 1440125) was cut into a circular pieces (0.5 cm diameter) and each piece was dipped into methanol solutions of polymer, AgPTS and polymer-nanocomposite solutions (all 50 mg/mL against *S. aureus* and 100 mg/mL against *E. coli*) to coat the paper. Bacterial suspension taken in PBS buffer (1 mL, ~10^8 CFU/mL) were spread onto the agar plate and allowed to dry for 2-3 min. The coated papers were then placed

on the agar plates and incubated at 37 ˚C for 24 h. After incubation, the agar plates were observed for the zone of inhibitin and imaged by Cell Biosciences gel documentation instrument. Images were captured under white light and processed using Alpha-imager software. A non-coated disk (dipped into methanol) was used as control experiment.

3B.4.11 Long lasting antibacterial activity

The long lasting antibacterial activity of the polymeric composites was evaluated by coating the **2c**-AgNP composite (1:1) onto glass cover slips. DMSO solution of solid nancomposites (50 μL, 50 mg/mL) was drop casted onto the cover glasses (12 mm diameter) and then dried to obtain thin films that contain fixed amount of the nanocomposite coatings. The coated cover slips were then taken into the wells of a 24 well plate and then bacterial (*S. aureus* and *E. coli*) suspensions (1 mL, 10^5 CFU/mL) in suitable broth were added to the wells. The plates were then incubated at 37 ˚C for about 24 h. After the incubation, all the media were carefully removed and then optical density of the media was recorded at 600 nm. Also, 20 μL of the solutions were directly plated on the agar plate to visualized bacterial growth. To the wells containing the coated cover slips, bacteria were similarly added and the method was repeated for at least 14 days.

3B.4.12 Release of Ag^+ ions from composite (Atomic emission spectroscopy)

The release of the silver ions from the polymer-silver nanocomposites was evaluated by coating the **2c**-AgNP composite (1:1) onto glass cover slips. The cover slips were coated similarly as described in the previous section. The coated cover slips were then taken into the wells of a 24 well plate and water and nutrient broth (0.5 mL) were added to the wells. The plates were then incubated at 37 ˚C for about 24 h. After the incubation, both water and the media were carefully collected. To the wells containing the coated cover slips, bacteria were similarly added and the method was repeated for at least 14 days. Finally, Ag^+ ion concentration in both water was determined using ICP-AES (Perkin Elmer Optima 7000UV) (Argon Plasma, excitation wavelengths: 224.874 and 328.068 nm, Ag sensitivity of 0.005 ppm).

3B.4.13 Biocompatibility of polymers

3B.4.13.1 Hemolytic activity of the composites

Hemolytic assay of the polymeric silver composites was evaluated following same protocol as described in the section 2A.4.10 in Chapter 2A.

3B.4.13.2 *In-vivo* toxicity

In-vivo toxicity of the nanocomposites was evaluated following same protocol as described in the section 2B.4.11.3 in Chapter 2B.

3B.4.14 *In-vivo* activity

In-vivo activity of the nanocomposites was evaluated following same protocol as described in the section 2B.4.12 in Chapter 2B.

BIBLIOGRAPHY

1. Sanderson, P. J. Infection in orthopaedic implants. *J. Hosp. Infect.* **1991,** *18 Suppl A*, 367-375.
2. Trampuz, A.; Widmer, A. F. Infections associated with orthopedic implants. *Curr. Opin. Infect. Dis.* **2006,** *19*, 349-356.
3. Darouiche, R. O. Treatment of infections associated with surgical implants. *N. Engl. J. Med.* **2004,** *350*, 1422-1429..
4. Goodman, S. B.; Yao, Z.; Keeney, M.; Yang, F. The future of biologic coatings for orthopaedic implants. *Biomaterials* **2013,** *34*, 3174-3183.
5. Darley, E. S.; MacGowan, A. P. Antibiotic treatment of gram-positive bone and joint infections. *J. Antimicrob. Chemother.* **2004,** *53*, 928-935.
6. van de Belt, H.; Neut, D.; Schenk, W.; van Horn, J. R.; van der Mei, H. C.; Busscher, H. J. Infection of orthopedic implants and the use of antibiotic-loaded bone cements - A review. *Acta Orthop. Scand.* **2001,** *72*, 557-571.
7. Costerton, J. W.; Stewart, P. S.; Greenberg, E. P. Bacterial biofilms: A common cause of persistent infections. *Science* **1999,** *284*, 1318-1322.
8. Bozic, K. J.; Kurtz, S. M.; Lau, E.; Ong, K.; Vail, T. P.; Berry, D. J. The epidemiology of revision total hip arthroplasty in the United States. *J. Bone Joint Surg. Am.* **2009,** *91A*, 128-133.
9. Kurtz, S. M.; Lau, E.; Watson, H.; Schmier, J. K.; Parvizi, J. Economic burden of periprosthetic joint infection in the United States. *J. Arthroplasty* **2012,** *27*, 61-65.
10. Bernard, L.; Hoffmeyer, P.; Assal, M.; Vaudaux, P.; Schrenzel, J.; Lew, D. Trends in the treatment of orthopaedic prosthetic infections. *J. Antimicrob. Chemother.* **2004,** *53*, 127-129.
11. Wong, S. Y.; Moskowitz, J. S.; Veselinovic, J.; Rosario, R. A.; Timachova, K.; Blaisse, M. R.; Fuller, R. C.; Klibanov, A. M.; Hammond, P. T. Dual functional polyelectrolyte multilayer coatings for implants: permanent microbicidal base with controlled release of therapeutic agents. *J. Am. Chem. Soc.* **2010,** *132*, 17840-17848.
12. Li, Z.; Lee, D.; Sheng, X. X.; Cohen, R. E.; Rubner, M. F. Two-level antibacterial coating with both release-killing and contact-killing capabilities. *Langmuir* **2006,** *22*, 9820-9823.
13. Sambhy, V.; MacBride, M. M.; Peterson, B. R.; Sen, A. Silver bromide nanoparticle/polymer composites: Dual action tunable antimicrobial materials. *J. Am. Chem. Soc.* **2006,** *128*, 9798-9808.
14. Min, J. H.; Choi, K. Y.; Dreaden, E. C.; Padera, R. F.; Braatz, R. D.; Spector, M.; Hammond, P. T. Designer dual therapy nanolayered implant coatings eradicate biofilms and accelerate bone tissue repair. *ACS Nano* **2016,** *10*, 4441-4450.
15. Rai, M.; Yadav, A.; Gade, A. Silver nanoparticles as a new generation of antimicrobials. *Biotechnol. Adv.* **2009,** *27*, 76-83.
16. Monteiro, D. R.; Gorup, L. F.; Takamiya, A. S.; Ruvollo, A. C.; Camargo, E. R.; Barbosa, D. B. The growing importance of materials that prevent microbial adhesion: antimicrobial effect of medical devices containing silver. *Int. J. Antimicrob. Agents* **2009,** *34*, 103-110.
17. Feng, Q. L.; Wu, J.; Chen, G. Q.; Cui, F. Z.; Kim, T. N.; Kim, J. O. A mechanistic study of the antibacterial effect of silver ions on Escherichia coli and Staphylococcus aureus. *J. Biomed. Mater. Res.* **2000,** *52*, 662-668.
18. Eckhardt, S.; Brunetto, P. S.; Gagnon, J.; Priebe, M.; Giese, B.; Fromm, K. M. Nanobio silver: its interactions with peptides and bacteria, and its uses in medicine. *Chem. Rev.* **2013,** *113*, 4708-4754.
19. Hachem, R. Y.; Wright, K. C.; Zermeno, A.; Bodey, G. P.; Raad, I. I. Evaluation of the silver iontophoretic catheter in an animal model. *Biomaterials* **2003,** *24*, 3619-3622.

20. Melaiye, A.; Sun, Z. H.; Hindi, K.; Milsted, A.; Ely, D.; Reneker, D. H.; Tessier, C. A.; Youngs, W. J. Silver(I)-imidazole cyclophane gem-diol complexes encapsulated by electrospun tecophilic nanofibers: formation of nanosilver particles and antimicrobial activity. *J. Am. Chem. Soc.* **2005,** *127*, 2285-2291.
21. Lu, Y.; Liu, G. L.; Lee, L. P. High-density silver nanoparticle film with temperature-controllable interparticle spacing for a tunable surface enhanced Raman scattering substrate. *Nano Lett.* **2005,** *5*, 5-9.
22. Dowling, D. P.; Donnelly, K.; McConnell, M. L.; Eloy, R.; Arnaud, M. P. Deposition of anti-bacterial silver coatings on polymeric substrates. *Thin Solid Films* **2001,** *398*, 602-606.
23. Jiang, H. Q.; Manolache, S.; Wong, A. C. L.; Denes, F. S. Plasma-enhanced deposition of silver nanoparticles onto polymer and metal surfaces for the generation of antimicrobial characteristics. *J. Appl. Polym. Sci.***2004,** *93*, 1411-1422.
24. Affinito, J.; Martin, P.; Gross, M.; Coronado, C.; Greenwell, E. Vacuum deposited polymer metal multilayer films for optical application. *Thin Solid Films* **1995,** *270*, 43-48.
25. Sharma, V. K.; Yngard, R. A.; Lin, Y. Silver nanoparticles: Green synthesis and their antimicrobial activities. *Adv. Colloid Interface Sci.* **2009,** *145*, 83-96.
26. Gao, G.; Lange, D.; Hilpert, K.; Kindrachuk, J.; Zou, Y.; Cheng, J. T.; Kazemzadeh-Narbat, M.; Yu, K.; Wang, R.; Straus, S. K.; Brooks, D. E.; Chew, B. H.; Hancock, R. E.; Kizhakkedathu, J. N. The biocompatibility and biofilm resistance of implant coatings based on hydrophilic polymer brushes conjugated with antimicrobial peptides. *Biomaterials* **2011,** *32*, 3899-3909.
27. Bostman, O.; Pihlajamaki, H. Clinical biocompatibility of biodegradable orthopaedic implants for internal fixation: a review. *Biomaterials* **2000,** *21*, 2615-2621.
28. Samuel, U.; Guggenbichler, J. P. Prevention of catheter-related infections: the potential of a new nano-silver impregnated catheter. *Int. J. Antimicrob. Agents* **2004,** *23 Suppl 1*, S75-78.

Chapter 4A

Membrane-Active Cationic Small Molecules with Multiple Non-Peptidic Amide groups as Potent Antibacterial and Antibiofilm Agents

Abstract

Chapter 4A *describes development of cationic small molecular biocides featuring two positive charges, multiple non-peptide amide groups positioned in different places of the molecules and variable hydrophobic/hydrophilic character which mimics the action of natural microbicidal peptides yet stable under plasma conditions and non-toxic towards mammalian cells. The molecules synthesized via facile inexpensive methodology not only displayed good antibacterial activity against wild-type bacteria but also showed activity against various drug-resistant bacteria such as methicillin-resistant Staphylococcus aureus (MRSA), vancomycin-resistant Enterococcus faecium (VRE) and β-lactam-resistant Klebsiella pneumoniae (minimum inhibitory concentration, MIC= 1-15 μg/mL). The biocides were also shown to eradicate established S. aureus, MRSA and E. coli biofilms, the most common bacteria that often form biofilms on various biotic surfaces (e,g. skin, urinary tract). Mechanistic studies revealed that the cationic molecules inactivated bacteria by disrupting the membrane integrity and were shown to hinder the propensity of their resistance development. Negligible toxicity against human red blood cells (hRBC) and human embryo kidney (HEK) cells were observed for the most active molecules. Further the molecules showed high 50% lethal doses (LD_{50}) upon intraperitonial (i.p.) and subcutaneous (s.c.) administration in mice (LD_{50} >55 mg/kg) and no skin toxicity upon application on skin. Notably, the optimised molecule was shown to reduce MRSA burden (5.3 log reduction) and eradicate preformed bacterial biofilm in murine model of superficial skin infection. Development of these novel non-toxic small molecules with high antibacterial and antibiofilm activities thus could lead to the new generation of therapeutics which would find applications in various healthcare especially topical treatments.*

Publications based on this work

(1) Hoque, J. *et al.* Membrane active small molecules show selective broad spectrum antibacterial activity with no detectable resistance and eradicate biofilms. *J. Med. Chem.* **2015**, *58,* 5486.

(2) Hoque, J. *et al.* 'Selective and broad spectrum amphiphilic small molecules to combat bacterial resistance and eradicate biofilms'. *Chem. Commun.* **2015**, *51*, 13670.

(3) Hoque, J. *et al.* Antibacterial and antibiofilm activity of cationic small molecules with spatial positioning of hydrophobicity: an in vitro and in vivo evaluation. *J. Med. Chem.* **2016**, *59*, 10750.

4A.1 Introduction

Coupled with the inexorable proliferation of drug-resistant microorganisms, the antimicrobial drugs getting approved by the Food and Drug Administration (FDA) are declining steadily.[1] This poses a grim scenario for the generation to come when most antimicrobials may prove ineffective, taking human medicine to the pre-antibiotic era. Antibiotics which in general target the cellular processes of bacteria are rendered ineffective due to point mutations, production of drug-inactivating enzymes and/or highly effective efflux pumps developed by bacteria.[2-4] Another major threat to human health is the formation of bacterial biofilm.[5,6] Pathogens living in biotic biofilm induce persistent chronic infections and significantly elevate bacterial resistance to antibiotics and host immune system as a result of the diffusion barrier due to extra-cellular matrix (EPS), slow metabolism, genetic mutation, persister cells and so on.[7] Compared with the planktonic cells, bacteria in biofilm state are 10-1000-times more resistant to host immune responses and conventional antibiotic treatment.[8,9] More importantly, bacterial biofilms account for over 80% of microbial infections in humans, e.g., endocarditis, periodontitis, and chronic lung infections in cystic fibrosis (CF) patients are some of the prominent diseases. In order to prevent infections associated with bacterial biofilms, various synthetic antibiofilm agents capable of inhibiting biofilm formation have been developed.[10-13] Nonetheless, from a clinical standpoint, infections caused by already established biofilms pose significant threat to human health as biofilms are inherently resistant to host immune system and conventional therapeutic antibiotics.[8, 14] It is therefore necessary to develop molecules that are capable of eradicating preformed bacterial biofilms while sparing the mammalian cells.

Antimicrobial peptides (AMPs) and lipopeptides are the nature's very own design of membrane-active agents.[15-17] Cationic AMPs and lipopeptides, composed of positively charged amino acids, hydrophobic moieties from hydrophobic amino acids or fatty acid and peptide (or amide) bonds, are known to interact with the bacterial cell membrane in a non-specific manner. Consequently, propensity of developing bacterial resistance against these agents is low. Further, these are also shown to have the potency to destroy preformed bacterial biofilms.[18] Thus they appear to be ideal antibacterial agents to supplement or to replace existing antibiotic arsenal. However, low *in-vivo* potency, high cost of manufacture, low stability in plasma and low selectivity towards mammalian cells limit the large-scale use of these natural peptides as clinical antibacterial agents. Non-natural peptidomimetic approaches that mimic AMPs/lipopeptides to improve plasma stability and selectivity may

circumvent the problems associated with the natural peptides. To this end, various synthetic mimics of these agents were developed such as α-peptoids, β-peptides, oligoureas, oligoacyl lysines, aryl-amide foldamers, antimicrobial polymers, alkylated peptoids, etc.[19-22] However, the rational design of these peptidomimitics often turns out to be complicated due to the involvement of a variety of molecular frameworks and functional groups in order to tune their structure-activity relationship and selectivity.[23] Furthermore, synthetic complexity associated with such molecules even limits their large-scale usage. Further, the biofilm disrupting ability of the synthetic molecules needs further investigation both in-vitro and in-vivo as the efficacy against established biofilms of most of these systems were not shown.

In this chapter, an initiative was taken to develop non-toxic and stable membrane-active cationic small molecular biocide which are easy to synthesis and mimic the basic structural and functional features of the AMPs. The molecules were designed to possess non-peptidic amide bonds (devoid of amino acids), two positive charges (quaternary ammonium groups) and varying hydrophobic and hence amphiphilic character along with spatial positioning of hydrophobicity. The biocides were synthesized quantitatively in 2-4 synthetic steps using commercially available diaminoalkanes and dibromoalkanes as framework. Antibacterial activity against various bacteria and toxicity against mammalian cells were evaluated both *in-vitro* and *in-vivo*. Membrane active mechanism of action, plasma stability studies, activity in presence of complex mammalian fluids and ability of these compounds to withstand bacterial resistance were evaluated. Further, the potential to destroy the preformed biofilm were evaluated *in-vitro* and *in-vivo* in murine model of superficial MRSA infections thus establishing these biocides as potent topical antimicrobials.

4A.2 Results and discussion

4A.2.1 Synthesis of the small molecular biocides

Some of the important structural features of AMPs are the presence of positive charges (due to cationic amino acids), hydrophobic moiety (due to hydrophobic amino acids) and peptidic-amide bonds between two amino acids. Recently other than expected electrostatic and hydrophobic interactions, amphiphilic antimicrobials with amide groups have been shown to interact with bacterial cell membrane via hydrogen bonding thereby leading to enhanced activity.[24] Keeping in mind about these structural features, simple cationic small molecular systems were designed. Thus, three different sets (set I-III) of cationic small molecular biocides with varying number and position of non-peptidic amide bonds along with varying

amphiphilic character were synthesized. Set I contained molecules that bear two positive charges, three lipophilic alkyl moieties (one confined in between two charges and the other two pending from both the charges) and four non-peptidic amide groups placed both in confined and pendent alkyl chains (Scheme 4A.1). Set II contained molecules that bear two positive charges, three lipophilic alkyl moieties (one confined in between two charges and the other two pending from both the charges) and two non-peptidic amide groups placed only in confined alkyl chains (Scheme 4A.2). Set III contained molecules that bear two positive charges, three lipophilic alkyl moieties (one confined in between two charges and the other two pending from both the charges) and two non-peptidic amide groups placed only in pendent alkyl chains (Scheme 4A.3).

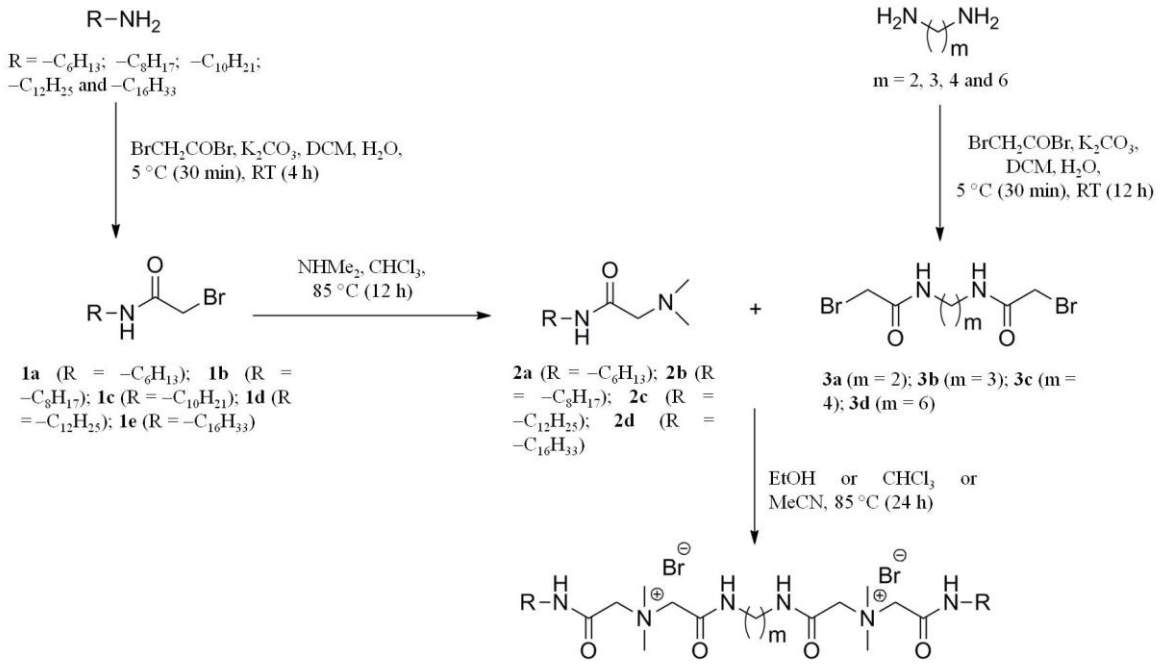

4a (m = 2, R = $–C_6H_{13}$); **4b** (m = 3, R = $–C_6H_{13}$); **4c** (m = 4, R = $–C_6H_{13}$); **4d** (m = 6, R = $–C_6H_{13}$); **5a** (m = 2, R = $–C_8H_{17}$); **5b** (m = 3, R = $–C_8H_{17}$); **5c** (m = 4, R = $–C_8H_{17}$); **5d** (m = 6, R = $–C_8H_{17}$); **6a** (m = 2, R = $–C_{12}H_{25}$); **6b** (m = 3, R = $–C_{12}H_{25}$); **6c** (m = 4, R = $–C_{12}H_{25}$); **6d** (m = 6, R = $–C_{12}H_{25}$); **7a** (m = 2, R = $–C_{16}H_{33}$); **7b** (m = 3, R = $–C_{16}H_{33}$); **7c** (m = 4, R = $–C_{16}H_{33}$); **7d** (m = 6, R = $–C_{16}H_{33}$)

Scheme 4A.1: Synthesis of lipophilic cationic small molecular biocides bearing non-peptidic amide groups both in the confined (spacer) and in the pendent alkyl chains.

Molecules of set I and II were synthesized using diaminoalkanes as framework whereas molecules of set III were synthesized using dibromoalkanes as framework. In order to assess the importance of amphiphilic balance, length of both pendent and confined lipophilic alkyl chains were varied in all three sets. To fine-tune the structure-activity relationship further,

positioning of confined hydrophobicity (restrained between two positive charges) was varied while keeping the hydrophobic/hydrophilic balance unchanged. To synthesize molecules of Set I, first various intermediates (**1a-1e**, **2a-2d** and **3a-3d**) were synthesized. Intermediates **1a-1e** were synthesized by reacting *N*-alkyl amines with bromoacetyl bromide in presence of aqueous K_2CO_3 (Scheme 4A.1). Intermediates **2a-2d** were synthesized with quantitative yields by the reacting **1a-1e** with *N,N*-dimethylamine at room temperature for 12 h and subsequent deprotonation with aqueous KOH. Intermediates **3a-3d** were prepared by reacting diaminoalkanes with bromoacetyl bromide following the protocol similar to the preparation of **1a-1e**. Finally, **2a-2d** were reacted individually with the **3a-3d** to give various cationic small molecular compounds with four amide bonds at different places in the molecules (**4a-4d, 5a-5d, 6a-6d** and **7a-7d**) (Scheme 4A.1). Molecules of set II were synthesized by reacting the intermediates **3a-3d** with *N,N*-dimethylalkyl amines with varying alkyl chains (Scheme 4A.2). This simple method thus allowed the introduction of non-peptidic amide functionality only in the confined spacer chain (**8a-8d, 9a-9d, 10a-10d** and **11a-11d**).

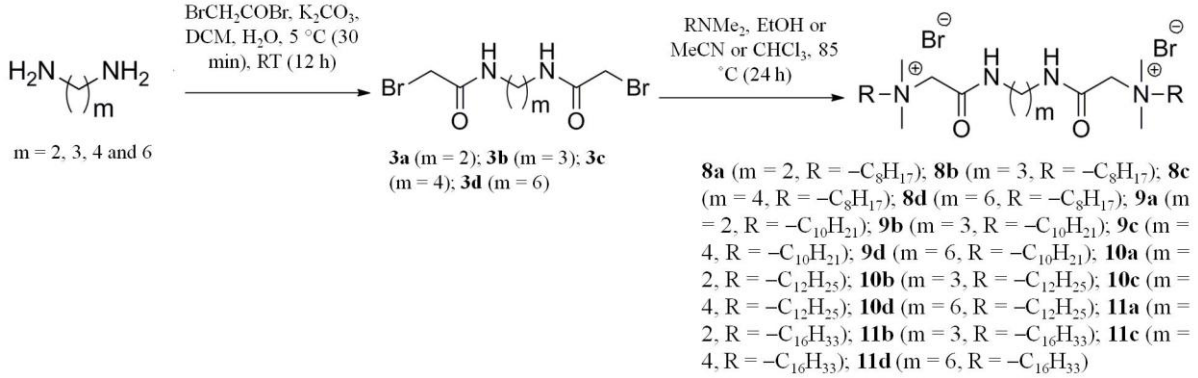

Scheme 4A.2: Synthesis of lipophilic cationic small molecular biocides bearing non-peptidic amide groups in the confined (spacer) chain.

Molecules of set III were synthesized in a simple three step method. First, intermediates (*N,N,N′,N′*-tetramethyl-α,ω-diaminoalkanes, **12a-12f**) were synthesized from α,ω-dibromoalkanes by reacting the bromoalkanes with *N,N*-dimethylamine. The length of the confined hydrocarbon chain in α,ω-dibromoalkanes was varied from a very low chain to high chain to obtain molecules with variable confined and pendent hydrophobicity. Finally, *N,N,N′,N′*-tetramethyl-α,ω-diaminoalkanes were reacted with *N*-alkyl-1-bromoethanamide to obtain the cationic small molecules (**13a-13f**, **14a-14f**, **15a-15f** and **16a-16f**) (Scheme 4A.3). The products were purified and isolated by precipitation to give more than 99% yield. All the final compounds were characterized by FT-IR, ^{1}H-NMR, ^{13}C-NMR and HRMS. An

important feature of these compounds is the inclusion of permanent positive charges instead of soft charges in AMPs/lipopeptides in addition to variable hydrophobic character and non-peptidic amide bonds.

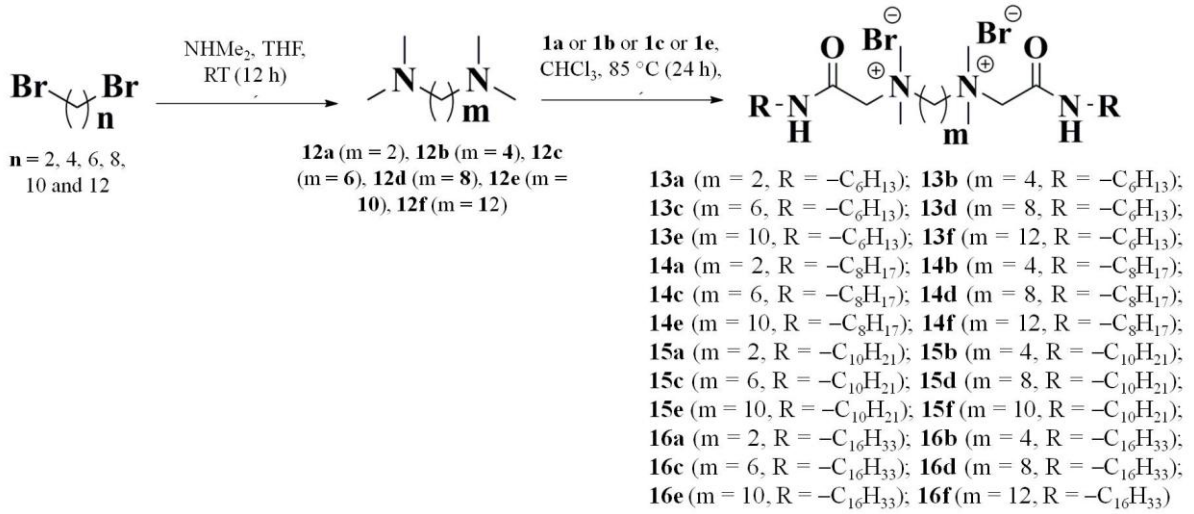

Scheme 4A.3: Synthesis of lipophilic cationic small molecular biocides bearing non-peptidic amide groups in the pendent alkyl chains.

4A.2.2 Antibacterial activity

The antibacterial efficacy was determined in suitable media by broth dilution method and expressed as minimum inhibitory concentration (MIC), i.e., the minimum concentration of the molecules required to inhibit the growth of bacteria.[25] All the cationic molecules were challenged against a wide spectrum of drug-sensitive bacteria such as *S. aureus*, *E. coli* and *P. aeruginosa* and drug-resistant bacteria such as methicillin-resistant *S. aureus* (MRSA), vancomycin-resistant *E. faecium* (VRE), β-lactam-resistant *K. pneumoniae*. A glycopetide antibiotic vancomycin and a lipopetide antibiotic colistin were also used in this study to compare the results. In general, all the compounds except molecules with very low or very high alkyl pendent chain ($-C_6H_{13}$ or $-C_{16}H_{33}$ lipophilic chain) showed good activity against all the bacteria tested (Table 4A.1, 4A.2 and 4A.3 respectively). For example in the case of set I, the range of MIC values for compounds **5a-5d** ($-C_8H_{17}$ lipophilic chain and m = 2-6) was 1-4 μg/mL against *S. aureus* and 2-24 μg/mL against *E. coli* respectively whereas the MIC values for compounds **4a-4d** ($-C_6H_{13}$ lipophilic chain and m = 2-6), **6a-6d** ($-C_{12}H_{25}$ lipophilic chain and m = 2-6) and **7a-7d** ($-C_{16}H_{33}$ lipophilic chain and m = 2-6) were 4-16 μg/mL, 3-4 μg/mL and 94-125 μg/mL against *S. aureus* and 24-62 μg/mL, 16-32 μg/mL and >1000 μg/mL against *E. coli* respectively. The above results thus suggested that an optimum lipophilic alkyl chain length is required to obtain maximum activity.

Table 4A.1 Antibacterial and hemolytic activities of molecules from set I

Biocides	MIC (μg/mL)						HC_{50} (μg/mL)
	Drug-sensitive bacteria			Drug-resistant bacteria			
	S. aureus	*E. coli*	*P. aeruginosa*	MRSA	VRE	K. *pneumoniae*	
4a	16	62	375	32	32	187	440
4b	16	32	187	24	24	125	420
4c	15	32	93	24	16	93	400
4d	4	24	48	8	7.8	93	338
5a	4	24	32	4	12	93	385
5b	4	12	32	4	6	48	330
5c	2	4	24	2	4	24	255
5d	0.9	2	16	1	1	16	132
6a	3.5	32	367	6	6	375	46
6b	2.8	24	367	3.9	4	375	44
6c	3.4	15.6	375	3.9	4	375	43
6d	4	31	375	3.9	4	375	41
7a	94	>1000	>1000	94	187	>1000	80
7b	94	>1000	>1000	94	187	>1000	52
7c	125	>1000	>1000	94	187	>1000	38
7d	125	>1000	>1000	125	250	>1000	36
Colistin	20	0.4	0.4	54	>199	1.2	> 250
Vancomycin	0.63	ND	ND	0.64	750	ND	>1000

MRSA = Methicillin-resistant *S. aureus* (ATCC 33591); VRE = vancomycin-resistant *Enterococcus faecium* (ATCC 51559); *K. pneumoniae* = beta lactam-resistant *K. pneumoniae* (ATCC 700603); HC_{50} = Hemolytic concentration at which 50% hemolysis occurs.

To understand the role of lipophilic alkyl chain more closely, the MIC values of the compounds of different alkyl chains and a particular spacer chain were compared. For example, **4d** (R = $–C_6H_{13}$), **5d** (R = $–C_8H_{17}$), **6d** (R = $–C_{12}H_{25}$) and **7d** (R = $–C_{16}H_{33}$), molecules with fixed spacer chain (m = 6) in set I, showed MIC values of 4 μg/mL, 0.9 μg/mL, 4 μg/mL and 125 μg/mL against *S. aureus* and 24 μg/mL, 2 μg/mL, 31 μg/mL and > 1000 μg/mL against *E. coli* respectively. In order to fine-tune the antibacterial activity of these small molecules further, amphiphilic balance was also varied by varying the lipophilic spacer chain length by one and/or two methylene units while keeping the optimum alkyl chain length constant. For example, **5a** (m = 2), **5b** (m = 3), **5c** (m = 4) and **5d** (m = 6), molecules with fixed pendent chain ($–C_{10}H_{21}$) in set I, showed MIC values of 4 μg/mL, 4 μg/mL, 2 μg/mL and 0.9 μg/mL against *S. aureus* and 24 μg/mL, 12 μg/mL, 4 μg/mL and 2 μg/mL against *E. coli* respectively. Thus an optimum confined and pended alkyl chain was

required to obtain the maximum antibacterial activity. Similar trends were observed for the molecules of set II and set III also (Table 4A.2 and 4A.3).

Table 4A.2 Antibacterial and hemolytic activities of molecules from set II

	MIC (μg/mL)						HC_{50}
	Drug-sensitive bacteria			Drug-resistant bacteria			
Biocides	*S. aureus*	*E. coli*	*P. aeruginosa*	MRSA	VRE	*K. pneumoniae*	(μg/mL)
8a	22	125	188	20	94	500	> 1000
8b	18	62.5	188	17	125	500	> 1000
8c	7.8	31.2	125	8	62	250	> 1000
8d	1.9	3.9	31.2	3	6	31.2	780
9a	2	3.9	6	1.5	1.5	8	200
9b	1.9	3.9	6	1	1	6	140
9c	1.5	3.9	6	1	1	4	110
9d	1.5	1.9	3	1	1	3	45
10a	2	3.9	9	3.9	2	6	53
10b	1.9	2	10	3.9	1.5	6	40
10c	1.9	2	14	3.9	1.5	6	33
10d	1.0	1.9	28	8	1.5	8	31
11a	125	>1000	250	47	188	530	49
11b	94	>1000	186	47	147	517	41
11c	62.5	>1000	186	47	137	500	37
11d	62.5	>1000	250	31	94	500	32

Notably, molecules were found to be more active towards Gram-positive bacteria than the Gram-negative bacteria. For example, the range of MIC values for **4a-4d, 5a-5d, 6a-6a-6d** and **7a-7d** were 1-125 μg/mL against Gram-positive *S. aureus* whereas the range of MIC values was 2-1000 μg/mL for Gram-negative *E. coli* (Table 4A.1). However, to be suitable for applications in healthcare settings, the molecules should selectively act on bacterial cells over the mammalian cells. One simplest way to check the toxicity of the molecules is to study their hemolytic activity against human red blood cells (hRBC). Being highly fragile to environmental change and devoid of any intracellular organelles, lysis of hRBC in the presence of active molecules represents an important tool to determine the toxicity of the molecules. Interestingly, when the hydrophobic character hence the overall amphiphilic balance of the molecules was varied, hemolytic activity expressed as HC_{50} (concentration at which 50% hemolysis occurs) was found to vary differently depending on the length of the alkyl chain. For example, when the length of confined spacer chain was increased for the

molecules with $-C_6H_{13}$ pendent chain in set III, hemolytic toxicity of the molecules were found to vary non-significantly (Table 4A.3).

Table 4A.3 Antibacterial and hemolytic activities of molecules from set III

Small molecules	MIC (μg/mL)						HC_{50} (μg/mL)
	Drug-sensitive bacteria			Drug-resistant bacteria			
	S. aureus	*E. coli*	*P. aeruginosa*	*MRSA*	*VRE*	*K. pneumoniae*	
13a	125	250	500	250	250	500	>1000
13b	62.5	125	250	125	250	500	>1000
13c	62.5	125	250	125	125	250	>1000
13d	15.6	31.2	250	31.2	62.5	125	>1000
13e	3.9	3.9	125	7.8	15.6	31.2	>1000
13f	1.0	2.0	31.2	2.0	3.9	15.6	805
14a	2.0	3.9	15.6	3.9	15.6	125	250
14b	2.0	3.9	15.6	3.9	15.6	125	250
14c	2.0	3.9	15.6	3.9	15.6	62.5	200
14d	1.0	1.0	7.8	3.9	7.8	15.6	125
14e	1.0	1.0	7.8	2.0	7.8	3.9	100
14f	1.0	2.0	7.8	1.0	7.8	3.9	50
15a	2.0	2.0	62.5	2.0	7.8	3.9	62
15b	2.0	2.0	62.5	2.0	7.8	3.9	55
15c	2.0	2.0	62.5	2.0	7.8	3.9	55
15d	2.0	3.9	62.5	2.0	7.8	7.8	55
15e	2.0	3.9	125	2.0	7.8	31.2	50
15f	31.2	500	>1000	2.0	7.8	>1000	48
16a	2.0	3.9	1000	31.2	15.6	62.5	55
16b	31.2	125	>1000	62.5	62.5	125	52
16e	31.2	250	>1000	125	125	>1000	50
16d	125	250	>1000	125	125	>1000	45
16e	62.5	500	>1000	31.2	15.6	500	44
16f	15.6	125	>1000	15.6	7.8	250	42

To illustrate, HC_{50} values of all the molecules with $-C_6H_{13}$ pendent chain (**13a-13f**) were close to or more than 1000 μg/mL. On the other hand, when length of the confined chain was increased for the molecules with $-C_8H_{17}$ pendent chain in the same set, hemolytic activity varied greatly. To illustrate, HC_{50} values of molecules with $-C_8H_{17}$ pendent chain (**14a-14f**) were 50-250 μg/mL (Table 4A.3). In summary above facts indicated that an optimum amphiphilic balance is important to obtain active yet non-toxic compounds. The most selective compounds (selectivity, $S = HC_{50}/MIC$) from all three sets were found to be **8d** and **13f**. While these molecules showed excellent antibacterial efficacy against both Gram-positive *S. aureus* and Gram-negative *E. coli* (MIC values of **8d** and **13f** were 1.9 and 1.0 μg/mL against *S. aureus* and 3.9 and 2.0 μg/mL *E. coli* respectively), negligible toxicity

towards hRBC was observed for both molecules (HC_{50} values of **8d** and **13f** were 780 and 805 μg/mL respectively). Thus molecules **8d** and **13f** were shown 205-410 and 402-805 times more selective towards bacteria than human erythrocytes. Thus among all the molecules synthesized, **13f** was found to be the most selective molecule. It should be mentioned that molecules with four non-peptidic amide bonds (set I) though provided active molecules but did not yield highly selective compounds.

Interestingly, the molecules showed activity against *P. aeruginosa*, a difficult-to-treat Gram-negative bacterium which causes many nosocomial infections and is known to show resistant to almost all the clinically approved drugs (Table 4A.1, 4A.2 and 4A.3).[38] The MIC values displayed by the two most optimized compounds **8d** and **13f** were 31.2 μg/mL each against *P. aeruginosa*. Not only active against drug-sensitive bacteria, the cationic molecules also showed activity against various drug-resistant bacteria. Like the drug-sensitive bacteria, the cationic molecules showed similar trends in their activity against drug-resistant bacteria upon variation in their amphiphilic balance (Table 4A.1, 4A.2 and 4A.3). The optimized compounds **8d** and **13f** displayed MIC values of 3 μg/mL and 2 μg/mL respectively against MRSA. The activity of **8d** and **13f** against VRE was also excellent as they exhibited MIC values of 6 μg/mL and 3.9 μg/mL respectively. These biocides were also found to be active against *β*-lactam-resistant *K. pneumoniae*. The MIC values of compounds **8d** and **13f** were 31.2 μg/mL and 15.6 μg/mL respectively against this Gram-negative drug-resistant bacterium.

4A.2.3. Plasma stability and activity in mammalian fluids

One of the major disadvantages of the natural antibacterial peptides is the loss of antibacterial efficacy due to protease degradation which in-turn results in decreased antibacterial activity in the blood plasma.[26] In order to determine the stability of the non-peptidic amide containing biocides under plasma condition, first one of the optimized and active compounds **13f** was treated in 50% human plasma for different period of time and subsequently antibacterial efficacy of the plasma-treated biocides was evaluated.[27] Interestingly **13f**, after treating with 50% plasma for 0 h, 3 h and 6 h respectively, did not reveal any significant loss in activity. The MIC values of **13f** were found to be 1 μg/mL after 0 h, 3 h and 6 h treatment in 50% plasma (Figure 4A.1A). Notably, MSI-78, a naturally occurring antimicrobial peptide, is known to show 2-fold increase in MIC in the presence of

50% human serum itself than in the absence of serum (100% media).[28] The above result thus indicated that the compound **13f** did not lose antibacterial efficacy under plasma condition.

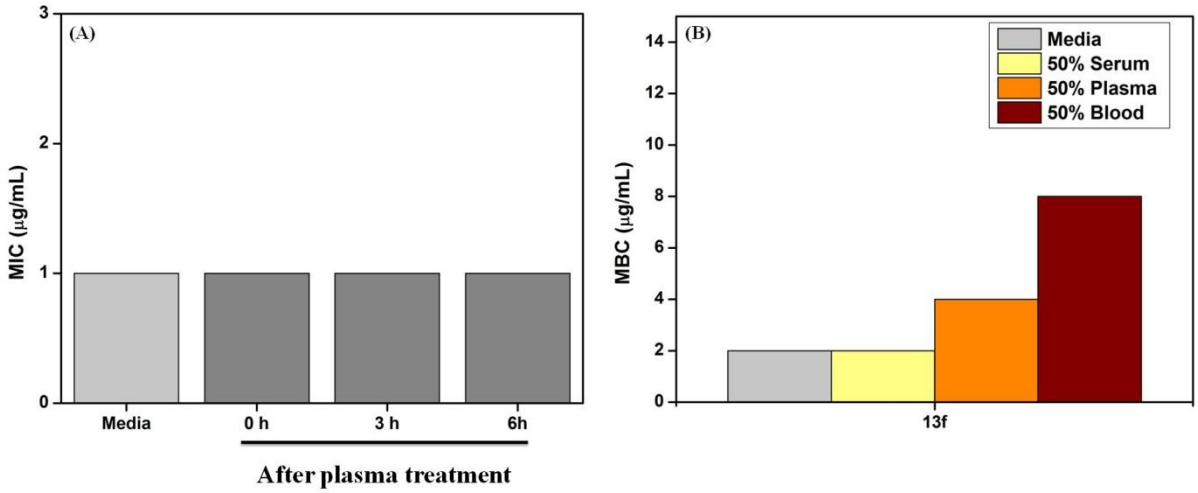

Figure 4A.1: Antibacterial activity after pre-incubating in plasma and activity in complex mammalian fluids systems of compound **13f**: (A) antibacterial efficacy of **13f** against *S. aureus* after pre-incubating in 50% plasma for different period of time (0 h, 3 h and 6 h; (B) minimum bactericidal concentrations (MBCs) of **13f** in 50% serum, 50% plasma and 50% blood against MRSA.

Another serious concern of the antibacterial agents is the loss of antibacterial activity in presence of complex mammalian fluids due to complexation and loss of bioavailability.[29] Hence the antibacterial efficacy of **13f** was directly investigated in various complex mammalian fluid systems (50% serum, 50% plasma and 50% blood) against MRSA-a drug-resistant Gram-positive bacterium causes many infections in humans. Antibacterial activity was investigated by determining the minimum bactericidal concentration (MBC) of the compound **13f** in 50% serum, 50% plasma and 50% blood supplemented with 50% minimum essential media (MEM) containing ~10^5 CFU/mL MRSA. Notably, the compound was found to be active in 50% serum, 50% plasma and 50% blood. The MBC values of **13f** were 2 μg/mL in 50% serum, 4 μg/mL in 50% plasma and 8 μg/mL 50% blood respectively (while the MBC value of **13f** was 2 μg/mL against *S. aureus* in nutrient media) (Figure 4A.1B). The above results indicated that the compound was able to retain its antibacterial activity even in very complex mammalian fluids like serum, plasma and blood thus implying its potential as an antibacterial agent. The 2-4 fold increase of MBC value could be possibly due to negatively charged proteins and macromolecules in human serum, plasma or blood that tightly bind to the cationic molecules, thereby deactivating it toward membrane disruption.

4A.2.4 Mechanism of action

4A.2.4.1 Cytoplasmic membrane depolarization

To confirm that these cationic small molecular biocides act by disrupting the bacterial cell membrane integrity, detailed molecular mechanism of action was investigated using both spectroscopic methods. To find out whether the biocides act by depolarizing the bacterial cell membrane and to establish the effect of molecular architecture on membrane depolarization, fluorescence spectroscopy was used using the membrane-potential sensitive dye 3,3'-dipropylthiadicarbocyanine iodide ($diSC_35$).[30] In general, due to potential gradient the dye is taken up the bacteria and accumulation in the membrane led to a decrease in fluorescence intensity due to self-quenching. However, when bacteria were treated with the biocides, an increase in fluorescence intensity was observed due to the displacement of $diSC_35$ into the solution against both *S. aureus* and *E. coli*. Thus the above fact indicated that the biocides dissipated the membrane potential of both types of bacteria. Further, different biocides showed different extent of dissipation of membrane potential. For example, biocides **14a-14f** (m = 2-12 and R = $–C_8H_{17}$) and **15a-15f** (m = 2-12 and R = $–C_{10}H_{21}$) showed the maximum membrane depolarization whereas biocides **13a-13f** (m = 2-6 and R = $–C_6H_{13}$) and **16a-16f** (m = 2-12 and R = $–C_{16}H_{33}$) exhibited less or negligible membrane depolarization against both *S. aureus* and *E. coli* (Figure 4A.2A and B). The above results further indicated that the biocides with $–C_8H_{17}$ and $–C_{10}H_{21}$ lipophilic moiety are more active in disrupting the potential than the biocides with $–C_6H_{13}$ and $–C_{16}H_{33}$ which are well correlated with their MIC values. However, it should be mentioned that as the mechanistic studies were performed in HEPES buffer where the activity of these compound might vary and be different than that of obtained in nutrient media.

4A.2.4.2 Membrane permeabilization

The ability of biocides to permeabilize the cytoplasmic membrane of bacteria was studied using propidium iodide (PI) dye.[31] PI is known to enter inside bacterial cell only through compromised membrane and fluoresces upon binding to the cellular DNA. Upon treatment with the biocides, an enhancement in the fluorescence intensity was found to observe against *S. aureus* and *E. coli*. Thus the biocides were efficient in permeabilizing the cytoplasmic membranes of both Gram-positive (*S. aureus*) and Gram-negative (*E. coli*) bacteria. All the biocides were found to show the membrane permeabilization against both the bacteria. Biocides **14a-14f** and **15a-15f** showed the maximum membrane permeabilization whereas

13a-13f and **16a-16f** exhibited less or negligible membrane permeabilization against *S. aureus*. On the other hand, all the biocides showed membrane permeabilization at the tested concentration against *E. coli*. However, biocides **15a-15f** and **16a-16f** showed higher cytoplasmic permeabilization (Figure 4A.2C and D) probably due to similar reason as explained earlier. In summary, all the above studies indicated that these cationic small molecules indeed interacted with the negatively charged bacterial cell membrane and disrupted the membrane integrity.

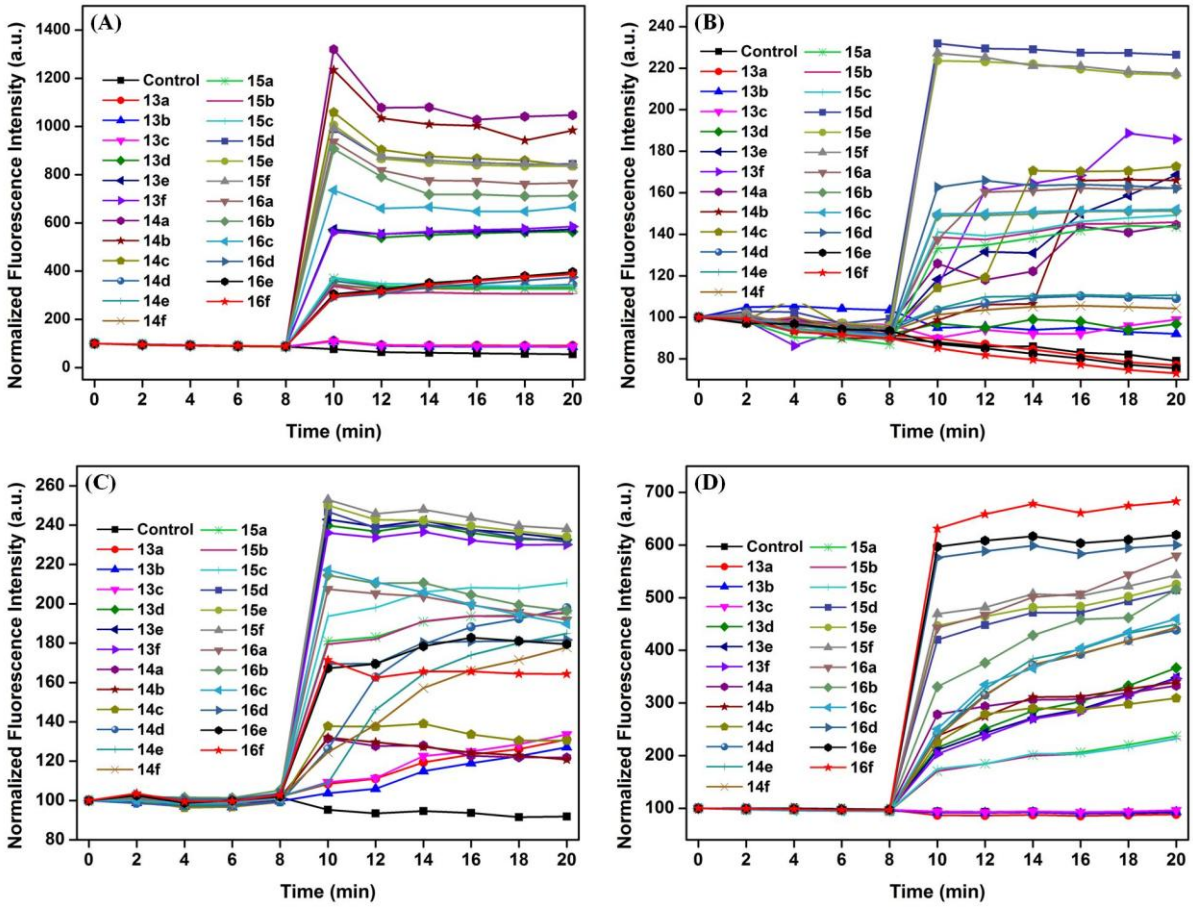

Figure 4A.2: Mechanism of antibacterial action of the cationic small molecular biocides at 40 μg/mL: (**A** and **B**) membrane depolarization against *S. aureus* and *E. coli* respectively using diSC3(5) dye as fluorescence probe and (**C** and **D**) cytoplasmic membrane permeabilization against *S. aureus* and *E. coli* respectively using propidium iodide (PI) as fluorescence probe.

4A.2.5 *In-vitro* biofilm eradication ability

The ability of the optimized non-toxic molecule to eradicate established bacterial biofilms was tested developing matured bacterial biofilms *in-vitro* and then treating the biofilm with the molecule. *S. aureus* and *E. coli* biofilms were treated with **13f** (at 32 μg/mL) and

analyzed for cell counting as well as observed by confocal laser scanning microscopy (CLSM).[32] Molecule **13f** was found to reduce 9.2 log bacterial burdens against *S. aureus* biofilm and 7.1 log against *E. coli* biofilm respectively under *in-vitro* conditions thus showing the ability to destroy biofilm-encased bacteria. The biofilm disrupting property of the molecule was further established by CLSM via staining with green fluorescent dye SYTO 9. In the untreated samples, thick and matured biofilms of thickness ~14-18 μm were seen (Figure 4A.3A and C) while treated samples showed scattered mono layered bacteria of only 2-3 μm thickness against both *S. aureus* and *E. coli* respectively (Figure 4A.3B and D). These results further demonstrated the ability of the molecules to eradicate establish bacterial biofilms.

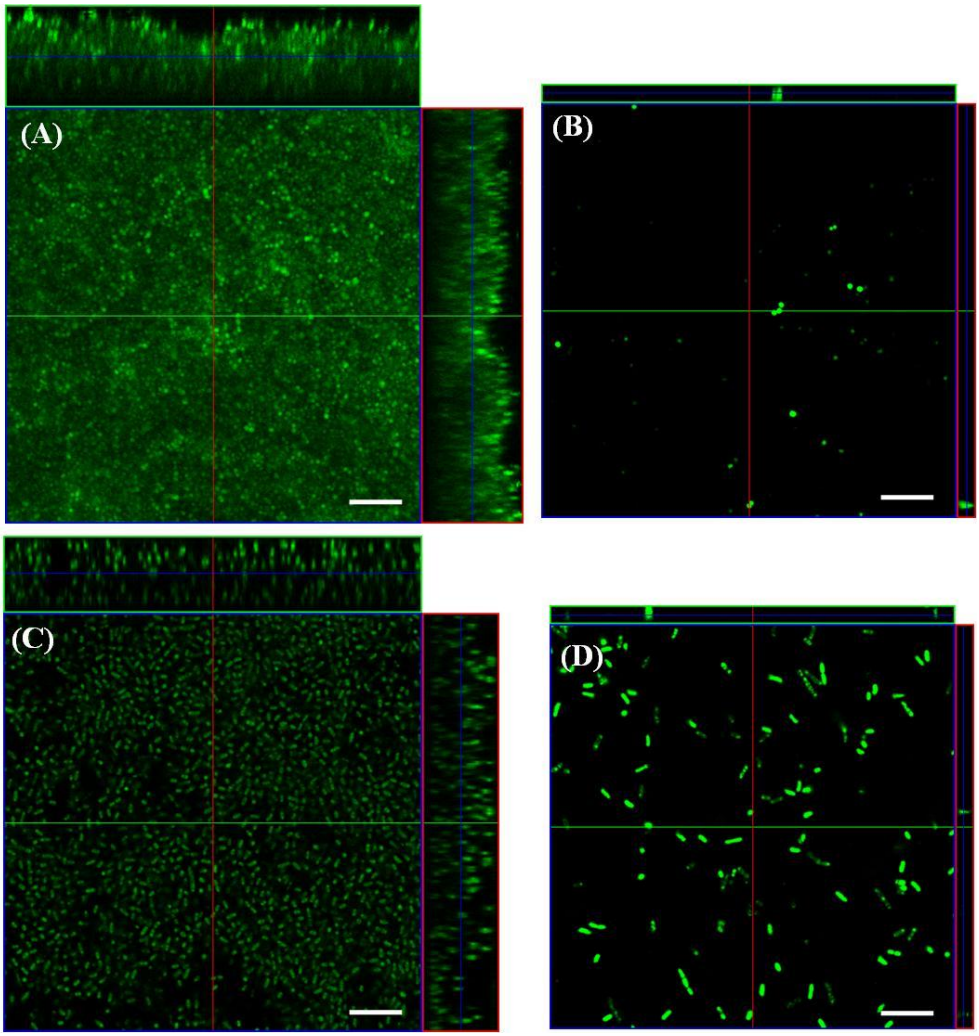

Figure 4A.3: *In-vitro* antibiofilm efficacy of molecule **13f**. CLSM images of (A and C) non-treated *S. aureus* and *E. coli* biofilm; (B and D) **13f** treated *S. aureus* and *E. coli* biofilm (at 32 μg/mL) after staining with SYTO 9. Scale bar 5 μm.

The minimum biofilm eradication concentration (MBEC) for the cationic molecules was also determined. MBEC values of **13f** were found to be 31.2-62.5 μg/mL against *S. aureus* and *E. coli*. The above results thus indicated that these molecules are capable of annihilating established biofilms completely. To evaluate the potential of these small molecules as antibiofilm agents, MBEC values were also compared with some common antiseptics (BAC-14 and DDAC-10) and cationic amphiphiles (DTAB and CTAB). Notably, the molecules showed similar or even better MBEC values compared to those of commercial quaternary compounds 31.2-125 μg/mL against *S. aureus* and *E. coli*.

4A.2.6 *In-vitro* toxicity against mammalian cells

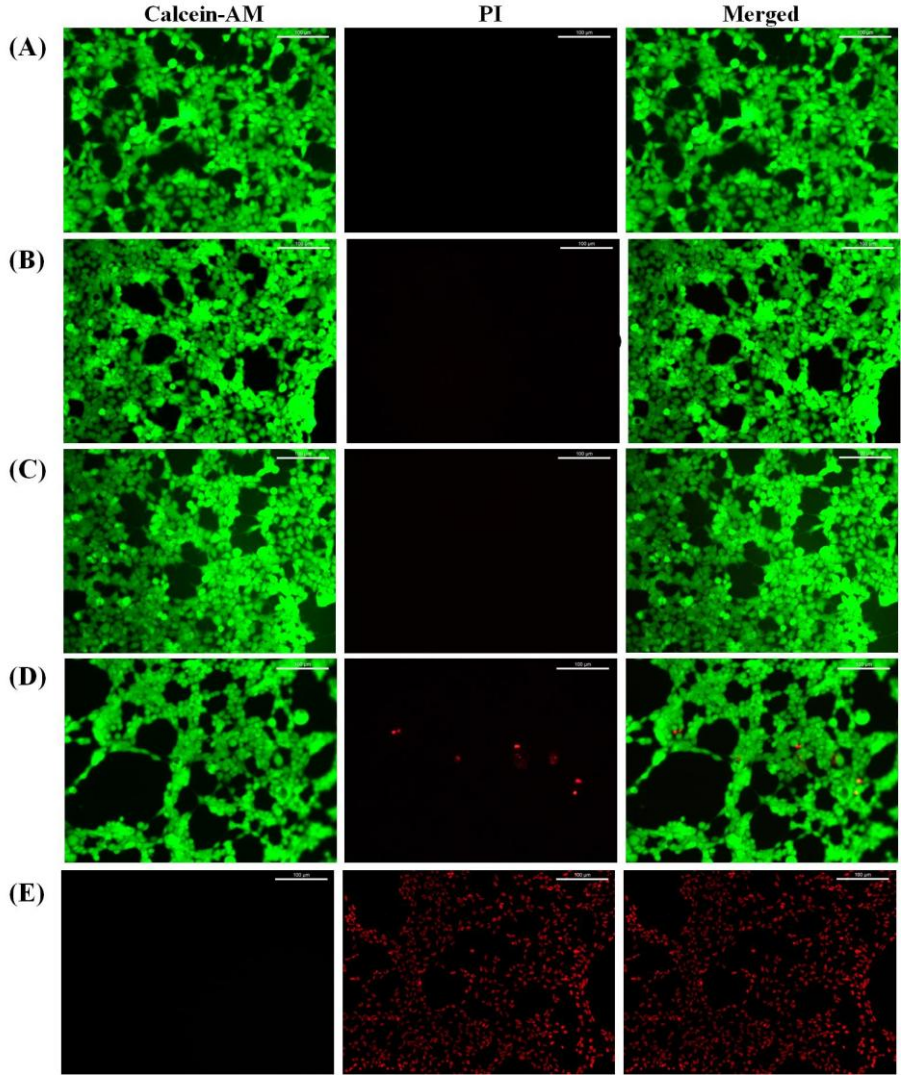

Figure 4A.4: Cytotoxicity of the small molecule. Fluorescence microscopy images of HEK 293 cells after treatment with the molecule for 24 h and staining with calcein AM and PI. Panel (A): non-treated cells (negative control); panel (B): cells treated with **13f** at 16 μg/mL; panel (C): cells treated with **13f** at 32 μg/mL; panel (D) cells treated with **13f** at 64 μg/mL; panel (E) cells treated with TX (0.1 vol%).

One of the major concerns in the development of clinically useful antibacterial agents for biomedical applications is their selectivity towards mammalian cells over bacterial cells. Previously the optimised molecule was shown to be highly hemocompatible. To strengthen the non-cytotoxic behaviour of the optimized molecule, human embryonic kidney (HEK 293) cells were treated with **13f** at 16 μg/mL, 32 μg/mL and 64 μg/mL and then imaged by fluorescence microscopy using membrane permeable green fluorescent dye calcein-AM and membrane impermeable red fluorescent dye propidium iodide (PI).[33] Untreated cells showed complete green fluorescence (Figure 4A.4A) thereby indicated the presence of live cells. Notably cells treated with molecule **13f** showed almost complete green fluorescence at all three tested concentrations (Figure 4A.4B-D). On the other hand, TX treated cells showed completely red fluorescence indicative of cell death (Figure 4A.4F). The above facts thus indicated the non-cytotoxic nature of the optimized molecule.

4A.2.7 *In-vivo* studies

4A.2.7.1 *In-vivo* toxicity

In-vivo toxicity of the cationic small molecules still remains a major concern for the molecules to be used in healthcare applications. The toxic effect of the optimized molecule was briefly evaluated by determining the lethal dose (LD_{50}) upon topical application in mice. LD_{50} value for **13f** was found to be more than 200 mg/kg in an acute dermal toxicity study (OECD 425). Also, no visible inflammation or abnormal skin reaction was observed for the molecule at 200 mg/kg when applied on the mice skin.

4A.2.7.2 *In-vivo* antibiofilm activity

Another important limitation of the antimicrobials is their relatively poor potency under *in-vivo* conditions. In general, it has been observed that small molecules lack the ability to eliminate preformed bacterial biofilms *in-vivo*, which has largely limited their pre-clinical entry. Thus *in-vivo* efficacy of the most potent molecule to eradicate preformed biofilm of MRSA (one of the leading biofilm forming and the most common bacteria that cause many nosocomial infections) was evaluated.[34] Importantly, the optimised molecule showed remarkable biofilm eradicating ability under *in-vivo* conditions. In a murine model of superficial skin infection and biofilm formation, a wound was first induced on the back of mice (dorsal midline) and then infected with MRSA.[6] The biofilms formed after 24 h of

infection were then treated by **3b** topically (40 mg/kg once a day) (Figure 4A.5A) for four days.

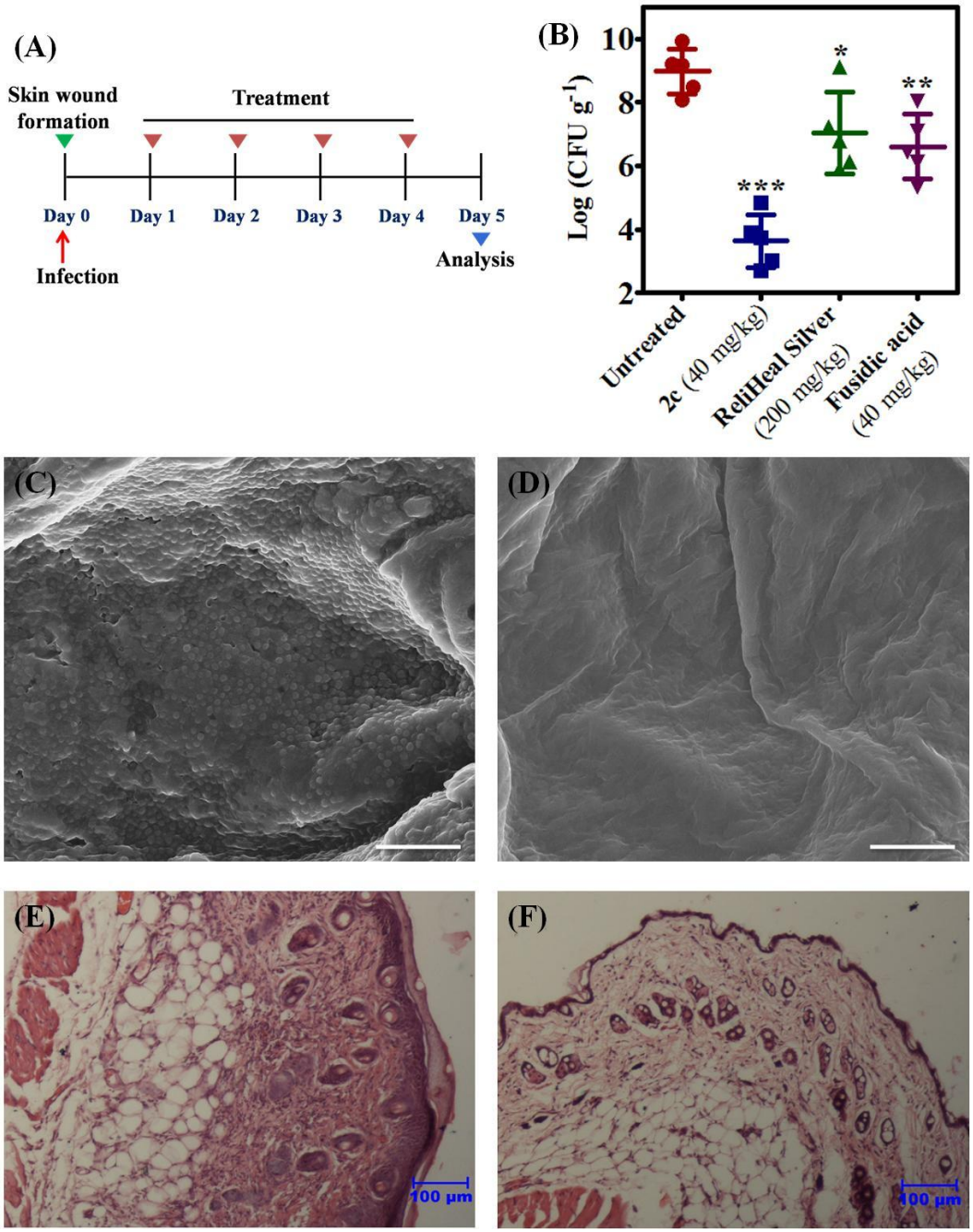

Figure 4A.5: *In-vivo* activity and antibiofilm efficacy of **13f**. (A) Experimental plan of murine model of superficial MRSA biofilm formation and treatment after mice were rendered neutropenic; (B) bacterial count of the treated and un-treated skin tissue sample from mice. Scanning electron microscopy images of the skin tissue samples representing bacteria (C) after 24 h of infection and (D) after 4 days of treatment with **13f** (at 40 mg/kg). Arrow indicates the bacterial cells; p values (*) are <0.0001, 0.0183 and 0.0025 for **13f**-, Reliheal silver- and fusidic acid- treated samples. Mice skin histopathology of (E) infected non-treated skin tissue and (F) treated skin tissue after haematoxylin and eosin staining.

After 18 h of the application of last dosage, mice were sacrificed and skin tissues were collected. Notably, **3b** treated skin tissue samples showed 5.3 log (> 99.999%) reduction of MRSA compared to the untreated tissue samples (p value <0.0001) (Figure 4A.5B). In contrast, fusidic acid and silver nanoparticle containing commercial ointment (ReliHeal) which are used in clinics to treat skin infections, were found to reduce MRSA count by 2.2 and 2.3 log reduction at 40 mg/kg and 200 mg/kg respectively (Figure 4A.5B) (p values were 0.0183 and 0.0025 respectively). The fact that the molecule **13f** was much more effective in comparison to the approved drug fusidic acid emphasizes on the clinical potential of the molecule. The ability of the small molecule in eradicating matured biofilm under *in-vivo* conditions was further established by imaging skin tissue samples with scanning electron microscopy. Tissue samples after 24 h of infection showed the presence of a thick dense MRSA layer thereby indicated the formation and persistence of biofilm (Figure 4A.5C). The treated skin tissue sample, on the other hand, showed negligible number of bacteria on the tissue surface (Figure 4A.5D). Histopathological responses of both untreated and molecule-treated skin tissues were recorded. While the MRSA infected mice showed mild infiltration of inflammatory cells mainly neutrophils in dermis layer (arrow), tissue treated with **13f** showed normal appearance of skin with thin layer of epidermis and hair follicles, sweat glands (arrow) (Figure 4A.5E-F). These result thus indicated the ability of the optimised molecule to eradicate bacterial biofilms under *in-vivo* conditions.

4A.2.8 Propensity to induce bacterial resistance

The ability of these biocides to suppress the development of resistance was evaluated by taking the most potent biocide (**13f**) against both Gram-positive *S. aureus* and Gram-negative *E. coli*. Norfloxacin, an antibiotic commonly used to treat the Gram-positive infections, was used as a positive control for *S. aureus*, whereas colistin, a lipopeptide antibiotic active against Gram-negative bacteria, was used in case of *E. coli*. These antibacterial agents were repeatedly challenged against bacteria at their sub-MIC values to allow bacteria to develop resistance. Interestingly, no change in the MIC of **13f** was observed against both *S. aureus* and *E. coli* even after 20 passages whereas around 810-fold and 248-fold increase in MIC was observed in case of norfloxacin and colistin respectively (Figure 4A.6). The above results thus indicated that bacteria find it difficult to develop resistance against this type of biocides within the experimental time period.

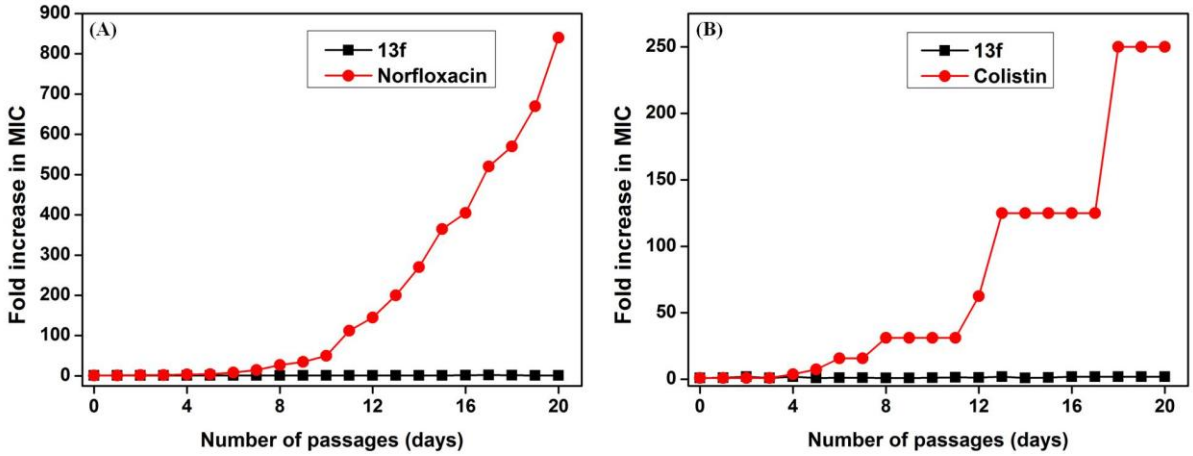

Figure 4A.6: Propensity of development of bacterial resistance against compound **13f**: (A) for *S. aureus* where norfloxacin was used as control (B) for *E. coli* where colistin was used as control.

4A.3. Conclusion

In conclusion, novel membrane-active small molecules have been developed via simple yet quantitative methodology. The compounds displayed excellent antibacterial activity against various wild-type and drug resistant bacteria (both Gram-positive and Gram-negative). Variation of amphiphilic nature of the compounds drastically improved their antibacterial activity and as well as selectivity. Additionally, the small molecules were found to be stable under plasma conditions and showed excellent activity in various complex mammalian fluids such as serum, plasma and blood. Further, these compounds were shown to eradicate established bacterial biofilms under *in-vitro* conditions. These molecules acted on bacteria rapidly by disrupting the membrane and did not allow bacteria to develop resistance. The compounds showed negligible toxicity against mammalian cells. Moreover, the molecule was also found to eradicate preformed bacterial biofilm under more complex *in-vivo* conditions without causing substantial skin toxicity. The results furnished herein thus emphasize the potential of this class of molecules to be useful in guiding and developing future antibacterial and antibiofilm small molecules with improved biocompatibility.

4A.4 Experimental Section

4A.4.1 Materials and instrumentation

1-Aminohexane, 1-aminooctane, 1-aminododecane, 1-aminohexadecane, *N*,*N*-dimethyl octylamine, *N*,*N*-dimethyl decylamine, *N*,*N*-dimethyl dodecylamine, *N*,*N*-dimethyl hexadecylamine, *N*,*N*,*N*′,*N*′-tetramethyl-1,2-diaminoethane, *N*,*N*,*N*′,*N*′-tetramethyl-1,4-

diaminobutane, 1,6-dibromohexane, 1,8-dibromooctane, 1,10-dibromodecane and 1,12-dibromododecane 1,2-diaminoethane, 1,3-diaminopropane, 1,4-diaminobutane, 1,6-diaminohexane, bromoacetyl bromide, 2-[4-(2-hydroxyethyl)piperazin-1-yl]ethanesulfonic acid (HEPES) and alpha D(+) glucose were purchased from Sigma-Aldrich and used as received. Anhydrous potassium carbonate (K_2CO_3), anhydrous sodium sulphate (Na_2SO_4), phosphorous pentaoxide (P_2O_5), calcium hydride (CaH_2), *N*,*N*-dimethylamine solution (40%), dichloromethane (DCM), chloroform, ethanol, acetonitrile, diethyl ether, acetone and molecular sieves (4 Å) were purchased from SD Fine, India and were of analytical grade. Acetonitrile, DCM and chloroform were dried over P_2O_5 and ethanol was dried over CaH_2 and stored over molecular sieves. Nuclear magnetic resonance (NMR) spectra were recorded using Bruker AMX-400 (400 MHz for ^{1}H NMR and 100 MHz for ^{13}C NMR) spectrometer. The chemical shift (δ) values are reported in parts per million (ppm). Mass spectra were recorded on a 6538-UHD Accurate mass Q-TOF LC-MS high resolution mass-spectrometer (HRMS). Infrared (IR) spectra were recorded by Bruker IFS66 V/s spectrometer on NaCl crystal for liquid compounds and KBr pellet for solid compounds. For optical density (O. D.) measurement, Tecan Infinite Pro series M200 Microplate Reader was employed. *Staphylococcus aureus* (MTCC 737) and *Escherichia coli* (MTCC 443) were purchased from MTCC (Chandigarh, India). *Pseudomonas aeruginosa* (ATCC 424), methicillin-resistant *Staphylococcus aureus* (ATCC 33591), vancomycin-resistant *Enterococcus faecium* (ATCC 51559) and β-lactam-resistant *Klebsiella pneumoniae* (ATCC 700603) were obtained from ATCC (Rockville, MD, USA).

4A.4.2 General synthetic procedure

4A.4.2.1 General procedure for the synthesis of 1a-1e

Intermediates **1a-1e** was synthesized from 1-aminoalkanes following the same protocol as described in the section 2B.4.2 of chapter 2B.

1a (2-Bromo-*N*-hexylethanamide)**:** FT-IR ($\bar{\nu}$): 3250 cm^{-1} (amide N–H str.), 2928 cm^{-1} (–CH_2– assym. str.), 2850 (–CH_2– sym. str.), 1680 cm^{-1} (Amide I, C=O str.), 1560 cm^{-1} (Amide II, N–H ben.), 1470 cm^{-1} (–CH_2– scissor); ^{1}H NMR: (400 MHz, $CDCl_3$): δ 0.859 (t, terminal –*CH*$_3$, 3H), 1.309 (m, –(*CH*$_2$)$_3$–, 6H), 1.530 (q, –*CH*$_2$(CH_2)$_3$–, 2H), 3.248 (m, –CONH*CH*$_2$–, 2H), 3.861 (s, –CO*CH*$_2$Br, 2H), 6.581 (br s, amide –*NH*CO, 1H); ^{13}C-NMR (100 MHz, $CDCl_3$): δ 14.190, 22.770, 26.912, 29.711, 31.994, 40.408, 165.589.

1b (2-Bromo-*N*-octylethanamide)**:** FT-IR ($\bar{\nu}$): 3252 cm^{-1} (amide N–H str.), 2929 cm^{-1} (–CH_2-assym. str.), 2851 (–CH_2– sym. str.), 1680 cm^{-1} (Amide I, C=O str.), 1556 cm^{-1} (Amide

II, N–H ben.), 1469 cm^{-1} (–CH_2– scissor); ^{1}H-NMR: (400 MHz, $CDCl_3$): δ 0.877 (t, terminal –*CH₃*, 3H), 1.291 (m, –(*CH₂*)$_5$–, 10H), 1.535 (q, –*CH₂*(CH_2)$_5$–, 2H), 3.252 (t, –CONH*CH₂*–, 2H), 3.865 (s, –CO*CH₂*Br, 2H), 6.565 (br s, amide –*NH*CO, 1H); ^{13}C-NMR (100 MHz, $CDCl_3$): δ 14.188, 22.698, 26.904, 29.411, 29,589, 29.998, 31.989, 40.402, 165.578.

1c (2-Bromo-*N*-decylethanamide)**:** FT-IR ($\bar{\nu}$): 3255 cm^{-1} (amide N–H str.), 2932 cm^{-1} (–CH_2-assym. str.), 2850 (–CH_2– sym. str.), 1685 cm^{-1} (Amide I, C=O str.), 1555 cm^{-1} (Amide II, N–H ben.), 1469 cm^{-1} (–CH_2– scissor); ^{1}H-NMR: (400 MHz, $CDCl_3$): δ 0.878 (t, terminal –*CH₃*, 3H), 1.292 (m, –(*CH₂*)$_7$–, 14H), 1.535 (q, –*CH₂*(CH_2)$_7$–, 2H), 3.258 (t, –CONH*CH₂*–, 2H), 3.874 (s, –CO*CH₂*Br, 2H), 6.585 (br s, amide –*NH*CO, 1H); ^{13}C-NMR (100 MHz, $CDCl_3$): δ 14.188.7, 22.699, 26.914, 29.411, 29,589, 29.978, 31.919, 40.412, 165.598.

1d (2-Bromo-*N*-dodecylethanamide)**:** FT-IR ($\bar{\nu}$): 3251 cm^{-1} (amide N–H str.), 2929 cm^{-1} (–CH_2–assym. str.), 2851 (–CH_2– sym. str.), 1685 cm^{-1} (Amide I, C=O str.), 1558 cm^{-1} (Amide II, N–H ben.), 1470 cm^{-1} (–CH_2– scissor); ^{1}H-NMR: (400 MHz, $CDCl_3$): δ 0.858 (t, terminal –*CH₃*, 3H), 1.289 (m, –(*CH₂*)$_9$–, 18H), 1.533 (q, –*CH₂*(CH_2)$_9$–, 2H), 3.278 (t, –CONH*CH₂*–, 2H), 3.881 (s, –CO*CH₂*Br, 2H), 6.475 (br s, amide –*NH*CO, 2H); ^{13}C-NMR (100 MHz, $CDCl_3$): δ 14.192, 22.765, 26.901, 29.321, 29.420, 29.585, 29.643, 29.705, 31.992, 40.401, 165.587.

1e (2-Bromo-*N*-hexadecylethanamide)**:** FT-IR ($\bar{\nu}$): 3250 cm^{-1} (amide N–H str.), 2927 cm^{-1} (–CH_2-assym. str.), 2849 (–CH_2– sym. str.), 1679 cm^{-1} (Amide I, C=O str.), 1562 cm^{-1} (Amide II, N–H ben.), 1468 cm^{-1} (–CH_2– scissor); ^{1}H-NMR: (400 MHz, $CDCl_3$): δ 0.878 (t, terminal –*CH₃*, 3H), 1.300 (m, –(*CH₂*)$_{13}$–, 26H), 1.547 (q, –*CH₂*(CH_2)$_{13}$–, 2H), 3.279 (t, –CONH*CH₂*–, 2H), 3.883 (s, –CO*CH₂*Br, 2H), 6.575 (br s, amide –*NH*CO, 2H); ^{13}C NMR (100 MHz, $CDCl_3$): δ 14.193, 22.769, 26.903, 29.334, 29.413, 29.578, 29.636, 29.718, 29.818, 32.095, 40.413, 165.567.

4A.4.2.2 General procedure for the synthesis of 2a-2d

N-Alkyl-1-bromoethanamide **1a-1d** (40 mmol) was dissolved in dry chloroform (40 mL) in a screw-top pressure tube. Dry $NHMe_2$ gas was collected to the solution of *N*-alkyl-1-bromoethanamide in chloroform at 0 °C until the volume of the resulting solution was roughly doubled (80 mL). Then the reaction mixture was stirred for 24 h at 80 °C overnight. After the reaction, the pressure tube was cooled and the reaction mixture was transferred to a round bottom (RB) flask and the final volume of the reaction mixture was made to 150 mL by adding chloroform. The unreacted gas was removed carefully by heating slowly until wet litmus paper no longer turns blue on exposure to the emerging vapors. The solution was washed with 2 M KOH solution (3 × 100 mL) in order to deprotonate the products. Finally, the organic layer was passed through anhydrous Na_2SO_4 and was dried to give yellow colored liquids with 100% yield. The products were characterized by FT-IR, ^{1}H NMR and ^{13}C NMR spectroscopy.

2a (2-(*N*,*N*-Dimethyl)-*N′*-hexylethanamide)**:** FT-IR ($\bar{\nu}$): 3230 cm^{-1} (amide N–H str.), 2926 cm^{-1} (–CH_2– assym. str.), 2852 cm^{-1} (–CH_2– sym. str.), 1680 cm^{-1} (Amide I, C=O str.), 1560 cm^{-1} (Amide II, N–H ben.), 1470 cm^{-1} (–CH_2– scissor); ^{1}H-NMR (400 MHz, $CDCl_3$): δ 0.879 (t, terminal –*CH*$_3$, 3H), 1.239 (m, CH_3*(*CH_2*)*$_3$–, 6H), 1.547 (q, $CH_3(CH_2)_3$*CH*$_2$–, 2H), 2.286 (s, (*CH*$_3$)$_2$N–, 6H), 2.883 (s, $(CH_3)_2N$*CH*$_2$CO–, 2H), 3.224 (q, –*CH*$_2$NHCO–, 2H), 7.137 (br s, amide –*NH*, 1H).

2b (2-(*N*,*N*-Dimethyl)-*N′*-octylethanamide)**:** FT-IR ($\bar{\nu}$): 3232 cm^{-1} (amide N–H str.), 2936 cm^{-1} (–CH_2– assym. str.), 2855 cm^{-1} (–CH_2– sym. str.), 1678 cm^{-1} (Amide I, C=O str.), 1560 cm^{-1} (Amide II, N–H ben.), 1470 cm^{-1} (–CH_2– scissor); ^{1}H-NMR (400 MHz, $CDCl_3$): δ 0.831 (t, terminal –*CH*$_3$, 3H), 1.237 (m, CH_3*(*CH_2*)*$_5$–, 10H), 1.489 (q, $CH_3(CH_2)_5$*CH*$_2$–, 2H), 2.236 (s, (*CH*$_3$)$_2$N–, 6H), 2.884 (s, $(CH_3)_2N$*CH*$_2$CO–, 2H), 3.274 (q, –*CH*$_2$NHCO–, 2H), 7.139 (br s, amide –*NH*, 1H).

2c (2-(*N*,*N*-Dimethyl)-*N′*-dodecylethanamide)**:** FT-IR ($\bar{\nu}$): 3229 cm^{-1} (amide N–H str.), 2934 cm^{-1} (–CH_2– assym. str.), 2856 cm^{-1} (–CH_2– sym. str.), 1680 cm^{-1} (Amide I, C=O str.), 1559 cm^{-1} (Amide II, N–H ben.), 1471 cm^{-1} (–CH_2– scissor); ^{1}H-NMR (400 MHz, $CDCl_3$): δ 0.869 (t, terminal –*CH*$_3$, 3H), 1.247 (m, CH_3*(*CH_2*)*$_9$–, 18H), 1.489 (q, $CH_3(CH_2)_9$*CH*$_2$–, 2H), 2.229 (s, (*CH*$_3$)$_2$N–, 6H), 2.926 (s, $(CH_3)_2N$*CH*$_2$CO–, 2H), 3.281 (q, –*CH*$_2$NHCO–, 2H), 7.136 (br s, amide –*NH*, 1H).

2d (2-(*N*,*N*-Dimethyl)-*N′*-hexadecylethanamide)**:** FT-IR ($\bar{\nu}$): 3228 cm^{-1} (amide N–H str.), 2935 cm^{-1} (–CH_2– assym. str.), 2859 cm^{-1} (–CH_2– sym. str.), 1681 cm^{-1} (Amide I, C=O str.), 1559 cm^{-1} (Amide II, N–H ben.), 1470 cm^{-1} (–CH_2– scissor); ^{1}H-NMR (400 MHz, $CDCl_3$): δ 0.871 (t, terminal –*CH*$_3$, 3H), 1.239 (m, CH_3*(*CH_2*)*$_{13}$–, 26H), 1.529 (q, $CH_3(CH_2)_{13}$*CH*$_2$–, 2H), 2.268 (s, (*CH*$_3$)$_2$N–, 6H), 2.934 (s, $(CH_3)_2N$*CH*$_2$CO–, 2H), 3.265 (q, –*CH*$_2$NHCO–, 2H), 7.120 (br s, amide –*NH*, 1H).

4A.4.2.3 General procedure for the synthesis of 3a-3d

Diaminoalkanes (50 mmol) was dissolved in chloroform (100 mL) and a solution of K_2CO_3 (20.7 g, 150 mmol) in water (100 mL) was added to it. The binary mixture was then cooled to 5 °C in a cold incubator. Bromoacetyl bromide (30.4 g, 150 mmol) was dissolved in chloroform (100 mL) and was added to the mixture drop wise for about 30 min. After the completion of addition, the reaction mixture was stirred at room temperature for 12 h. After the reaction, the insoluble solid was filtered through a sintered glass funnel and washed repeatedly with water. Finally, the precipitate was dried in vacuum oven at 60 °C to obtain white colored products (1st collection). Also, organic layer from the reaction mixture after the filtration was separated using a separating funnel and the aqueous layer was subjected to repeated wash with chloroform (2 × 50 mL). All the organic solutions were then combined and washed with water (3 × 75 mL). The final organic layer was passed through anhydrous Na_2SO_4. The organic solvent was evaporated to obtain white products (2nd collection). The products were characterized by FT-IR, ^{1}H-NMR and 13C-NMR spectroscopy. The products

obtained in both ways (from precipitate and solution) were same and combined weight gave quantitative (100%) yield of **3a-3d**.

3a: FT-IR ($\overline{\nu}$): 3294 cm^{-1} (amide N–H str.), 2938 cm^{-1} (–CH_2– assym. str.), 2860 cm^{-1} (–CH_2– sym. str.), 1645 cm^{-1} (Amide I, C=O str.), 1542 cm^{-1} (Amide II, N–H ben.), 1480 cm^{-1} (–CH_2– scissor); ^{1}H-NMR: (400 MHz, $CDCl_3$): δ 3.290 (m, –NH*(CH₂)₂*NH–, 4H), 3.873 (s, –*CH₂*CONH$(CH_2)_2$NHCO*CH₂*–, 4H), 6.551 (br s, amide –CO*NH*$(CH_2)_2$*NH*CO–, 2H); ^{13}C-NMR (100 MHz, $CDCl_3$): δ 29.495, 40.134, 165.531.
3b: FT-IR ($\overline{\nu}$): 3295 cm^{-1} (amide N–H str.), 2942 cm^{-1} (–CH_2– assym. str.), 2863 cm^{-1} (–CH_2– sym. str.), 1645 cm^{-1} (Amide I, C=O str.), 1544 cm^{-1} (Amide II, N–H ben.), 1485 cm^{-1} (–CH_2– scissor); ^{1}H-NMR: (400 MHz, $CDCl_3$): δ 1.542 (m, –CH_2*CH_2*CH_2–, 4H), 3.291 (m, –NH*CH_2*CH_2*CH_2*NH–, 4H), 3.876 (s, –*CH_2*CONH$(CH_2)_3$NHCO*CH_2*–, 4H), 6.589 (br s, amide –CO*NH*$(CH_2)_3$*NH*CO–, 2H); ^{13}C-NMR (100 MHz, $CDCl_3$): δ 29.239, 29.482, 40.194, 165.538.

3c: FT-IR ($\overline{\nu}$): 3294 cm^{-1} (amide N–H str.), 2939 cm^{-1} (–CH_2– assym. str.), 2859 cm^{-1} (–CH_2– sym. str.), 1642 cm^{-1} (Amide I, C=O str.), 1545 cm^{-1} (Amide II, N–H ben.), 1480 cm^{-1} (–CH_2– scissor); ^{1}H-NMR: (400 MHz, $CDCl_3$): δ 1.541 (m, –CH_2*(CH₂)₂*CH_2–, 4H), 3.293 (q, –*CH_2*$(CH_2)_2$*CH_2*–, 4H), 3.874 (s, –*CH_2*CONH$(CH_2)_4$NHCO*CH_2*–, 4H), 6.554 (br s, amide –CO*NH*$(CH_2)_4$*NH*CO–, 2H); ^{13}C-NMR (100 MHz, $CDCl_3$): δ 29.254, 29.479, 40.294, 165.540.

3d: FT-IR ($\overline{\nu}$): 3295 cm^{-1} (amide N–H str.), 2937 cm^{-1} (–CH_2– assym. str.), 2858 cm^{-1} (–CH_2– sym. str.), 1639 cm^{-1} (Amide I, C=O str.), 1540 cm^{-1} (Amide II, N–H ben.), 1483 cm^{-1} (–CH_2– scissor); ^{1}H-NMR: (400 MHz, $CDCl_3$): δ 1.369 (m, –CH_2CH_2*(CH₂)₂*CH_2CH_2–, 4H), 1.539 (m, –CH_2*CH_2*$(CH_2)_2$*CH_2*CH_2–, 4H), 3.293 (q, –*CH_2*$CH_2(CH_2)_2CH_2$*CH_2*–, 4H), 3.877 (s, –*CH_2*CONH$(CH_2)_6$NHCO*CH_2*–, 4H), 6.548 (br s, amide –CO*NH*$(CH_2)_6$*NH*CO–, 2H); ^{13}C-NMR (100 MHz, $CDCl_3$): δ 26.268, 29.264, 29.485, 40.034, 165.531.

4A.4.2.4 General procedure for the synthesis of 4a-4d, 5a-5d, 6a-6d and 7a-7d

To the individual solutions of **3a-3d** (4 mmol) in organic solvents (EtOH for **3a**, $CHCl_3$ for **3b** and MeCN for **3c** and **3d**, 50 mL) were added **2a-2d** (12 mmol) separately and the reaction mixtures were stirred at 85 °C for about 24 h. After the reaction, the mixtures were cooled to room temperature and transferred to RB. Then the volume of the reaction mixtures was reduced to $1/10^{th}$ to its original volume by rotary evaporator. Finally, the products were precipitated with excess of diethyl ether/acetone (150 mL). Either the organic solvent was decanted off and the precipitate was washed three times with diethyl ether or the precipitates were filtered through sintered glass funnel and washed repeatedly with diethyl ether and vacuum dried to give more than 99% yield. All the final products (**4a-4d, 5a-5d, 6a-6d** and **7a-7d**) were characterized by FT-IR, ^{1}H-NMR, ^{13}C-NMR and HRMS. The purity of the compounds checked by reverse phase high performance liquid chromatography (HPLC)

using 0.1% trifluoroacetic acid (TFA) in water/acetonitrile (0-100%) as mobile phase and was found to be more than 95%.

4a: FT-IR ($\overline{\nu}$): 3208 cm^{-1} (amide N–H str.), 2909 cm^{-1} (–CH_2– assym. str.), 2860 cm^{-1} (–CH_2– sym. str.), 1675 cm^{-1} (amide I, C=O str.), 1555 cm^{-1} (amide II, N–H ben.), 1468 cm^{-1} (–CH_2– scissor); ^{1}H-NMR (400 MHz, $CDCl_3$): δ 0.875 (t, terminal –*CH_3*, 6H), 1.259 (m, –CH_3*$(CH_2)_3$*CH_2–, 12H), 1.581 (m, $CH_3(CH_2)_3$*CH_2*CH_2–, 4H), 3.231 (m, $CH_3(CH_2)_3CH_2$*CH_2*–, 4H), 3.439 (m, –NH*CH_2CH_2*NH–, 4H), 3.611 (s, –CH_2N^+*$(CH_3)_2$*CH_2–, 12H), 4.630 (s, –*CH_2*$N^+(CH_3)_2$*CH_2*–, 4H), 8.219 (br s, $CH_3(CH_2)_5$*NH*CO–, 2H), 8.684 (br s, –CO*NH*CH_2–, 2H); ^{13}C-NMR (100 MHz, $CDCl_3$): δ 14.219, 22.777, 27.281, 29.225, 29.415, 38.941, 40.409, 52.829, 64.182, 66.226, 162.664, 162.880; HRMS (ESI): m/z calculated for $C_{26}H_{54}N_6O_4Br_2$ $[M–Br]^+$ and $[M–2Br]^{2+}$: 593.3571, 595.3571 and 257.2194 Found: 593.3394, 595.3379 and 257.2112.

4b: FT-IR ($\overline{\nu}$): 3212 cm^{-1} (amide N–H str.), 2928 cm^{-1} (–CH_2– assym. str.), 2860 cm^{-1} (–CH_2– sym. str.), 1685 cm^{-1} (amide I, C=O str.), 1565 cm^{-1} (amide II, N–H ben.), 1465 cm^{-1} (–CH_2– scissor); ^{1}H-NMR (400 MHz, $CDCl_3$): δ 0.862 (t, terminal –*CH_3*, 6H), 1.269 (m, –CH_3*$(CH_2)_3$*CH_2–, 12H), 1.615 (m, $CH_3(CH_2)_3$*CH_2*CH_2–, 4H), 1.851 (m, –$NHCH_2$*CH_2*CH_2NH–, 2H), 3.231 (m, $CH_3(CH_2)_3CH_2$*CH_2*–, 4H), 3.381 (m, –NH*CH_2*CH_2*CH_2*NH–, 4H), 3.580 (s, –CH_2N^+*$(CH_3)_2$*CH_2–, 12H), 4.614 (s, –*CH_2*$N^+(CH_3)_2$*CH_2*–, 4H), 8.208 (br s, $CH_3(CH_2)_5$*NH*CO–, 2H), 8.665 (br s, –CO*NH*CH_2–, 2H); ^{13}C-NMR (100 MHz, $CDCl_3$): δ 14.209, 22.707, 26.138 27.278, 29.224, 29.409, 38.978, 40.412, 52.838, 64.194, 66.234, 162.647, 162.856; HRMS (ESI): m/z calculated for $C_{27}H_{56}N_6O_4Br_2$ $[M–Br]^+$ and $[M–2Br]^{2+}$: 607.3726, 609.3726 and 264.2272. Found: 607.2185, 609.3509 and 264.2185.

4c: FT-IR ($\overline{\nu}$): 3210 cm^{-1} (amide N–H str.), 2920 cm^{-1} (–CH_2– assym. str.), 2860 cm^{-1} (–CH_2– sym. str.), 1678 cm^{-1} (amide I, C=O str.), 1557 cm^{-1} (amide II, N–H ben.), 1470 cm^{-1} (–CH_2– scissor); ^{1}H-NMR (400 MHz, $CDCl_3$): δ 0.872 (t, terminal –*CH_3*, 6H), 1.254 (m, –CH_3*$(CH_2)_3$*CH_2–, 12H), 1.534 (m, $CH_3(CH_2)_3$*CH_2*CH_2–, 4H), 1.578 (m, –$NHCH_2$*$(CH_2)_2$*CH_2NH–, 4H), 3.220 (m, $CH_3(CH_2)_3CH_2$*CH_2*–, 4H), 3.321 (m, –NH*CH_2*$(CH_2)_2$*CH_2*NH–, 4H), 3.558 (s, –CH_2N^+*$(CH_3)_2$*CH_2–, 12H), 4.610 (s, –*CH_2*$N^+(CH_3)_2$*CH_2*–, 4H), 8.205 (br s, $CH_3(CH_2)_7$*NH*CO–, 2H), 8.447 (br s, –CO*NH*CH_2–, 2H); ^{13}C-NMR (100 MHz, $CDCl_3$): δ 14.221, 22.760, 26.108, 27.144, 27.173, 29.308, 29.336, 31.160, 40.056, 52.788, 64.447, 65.532, 162.773, 162.943; HRMS (ESI): m/z calculated for $C_{28}H_{58}N_6O_4Br_2$ $[M–Br]^+$ and $[M–2Br]^{2+}$: 677.4510, 679.4510 and 299.2663. Found: 677.4306, 679.4290 and 299.2618.

4d: FT-IR ($\overline{\nu}$): 3207 cm^{-1} (amide N–H str.), 2914 cm^{-1} (–CH_2– assym. str.), 2855 cm^{-1} (–CH_2– sym. str.), 1675 cm^{-1} (amide I, C=O str.), 1558 cm^{-1} (amide II, N–H ben.), 1470 cm^{-1} (–CH_2– scissor); ^{1}H-NMR (400 MHz, $CDCl_3$): δ 0.875 (t, terminal –*CH_3*, 6H), 1.262 (m, –CH_3*$(CH_2)_5$*CH_2–, 20H), 1.414 (m, –$NHCH_2CH_2$*$(CH_2)_2$*CH_2CH_2NH–, 4H), 1.554-1.571 (m, –$CH_3(CH_2)_5$*CH_2*CH_2– and –$NHCH_2$*CH_2*$(CH_2)_2$*CH_2*CH_2NH–, 8H), 3.241-3.316 (m, $CH_3(CH_2)_5CH_2$*CH_2*– and –NH*CH_2*$(CH_2)_4$*CH_2*NH–, 8H), 3.586 (s, –CH_2N^+*$(CH_3)_2$*CH_2–, 12H), 4.641 (s, –*CH_2*$N^+(CH_3)_2$*CH_2*–, 4H), 8.229 (br s, $CH_3(CH_2)_7$*NH*CO–, 2H), 8.440 (br s, –CO*NH*CH_2–, 2H); ^{13}C-NMR (100 MHz, $CDCl_3$): δ 14.206, 22.743, 26.198, 27.129, 28.308, 29.156, 29.297, 29.320, 39.313, 40.040, 52.621, 64.782, 65.243, 162.765, 162.862; HRMS

(ESI): m/z calculated for $C_{30}H_{62}N_6O_4Br_2$ $[M–Br]^+$ and $[M–2Br]^{2+}$: 649.4197, 651.4197 and 285.2507 Found: 649.4109, 651.4098 and 285.2493.

5a: FT-IR ($\overline{\nu}$): 3215 cm^{-1} (amide N–H str.), 2918 cm^{-1} (–CH_2– assym. str.), 2855 cm^{-1} (–CH_2– sym. str.), 1678 cm^{-1} (amide I, C=O str.), 1560 cm^{-1} (amide II, N–H ben.), 1465 cm^{-1} (–CH_2– scissor); ^{1}H-NMR (400 MHz, $CDCl_3$): δ 0.866 (t, terminal –*CH_3*, 6H), 1.266 (m, –CH_3*$(CH_2)_5$*CH_2–, 20H), 1.564 (m, $CH_3(CH_2)_5$*CH_2*CH_2–, 4H), 3.229 (m, $CH_3(CH_2)_5CH_2$*CH_2*–, 4H), 3.459 (m, –NH*CH_2CH_2*NH–, 4H), 3.605 (s, –CH_2N^+*$(CH_3)_2$*CH_2–, 12H), 4.629 (s, –*CH_2*$N^+(CH_3)_2$*CH_2*–, 4H), 8.234 (br s, $CH_3(CH_2)_7$*NH*CO–, 2H), 8.734 (br s, –CO*NH*CH_2–, 2H); ^{13}C-NMR (100 MHz, $CDCl_3$): δ 14.228, 22.767, 27.163, 29.180, 29.313, 29.338, 31.939, 38.822, 40.403, 52.829, 64.122, 66.238, 162.765, 163.380; HRMS (ESI): m/z calculated for $C_{30}H_{62}N_6O_4Br_2$ $[M–Br]^+$ and $[M–2Br]^{2+}$: 649.4197, 651.4197 and 285.2507 Found: 649.4109, 651.4098 and 285.2493.

5b: FT-IR ($\overline{\nu}$): 3210 cm^{-1} (amide N–H str.), 2925 cm^{-1} (–CH_2– assym. str.), 2860 cm^{-1} (–CH_2– sym. str.), 1680 cm^{-1} (amide I, C=O str.), 1565 cm^{-1} (amide II, N–H ben.), 1470 cm^{-1} (–CH_2– scissor); ^{1}H-NMR (400 MHz, $CDCl_3$): δ 0.860 (t, terminal –*CH_3*, 6H), 1.264 (m, –CH_3*$(CH_2)_5$*CH_2–, 20H), 1.555 (m, $CH_3(CH_2)_5$*CH_2*CH_2–, 4H), 1.848 (m, –$NHCH_2$*CH_2*CH_2NH–, 2H), 3.241 (m, $CH_3(CH_2)_5CH_2$*CH_2*–, 4H), 3.377 (m, –NH*CH_2*CH_2*CH_2*NH–, 4H), 3.583 (s, –CH_2N^+*$(CH_3)_2$*CH_2–, 12H), 4.666 (s, –*CH_2*$N^+(CH_3)_2$*CH_2*–, 4H), 8.178 (br s, $CH_3(CH_2)_7$*NH*CO–, 2H), 8.601 (br s, –CO*NH*CH_2–, 2H); ^{13}C-NMR (100 MHz, $CDCl_3$): δ 14.201, 22.790, 26.128, 27.134, 27.189, 29.412, 29.289, 31.260, 40.456, 52.898, 64.401, 65.516, 162.768, 162.848; HRMS (ESI): m/z calculated for $C_{31}H_{64}N_6O_4Br_2$ $[M–Br]^+$ and $[M–2Br]^{2+}$: 663.4354, 665.4354 and 292.2585. Found: 663.4164, 665.4133 and 292.2564.

5c: FT-IR ($\overline{\nu}$): 3205 cm^{-1} (amide N–H str.), 2915 cm^{-1} (–CH_2– assym. str.), 2852 cm^{-1} (–CH_2– sym. str.), 1674 cm^{-1} (amide I, C=O str.), 1560 cm^{-1} (amide II, N–H ben.), 1468 cm^{-1} (–CH_2– scissor); ^{1}H-NMR (400 MHz, $CDCl_3$): δ 0.864 (t, terminal –*CH_3*, 6H), 1.262 (m, –CH_3*$(CH_2)_5$*CH_2–, 20H), 1.544 (m, $CH_3(CH_2)_5$*CH_2*CH_2–, 4H), 1.580 (m, –$NHCH_2$*$(CH_2)_2$*CH_2NH–, 4H), 3.213 (m, $CH_3(CH_2)_5CH_2$*CH_2*–, 4H), 3.316 (m, –NH*CH_2*$(CH_2)_2$*CH_2*NH–, 4H), 3.558 (s, –CH_2N^+*$(CH_3)_2$*CH_2–, 12H), 4.610 (s, –*CH_2*$N^+(CH_3)_2$*CH_2*–, 4H), 8.205 (br s, $CH_3(CH_2)_7$*NH*CO–, 2H), 8.447 (br s, –CO*NH*CH_2–, 2H); ^{13}C-NMR (100 MHz, $CDCl_3$): δ 14.221, 22.760, 26.108, 27.144, 27.173, 29.308, 29.336, 31.160, 40.056, 52.788, 64.447, 65.532, 162.773, 162.943; HRMS (ESI): m/z calculated for $C_{32}H_{66}N_6O_4Br_2$ $[M–Br]^+$ and $[M–2Br]^{2+}$: 677.4510, 679.4510 and 299.2663. Found: 677.4306, 679.4290 and 299.2618.

5d: FT-IR ($\overline{\nu}$): 3207 cm^{-1} (amide N–H str.), 2914 cm^{-1} (–CH_2– assym. str.), 2855 cm^{-1} (–CH_2– sym. str.), 1675 cm^{-1} (amide I, C=O str.), 1558 cm^{-1} (amide II, N–H ben.), 1470 cm^{-1} (–CH_2– scissor); ^{1}H-NMR (400 MHz, $CDCl_3$): δ 0.875 (t, terminal –*CH_3*, 6H), 1.262 (m, –CH_3*$(CH_2)_5$*CH_2–, 20H), 1.414 (m, –$NHCH_2CH_2$*$(CH_2)_2$*CH_2CH_2NH–, 4H), 1.554-1.571 (m, –$CH_3(CH_2)_5$*CH_2*CH_2– and –$NHCH_2$*CH_2*$(CH_2)_2$*CH_2*CH_2NH–, 8H), 3.241-3.316 (m, $CH_3(CH_2)_5CH_2$*CH_2*– and –NH*CH_2*$(CH_2)_4$*CH_2*NH–, 8H), 3.586 (s, –CH_2N^+*$(CH_3)_2$*CH_2–, 12H), 4.641 (s, –*CH_2*$N^+(CH_3)_2$*CH_2*–, 4H), 8.229 (br s, $CH_3(CH_2)_7$*NH*CO–, 2H), 8.440 (br s, –CO*NH*CH_2–, 2H); ^{13}C-NMR (100 MHz, $CDCl_3$): δ 14.206, 22.743, 26.198, 27.129, 28.308, 29.156, 29.297, 29.320, 39.313, 40.040, 52.621, 64.782, 65.243, 162.765, 162.862; HRMS (ESI): m/z calculated for $C_{34}H_{70}N_6O_4Br_2$ $[M–Br]^+$ and $[M–2Br]^{2+}$: 705.4824, 707.4824 and 313.2820. Found: 705.4618, 707.4602 and 313.2761.

6a: FT-IR ($\overline{\nu}$): 3212 cm^{-1} (amide N–H str.), 2920 cm^{-1} (–CH_2– assym. str.), 2860 cm^{-1} (–CH_2– sym. str.), 1682 cm^{-1} (amide I, C=O str.), 1565 cm^{-1} (amide II, N–H ben.), 1468 cm^{-1} (–CH_2– scissor); ^{1}H-NMR (400 MHz, $CDCl_3$): δ 0.886 (t, terminal –*CH_3*, 6H), 1.259 (m, –CH_3*$(CH_2)_9$*CH_2–, 36H), 1.589 (m, $CH_3(CH_2)_9$*CH_2*CH_2–, 4H), 3.219 (m, $CH_3(CH_2)_9CH_2$*CH_2*–, 4H), 3.459 (m, –NH*CH_2CH_2*NH–, 4H), 3.612 (s, –CH_2N^+*$(CH_3)_2$*CH_2–, 12H), 4.627 (s, –*CH_2*$N^+(CH_3)_2$*CH_2*–, 4H), 8.229 (br s, $CH_3(CH_2)_{11}$*NH*CO–, 2H), 8.824 (br s, –CO*NH*CH_2–, 2H); ^{13}C-NMR (100 MHz, $CDCl_3$): δ 14.198, 22.801, 27.098, 29.280, 29.320, 29.431, 29.615, 29.718, 32.401, 38.816, 40.415, 52.909, 64.221, 66.285, 162.749, 163.258; HRMS (ESI): m/z calculated for $C_{38}H_{78}N_6O_4Br_2$ $[M–Br]^+$ and $[M–2Br]^{2+}$: 761.5450, 763.5450 and 341.3133 Found: 761.5241, 763.5229 and 341.3037.

6b: FT-IR ($\overline{\nu}$): 3214 cm^{-1} (amide N–H str.), 2929 cm^{-1} (–CH_2– assym. str.), 2862 cm^{-1} (–CH_2– sym. str.), 1681 cm^{-1} (amide I, C=O str.), 1562 cm^{-1} (amide II, N–H ben.), 1468 cm^{-1} (–CH_2– scissor); ^{1}H-NMR (400 MHz, $CDCl_3$): δ 0.877 (t, terminal –*CH_3*, 6H), 1.264 (m, –CH_3*$(CH_2)_9$*CH_2–, 36H), 1.521 (m, $CH_3(CH_2)_9$*CH_2*CH_2–, 4H), 1.839 (m, –$NHCH_2$*CH_2*CH_2NH–, 2H), 3.250 (m, $CH_3(CH_2)_9CH_2$*CH_2*–, 4H), 3.379 (m, –NH*CH_2*CH_2*CH_2*NH–, 4H), 3.579 (s, –CH_2N^+*$(CH_3)_2$*CH_2–, 12H), 4.689 (s, –*CH_2*$N^+(CH_3)_2$*CH_2*–, 4H), 8.210 (br s, $CH_3(CH_2)_{11}$*NH*CO–, 2H), 8.612 (br s, –CO*NH*CH_2–, 2H); ^{13}C-NMR (100 MHz, $CDCl_3$): δ 14.218, 22.789, 27.112, 29.310, 29.318, 29.428, 29.595, 29.710, 32.412, 38.821, 40.421, 52.913, 64.230, 66.290, 162.752, 163.308; HRMS (ESI): m/z calculated for $C_{39}H_{80}N_6O_4Br_2$ $[M–Br]^+$ and $[M–2Br]^{2+}$: 775.1874, 777.1874 and 348.1345. Found: 775.1396, 777.1381 and 348.1123.

6c: FT-IR ($\overline{\nu}$): 3210 cm^{-1} (amide N–H str.), 2912 cm^{-1} (–CH_2– assym. str.), 2855 cm^{-1} (–CH_2– sym. str.), 1675 cm^{-1} (amide I, C=O str.), 1563 cm^{-1} (amide II, N–H ben.), 1470 cm^{-1} (–CH_2– scissor); ^{1}H-NMR (400 MHz, $CDCl_3$): δ 0.878 (t, terminal –*CH_3*, 6H), 1.257 (m, –CH_3*$(CH_2)_9$*CH_2–, 36H), 1.539 (m, $CH_3(CH_2)_9$*CH_2*CH_2–, 4H), 1.578 (m, –$NHCH_2$*$(CH_2)_2$*CH_2NH–, 4H), 3.218 (m, $CH_3(CH_2)_9CH_2$*CH_2*–, 4H), 3.320 (m, –NH*CH_2*$(CH_2)_2$*CH_2*NH–, 4H), 3.560 (s, –CH_2N^+*$(CH_3)_2$*CH_2–, 12H), 4.612 (s, –*CH_2*$N^+(CH_3)_2$*CH_2*–, 4H), 8.218 (br s, $CH_3(CH_2)_{11}$*NH*CO–, 2H), 8.451 (br s, –CO*NH*CH_2–, 2H); ^{13}C-NMR (100 MHz, $CDCl_3$): δ 14.220, 22.791, 27.110, 29.312, 29.321, 29.425, 29.598, 29.707, 32.417, 38.821, 40.418, 52.924, 64.232, 66.288, 162.756, 163.310; HRMS (ESI): m/z calculated for $C_{40}H_{82}N_6O_4Br_2$ $[M–Br]^+$ and $[M–2Br]^{2+}$: 789.763, 791.5763 and 355.329. Found: 789.5557, 791.5545 and 355.3197.

6d: FT-IR ($\overline{\nu}$): 3210 cm^{-1} (amide N–H str.), 2918 cm^{-1} (–CH_2– assym. str.), 2858 cm^{-1} (–CH_2– sym. str.), 1676 cm^{-1} (amide I, C=O str.), 1560 cm^{-1} (amide II, N–H ben.), 1465 cm^{-1} (–CH_2– scissor); ^{1}H-NMR (400 MHz, $CDCl_3$): δ 0.879 (t, terminal –*CH_3*, 6H), 1.258 (m, –CH_3*$(CH_2)_9$*CH_2–, 36H), 1.421 (m, –$NHCH_2CH_2$*$(CH_2)_2$*CH_2CH_2NH–, 4H), 1.552-1.574 (m, –$CH_3(CH_2)_9$*CH_2*CH_2– and –$NHCH_2$*CH_2*$(CH_2)_2$*CH_2*CH_2NH–, 8H), 3.240-3.318 (m, $CH_3(CH_2)_9CH_2$*CH_2*– and –NH*CH_2*$(CH_2)_4$*CH_2*NH–, 8H), 3.588 (s, –CH_2N^+*$(CH_3)_2$*CH_2–, 12H), 4.642 (s, –*CH_2*$N^+(CH_3)_2$*CH_2*–, 4H), 8.227 (br s, $CH_3(CH_2)_{11}$*NH*CO–, 2H), 8.438 (br s, –CO*NH*CH_2–, 2H); ^{13}C-NMR (100 MHz, $CDCl_3$): δ 14.218, 22.786, 27.108, 29.318, 29.341, 29.435, 29.599, 29.714, 32.423, 38.828, 40.419, 52.928, 64.241, 66.294, 162.757, 163.312; HRMS (ESI): m/z calculated for $C_{42}H_{86}N_6O_4Br_2$ $[M–Br]^+$ and $[M–2Br]^{2+}$: 817.6076, 819.6076 and 369.3446. Found: 817.5849, 819.5837 and 369.3339.

7a: FT-IR ($\overline{\nu}$): 3208 cm^{-1} (amide N–H str.), 2925 cm^{-1} (–CH_2– assym. str.), 2862 cm^{-1} (–CH_2– sym. str.), 1680 cm^{-1} (amide I, C=O str.), 1560 cm^{-1} (amide II, N–H ben.), 1467 cm^{-1} (–CH_2– scissor); ^{1}H-NMR (400 MHz, $CDCl_3$): δ 0.880 (t, terminal –*CH_3*, 6H), 1.249 (m, –

CH_3*$(CH_2)_{13}$*CH_2–, 52H), 1.580 (m, $CH_3(CH_2)_{13}$*CH_2*CH_2–, 4H), 3.217 (m, $CH_3(CH_2)_{13}CH_2$*CH_2–, 4H), 3.458 (m, –NH*CH_2CH_2*NH–, 4H), 3.618 (s, –CH_2N^+*$(CH_3)_2$*CH_2–, 12H), 4.628 (s, –*CH_2*$N^+(CH_3)_2$*CH_2*–, 4H), 8.224 (br s, $CH_3(CH_2)_{15}$*NH*CO–, 2H), 8.828 (br s, –CO*NH*CH_2–, 2H); ^{13}C-NMR (100 MHz, $CDCl_3$): δ 14.212, 22.745, 27.112, 29.321, 29.347, 29.429, 29.578, 29.726, 32.420, 38.824, 40.422, 52.931, 64.244, 66.289, 162.754, 163.307; HRMS (ESI): m/z calculated for $C_{46}H_{94}N_6O_4Br_2$ $[M–Br]^+$ and $[M–2Br]^{2+}$: 873.6703, 875.6703 and 397.6760 Found: 873.6499, 875.6489 and 397.3687.

7b: FT-IR ($\overline{\nu}$): 3215 cm^{-1} (amide N–H str.), 2930 cm^{-1} (–CH_2– assym. str.), 2860 cm^{-1} (–CH_2– sym. str.), 1682 cm^{-1} (amide I, C=O str.), 1565 cm^{-1} (amide II, N–H ben.), 1465 cm^{-1} (–CH_2– scissor); ^{1}H-NMR (400 MHz, $CDCl_3$): δ 0.881 (t, terminal –*CH_3*, 6H), 1.260 (m, –CH_3*$(CH_2)_{13}$*CH_2–, 52H), 1.531 (m, $CH_3(CH_2)_{13}$*CH_2*CH_2–, 4H), 1.842 (m, –$NHCH_2$*CH_2*CH_2NH–, 2H), 3.252 (m, $CH_3(CH_2)_{13}CH_2$*CH_2*–, 4H), 3.368 (m, –NH*CH_2CH_2*CH_2*NH*–, 4H), 3.584 (s, –CH_2N^+*$(CH_3)_2$*CH_2–, 12H), 4.682 (s, –*CH_2*$N^+(CH_3)_2$*CH_2*–, 4H), 8.206 (br s, $CH_3(CH_2)_{15}$*NH*CO–, 2H), 8.624 (br s, –CO*NH*CH_2–, 2H); ^{13}C-NMR (100 MHz, $CDCl_3$): δ 14.220, 22.789, 23.878, 27.142, 29.321, 29.334, 29.438, 29.584, 29.714, 32.425, 38.829, 40.427, 52.920, 64.238, 66.297, 162.757, 163.314; HRMS (ESI): m/z calculated for $C_{47}H_{96}N_6O_4Br_2$ $[M–Br]^+$ and $[M–2Br]^{2+}$: 887.6859, 889.6859 and 404.3838. Found: 887.6662, 889.6652 and 404.3786.

7c: FT-IR ($\overline{\nu}$): 3205 cm^{-1} (amide N–H str.), 2910 cm^{-1} (–CH_2– assym. str.), 2850 cm^{-1} (–CH_2– sym. str.), 1674 cm^{-1} (amide I, C=O str.), 1560 cm^{-1} (amide II, N–H ben.), 1464 cm^{-1} (–CH_2– scissor); ^{1}H-NMR (400 MHz, $CDCl_3$): δ 0.869 (t, terminal –*CH_3*, 6H), 1.251 (m, –CH_3*$(CH_2)_{13}$*CH_2–, 52H), 1.537 (m, $CH_3(CH_2)_{13}$*CH_2*CH_2–, 4H), 1.581 (m, –$NHCH_2$*$(CH_2)_2$*CH_2NH–, 4H), 3.220 (m, $CH_3(CH_2)_{13}CH_2$*CH_2*–, 4H), 3.324 (m, –NH*CH_2*$(CH_2)_2$*CH_2*NH–, 4H), 3.556 (s, –CH_2N^+*$(CH_3)_2$*CH_2–, 12H), 4.607 (s, –*CH_2*$N^+(CH_3)_2$*CH_2*–, 4H), 8.211 (br s, $CH_3(CH_2)_{15}$*NH*CO–, 2H), 8.454 (br s, –CO*NH*CH_2–, 2H); ^{13}C-NMR (100 MHz, $CDCl_3$): δ 14.217, 22.788, 23.867, 27.151, 29.318, 29.328, 29.441, 29.542, 29.708, 32.418, 38.820, 40.420, 52.918, 64.228, 66.290, 162.753, 163.322; HRMS (ESI): m/z calculated for $C_{48}H_{98}N_6O_4Br_2$ $[M–Br]^+$ and $[M–2Br]^{2+}$: 901.7016, 903.7016 and 411.3916. Found: 901.6819, 903.6814 and 411.3865.

7d: FT-IR ($\overline{\nu}$): 3208 cm^{-1} (amide N–H str.), 2920 cm^{-1} (–CH_2– assym. str.), 2860 cm^{-1} (–CH_2– sym. str.), 1675 cm^{-1} (amide I, C=O str.), 1563 cm^{-1} (amide II, N–H ben.), 1467 cm^{-1} (–CH_2– scissor); ^{1}H-NMR (400 MHz, $CDCl_3$): δ 0.889 (t, terminal –*CH_3*, 6H), 1.254 (m, –CH_3*$(CH_2)_{13}$*CH_2–, 52H), 1.429 (m, –$NHCH_2CH_2$*$(CH_2)_2$*CH_2CH_2NH–, 4H), 1.550-1.575 (m, –$CH_3(CH_2)_{13}$*CH_2CH_2– and –$NHCH_2$*CH_2*$(CH_2)_2$*CH_2CH_2NH–, 8H), 3.241-3.320 (m, $CH_3(CH_2)_{13}CH_2$*CH_2*– and –NH*CH_2*$(CH_2)_4$*CH_2*NH–, 8H), 3.591 (s, –CH_2N^+*$(CH_3)_2$*CH_2–, 12H), 4.640 (s, –*CH_2*$N^+(CH_3)_2$*CH_2*–, 4H), 8.225 (br s, $CH_3(CH_2)_{15}$*NH*CO–, 2H), 8.451 (br s, –CO*NH*CH_2–, 2H); ^{13}C-NMR (100 MHz, $CDCl_3$): δ 14.220, 22.784, 23.860, 27.150, 29.314, 29.324, 29.440, 29.540, 29.712, 32.422, 38.814, 40.425, 52.925, 64.230, 66.294, 162.758, 163.323; HRMS (ESI): m/z calculated for $C_{50}H_{102}N_6O_4Br_2$ $[M–Br]^+$ and $[M–2Br]^{2+}$: 929.7329, 931.7329 and 425.4073. Found: 929.7130, 931.7121 and 425.4075.

4A.4.2.5 General procedure for the synthesis of 8a-8d, 9a-9d, 10a-10d and 11a-11d

N,*N*-Dimethylalkylamines (15 mM) were added to the organic solutions of intermediates **3a-3d** (5 mM; EtOH for **3a**, $CHCl_3$ for **3b** and MeCN for **3c** and **3d**, 50 mL) separately in screw top pressure tubes and the reaction mixtures were stirred at 85 °C for about 24 h. After the

reaction, the mixtures were allowed to cool down to room temperature and transferred to round bottom flask. Then, the organic solvents were removed and volume of the reaction mixtures was reduced to $1/10^{th}$ to its original volume. Finally, the products were precipitated in excess of dry diethyl ether/acetone (150 mL). The precipitates were filtered and washed repeatedly with diethyl ether/acetone. The white precipitates were vacuum dried to give more than 99% yield of **8a-8d, 9a-9d, 10a-10d** and **11a-11d**. All the final products were characterized by FT-IR, ^{1}H-NMR, ^{13}C-NMR and HRMS.

8a: FT-IR ($\overline{\nu}$): 3215 cm^{-1} (amide N–H str.), 2922 cm^{-1} (–CH_2– assym. str.), 2861 cm^{-1} (–CH_2– sym. str.), 1685 cm^{-1} (amide I, C=O str.), 1560 cm^{-1} (amide II, N–H ben.), 1468 cm^{-1} (–CH_2– scissor); ^{1}H-NMR (400 MHz, $CDCl_3$): δ 0.868 (t, terminal –*CH_3*, 6H), 1.288 (m, –CH_3*$(CH_2)_5$*CH_2–, 20H), 1.789 (m, $CH_3(CH_2)_5$*CH_2*CH_2–, 4H), 3.392-3.515 (m, –CH_2N^+*$(CH_3)_2$*CH_2– and $CH_3(CH_2)_5CH_2$*CH_2*–, 16H), 3.619 (m, –NH*CH_2CH_2*NH–, 4H), 4.663 (s, –$N^+(CH_3)_2$*CH_2*CO–, 4H), 8.882 (br s, –CO*NH*CH_2–, 2H); ^{13}C-NMR (100 MHz, $CDCl_3$): δ 14.217, 22.782, 26.350, 29.424, 29.591, 29.678, 31.978, 38.514, 52.265, 63.624, 66.502, 163.623; HRMS (ESI): m/z calculated for $C_{26}H_{56}N_4O_2Br_2$ $[M–Br]^+$ and $[M–2Br]^{2+}$: 535.3575, 537.3554 and 228.2196 Found: 535.3619, 537.3605 and 228.2268.

8b: FT-IR ($\overline{\nu}$): 3222 cm^{-1} (amide N–H str.), 2930 cm^{-1} (–CH_2– assym. str.), 2865 cm^{-1} (–CH_2– sym. str.), 1685 cm^{-1} (amide I, C=O str.), 1565 cm^{-1} (amide II, N–H ben.), 1471 cm^{-1} (–CH_2– scissor); ^{1}H-NMR (400 MHz, $CDCl_3$): δ 0.887 (t, terminal –*CH_3*, 6H), 1.298 (m, –CH_3*$(CH_2)_5$*CH_2–, 20H), 1.789 (m, $CH_3(CH_2)_5$*CH_2*CH_2–, 4H), 1.882 (m, –$NHCH_2$*CH_2*CH_2NH–, 2H), 3.269-3.466 (m, –CH_2N^+*$(CH_3)_2$*CH_2– and $CH_3(CH_2)_5CH_2$*CH_2*–, 16H), 3.678 (m, –NH*CH_2*CH_2*CH_2*NH–, 4H), 4.687 (s, –$N^+(CH_3)_2$*CH_2*CO–, 4H), 8.860 (br s, –CO*NH*CH_2–, 2H); ^{13}C-NMR (100 MHz, $CDCl_3$): δ 14.201, 22.675, 22.981, 26.267, 27.779, 29.201, 29.439, 29.475, 31.920, 52.106, 63.543, 65.913, 163.207; HRMS (ESI): m/z calculated for $C_{27}H_{58}N_4O_2Br_2$ $[M–Br]^+$ and $[M–2Br]^{2+}$: 549.3137, 551.3116 and 235.2274. Found: 549.3729, 551.3712 and 235.2274.

8c: FT-IR ($\overline{\nu}$): 3215 cm^{-1} (amide N–H str.), 2915 cm^{-1} (–CH_2– assym. str.), 2859 cm^{-1} (–CH_2– sym. str.), 1675 cm^{-1} (amide I, C=O str.), 1560 cm^{-1} (amide II, N–H ben.), 1476 cm^{-1} (–CH_2– scissor); ^{1}H-NMR (400 MHz, $CDCl_3$): δ 0.889 (t, terminal –*CH_3*, 6H), 1.290 (m, –CH_3*$(CH_2)_5$*CH_2–, 20H), 1.639 (m, $CH_3(CH_2)_5$*CH_2*CH_2–, 4H), 1.781 (m, –$NHCH_2$*$(CH_2)_2$*CH_2NH–, 4H), 3.302 (m, –NH*CH_2*$(CH_2)_2$*CH_2*NH–, 4H), 3.423 (s, –CH_2N^+*$(CH_3)_2$*CH_2–, 12H), 3.624 (m, $CH_3(CH_2)_5CH_2$*CH_2*–, 4H), 4.641 (s, –$N^+(CH_3)_2$*CH_2*CO–, 4H), 8.6798 (br s, –CO*NH*CH_2–, 2H); ^{13}C-NMR (100 MHz, $CDCl_3$): δ 14.241, 22.829, 26.270, 26.344, 29.245, 29.448, 29.569, 32.123, 38.890, 52.201, 63.609, 66.403, 163.179; HRMS (ESI): m/z calculated for $C_{28}H_{60}N_4O_2Br_2$ $[M–Br]^+$ and $[M–2Br]^{2+}$: 563.3961, 565.3886 and 242.2353. Found: 563.3961, 565.3946 and 242.2427.

8d: FT-IR ($\overline{\nu}$): 3216 cm^{-1} (amide N–H str.), 2921 cm^{-1} (–CH_2– assym. str.), 2862 cm^{-1} (–CH_2– sym. str.), 1675 cm^{-1} (amide I, C=O str.), 1561 cm^{-1} (amide II, N–H ben.), 1465 cm^{-1} (–CH_2– scissor); ^{1}H-NMR (400 MHz, $CDCl_3$): δ 0.849 (t, terminal –*CH_3*, 6H), 1.278 (m, –CH_3*$(CH_2)_5$*CH_2–, 20H), 1.418 (m, –$NHCH_2CH_2$*$(CH_2)_2$*CH_2CH_2NH–, 4H), 1.544 (m, $CH_3(CH_2)_5$*CH_2*CH_2–, 4H), 1.769 (m, –$NHCH_2$*CH_2*$(CH_2)_2$*CH_2*CH_2NH–, 4H), 3.267 (m, –NH*CH_2*$(CH_2)_4$*CH_2*NH–, 4H), 3.487 (s, –CH_2N^+*$(CH_3)_2$*CH_2–, 12H), 3.667 (m,

$CH_3(CH_2)_5CH_2\mathit{CH_2}$–, 4H), 4.667 (m, –$N^+(CH_3)_2\mathit{CH_2}$CO–, 4H), 8.691 (br s, –CO*NH*CH_2–, 2H); ^{13}C-NMR (100 MHz, $CDCl_3$): δ 14.211, 22.817, 23.226, 26.423, 28.201, 29.317, 29.518, 29.614, 29.696, 32.160, 39.479, 52.209, 63.392, 66.116, 163.219; HRMS (ESI): m/z calculated for $C_{30}H_{64}N_4O_2Br_2$ $[M–Br]^+$ and $[M–2Br]^{2+}$: 591.4203, 593.4182 and 256.2510. Found: 591.4242, 593.4228 and 256.2595.

9a: FT-IR ($\overline{\nu}$): 3215 cm^{-1} (amide N–H str.), 2925 cm^{-1} (–CH_2– assym. str.), 2858 cm^{-1} (–CH_2– sym. str.), 1685 cm^{-1} (amide I, C=O str.), 1560 cm^{-1} (amide II, N–H ben.), 1468 cm^{-1} (–CH_2– scissor); ^{1}H-NMR (400 MHz, $CDCl_3$): δ 0.856 (t, terminal –*CH_3*, 6H), 1.288 (m, –$CH_3\mathit{(CH_2)_7}CH_2$–, 28H), 1.765 (m, $CH_3(CH_2)_7\mathit{CH_2}CH_2$–, 4H), 3.402-3.465 (m, –$CH_2N^+\mathit{(CH_3)_2}CH_2$– and $CH_3(CH_2)_7CH_2\mathit{CH_2}$–, 16H), 3.620 (m, –NH$\mathit{CH_2CH_2}$NH–, 4H), 4.654 (s, –$N^+(CH_3)_2\mathit{CH_2}$CO–, 4H), 8.889 (br s, –CO*NH*CH_2–, 2H); ^{13}C-NMR (100 MHz, $CDCl_3$): δ 14.220, 22.778, 23.105, 26.297, 29.329, 29.514, 29.554, 29.787, 31.987, 38.511, 52.248, 63.614, 66.410, 163.613; HRMS (ESI): m/z calculated for $C_{30}H_{64}N_4O_2Br_2$ $[M–Br]^+$ and $[M–2Br]^{2+}$: 591.4203, 593.4182 and 256.2510. Found: 591.4244, 593.4218 and 256.2504.

9b: FT-IR ($\overline{\nu}$): 3215 cm^{-1} (amide N–H str.), 2930 cm^{-1} (–CH_2– assym. str.), 2865 cm^{-1} (–CH_2– sym. str.), 1680 cm^{-1} (amide I, C=O str.), 1565 cm^{-1} (amide II, N–H ben.), 1470 cm^{-1} (–CH_2– scissor); ^{1}H-NMR (400 MHz, $CDCl_3$): δ 0.887 (t, terminal –*CH_3*, 6H), 1.285 (m, –$CH_3\mathit{(CH_2)_7}CH_2$–, 28H), 1.787 (m, $CH_3(CH_2)_7\mathit{CH_2}CH_2$–, 4H), 1.877 (m, –$NHCH_2\mathit{CH_2}CH_2NH$–, 2H), 3.264-3.455 (m, –$CH_2N^+\mathit{(CH_3)_2}CH_2$– and $CH_3(CH_2)_7CH_2\mathit{CH_2}$–, 16H), 3.648 (m, –NH$\mathit{CH_2}CH_2\mathit{CH_2}$NH–, 4H), 4.678 (s, –$N^+(CH_3)_2\mathit{CH_2}$CO–, 4H), 8.859 (br s, –CO*NH*CH_2–, 2H); ^{13}C-NMR (100 MHz, $CDCl_3$): δ 14.147, 22.710, 22.957, 26.277, 27.790, 29.165, 29.434, 29.472, 31.915, 52.104, 63.347, 65.884, 163.128; HRMS (ESI): m/z calculated for $C_{31}H_{66}N_4O_2Br_2$ $[M–Br]^+$ and $[M–2Br]^{2+}$: 605.4359, 607.4338 and 263.2588. Found: 605.4347, 607.4333 and 263.2598.

9c: FT-IR ($\overline{\nu}$): 3215 cm^{-1} (amide N–H str.), 2925 cm^{-1} (–CH_2– assym. str.), 2862 cm^{-1} (–CH_2– sym. str.), 1675 cm^{-1} (amide I, C=O str.), 1563 cm^{-1} (amide II, N–H ben.), 1478 cm^{-1} (–CH_2– scissor); ^{1}H-NMR (400 MHz, $CDCl_3$): δ 0.874 (t, terminal –*CH_3*, 6H), 1.284 (m, –$CH_3\mathit{(CH_2)_7}CH_2$–, 28H), 1.644 (m, $CH_3(CH_2)_7\mathit{CH_2}CH_2$–, 4H), 1.788 (m, –$NHCH_2\mathit{(CH_2)_2}CH_2NH$–, 4H), 3.311 (m, –NH$\mathit{CH_2}(CH_2)_2\mathit{CH_2}$NH–, 4H), 3.420 (s, –$CH_2N^+\mathit{(CH_3)_2}CH_2$–, 12H), 3.630 (m, $CH_3(CH_2)_7CH_2\mathit{CH_2}$–, 4H), 4.639 (s, –$N^+(CH_3)_2\mathit{CH_2}$CO–, 4H), 8.670 (br s, –CO*NH*CH_2–, 2H); ^{13}C-NMR (100 MHz, $CDCl_3$): δ 14.230, 22.804, 23.145, 26.270, 26.344, 29.239, 29.512, 29.550, 29.711, 32.113, 38.965, 52.194, 63.549, 66.370, 163.179; HRMS (ESI): m/z calculated for $C_{32}H_{68}N_4O_2Br_2$ $[M–Br]^+$ and $[M–2Br]^{2+}$: 619.4516, 621.4495 and 270.2666. Found: 619.4498, 621.4482 and 270.2674.

9d: FT-IR ($\overline{\nu}$): 3212 cm^{-1} (amide N–H str.), 2922 cm^{-1} (–CH_2– assym. str.), 2860 cm^{-1} (–CH_2– sym. str.), 1675 cm^{-1} (amide I, C=O str.), 1565 cm^{-1} (amide II, N–H ben.), 1468 cm^{-1} (–CH_2– scissor); ^{1}H-NMR (400 MHz, $CDCl_3$): δ 0.866 (t, terminal –*CH_3*, 6H), 1.291 (m, –$CH_3\mathit{(CH_2)_7}CH_2$–, 28H), 1.410 (m, –$NHCH_2CH_2\mathit{(CH_2)_2}CH_2CH_2NH$–, 4H), 1.574 (m, $CH_3(CH_2)_7\mathit{CH_2}CH_2$–, 4H), 1.809 (m, –$NHCH_2\mathit{CH_2}(CH_2)_2\mathit{CH_2}CH_2NH$–, 4H), 3.287 (m, –NH$\mathit{CH_2}(CH_2)_4\mathit{CH_2}$NH–, 4H), 3.432 (s, –$CH_2N^+\mathit{(CH_3)_2}CH_2$–, 12H), 3.649 (m, $CH_3(CH_2)_7CH_2\mathit{CH_2}$–, 4H), 4.691 (m, –$N^+(CH_3)_2\mathit{CH_2}$CO–, 4H), 8.670 (br s, –CO*NH*CH_2–, 2H); ^{13}C-NMR (100 MHz, $CDCl_3$): δ 14.206, 22.783, 23.126, 26.343, 26.720, 28.192, 29.225, 29.440, 29.554, 29.706, 32.120, 39.532, 52.219, 63.402, 66.116, 163.209; HRMS (ESI): m/z calculated for $C_{34}H_{72}N_4O_2Br_2$ $[M–Br]^+$ and $[M–2Br]^{2+}$: 647.4516, 649.4495 and 284.3192. Found: 647.4813, 649.4800 and 284.2868.

10a: FT-IR ($\overline{\nu}$): 3215 cm^{-1} (amide N–H str.), 2922 cm^{-1} (–CH_2– assym. str.), 2861 cm^{-1} (–CH_2– sym. str.), 1685 cm^{-1} (amide I, C=O str.), 1560 cm^{-1} (amide II, N–H ben.), 1470 cm^{-1} (–CH_2– scissor); ^{1}H-NMR (400 MHz, $CDCl_3$): δ 0.859 (t, terminal –*CH_3*, 6H), 1.279 (m, –CH_3*$(CH_2)_9$*CH_2–, 36H), 1.764 (m, $CH_3(CH_2)_9$*CH_2*CH_2–, 4H), 3.412-3.445 (m, –CH_2N^+*$(CH_3)_2$*CH_2– and $CH_3(CH_2)_9CH_2$*CH_2*–, 16H), 3.619 (m, –NH*CH_2CH_2*NH–, 4H), 4.653 (s, –$N^+(CH_3)_2$*CH_2*CO–, 4H), 8.878 (br s, –CO*NH*CH_2–, 2H); ^{13}C-NMR (100 MHz, $CDCl_3$): δ 14.214, 22.780, 23.005, 26.347, 29.229, 29.419, 29.503, 29.544, 29.687, 31.999, 38.509, 52.255, 63.603, 66.401, 163.603; HRMS (ESI): m/z calculated for $C_{34}H_{72}N_4O_2Br_2$ $[M–Br]^+$ and $[M–2Br]^{2+}$: 647.4516, 649.4495 and 284.3192. Found: 647.4601, 649.4594 and 284.2854.

10b: FT-IR ($\overline{\nu}$): 3215 cm^{-1} (amide N–H str.), 2930 cm^{-1} (–CH_2– assym. str.), 2865 cm^{-1} (–CH_2– sym. str.), 1685 cm^{-1} (amide I, C=O str.), 1565 cm^{-1} (amide II, N–H ben.), 1470 cm^{-1} (–CH_2– scissor); ^{1}H-NMR (400 MHz, $CDCl_3$): δ 0.881 (t, terminal –*CH_3*, 6H), 1.305 (m, –CH_3*$(CH_2)_9$*CH_2–, 36H), 1.790 (m, $CH_3(CH_2)_9$*CH_2*CH_2–, 4H), 1.880 (m, –$NHCH_2$*CH_2*CH_2NH–, 2H), 3.270-3.453 (m, –CH_2N^+*$(CH_3)_2$*CH_2– and $CH_3(CH_2)_9CH_2$*CH_2*–, 16H), 3.649 (m, –NH*CH_2*CH_2*CH_2*NH–, 4H), 4.677 (s, –$N^+(CH_3)_2$*CH_2*CO–, 4H), 8.857 (br s, –CO*NH*CH_2–, 2H); ^{13}C-NMR (100 MHz, $CDCl_3$): δ 14.131, 22.690, 22.950, 26.270, 27.793, 29.161, 29.334, 29.432, 29.471, 31.911, 52.006, 63.343, 65.893, 163.127; HRMS (ESI): m/z calculated for $C_{34}H_{70}N_4O_2Br_2$ $[M–Br]^+$ and $[M–2Br]^{2+}$: 661.4986, 663.4964 and 291.2901. Found: 661.4959, 661.4945 and 291.2890.

10c: FTIR ($\overline{\nu}$): 3212 cm^{-1} (amide N–H str.), 2915 cm^{-1} (–CH_2– assym. str.), 2858 cm^{-1} (–CH_2– sym. str.), 1675 cm^{-1} (amide I, C=O str.), 1560 cm^{-1} (amide II, N–H ben.), 1475 cm^{-1} (–CH_2– scissor); ^{1}H-NMR (400 MHz, $CDCl_3$): δ 0.869 (t, terminal –*CH_3*, 6H), 1.288 (m, –CH_3*$(CH_2)_9$*CH_2–, 36H), 1.646 (m, $CH_3(CH_2)_9$*CH_2*CH_2–, 4H), 1.776 (m, –$NHCH_2$*$(CH_2)_2$*CH_2NH–, 4H), 3.302 (m, –NH*CH_2*$(CH_2)_2$*CH_2*NH–, 4H), 3.419 (s, –CH_2N^+*$(CH_3)_2$*CH_2–, 12H), 3.624 (m, $CH_3(CH_2)_9CH_2$*CH_2*–, 4H), 4.641 (s, –$N^+(CH_3)_2$*CH_2*CO–, 4H), 8.699 (br s, –CO*NH*CH_2–, 2H); ^{13}C-NMR (100 MHz, $CDCl_3$): δ 14.237, 22.804, 23.045, 26.270, 26.341, 29.235, 29.440, 29.503, 29.555, 29.705, 32.023, 38.980, 52.197, 63.449, 66.363, 163.171; HRMS (ESI): m/z calculated for $C_{36}H_{76}N_4O_2Br_2$ $[M–Br]^+$ and $[M–2Br]^{2+}$: 675.5142, 677.5121 and 298.2979. Found: 675.5119, 677.5104 and 298.2942.

10d: FT-IR ($\overline{\nu}$): 3212 cm^{-1} (amide N–H str.), 2920 cm^{-1} (–CH_2– assym. str.), 2860 cm^{-1} (–CH_2– sym. str.), 1675 cm^{-1} (amide I, C=O str.), 1560 cm^{-1} (amide II, N–H ben.), 1465 cm^{-1} (–CH_2– scissor); ^{1}H-NMR (400 MHz, $CDCl_3$): δ 0.869 (t, terminal –*CH_3*, 6H), 1.288 (m, –CH_3*$(CH_2)_9$*CH_2–, 36H), 1.414 (m, –$NHCH_2CH_2$*$(CH_2)_2$*CH_2CH_2NH–, 4H), 1.586 (m, $CH_3(CH_2)_9$*CH_2*CH_2–, 4H), 1.779 (m, –$NHCH_2$*CH_2*$(CH_2)_2$*CH_2*CH_2NH–, 4H), 3.284 (m, –NH*CH_2*$(CH_2)_4$*CH_2*NH–, 4H), 3.429 (s, –CH_2N^+*$(CH_3)_2$*CH_2–, 12H), 3.653 (m, $CH_3(CH_2)_9CH_2$*CH_2*–, 4H) 4.701 (m, –$N^+(CH_3)_2$*CH_2*CO–, 4H), 8.688 (br s, –CO*NH*CH_2–, 2H); ^{13}C-NMR (100 MHz, $CDCl_3$): δ 14.236, 22.803, 23.046, 26.343, 26.720, 28.191, 29.227, 29.439, 29.498, 29.554, 29.706, 32.020, 39.529, 52.119, 63.412, 66.106, 163.119; HRMS (ESI): m/z calculated for $C_{38}H_{80}N_4O_2Br_2$ $[M–Br]^+$ and $[M–2Br]^{2+}$: 703.5456, 705.5434 and 312.3136. Found: 703.5440, 705.5427 and 312.3124.

11a: FT-IR ($\overline{\nu}$): 3219 cm^{-1} (amide N–H str.), 2928 cm^{-1} (–CH_2– assym. str.), 2861 cm^{-1} (–CH_2– sym. str.), 1680 cm^{-1} (amide I, C=O str.), 1555 cm^{-1} (amide II, N–H ben.), 1470 cm^{-1} (–CH_2– scissor); ^{1}H-NMR (400 MHz, $CDCl_3$): δ 0.872 (t, terminal –*CH_3*, 6H), 1.311 (m, –CH_3*$(CH_2)_{13}$*CH_2–, 52H), 1.780 (m, $CH_3(CH_2)_{13}$*CH_2*CH_2–, 4H), 3.410-3.456 (m, –CH_2N^+*$(CH_3)_2$*CH_2– and $CH_3(CH_2)_{13}CH_2$*CH_2*–, 16H), 3.611 (m, –NH*CH_2*CH_2*NH–, 4H),

4.671 (s, –$N^+(CH_3)_2CH_2CO$–, 4H), 8.943 (br s, –CO*NH*CH_2–, 2H); ^{13}C-NMR (100 MHz, $CDCl_3$): δ 14.256, 22.830, 23.026, 26.371, 29.248, 29.503, 29.530, 29.583, 29.727, 29.801, 29.839, 32.066, 38.452, 52.311, 63.523, 66.112, 163.453; HRMS (ESI): m/z calculated for $C_{42}H_{88}N_4O_2Br_2$ $[M–Br]^+$ and $[M–2Br]^{2+}$: 759.6082, 761.6061 and 340.3449 Found: 759.6044, 761.6035 and 340.3584.

11b: FT-IR ($\bar{\nu}$): 3215 cm^{-1} (amide N–H str.), 2929 cm^{-1} (–CH_2– assym. str.), 2865 cm^{-1} (–CH_2– sym. str.), 1683 cm^{-1} (amide I, C=O str.), 1565 cm^{-1} (amide II, N–H ben.), 1475 cm^{-1} (–CH_2– scissor); ^{1}H-NMR (400 MHz, $CDCl_3$): δ 0.871 (t, terminal –*CH_3*, 6H), 1.325 (m, –CH_3*$(CH_2)_{13}$*CH_2–, 52H), 1.785 (m, $CH_3(CH_2)_{13}$*CH_2*CH_2–, 4H), 1.883 (m, –$NHCH_2$*CH_2*CH_2NH–, 2H), 3.383-3.425 (m, –CH_2N^+*$(CH_3)_2$*CH_2– and $CH_3(CH_2)_{13}CH_2$*CH_2*–, 16H), 3.604 (m, –NH*CH_2*CH_2*CH_2*NH–, 4H), 4.814 (s, –$N^+(CH_3)_2$*CH_2*CO–, 4H), 8.876 (br s, –CO*NH*CH_2–, 2H); ^{13}C-NMR (100 MHz, $CDCl_3$): δ 14.250, 22.824, 22.989, 26.354, 27.646, 29.213, 29.497, 29.564, 29.717, 29.802, 29.828, 32.059, 52.088, 63.518, 66.144, 163.252; HRMS (ESI): m/z calculated for $C_{43}H_{90}N_4O_2Br_2$ $[M–Br]^+$ and $[M–2Br]^{2+}$: 773.6238, 775.6218 and 347.3527. Found: 773.6192, 775.6183 and 347.3605.

11c: FT-IR ($\bar{\nu}$): 3215 cm^{-1} (amide N–H str.), 2925 cm^{-1} (–CH_2– assym. str.), 2861 cm^{-1} (–CH_2– sym. str.), 1675 cm^{-1} (amide I, C=O str.), 1565 cm^{-1} (amide II, N–H ben.), 1475 cm^{-1} (–CH_2– scissor); ^{1}H-NMR (400 MHz, $CDCl_3$): δ 0.868 (t, terminal –*CH_3*, 6H), 1.289 (m, –CH_3*$(CH_2)_{13}$*CH_2–, 52H), 1.645 (m, $CH_3(CH_2)_{13}$*CH_2*CH_2–, 4H), 1.787 (m, –$NHCH_2$*$(CH_2)_2$*CH_2NH–, 4H), 3.299 (m, –NH*CH_2*$(CH_2)_2$*CH_2*NH–, 4H), 3.418 (s, –CH_2N^+*$(CH_3)_2$*CH_2–, 12H), 3.624 (m, $CH_3(CH_2)_9CH_2$*CH_2*–, 4H), 4.648 (s, –$N^+(CH_3)_2$*CH_2*CO–, 4H), 8.711 (br s, –CO*NH*CH_2–, 2H); ^{13}C-NMR (100 MHz, $CDCl_3$): δ 14.243, 22.816, 23.048, 26.278, 26.350, 29.247, 29.487, 29.516, 29.574, 29.720, 29.784, 29.807, 29.826, 32.053, 38.974, 52.1990, 63.453, 66.379, 163.179; HRMS (ESI): m/z calculated for $C_{44}H_{92}N_4O_2Br_2$ $[M–Br]^+$ and $[M–2Br]^{2+}$: 787.6395, 789.6374 and 354.3606. Found: 787.6352, 789.6343 and 354.3759.

11d: FT-IR ($\bar{\nu}$): 3215 cm^{-1} (amide N–H str.), 2921 cm^{-1} (–CH_2– assym. str.), 2865 cm^{-1} (–CH_2– sym. str.), 1674 cm^{-1} (amide I, C=O str.), 1560 cm^{-1} (amide II, N–H ben.), 1465 cm^{-1} (–CH_2– scissor); ^{1}H-NMR (400 MHz, $CDCl_3$): δ 0.876 (t, terminal –*CH_3*, 6H), 1.337 (m, –CH_3*$(CH_2)_{13}$*CH_2–, 52H), 1.421 (m, –$NHCH_2CH_2$*$(CH_2)_2$*CH_2CH_2NH–, 4H), 1.587 (m, $CH_3(CH_2)_{13}$*CH_2*CH_2–, 4H), 1.779 (m, –$NHCH_2$*CH_2*$(CH_2)_2$*CH_2*CH_2NH–, 4H), 3.299 (m, –NH*CH_2*$(CH_2)_4$*CH_2*NH–, 4H), 3.429 (s, –CH_2N^+*$(CH_3)_2$*CH_2–, 12H), 3.644 (m, $CH_3(CH_2)_{13}CH_2$*CH_2*–, 4H), 4.681 (m, –$N^+(CH_3)_2$*CH_2*CO–, 4H), 8.682 (br s, –CO*NH*CH_2–, 2H); ^{13}C-NMR (100 MHz, $CDCl_3$): δ 14.241, 22.815, 23.050, 26.350, 26.737, 28.180, 29.237, 29.486, 29.511, 29.571, 29.717, 29.783, 29.805, 29.824, 32.052, 39.538, 52.122, 63.420, 66.111, 163.136; HRMS (ESI): m/z calculated for $C_{46}H_{96}N_4O_2Br_2$ $[M–Br]^+$ and $[M–2Br]^{2+}$: 815.6708, 817.6687 and 368.3763. Found: 815.6661, 817.6652 and 368.3823.

4A.4.2.6 General Synthesis of 12a-12f

$NHMe_2$ gas was collected into dry $CHCl_3$ (40 mL) in a screw-top pressure tube set at 0 °C until the volume of the resulting solution became 1.5 fold (~60 mL). Dibromoalkane (10 g) was then added through syringe and stirred for 24 h at room temperature. After cooling, the reaction mixture was transferred into a round bottomed flask quantitatively. Excess gas was removed by heating the reaction mixture slowly. Finally, the mixture was diluted with $CHCl_3$

followed by washing with NaOH (2 M, 100 mL × 2) solution. Organic layer was then collected and passed through anhydrous Na_2SO_4. Finally, the organic solution was dried and light yellow gummy liquid was obtained as product with quantitative yield. **12a** and **12b** were obtained from commercial source.

12c (*N,N,N′,N′*-Tetramethyl-1,6-diaminohexane)**:** ^{1}H-NMR (400 MHz, $CDCl_3$): δ 1.288-1.342 (m, $-CH_2CH_2CH_2NMe_2$, 4H), 1.421-1.476 (m, $-CH_2CH_2CH_2NMe_2$, 4H), 2.204-2.255 (br. m, $-CH_2CH_2N(CH_3)_2$ and $-CH_2CH_2CH_2NMe_2$, 16H); ^{13}C NMR (100 MHz, $CDCl_3$): δ 27.636, 27.879, 45.656, 60.030.

12d (*N,N,N′,N′*-Tetramethyl-1,8-diaminoctane)**:** ^{1}H-NMR (400 MHz, $CDCl_3$): δ 1.223-1.314 (br. m, $-(CH_2)_2CH_2CH_2NMe_2$, 8H), 1.398-1.451 (m, $-(CH_2)_2CH_2CH_2NMe_2$, 4H), 2.179-2.228 (br. m, $-CH_2CH_2N(CH_3)_2$ and $-(CH_2)_2CH_2CH_2NMe_2$, 16H); ^{13}C NMR (100 MHz, $CDCl_3$): δ 27.615, 27.877, 29.685, 45.638, 60.092.

12e (*N,N,N′,N′*-Tetramethyl-1,10-diaminodecane)**:** ^{1}H-NMR (400 MHz, $CDCl_3$): δ 1.257 (br. m, $-(CH_2)_3CH_2CH_2NMe_2$, 12H), 1.409-1.444 (m, $-(CH_2)_3CH_2CH_2NMe_2$, 4H), 2.192-2.242 (br. m, $-CH_2CH_2N(CH_3)_2$ and $-(CH_2)_3CH_2CH_2NMe_2$, 16H); ^{13}C NMR (100 MHz, $CDCl_3$): δ 27.671, 27.908, 29.703, 29.753, 45.643, 60.119.

12f (*N,N,N′,N′*-Tetramethyl-1,12-diaminododecane)**:** ^{1}H-NMR (400 MHz, $CDCl_3$): δ 1.246-1.262 (br. m, $-(CH_2)_4CH_2CH_2NMe_2$, 16H), 1.410-1.445 (m, $-(CH_2)_4CH_2CH_2NMe_2$, 4H), 2.190-2.231 (br. m, $-CH_2CH_2N(CH_3)_2$ and $-(CH_2)_4CH_2CH_2NMe_2$ and, 16H); ^{13}C NMR (100 MHz, $CDCl_3$): δ 27.682, 27.922, 29.753, 29.775, 45.652, 60.130.

4A.4.2.7 General synthesis of 13a-13f, 14a-14f, 15a-15f and 16a-16f

N,N,N′,N′-Tetramethyl-α,ω-diaminoalkanes (5 mmol) was reacted with *N*-alkyl-1-bromoethanamide (15 mmol) in dry $CHCl_3$ (40 mL) in a screw-top pressure tube at 85 °C for about 24 h. After the reaction, the solvent was evaporated and the product was precipitated using excess diethylether. Finally the product was filtered and washed multiple times with diethylether. The precipitate was then dried overnight in vacuum oven at 55 °C to give **13a-13f, 14a-14f, 15a-15f** and **16a-16f** quantitatively.

13a: FT-IR ($\bar{\nu}$): 3263 cm^{-1} (NH str.), 2925 cm^{-1} (CH_2 assym. str.), 2852 cm^{-1} (CH_2 sym. str.), 1688 cm^{-1} (amide I, C=O str.), 1562 cm^{-1} (amide II, NH ben.), 1481 cm^{-1} (CH_2 scissor); ^{1}H-NMR (400 MHz, $CDCl_3$): δ 0.88 (t, terminal $-CH_3$, 6H), 1.26-1.35 (m, $-CH_2(CH_2)_3CH_3$, 12H), 1.57 (m, $-CH_2(CH_2)_3CH_3$ 4H), 3.24 (m, $-CONHCH_2-$, 4H), 3.62 (s, $-(CH_3)_2N^+-$, 12H), 4.67 (br. m, $-(Me)_2{}^+NCH_2-$, 4H), 4.79 (s, $-NHCOCH_2-$, 4H), 8.81 (br. s, amide $-NH$, 2H); ^{13}C-NMR (100 MHz, $CDCl_3$): δ 14.3, 22.6, 26.8, 29.1, 31.5, 40.2, 53.1, 63.2, 162.2; HRMS: calculated m/z 479.2955, 481.2940 $[M–Br^-]^+$, 200.1883 $[M–2Br^-]^{2+}$; observed m/z 479.2954, 481.2938 $[M–Br^-]^+$, 200.1886 $[M–2Br^-]^{2+}$.

13b: FT-IR ($\overline{\nu}$): 3260 cm^{-1} (NH str.), 2928 cm^{-1} (CH_2 assym. str.), 2860 cm^{-1} (CH_2 sym. str.), 1681 cm^{-1} (amide I, C=O str.), 1556 cm^{-1} (amide II, NH ben.), 1484 cm^{-1} (CH_2 scissor); ^{1}H-NMR (400 MHz, $CDCl_3$): δ 0.89 (t, terminal –*CH_3*, 6H), 1.26-1.29 (br. m, –CH_2*$(CH_2)_3$*CH_3 12H), 1.54 (m, –*CH_2*$(CH_2)_3CH_3$, 4H), 2.14 (br. m, –*CH_2*$CH_2N^+Me_2$, 4H) 3.25 (m, –CONH*CH_2*–, 4H), 3.47 (s, –*$(CH_3)_2$*N^+–, 12H), 3.91 (br. m, –$(Me)_2^+$N*CH_2*–, 4H), 4.46 (s, –NHCO*CH_2*–, 4H), 8.51 (br. s, amide –*NH*, 2H); ^{13}C-NMR (100 MHz, $CDCl_3$): δ 14.1, 20.4, 22.6, 26.7, 29.1, 31.4, 40.1, 52.2, 63.1, 65.5, 162.6; HRMS: calculated m/z 507.3268, 509.3291 $[M–Br^–]^+$, 214.2039 $[M–2Br^–]^{2+}$; observed m/z 507.3250, 509.3285 $[M–Br^–]^+$, 214.2063 $[M–2Br^–]^{2+}$.

13c: FT-IR ($\overline{\nu}$): 3261 cm^{-1} (NH str.), 2925 cm^{-1} (CH_2 assym. str.), 2850 cm^{-1} (CH_2 sym. str.), 1680 cm^{-1} (amide I, C=O str.), 1560 cm^{-1} (amide II, NH ben.), 1482 cm^{-1} (CH_2 scissor); ^{1}H-NMR (400 MHz, $CDCl_3$): δ 0.87 (t, terminal –*CH_3*, 6H), 1.26-1.37 (m, –CH_2*$(CH_2)_3$*CH_3, 12H), 1.55 (m, –*CH_2*$(CH_2)_3CH_3$ and –*$(CH_2)_2$*$CH_2CH_2N^+Me_2$, 8H), 2.1 (br. m, –*CH_2*$CH_2N^+Me_2$, 4H) 3.25 (m, –CONH*CH_2*–, 4H), 3.44 (s, –*$(CH_3)_2$*N^+–, 12H), 3.74 (br. m, –$(Me)_2^+$N*CH_2*–, 4H), 4.58 (s, –NHCO*CH_2*–, 4H), 8.61 (br. s, amide –*NH*, 2H); ^{13}C-NMR (100 MHz, $CDCl_3$): δ 14.1, 21.8, 22.6, 24.5, 26.7, 29.1, 31.4, 39.9, 52.3, 62.8, 66.8, 162.8; HRMS: calculated m/z 535.3581, 537.3569 $[M–Br^–]^+$, 228.2196 $[M–2Br^–]^{2+}$; observed m/z 535.3593, 537.3576 $[M–Br^–]^+$, 228.2207 $[M–2Br^–]^{2+}$.

13d: FT-IR ($\overline{\nu}$): 3260 cm^{-1} (NH str.), 2930 cm^{-1} (CH_2 assym. str.), 2860 cm^{-1} (CH_2 sym. str.), 1685 cm^{-1} (amide I, C=O str.), 1552 cm^{-1} (amide II, NH ben.), 1480 cm^{-1} (CH_2 scissor); ^{1}H-NMR (400 MHz, $CDCl_3$): δ 0.87 (t, terminal –*CH_3*, 6H), 1.28-1.35 (br. m, –CH_2*$(CH_2)_3$*CH_3 12H), 1.48 (m, –CH_2*$(CH_2)_4$*CH_2–, 8H), 1.59 (m, –*CH_2*$(CH_2)_3CH_3$, 4H), 1.95 (br. m, –*CH_2*$CH_2N^+Me_2$, 4H) 3.26 (m, –CONH*CH_2*–, 4H), 3.41 (s, –*$(CH_3)_2$*N^+–, 12H), 3.70 (br. m, –$(Me)_2^+$N*CH_2*–, 4H), 4.55 (s, –NHCO*CH_2*–, 4H), 8.76 (br. s, amide –*NH*, 2H); ^{13}C-NMR (100 MHz, $CDCl_3$): δ 15.9, 24.5, 24.6, 27.8, 28.3, 30.4, 30.5, 33.2, 42.1, 54.9, 65.3, 67.8, 162.8; HRMS: calculated m/z 563.3894, 565.3878 $[M–Br^–]^+$, 242.2352 $[M–2Br^–]^{2+}$; observed m/z 563.3900, 565.3885 $[M–Br^–]^+$, 242.2359 $[M–2Br^–]^{2+}$.

13e: FT-IR ($\overline{\nu}$): 3257 cm^{-1} (NH str.), 2925 cm^{-1} (CH_2 assym. str.), 2850 cm^{-1} (CH_2 sym. str.), 1679 cm^{-1} (amide I, C=O str.), 1555 cm^{-1} (amide II, NH ben.), 1480 cm^{-1} (CH_2 scissor); ^{1}H-NMR (400 MHz, $CDCl_3$): δ 0.87 (t, terminal –*CH_3*, 6H), 1.28-1.43 (m, –CH_2*$(CH_2)_3$*CH_3, and –*$(CH_2)_6$*$CH_2CH_2N^+Me_2$, 24H), 1.59 (m, –*CH_2*$(CH_2)_3CH_3$ 4H), 1.87 (br. m, –*CH_2*$CH_2N^+Me_2$, 4H) 3.25 (m, –CONH*CH_2*–, 4H), 3.39 (s, –*$(CH_3)_2$*N^+–, 12H), 3.68 (br. m, –$(Me)_2^+$N*CH_2*–, 4H), 4.56 (s, –NHCO*CH_2*–, 4H), 8.82 (br. s, amide –*NH*, 2H); ^{13}C-NMR (100 MHz, $CDCl_3$): δ 14.1, 22.6, 22.6, 25.8, 26.7, 28.2, 28.4, 29.1, 31.4, 39.942, 52.1, 63.323, 66.4, 162.8; HRMS: calculated m/z 591.4207, 593.4188 $[M–Br^–]^+$, 256.2509 $[M–2Br^–]^{2+}$; observed m/z 591.4206, 593.4192 $[M–Br^–]^+$, 256.2524 $[M–2Br^–]^{2+}$.

13f: FT-IR ($\overline{\nu}$): 3260 cm^{-1} (NH str.), 2928 cm^{-1} (CH_2 assym. str.), 2855 cm^{-1} (CH_2 sym. str.), 1680 cm^{-1} (amide I, C=O str.), 1555 cm^{-1} (amide II, NH ben.), 1480 cm^{-1} (CH_2 scissor); ^{1}H-NMR (400 MHz, $CDCl_3$): δ 0.87 (t, terminal –*CH_3*, 6H), 1.28-1.39 (br. m, –CH_2*$(CH_2)_3$*CH_3 and –*$(CH_2)_8$*$CH_2CH_2N^+Me_2$, 28H), 1.56 (m, –*CH_2*$(CH_2)_3CH_3$, 4H), 1.83 (br. m, –*CH_2*$CH_2N^+Me_2$, 4H) 3.27 (m, –CONH*CH_2*–, 4H), 3.37 (s, –*$(CH_3)_2$*N^+–, 12H), 3.65 (br. m, –$(Me)_2^+$N*CH_2*–, 4H), 4.58 (s, –NHCO*CH_2*–, 4H), 8.89 (br. s, amide –*NH*, 2H); ^{13}C-NMR (100 MHz, $CDCl_3$): δ 14.1, 22.6, 22.6, 22.9, 26.1, 26.5, 26.8, 28.6, 28.7, 28.7, 29.1, 29.3,

31.5, 40.1, 49.8, 52.1, 63.4, 162.8; HRMS: calculated m/z 619.4520, 621.4520 $[M–Br^-]^+$, 270.2665 $[M–2Br^-]^{2+}$; observed m/z 619.4527, 621.4516 $[M–Br^-]^+$, 270.2687 $[M–2Br^-]^{2+}$.

14a: FT-IR ($\overline{\nu}$): 3265 cm^{-1} (NH str.), 2927 cm^{-1} (CH_2 assym. str.), 2860 cm^{-1} (CH_2 sym. str.), 1675 cm^{-1} (amide I, C=O str.), 1550 cm^{-1} (amide II, NH ben.), 1474 cm^{-1} (CH_2 scissor); ^{1}H-NMR (400 MHz, $CDCl_3$): δ 0.88 (t, terminal $–CH_3$, 6H), 1.26-1.31 (br. m, $–CH_2(CH_2)_5CH_3$, 20H), 1.57 (m, $–CH_2(CH_2)_5CH_3$, 4H), 3.23 (m, –CONHCH_2–, 4H), 3.62 (s, $–(CH_3)_2N^+–$, 12H), 4.68 (br. m, $–(Me)_2{}^+NCH_2–$, 4H), 4.81 (s, –NHCOCH_2–, 4H), 8.37 (br. s, amide –*NH*, 2H); ^{13}C-NMR (100 MHz, $CDCl_3$): δ 14.2, 22.7, 27.1, 29.1, 29.3, 29.4, 31.9, 40.2, 53.1, 58.1, 63.1, 162.2; HRMS: calculated m/z 535.3581, 537.3569 $[M–Br^-]^+$, 228.2196 $[M–2Br^-]^{2+}$; observed m/z 535.3592, 537.3578 $[M–Br^-]^+$, 228.2203 $[M–2Br^-]^{2+}$.

14b: FT-IR ($\overline{\nu}$): 3269 cm^{-1} (NH str.), 2933 cm^{-1} (CH_2 assym. str.), 2855 cm^{-1} (CH_2 sym. str.), 1685 cm^{-1} (amide I, C=O str.), 1555 cm^{-1} (amide II, NH ben.), 1480 cm^{-1} (CH_2 scissor); ^{1}H-NMR (400 MHz, $CDCl_3$): δ 0.87 (t, terminal $–CH_3$, 6H), 1.26-1.34 (br. m, $–CH_2(CH_2)_5CH_3$, 20H), 1.44 (m, $–(CH_2)_4CH_2CH_2N^+Me_2$, 8H), 1.58 (m, $–CH_2(CH_2)_5CH_3$, 4H), 2.15 (br. m, $–CH_2CH_2N^+Me_2$, 4H) 3.23 (m, –CONHCH_2–, 4H), 3.46 (s, $–(CH_3)_2N^+–$, 12H), 3.92 (br. m, $–(Me)_2{}^+NCH_2–$, 4H), 4.47 (s, –NHCOCH_2–, 4H), 8.52 (br. s, amide –*NH*, 2H); ^{13}C-NMR (100 MHz, $CDCl_3$): δ 14.2, 20.4, 22.7, 27.2, 29.1, 29.3, 29.3, 31.9, 40.1, 52.3, 63.1, 65.7, 162.6; HRMS: calculated m/z 563.3894, 565.3878 $[M–Br^-]^+$, 242.2352 $[M–2Br^-]^{2+}$; observed m/z 563.3895, 565.3881 $[M–Br^-]^+$, 242.2356 $[M–2Br^-]^{2+}$.

14c: FT-IR ($\overline{\nu}$): 3260 cm^{-1} (NH str.), 2922 cm^{-1} (CH_2 assym. str.), 2850 cm^{-1} (CH_2 sym. str.), 1680 cm^{-1} (amide I, C=O str.), 1554 cm^{-1} (amide II, NH ben.), 1480 cm^{-1} (CH_2 scissor); ^{1}H-NMR (400 MHz, $CDCl_3$): δ 0.87 (t, terminal $–CH_3$, 6H), 1.26-1.29 (m, $–CH_2(CH_2)_5CH_3$, 20H), 1.56-1.62 (m, $–CH_2(CH_2)_5CH_3$ and $–(CH_2)_2CH_2CH_2N^+Me_2$, 8H), 2.12 (br. m, $–CH_2CH_2N^+Me_2$, 4H) 3.21 (m, –CONHCH_2–, 4H), 3.61 (s, $–(CH_3)_2N^+–$, 12H), 4.68 (br. m, $–(Me)_2{}^+NCH_2–$, 4H), 4.81 (s, –NHCOCH_2–, 4H), 8.69 (br. s, amide –*NH*, 2H); ^{13}C-NMR (100 MHz, $CDCl_3$): δ 14.1, 21.9, 22.7, 24.7, 27.1, 29.1, 29.2, 29.3, 31.8, 39.9, 62.9, 66.2, 162.9; HRMS: calculated m/z 591.4207, 593.4188 $[M–Br^-]^+$, 256.2509 $[M–2Br^-]^{2+}$; observed m/z 591.4214, 593.4202 $[M–Br^-]^+$, 256.2522 $[M–2Br^-]^{2+}$.

14d: FT-IR ($\overline{\nu}$): 3259 cm^{-1} (NH str.), 2927 cm^{-1} (CH_2 assym. str.), 2854 cm^{-1} (CH_2 sym. str.), 1685 cm^{-1} (amide I, C=O str.), 1555 cm^{-1} (amide II, NH ben.), 1479 cm^{-1} (CH_2 scissor); ^{1}H-NMR (400 MHz, $CDCl_3$): δ 0.87 (t, terminal $–CH_3$, 6H), 1.25-1.28 (br. m, $–CH_2(CH_2)_5CH_3$, 20H), 1.44 (m, $–(CH_2)_4CH_2CH_2N^+Me_2$, 8H), 1.58 (m, $–CH_2(CH_2)_5CH_3$, 4H), 1.95 (br. m, $–CH_2CH_2N^+Me_2$, 4H) 3.24 (m, –CONHCH_2–, 4H), 3.40 (s, $–(CH_3)_2N^+–$, 12H), 3.71 (br. m, $–(Me)_2{}^+NCH_2–$, 4H), 4.55 (s, –NHCOCH_2–, 4H), 8.79 (br. s, amide –*NH*, 2H); ^{13}C-NMR (100 MHz, $CDCl_3$): δ 14.1, 22.3, 22.6, 25.5, 27.1, 27.7, 29.1, 29.2, 29.2, 31.8, 39.8, 52.2, 63.1, 66.2, 162.9; HRMS: calculated m/z 619.4520, 621.4520 $[M–Br^-]^+$, 270.2665 $[M–2Br^-]^{2+}$; observed m/z 619.4522, 621.4511 $[M–Br^-]^+$, 270.2679 $[M–2Br^-]^{2+}$.

14e: FT-IR ($\overline{\nu}$) : 3260 cm^{-1} (NH str.), 2935 cm^{-1} (CH_2 assym. str.), 2855 cm^{-1} (CH_2 sym. str.), 1685 cm^{-1} (amide I, C=O str.), 1555 cm^{-1} (amide II, NH ben.), 1480 cm^{-1} (CH_2 scissor); ^{1}H-NMR (400 MHz, $CDCl_3$): δ 0.87 (t, terminal $–CH_3$, 6H), 1.26-1.35 (br. m, $–CH_2(CH_2)_5CH_3$ and $–(CH_2)_4CH_2CH2CH2N^+Me_2$, 24H), 1.43 (m, $–(CH_2)_4CH_2CH2CH2N^+Me_2$, 8H), 1.54 (m, $–CH_2(CH_2)_5CH_3$, 4H), 1.87 (br. m, $–CH_2CH_2N^+Me_2$, 4H) 3.25 (m, –CONHCH_2–, 4H), 3.39 (s, $–(CH_3)_2N^+–$, 12H), 3.70 (br. m,

–$(Me)_2{}^+NCH_2$–, 4H), 4.57 (s, –NHCOCH_2–, 4H), 8.84 (br. s, amide –*NH*, 2H); ^{13}C-NMR (100 MHz, $CDCl_3$): δ 14.1, 22.7, 25.7, 27.1, 28.1, 28.2, 29.1, 29.3, 31.9, 40.1, 52.1, 63.4, 66.9, 162.8; HRMS: calculated m/z 647.4833, 649.4815, $[M–Br^-]^+$, 284.2822 $[M–2Br^-]^{2+}$; observed m/z 647.4835, 649.4819, $[M–Br^-]^+$, 284.2877 $[M–2Br^-]^{2+}$.

14f: FT-IR ($\overline{\nu}$): 3263 cm^{-1} (NH str.), 2935 cm^{-1} (CH_2 assym. str.), 2860 cm^{-1} (CH_2 sym. str.), 1682 cm^{-1} (amide I, C=O str.), 1555 cm^{-1} (amide II, NH ben.), 1480 cm^{-1} (CH_2 scissor); ^{1}H-NMR (400 MHz, $CDCl_3$): δ 0.86 (t, terminal –CH_3, 6H), 1.25-1.29 (br. m, –$CH_2(CH_2)_5CH_3$ and –$(CH_2)_8CH_2CH_2N^+Me_2$, 36H), 1.57 (m, –$CH_2(CH_2)_3CH_3$, 4H), 1.82 (br. m, –$CH_2CH_2N^+Me_2$, 4H) 3.26 (m, –CONHCH_2–, 4H), 3.38 (s, –$(CH_3)_2N^+$–, 12H), 3.66 (br. m, –$(Me)_2{}^+NCH_2$–, 4H), 4.57 (s, –NHCOCH_2–, 4H), 8.81 (br. s, amide –*NH*, 2H); ^{13}C-NMR (100 MHz, $CDCl_3$): δ 14.1, 22.7, 22.9, 26.1, 27.2, 28.7, 28.8, 29.1, 29.3, 29.5, 29.6, 31.9, 39.9, 52.1, 63.4, 66.3, 162.8; HRMS: calculated m/z 675.5148, 677.5130 $[M–Br^-]^+$, 298.2978 $[M–2Br^-]^{2+}$; observed m/z 675.5148, 677.5133 $[M–Br^-]^+$, 298.3002 $[M–2Br^-]^{2+}$.

15a: FT-IR ($\overline{\nu}$): 3258 cm^{-1} (NH str.), 2920 cm^{-1} (CH_2 assym. str.), 2848 cm^{-1} (CH_2 sym. str.), 1685 cm^{-1} (amide I, C=O str.), 1550 cm^{-1} (amide II, NH ben.), 1472 cm^{-1} (CH_2 scissor); ^{1}H-NMR (400 MHz, $CDCl_3$): δ 0.84 (t, terminal –CH_3, 6H), 1.26 (m, –$CH_2(CH_2)_7CH_3$, 28H), 1.52 (m, –$CH_2(CH_2)_7CH_3$, 4H), 3.21 (m, –CONHCH_2–, 4H), 3.61 (s, –$(CH_3)_2N^+$–, 12H), 4.68 (br. m, –$CH_2N^+Me_2$–, 4H), 4.81 (s, –NHCOCH_2–, 4H), 8.34 (br. s, amide –*NH*, 2H); ^{13}C-NMR (100 MHz, $CDCl_3$): δ 14.1, 22.7, 27.1, 29.1, 29.3, 29.4, 29.6, 31.9, 40.1, 57.9, 63.0, 162.1; HRMS: calculated m/z 591.4207, 593.4188 $[M–Br^-]^+$, 256.2509 $[M–2Br^-]^{2+}$; observed m/z 591.4212, 593.4198 $[M–Br^-]^+$, 256.2529 $[M–2Br^-]^{2+}$.

15b: FT-IR ($\overline{\nu}$): 3261 cm^{-1} (NH str.), 2928 cm^{-1} (CH_2 assym. str.), 2851 cm^{-1} (CH_2 sym. str.), 1682 cm^{-1} (amide I, C=O str.), 1554 cm^{-1} (amide II, NH ben.), 1476 cm^{-1} (CH_2 scissor); ^{1}H-NMR (400 MHz, $CDCl_3$): δ 0.87 (t, terminal –CH_3, 6H), 1.29 (br. m, –$CH_2(CH_2)_7CH_3$, 28H), 1.55 (m, –$CH_2(CH_2)_7CH_3$, 4H), 2.21 (br. m, –$CH_2CH_2N^+Me_2$–, 4H), 3.27 (m, –CONHCH_2–, 4H), 3.45 (s, –$(CH_3)_2N^+$–, 12H), 3.89 (br. m, –$CH_2CH_2N^+Me_2$–, 4H), 4.44 (s, –NHCOCH_2–, 4H), 8.56 (br. s, amide –*NH*, 2H); ^{13}C-NMR (100 MHz, $CDCl_3$): δ 14.2, 20.4, 22.7, 27.2, 29.2, 29.4, 29.4, 29.7, 31.9, 40.1, 63.1, 65.5, 162.6; HRMS: calculated m/z 619.4520, 621.4520 $[M–Br^-]^+$, 270.2665 $[M–2Br^-]^{2+}$; observed m/z 619.4525, 621.4521 $[M–Br^-]^+$, 270.2683 $[M–2Br^-]^{2+}$.

15c: FT-IR ($\overline{\nu}$): 3255 cm^{-1} (NH str.), 2925 cm^{-1} (CH_2 assym. str.), 2852 cm^{-1} (CH_2 sym. str.), 1680 cm^{-1} (amide I, C=O str.), 1555 cm^{-1} (amide II, NH ben.), 1470 cm^{-1} (CH_2 scissor); ^{1}H-NMR (400 MHz, $CDCl_3$): δ 0.87 (t, terminal –CH_3, 6H), 1.24-1.29 (m, –$CH_2(CH_2)_7CH_3$, 28H), 1.53-1.58 (m, –$CH_2(CH_2)_7CH_3$ and –$(CH_2)_2CH_2CH_2N^+Me_2$, 8H), 1.94 (br. m, –$CH_2CH_2N^+Me_2$, 4H), 3.25 (m, –CONHCH_2–, 4H), 3.44 (s, –$(CH_3)_2N^+$–, 12H), 3.75 (br. m, –$CH_2N^+Me_2$–, 4H), 4.57 (s, –NHCOCH_2–, 4H), 8.61 (br. s, amide –*NH*, 2H); ^{13}C-NMR (100 MHz, $CDCl_3$): δ 14.2, 21.7, 22.7, 24.4, 27.2, 29.1, 29.4, 29.4, 29.6, 32.1, 40.1, 52.4, 62.9, 66.9, 162.9; HRMS: calculated m/z 647.4833, 649.4815, $[M–Br^-]^+$, 284.2822 $[M–2Br^-]^{2+}$; observed m/z 647.4830, 649.4813, $[M–Br^-]^+$, 284.2827 $[M–2Br^-]^{2+}$.

15d: FT-IR ($\overline{\nu}$): 3257 cm^{-1} (NH str.), 2925 cm^{-1} (CH_2 assym. str.), 2849 cm^{-1} (CH_2 sym. str.), 1682 cm^{-1} (amide I, C=O str.), 1555 cm^{-1} (amide II, NH ben.), 1482 cm^{-1} (CH_2 scissor); ^{1}H-NMR (400 MHz, $CDCl_3$): δ 0.87 (t, terminal –CH_3, 6H), 1.25-1.48 (m, –$CH_2(CH_2)_7CH_3$, 28H), 1.53-1.61 (m, –$(CH_2)_4CH_2CH_2N^+Me_2$, 8H), 1.96 (br. m, –$CH_2CH_2N^+Me_2$, 4H) 3.23

(m, –CONH*CH*$_2$–, 4H), 3.42 (s, –*(CH*$_3$*)*$_2$N$^+$–, 12H), 3.72 (br. m, –(Me)$_2^+$N*CH*$_2$–, 4H), 4.55 (s, –NHCO*CH*$_2$–, 4H), 8.74 (br. s, amide –*NH*, 2H); ^{13}C-NMR (100 MHz, $CDCl_3$): δ 14.1, 21.7, 22.8, 24.5, 27.2, 29.2, 29.4, 29.5, 29.6, 32.1, 40.2, 52.5, 62.9, 66.9, 162.7; HRMS: calculated m/z 675.5148, 677.5130 $[M–Br^-]^+$, 298.2978 $[M–2Br^-]^{2+}$; observed m/z 675.5146, 677.5133 $[M–Br^-]^+$, 298.3002 $[M–2Br^-]^{2+}$.

15e: FT-IR ($\overline{\nu}$): 3260 cm^{-1} (NH str.), 2920 cm^{-1} (CH_2 assym. str.), 2849 cm^{-1} (CH_2 sym. str.), 1682 cm^{-1} (amide I, C=O str.), 1555 cm^{-1} (amide II, NH ben.), 1477 cm^{-1} (CH_2 scissor); ^{1}H-NMR (400 MHz, $CDCl_3$): δ 0.88 (t, terminal –*CH*$_3$, 6H), 1.27-1.35 (m, –CH_2*(CH*$_2$*)*$_7$$CH_3$ and –*CH*$_2$(CH_2)$_4$$CH_2CH_2N^+Me_2$, 32H), 1.43 (m, –$CH_2$*(CH*$_2$*)*$_4$$CH_2CH_2N^+Me_2$, 8H), 1.58 (m, –*CH*$_2$($CH_2$)$_7$$CH_3$, 4H), 1.87 (br. m, –*CH*$_2$$CH_2N^+Me_2$, 4H), 3.26 (m, –CONH*CH*$_2$–, 4H), 3.39 (s, –*(CH*$_3$*)*$_2$N$^+$–, 12H), 3.70 (br. m, –*CH*$_2$N$^+$$Me_2$–, 4H), 4.57 (s, –NHCO*CH*$_2$–, 4H), 8.84 (br. s, amide –*NH*, 2H); ^{13}C-NMR (100 MHz, $CDCl_3$): δ 14.2, 22.5, 22.8, 25.7, 27.2, 28.1, 28.2, 29.1, 29.3, 29.7, 32.1, 40.1, 52.1, 63.4, 66.9, 162.8; HRMS: calculated m/z 703.5459, 705.5450 $[M–Br^-]^+$, 312.3135 $[M–2Br^-]^{2+}$; observed m/z 703.5467, 705.5454 $[M–Br^-]^+$, 312.3177 $[M–2Br^-]^{2+}$.

15f: FT-IR ($\overline{\nu}$): 3267 cm^{-1} (NH str.), 2931 cm^{-1} (CH_2 assym. str.), 2854 cm^{-1} (CH_2 sym. str.), 1688 cm^{-1} (amide I, C=O str.), 1550 cm^{-1} (amide II, NH ben.), 1480 cm^{-1} (CH_2 scissor); ^{1}H-NMR (400 MHz, $CDCl_3$): δ 0.87 (t, terminal –*CH*$_3$, 6H), 1.25-1.30 (m, –CH_2*(CH*$_2$*)*$_5$$CH_3$ and –*(CH*$_2$*)*$_4$(CH_2)$_4$$CH_2CH_2N^+Me_2$, 36H), 1.39 (m, –($CH_2$)$_4$*(CH*$_2$*)*$_4$$CH_2CH_2N^+Me_2$, 8H), 1.56-1.61 (m, –*CH*$_2$(CH_2)$_5$$CH_3$, 4H), 1.85 (br. m, –*CH*$_2$$CH_2N^+Me_2$, 4H), 3.25 (m, –CONH*CH*$_2$–, 4H), 3.37 (s, –*(CH*$_3$*)*$_2$N$^+$–, 12H), 3.64 (br. m, –(Me)$_2^+$N*CH*$_2$–, 4H), 4.58 (s, –NHCO*CH*$_2$–, 4H), 8.88 (br. s, amide –*NH*, 2H); ^{13}C-NMR (100 MHz, $CDCl_3$): δ 14.2, 22.4, 22.8, 25.7, 27.2, 28.1, 28.3, 29.2, 29.4, 29.7, 32.2, 41.1, 52.6, 63.5, 66.9, 162.7; HRMS: calculated m/z 731.5772, 733.5759 $[M–Br^-]^+$, 326.3291 $[M–2Br^-]^{2+}$; observed m/z 731.5776, 733.5761 $[M–Br^-]^+$, 326.3290 $[M–2Br^-]^{2+}$.

16a: FT-IR ($\overline{\nu}$): 3258 cm^{-1} (NH str.), 2920 cm^{-1} (CH_2 assym. str.), 2848 cm^{-1} (CH_2 sym. str.), 1685 cm^{-1} (amide I, C=O str.), 1550 cm^{-1} (amide II, NH ben.), 1472 cm^{-1} (CH_2 scissor); ^{1}H-NMR (400 MHz, $CDCl_3$): δ 0.84 (t, terminal –*CH*$_3$, 6H), 1.26 (m, –CH_2*(CH*$_2$*)*$_7$$CH_3$, 28H), 1.52 (m, –*CH*$_2$($CH_2$)$_7$$CH_3$, 4H), 3.21 (m, –CONH*CH*$_2$–, 4H), 3.61 (s, –*(CH*$_3$*)*$_2$N$^+$–, 12H), 4.68 (br. m, –*CH*$_2$N$^+$$Me_2$–, 4H), 4.81 (s, –NHCO*CH*$_2$–, 4H), 8.34 (br. s, amide –*NH*, 2H); ^{13}C-NMR (100 MHz, $CDCl_3$): δ 14.1, 22.7, 27.1, 29.1, 29.3, 29.4, 29.6, 31.9, 40.1, 57.9, 63.0, 162.1; HRMS: calculated m/z 591.4207, 593.4188 $[M–Br^-]^+$, 256.2509 $[M–2Br^-]^{2+}$; observed m/z 591.4212, 593.4198 $[M–Br^-]^+$, 256.2529 $[M–2Br^-]^{2+}$.

16b: FT-IR ($\overline{\nu}$): 3261 cm^{-1} (NH str.), 2928 cm^{-1} (CH_2 assym. str.), 2851 cm^{-1} (CH_2 sym. str.), 1682 cm^{-1} (amide I, C=O str.), 1554 cm^{-1} (amide II, NH ben.), 1476 cm^{-1} (CH_2 scissor); ^{1}H-NMR (400 MHz, $CDCl_3$): δ 0.87 (t, terminal –*CH*$_3$, 6H), 1.29 (br. m, –CH_2*(CH*$_2$*)*$_7$$CH_3$, 28H), 1.55 (m, –*CH*$_2$($CH_2$)$_7$$CH_3$, 4H), 2.21 (br. m, –*CH*$_2$$CH_2N^+Me_2$–, 4H), 3.27 (m, –CONH*CH*$_2$–, 4H), 3.45 (s, –*(CH*$_3$*)*$_2$N$^+$–, 12H), 3.89 (br. m, –CH_2*CH*$_2$N$^+$$Me_2$–, 4H), 4.44 (s, –NHCO*CH*$_2$–, 4H), 8.56 (br. s, amide –*NH*, 2H); ^{13}C-NMR (100 MHz, $CDCl_3$): δ 14.2, 20.4, 22.7, 27.2, 29.2, 29.4, 29.4, 29.7, 31.9, 40.1, 63.1, 65.5, 162.6; HRMS: calculated m/z 619.4520, 621.4520 $[M–Br^-]^+$, 270.2665 $[M–2Br^-]^{2+}$; observed m/z 619.4525, 621.4521 $[M–Br^-]^+$, 270.2683 $[M–2Br^-]^{2+}$.

16c: FT-IR ($\overline{\nu}$): 3255 cm^{-1} (NH str.), 2925 cm^{-1} (CH_2 assym. str.), 2852 cm^{-1} (CH_2 sym. str.), 1680 cm^{-1} (amide I, C=O str.), 1555 cm^{-1} (amide II, NH ben.), 1470 cm^{-1} (CH_2 scissor); ^{1}H-NMR (400 MHz, $CDCl_3$): δ 0.87 (t, terminal –*CH_3*, 6H), 1.24-1.29 (m, –CH_2*$(CH_2)_7$*CH_3, 28H), 1.53-1.58 (m, –*CH_2*$(CH_2)_7CH_3$ and –*$(CH_2)_2$*$CH_2CH_2N^+Me_2$, 8H), 1.94 (br. m, –*CH_2*$CH_2N^+Me_2$, 4H), 3.25 (m, –CONH*CH_2*–, 4H), 3.44 (s, –*$(CH_3)_2$*N^+–, 12H), 3.75 (br. m, –*CH_2*N^+Me_2–, 4H), 4.57 (s, –NHCO*CH_2*–, 4H), 8.61 (br. s, amide –*NH*, 2H); ^{13}C-NMR (100 MHz, $CDCl_3$): δ 14.2, 21.7, 22.7, 24.4, 27.2, 29.1, 29.4, 29.4, 29.6, 32.1, 40.1, 52.4, 62.9, 66.9, 162.9; HRMS: calculated m/z 647.4833, 649.4815, $[M–Br^–]^+$, 284.2822 $[M–2Br^–]^{2+}$; observed m/z 647.4830, 649.4813, $[M–Br^–]^+$, 284.2827 $[M–2Br^–]^{2+}$.

16d: FT-IR ($\overline{\nu}$): 3257 cm^{-1} (NH str.), 2925 cm^{-1} (CH_2 assym. str.), 2849 cm^{-1} (CH_2 sym. str.), 1682 cm^{-1} (amide I, C=O str.), 1555 cm^{-1} (amide II, NH ben.), 1482 cm^{-1} (CH_2 scissor); ^{1}H-NMR (400 MHz, $CDCl_3$): δ 0.87 (t, terminal –*CH_3*, 6H), 1.25-1.48 (m, –CH_2*$(CH_2)_7$*CH_3, 28H), 1.53-1.61 (m, –*$(CH_2)_4$*$CH_2CH_2N^+Me_2$, 8H), 1.96 (br. m, –*CH_2*$CH_2N^+Me_2$, 4H) 3.23 (m, –CONH*CH_2*–, 4H), 3.42 (s, –*$(CH_3)_2$*N^+–, 12H), 3.72 (br. m, –$(Me)_2{}^+N$*CH_2*–, 4H), 4.55 (s, –NHCO*CH_2*–, 4H), 8.74 (br. s, amide –*NH*, 2H); ^{13}C-NMR (100 MHz, $CDCl_3$): δ 14.1, 21.7, 22.8, 24.5, 27.2, 29.2, 29.4, 29.5, 29.6, 32.1, 40.2, 52.5, 62.9, 66.9, 162.7; HRMS: calculated m/z 675.5148, 677.5130 $[M–Br^–]^+$, 298.2978 $[M–2Br^–]^{2+}$; observed m/z 675.5146, 677.5133 $[M–Br^–]^+$, 298.3002 $[M–2Br^–]^{2+}$.

16e: FT-IR ($\overline{\nu}$): 3260 cm^{-1} (NH str.), 2920 cm^{-1} (CH_2 assym. str.), 2849 cm^{-1} (CH_2 sym. str.), 1682 cm^{-1} (amide I, C=O str.), 1555 cm^{-1} (amide II, NH ben.), 1477 cm^{-1} (CH_2 scissor); ^{1}H-NMR (400 MHz, $CDCl_3$): δ 0.88 (t, terminal –*CH_3*, 6H), 1.27-1.35 (m, –CH_2*$(CH_2)_7$*CH_3 and –*CH_2*$(CH_2)_4CH_2CH_2N^+Me_2$, 32H), 1.43 (m, –CH_2*$(CH_2)_4$*$CH_2CH_2N^+Me_2$, 8H), 1.58 (m, –*CH_2*$(CH_2)_7CH_3$, 4H), 1.87 (br. m, –*CH_2*$CH_2N^+Me_2$, 4H), 3.26 (m, –CONH*CH_2*–, 4H), 3.39 (s, –*$(CH_3)_2$*N^+–, 12H), 3.70 (br. m, –*CH_2*N^+Me_2–, 4H), 4.57 (s, –NHCO*CH_2*–, 4H), 8.84 (br. s, amide –*NH*, 2H); ^{13}C-NMR (100 MHz, $CDCl_3$): δ 14.2, 22.5, 22.8, 25.7, 27.2, 28.1, 28.2, 29.1, 29.3, 29.7, 32.1, 40.1, 52.1, 63.4, 66.9, 162.8; HRMS: calculated m/z 703.5459, 705.5450 $[M–Br^–]^+$, 312.3135 $[M–2Br^–]^{2+}$; observed m/z 703.5467, 705.5454 $[M–Br^–]^+$, 312.3177 $[M–2Br^–]^{2+}$.

16f: FT-IR ($\overline{\nu}$): 3267 cm^{-1} (NH str.), 2931 cm^{-1} (CH_2 assym. str.), 2854 cm^{-1} (CH_2 sym. str.), 1688 cm^{-1} (amide I, C=O str.), 1550 cm^{-1} (amide II, NH ben.), 1480 cm^{-1} (CH_2 scissor); ^{1}H-NMR (400 MHz, $CDCl_3$): δ 0.87 (t, terminal –*CH_3*, 6H), 1.25-1.30 (m, –CH_2*$(CH_2)_5$*CH_3 and –*$(CH_2)_4$*$(CH_2)_4CH_2CH_2N^+Me_2$, 36H), 1.39 (m, –$(CH_2)_4$*$(CH_2)_4$*$CH_2CH_2N^+Me_2$, 8H), 1.56-1.61 (m, –*CH_2*$(CH_2)_5CH_3$, 4H), 1.85 (br. m, –*CH_2*$CH_2N^+Me_2$, 4H), 3.25 (m, –CONH*CH_2*–, 4H), 3.37 (s, –*$(CH_3)_2$*N^+–, 12H), 3.64 (br. m, –$(Me)_2{}^+N$*CH_2*–, 4H), 4.58 (s, –NHCO*CH_2*–, 4H), 8.88 (br. s, amide –*NH*, 2H); ^{13}C-NMR (100 MHz, $CDCl_3$): δ 14.2, 22.4, 22.8, 25.7, 27.2, 28.1, 28.3, 29.2, 29.4, 29.7, 32.2, 41.1, 52.6, 63.5, 66.9, 162.7; HRMS: calculated m/z 731.5772, 733.5759 $[M–Br^–]^+$, 326.3291 $[M–2Br^–]^{2+}$; observed m/z 731.5776, 733.5761 $[M–Br^–]^+$, 326.3290 $[M–2Br^–]^{2+}$.

4A.4.3 *In-vitro* antibacterial assay

Bacteria were grown for 6 h grown (about 10^9 CFU/mL). The bacterial cultures were diluted to give ~10^5 CFU/mL in the respective media/buffer and used for determining antibacterial efficacy. Most of the final compounds were water soluble at room temperature. Some

compounds were solubilized in water by heating. Stock solutions were prepared by serial dilution of the compounds using sterilized Milli-Q water. The aqueous solution of serial dilutions (50 μL) were added to the wells of 96 well plate followed by the addition of about 150 μL of bacterial suspension (10^5 CFU/mL). The plates were then incubated at 37 °C for 24 h in shaker incubator. The optical density (OD) of the bacterial suspension was recorded using TECAN (Infinite series, M200 pro) Plate Reader at 600 nm. Each concentration had triplicate values and the whole experiment was repeated at least twice and the antibacterial efficacy was determined by taking the average of triplicate OD values for each concentration and plotting it against concentration. A glycopeptides antibiotic vancomycin and a lipopeptide colistin, were used in this study to compare the antibacterial efficacy.

4A.4.4 Antibacterial activity in presence of human plasma

Bacteria (*S. aureus*) was grown similarly as mentioned earlier and finally diluted in the respective media to give 10^5 CFU/mL. Fresh human blood donated by a healthy donor was centrifuged at 3500 rpm for 5 min. The plasma, which was separated from the blood cells, was carefully collected. The test compound **13f** was dissolved in sterile water at a concentration of 2000 μg/mL. This was further diluted 2-fold into the plasma so that the final concentration of compound **13f** was 1000 μg/mL in 50% plasma. Three such test samples were pre-incubated in 50% plasma for 0 h, 3 h and 6 h respectively at 37 °C. Then 50 μL of the above solutions was added to wells of a 96-well plate and 150 μL of the bacterial suspension (10^5 CFU/mL) was added to wells containing the test samples in 50% plasma. The plate was then incubated for 24 h at 37 °C and antibacterial efficacy of the test compound was determined as described above.

4A.4.5 Antibacterial activity in complex mammalian fluids

Blood (sodium heparin as anticoagulant) was donated by a healthy human donors. Plasma was isolated by centrifugation of the blood at 3500 rpm for 5 min as mentioned above. Serum was obtained by using SST^{TM} II Advance serum tube (BD vacutainer) (Ref. 367956) containing human blood and then centrifuging the blood at 3500 rpm for 5 min. Methicillin-resistant *S. aureus* (MRSA) was grown similarly as above at nutrient broth for 6 h to give ~ 10^9 CFU/mL. Finally, MRSA was diluted in minimum essential medium (MEM) and mixed with the mammalian systems individually in a way to give 10^5 CFU/mL in 50% serum, 50% plasma, and 50% blood supplemented with 50% MEM. The test compound **13f** was dissolved

in sterile water at a concentration of 4000 μg/mL. This was further diluted 2-fold and then 50 μL of the solutions was added to wells of a 96-well plate. Bacterial suspension (150 μL, 10^5 CFU/mL) in 50% serum, 50% plasma and 50% blood was added individually to the wells containing the test solutions. The plates were then incubated for 24 h at 37 °C and antibacterial efficacy of the test compound was determined by plating the bacterial suspension (20 μL) directly from the wells onto nutrient agar plate. The agar plates were incubated at 37 °C for 24 h and colonies were observed to determine the minimum bactericidal concentration (MBC) (the minimum concentration at which the compound killed all the bacterial cells).

4A.4.6 Mechanism of action

4A.4.6.1 Cytoplasmic membrane depolarization assay

The 6 h grown bacteria (midlog phase) were harvested (3500 rpm, 5 min), washed in a mixture of 5 mM glucose and 5 mM HEPES buffer (pH = 7.2) (1:1) and resuspended in a mixture of 5 mM HEPES buffer, 5 mM glucose and 100 mM KCl solution (1:1:1) to give ~10^8 CFU/mL. Bacterial suspension (150 μL) was added to wells of a 96-well plate (Black plate, clear bottom with lid). Then 8 μM of 3, 3′-dipropylthiadicarbocyanine iodide ($diSC_35$) (50 μL) was added to the wells containing bacterial suspension and pre-incubated for 30 min for *S. aureus* and 60 min for *E. coli* (additional 50 μL of 200 μM of EDTA was also added in case of *E. coli*). After the incubation, fluorescence was measured for about 8 min at every 2 min interval at an excitation wavelength of 622 nm (slit width: 10 nm) and emission wavelength of 670 nm (slit width: 5 nm). Then, the bacterial suspensions were transferred to another well-plate containing 10 μL of 840 μg/mL of biocides and fluorescence intensity was monitored similarly for another 12 min. A control experiment was performed by treating the preincubated bacterial and dye solution only with Milli-Q water (10 μL).

4A.4.6.2 Membrane permeabilization assay

Bacteria (*S. aureus* and *E. coli*, midlog phase) of were harvested (3500 rpm, 5 min), washed, and resuspended in a mixture of 5 mM glucose and 5 mM HEPES buffer (pH = 7.2) (1:1). Bacterial suspension (150 μL) was added to wells of a 96-well plate (Black plate, clear bottom with lid). Then 10 μM of propidium iodide (PI) (50 μL) was added to the wells containing bacterial suspension and pre-incubated for 30 min for *S. aureus* and 60 min for *E. coli*. After the incubation, fluorescence was measured for about 8 min at every 2 min

interval at excitation wavelength of 535 nm (slit width: 10 nm) and emission wavelength of 617 nm (slit width: 5 nm). Then, the bacterial suspensions were transferred to another well-plate containing 10 μL of 840 μg/mL of biocides and fluorescence intensity was monitored similarly for another 12 min. A control experiment was performed by treating the preincubated bacterial and dye solution only with Milli-Q water (50 μL).

4A.4.7 Biofilm disruption assay

Glass cover slips were sterilised by dipping them in ethanol and then drying in flame. The sterilised cover slips were placed in the wells of a 6-well plate. Bacteria (6 h grown) were then diluted to ~10^5 CFU/mL in nutrient medium supplemented with 1% glucose and 1% NaCl for *S. aureus* and M9 medium supplemented with 0.5% glycerol and 0.02% casamino acid for *E. coli* respectively and were added to the wells containing cover slips (2 mL). The well plate was then incubated under stationary conditions at 37 ˚C for about 24 h for *S. aureus* and 72 h for *E. coli* respectively. After incubation, medium was removed and planktonic bacteria were carefully washed once with PBS (pH = 7.4). Cover slips containing biofilms were then placed into the wells of another 6-well plate and 2 mL of test compound **3b** dissolved in the above respective media (at 32 μg/mL) was added to the wells containing the cover slips with already established bacterial biofilm. The plate was then allowed to incubate under stationary conditions at 37 ˚C for 24 h. Only 2 mL of the respective media was used as negative control. After 24 h, medium was discarded and cover slips were washed with PBS. Then trypsin-EDTA solution (100 μL) was added to the wells containing treated and non-treated cover slips to dissolve the biofilm matrix. Bacterial count was performed by serially diluting the suspension (10-fold dilution) and then plating on nutrient agar plates. Bacterial colonies grown on the plate after 24 h were counted and viability of the cell within the matrix was expressed as $\log_{10}$ (CFU/mL). For imaging via CLSM, cover slips were stained with green fluorescent dye SYTO 9 (5 μM, 10 μL) and imaged using a confocal laser-scanning microscopy (Zeiss 510 Meta Confocal Microscope).

4A.4.8 Toxicity assay

4A.4.8.1 Hemolytic assay

Studies on human subjects were performed according to the guidelines approved by Institutional Bio-Safety Committee (IBSC) at Jawaharlal Nehru Centre for Advanced Scientific Research (JNCASR). Blood was donated by a healthy human donor and red blood

cells (RBCs) were isolated from the heparinised blood. The cells were then washed twice and finally resuspended in PBS (5 vol%). Cell suspension (150 μL) was then added to solutions of serially diluted small molecules taken in wells of a 96-well plate (50 μL). Two controls were prepared, one without the compounds (only 50 μL water) and the other with 0.1 vol% solution of Triton X-100 (TX, 50 μL). The plate was then incubated at 37 °C for 1 h. Next, cells were centrifuged at 3500 rpm for 5 minutes. Supernatant from the wells (~100 μL) was then transferred to a new 96-well plate and absorbance of the supernatant was recorded at 540 nm. Percentage of hemolysis was calculated as $(A–A_o)/(A_{total}–A_o)\times100$, where A is the absorbance for the test samples, A_o is the absorbance for the wells contained only water and RBC suspension , and A_{total} the absorbance of fully lysed cells (wells with TX), all at 540 nm.

4A.4.8.2 Cytotoxicity assay

Human embryo kidney (HEK 293) cells were seeded onto the wells of a tissue culture treated 96-well plate (~10^4 cells/well). The seeded cellswere then treated with the small molecules at 32 μg/mL. 0.1% Triton-X was used as positive control whereas untreated cells were used as negative controls. Both the treated and untreated cells were then washed once with PBS and stained with calcein AM (2 μM, Fluka) and propidium iodide (PI, 4.5 μM) (Sigma-Aldrich) for 15 min at 37 °C under 5% CO_2-95% atmosphere (50 μL of 1:1 calcein AM:PI). Finally, the cells were washed with PBS to remove the excess dyes and images were captured with a 20X objective in Leica DM2500 fluorescence microscope using. A band-pass filter for calcein AM at 500-550 nm and a long-pass filter for PI at 590-800 nm were used while imaging.

4A.4.8.3 *In-vivo* toxicity

The numbers of animals per groups, dosage of polymers etc. were used according to the Organisation for Economic Cooperation and Development (OECD) Guidelines for the Testing of Chemicals (OECD 425). BALB/c mice (female, 6-8 weeks, 18-21 g) were used for the systemic toxicity studies. Mice were divided into control and test groups with 5 mice per group. Various doses (5.5, 17.5, 55 and 175 mg/kg) of the test polymer, HTCC, were used as per the OECD guidelines. Solution (200 μL) of small molecular biocide in sterilized saline was injected into each mouse (5 mice per group) via intra-peritoneal (i.p.) and subcutaneous (s.c.) routes of administration. All the mice were monitored for the next 14 days after the administration of the polymer. During the observation period of 14 days, onset abnormality

was monitored for all the tested amounts. Saline (200 μL) was used as control. For the acute dermal toxicity studies, fur of the mice was shaved 24 h before the experiment. To the shaved region, the biocide solution (40 μL) of different concentration was applied. Adverse effect on the skin of mice was monitored along with mortality rate for 14 days post treatment.

4A.4.9 *In-vivo* activity

BALB/c mice (female, 6 to 8 weeks old, 18-22g) were used for the experiments. First, the mice were rendered neutropenic (~100 neutrophils/mL) by injecting two doses of cyclophosphamide intraperitoneally (i.p.) (150 mg/kg first dose and 100 mg/kg after 3 days of the first dose). After 24 h of the second dose, mice were anesthetized by ketamine-xylazine (40 mg/kg ketamine and 2 mg/kg) mixture i.p.) The back of each mouse was clipped and then shaved using a razor. While shaving, a wound (reddening and glistening of the skin without bleeding) was introduced on the dorsal midline of each mouse. To the wound site, methicillin-resistant *S. aureus* (MRSA) was added drop wise (~10^9 cells/mL, 20 μL) and allowed to dry to ensure that the bacteria remained within the shaved area. Mice (n = 5 in each group) were left for 24 h of the infection to allow to form the biofilm. Next, mice were treated with **3b** (40 mg/kg), fusidic acid (40 mg/kg), and ReliHeal-Silver ointment (Carboxymethylcellulose IP 3.5% w/w, colloidal silver nanoparticle 50 ppm, Reliance Life Advances, India) (200 mg/kg) at the site of infection. The compound solution was carefully added and spread on the entire wound surface to avoid any loss of solution. The dosages were continued for four days (per day one dose). One group of mice (n = 5) were left untreated and used as a control. Mice were sacrificed 18 h after the last dose using isofluorane and the infected skin was collected, homogenized, diluted and plated for cell counting. The bacterial count was finally expressed as log CFU/g of the tissue collected and expressed as mean ± standard error of mean. For imaging the skin tissue by SEM, some portion of skin tissue samples were fixed in formalin for 24 h, dried subsequently using 30, 50, 70, 90 and 100% ethanol. The skin tissue samples were then adhered on silicon wafers; sputter coated with gold and imaged by Quanta 3D FEG, FEI field emission scanning electron microscope.

4A.4.10 Resistance development studies

Propensity of developing bacterial resistance was studied against both *S. aureus* and *E. coli* following earlier protocol as described in the section 2A.4.9 of Chapter 2A.

BIBLIOGRAPHY

1. Taubes, G. The bacteria fight back. *Science* **2008**, *321*, 356-361.
2. Walsh, C. Molecular mechanisms that confer antibacterial drug resistance. *Nature* **2000**, *406*, 775-781.
3. Alekshun, M. N.; Levy, S. B. Molecular mechanisms of antibacterial multidrug resistance. *Cell* **2007**, *128*, 1037-1050.
4. Bush, K. *et al.* Tackling antibiotic resistance. *Nature Rev. Microbiol.* **2011**, *9*, 894-896.
5. Hall-Stoodley, L.; Costerton, J. W.; Stoodley, P. Bacterial biofilms: From the natural environment to infectious diseases. *Nature Rev. Microbiol.* **2004**, *2*, 95-108.
6. Flemming, H. C.; Wingender, J. The biofilm matrix. *Nature Rev. Microbiol.* **2010**, *8*, 623-633.
7. Fux, C. A.; Costerton, J. W.; Stewart, P. S.; Stoodley, P. Survival strategies of infectious biofilms. *Trends Microbiol.* **2005**, *13*, 34-40.
8. Hoiby, N.; Bjarnsholt, T.; Givskov, M.; Molin, S.; Ciofu, O. Antibiotic resistance of bacterial biofilms. *Int. J. Antimicrob. Agents* **2010**, *35*, 322-332.
9. Davies, D. Understanding biofilm resistance to antibacterial agents. *Nat. Rev. Drug Discov.* **2003**, *2*, 114-122.
10. Joseph, R.; Naugolny, A.; Feldman, M.; Herzog, I. M.; Fridman, M.; Cohen, Y. Cationic pillararenes potently inhibit biofilm formation without affecting bacterial growth and viability. *J. Am.Chem.Soc.* **2016**, *138*, 754-757.
11. Peng, L. L.; DeSousa, J.; Su, Z. M.; Novak, B. M.; Nevzorov, A. A.; Garland, E. R.; Melander, C. Inhibition of Acinetobacter baumannii biofilm formation on a methacrylate polymer containing a 2-aminoimidazole subunit. *Chem.Comm.* **2011**, *47*, 4896-4898.
12. Huigens, R. W.; Richards, J. J.; Parise, G.; Ballard, T. E.; Zeng, W.; Deora, R.; Melander, C. Inhibition of Pseudomonas aeruginosa biofilm formation with bromoageliferin analogues. *J. Am. Chem.Soc.* **2007**, *129*, 6966-6967.
13. Reymond, J. L.; Bergmann, M.; Darbre, T. Glycopeptide dendrimers as Pseudomonas aeruginosa biofilm inhibitors. *Chem. Soc. Rev.* **2013**, *42*, 4814-4822.
14. Stewart, P. S.; Costerton, J. W. Antibiotic resistance of bacteria in biofilms. *Lancet* **2001**, *358*, 135-138.
15. Zasloff, M. Antimicrobial peptides of multicellular organisms. *Nature* **2002**, *415*, 389-395.
16. Hancock, R. E. W.; Sahl, H. G. Antimicrobial and host-defense peptides as new anti-infective therapeutic strategies. *Nature Biotechnol.* **2006**, *24*, 1551-1557.
17. Bionda, N.; Pastar, I.; Davis, S. C.; Cudic, P. In vitro and in vivo activities of novel cyclic lipopeptides against Staphylococcal biofilms. *Protein Pept. Lett.* **2014**, *21*, 352-356.
18. Luca, V.; Stringaro, A.; Colone, M.; Pini, A.; Mangoni, M. L. Esculentin(1-21), an amphibian skin membrane-active peptide with potent activity on both planktonic and biofilm cells of the bacterial pathogen Pseudomonas aeruginosa. *Cell. Mol. Life Sci.* **2013**, *70*, 2773-2786.
19. Chen, Y. X.; Mant, C. T.; Farmer, S. W.; Hancock, R. E. W.; Vasil, M. L.; Hodges, R. S. Rational design of alpha-helical antimicrobial peptides with enhanced activities and specificity/therapeutic index. *J. Biol.Chem.* **2005**, *280*, 12316-12329.
20. Porter, E. A.; Wang, X. F.; Lee, H. S.; Weisblum, B.; Gellman, S. H. Antibiotics - Non-haemolytic beta-amino-acid oligomers. *Nature* **2000**, *404*, 565-565.

21. Radzishevsky, I. S.; Rotem, S.; Bourdetsky, D.; Navon-Venezia, S.; Carmeli, Y.; Mor, A. Improved antimicrobial peptides based on acyl-lysine oligomers. *Nature Biotechnol.* **2007**, *25*, 657-659.
22. Tang, H. Z.; Doerksen, R. J.; Tew, G. N. Synthesis of urea oligomers and their antibacterial activity. *Chem. Comm.* **2005**, 28, 1537-1539.
23. Goodman, C. M.; Choi, S.; Shandler, S.; DeGrado, W. F. Foldamers as versatile frameworks for the design and evolution of function. *Nat.Chem.Biol.* **2007**, *3*, 252-262.
24. Uppu, D. S. S. M.; Konai, M. M.; Baul, U.; Singh, P.; Siersma, T. K.; Samaddar, S.; Vemparala, S.; Hamoen, L. W.; Narayana, C.; Haldar, J. Isosteric substitution in cationic-amphiphilic polymers reveals an important role for hydrogen bonding in bacterial membrane interactions. *Chem. Sci.* **2016**, *7*, 4613-4623.
25. Wiegand, I.; Hilpert, K.; Hancock, R. E. W. Agar and broth dilution methods to determine the minimal inhibitory concentration (MIC) of antimicrobial substances. *Nat. Protoc.* **2008**, *3*, 163-175.
26. Haug, B. E.; Stensen, W.; Kalaaji, M.; Rekdal, O.; Svendsen, J. S. Synthetic antimicrobial peptidomimetics with therapeutic potential. *J. Med. Chem.* **2008**, *51*, 4306-4314.
27. Konai, M. M.; Ghosh, C.; Yarlagadda, V.; Samaddar, S.; Haldar, J. Membrane active phenylalanine conjugated lipophilic norspermidine derivatives with selective antibacterial activity. *J. Med. Chem.* **2014**, *57*, 9409-9423.
28. Ge, Y.; MacDonald, D. L.; Holroyd, K. J.; Thornsberry, C.; Wexler, H.; Zasloff, M. In vitro antibacterial properties of pexiganan, an analog of magainin. *Antimicrob. Agents Chemother.* **1999**, *43*, 782-788.
29. Kim, H.; Jang, J. H.; Kim, S. C.; Cho, J. H. De novo generation of short antimicrobial peptides with enhanced stability and cell specificity. *J. Antimicrob. Chemother.* **2014**, *69*, 121-132.
30. Hu, Y.; Amin, M. N.; Padhee, S.; Wang, R. E.; Qiao, Q.; Bai, G.; Li, Y.; Mathew, A.; Cao, C.; Cai, J. Lipidated peptidomimetics with improved antimicrobial activity. *ACS Med. Chem. Lett.* **2012**, *3*, 683-686.
31. Makovitzki, A.; Avrahami, D.; Shai, Y. Ultrashort antibacterial and antifungal lipopeptides. *Proc. Natl. Acad. Sci. U S A* **2006**, *103*, 15997-16002.
32. Konai, M. M.; Adhikary, U.; Samaddar, S.; Ghosh, C.; Haldar, J. Structure-activity relationship of amino Acid tunable lipidated norspermidine conjugates: disrupting biofilms with potent activity against bacterial persisters. *Bioconjugate Chem.* **2015**, *26*, 2442-2453.
33. Konai, M. M.; Ghosh, C.; Yarlagadda, V.; Samaddar, S.; Haldar, J. Membrane active phenylalanine conjugated lipophilic norspermidine derivatives with selective antibacterial activity. *J. Med. Chem.* **2014**, *57*, 9409-9423.
34. Ghosh, C.; Manjunath, G. B.; Konai, M. M.; Uppu, D. S. S. M.; Hoque, J.; Paramanandham, K.; Shome, B. R.; Haldar, J. Aryl-alkyl-lysines: agents that kill planktonic cells, persister cells, biofilms of MRSA and protect mice from skin-infection. *PLoS One* **2015**, *10*, e0144094.

Chapter 4B

Dextran-Based Antibacterial Hydrogels for Extended Release of Cationic Small Molecular Biocide and Eradication of Topical Biofilms

Abstract

Chapter 4B *describes development of antibacterial and antibiofilm hydrogels capable of eradicating established topical bacterial biofilms without causing substantial skin toxicity. The hydrogels were developed using dextran methacrylate (Dex-MA), a highly biocompatible and photopolymerizable polymer, and the optimised cationic biocide (**13f**) developed in Chapter 4A. The antibacterial gels were prepared by UV polymerization of Dex-MA along with the small molecular biocide (**13f**) thus allowing direct loading of the biocide with desired and controlled amounts. The biocide impregnated gels displayed strong antibacterial activity (7-log reduction) against both drug-sensitive (Staphylococcus aureus and E. coli) and drug-resistant bacteria such as methicillin-resistant Staphylococcus aureus (MRSA). The gels were shown to release the biocide for an extended period of time and killed bacteria by releasing the biocide into the surroundings (till day 5). Moreover, the gels not only eradicated established bacterial biofilms in-vitro but also shown to be highly efficacious in clearing established MRSA biofilm in a mice model of superficial skin infection. Notably, excellent skin compatibility was observed for all the hydrogel formulations in different animal models (high lethal dose in rat model, no skin sensitization in guinea pig model and negligible skin irritation in rabbit model). The biocompatible antibiofim gels developed in this chapter might hold great promise to be used in removing bacterial biofilms and treating topical infections.*

Publication based on this work

1. Hoque, J. *et al.* Direct synthesis of dextran-based antibacterial hydrogels for extended release of biocides and eradication of biofilms. Manuscript submitted.

4B.1 Introduction

Skin, the largest organ among all the protecting systems in human, is a natural barrier to the interior body parts which protects internal organs from pathogens and dehydration.[1] However, being the most exposed organ towards external environment it is very much prone to get infections. Among various microorganisms, bacterial skin infections are the most common and known to affect about 155 million people and occur in about 600 million people worldwide.[2,3] Upon adherence to the skin, bacteria form a complex community known as biofilm.[4,5] Notably biofilms, covered by self-secreted exo-polymeric substances (EPS), are inherently immune to the host defence systems.[6] Moreover antibiotics, commonly used to prevent and treat infections, are known to be ineffective against biofilms.[7,8] Commercially used topical antimicrobials (e.g., fusidic acid based ointments, lipopeptides based gels, silver containing gels, etc.) are limited individually or collectively due to bacterial resistance development, narrow-spectrum activity, toxicity towards mammalian cells and inability to eradicate established bacterial biofilms *in-vivo*, etc.[9,10]

Synthetic cationic antibacterial scaffolds that disrupt biofilm matrix are considered as potential candidates because of their ability to act on encased bacteria by dissipating the membrane-integrity and stall bacterial resistance development.[11-15] However, the impact of the amphiphilic biocides in antibiofilm treatment is largely limited due to lack of a suitable delivery system that can ensure sustained and effective release of the biocides locally. Hydrogel, a highly cross-linked three dimensional matrix, is considered as an important platform to deliver antibacterial agents and to combat biofilm-associated infections. Because of the porous, moist and robust structure, hydrogels not only act as potent wound healing materials but also act as ideal delivery vehicles to combat infections.[16-20] This chapter therefore deals with the development of biocide-encapsulated antibacterial and antibiofilm hydrogel capable of eradicating topical bacterial biofilms.

In chapter 4A, highly effective and non-toxic small molecular biocides with excellent biofilm eradicating ability have been developed. In chapter 4B, biocompatible antibacterial and antibiofilm hydrogels were developed via direct loading of the optimised biocide developed in Chapter 4A in a highly cross linked network of dextran methyacrylate (Dex-MA). Cross-linked dextran is known to be biocompatible towards mammalian cells and capable of mitigating bacterial biofilm thus making it a promising material to be used as delivery vehicle in infection treatment and prevention.[21,22] The photo-polymerization of dextran methacrylate was performed along with the biocide which allowed direct

encapsulation of the molecule into the gel with known amounts. The hydrogels were shown to release the biocide gradually over time and kill bacteria including drug-resistant MRSA. Eradication of bacterial biofilms was observed when the established bacterial biofilms were treated repeatedly with the biocide upon release from the hydrogel. Also, one of the most active gels was shown to annihilate preformed MRSA biofilm in a murine model of superficial infection. Notably, the gels displayed excellent skin biocompatibility in various animal models.

4B.2 Results and discussion

4B.2.1 Synthesis and characterization of hydrogels

In order to prepare the gel, first dextran methacrylate (Dex-MA) was synthesized by reacting dextran with glycidyl methacrylate to introduce the UV-polymerizable methacrylate group into the polymer (Scheme 4B.1 and Figure 4B.1A).[23]

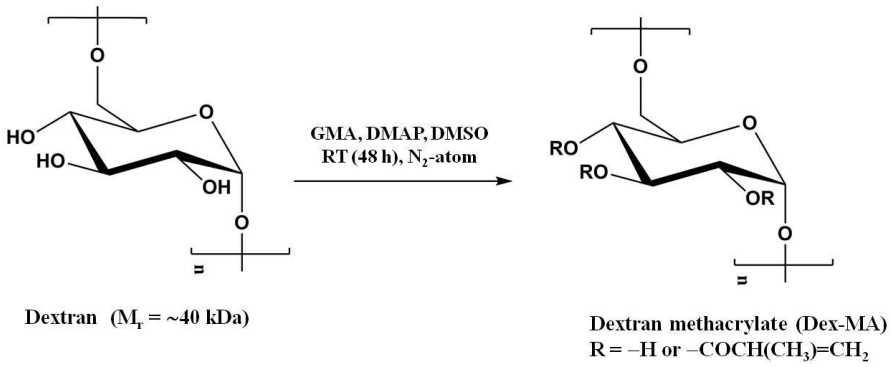

Scheme 4B.1: Synthesis of dextran methacrylate from dextran. GMA, glycidyl methacrylate; DMAP, 4-dimethylaminopyridine and DMSO, dimethyl sulfoxide.

Introduction of the methacrylate moiety was confirmed by FT-IR as the spectrum clearly revealed the appearance of peaks at around 1712 cm^{-1} and 1637 cm^{-1} corresponding to stretching frequencies of C=O bond in ester group and C=C bond of methacrylate group respectively. However, the stretching broad band (3100 cm^{-1}-3600 cm^{-1}) of the hydroxyl group was not reduced significantly due to incorporation of the methacrylate moiety into the dextran thus indicating that a large number of unreacted free hydroxyl groups are still present in dextran methacrylate. The degree of methacrylation in Dex-MA was calculated by ^{1}H NMR and found to be ~15%. Since the biocide-loaded hydrogels were prepared by photo-polymerization at 365 nm, first stability of the optimised cationic biocide developed in Chapter 4A (**13f**, Figure 4B.1B) was studied under UV using high performance liquid

chromatography (HPLC) and also by determining the antibacterial activity before and after UV treatment. HPLC traces of the molecule showed appearance of no other peaks except the molecular peak at 14.6 min even after irradiating the molecule for 1 h at 365 nm. Further, the molecule was shown to retain its activity (minimum inhibitory concentration, MIC = 1-2 μg/mL) after the UV-treatment which demonstrated that the molecule is indeed stable under UV.

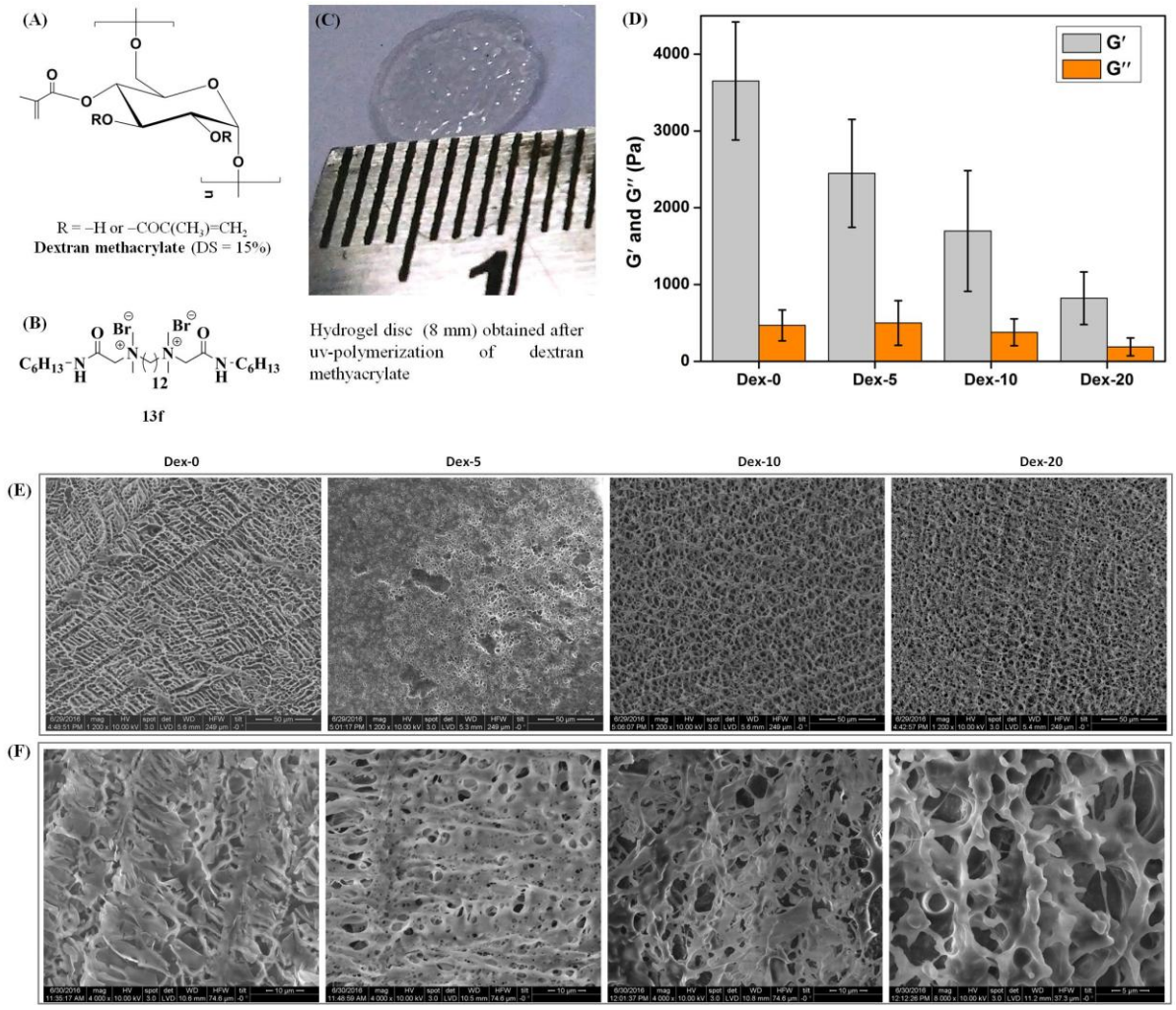

Figure 4B.1: Synthesis and characterization of gels. (A) Structures of dextran methyacrylate; (B) structures of the amphiphilic small molecular biocide; (C) hydrogel disk obtained after UV polymerization of dextran methacrylate (Dex-10); (D) storage (G′) and loss modulii (G″) of the hydrogels prepared by varying the amount of the biocide. Morphology of the hydrogel via scanning electron microscopy (E) top view and (F) cross sectional view.

Next, hydrogels were prepared using the Dex-MA solution (200 mg/mL in 0.2 M sodium citrate buffer of pH 5.2) in presence of a photo-initiator 2-hydroxy-4′-(2-hydroxyethoxy)-2-methylpropiophenone (0.05% w/v) with or without the biocides (Figure

4B.1C). Four different formulations were made wherein the biocide content was varied from 0 wt% to 20 wt% (Dex-0: gel with 0 wt% biocide; Dex-5: gel with 5 wt% biocide; Dex-10: gel with 10 wt% biocide and Dex-20: gel with 20 wt% biocide, all with respect to Dex-MA). With respect to the overall hydrogel weight, the biocide content were 0.8 wt%, 1.6 wt% and 3.2 wt% receptively in Dex-5, Dex-10 and Dex-20 gels (These values are indeed very low amounts suitable for clinical applications). The fact that photo-polymerization due to UV-cross-linking led to the consumption of the double bonds of Dex-MA was revealed by FT-IR spectra.

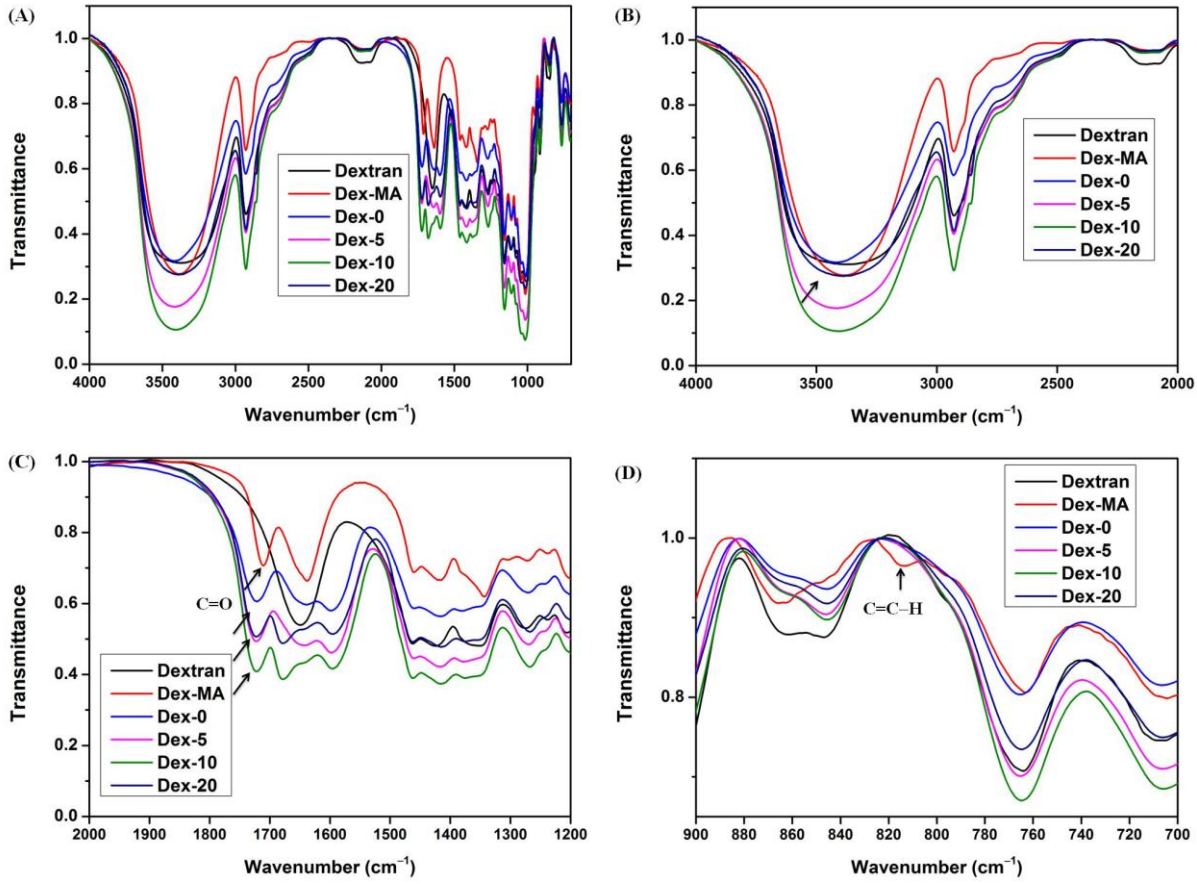

Figure 4B.2: FT-IR spectra of precursor polymer or dried dextran hydrogels. (A) Full spectra from 4000 to 500 cm^{-1}; (B) expanded spectra from 2000 to 1200 cm^{-1}; (C) expanded spectra from 2000 to 1200 cm^{-1}; (D) expanded spectra from 900 to 700 cm^{-1} of dextran, all for Dex-MA, Dex-0 xerogel, Dex-5 xerogel, Dex-10 xerogel and Dex-20 xerogel repectively.

Notably, a decrease in peak intensity in the double bonds regions at 1637 cm^{-1} (C=C stretching) and 814 cm^{-1} (C=C–H bending) was observed for all the hydrogel formulations (Figure 4B.2). As the native dextran has a peak at around 1649 cm^{-1}, the peak at 814 cm^{-1} (C=C–H bending) was used as an indicator of double bond consumption of dextran

methacrylate. The complete reduction of the 814 cm^{-1} peak in the IR spectra of the xerogels suggested that all the double bonds were fully consumed during hydrogel preparation. Further, presence of the carbonyl group in all the gels at 1724 cm^{-1} (C=O stretching) suggested that the carbonyl group during photo-irradiation remained intact. Moreover, shifting of the peak towards higher wave number (from 1712 cm^{-1} to 1724 cm^{-1}) also suggested the disappearance of conjugated double bond (Figure 4B.2). The viscoelastic properties of the gels were evaluated by rheologic determination of both storage modulus (G′) and loss modulus (G″) as a function of frequency. G′ value of Dex-0 gel at equilibrium was found to be 3652 ± 765 Pa. G′ Values of Dex-5, Dex-10 and Dex-20, on the other hand, were found to be 2448 ± 702 Pa, 1698 ± 786 Pa and 823 ± 342 Pa respectively (Figure 4B.1D). Thus excessive loading of the biocide into the gel matrix reduced the stiffness of the materials. This could be due to the fact that when considerable amount of biocide is included, the rigidity of those gels gets affected. The above results further indicated that for a particular degree of methacrylation in Dex-MA, the physical properties of the gels as well as the extent of biocide-loading can be tuned with precursors' concentration and stoichiometric ratio. However, it should be noted that the G′ values of the gels were found to be linear over the entire frequency sweep and always higher than G″ thus indicating formation of elastic and hydrogel network (Figure 4B.1D). The surface and cross sectional morphologies of the gels were visualized by field emission scanning electron microscopy (FESEM). All the gels when imaged after freeze drying and gold sputtering showed highly interconnected structures and pores thereby indicated porous yet extensively cross-linked polymer network due to photo-polymerization (Figure 4B.1E). The pore sizes were found to increase with the increase in biocide content.

4B.2.2 *In-vitro* antibacterial activity

The hydrogels were cut into 8 mm disks and were used for biological activity evaluation (Figure 4B.1C). The disks have weight of ~69.3±6.1 mg for Dex-0, 69.9±3.4 mg for Dex-5, ~70.8±5.8 mg for Dex-10 and ~71.3±6.5 mg for Dex-20 respectively while the weight of dried disk was ~13.4±1.2 mg for Dex-0, 13.6±1.4 mg for Dex-5, ~14.8±1.8 mg for Dex-10 and ~14.8±0.8 mg for Dex-20 respectively. The amount of the biocide present Dex-5, Dex-10 and Dex-20 hydrogel disks were approximately 1.0 ± 0.2 mg, 1.9 ± 0.2 mg and 4.1 ± 0.4 mg respectively. The antibacterial activity of all the gel formulations was evaluated by adding the

gel disks directly into bacterial suspension followed by determining the bacterial cell viability.

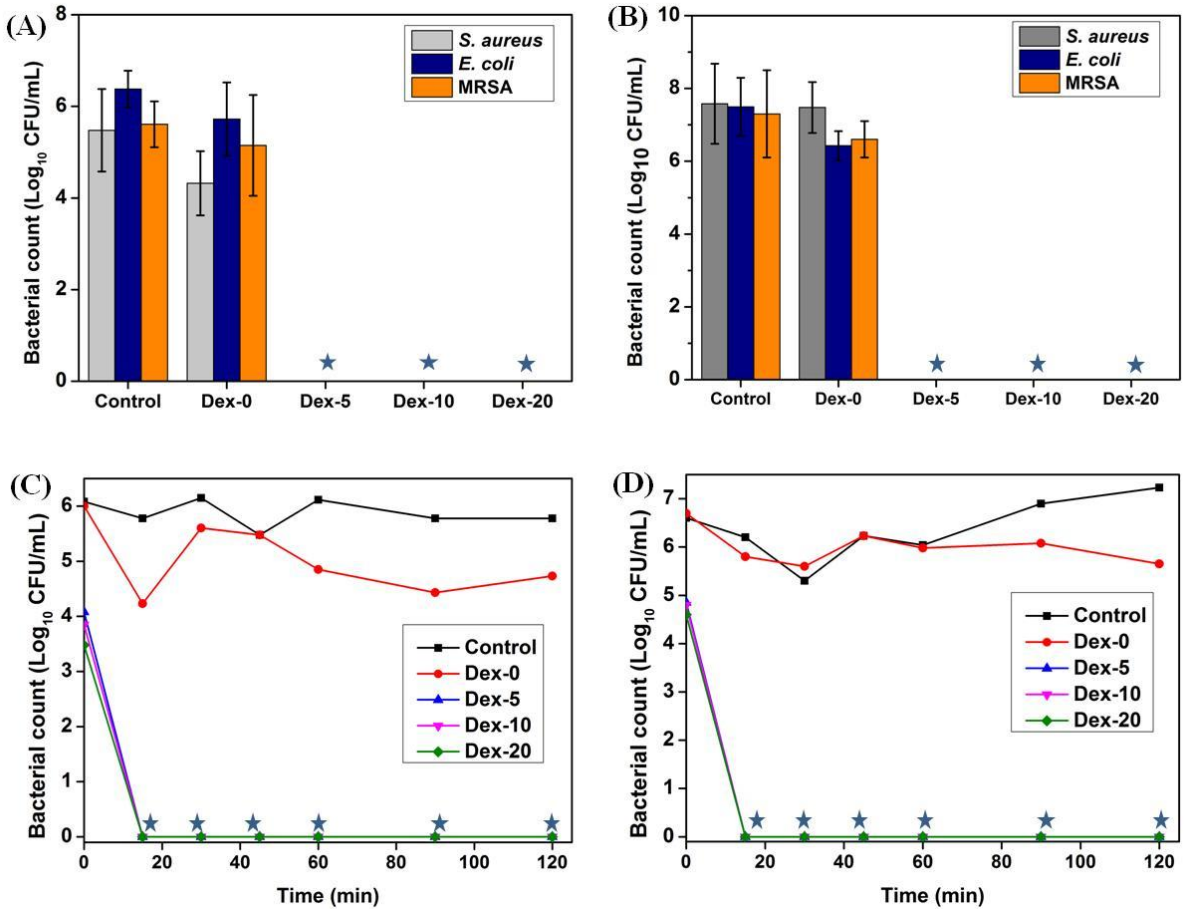

Figure 4B.3: *In-vitro* antibacterial activity of the hydrogels. (A and B) Cell viability after 2 h incubation with the gel against different bacteria with an initial ~10^6 CFU/mL and ~10^8 CFU/mL. (C and D). Antibacterial kinetics of the gels against *S. aureus* and *E. coli* respectively. Star represents less than 50 CFU/mL.

All the gels loaded with the biocides were found to kill both *S. aureus* and *E. coli* completely within 2 h when incubated with ~10^6 CFU/mL of bacteria (Figure 4B.3A). Notably, 100% killing observed by all three biocide loaded gels against MRSA, one of the most common bacteria that cause skin infections. The gels showed a reduction of 5.4 ± 0.9 log *S. aureus*, 6.3 ± 0.4 log *E. coli* and 5.6 ± 0.5 log MRSA respectively after 2 h (Figure 4B.3A). Interestingly, the gel showed complete killing even when the initial bacterial amount was high (~10^8 CFU/mL). The gels reduced 7.5 ± 1.1 log *S. aureus*, 7.1 ± 0.8 log *E. coli* and 7.3 ± 1.2 log MRSA respectively after 2 h (Figure 4B.3B). It should be mentioned that the dextran gel without any biocide showed negligible antibacterial activity thereby indicated that

it is the biocide which killed the bacteria. Further, when the disks were crushed and plated for bacterial count, disk of Dex-5, Dex-10 and Dex-20 did not show any bacterial colony whereas Dex-0 showed considerable amount of bacterial colonies thereby indicated bacterial adherence to the gel's surface. Interestingly, all the gels (Dex-5, Dex-10 and Dex-20) were found to kill both *S. aureus* and *E. coli* within 15 min of incubation when studied for killing kinetics thus suggested that these materials have rapid rate of killing necessary for an immediate and effective control of infections (Figure 4B.3C and D).

4B.2.3 Release kinetics and extended antibacterial activity

The release kinetics of the biocide and extended antibacterial activity were studied for the hydrogels via both chemical and biological assays. First, % of release of biocide from the gels at different time intervals was determined by immersing the disk in water and then evaluating the biocide content in water using high-performance liquid chromatography (HPLC). It was observed that 72-78% of the biocide got released from all the gels (Dex-5, Dex-10 and Dex-20) within 24 h. However, the gels were shown to release the biocide till day 5. Notably, more than 99% biocide was released by day 5 from all the gel formulations (Figure 4B.4A). The fact that these gels release biocide for an extended period of time was further studied by immersing the disk in nutrient medium (1 mL) and then determining the antibacterial activity with the released medium collected at different time intervals (the medium was exchanged after 24 h every day). Notably, the medium inactivated MRSA till day 5 (Figure 4B.4B-D). It should be mentioned that the released amounts of the biocide from the gels were higher than the MIC values (1-2 μg/mL) which allowed these gels to display antibacterial activity for this extended period of time. When tested, the released medium failed to display antibacterial activity at day 6 suggesting almost complete depletion of the biocide from the gels. Importantly, when the hydrogel disks after removing from the medium were placed in bacterial suspension (0.5 mL, ~10^5 CFU/mL), the disks were also shown to kill bacteria upto day 5 which indicated retention of the biocide within the matrix for the same period of time. It should be mentioned that the gel showed an initial burst release of the biocide probably due to non-covalent loading into the matrix. However, it is known that an initial 6 h of the post-contamination is very crucial to prevent infection and also an initial burst release is required to provide sufficient therapeutic amount for the eradication of infections associated with biofilms. The above results thus suggested that the biocide encapsulated gels would be potential candidates in combating infections.

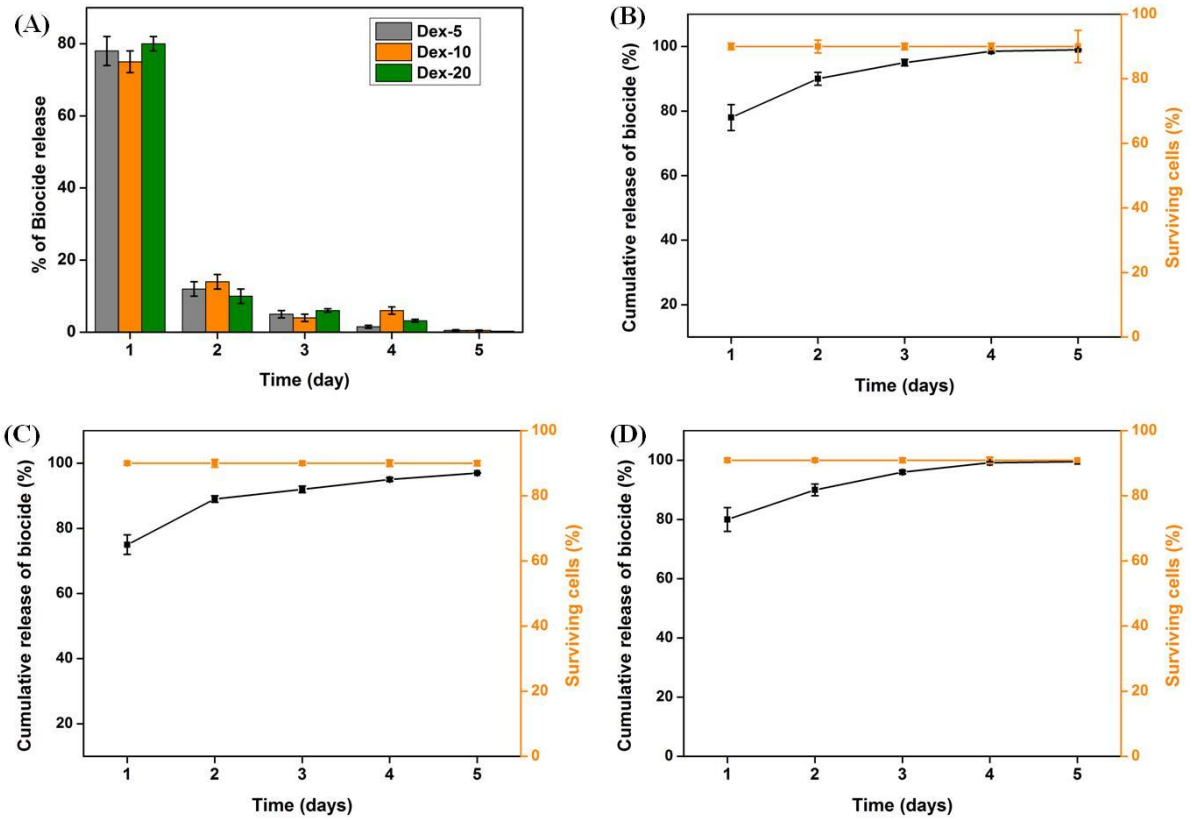

Figure 4B.4: Release kinetics and antibacterial activity of the biocide by the gels. (A) Release kinetics of the biocide from the hydrogels determined via HPLC; (B-D) extended release of the antibacterial biocide and bacterial cell viability determined with the released medium from the gels (B: Dex-5, C: Dex-10 and D:Dex-20) against MRSA.

4B.2.4 *In-vitro* antibiofilm activity

The antibiofilm efficacy of the gels was then evaluated by studying the ability of the released medium to eradicate established bacterial biofilms.[19] First matured biofilms of both *S. aureus* and *E. coli* were formed on glass cover slips (*S. aureus* biofilm was formed for 24 h whereas *E. coli* biofilm was formed for 72 h) and were characterized by confocal laser scanning electron microscopy (CLSM). The CLSM images showed highly thick and dense biofilm of ~15 μm for *S. aureus* and ~11 μm for *E. coli* respectively (Figure 4B.5A and D). The hydrogel disks of Dex-10 were first immersed in the respective biofilm media (nutrient broth supplemented with 1% glucose and 1% NaCl for *S. aureus* and M9 broth supplemented with 0.5% glycerol and 0.02% casamino acid for *E. coli* respectively, 1 mL). Then the media were collected after 24 h and replaced with the fresh medium. When the preformed biofilms were treated with the released medium collected at day 1, only mono-layered bacteria with 2-3 μm of thickness was observed on the glass surface for both *S. aureus* and *E. coli* (Figure 4B.5B and E). Further, when the same surfaces were treated with the medium collected at day 2,

negligible amount of cells for both the bacteria were observed (Figure 4B.5C and F). Notably, similar effects were observed for the drug-resistant bacteria MRSA. The hydrogel completely eradicated established MRSA biofilm when treated successively with the released medium from Dex-10 at day 1 and day 2 (Figure 4B.5G-I). The above facts thus indicated that the dextran based hydrogels developed in this chapter by impregnating the cationic biocide are capable of eradicating established bacterial biofilms and could be used in clinical settings to combat biofilm associated infections.

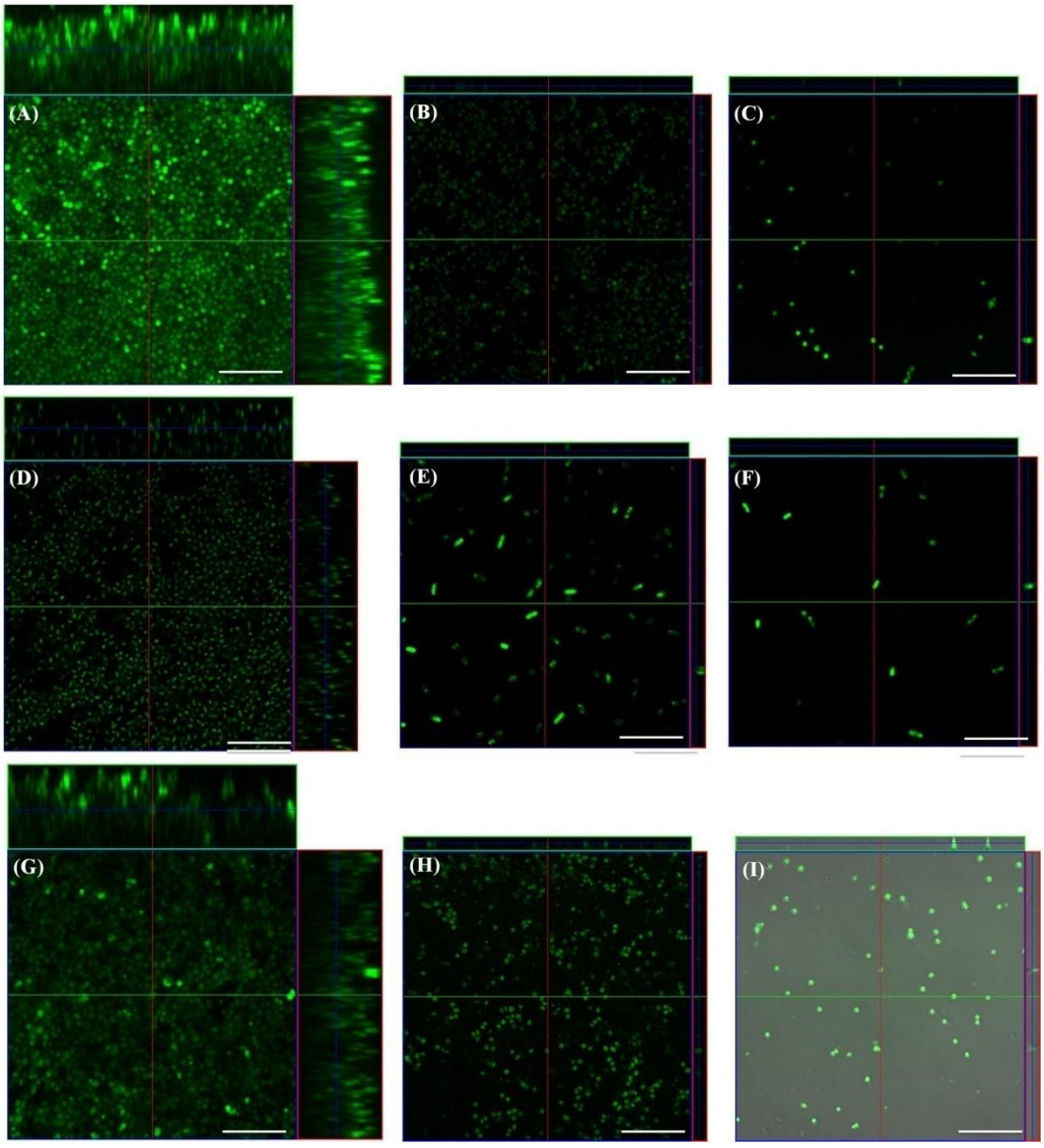

Figure 4B.5: *In-vitro* antibiofilm efficacy of the hydrogels. Biofilm disrupting ability of the hydrogel (Dex-10) determined with the released biocide from the gel at different time intervals. (A, D and G) Biofilm grown on non-coated glass slide; (B, E and H) treated biofilm with the released medium of day 1 and (C, F and I) treated biofilm with the released medium of day 2. (A-C) for *S. aureus*; (D-F) for *E. coli* and (G-I) for MRSA respectively. Scale bar 10 μm.

4B.2.5 *In-vivo* toxicity

One of the major concerns that largely limits the application of the topical antimicrobials into clinics is the toxicity towards mammalian tissues. To evaluate the toxic effects of **13f** loaded dextran-based hydrogels, acute dermal toxicity in rat, skin sensitization in guinea pigs and skin irritation in rabbits were performed. Acute dermal toxicity evaluated in rats by applying the gel on the rat's skin. Interestingly, the 50% lethal doses (LD_{50}) were found to be greater than 2000 mg/kg for all the hydrogels (Dex-5, Dex-10 and Dex-20). Further no adverse skin reaction was observed for the gels at the same dose. Moreover, none of the gels showed any adverse effects on the skin in guinea pigs studied by applying the gels repeatedly on pig's skin. Further, when the gels were applied on rabbit's skin topically, no erythema/oedema formation was observed for all three gels. However, mild reddening of the skin was observed for Dex-20 whereas Dex-5 and Dex-10 showed no such effect. The dextran based gels specially Dex-5 and Dex-10 thus displayed high skin compatibility in all three animal models demonstrating their potential to be used as topical antimicrobials.

4B.2.6 *In-vivo* activity

One of the major limitations of the currently used topical antimicrobials is their relatively poor activity under *in-vivo* conditions. In general, commonly/commercially used topical antimicrobials lack the ability to eradicate established bacterial biofilms in real scenario, which largely limits their applications. Herein, we evaluated the efficacy of the non-toxic gels (Dex-5 and Dex-10) in eliminating preformed biofilm in a murine model of superficial MRSA infections. First, a wound was created on the back of neutropenic mice, infected with MRSA (20 μL, 10^9 CFU/mL) and then allowed to form biofilms for about 24 h. The infected skin was then treated with the hydrogels (Dex-5 and dex-10) topically (two disks were placed at the site of infection on either side of the dorsal midline and then fixed with adhesive bandage). The gels were kept for four days (Figure 4B.6A). Finally, the animals were sacrificed and the skin tissues from the infected area were collected. Notably, Dex-5 treated skin samples showed 3.1 log (> 99.9%) reduction and Dex-10 treated skin samples showed 4.8 log (> 99.99%) reduction of MRSA compared to the non-treated skin samples. In contrary, the commercially used silver nanoparticle containing gel (ReliHeal) showed only 2.4 log MRSA reduction even after applying everyday for 4 days (Figure 4B.6B). This indicated the biocide loaded dextran hydrogels were highly effective in clearing topical infections.

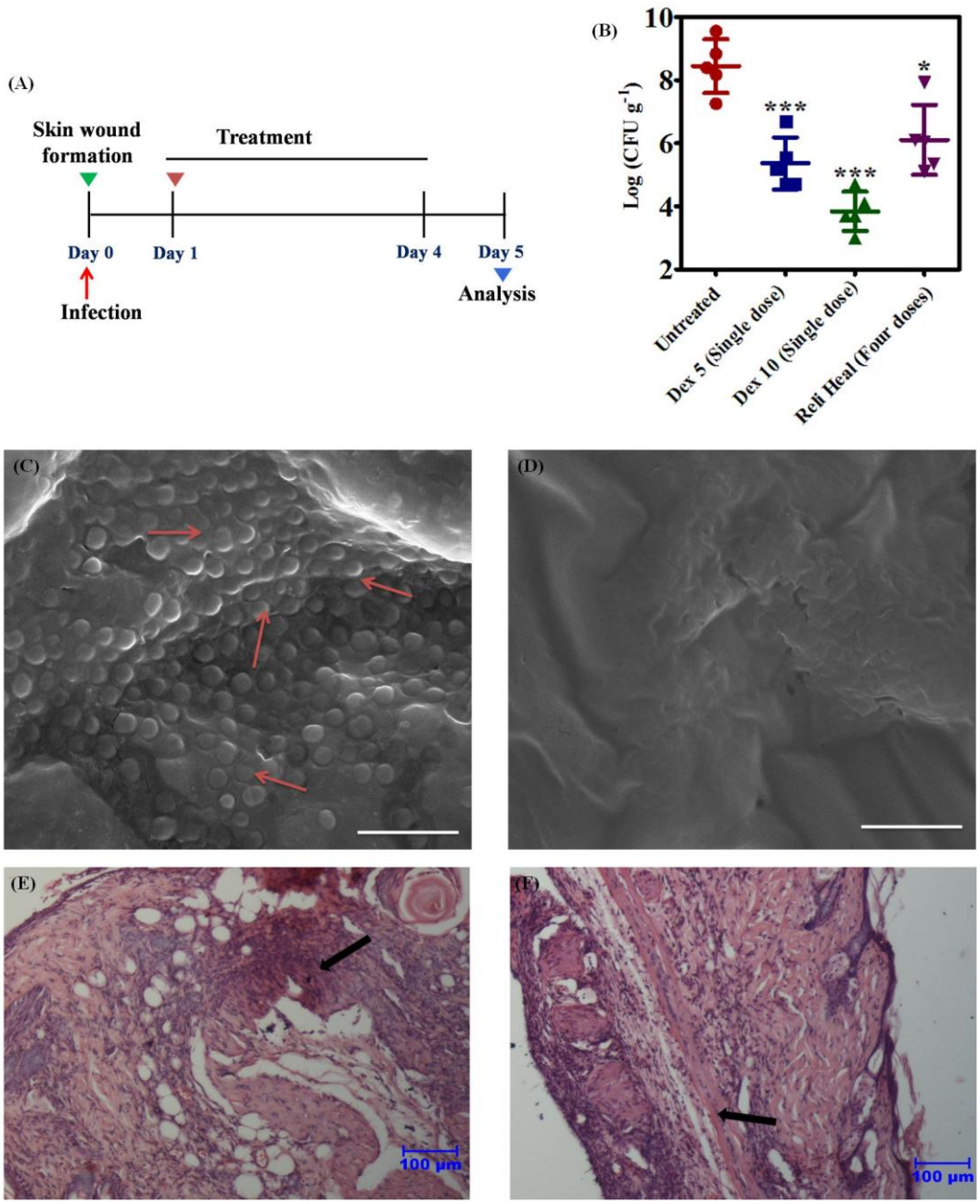

Figure 4B.6: *In-vivo* activity and antibiofilm efficacy of biocide loaded gel (Dex-10). (A) Experimental plan of murine model of superficial MRSA biofilm formation and treatment after mice were made neutropenic; (B) bacterial count of the treated and non-treated skin tissue samples from mice; p values (*) are <0.0001, <0.0001 and 0.005 for Dex-5-, Dex-10- and ReliHeal- treated samples. Scanning electron microscopy images of the skin samples C) after 24 h of infection; (D) after 4 days of treatment with Dex-10 respectively. Mice skin histopathology of (E) infected non-treated skin tissue and (F) treated skin tissue after haematoxylin and eosin staining.

The ability of the hydrogels to eradicate established biofilm under complex *in-vivo* conditions was further studied by imaging the skin samples via FESEM. The SEM image showed the formation of a thick and dense layer of MRSA on the skin indicating the survival

as well as biofilm formation in infected mice (Figure 4B.6C). Notably, the treated skins showed no detectable number of bacteria on the skin surfaces (Figure 4B.6D). The activity was further evaluated by studying the histopathological responses from the skin tissues. MRSA infected untreated skin tissue showed severe infiltration of inflammatory cells mainly neutrophils in dermis layer (arrow), with damage to the cells and appearance of cell nest with keratin layer. Gel treated skin tissue, on the other hand, showed normal appearance of skin with thin layer of epidermis, hair follicles, sweat glands with mild infiltration of inflammatory cells in the dermis layer (arrow). These results thus demonstrated the ability of the non-toxic hydrogels to eliminate established bacterial biofilms such as MRSA biofilm.

4B.3 Conclusion

In summary, photo-polymerized dextran based antibacterial and antibiofilm hydrogels *in-situ* via direct loading of a non-toxic cationic biocide was developed. The gels displayed strong antibacterial activity (100% killing) against both Gram-positive and Gram-negative bacteria including drug-resistant MRSA. Notably, the gels were shown to release the biocide for an extended period of time (till day 5) and shown to kill the bacteria by releasing the active molecule into the surroundings. The gels not only eradicated established bacterial biofilms *in-vitro* but also were shown to be highly efficacious in clearing established bacterial biofilm in superficial skin infection. Further, the gels showed excellent skin compatibility in various animal models. The antibacterial and antibiofim hydrogels developed in this chapter could be used to deliver active antimicrobial topically hence might hold promise in treating topical infections.

4B.4 Experimental section

4B.4.1 Materials and instrumentation

Dextran, glycidyl methacrylate, 4-dimethylaminopyridine (DMAP), 1,12-dibromododecane, 1-aminohexane, bromoacetyl bromide, anhydrous DMSO were purchased from Sigma-Aldrich and used as received. Anhydrous potassium carbonate (K_2CO_3), anhydrous sodium sulphate (Na_2SO_4), phosphorous pentaoxide (P_2O_5), dichloromethane, acetonitrile (CH_3CN) and anhydrous diethylether were purchased from Spectrochem, India and were of analytical grade. CH_3CN was dried over P_2O_5 and stored over activated molecular sieves (4 Å). Nuclear magnetic resonance (NMR) spectra were recorded using Bruker AMX-400 spectrometer in suitable deuterated solvents (400 MHz for ^1H NMR and 100 MHz for ^{13}C NMR). Fourier

transform infrared (FT-IR) spectra were recorded on an IFS66 V/s spectrometer (Bruker) using KBr pellets. High performance liquid chromatography (HPLC) was performed in SPD-M20A Shimadzu instrument. For optical density (OD) and fluorescence measurements, Tecan Infinite Pro series M200 microplate reader was used. *Staphylococcus aureus* (MTCC 737) and *Escherichia coli* (MTCC 443) were obtained from MTCC (Chandigarh, India). Methicillin-resistant *Staphylococcus aureus* (MRSA) (ATCC 33591), were purchased from ATCC (Rockville, MD, USA). Bacterial growth media and agar were provided by HIMEDIA, India. Studies on animals were performed in accordance with the protocols approved by the Institutional Animal Ethics Committee (IAEC) at Jawaharlal Nehru Centre for Advanced Scientific Research (JNCASR).

4B.4.2 Synthesis of small molecular biocide

The small molecular biocide (**13f**) was synthesized following the protocol as mentioned in the section 4A.4.8 in Chapter 4A.

4B.4.3 Synthesis of dextran methacrylate (Dex-MA)

Dextran (from Leuconostoc spp., M_r~40 kDa) (5 g, 30.8 mmol) was dissolved in anhydrous DMSO (100 mL) at room temperature under oxygen free nitrogen (OFN) atmosphere. Once the polymer, was dissolved, DMAP (1 g, 8.2 mmol) was added. After 2 h known amount (876 mg, 6.1 mmol) of glycidyl methacrylate was added. The reaction was carried out at room temperature under dark with constant stirring for about 48 h. Finally, the reaction mixture was subjected to extensive dialysis for about 3 days to replace DMSO and other small molecules. The aqueous dialysed solution was then freeze dried and kept at –20 ˚C for further use. The degree of substitution (DS) was determined by ^{1}H-NMR analysis from the ratio of integration of methacrylate proton and C-1 ring proton.

Dex-MA: FT-IR ($\overline{\nu}$): 3200-3600 cm^{-1} (OH str.), 2930 cm^{-1} (CH_2 assym. str.), 1710 cm^{-1} (C=O str.), 1639 cm^{-1} (C=C str.), 815 cm^{-1} (C=C–H ben.); ^{1}H NMR (400 MHz, $CDCl_3$): δ 1.99 (CH_2=CH(CH_3)CO–, 3H), 3.521-4.023 (C2–, C3–, C4–, C5– and C6–H, 7H), 5.01 (C6–H, 1 H), 5.82 (CH_2=CH(CH_3)CO–), 6.24 (CH_2=CH(CH_3)CO–).

4B.4.4 Determination of UV stability of biocide via HPLC

The biocide was first dissolved in water at 10 mg/mL. The solution was divided into four parts wherein 1st part was left without any treatment. The other three parts were subjected to UV-irradiation at 386 nm for 15 min, 30 min and 60 min respectively. All the fractions were

then injected in an HPLC instrument and ran with water-acetonitrile binary solvent solvent system (with 0.1% trifluoroacetic acid) to check the stability of the molecule. The run time was 20 min where at 0 min 100% water was used and gradually % of acetonitrile was increased with a flow rate of 8 mL/min. If the molecule is UV stable, no additional peak should appear in the HPLC trace.

4B.4.5 Minimum inhibitory concentration (MIC)

Minimum inhibitory concentration of the biocide was determined following the protocol as mentioned in the section 4A.4.9 in Chapter 4A.

4B.4.6 Preparation of the hydrogels

Hydrogels with or without biocide were prepared as follows. First, dextran methacrylate (400 mg) was dissolved in 0.2 M sodium citrate buffer (1.8 mL, pH 5.2). Small molecular biocide, on the other hand, was dissolved in varying amount (20, 40 and 80 mg/mL) in an aqueous solution that already contains 0.5 wt% 2-hydroxy-1-[4-(hydroxyethoxy) phenyl]-2-methyl-1-propanone photo-initiator. Then the photo-initiator containing biocide solution (200 μL) was added to the dextran methacrylate solution. The solution was then transferred into a 35 mm petri dish and then photo-polymerized at 365 nm (~5 mW/cm^2) for about 15 min. The gel was cut by using 8 mm biopsy punches to yield disks with 8 mm diameter. For the preparation of dextran based hydrogels without any biocide, the same procedure was followed without any biocide in the photo-initiator solution. The above formulations provided gels with varying amount of biocide content (0%, 5%, 10% and 20%, all with respect to Dex-MA). Gels without any biocide were designated as Dex-0, and the other formulations were designated as Dex-5, Dex-10 and Dex-20 depending on the amount of biocide loading into gel with respect to dextran methacrylate.

4B.4.7 Characterization of the hydrogels

4B.4.7.1 Morphological characterization

Morphologies of the gels were characterized by field emission scanning electron microscopy (FESEM). The hydrogels were prepared in petri dish as mentioned earlier and cut into small circular disks (8 mm diameter). The disks were then freeze-dried to obtain xerogels. These dried gels were then sputter coated with gold before imaging. Both the surface and cross-

sectional morphologies of all the formulation (Dex-0, Dex-5, Dex-10 and Dex-20) were imaged using Quanta 3D FEG, FEI FESEM at 10 kV operating voltage.

4B.4.7.2 Infrared (IR) spectroscopy

Fourier transformed infrared (FTIR) spectra of the polymer, small molecular biocide and all the xerogels were recorded using KBr pellets following the method as described in 4A.4.1 in chapter 4A.

4B.4.7.3 Viscoelastic properties

Viscoelastic properties of the hydrogels were measured using an oscillatory rheometer on the preformed gels using a DHR-2 rheometer (TA Instruments) with 25 mm stainless steel parallel plate geometry. The freshly prepared gels were transferred to the stainless steel plate of the rheometer pre-equilibrated at ~25 ˚C. A gap height of 1.0 mm was maintained between the plates before the measurements. For the equilibration of the gel, first a dynamic time sweep was applied at an angular frequency of 6 rad/s and at 0.2% strain for 10 min. Finally, a frequency sweep from 1 to 100 rad/s with 0.2% strain was used to record the viscoelastic behaviours. The storage modulus (G′) and loss modulus (G′′) were calculated as a function of angular frequency at every point.

4B.4.8 Antibacterial activity of the hydrogel

4B.4.8.1 Antibacterial activity due to direct exposure

Hydrogel disks (8 mm diameter) were placed in the wells of a 48-well tissue culture treated polystyrene plate (TCTP). To the disks, 200 μL of bacterial suspension (~10^6 or 10^8 cells in nutrient media) were added. The plates were the incubated for 2 h at 37 ˚C under constant shaking at 100 rpm. After the incubation, the hydrogel disks were removed, the medium was serially diluted by 10-fold and then plated on suitable agar plate (50 μL). Finally, bacterial colonies were counted for all the hydrogel formulations. Two controls were made wherein in one control no gel disk was added to bacterial suspension and in other control dextran hydrogel devoid of any biocide (Dex-0) was used. Also, the disks after the incubation were washed gently with PBS (2 × 500 μL) to remove any non-adherent bacterial cells. Then the disks were crushed and stirred vigorously in 0.5 mL of PBS. Finally, the suspension was plated and colonies on agar plates were observed.

4B.4.8.2 Antibacterial activity with the released biocide

To assess the long lasting antibacterial efficacy of the biocide loaded hydrogels, gel disks were immersed in 1 mL of nutrient medium with and incubated at 100 rpm at 37 ˚C. At different intervals (after 24 h), the medium was completely removed, and the disks were immersed in the fresh medium. To 450 μL of nutrient medium collected at each time interval, 50 μL of fresh nutrient medium containing ~10^7 CFU/mL bacteria (MRSA) were added. The mixture was then incubated at 37 ˚C for about 24 h. Finally, the OD values of the solutions were recorded. Also the solutions were directly plated to determine the bactericidal effect of the released medium.

4B.4.8.3 Antibacterial kinetics

Hydrogel disks (8 mm diameter) were similarly placed in the wells of a 48-well tissue culture treated polystyrene plate as mentioned previously. To the disks, 200 μL of bacterial suspension (~10^6 bacterial cells in nutrient media) were added. The plates were the incubated at 37 ˚C under constant shaking at 100 rpm. At different time intervals (0, 15, 30, 45, 60, 90 and 120 min), 10 μL of aliquots from the medium was taken out and subjected to 10-fold serial dilution in 0.9 % saline. Then 50 μL of the solutions was plated on agar plates and incubated for 24 h at 37 ºC. The bacterial colonies grown on the agar plates were counted and the reduction in bacterial count was represented in the logarithmic scale, i.e. $\log_{10}$ (CFU/mL) *vs* time (in min).

4B.4.9 Quantification of the biocide-release via HPLC

Hydrogel disks (8 mm) were taken in eppendorf tube and then 1 mL of water was added to the tube. The aqueous solution was replaced every day with water and the process was repeated till 7 days. Finally, release kinetics of the biocide from the gel was determined by HPLC. First, a standard curve of intensity vs known concentration of the biocide was prepared. Absorbance intensity of the biocide released in the aqueous solution was then used to determine the amount released in water at different time interval.

4B.4.10 Biofilm disruption assay

Biofilm disruption assay with the released biocide was performed following the protocol as mentioned in the section 4A.4.7 in Chapter 4A

4B.4.11 Skin toxicity

4B.4.11.1 Acute dermal toxicity (rat model)

Acute dermal toxicity of the gel was determined following OECD guidelines. Briefly, 20 Wistar rats (10 female: 180-220 g; 5 male: 290-420 g; 5 rats in each group) were used for the experiment. All animals were handled in accordance with protocols approved by the Institutional Animal Ethics Committee (IAEC) at the Jawaharlal Nehru Centre for Advanced Scientific Research (JNCASR). The rats were grouped for at least 3 days prior to the test. Approximately 24 hours before the test, fur in the dorsal midline area of each rat was removed (more than 10% of the body area). The rats were then weighed prior to the dosing. The gels were applied topically on the shaved area of each rat and held in contact with the shaved skin using a sterile gauze patch secured via occlusive dressing. The doses were approximately 2000 mg/kg with respect to the body weight of each rat. The gels were exposed for about 24 hours. Finally, any adverse effect on the skin was monitored up to 14 days. Also the body weight of the rats was measured after every 7 days.

4B.4.11.2 Skin sensitization (guinea pig model)

Skin sensitization of the gels was determined using female guinea pigs (albino; 300-500 g). The animals were divided into control (5) and test (10) groups. Each guinea pig from both groups had its fur clipped on the back prior to the test. The hydrogel (0.1-0.2 g) and 0.9% NaCl saline (the negative control, 0.1-0.2 mL) were applied topically on the clipped dorsal region of each guinea pig, and covered by a gauze patch secured with occlusive dressing. After 6 hours of exposure, the gauze patch with dressing was removed, and the residual test material was washed away with water. The skin was carefully dried. The hydrogel and saline were given for three weeks on the first three days in each week. At two weeks after the last treatment, the guinea pigs in both groups were challenged with the hydrogel (0.1-0.2 g), on a shaved naïve region of each animal. The treated area was covered by a gauze patch secured with occlusive dressing. After 6 hour, the gauze patch with dressing was removed. The area was washed with water, and dried carefully. Observation was made at 24 and 48 hours after the completion of the challenge phase. Description and grading of the skin reactions for the erythema formation were conducted according to the Magnusson and Kligman grading scale. The percentage of the guinea pigs showing Magnusson and Kligman grades of 1 or greater in the test and control groups is 0% at 24 and 48 hours after the completion of the challenge phase, demonstrating that no skin sensitization was produced on the guinea pigs.

4B.4.11.3 Skin irritation (rabbit model)

Skin irritation of the gels was determined following earlier report using New Zealand white female/male rabbits. Fur on both sides of three rabbit's spine was clipped approximately 24 h before the test. Each of the clipped areas was about 10 cm × 15 cm. Hydrogel and 0.9% NaCl saline (the negative control) were applied to the four areas on the back of each rabbit: two for the hydrogel and two for the negative control. The doses of the hydrogel and the negative control for each area were 0.5 g and 0.5 mL respectively. Each application site was then covered by a gauze patch secured with occlusive dressing. After 4 hours of exposure, the gauze patch and dressing were removed. The residual hydrogel was removed by washing with water and the skin was dried carefully. Observation was made at 1, 24, 48 and 72 h after the removal of the test and control substances. The erythema/eschar and oedema formation were rated in all the application sites based on the Draize grading scale. The average scores of the erythema and oedema formation were 0 during the 72-hour observation period, proving that the skin irritation response of the hydrogel is negligible.

4B.4.12 *In-vivo* activity and biofilm eradication ability

Female BALB/c mice (6 to 8 weeks old, 18-24 g) were used for the experiments. First, the mice were made neutropenic (approximately 100 neutrophils/mL) by injecting two doses of cyclophosphamide via intraperitoneal injection (first dose was at 150 mg/kg and the second dose at 100 mg/kg after 3 days of the first dose). Next, after 24 h of second dose, mice were anesthetized by ketamine-xylazine mixture. The fur at the back of each mouse was clipped and then shaved using a razor. While shaving, mild wound (reddening of the skin without bleeding) was introduced on the dorsal midline of each mouse. To the wound, MRSA was added (20 μL, ~10^9 cells/mL). Mice (n = 5 in each group) were left for 24 h of the post-infection to allow the biofilm formation. Next, hydrogel disks (8 mm) were applied on the infected area (one disk on either side of the flank) and then covered with sterile gauge patch and secured with occlusive dressing. The gels were kept for about 96 h. One group of mice (n = 5) were left untreated and used as a control. Mice were then sacrificed using isoflurane and the infected skin was collected in saline. Then the skin was homogenized, diluted and finally plated for cell counting. The bacterial count was represented as log CFU/g of the skin tissue collected and shown as mean ± standard error of mean. SEM images of the skin tissues were recorded following the similar procedure as described in the section 4A.4.15 of Chapter 4A.

Histopathological responses were recorded after collecting the tissue sample and fixing it with formalin and then following the similar procedure as described in the section 4A.4.9 of Chapter 4A.

BIBLIOGRAPHY

1. Huang, X.; Zhang, Y.; Zhang, X.; Xu, L.; Chen, X.; Wei, S. Influence of radiation crosslinked carboxymethyl-chitosan/gelatin hydrogel on cutaneous wound healing. *Mater. Sci. Eng. C Mater. Biol. Appl.* **2013,** *33*, 4816-4824.
2. Tognetti, L.; Martinelli, C.; Berti, S.; Hercogova, J.; Lotti, T.; Leoncini, F.; Moretti, S. Bacterial skin and soft tissue infections: review of the epidemiology, microbiology, aetiopathogenesis and treatment. *J. Eur. Acad. Dermatol. Venereol.* **2012,** *26*, 931-941.
3. Vos, T. *et al.* Global, regional, and national incidence, prevalence, and years lived with disability for 301 acute and chronic diseases and injuries in 188 countries, 1990-2013: a systematic analysis for the global burden of disease study 2013. *Lancet* **2015,** *386*, 743-800.
4. Flemming, H. C.; Wingender, J. The biofilm matrix. *Nature Rev. Microbiol.* **2010,** *8*, 623-633.
5. Battin, T. J.; Besemer, K.; Bengtsson, M. M.; Romani, A. M.; Packmann, A. I. The ecology and biogeochemistry of stream biofilms. *Nature Rev. Microbiol.* **2016,** *14*, 251-263.
6. Fux, C. A.; Costerton, J. W.; Stewart, P. S.; Stoodley, P. Survival strategies of infectious biofilms. *Trends Microbiol.* **2005,** *13*, 34-40.
7. Hoiby, N.; Bjarnsholt, T.; Givskov, M.; Molin, S.; Ciofu, O. Antibiotic resistance of bacterial biofilms. *Int. J. Antimicrob. Agents* **2010,** *35*, 322-332.
8. Anderson, G. G.; O'Toole, G. A. Innate and induced resistance mechanisms of bacterial biofilms. *Bacterial Biofilms* **2008,** *322*, 85-105.
9. Davies, J.; Davies, D. Origins and evolution of antibiotic resistance. *Microbiol. Mol. Biol. Rev.* **2010,** *74*, 417-433.
10. Glasser, J. S.; Guymon, C. H.; Mende, K.; Wolf, S. E.; Hospenthal, D. R.; Murray, C. K. Activity of topical antimicrobial agents against multidrug-resistant bacteria recovered from burn patients. *Burns* **2010,** *36*, 1172-1184.
11. Bottcher, T.; Kolodkin-Gal, I.; Kolter, R.; Losick, R.; Clardy, J. Synthesis and activity of biomimetic biofilm disruptors. *J. Am. Chem. Soc.* **2013,** *135*, 2927-2930.
12. Jennings, M. C.; Ator, L. E.; Paniak, T. J.; Minbiole, K. P. C.; Wuest, W. M. Biofilm-eradicating properties of quaternary ammonium amphiphiles: simple mimics of antimicrobial peptides. *ChemBioChem* **2014,** *15*, 2211-2215.
13. Ghosh, C.; Haldar, J. Membrane-active small molecules: designs inspired by antimicrobial peptides. *ChemMedChem* **2015,** *10*, 1606-1624.
14. Duncan, B.; Li, X. N.; Landis, R. F.; Kim, S. T.; Gupta, A.; Wang, L. S.; Ramanathan, R.; Tang, R.; Boerth, J. A.; Rotello, V. M. Nanoparticle-stabilized capsules for the treatment of bacterial biofilms. *ACS Nano* **2015,** *9*, 7775-7782.
15. Jennings, M. C.; Minbiole, K. P. C.; Wuest, W. M. Quaternary ammonium compounds: an antimicrobial mainstay and platform for innovation to address bacterial resistance. *ACS Infect. Dis.* **2015,** *1*, 288-303.
16. Ng, V. W. L.; Chan, J. M. W.; Sardon, H.; Ono, R. J.; Garcia, J. M.; Yang, Y. Y.; Hedrick, J. L. Antimicrobial hydrogels: a new weapon in the arsenal against multidrug-resistant infections. *Adv. Drug Deliv. Rev.* **2014,** *78*, 46-62.
17. Veiga, A. S.; Schneider, J. P. Antimicrobial hydrogels for the treatment of infection. *Biopolymers* **2013,** *100*, 637-644.
18. Zumbuehl, A.; Ferreira, L.; Kuhn, D.; Astashkina, A.; Long, L.; Yeo, Y.; Iaconis, T.; Ghannoum, M.; Fink, G. R.; Langer, R.; Kohane, D. S. Antifungal hydrogels. *Proc. Natl. Acad. Sci. USA* **2007,** *104*, 12994-12998.
19. Li, Y.; Fukushima, K.; Coady, D. J.; Engler, A. C.; Liu, S. Q.; Huang, Y.; Cho, J. S.; Guo, Y.; Miller, L. S.; Tan, J. P. K.; Ee, P. L. R.; Fan, W. M.; Yang, Y. Y.; Hedrick, J. L.

Broad-spectrum antimicrobial and biofilm-disrupting hydrogels: stereocomplex-driven supramolecular assemblies. *Angew.Chem.Int. Ed.* **2013,** *52*, 674-678.
20. Li, P.; Poon, Y. F.; Li, W. F.; Zhu, H. Y.; Yeap, S. H.; Cao, Y.; Qi, X. B.; Zhou, C. C.; Lamrani, M.; Beuerman, R. W.; Kang, E. T.; Mu, Y. G.; Li, C. M.; Chang, M. W.; Leong, S. S. J.; Chan-Park, M. B. A polycationic antimicrobial and biocompatible hydrogel with microbe membrane suctioning ability. *Nat. Mater.* **2011,** *10*, 149-156.
21. De Groot, C. J.; Van Luyn, M. J. A.; Van Dijk-Wolthuis, W. N. E.; Cadee, J. A.; Plantinga, J. A.; Den Otter, W.; Hennink, W. E. In vitro biocompatibility of biodegradable dextran-based hydrogels tested with human fibroblasts. *Biomaterials* **2001,** *22*, 1197-1203.
22. Park, J. Y.; Yeom, J.; Kim, J. S.; Lee, M.; Lee, H.; Nam, Y. S. Cell-repellant dextran coatings of porous titania using mussel adhesion chemistry. *Macromol. Biosci.* **2013,** *13*, 1511-1519.
23. Vandijkwolthuis, W. N. E.; Franssen, O.; Talsma, H.; Vansteenbergen, M. J.; Vandenbosch, J. J. K.; Hennink, W. E. Synthesis, characterization, and polymerization of glycidyl methacrylate derivatized dextran. *Macromolecules* **1995,** *28*, 6317-6322.

Chapter 5A

An Injectable Bioadhesive and Hemostatic Hydrogel with Innate Wound Healing and Antibacterial Properties

Abstract

Chapter 5A *describes the development of a biocompatible injectable hydrogel with inherent bioadhesive, antibacterial, wound healing and hemostatic capabilities suitable in wound sealing and wound infection treatment at the tissue level. The two component injectable hydrogels were prepared in-situ from an antibacterial N-(2-hydroxypropyl)-3-trimethylammonium chitosan chloride (HTCC) and bioadhesive polydextran aldehyde (PDA). The components upon mixing reacted with other via imine bond formation leading to hydrogelation and also reacted with the amine groups of extracellular matrix (ECM) when present thus providing the bioadhesive properties. The gels were shown to be active against both Gram-positive and Gram-negative bacteria including drug-resistant ones such as methicillin-resistant Staphylococcus aureus (MRSA), vancomycin-resistant Enterococcus faecium (VRE) and beta-lactam-resistant Klebsiela pneumoniae. Mechanistic studies revealed that the gels killed bacteria upon contact by disrupting the membrane integrity of pathogen. Importantly, the gels were shown to be efficacious in preventing sepsis in a cecum ligation and puncture (CLP) model in mice. While only 12.5% animal survived in the case of mice with punctured cecam but with no gel on the punctured area (control), 62.5% mice survived when the adhesive gel was applied to the punctured area. The gels were also shown to be effective in facilitating wound healing in rats and ceasing bleeding from a damaged liver in mice. Notably, the gel showed negligible toxicity towards human red blood cells (only 2-3% hemolysis) and no inflammation to the surrounding tissue upon subcutaneous implantation in mice thereby proving it as a safe and effective antibacterial sealant.*

Publication based on this work

1. Hoque, J. *et al.* Chitosan derivatives active against multidrug-resistant bacteria and pathogenic fungi: in vivo evaluation as topical antimicrobials. *Mol. Pharmaceutics* **2016**, *13*, 3578.

2. Hoque, J. *et al.* A biocompatible injectable hydrogel with potent wound healing and antibacterial properties. Manuscript submitted.

5A.1 Introduction

In-situ forming hydrogels that rapidly cross-link with tissues have drawn significant attention as potent bioadhesive materials. These materials are required to carry out a variety of functions such as sealing leaks, i.e., as sealants, stopping unwanted bleeding, i.e., as hemostatic agents, binding tissues together, i.e., as bioadhesives and if possible, facilitating a rapid healing process.[1-6] Considerable efforts have been given to develop naturally derived tissue adhesives, e.g., directly extracted from biological sources (fibrin glues), proteins (gelatine based glues), carbohydrates (alginate) or synthetic-material-based adhesives (cyanoacrylates and poly(ethylene glycol) based bioadhesives, mussel-inspired adhesives) etc.[7-18] However, traditional bioadhesives either normally suffer from relatively poor adhesive strength or higher toxicity.[19-21] Another major concern for the wound repair is the bacterial infections at the wound sites. These infections can reach as high as 41.9% and delay the natural healing process, cause abscess formation and even can lead to life-threatening sepsis.[22,23] The wound site infections therefore impose significant burden to healthcare systems, along with high morbidity and mortality.[24] Since commonly used sealant materials generally lack antibacterial properties, additional treatment of the wound infection is often required. However, systemic antibiotic therapy is limited due to ineffectiveness of antibiotics to reach to damaged tissue because of ruptured vascularity, resistance development by bacteria and toxicity (e.g., nephrotoxicity).

Bioadhesive materials with antibacterial activity have therefore been developed by encapsulating antibacterial agents such as antibiotics, metal nanoparticles, etc. into the matrix.[25-31] However, the materials lack permanent antibacterial activity, cause toxicity and might suffer from uncontrolled and unwanted release of the antibacterial agents. Thus there is a pressing need to develop biocompatible materials with intrinsic antibacterial activity that act can also as strong tissue-adhesives, hemostatic agents and wound healing materials. In the previous chapter, cationic chitosan detivatives, *N*-(2-hydroxypropyl)-3-trimethylammonium chitosan chlorides (HTCC) were developed and shown to be active against human pathogenic bacteria including multi-drug-resistant clinical isolates while being exceptionally compatible towards mammalian cells. Importantly, chitosan is already known to possess potent hemostatic and wound healing properties.[32-34] Further, quaternary chitosan derivatives contain free amine groups which can react with aldehydes groups of a polyaldehyde and subsequently can lead to hydrogelation due to extensive cross linking. Thus upon mixing

HTCC and polyaldehyde solution together via dual barrel syringe is expected to form hydrogel.

Herein, chapter 5B describes successful development of injectable hydrogels incorporated cationic HTCC and polydextran aldehyde (PDA). Effect of HTCC content on gelation and bioadhesive properties were studied to obtain the optimum formulations. Further, broad-spectrum activity against both drug-sensitive and drug-resistant bacteria with negligible toxicity towards mammalian cells was demonstrated *in-vitro*. The gels were shown to possess strong bioadhesive property and cease bleeding from a punctured liver in mice model. Also, the gels were shown to facilitate faster wound healing in a rat model. One of the most active formulations displayed negligible toxicity towards mammalian cells both *in-vitro* and *in-vivo* thereby proving it as safe and potent wound sealing and disinfecting materials.

5A.2 Results and discussion

5A.2.1 Synthesis of and optimization of precursor polymers

The quaternary chitosan derivatives were prepared by reacting chitosan with glycidyltrimethylammonium chloride (GTMAC) under aqueous acidic conditions (Scheme 5A.1).[35] The homogenous conditions favored the substitution of the sugar units of chitosan with selective grafting only onto the primary amine groups (as amines are more nucleophilic than the hydroxyl groups). The introduction of the quaternary ammonium groups onto chitosan and the selective substitution at the primary amine groups were confirmed by ^{1}H and ^{13}C CP-MAS NMR spectroscopy as the spectra showed the presence of the $–N^{+}Me_3$ group in the polymer chain (the presence of $–N^{+}Me_3$ group was confirmed by an intense peak at 3.2 ppm in ^{1}H-NMR spectrum and ~55.3 ppm in ^{13}C CP-MAS spectrum). However, due to overlapping of the signals from the protons of substituent group and the polymeric backbone in ^{1}H-NMR, the degree of substitution (DS with respect to only primary amine groups) was not calculated from the proton spectra. The DS of the polymers was determined by conductometric titration of $Cl^{–}$ ions with $AgNO_3$ solution.[36] Six derivatives were prepared all under identical reaction temperature, time, and concentration of polymer and only by varying the mole ratio of GTMAC to sugar unit of chitosan and the molecular weight of chitosan. Mole ratio of GTMAC to sugar unit was used as 4:1, 6:1 and 8:1, which led to three quaternary polymers from chitosan of a particular molecular weight. Two different molecular weights of chitosan were used (relatively lower molecular weight chitosan of 15 kDa and of higher molecular weight chitosan of 50-190 kDa). The DS values ranged from 0.35 to 0.55.

(Scheme 5A.1). All the derivatives were found to be soluble in water till 40 mg/mL. However, polymers with lower DS were found to form gel at higher concentrations (> 40 mg/mL) and thus heated to obtain clear aqueous solution when needed.

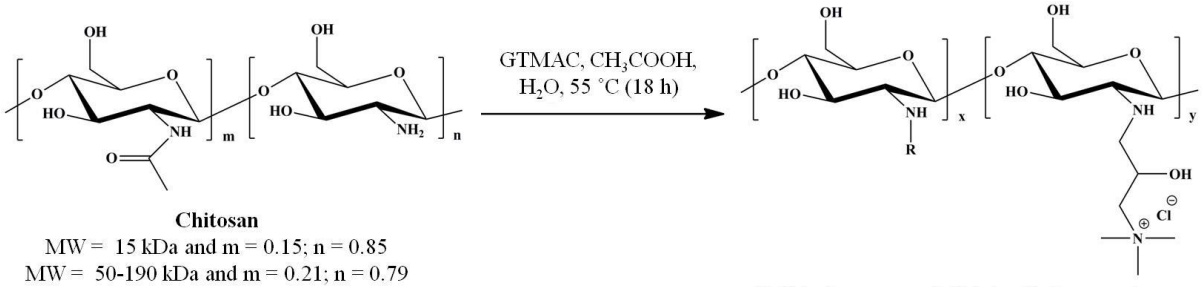

Chitosan
MW = 15 kDa and m = 0.15; n = 0.85
MW = 50-190 kDa and m = 0.21; n = 0.79

***N*-(2-hydroxypropyl)-3-trimethylammonium chitosan chloride (HTCC);**
R = –H and –$COCH_3$;
HTCC 1 (DS = 31, MW of chitosan = 15 kDa)
HTCC 2 (DS = 48, MW of chitosan = 15 kDa)
HTCC 3 (DS = 58, MW of chitosan = 15 kDa)
HTCC 4 (DS = 29, MW of chitosan = 50-190 kDa)
HTCC 5 (DS = 45, MW of chitosan = 50-190 kDa)
HTCC 6 (DS = 54, MW of chitosan = 50-190 kDa)

Scheme 5A.1: Synthesis of quaternary chitosan derivatives. GTMAC = glycidyl trimethylammonium chloride.

The bioadhesive polymer PDA was synthesized by oxidising dextran with sodium periodate ($NaIO_4$). Periodate is known to oxidize the adjacent hydroxyl groups of sugar ring of dextran to dialdehydes, thereby opening the ring to form bisaldehyde derivative (Scheme 5A.2). PDA was characterized by FT-IR, ^{1}H-NMR and ^{13}C-NMR spectroscopy. However, as no detectable signal from aldehyde functionality was observed in ^{1}H NMR due to hemiacetyl formation, the amount of bisaldehyde functionality in PDA was determined by colorimetric method and was found to be 51 ± 1%.[37]

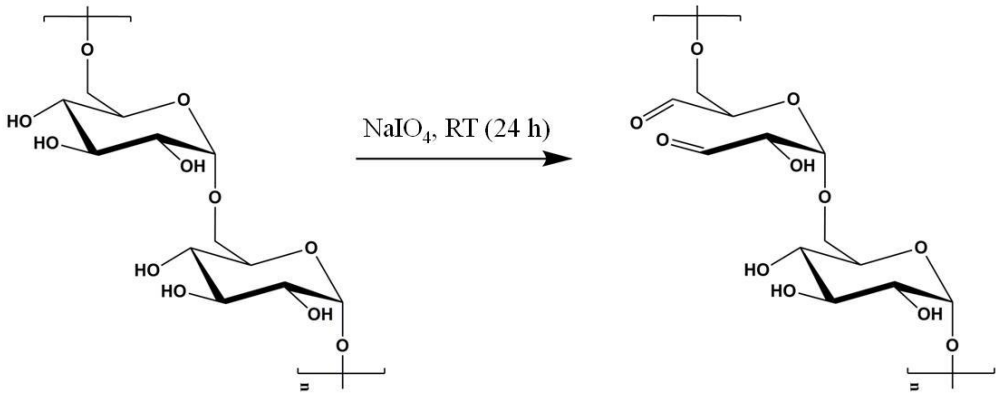

Scheme 5A.2: Synthesis of polydextran aldehyde (PDA) from naturally occurring dextran.

To find out the best polymer among all the chitosan derivatives, antibacterial efficacy of all the polymers was evaluated against a wide spectrum of drug-sensitive bacteria such as *S. aureus*, *E. coli* and *A. baumannii* and drug-resistant bacteria such as methicillin-resistant *Staphylococcus aureus* (MRSA), vancomycin-resistant *Enterococcus faecium* (VRE), *β*-lactam-resistant *K. pneumoniae*. In general, the polymers showed activity against all the bacteria tested (Table 5A.1). The range of minimum inhibitory concentration (MIC) values of the polymers varied from 125-1000 μg/mL. Variation of DS and molecular weight of chitosan derivatives were found to have slight effect on the antibacterial activity. For example, **HTCC 1** (with DS 31% obtained from chitosan of 15 kDa) showed MIC values of 250 μg/mL and 500 μg/mL against *S. aureus* and *E. coli* respectively whereas **HTCC 3** (with DS 58% obtained from chitosan of 15 kDa) showed MIC values of 125 μg/mL and 250 μg/mL against *S. aureus* and *E. coli* respectively. On the other hand, **HTCC 3** (with DS 58% obtained from chitosan of 15 kDa) and **HTCC 6** (with DS 54% obtained from chitosan of 50-190 kDa) showed similar MIC values against both *S. aureus* and *E. coli* (MIC = 125 μg/mL and 250 μg/mL against *S. aureus* and *E. coli* respectively). In general, the polymers were found to be more active towards Gram-positive bacteria than Gram-negative bacteria. For example, the range of MIC values for the polymers were 125-250 μg/mL against Gram-positive bacteria whereas the range of MIC values was 250-1000 μg/mL against Gram-negative bacteria for both low and high molecular weight HTCC polymers (Table 5A.1).

Table 5A.1 Antibacterial activity of cationic chitosan derivatives

Polymer	MIC (μg/mL)						HC_{50} (μg/mL)
	Drug-sensitive bacteria			Drug-resistant bacteria			
	S. aureus	*E. coli*	*P. aeruginosa*	MRSA	VRE	*K. pneumoniae*	
HTCC 1	250	1000	1000	250	250	1000	>10000
HTCC 2	250	500	500	250	250	500	>10000
HTCC 3	125	250	250	125	125	250	>10000
HTCC 4	250	500	500	250	250	500	>10000
HTCC 5	250	250	500	250	250	500	>10000
HTCC 6	125	250	250	125	125	250	>10000

MRSA = Methicillin-resistant *S. aureus* (ATCC 33591); VRE = vancomycin-resistant *Enterococcus faecium* (ATCC 51559); *K. pneumoniae* = beta lactam-resistant *K. pneumoniae* (ATCC 700603); HC_{50} = Hemolytic concentration at which 50% hemolysis occurs

Like drug-sensitive bacteria, the polymers showed similar activity against drug-resistant bacteria such as MRSA, VRE and *K. pneumoniae*. The two most active polymers (**HTCC 3** and **HTCC 6**) displayed MIC values of 125 μg/mL each against MRSA and VRE, and 500 μg/mL each against *K. pneumoniae* respectively (Table 1). The relatively low antibacterial activity of chitosan derivatives could be attributed to the lack of sufficient hydrophobicity.[46] In order to be used in clinical settings, the polymers should be active towards microbial cells and non-active towards mammalian cells. To evaluate the cytotoxic effects of the polymers, hemolytic activity against human red blood (hRBC) cells was evaluated. In general, HC_{50} of all the polymers was found to be more than 10000 μg/mL (Table 5A.1). This showed that these cationic polymers were 40-80 times more selective (selectivity = HC_{50}/MIC) towards bacteria over mammalian cells. Notably, all the polymers showed negligible hemolysis even at 8000 μg/mL (32-64 times more than their MIC values). Thus **HTCC 3** and **HTCC 6** were found to be most active polymers. However, because of the relatively higher aqueous solubility and less viscosity, **HTCC 3** was used in hydrogel preparation.

Table 5A.2 Effect of **HTCC 3** on liver and kidney functions as well as balance of electrolytes in the blood

Clinical biochemistry parameters		Treatment			
		Saline	**HTCC 3** (55 mg/kg) after day 2	**HTCC 3** (55 mg/kg) after day 14	Laboratory range
Liver functions	ALT (IU/L)	62.4 ± 19.1	56.3± 25.2	77.8 ± 29.1	50 ± 27
	AST (IU/L)	80.9 ± 18.7	87.6 ± 15.3	101.4 ± 23.2	100 ± 50
Kidney Function	Creatinine (mg/dL)	0.23 ± 0.07	0.23 ± 0.07	0.41 ± 0.13	0.38 ± 0.12
	Urea nitrogen (mg/dL)	18.4 ± 3.4	21.5 ± 2.9	20.3 ± 5.8	16 ± 7.2
Electrolyte Balance	Sodium ion (mg/dL)	143 ± 1.6	147.4 ± 1.01	151.3 ± 1.64	152.3 ± 17
	Potassium ion (mg/dL)	7.2 ± 0.7	5.7 ± 0.7	6.7 ± 0.3	8.9 ± 1.5
	Chloride ion (mg/dL)	111.5 ± 1.8	110.8 ± 2.2	108.9 ± 1.5	119.3 ± 13.5

The data are expressed as mean ± standard deviation, based on values obtained from 10 mice (n = 10). ALT = alanine transaminase, AST = aspartate transaminase, IU = international unit

Since the injectable hydrogels would be used in tissue level infection, the toxicity of **HTCC 3** was evaluated under in-vivo conditions as well. The cationic polymer showed very

high 50% lethal doses upon both intraperitoneal (i.p.) and subcutaneous (s.c.) administration in mice (LD_{50} = >175 mg/kg). The polymer also shown to cause negligible toxicity to major organs like liver and kidney as the functions of both the organs such as ALT (alanine transaminase), AST (aspartate aminotransferase), creatinine and urea nitrogen, etc. were found to be similar like untreated samples. Also the polymer did not interfere significantly with the balance of blood electrolytes such as sodium, potassium and chloride ions even at 55 mg/kg upon i.p. administration in mice (Table 5A.2).

5A.2.2 Preparation and characterization of hydrogels

PDA with ~50% dialdehyde functionality and **HTCC 3** with 46% quaternary ammonium group, 39% primary amine group and 15% of *N*-acetyl group were used to prepare the hydrogels (Figure 5A.1A and B). Finally, the hydrogels were prepared by mixing phosphate buffered (23.5 mM NaH_2PO_4, 80.5 mM Na_2HPO_4) solution of PDA and aqueous solution of **HTCC 3** either by simple mixing or by mixing with a dual barrel syringe in equal volumes (Figure 5A.1C). Four different gel compositions were made by varying the HTCC content from 1.0-2.5 wt% (1 wt%, 1.5 wt%, 2 wt% and 2.5 wt% respectively) while keeping the amount of PDA constant (2.5 wt%). The average gelation time of the hydrogels (t_{gel}) was found to be 10-60 sec, and was found to decrease with the increase in HTCC content (Table 5A.3). This is because of the greater number of amine groups available for imine bond formation at the higher amount of HTCC. The formation of imine bond upon mixing of PDA and **HTCC 3** was characterized by FT-IR spectroscopy. The spectra clearly revealed the peak corresponding to imine bond at ~1645 cm^{-1}. Not only in wet conditions, the gels showed the presence of imine bond even in the dry state along with the other functional groups (peak at ~1650 cm^{-1} was assigned to the imine group in xerogel). The gels were further characterized by field emission scanning electron microscope (FESEM) to visualize the surface and cross sectional morphologies.[38] All the hydrogels displayed a highly porous and interconnected structure. However, as the HTCC content in the gels increased, the pore size was found to decrease (Figure 5A.1D and E). Due to the interconnected pores which are mutually penetrating, the adhesives are expected to have a good permeability for nutrients and to support cellular growth. The viscoelastic properties such as storage modulus (G′) and loss modulus (G″) of each formulation were determined using pre-formed gels by oscillatory rheometer. As the wt% of HTCC content increases, the mechanical stiffness of the hydrogels increases from 175 Pa to 1528 Pa as observed by the gradual increase in storage modulus (G′)

values (Figure 5A.1F). This indicated that the gel formulations with higher amount of **HTCC 3** formed more imine bonds with the aldehyde groups of PDA, thereby enhancing the stiffness of the materials.

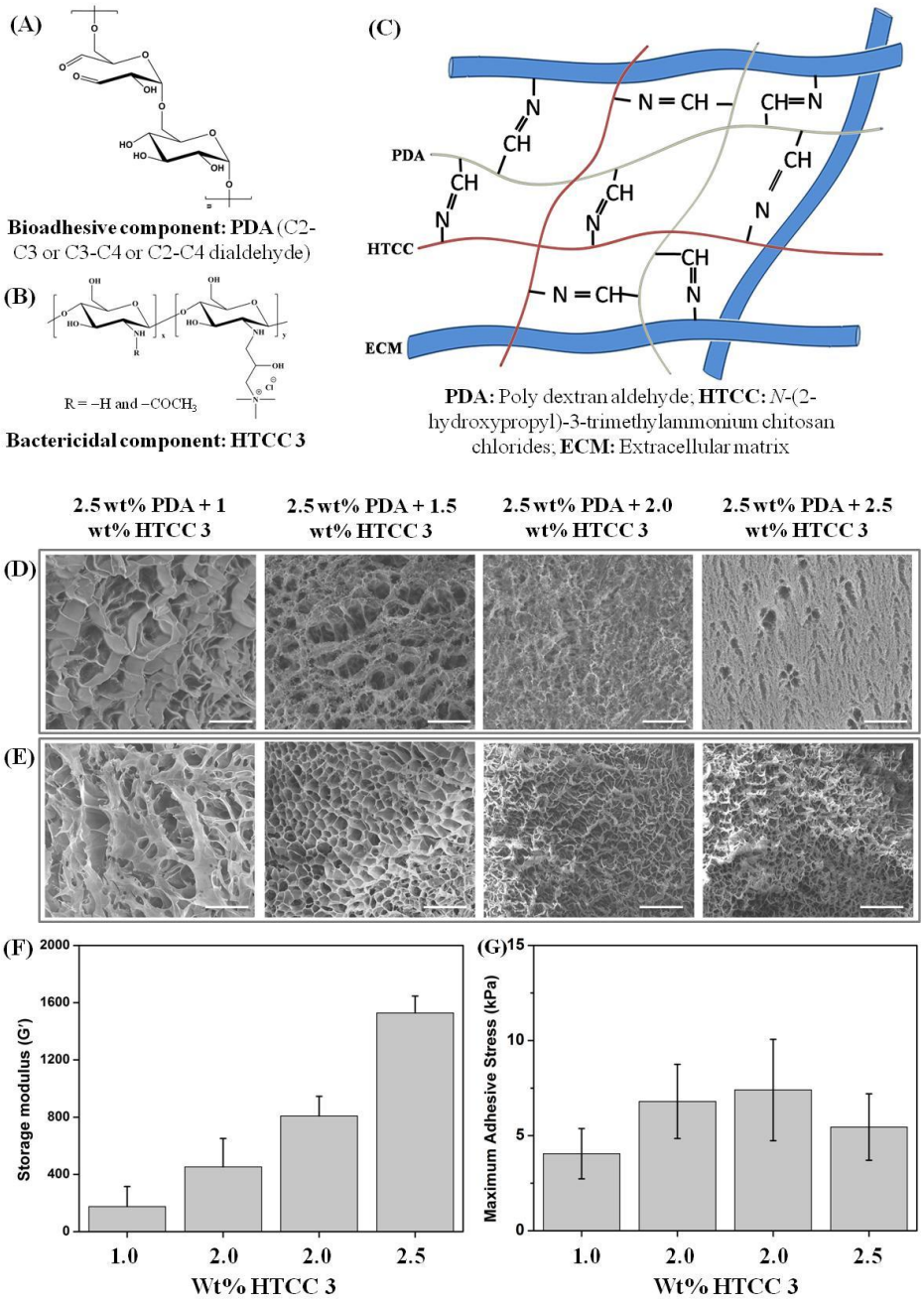

Figure 5A.1: Design, synthesis and characterization of injectable hydrogels. (A and B) The precursors of the hydrogels, PDA and **HTCC 3** as adhesive and antibacterial components respectively. (C) Schematic representation of hydrogel cross-linking designed through imine bond formation of among PDA and **HTCC 3** and extracellular matrix. SEM photographs of freeze-dried hydrogels: (D) surface morphologies of hydrogels with 2.5 wt% PDA and 1, 1.5, 2.0 and 2.5 wt% of **HTCC 3**; (E) cross-sectional morphologies of hydrogels with 2.5 wt% PDA and 1, 1.5, 2.0 and 2.5 wt% of **HTCC 3** respectively. Scale bar 50 μm. (F) Storage modulus of the hydrogels as a function of varying HTCC content keeping the PDA content constant. (G) Adhesive strength of the hydrogels measured using porcine skin.

It should be mentioned that G′ values for all the formulations were found to be much greater than G′′ values thereby indicated strong gel formation for all the combinations.

5A.2.3 Determination of adhesive stress

The adhesive nature of the hydogels was determined by uniaxial loading of the hydrogels adhered between two sections of porcine skin towards epidermis layers followed by lap-shear analysis.[39] The maximum adhesive stress for all the gels was found to vary slightly (4.05-7.4 kPa) (Figure 5A.1G). This is possibly due to the fact that PDA for all the adhesive formulations react strongly and almost invariably with the large content of amine groups of ECM. It was also observed that the bond failure for the gels was mainly cohesive in nature thus suggesting that bonds within the adhesive and antibacterial component fail first than the bonds between the material tissue interfaces.

5A.2.4 *In-vitro* antibacterial activity

The antibacterial activity of the hydrogels was evaluated against both drug-sensitive and drug-resistant bacteria.[40] To the gel surfaces prepared onto the wells of 96-well plate, ~10^5 CFU/mL bacterial suspension (100 μL) was added and optical density was recorded after inoculating for 24 h at 37 ˚C. Wells without the hydrogels but equal volume of bacterial suspension and wells with gels containing equal volume of only media were used as controls. Interestingly, all the hydrogels showed activity against both Gram-positive *S. aureus* and Gram-negative *E. coli* respectively (Figure 5A.2A and B). Moreover, the activity of the adhesives was found to depend on the wt% of the antibacterial component HTCC. The adhesive surfaces of all the formulations showed more than 99% reduction of viable bacteria against *S. aureus* whereas surfaces with 1.0 wt%, 1.5 wt%, 2.0 wt% and 2.5 wt% HTCC content showed 92%, 90%, 95% and 98% reduction against *E. coli* with respect to the untreated surface. Thus hydrogel with 2.5 wt% HTCC content was found to be the most active. Notably, when the gels were challenged with higher amount bacteria (~10^7, 10^8 and 10^9 CFU/mL), the surfaces were still found to inhibit the growth of both *S. aureus* and *E. coli* thereby demonstrated the efficacy of the gel (Figure 5A.2A and B). For example, the gels that contain 1 wt% and 1.5 wt% HTCC were shown to be moderately active (83-90% reduction of viable *S. aureus* and 67-87% reduction of viable *E. coli*) while the gels that contain 2 wt% and 2.5 wt% HTCC were shown to be more effective (93-98% reduction of viable *S. aureus*

and 88-94% reduction of viable *E. coli*) when the gels were challenged with higher amount of bacteria (Figure 5A.2A and B). It should be mentioned that all the gels were shown to be more active against Gram-positive *S. aureus* than Gram-negative *E. coli*.

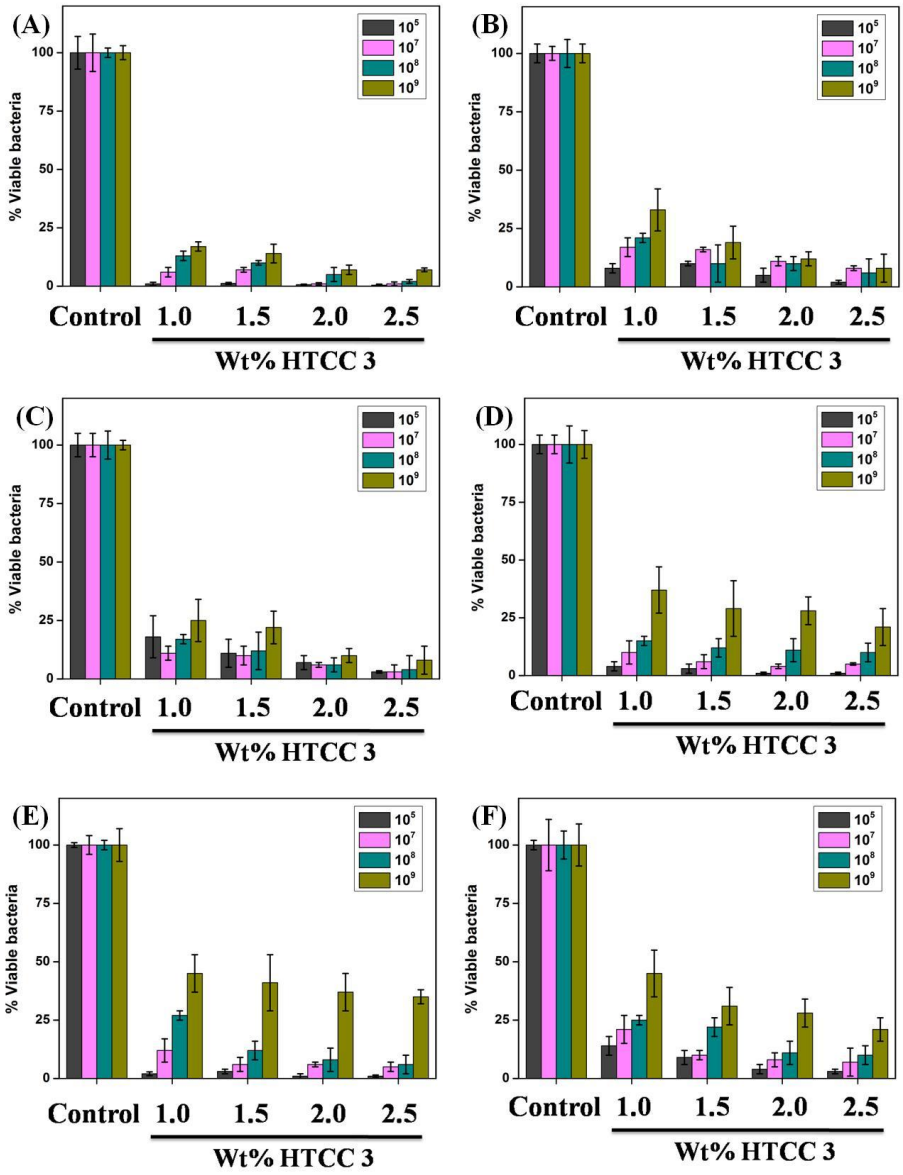

Figure 5A.2: Antibacterial activity of the hydrogels. % of Viable bacteria as evaluated with respect to control for different hydrogels with variable amount of HTCC content after challenging with (A) *S. aureus* and (B) *E. coli*; (C) *P. aeruginosa*; (D) MRSA; (E) VRE and (F) beta-lactam-resistant *K. pneumoniae* respectively.

Importantly, the gels were shown to be active against *P. aeruginosa*-an opportunistic Gram-negative bacterium which causes many nosocomial infections and is generally difficult to treat (Figure 5A.2C). The gels were also found to be active against drug-resistant bacteria such as methicillin-resistant *Staphylococcus aureus* (MRSA), vancomycin-resistant

Enterococcus faecium (VRE) and beta-lactam-resistant *Klebsiella pneumoniae*. The gels inhibited the growth of all three bacteria when challenged with ~10^5 CFU/mL (Figure 5A.2C-F). Notably, these materials were shown to be efficacious in reducing cell viability even at the higher amount of bacteria. For example, one of the most potent gel (2.5 wt% PDA cross linked with 2.5 wt% **HTCC 3**) showed 96%, 90% and 79% reduction against 10^7, 10^8 and 10^9 CFU/mL of MRSA; 98%, 94% and 75% reduction against 10^7, 10^8 and 10^9 CFU/mL of VRE and 93%, 90% and 78% reduction against 10^7, 10^8 and 10^9 CFU/mL of *K. pneumoniae* respectively (Figure 5A.2C-F).

5A.2.5 Contact based mode of action

In order to establish that the gel inactivates bacteria upon contact and not by releasing its components, hydrogel (2.5 wt% HTCC cross-linked with 2.5 wt% **HTCC 3**) was prepared in 6.5 mm trans-well cell culture inserts with polycarbonate membrane of 0.4 μm pore size.[32] The inserts were then kept over bacterial suspension in suitable growth media taken in the wells of the culture plate. The volume of the media was chosen in such that the polycarbonate membrane along with the gel was under the media without touching the bottom of the wells. So if there is any leakage of the polymers from the gel into the suspension, bacterial proliferation should get inhibited. However, after inoculation of bacteria (10^4 CFU/mL, 500 μL) for about 24 h, substantial amount of growth was observed for both *S. aureus* and *E. coli* (Figure 5A.3A and B). When an equal volume of only **HTCC 3** polymer solutions was placed in the cell culture inserts and incubated with bacteria, no growth was observed for both *S. aureus* and *E. coli* respectively (Figure 5A.3A and B). Thus the above results indicated that the bacterial attachment onto surface of gel is necessary to have antibacterial activity.

As the gel surface is positively charged due to the presence of quaternary trimethylammonium group in **HTCC 3**, the surfaces are expected to interact with the negatively charged membrane of bacteria thus causing membrane disruption. To substantiate the mode of action, we studied the membrane permeabilization of bacteria by fluorescence microscopy using green fluorescent membrane permeable dye SYTO 9 and red fluorescent membrane impermeable dye propidium iodide.[41] While the untreated bacteria showed completely green fluorescence thereby indicated only live bacteria (Figure 5A.3C and E), both *S. aureus* and *E. coli* showed significant red fluorescence upon treatment with the adhesive surface thereby indicating the presence of membrane-compromised bacteria (Figure

5A.3D and F). It should be mentioned that cationic **HTCC 3** which possesses good activity against bacteria (minimum inhibitory concentration, MIC values were 125-250 μg/mL) and inactivates them by interacting with the negatively charged cell membrane might play as the major antibacterial component for the adhesive. Since, PDA is also shown to possess activity against bacteria (MIC of PDA is 4000 μg/mL and 32000 μg/mL against *S. aureus* and *E. coli* respectively), the contribution from PDA towards gel's antibacterial efficacy cannot be ignored.

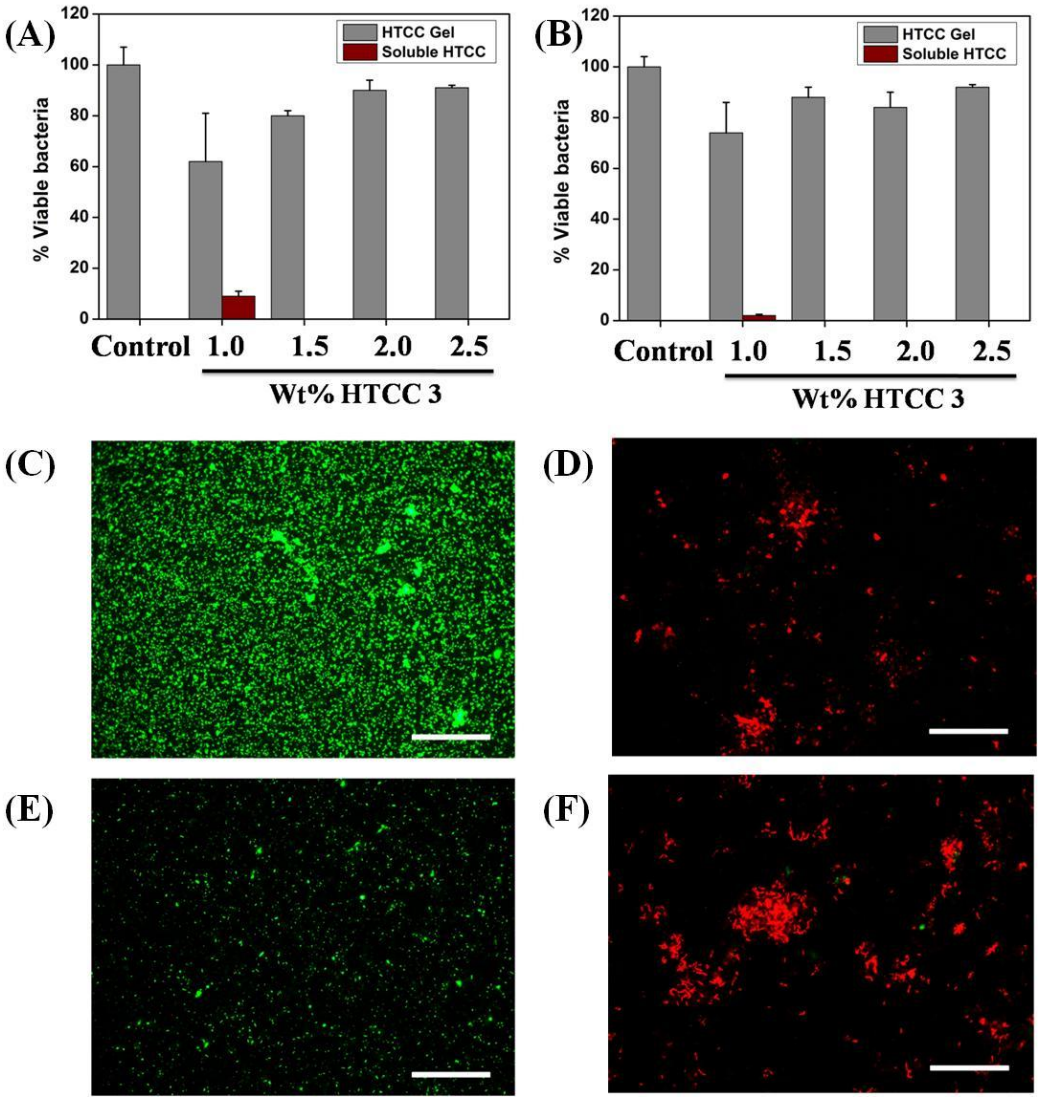

Figure 5A.3: Mode of action of the hydrogels. Contact based mode of action of the hydrogels: (A) *S. aureus* and (B) *E. coli* exposed to cell culture inserts bearing hydrogels or soluble **HTCC 3** of same volume and concentration used to prepare the gels. Mechanism of action of the gel: fluorescence microscopy images of non-treated (C) *S. aureus* and (E) *E. coli* and treated (D) *S. aureus* and (F) *E. coli* respectively after staining with SYTO 9 and propidium iodide. Scale bar 10 μm.

5A.2.6 *In-vitro* and *in-vivo* toxicity

Hemocompatibility of the hydrogels was evaluated by exposing the gel's surfaces with human red blood cells (hRBC) and determining the percentage of hemolysis with respect to a highly toxic surfactant triton-X (TX-100).

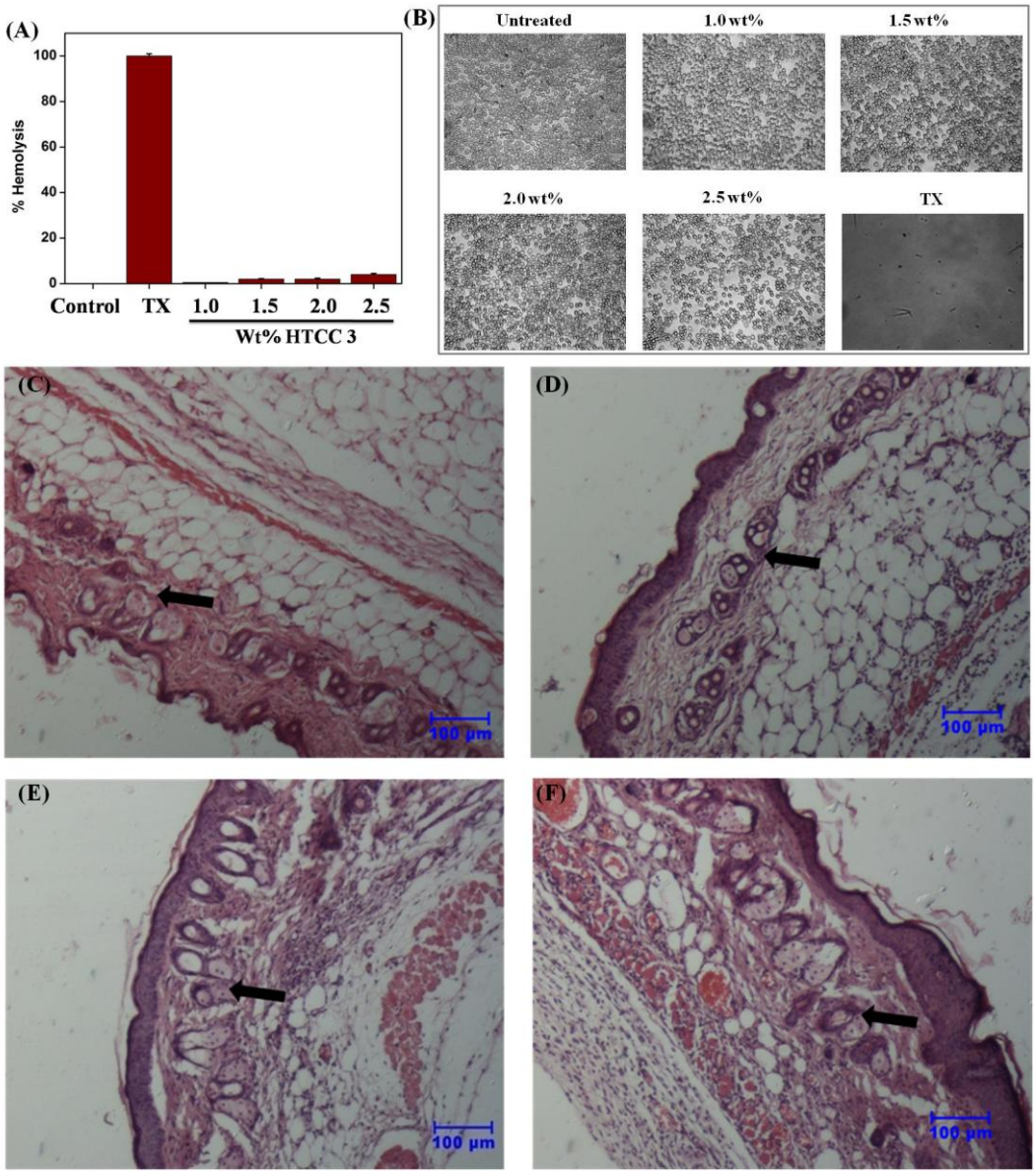

Figure 5A.4: *In-vitro* biocompatibility of the hydrogels. (A) Hemolytic activity of the hydrogels as a function of varying HTCC content and the controls (untreated and TX-100); (B) optical micrograph images of hRBC images from the various gel and control surfaces. *In-vivo* biocompatibility of the bioadhesive hydrogels Mice skin and subcutaneous tissue histopathology: (C and D) untreated skin tissue showing normal architecture of epidermis, dermis and subcutaneous tissues (after 3 and 7 days of saline injection); sweat gland, sebaceous gland was seen (arrow). (E and F) Hydrogel treated skin tissue showing normal dermis layer with sweat and sebaceous gland along with normal adipose tissue (arrow) (after 3 and 7 days of injection of the hydrogel).

Notably, all the adhesives showed negligible hemolysis (Figure 5A.4A). The most active adhesive (containing 2.5 wt% **HTCC 3**) showed only 2-4% hemolysis. This emphasized that the gels were hemocompatible against human erythrocytes. To have better insight, blood cells were also imaged after exposing to the gel's surfaces. The treated cells were found to have round morphology typical of healthy blood cells as observed in the non-treated wells. In contrast, wells treated with TX-100 showed no survival of RBC as no cells were observed under the microscope (Figure 5A.4B). The above facts further indicated the non-cytotoxic nature of the adhesive surfaces suitable for biomedical applications. The cytotoxic effect of the hydrogel was also evaluated *in-vivo* by injecting the gel subcutaneously in mice and then studying histopathological responses after 3 and 7 days of implantation via haematoxylin and eosin staining. Notably, tissue surrounding the gel (2.5 wt% PDA and 2.5 wt% **HTCC 3**) showed no inflammation and showed normal architecture of epidermis, dermis and subcutaneous tissues like the untreated tissue samples after 3 and 7 days post injection (Figure 5A.4C-F). The above facts therefore indicated that gels are indeed non-toxic towards mammalian cells.

5A.2.7 Hemostatic properties

In order to be used as effective sealant, the gels are requisite to seal the blood leakage thus act as anti-haemorrhaging agent.[42] The hemostatic ability of the hydrogels was studied by puncturing the liver of mice with a needle and instantaneously applying the adhesive on the punctured area. While the punctured liver without gel showed leakage of significant amount of blood collected on the paper, punctured liver with the gel showed negligible amount of blood loss **(**Figure 5A.5A**)**. The total blood loss from the control liver was about 168 mg for 3 min after the liver was pricked. In contrast, the bleeding was significantly arrested by the gels, the loss of blood being reduced to 50 mg (Figure 5A.5B). Thus the above result demonstrates that the hydrogels when cross linked *in situ* can serve as an effective anti-haemorrhaging agent.

5A.2.8 Wound healing activity

The wound healing abilities of the gel was studied by creating a spherical wound (~18 mm diameter) on the back of Wistar rats by skin incision and removal.[3] While the control group have no significant effects on the wound size after day 5 and day 10, gel with 2.5 wt% PDA and 2.5 wt% **HTCC 3** was able to reduce the wound size by 14 ± 4% and 31 ± 8%,

respectively (Figure 5A.5C and D). Notably, after day 15 and day 20, wound in the treated groups almost repaired in sharp contrast to control. The adhesive has a wound healing ratio of 78 ± 9%, much higher than that of the control group which showed a healing ratio of 58 ± 7% (Figure 5A.5C and D). In summary, the adhesive exhibited faster wound-healing performance over a very short period (Figure 5A.5E).

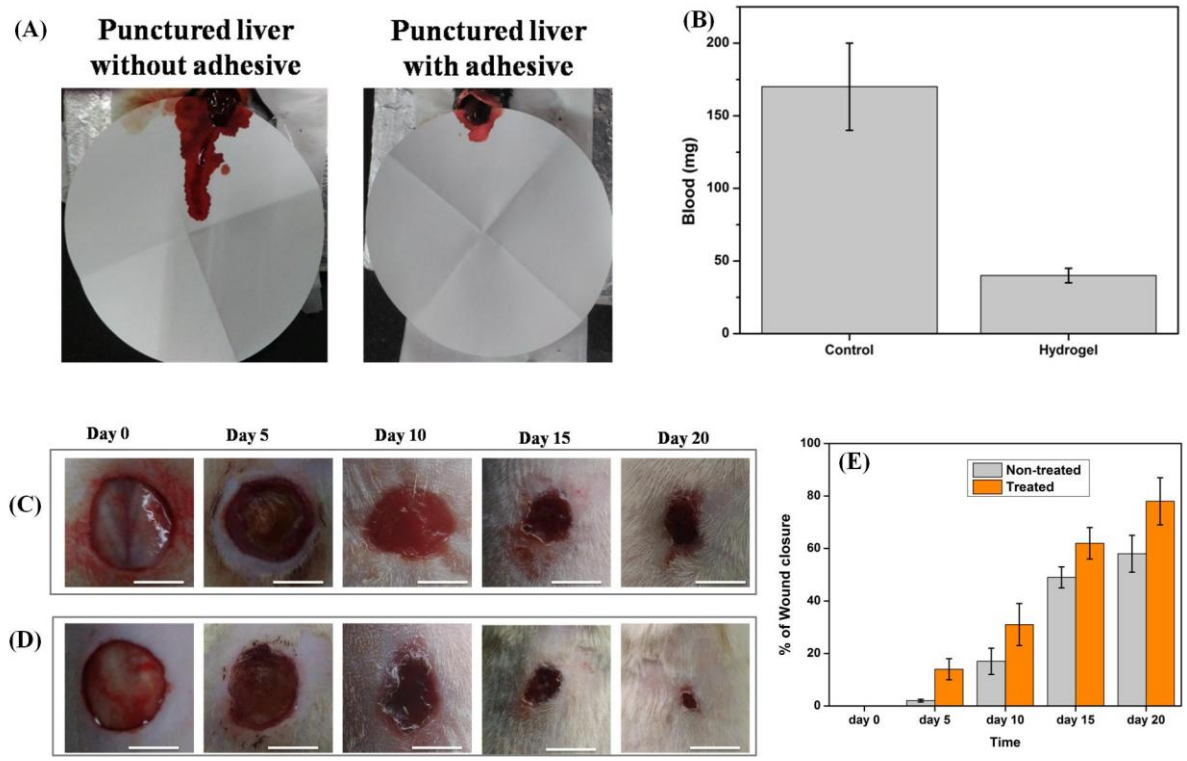

Figure 5A.5: *In-vivo* activity of the hydrogels. Hemostatic ability of the hydrogel: (A) Images of the paper after collecting blood after pricking the liver of mice without and with hydrogel; (B) loss of blood from the damaged livers after 3 min. Wound healing ability of the injectable hydrogel: representative photographs of 18 mm diameter wounds excised on rats (C) without any hydrogel and (D) treated with the hydrogel. Scale bar 10 mm. % of Wound closure at different time interval for both untreated and gel treated wound.

5A.2.9 *In-vivo* antibacterial activity

In order to evaluate the ability of the gel to prevent infections under *in-vivo* condition, cecal ligation and puncture (CLP) model of sepsis was performed in mice.[41] Cecam, an intra-peritoneal pouch, contains a variety of microbes including both Gram-positive and gram-negative bacteria. Puncture of cecam would thus allow the bacterial leakage from the intestine which would ultimately results in sepsis and death. Application of the hydrogel to the punctured area are expected to form a barrier between the cecam and the peritoneal cavity

thus inhibiting bacterial infiltration and translocation, and if possible kill bacteria which are on contact.

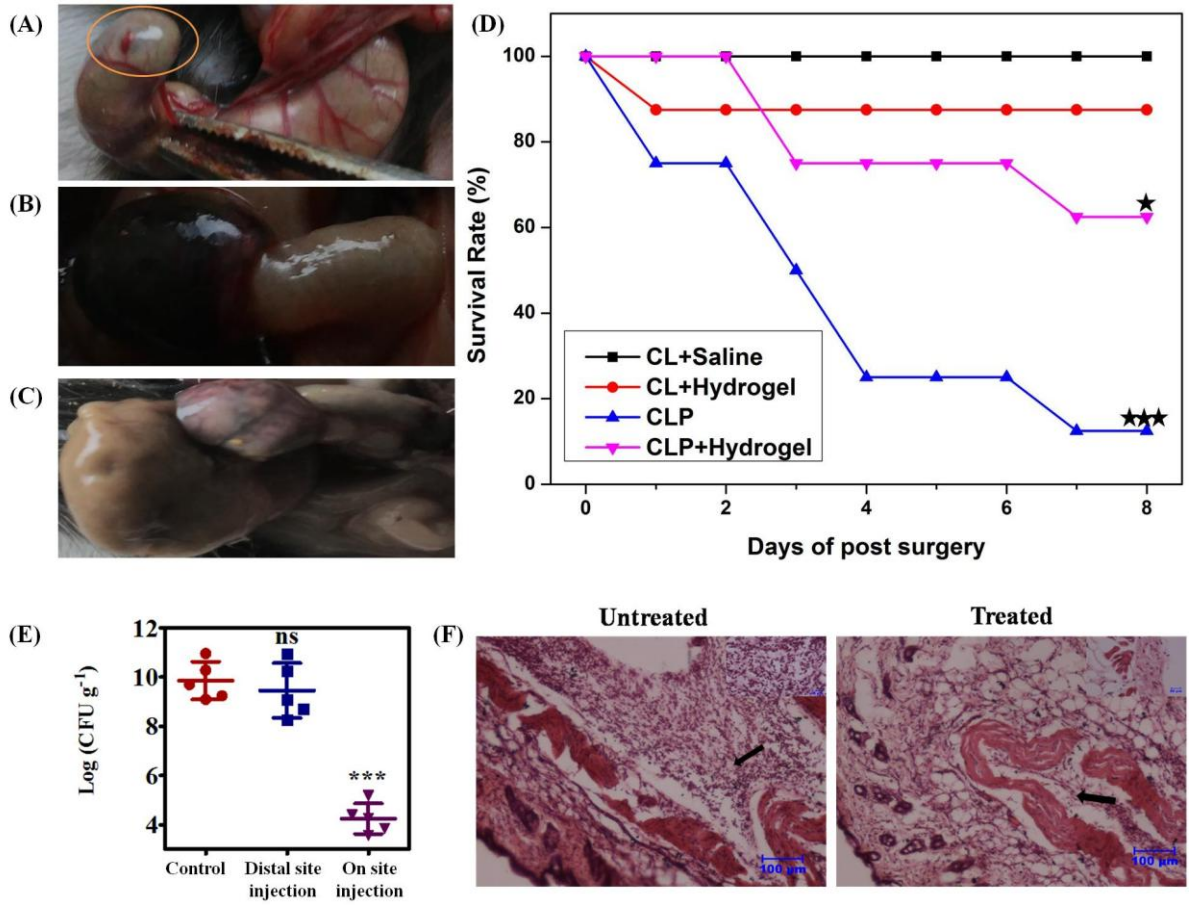

Figure 5A.6: *In-vivo* activity of the hydrogels. Efficacy of the hydrogel in sealing leaks and preventing sepsis by cecal ligation and puncture model: (A) application of the hydrogel to the punctured area of cecam during surgery. Isolated punctured ceca after 24 h of surgery (B) cecam with no gel and (C) cecam that was treated with the gel; (D) survival rates of mice for saline treated cecam with ligation, gel treated cecam with ligation, cecam with both ligation and puncture, and gel treated cecam with ligation and puncture respectively (saline or gel were applied on the punctured area). P values (∗ and ∗∗∗) are 0.0330 and 0.0009 for CLP and CLP+hydrogel with respect to CL+hydrogel. Evaluation of antibacterial activity upon injection of MRSA into gel subcutaneously in mice: (E) MRSA count after 72 h of infection; p value (*) are <0.0001 for treated samples (F) mice skin and subcutaneous tissue histopathology after hematoxylin and eosin staining.

Herein, the caeca of mice were ligated and then punctured with a needle. Next one of the active hydrogels (containing 2.5 wt% PDA and 2.5 wt% **HTCC 3**) was applied onto the punctured area of caeca (Figure 5A.6A) and then returned back into the peritoneal cavity. Mice having punctured caeca without any adhesives were used as controls. To visualize the differences between treated and non-treated cecam, caeca of animals were imaged after 24 h

of the application of gel. While the punctured cecam with no hydrogel was found to be highly erythematous and black in colour indicative of severe infection (Figure 5A.6B), punctured cecum with the gel was found to be healthy and normal in colour (Figure 5A.6C). The above facts therefore suggested that the hydrogel formed an efficient barrier to infection. Further survival rate of the mice were also studied for the 8-post-operative days to determine the efficacy of the gels towards sepsis prevention. While only 1 mice out of 8 (12.5%) survived in the control group, 5 mice (62.5%) survived when the punctured area were treated with gel (Figure 5A.6D). The above results thus indicated that the gels are able to seal the leakage and prevent the infection. Interestingly, when the gel is applied to mice without puncturing the cecum, survival rate was found to be very high (87.5-100%). Moreover, all animals were found to recover the initial weight loss after 4-5 days. These observations further suggested that the gels are non-toxic *in-vivo* and cause negligible organ toxicity.

The efficacy of the hydrogel was also evaluated in a subcutaneous injection and subsequent infection of the gel in mice model.[41] The gel (2.5 wt% PDA and 2.5 wt% **HTCC 3**) were injected subcutaneously in neutropenic mice. Bacteria (40 μL of 10^7 CFU/mL MRSA) were then directly injected directly into the gel. Bacteria were also injected subcutaneously without the gel and at distal site far from the gel. After 72 h, mice were sacrificed and tissue surrounding the gel was collected for cell enumeration. Notably, skin tissue (without gel) showed 5.6 log less bacteria as compared to the untreated skin tissue (Figure 5A.6E). Further, no reduction of MRSA count was observed for mice where bacteria were injected at different site from the gel thereby indicated that the gel acts only on contact. The efficacy of the gel was further established by histopathology examination of both treated and untreated tissue samples. While the control tissue samples showed severe infiltration of inflammatory cells mostly neutrophils and mononuclear cells in the subcutaneous tissues (arrow) with congestion of blood vessels (inset), tissue surrounding the gel showed normal skin morphology with minimal inflammation (Figure 5A.6F). Also, it was noted that 2.1 log reduction of MRSA count was observed compared to untreated sample when the tissue along with the gel was enumerated for cell counting. In general, the above results indicated that the gel was able to prevent the spreading of infection in the surrounding tissue as well as was able to reduce infection.

5A.3. Conclusion

In summary, bioadhesive injectable hydrogels developed from two naturally occurring polymer derivatives were shown to act as potent antibacterial agents. The hydrogels were found to inactivate both drug-sensitive and drug-resistant bacteria such MRSA, VRE and beta lactam-resistant *K. pneumoniae*. Mechanistic studies revealed that the gels mainly acted by disrupting the membrane integrity of the pathogen upon contact. These materials were found to be efficacious in sealing leaks and preventing infection *in-vivo*. Further, the materials were also shown to be effective in facilitating wound healing and preventing haemorrhage. Importantly, they were shown to be non-toxic towards human erythrocytes and caused no organ toxicity when applied internally. No inflammation was observed to the surrounding tissue upon subcutaneous implantation in mice. The bioadhesive hydrogels developed herein thus can be used as safe and effective sealant to prevent wound site infections at the tissue level.

5A.4. Experimental section

5A.4.1 Materials and instrumentation

Dextran from *Leuconostic* spp. (M_r ~40 kDa), glycidyltrimethylammonium chloride (GTMAC), acetic acid, sodium periodate ($NaIO_4$), hydroxyl amine, methyl orange were purchased from Sigma-Aldrich, USA as used as received. Chitosan with a degree of acetylation (DA) ~85% (molecular weight = 15 kDa) was purchased from Polysciences, USA. Acetone, ethanol and other organic solvents were of analytical grade and purchased from Spectrochem, India. The water used in all experiments was Millipore water with a resistivity of 18.6 MΩ cm. Bacterial strains such as *S. aureus* (MTCC 737), *E. coli* (MTCC 443) and *P. aeruginosa* (MTCC 424) were purchased from MTCC (Chandigarh, India). Drug-resistant bacteria such as vancomycin-resistant *Enterococcus faecium* (VRE) (ATCC 51559), methicilin-resistant *S. aureus* (MRSA) (ATCC 33591) and *β*-lactum resistant *Klebsiella pneumoniae* (ATCC 700603) were obtained from ATCC (Rockvillei, Md). Bacterial growth media and agar were supplied by HIMEDIA, India. Nuclear magnetic resonance spectra (^{1}H-NMR and ^{13}C-NMR) were recorded on a Bruker AMX-400 instrument (400 MHz) in deuterated solvents. Solid state NMR (^{13}C cross polarization magic angle spinning, ^{13}C CP-MAS), was performed in Bruker Avance III spectrometer. FT-IR spectra of the solid compounds were recorded on Bruker IFS66 V/s spectrometer using KBr pellets and the IR spectra of the hydrogels were recorded in attenuated total reflectance (ATR) FTIR

instrument using diamond crystal (Perkin Elmer, BS EN 60825-1). Electron microscopy images were captured in using field emission scanning electron microscope (Quanta 3D FEG, FEI). An Olympus microscope (Model BX51) and Leica DM2500 fluorescent microscope was used for imaging of bacterial cells. Oscillatory rheology experiments were performed on preformed adhesive gels using a TA Instrument AR-G2 rheometer, using a 25 mm diameter stainless steel parallel plate tool. Adhesive strength of the gels was performed using Q800 dynamic mechanical analyser (DMA) (TA, Instruments). Eppendorf 5810R centrifuge was used for centrifugation. TECAN (Infinite series, M200 pro) Plate Reader was used to measure optical density. Studies on animal subjects were performed following the protocols approved by Institutional Bio-safety Committee (IBSC) of Jawaharlal Nehru Centre for Advanced Scientific Research (JNCASR). Studies with the animals were performed following protocols approved by the Institutional Animal Ethics Committee (IAEC) in the institute (Jawaharlal Nehru Centre for Advanced Scientific Research).

5A.4.2. Synthesis and characterization of polymers

5A.4.2.1 Synthesis of HTCC

Chitosan (2.5 g) was suspended in Millipore water (200 mL), and then acetic acid (1 mL, 0.5%, v/v) was added to the suspension. The chitosan-acetic acid mixture was stirred for about 12 hat room temperature to obtain a clear polymer solution. GTMAC was added to the polymer solution in three portions at nearly two-hour intervals. The GTMAC to chitosan mole ratio was varied from 4:1 to 8:1. The reaction was allowed to proceed at 55 °C for 18 h after the final addition of GTMAC. The reaction mixture was then diluted with 300 mL water and the product was precipitated with excess of acetone. The chitosan derivatives were filtered through a sintered glass funnel and washed with acetone repeatedly. The products were characterized by ^{1}H-NMR, ^{13}C cross-polarization magic-angle spinning (CP-MAS) NMR and FT-IR spectroscopy (yields higher than 90%). The degrees of substitutions (DS) of the quaternary chitosan derivatives were determined by conductivity measurements.

HTCC 1: FT-IR ($\overline{\nu}$): 3450-3100 cm^{-1} (–OH and –NH_2 or –NH–),1686 cm^{-1} (amide I, C=O str.), 1559 cm^{-1} (amide II, NH ben.), 1477 cm^{-1} (–$N^+(CH_3)_3$ ben.); ^{1}H-NMR (400 MHz, $CDCl_3$, 25 ˚C): δ = 1.908 (s, –*CH_3*COO–), 2.068 (s, –*CH_3*CO–), 2.568-2.939 (m, –NH*CH_2*CH(OH)CH_2– and Cell C2*H*), 3.227 (s, –CH(OH)CH_2N^+*$(CH_3)_3$*), 3.408-3.993 (m, Cell C3*H*-C5*H*, –CH(OH)*CH_2*$N^+(CH_3)_3$), 4.290 (s, –CH_2*CH*(OH)CH_2–), 4.542 (s, Cell C1*H*); ^{13}C-NMR (CP-MAS, 100 MHz): δ = 24.161, 55.297, 557.574, 61.925, 63.812, 64.170, 64.917, 75.225, 84.513, 105.657, 106.061, 174.107.

HTCC 2: FT-IR ($\overline{\nu}$): 3440-3160 cm^{-1} (–OH and $–NH_2$ or –NH–),1684 cm^{-1} (amide I, C=O str.), 1560 cm^{-1} (amide II, NH ben.), 1480 cm^{-1} ($–N^+(CH_3)_3$ ben.); ^{1}H-NMR (400 MHz, $CDCl_3$, 25 ˚C): δ = 1.908 (s, $–CH_3COO–$), 2.067 (s, $–CH_3CO–$), 2.565-2.935 (m, $–NHCH_2CH(OH)CH_2–$ and Cell C2*H*), 3.225 (s, $–CH(OH)CH_2N^+(CH_3)_3$), 3.409-3.969 (m, Cell C3*H*-C5*H*, $–CH(OH)CH_2N^+(CH_3)_3$), 4.289 (s, $–CH_2CH(OH)CH_2–$), 4.504 (s, Cell C1*H*); ^{13}C-NMR (CP-MAS, 100 MHz): δ = 24.345, 55.308, 62.022, 62.719, 62.983, 63.723, 64.310, 64.660, 64.982, 75.123, 84.570, 104.617, 105.770, 174.068.

HTCC 3: FT-IR ($\overline{\nu}$): 3445-3162 cm^{-1} (–OH and $–NH_2$ or –NH–),1682 cm^{-1} (amide I, C=O str.), 1555 cm^{-1} (amide II, NH ben.), 1478 cm^{-1} ($–N^+(CH_3)_3$ ben.); ^{1}H-NMR (400 MHz, $CDCl_3$, 25 ˚C): δ = 1.910 (s, $–CH_3COO–$), 2.068 (s, $–CH_3CO–$), 2.568-2.939 (m, $–NHCH_2CH(OH)CH_2–$ and Cell C2*H*), 3.228 (s, $–CH(OH)CH_2N^+(CH_3)_3$), 3.412-3.991 (m, Cell C3*H*-C5*H*, $–CH(OH)CH_2N^+(CH_3)_3$), 4.292 (s, $–CH_2CH(OH)CH_2–$), 4.546 (s, Cell C1*H*); ^{13}C-NMR (CP-MAS, 100 MHz): δ = 24.064, 55.265, 61.417, 61.715, 62.023, 63.922, 64.293, 64.953, 75.050, 84.552, 104.858, 105.633, 174.047.

HTCC 4: FT-IR ($\overline{\nu}$): 3455-3160 cm^{-1} (–OH and $–NH_2$ or –NH–),1679 cm^{-1} (amide I, C=O str.), 1559 cm^{-1} (amide II, NH ben.), 1472 cm^{-1} ($–N^+(CH_3)_3$ ben.); ^{1}H-NMR (400 MHz, $CDCl_3$, 25 ˚C): δ = 1.915 (s, $–CH_3COO–$), 2.069 (s, $–CH_3CO–$), 2.567-2.966 (m, $–NHCH_2CH(OH)CH_2–$ and Cell C2*H*), 3.227 (s, $–CH(OH)CH_2N^+(CH_3)_3$), 3.571-3.969 (m, Cell C3*H*-C5*H*, $–CH(OH)CH_2N^+(CH_3)_3$), 4.281 (s, $–CH_2CH(OH)CH_2–$), 4.537 (s, Cell C1*H*); ^{13}C-NMR (CP-MAS, 100 MHz): δ = 24.048, 55.225, 61.326, 61.720, 62.041, 62.337, 63.047, 63.716, 64.079, 64.799, 74.838, 84.402, 104.864, 106.168, 173.521.

HTCC 5: FT-IR ($\overline{\nu}$): 3475-3140 cm^{-1} (–OH and $–NH_2$ or –NH–),1680 cm^{-1} (amide I, C=O str.), 1560 cm^{-1} (amide II, NH ben.), 1481 cm^{-1} ($–N^+(CH_3)_3$ ben.); ^{1}H-NMR (400 MHz, $CDCl_3$, 25 ˚C): δ = 1.911 (s, $–CH_3COO–$), 2.071 (s, $–CH_3CO–$), 2.570-2.943 (m, $–NHCH_2CH(OH)CH_2–$ and Cell C2*H*), 3.231 (s, $–CH(OH)CH_2N^+(CH_3)_3$), 3.414-3.974 (m, Cell C3*H*-C5*H*, $–CH(OH)CH_2N^+(CH_3)_3$), 4.287 (s, $–CH_2CH(OH)CH_2–$), 4.541 (s, Cell C1*H*); ^{13}C-NMR (CP-MAS, 100 MHz): δ = 24.073, 55.115, 58.124, 61.817, 62.151, 64.014, 64.213, 64.873, 75.225, 84.256, 105.504, 105.890, 173.939.

HTCC 6: FT-IR ($\overline{\nu}$): 3462-3158 cm^{-1} (–OH and $–NH_2$ or –NH–),1688 cm^{-1} (amide I, C=O str.), 1551 cm^{-1} (amide II, NH ben.), 1474 cm^{-1} ($–N^+(CH_3)_3$ ben.); ^{1}H-NMR (400 MHz, $CDCl_3$, 25 ˚C): δ = 1.909 (s, $–CH_3COO–$), 2.059 (s, $–CH_3CO–$), 2.588-2.929 (m, $–NHCH_2CH(OH)CH_2–$ and Cell C2*H*), 3.224 (s, $–CH(OH)CH_2N^+(CH_3)_3$), 3.409-3.989 (m, Cell C3*H*-C5*H*, $–CH(OH)CH_2N^+(CH_3)_3$), 4.278 (s, $–CH_2CH(OH)CH_2–$), 4.541 (s, Cell C1*H*); ^{13}C-NMR (CP-MAS, 100 MHz): δ = 24.148, 55.029, 60.921, 61.421, 63.183, 63.817, 64.171, 64.623, 74.847, 84.414, 105.108, 105.363, 174.729.

5A.4.2.2 Determination of degree of substitution (DS)

DS of the polymers was calculated by titrating the amount of chloride ($Cl^–$) ions on the polymers with aqueous $AgNO_3$ solution. The moles of reacted GTMAC to the mole of repeating sugar unit of chitosan was defined as DS. HTCCs (0.025 g) were dissolved in Millipore water (50 mL) an aqueous solution of $AgNO_3$ (0.02 M) was used to titrate the

aqueous solution of polymers. The DS of HTCC polymers was calculated using the following Equation 1:

$$C_{AgNO3} \times V_{AgNO3} = m_{HTCC} \times DS)/[(DS \times M_3) + \{(1-DS-DA) \times M_1\} + (DA \times M_2)] \quad (1)$$

In this equation, C_{AgNO3} is the concentration of $AgNO_3$, V_{AgNO3} is the volume of the $AgNO_3$ solution at the point of equivalence, m is the mass of HTCC used for titration, M_1 is the molecular weight of the glucosamine repeating unit, M_2 is the molecular weight of the *N*-acetyl glucosamine repeating unit, M_3 is the molecular weight of GTMAC substituted repeating unit, i.e., quaternary unit, DA is the degree of acetylation of the native chitosan (0.15 or 0.21).

5A.4.2.3 Synthesis of polydextran aldehyde (PDA)

Dextran (40 kDa, 10 g, 61.7 mol/repeating unit) was dissolved in Millipore water (400 mL). Then of sodium periodate (9.9 g, 46.3 mol) dissolved in Millipore water (100 mL) was added to the dextran solution and stirred for 24 h at room temperature under dark condition. After the reaction, the mixture was dialyzed (Mol. Wt. cut off ~10 kDa) using Millipore water over a period of 4 days changing water thrice a day. The solution was then freeze dried to obtain oxidized dextran as white fluffy powder. Oxidation of dextran with $NaIO_4$ generates various aldehyde and hemiacetals species in the polymer. These species generally remain in equilibrium when PDA is dissolved in aqueous buffer solution.

The percentage of aldehyde functionality was determined by colorimetric method following an earlier report by dissolving PDA (100 mg) in 0.25 N hydroxylamine hydrochloride (25 mL) containing methyl orange (~0.007 w/v%) (pH ~4).[4] Hydroxylamine reacts with aldehyde thereby consumes both aldehyde and hemiacetal. The mixture was stirred for 2 h, after which the solution was titrated with NaOH (0.1 N). The volume of NaOH solution required to titrate (where the first colour change was observed) was recorded. The percent of aldehyde functionality was calculated by:

$$\% \text{ of aldehyde} = (V_{NaOH} \times C_{NaOH} \times 0.5)/(m_{dextran}/162) \quad (2)$$

Here, V_{NaOH} = volume of NaOH required to titrate the solution, C_{NaOH} = concentration of NaOH solution and $m_{dextran}$ = weight of PDA used in titration. The aldehyde content in PDA was found to be 51±1%.

PDA: FT-IR ($\overline{\nu}$): 3620-3260 cm^{-1} ($-NH_2$ or –NH– or –OH), 2972 cm^{-1} (C–H str.), 1780 cm^{-1} (amide I, C=O str.), 1552 cm^{-1} (amide II, NH ben.), 1480 cm^{-1} ($-N^+(CH_3)_3$ ben.); ^{1}H-NMR (400 MHz, D_2O, 70 ˚C): δ = 3.574-4.468 (m, Cell C2*H*–C6*H*), 4.965 (s, Cell C1*H*),

5.131-5.612 (m, hemiacetyl protons); ^{13}C-NMR (100 MHz, D_2O): δ = 68.056, 72.102, 72.416, 72.803, 73.955, 75.884, 82.044, 89.059, 90.569, 92.042, 93.825, 96.196, 97.133, 97.676, 98.633, 100.277, 100.460, 100.778, 103.583.

5A.4.3 Preparation of hydrogels

Hydrogels were prepared by first dissolving 50 mg of PDA in 1 mL of phosphate buffer (23.5 mM NaH_2PO_4, 80.5 mM Na_2HPO_4) which gave 5 wt% solution of PDA in the buffer. To this, an equal volume of 20 mg/mL or 30 mg/mL 40 mg/mL or 50 mg/mL (2.0 or 3.0 or 4.0 or 5.0 wt%) aqueous solution of **HTCC 3** was added. The mixture was kept in an incubator for 15 min at 37 ˚C to allow hydrogel formation. So four different hydrogel compositions were prepared where the wt% of PDA was held constant while wt% of **HTCC 3** was varied (2.5 wt% PDA + 1.0 wt% of **HTCC 3**; 2.5 wt% PDA + 1.5 wt% of **HTCC 3**; 2.5 wt% PDA + 2.0 wt% of **HTCC 3** and 2.5 wt% PDA + 2.5 wt% of **HTCC 3**).

5A.4.4 Characterization of hydrogels

5A.4.4.1 Gelation time

The gelation time (t_{gel}) of the hydrogel was measured by vial inversion method. The hydrogel components at the above concentrations and volumes (50 μL PDA + 50 μL **HTCC 3**) were mixed in a glass sample vial and vortexed gently (immediately after mixing the components). The time of addition of components was noted and the gelation time was calculated as the time required when no flow observed for each formulation.

5A.4.4.2 Morphology (Scanning electron microscopy)

Morphologies of the hydrogels were characterized by field emission scanning electron microscopy (FESEM) after hydrogel formation. The hydrogels were prepared in petri dish (1 mL PDA + 1 mL **HTCC 3**) and cut into small circular disks (6 mm diameter). The disks were then freeze-dried and sputter coated with gold. Both surface and cross-sectional morphologies were then imaged using Quanta 3D FEG, FEI field emission scanning electron microscopy at 10 kV operating voltage.

5A.4.4.3 Fourier transformed infrared (FT-IR) spectroscopy

FT-IR spectra of PDA, **HTCC 3** and hydrogel were recorded to identify the functional groups present in the polymers or hydrogels. IR spectra of the solid compounds were recorded on IFS66 V/s spectrometer (Bruker) using KBr pellets

5A.4.4.4 Viscoelastic properties

Viscoelastic properties were measured using an oscillatory rheometer on preformed hydrogels using a DHR-2 rheometer (TA Instruments) with 25 mm stainless steel (SS) parallel plate geometry. PDA was dissolved in phosphate buffer (at 50 mg/mL) and 200 μL of this solution was then transferred in a sample vial. To this, **HTCC 3** solution (200 μL of 20 mg/mL or 30 mg/mL or 40 mg/mL or 50 mg/mL) was added. The resulting hydrogels were transferred to the SS plate of the rheometer pre-equilibrated at 25 ˚C. A gap height of 1.0 mm was maintained before the measurements. For the equilibration of the gel, first a dynamic time sweep was applied at 6.3 rad/s angular frequency and 0.2% strain for 10 min. Then a frequency sweep from 0.1 to 100 rad/s with 0.2% strain was applied. The storage modulus (G′) and loss modulus (G′′) were calculated as a function of angular frequency at each point. The G′ and G′′ values were calculated at 6.3 rad/s which was in the linear regime and the average of three such independent measurements were reported.

5A.4.5 Determination of adhesive stress

Porcine skin was collected from local slaughter house. The fat was then removed from the dermal tissue layer. Skin sections (3.2 mm thickness) were then cut to a size of 55 mm of length and 10 mm of width. The sections were then soaked in PBS overnight at 4 ˚C. Before the measurement, skin samples were taken out from PBS and were allowed to come to room temperature. Hydrogels (50 μL of 50 mg/mL PDA + 50 μL of 20 mg/mL, 30 mg/mL, 40 mg/mL and 50 mg/mL HTCC separately) was applied between two tissue samples (contact area 10 mm × 6 mm). The samples were then incubated at 37 ˚C for 60 min. Samples were allowed to come to room temperature and adhesion stress measurements were performed on Q800 dynamic mechanical analyser (DMA) using film tension clamp (TA Instruments). A tensile load was applied to the adhesive sample at a rate of 0.1 N/min and the adhesive stress was monitored (ramp force was set up to 18.0000 N). The maximum adhesive stress was taken as the stress at which the two skin sample became completely separated thus indicated bond failure.

5A.4.6 *In-vitro* antibacterial activity

Minimum inhibitory concentration of the HTCC polymers was determined following the same protocol as described in the section of 4A.4.5 in Chapter 4A. Antibacterial activity of

the hydrogels was determined by preparing the gel into 96-well plate followed by exposing bacteria onto gel's surface. First, PDA (50 μL, 50 mg/mL) was taken in the wells of the well plate. Then **HTCC 3** (50 μL, 20 mg/mL, 30 mg/mL, 40 mg/mL and 50 mg/mL) was added to the wells and the mixture was mixed with a sterile tip and then gels were allowed form for 15 min in an incubator (37 ˚C). The hydrogels were repeatedly washed with PBS to remove any non-cross-linked **HTCC 3** (100 μL × 3, before each washing the gels were at least incubated for 10 min with PBS). Finally, bacteria (~10^5 CFU/mL, 100 μL) in nutrient media were added to the hydrogel surface or to the wells without any gel as control. The plates were then incubated at 37 ˚C for 24 h after which optical density (OD) of the nutrient media along with the gel was measured at 600 nm. To determine the antibacterial activity, OD value of the hydrogel containing only media (without any bacteria) was also recorded and subtracted from the OD values of the test samples. Finally, bacterial cell viability was calculated using the following equation:

$$\text{Cell viability} = \{\text{OD from hydrogel surface}_{(\text{Media+Bacteria})} - \text{OD from hydrogel surface}_{(\text{Media})}\} / \{\text{OD from well without gel}_{(\text{Media+Bacteria})} - \text{OD from well without gel}_{(\text{Media})}\} \times 100\% \quad (1)$$

5A.4.7 Determination of contact-based activity

In order to assess that the hydrogels act only by contact based mechanism (i.e., the antibacterial component of the gel, **HTCC 3**, does not leach out from the hydrogel matrix thus kill bacteria only on contact), the following experiment was performed. Hydrogels were prepared in inserts of a trans-well cell culture plate (24-well) at a volume of 400 μL. The surfaces of the gels were washed by 1 mL of PBS to the bottom of the wells in the 24-well plate. PBS (100 μL) was added onto the surface of the gel. The plates were then kept for 15 min in an incubator set at 37 ˚C and the PBS solutions from the bottom and top of the gels were removed. Similarly, the gels were further washed two more times. Bacteria (500 μL, 10^4 CFU/mL of *S. aureus* and *E. coli*) were added to the bottom of wells of the trans-well cell culture plate and then the inserts containing freshly prepared hydrogels were placed above the bacterial suspension. Nutrient media without bacteria (100 μL) was also added onto the surface of the hydrogel. Only **HTCC 3** at the same volume and concentration was added to the inserts and incubated similarly above the bacterial suspension. Another control was made where only bacteria (500 μL, 10^4 CFU/mL of *S. aureus* and *E. coli*) were incubated. Then the well plate was incubated at 37 ˚C for about 24 h. Finally, bacterial growth was determined by

measuring the OD values of the bacterial suspension. Cell viability was then calculated as mentioned previously.

5A.4.8 Mechanism of action

Hydrogel (2.5 wt% PDA and 2.5 wt% **HTCC 3**) was prepared onto the wells of a 96-well plate and washed with PBS to remove non-reacted **HTCC 3**. Then freshly grown bacteria (150 μL, ~10^7 CFU/mL) were added to the surface of the gel and incubated for about 6 h at 37 ˚C under constant shaking. Then the suspension were collected in an eppendorf tube, centrifuged at 12000 rpm for 1 min, washed twice with PBS, resuspended again in PBS. SYTO 9 (a membrane permeable green fluorescent dye) and propidium iodide (PI, a membrane impermeable red fluorescent dye) were added (3.0 μM of SYTO 9 and 15.0 μM of PI, 1:1 v/v) to the bacterial solution. The mixture was then incubated for 15 min in dark and 5 μL of the mixture was then placed on glass slide. The solution was then covered by a clean cover slip, sealed, and imaged via a fluorescence microscope (excitation = 488 nm and 543 nm for SYTO 9 and PI respectively; emission = 500-550 nm and 590-800 nm for SYTO 9 and PI respectively). Leica DM 2500 fluorescence microscope was used to image bacteria.

5A.4.9 Hemolytic assay

Hemolytic activity was determined by making the gels onto the wells of a 96-well plate (as described earlier) and then hemolytic activity was determined by following the same protocol as described in the section 2A.4.10 in chapter 2A.

5A.4.10 *In-vivo* toxicity

5A.4.10.1 Systemic toxicity with HTCC

Systemic toxicity of the HTCC polymers was determined following the same protocol as described in the section of 4A.4.14.3 in Chapter 4A.

5A.4.10.2 Sub-chronic toxicity with HTCC

BALB/c mice were used for the sub-chronic toxicity studies (four groups of mice, 10 mice in each group). Polymer solution in sterilized saline (200 μL) was given via i.p. injection of **HTCC 3** at a dosage of 55 mg/kg in two groups and the remaining two groups were used as control. After 2 days, blood was collected from both control and treated mice (10 mice for HTCC, 10 mice for control), and analyzed for different parameters like ALT (alanine

transaminase), AST (aspartate transaminase), creatinine, blood urea nitrogen, and electrolytes like sodium ion, potassium ion and chloride ion. Also after 14 days, blood was collected similarly from the remaining 20 mice (10 mice for **HTCC 3**, 10 mice for control) and analyzed for the above mentioned parameters. The data are presented as mean ± standard deviation, based on the values obtained from 10 mice (n = 10 for the data from this report). Student's t-test was used for statistical analysis. Differences are considered statistically significant with probability (p) < 0.05.

5A.4.10.3 Toxicity of the hydrogel

Mice were divided into control and test groups with 5 mice per group. In the test groups, 100 μL of the gel solution (after immediate mixing of both the components) was injected subcutaneously in each animal above the thoracic midline (dorsal). In control groups, 100 μL of saline was injected similarly. After 3 and 7 days, mice were sacrificed; tissue surrounding the gel was collected, fixed in 10% formalin and analyzed for histopathological studies following same protocol as described in section 2B.4.11.3 in Chapter 2B.

5A.4.11 Wound healing activity

The wound healing abilities of the injectable hydrogels were performed in a rat model.[3,10] Wistar rats (male, 250-300 g) were used for the experiment. Animals were divided into two groups: control and test groups. In each group 5 rats were used. The animals were anesthetized by intraperitoneal injection of the cocktail of ketamine (40-50 mg/kg) and xylaxin (2-3 mg/kg) body weight. Skin above the dorsal midline of the animals was shaved aseptically. Wounds of 18 mm diameter were prepared by excising the dorsum of the rats. The hydrogel (2.5 wt% PDA and 2.5 wt% **HTCC 3**, 400 μL) was then applied at the wound site via a syringe after immediate mixing of both the components. Then gels were spread on the entire wound area with the help of a glass rod. The rats of the tests groups were covered with sterile gauze. Then elastic adhesive bandage (Dynaplast, Johnson & Johnson) was used to fix the gauze. Wounds were also covered with the gauze and fixed with adhesive bandage without gel and used as controls. The animals were then kept in separate cages and allowed to have access of food and water. After the predetermined time interval (after postsurgical day 5, 10, 15 and 20) rats were sacrificed. Finally wounds were grossly observed and photographed to measure the reduction of wound size.

5A.4.12 Hemostatic ability

To evaluate the hemostatic potential of the hydrogels, a hemorrhaging liver mouse model was used (C57BL/6 mouse, 22-25 g, 5 weeks, male). Mice were anesthetized by intraperitoneal injection of the cocktail of ketamine and xylaxin. The liver of the mouse was exposed by abdominal incision, and serous fluid around the liver was carefully removed to prevent inaccuracies in estimation of the subsequent blood weight obtained by the filter paper. A pre-weighted filter paper on a paraffin film was placed beneath the liver. Bleeding from the liver was induced using a 20 G needle with the corkboard tilted at about 30˚ and 50 μL of hydrogel (2.5 wt% PDA and 2.5 wt% **HTCC 3**) was immediately applied to the bleeding site using the dual syringe kit filled with the gel solutions. After 3 min, the weight of the filter paper with absorbed blood was measured and compared with a control group (no treatment after pricking the liver).

5A.4.13 Cecal ligation and puncture (CLP) model of sepsis

Mice (C57BL/6, male, 6-8 weeks old) were used for this experiment (8 mice per group). Animals were anaesthetized by intraperitoneal injection of the cocktail of ketamine and xylaxin. Then the abdomen was shaved and disinfected by first applying betadine solution followed by wiping with a 70% alcohol swab. All procedures were performed under clean but not sterile conditions. Midline laparotomy (1.5 cm) was performed to expose the cecum. Next, the cecal pole was tightly ligated with a 6.0 silk suture at 0.5 cm from its tip, and then perforated once with a 20 G needle. In the experimental group, the cecum was covered with the adhesive gel (2.5 wt% PDA and 2.5 wt% **HTCC 3**) before returning it back to the peritoneal cavity, whereas in the control group the cecum was directly returned to the peritoneal cavity. The abdominal wall was then closed in layers using a 6.0 silk running suture for the peritoneum and a 6.0 nylon suture for the skin. All animals were resuscitated by injecting 1 mL of saline solution subscutaneously. Buprenorphine (0.05 mg/kg) was injected subcutaneously for postoperative analgesia. The animals were then left for full recovery. Free access to food and water was ensured post surgery. Mice were monitored every 12 h for survival and weight loss.

5A.4.14 Subcutaneous infection model

Female BALB/c mice (6 to 7 weeks old, 18-21g) were used for the experiment. The mice were first rendered neutropenic (~100 neutrophils/mL) by injecting cyclophosphamide, i.p.

(first dose at 150 mg/kg and then second dose at 100 mg/kg after 3 days of the first dose). Fur above the thorasic midline of mice was clipped. Then hydrogel (2.5 wt% PDA and 2.5 wt% **HTCC 3**, 100 μL) was injected subcutaneously. To infect the hydrogel, MRSA (~10^7 CFU/mL, 40 μL) was injected directly into the gel. Two control groups were made where in one group bacteria were injected at a distal site far from the gel while in other group only bacteria (100 μL saline + 40 μL 10^7CFU/mL MRSA) were injected. After 3 days, the mice were sacrificed and skin tissue from the injection sites with or without the gels were collected. Tissue samples were then homogenized, and used for cell counting by plating the homogenized solution on nutrient agar plate. The MRSA count was then expressed as log CFU/g of skin tissue and expressed as mean ± standard error of mean. A small section of the skin tissue from the injection site was also fixed in 10% formalin to study the histological responses in a similar manner as described in section 2B.4.12 in chapter 2B.

BIBLIOGRAPHY

1. Mehdizadeh, M.; Yang, J. Design strategies and applications of tissue bioadhesives. *Macromol. Biosci.* **2013,** *13*, 271-288.
2. Führmann, T.; Tam, R. Y.; Ballarin, B.; Coles, B.; Elliott Dongahue, I.; van der Kooy, D.; Nagy, A.; Morshead, C. M.; Shoichet, M. S. Injectable hydrogel promotes early survival of induced pluripotent stem cell-derived oligodendrocytes and attenuates long term teratoma formation in a spinal cord injury model. *Biomaterials* **2016**, *83*, 23-36.
3. Balakrishnan, B.; Mohanty, M.; Umashankar, P. R.; Jayakrishnan, A. Evaluation of an in situ forming hydrogel wound dressing based on oxidized alginate and gelatin. *Biomaterials* **2005,** *26*, 6335-6342.
4. Navath, R. S.; Menjoge, A.R.; Dai, H.; Romero, R.; Kannan, S.; Kannan, R. M. Injectable PAMAM dendrimer-PEG hydrogels for the treatment of genital infections: formulation and in vitro and in vivo evaluation. *Mol. Pharmaceutics* **2011**, *8*, 1209-1223.
5. Yamada, Y.; Schneider, J. P. Fragmentation of injectable bioadhesive hydrogels affords chemotherapeutic macromolecules. *Biomacromolecules* **2016,** *17*, 2634-2641.
6. Purcell, B. P.; Lobb, D.; Charati, M. B.; Dorsey, S. M.; Wade, R. J.; Zellars, K. N.; Doviak, H.; Pettaway, S.; Logdon, C. B.; Shuman, J. A.; Freels, P. D.; Gorman III, J. H.; Gorman, R. C.; Spinale, F. G.; Burdick, J. A. Injectable and bioresponsive hydrogels for on-demand matrix metalloproteinase inhibition. *Nat. Mater.* **2014**, *13*, 653-661.
7. Ryu, J. H.; Lee, Y.; Kong, W. H.; Kim, T. G.; Park, T. G.; Lee, H. Catechol-functionalized chitosan/pluronic hydrogels for tissue adhesives and hemostatic materials. *Biomacromolecules* **2011,** *12*, 2653-2659.
8. Spotnitz, W. D. Fibrin sealant: past, present, and future: a brief review. *World J. Surg.* **2010,** *34*, 632-634.
9. Salick, D. A.; Pochan, D. J.; Schneider, J. P. Design of an injectable beta-hairpin peptide hydrogel that kills methicillin-resistant *Staphylococcus aureus*. *Adv. Mater.* **2009,** *21*, 4120-4123.
10. Lih, E.; Lee, J. S.; Park, K. M.; Park, K. D. Rapidly curable chitosan-PEG hydrogels as tissue adhesives for hemostasis and wound healing. *Acta Biomater.* **2012,** *8*, 3261-3269.
11. Lee, H.; Lee, B. P.; Messersmith, P. B. A reversible wet/dry adhesive inspired by mussels and geckos. *Nature* **2007,** *448*, 338-341.
12. Mehdizadeh, M.; Weng, H.; Gyawali, D.; Tang, L. P.; Yang, J. Injectable citrate-based mussel-inspired tissue bioadhesives with high wet strength for sutureless wound closure. *Biomaterials* **2012,** *33*, 7972-7983.
13. Tseng, T. C.; Tao, L.; Hsieh, F. Y.; Wei, Y.; Chiu, I. M.; Hsu, S. H. An injectable, self-healing hydrogel to repair the central nervous system. *Adv. Mater.* **2015,** *27*, 3518-3524.
14. Pritchard, C. D.; O'Shea, T. M.; Siegwart, D. J.; Calo, E.; Anderson, D. G.; Reynolds, F. M.; Thomas, J. A.; Slotkin, J. R.; Woodard, E. J.; Langer, R. An injectable thiol-acrylate poly(ethylene glycol) hydrogel for sustained release of methylprednisolone sodium succinate. *Biomaterials* **2011,** *32*, 587-597.
15. Singer, A. J.; Quinn, J. V.; Hollander, J. E. The cyanoacrylate topical skin adhesives. *Am. J. Emerg. Med.* **2008,** *26*, 490-496.
16. Ito, T.; Yeo, Y.; Highley, C. B.; Bellas, E.; Kohane, D. S. Dextran-based in situ cross-linked injectable hydrogels to prevent peritoneal adhesions. *Biomaterials* **2007,** *28*, 3418-3426.
17. Liu, Y.; Meng, H.; Konst, S.; Sarmiento, R.; Rajachar, R.; Lee, B. P. Injectable dopamine-modified poly(ethylene glycol) nanocomposite hydrogel with enhanced adhesive property and bioactivity. *ACS Appl. Mater. Interfaces* **2014,** *6*, 16982-16992.

18. Cao, L. P.; Li, Q. L.; Zhang, C.; Wu, H. C.; Yao, L. Q.; Xu, M. D.; Yu, L.; Ding, J. D. Safe and efficient colonic endoscopic submucosal dissection using an injectable hydrogel. *ACS Biomater. Sci. Eng.* **2016,** *2*, 393-402.
19. Leggat, P. A.; Smith, D. R.; Kedjarune, U. Surgical applications of cyanoacrylate adhesives: a review of toxicity. *ANZ J. Surg.* **2007,** *77*, 209-213.
20. MacGillivray, T. E. Fibrin sealants and glues. *J. Card. Surg.* **2003,** *18*, 480-485.
21. Bae, K. H.; Wang, L. S.; Kurisawa, M. Injectable biodegradable hydrogels: progress and challenges. *J. Mater. Chem. B* **2013,** *1*, 5371-5388.
22. Owens, C. D.; Stoessel, K. Surgical site infections: epidemiology, microbiology and prevention. *J. Hosp. Infect.* **2008,** *70*, 3-10.
23. Reichman, D. E.; Greenberg, J. A. Reducing surgical site Infections: a review. *Rev. Obstet. Gynecol.* **2009,** *2*, 212-221.
24. Cosgrove, S. E. Antimicrobial resistance and patient outcomes: mortality, length of hospital stay, and health care costs. *Clin. Infect. Dis.* **2006,** *42*, S82-S89.
25. Hudson, S. P.; Langer, R.; Fink, G. R.; Kohane, D. S. Injectable in Situ cross-linking hydrogels for local antifungal therapy. *Biomaterials* **2010,** *31*, 1444-1452.
26. Guo, J. S.; Wang, W.; Hu, J. Q.; Xie, D. H.; Gerhard, E.; Nisic, M.; Shan, D. Y.; Qian, G. Y.; Zheng, S. Y.; Yang, J. Synthesis and characterization of anti-bacterial and anti-fungal citrate-based mussel-inspired bioadhesives. *Biomaterials* **2016,** *85*, 204-217.
27. Burke, K. A.; Roberts, D. C.; Kaplan, D. L. Silk fibroin aqueous-based adhesives inspired by mussel adhesive proteins. *Biomacromolecules* **2016**, *17*, 237-245.
28. Zhang, Y.; Zhang, J.; Chen, M.; Gong, H.; Thamphiwatana, S.; Eckmann, L.; Gao, W.; Zhang, L. A bioadhesive nanoparticle-hydrogel hybrid system for localized antimicrobial drug delivery. *ACS Appl. Mater. Interfaces* **2016,** *8*, 18367-18374.
29. Sivakumaran, D.; Maitland, D.; Hoare, T. Injectable microgel-hydrogel composites for prolonged small-molecule drug delivery. *Biomacromolecules* **2011**, *12*, 4112-4120.
30. Cuggino, J. C.; Contreras, C. B.; Jimenez-Kairuz, A.; Maletto, B. A.; Igarzabal, C. I. A. Novel poly(NIPA-co-AAc) functional hydrogels with potential application in drug controlled release. *Mol. Pharmaceutics* **2014**, *11*, 2239-2249.
31. Ma, L.; Cheng, C.; He, C.; Nie, C. X.; Deng, J.; Sun, S. D.; Zhao, C. S. Substrate-independent robust and heparin-mimetic hydrogel thin film coating via combined LbL self-assembly and mussel-inspired post-cross-linking. *ACS Appl. Mater. Interfaces* **2015,** *7*, 26050-26062.
32. Sahariah, P.; Benediktssdottir, B. E.; Hjalmarsdottir, M. A.; Sigurjonsson, O. E.; Sorensen, K. K.; Thygesen, M. B.; Jensen, K. J.; Masson, M. Impact of chain length on antibacterial activity and hemocompatibility of quaternary *N*-alkyl and *N,N*-dialkyl chitosan derivatives. *Biomacromolecules* **2015,** *16*, 1449-1460.
33. Kaminski, K.; Szczubialka, K.; Zazakowny, K.; Lach, R.; Nowakowska, M. Chitosan derivatives as novel potential heparin reversal agents. *J. Med. Chem.* **2010,** *53*, 4141-4147.
34. Cui, D.; Szarpak, A.; Pignot-Paintrand, I.; Varrot, A.; Boudou, T.; Detrembleur, C.; Jerome, C.; Picart, C.; Auzely-Velty, R. Contact-killing polyelectrolyte microcapsules based on chitosan derivatives. *Adv. Funct. Mater.* **2010,** *20*, 3303-3312.

35. Draye, J. P.; Delaey, B.; Van de Voorde, A.; Van Den Bulcke, A.; De Reu, B.; Schacht, E. In vitro and In vivo biocompatibility of dextran dialdehyde cross-linked gelatin hydrogel films. *Biomaterials* **1998,** *19*, 1677-1687.
37. Kumar, M. N. V. R.; Muzzarelli, R. A. A.; Muzzarelli, C.; Sashiwa, H.; Domb, A. J. Chitosan chemistry and pharmaceutical perspectives. *Chem. Rev.* **2004,** *104*, 6017-6084.
38. Borden, B. A.; Yockman, J.; Kim, S. W. Thermo responsive hydrogel as a delivery scaffold for transfected Rat mesenchymal stem cells. *Mol. Pharmaceutics* **2010**, *7*, 963-968.

39. Paez, J. I.; Ustahü seyin , O.; Serrano, C.; Ton, X.-A.; Shafiq, Z.; Auernhammer, G. K.; d'Ischia, M.; del Campo. A. Gauging and tuning cross-linking kinetics of catechol-PEG adhesives via catecholamine functionalization. *Biomacromolecules* **2015**, *16*, 3811-3818.
40. Liu, S. Q.; Yang, C.; Huang, Y.; Ding, X.; Li, Y.; Fan, W. M.; Hedrick, J. L.; Yang, Y. Y. Antimicrobial and antifouling hydrogels formed in situ from polycarbonate and poly(ethylene glycol) via michael addition. *Adv. Mater.* **2012,** *24*, 6484-6489.
41. Giano, M. C.; Ibrahim, Z.; Medina, S. H.; Sarhane, K. A.; Christensen, J. M.; Yamada, Y.; Brandacher, G.; Schneider, J. P. Injectable bioadhesive hydrogels with innate antibacterial properties. *Nat. Commun.* **2014,** *5*, 4095.
42. Hsu, B. B.; Hagerman, S. R.; Jamieson, K.; Castleberry, S. A.; Wang, W.; Holler, E.; Ljubimova, J. Y.; Hammond, P. T. Multifunctional self-assembled films for rapid hemostat and sustained anti-infective delivery. *ACS Biomater. Sci. Eng.* **2015**, *1*, 148-156.

Chapter 5B

Vancomycin-loaded Injectable Bioadhesive Hydrogels that Deliver Antibiotic Locally and Kill Bacteria Efficiently

Abstract

Chapter 5B *deals with the development of a dual action antibacterial injectable hydrogel for controlled release of antibiotics and delivering the drug locally to treat infections in relatively less vascular tissues (e.g., bone tissue infections), in avascular tissues (e.g., cartilage tissue infections) or in necrotic tissues (e.g., surgical site infections, SSI). The syringe deliverable bioadhesive hydrogel was prepared by mixing a buffer solution of PDA containing the antibiotic vancomycin and an aqueous solution of the antibacterial polymer* ***HTCC 3*** *developed in Chapter 5A. The antibiotic was loaded via primarily (more than 85%) covalent (imine) bond formed between the aldehyde group of PDA and amine group of vancomycin. The gel was shown to release the antibiotic over an extended period of time (50-60% release till day 14) at different pH (5.5, 6.2 and 7.2). Importantly, antibiotic loaded gels showed much higher activity than the gel alone against S. aureus and methicillin-resistant S. aureus (MRSA), two of the most common bacteria that cause infections in humans (e.g., surgical site infections). Further, the gel showed activity for an extended period of time (active till day 14 as tested). The gels were also shown to be impressively active under in-vivo conditions against MRSA when the bacteria were directly injected into the gel. Notably, when MRSA was injected at a distal site far from the gel, the vancomycin loaded gel was shown to eradicate MRSA infection in a subcutaneous infection model in mice. One of the most active formulations (2.5 wt% PDA with 0.3 wt% vancomycin and 2.0%* ***HTCC 3****) showed no toxicity towards human red blood cells (hRBC) and to the surrounding tissue upon subcutaneous injection in mice. The dual action injectable bioadhesive gel prepared in this chapter therefore might hold promise in combating infections at less vascular or avascular tissue level.*

Publication based on this work

(1) Hoque, J. *et al.* Dual action injectable bioadhesive hydrogel for extended release of antibiotics and effective killing of bacteria. Manuscript submitted.

5B.1 Introduction

Infections due to surgical procedure or by other means such as diffusion of skin microbes in relatively less vascular tissues (e.g., bone tissue infections), in avascular tissues (e.g., cartilage tissue infections) or in necrotic tissues (e.g., surgical site infections, SSI) are very challenging because of the limited penetration of antibiotics into the target tissues.[1-4] The risk further increases with the introduction of a surgical device or implant due to the biofilm formation on the easily colonisable surfaces of the devices.[5,6] Generally, treatment of these infections is carried out via prolonged course of oral or intravenous antibiotics which require use of the drugs from weeks to months in order to combat infections.[7,8] Despite the systemic treatment, severe infections can emerge because of the less diffusion of antibiotics to the less or avascular tissues and difficult-to-eliminate bacterial biofilms which in extreme cases can cause whole body infections known as sepsis.[9] Furthermore, systemic delivery of antibiotics with extensive and higher doses can have lethal side effects at the tissue level and also are prone to resistance development.[10-12] Thus there is pressing demand to develop delivery vehicles that can deliver antibiotics effectively at the target site for the required period of time.

Bioadhesive injectable hydrogels with innate antibacterial activity offer great advantages as these materials can integrate well with the tissue without any invasive surgery thereby acting as local therapeutics.[13-16] However, these gels require direct bacterial contact to impart activity and therefore are not fully suitable for infections in relatively less vascular or avascular tissues where bacteria could be far away from the target site. On the other, injectable hydrogel with encapsulated antibiotics/active antimicrobials were also developed.[17,18] However, uncontrolled release of the active moiety and poor activity of the gel matrix itself make these materials unsuitable for the applications. An inherently antibacterial injectable hydrogel loaded with antibiotics thus combining the properties of both the materials would be ideal to combat such infections wherein the gel can act simultaneously with dual (both release-active and contact-active) mode of action. Furthermore, it will not only deliver antibiotics into the target site locally but also can display higher or synergistic efficacy than the individual components and can act as tissue sealant, wound healing and hemostatic materials simultaneously.

Herein chapter 5B describe the development of an injectable hydrogel with dual mechanism of action by loading vancomycin into an inherently antibacterial hydrogel matrix developed in chapter 5A. Vancomycin, one of the most potent antibiotics, commonly used to

treat Gram-positive bacterial infection and is considered as the drug of last resort. However, the efficacy of systemic vancomycin is largely inhibited by unpredictable exposure of the drug in the tissue as the serum concentrations have been shown to be poorly correlated to the vancomycin levels within tissues.[19,20] Further, the systemic toxicity and quick elimination have been the other limitations of the drug.[21] In this chapter, vancomycin has been successfully loaded into injectable bioadhesive hydrogel using bioadhseive polydextran aldehyde (PDA) and antibacterial chitosan derivative *N*-(2-hydroxy) propyl-3-trimethylammonium chitosan chloride (**HTCC 3** from chapter 5A) and shown to be delivered locally with excellent combined antibacterial efficacy. Further, a pH dependent release of the antibiotic was observed wherein the gel released vancomycin at a relatively lower rate at acidic pH than neutral (infection sites are generally acidic in nature and is therefore believed to be highly suitable for application in such site). Further, the gel was shown to be impressively effective in killing MRSA when bacteria were injected not only into the gel but also at distal site (far from the gel) while being highly biocompatible in animal model. Importantly the gel was also shown to be efficacious in sealing leaks and preventing sepsis in a cecum ligation and puncture model.

5B.2 Results and discussion

5B.2.1 Synthesis and characterization of the hydrogels

Antibiotic loaded injectable hydrogel was prepared by encapsulating vancomycin in 2.5 wt% PDA (having ~50% dialdehyde functionality) and 2.0 wt% **HTCC 3** (having 46% quaternary ammonium group, 39% primary amine group and 15% of *N*-acetyl group) hydrogel matrix as developed in Chapter 5A (Figure 5B.1). In order to prepare vancomycin containing hydrogels, the antibiotic was dissolved in phosphate buffer (pH 7.2) at 1 mg/mL, 6 mg/mL and 12 mg/mL respectively. Solid PDA was then added to the each antibiotic containing buffer solutions individually to obtain 50 mg/mL of PDA. After 1 h, 40 mg/mL of **HTCC 3** dissolved in Millipore water was added to the polymer-antibiotic solutions in equal volume via dual barrel syringe which led to the formation of hydrogels within 10-15 seconds (**Table 1**). Thus three different vancomycin (V) containing injectable hydrogels (IH) named as IHV-1 (50 mg/mL PDA with 1 mg/mL vancomycin and 40 mg/mL **HTCC 3**; 1:1 v/v), IHV-2 (50 mg/mL PDA with 6 mg/mL vancomycin and 40 mg/mL **HTCC 3**; 1:1 v/v) and IHV-3 (50 mg/mL PDA with 12 mg/mL vancomycin and 40 mg/mL **HTCC 3**; 1:1 v/v) were obtained. Hydrogel with no vancomycin was named as IHV-0.

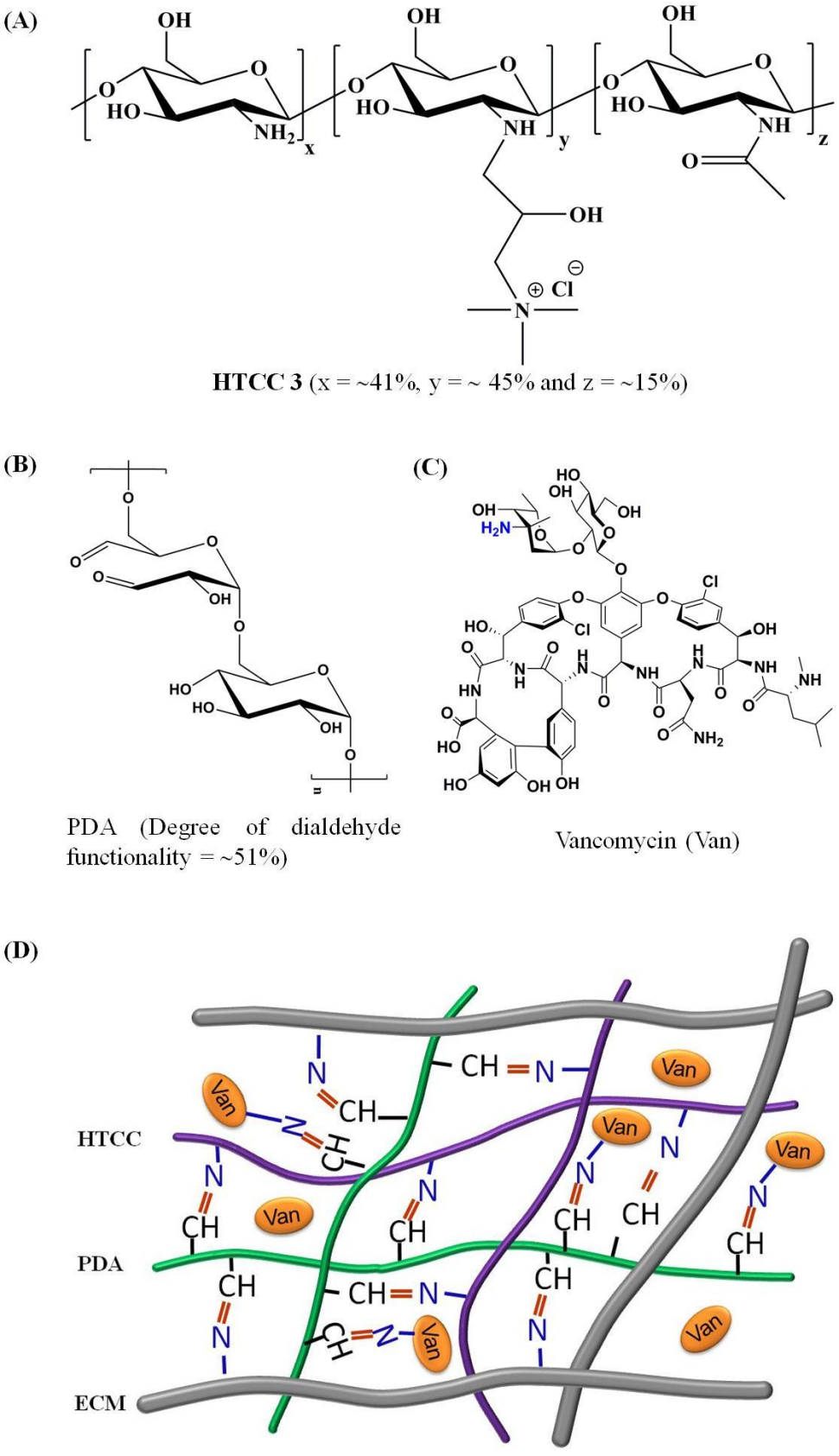

Figure 5B.1: Structures of hydrogel precursors and schematic representation of the antibiotic loaded hydrogels. (A) Structure of **HTCC 3**; (B) structure of PDA; (C) structure of vancomycin. (D) Schematic representation of the antibiotic loaded hydrogels showing both covalent and non-covalent encapsulation.

Since vancomycin contains free amine groups in its structure, thus it can react with the –CHO groups of PDA and are therefore expected to be conjugated covalently and/or non-covalently depending on the amount of antibiotic/PDA ratio. To evaluate the extent of covalent coupling of vancomycin with PDA, the polymer-antibiotic mixtures were kept for 1 h and then dialysed to remove non-conjugated antibiotic if there was any and then freeze dried. The covalent coupling of vancomycin with PDA was confirmed and quantified by FT-IR, ^{1}H-NMR and elemental analysis. Though the peak of amide I (C=O stretching) from vancomycin and the imine bond (C=N stretching) formed between vancomycin and PDA came at around 1644 cm^{-1}, the presence of amide II peak at 1583 cm^{-1} from vancomycin was clearly evident in the IR spectra of all the PDA-antibiotic combinations. Further, the IR spectra showed the presence of aromatic ring stretch (C=C stretching) at 1506 cm^{-1} which were absent in the non-conjugated PDA and originated from the coupled vancomycin (for vancomycin the same peak was observed at 1507 cm^{-1}). ^{1}H-NMR spectra also showed the presence of aromatic protons in the regions of 7.2 to 7.8 ppm which indicated the presence of benzene ring of vancomycin along with the other protons of either vancomycin or PDA in the region of 2.5-6.5 ppm. The % of antibiotic coupling was quantified from the elemental analysis of the PDA-antibiotic conjugates and it was found to be 100% for IHV-1, 85% for IHV-2 and 91% for IHV-3.

The viscoelastic properties of the hydrogels were studied by determining the elastic modulus (G′) and loss modulus (G′′) using pre-formed gels via oscillatory rheology as a function of frequency. Notably, G′ values of all the vancomycin loaded hydrogels (IHV-1, IHV-2 and IHV-3) were found to be closure to that of the gel without vancomycin (IHV-0) (Figure 5B.2A and B). While the IHV-0 showed G′ value of 830 ± 120 kPa, the elastic modulus values of IHV-1, IHV-2 and IHV-3 were 847 ± 87 kPa, 887 ± 141 kPa and 849 ± 110 kPa respectively. Further, all the formulation indicated gel formation as the G′ values were found to be higher than the G′′ values over the entire frequency range (1-100 rad/s) (Figure 5B.2A and B). The above results thus indicated that vancomycin loading has negligible effect of the mechanical stiffness of the gels. The surface as well as cross-sectional morphologies of the gels was observed by scanning electron microscopy after freeze-drying the gel disks followed by gold-sputtering (Figure 5B.2C and D). The surface morphologies of all the hydrogels showed a thin polymer layer which is probably due to the collapse of surface pores during the freeze-drying process (Figure 5B.2C). However, the cross-sectional

morphologies of all the gels showed characteristic sponge-like interconnected and porous structures with a number of irregular lamellar features (Figure 5B.2D).

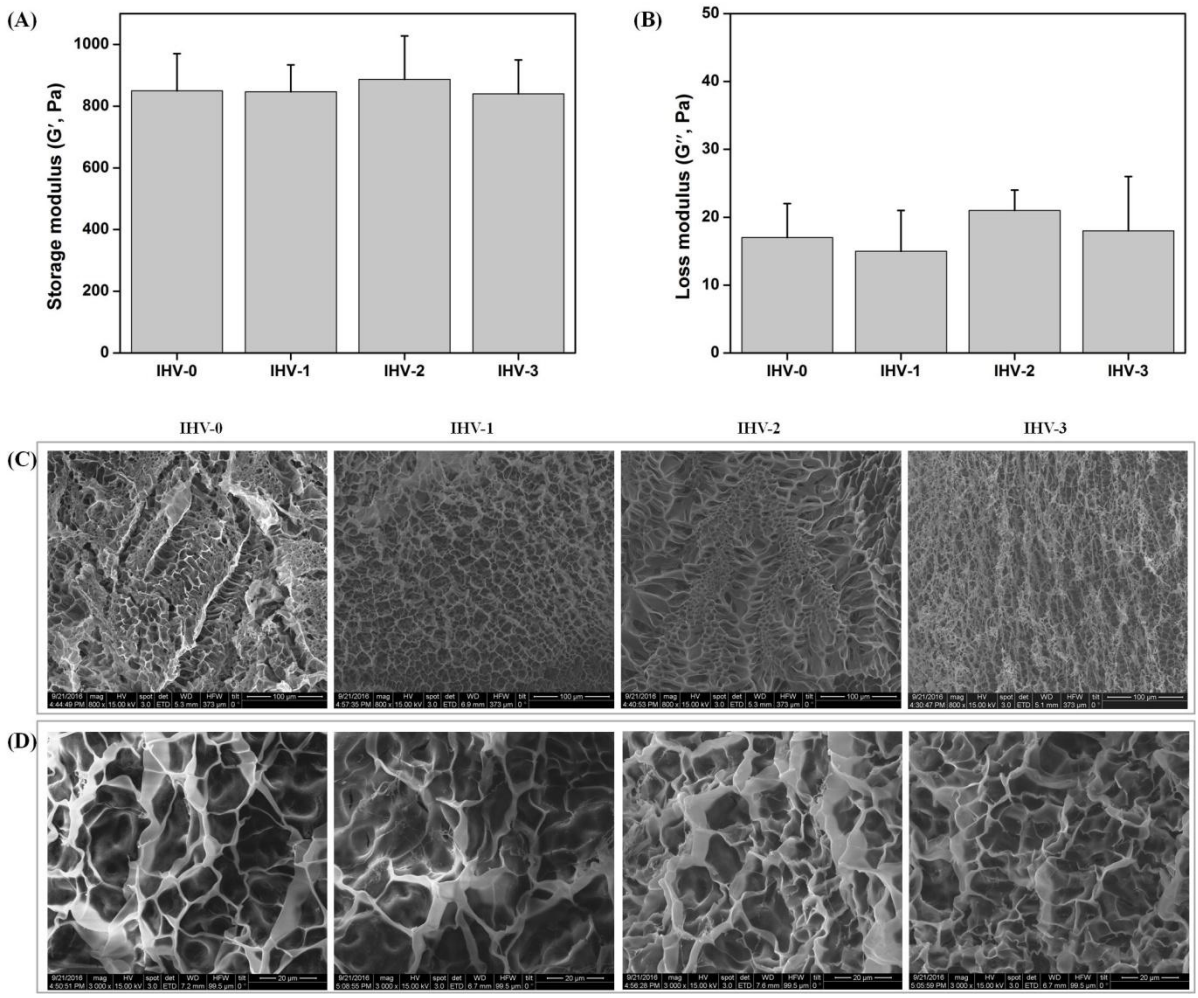

Figure 5B.2: Physical characterization of the vancomycin loaded gels. (A and B) Storage and loss modulii of the hydrogels as a function of varying vancomycin content keeping the PDA content constant. SEM photographs of freeze-dried hydrogels: (C) surface morphologies of hydrogels (D) cross-sectional morphologies of hydrogels.

FTIR spectroscopy was employed to identify the functional groups within the gels. Though PDA showed a peak at 1640 cm^{-1} in the IR spectra, the peak at 1650 cm^{-1} was assumed to be imine bond (C=N stretching) formed between vancomycin or HTCC and PDA. Also, the presence of amide II peak at 1586 cm^{-1} was clearly evident from the spectra that originated from vancomycin amide group (amide II stretching). Further, the IR spectra showed the presence of aromatic ring stretch (C=C stretching) at 1479 cm^{-1} thus confirming the encapsulation of antibiotic within the hydrogel matrix. Finally, the adhesive properties of the gels were measured by fixing the gels between two sections of porcine skins followed by lap-

shear analysis. The adhesive strength was found to be almost invariant with the variation of encapsulated antibiotics (the adhesive strength of IHV-0, IHV-1, IHV-2 and IHV-3 was 3.5 ± 1.2 to 6.9 ± 1.7 kPa). The above results thus indicated that these gels can be applied at the site of interests without any surgical procedure and therefore can be used as sealant.

5B.2.2 *In-vitro* antibacterial activity

Next the antibacterial efficacy of the hydrogels was evaluated by exposing the gel's surface to bacterial suspension. First the gels were prepared with or without antibiotic in a 96-well plate (100 μL of IHV-0, IHV-1, IHV-2 and IHV-3) and then challenged with 150 μL of 1.7×10^5 CFU/mL of a drug-sensitive *Staphylococcus aureus* and a drug-resistant *Staphylococcus aureus* (methicillin-resistant *S. aureus*, MRSA). Bacterial viability was then determined by plating the suspension on suitable agar plate after 6 h of treatment and then counting the colonies for each formulation. Blank well without any gels were used as control. Interestingly, all the gels reduced viability of both the bacteria significantly. While the control wells showed 9.5 ± 0.9 log CFU/mL *S. aureus*, IHV-0 (gel without any antibiotic) showed 3.4 ± 0.5 log CFU/mL bacteria after 6 h of treatment. Notably, gels with vancomycin (IHV-1, IHV-2 and IHV-3) showed complete killing of *S. aureus* (Figure 5B.3A). Similar results were obtained for the drug-resistant bacteria when the gels were challenged with 150 μL of 1.2×10^4 CFU/mL of MRSA. While the control wells was shown to have 6.8.5 ± 0.7 log CFU/mL MRSA after 6 h, IHV-0, IHV-1, IHV-2 and IHV-3 showed complete killing of bacteria (Figure 5B.3B). Interestingly, when the gel's surfaces were treated with higher amount of bacteria, vancomycin loaded gels showed far superior activity than the gel alone. For example, while the control wells showed 10.2 ± 1.1 log CFU/mL of bacteria after 6 h when incubated with an initial amount of 1.67×10^7 CFU/mL of *S. aureus*, gels with no or less antibiotic such as IHV-0 and IHV-1 showed 3.8 ± 0.8 log CFU/mL and 2.4 ± 0.4 log CFU/mL of bacteria. However, no bacteria were observed for the gels with higher amount of antibiotic, e.g., IHV-2 and IHV-3 (Figure 5B.3C). Not only against drug-sensitive bacteria, gels with antibiotic showed remarkably better efficiency than gels with no or less antibiotic against higher amount of drug-resistant bacteria. For example, while the control wells showed 8.7 ± 1.1 log CFU/mL of MRSA after 6 h for an initial amount of 1.1×10^6 CFU/mL of MRSA, IHV-0 and IHV-1 showed 2.8 ± 0.4 log CFU/mL and 2.3 ± 0.7 log CFU/mL of bacteria. IHV-2 and IHV-3, on the other hand, showed no bacteria thus indicating complete eradication of MRSA (Figure 5B.3D). The above results thereby suggested that the antibiotic

encapsulated gels are acting more effectively possibly by killing bacteria upon contact as well as by releasing vancomycin in the media. The above results also indicated that gel with an optimum amount of antibiotic (as in the case of IHV-2 which contains 0.3 wt% of antibiotic) is required for utmost efficacy.

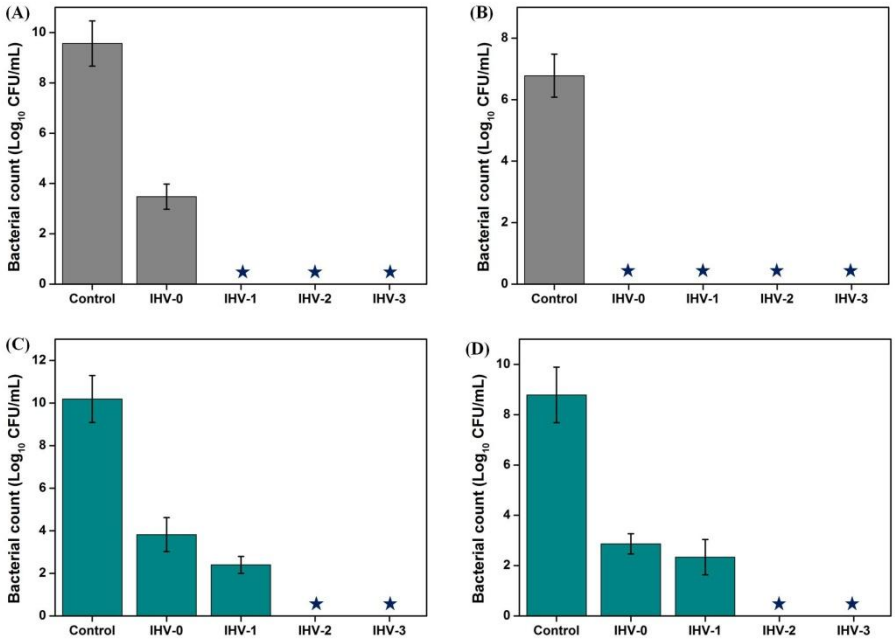

Figure 5B.3: Antibacterial activity of the hydrogels. Bacterial count after 6 h when 150 μL of the pathogen was challenged against the hydrogel's surface: (A) *S. aureus* count with an initial amount 1.7×10^5 CFU/mL (150 μL); (B) MRSA count with an initial amount 1.2×10^4 CFU/mL; (C) *S. aureus* count with an initial amount 1.67×10^7 CFU/mL and (D) MRSA count with an initial amount 1.1×10^6 CFU/mL. Stars represent less than 50 CFU/mL.

In order to establish that the gels released antibiotic into the surroundings, zone of inhibition (ZOI) experiment was performed.[22] This was done by preparing the gel on a suitable agar plate after removing a circular portion of agar, spreading MRSA (1 mL of ~10^8 CFU/mL) on the plate and then allowing to form bacterial lawns for about 24 h at 37 ˚C. As expected IHV-0 did not show any zone of clearance though it showed no colonies on the gel's surface thus inactivate bacteria only upon contact (Figure 5B.4A). IHV-1, IHV-2 and IHV-3, on the other hand, displayed significant zone of inhibition against MRSA lawns grown on the agar plate thereby suggested the diffusion of vancomycin to the surroundings which inactivated bacteria in the respective areas (Figure 5B.4B-D). Furthermore, IHV-3 with highest amount of encapsulated drug showed maximum zone of inhibition while IHV-1 with lowest amount of encapsulated drug showed minimum inhibition zone. The above

results thus suggested that diffusion of antibiotic is dependent on the initial amount of antibiotic loading.

In order to assess further that the gel without any antibiotic killed bacteria only upon contact whereas gels with antibiotic kill bacteria by both release and contact active mechanism, the gels were prepared within the separate inserts of a transwell cell culture plate.[15]

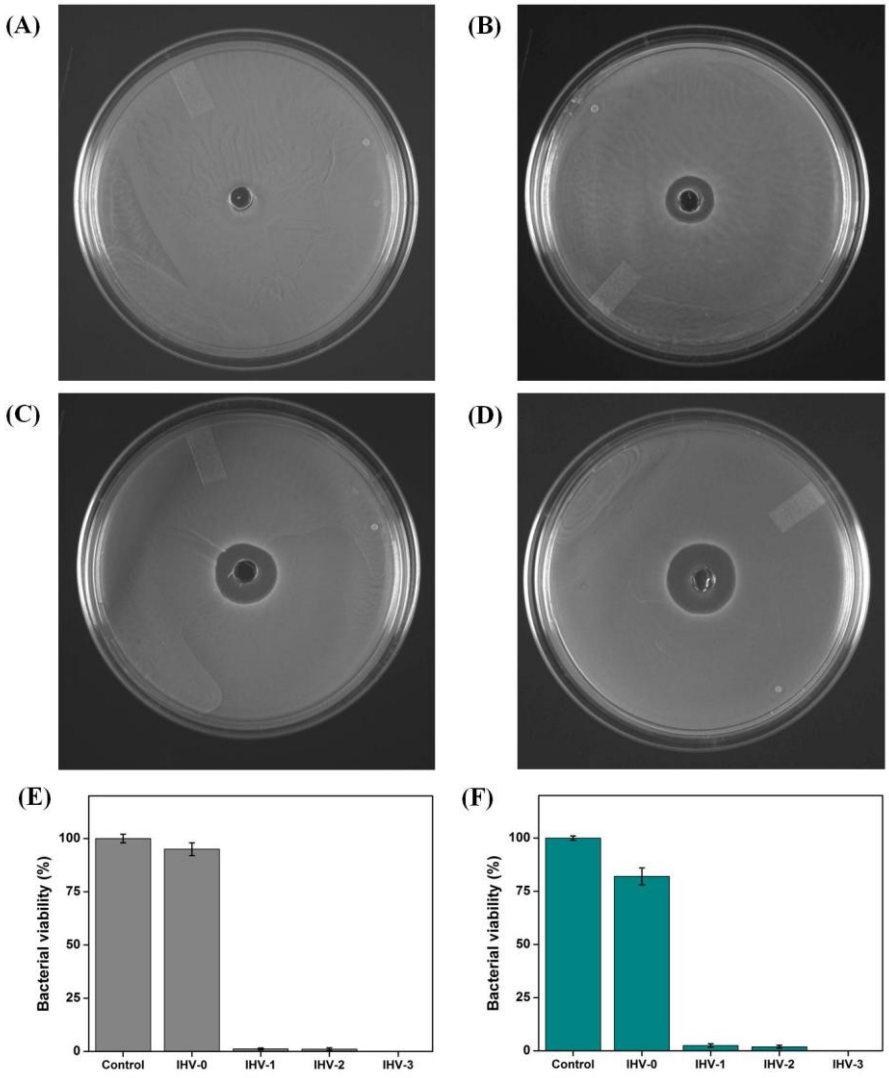

Figure 5B.4: Inhibition of bacterial lawn growth induced by releasing the antibiotic (vancomycin) containing hydrogels. Each plate has a confluent lawn of MRSA cells where the antibiotic diffused out from the central hydrogel disc and killed the surrounding bacteria leaving a clear zone. The hydrogels consisted of PDA and HTCC containing (A) 2.5 wt% PDA with 0 wt% vancomycin and 2.0 wt% HTCC (IHV-0); (B) 2.5 wt% PDA with 0.05 wt% vancomycin and 2.0 wt% HTCC (IHV-1); (C) 2.5 wt% PDA with 0.3 wt% vancomycin and 2.0 wt% HTCC (IHV-2) and (D) 2.5 wt% PDA with 0.6 wt% vancomycin and 2.0 wt% HTCC (IHV-3). Activity due to release of antimicrobials from the hydrogels against (E) *S. aureus* and (F) MRSA respectively.

The inserts were then placed in the wells which were spatially separated from the bacteria proliferating below in the wells of a tissue culture polystyrene plate. Like the control wells, substantial bacterial growth was observed in the wells with inserts containing IHV-0 after 24 h. If there was any release of HTCC from IHV-0, the bacterial growth should have been inhibited. The above results thus suggested that IHV-0 is capable of reducing bacterial count only on contact (Figure 5B.4E and F). Interestingly, wells with inserts that contained IHV-1, IHV-2 and IHV-3 showed no growth of bacteria thus indicated that these gels released vancomycin in the bottom solution leading to bacterial inhibition (Figure 5B.4E and F).

5B.2.3 Extended release of antibiotic and long lasting antibacterial activity

As most of the antibiotic was primarily incorporated via imine bond formation (100% for IHV-1 and more than 85% for IHV-2 and IHV-3) into the hydrogel matrix, it is expected that the gels will release the antibiotic over a period of time and hence will be able to display long lasting antibacterial activity required to eliminate infections completely especially in the less or no vascular tissues. The antibiotic release kinetics was studied by taking all three hydrogels (400 μL) wherein IHV-1, IHV-2 and IHV-3 contained 200 μg, 1200 μg and 2400 μg of the antibiotic respectively. Since the infection sites are commonly acidic in nature, the release kinetic was studied at three different pHs starting from neutral to acidic (pH 7.2, 6.2 and 5.5 respectively). First, 1 mL of buffer was added to the eppendorp tubes containing the gels and allowed to be in contact for 24 h. Then, the buffer solutions were collected and fresh buffer was added. Finally, the amount vancomycin released was quantified by UV-visible spectroscopy (vancomycin absorbed at 281 nm). Notably, gels were shown to release the antibiotic continuously over 14 days as tested (Figure 5B.5). The release of vancomycin was found to be dependent on the initial amount of loading (Figure 5B.5A-C). Interestingly, the release kinetics was found to be dependent on pH of the buffer as well. At pH 7.2, all the gels released higher amount of antibiotic. For example, while IHV-2 showed ~49-50% release at pH 5.5 and 6.2, 62% release was observed at pH 7.2 after 14 days (Figure 5B.5D-F). It should be mentioned that after 11 days, the UV-absorption spectra of the release buffer showed the presence of a weak absorption peak at 290-300 nm in addition to a peak at 281 nm at lower pHs (pH 5.5 or 6.2). This indicated that a minor amount of PDA-van conjugates with imine bonds got released from the gels along with the free antibiotics. Thus the studies were conducted till 14 days at all three pHs. It should also be mentioned that the IHV-2 and IHV-3 gels released slightly higher proportion of the antibiotic in the first 1-2 days possibly

by combined release of the covalently bonded vancomycin as well as diffusion of non-covalently bonded antibiotic (Figure 5B.5). However, the rate of release was found to be almost linear for all three formulations possibly due to the drug release being mostly controlled by the opening of the covalent imine bonds. In general, the above results indicated that an extended release of the drug was achievable by encapsulating antibiotics in the hydrogel network. Interestingly, gels with higher amount of vancomycin (IHV-2 or IHV-3) were shown to release the antibiotic till 40 days (at pH 7.2) which indicated the effectiveness of the matrix in controlling the release behavior of the antibiotic (for IHV-1 it was difficult to detect the vancomycin as the peak intensity at 281 nm was found to be very poor after 12 days).

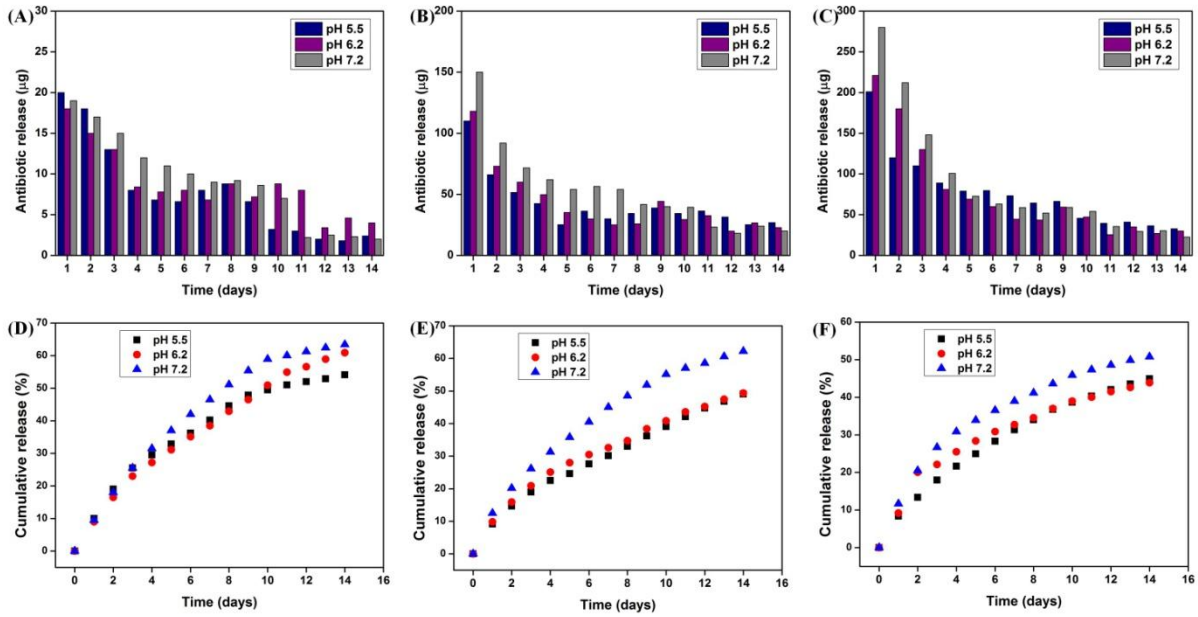

Figure 5B.5: Antibiotic release from the vancomycin-containing hydrogels. The amount of antibiotic released at different time interval from (A) IHV-1; (B) IHV-2 and (C) IHV-3 respectively. IHV-1, IHV-2 and IHV-3 contained an initial 200 μg, 1200 μg and 2400 μg of vancomycin and were used for release kinetics by adding 1 mL of buffer solution at varying pH and replacing the old buffer with fresh one after every 24 h. The amount antibiotic content in the solution was then determined by UV-visible absorption spectroscopy. Cumulative release of vancomycin from (D) IHV-1; (E) IHV-2 and (F) IHV-3 respectively.

A drug-carrier must retain the bioactivity of the encapsulated drug during and/or after fabrication.[23] Herein we tested the antibacterial activity of the released vancomycin collected in nutrient media with one of the most active formulations (IHV-2). Notably, the release media inactivated MRSA completely till 14 days as tested. These results thus portrayed the

utilities of the vancomycin-loaded hydrogels as dual action drug-carrier with effective and sustained release properties.

5B.2.4 *In-vitro* and *in-vivo* toxicity

It is known that the cationic polymers or hydrogels interact with the mostly negatively charged bacterial cell membrane leading cellular inactivation. However unlike bacterial cell membranes, mammalian cell membranes are mostly composed of zwitterionic lipids thus relatively less susceptible towards quaternary ammonium moiety. Though the differences in bacterial and mammalian cell membrane are significant, cationic hydrogels with substantial amount of antibiotic might also cause toxicity towards mammalian cells.

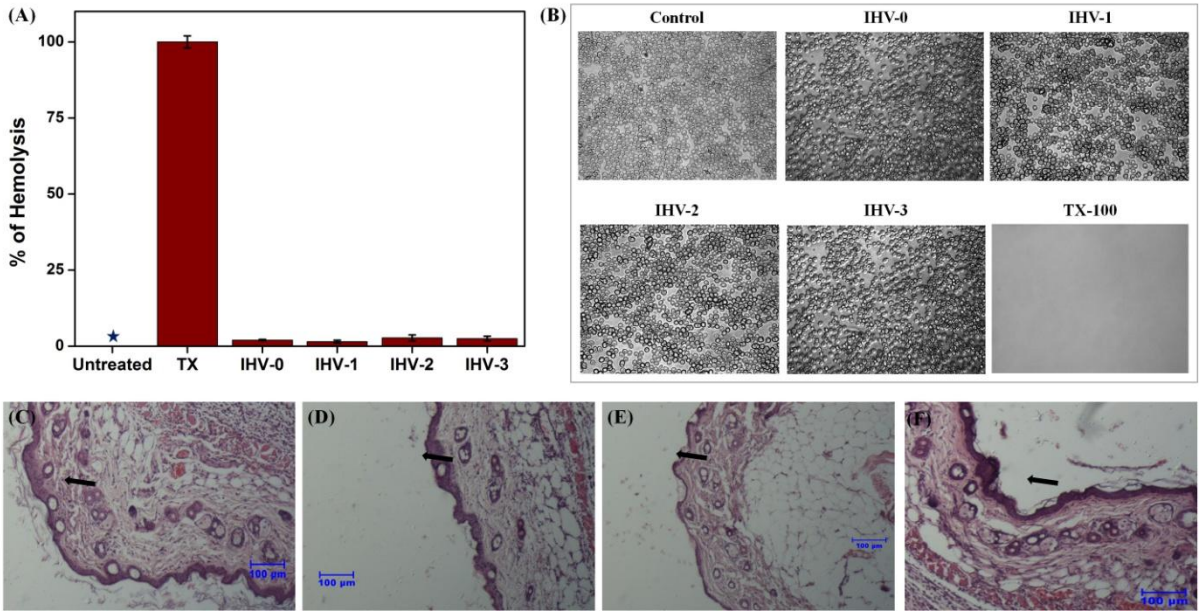

Figure 5B.6: *In-vitro* and *in-vivo* biocompatibility of the hydrogels. (A) Hemolytic activity of the gels as a function of increasing antibiotic content and the controls (untreated and TX-100); (B) optical micrograph images of hRBC collected from the surface of all the hydrogels including controls. *In-vivo* biocompatibility of the gels upon subcutaneous implanation in mice. Mice skin and subcutaneous tissue histopathology: (C) untreated skin tissue showing normal architecture of epidermis, dermis and subcutaneous tissues after 3 days; sweat gland, sebaceous gland was seen (arrow). (D, E and F) skin tissues showing normal dermis layer with sweat and sebaceous gland along with normal adipose tissue (arrow) for IHV-1, IHV-2 and IHV-3 respectively.

The compatibility of the gels *in-vitro* against human red blood cells (hRBC) and *in-vivo* via subcutaneous implantation in mice was therefore studied.[15] Hemocompatibility of the gels was evaluated by exposing the gel's surfaces with hRBC and finding out the percentage of

hemolysis occurred with respect to a toxic surfactant triton-X (TX-100). All the vancomycin-loaded hydrogels (IHV-1, IHV-2 and IHV-3) showed negligible hemolysis like the gel without any antibiotic (IHV-0). Only 2-3% hemolysis was observed for all the hydrogel formulations (Figure 5B.6A). This implied that the gels were compatible against human erythrocytes. In order to have visual insight, blood cells were also imaged via optical microscopy after exposing them to the gel's surface. Notably, treated cells were found to have healthy and round morphology typical of normal blood cells as observed in the case of control (non-treated hRBC). In contrast, TX-100 treated samples showed complete killing of cells as no RBCs were observed under microscope (Figure 5B.6B). The above facts therefore further indicated the hemocompatible nature of the hydrogels. The biocompatibility of the hydrogels was then evaluated *in-vivo* by injecting one of the most potent antibiotic-loaded gels (IHV-2) subcutaneously in mice. After 3 days and 7 days of post-implantation the histopathological responses in the surrounding tissue was recorded via haematoxylin and eosin staining. Interestingly, the tissue surrounding the gel showed negligible inflammation and normal architecture of dermis, epidermis and subcutaneous tissues like the saline treated tissue samples (Figure 5B.6C-F). The above results therefore suggested that gels were indeed non-toxic towards mammalian cells.

5B.2.5 *In-vivo* activity (cecam ligation and puncture model of sepsis)

To evaluate the potency of the gel in preventing infections under *in-vivo* conditions, cecal ligation and puncture (CLP) model of sepsis was performed similarly as described in the previous chapter for the hydrogel without vancomycin.[15] Here, after puncturing the ceca of mice, one of the most active formulations IHV-2 was applied in the punctured area and then returned back into the abdominal cavity. Only ligated ceca with gel and in another case punctured and ligated ceca without any gel were used as controls. After 24 h, first ceca of animals were imaged to visualize the effect. Notably, the punctured ceca with no gel were found to be black in colour suggesting severe infection (Figure 5B.7A) whereas ceca with the gel were found to be normal in colour (Figure 5B.7B). The above facts therefore suggested that the gel formed an efficient barrier to infection. When the survival rate of the mice was also monitored for the 8 post-operative days, merely 1-2 animal from a group of 8 survived in the control group without gel (survival rate 12.5-25%). However, 5-6 mice were found to survive in the case of gel treated group (survival rate 62.5-75%) (Figure 5B.7C). The above results therefore suggested that the gel was able to seal the leakage and prevent sepsis. Furthermore, when the gel was applied on the ceca without puncturing it, survival rate was

very high (87.5-100%). These observations further suggested that the gels were non-toxic at the organ level.

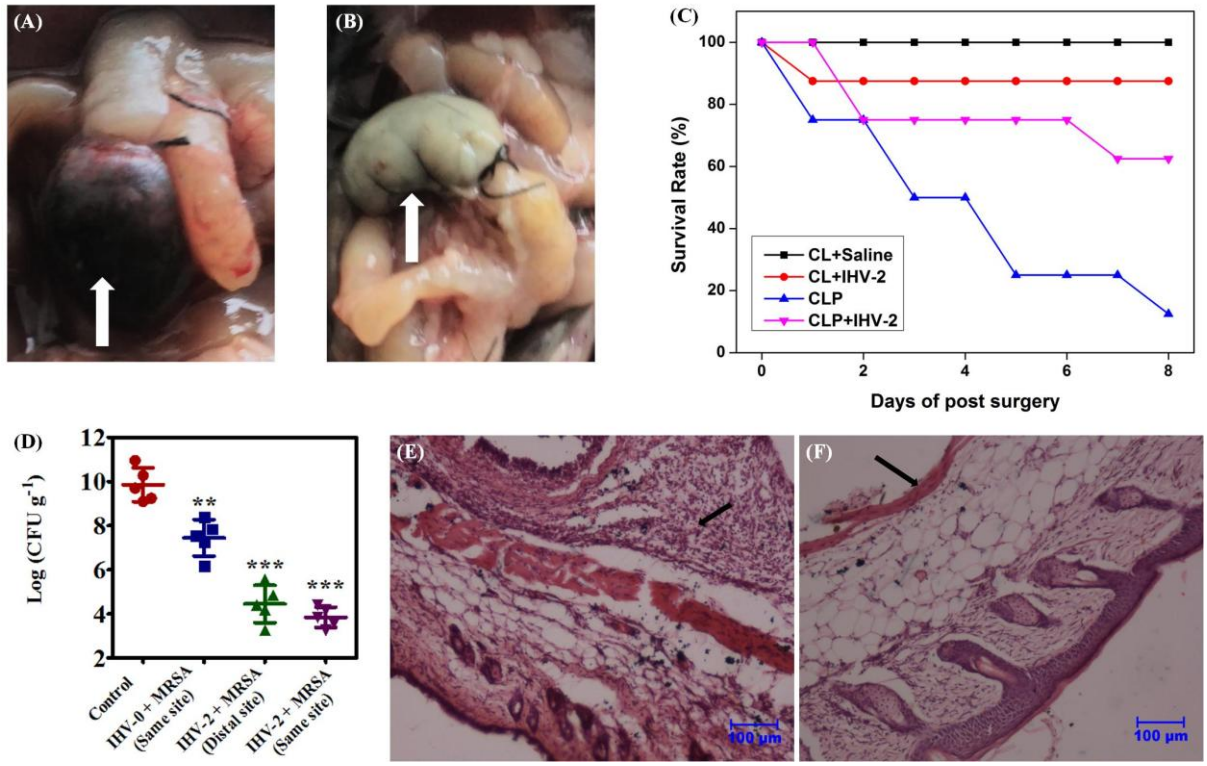

Figure 5B.7: *In-vivo* activity of the hydrogels. Efficacy of the hydrogel in sealing leaks and preventing sepsis by cecal ligation and puncture model: (A) isolated punctured cecam after 24 h of surgery treated with no gel and (B) punctured cecam after 24 h of surgery treated with the gel; (C) survival rates of the animals at different conditions with punctured and ligated caca with or without the gel (IHV-2). Evaluation of antibacterial activity upon injection of MRSA subcutaneously in mice: (D) MRSA count after 72 h of infection at different conditions; p values (*) are 0.002, <0.0001 and <0.0001 for IHV-0, IHV-2 (same site) and IHV-2 (distal site) samples. Mice skin and subcutaneous tissue histopathology after hematoxylin and eosin staining: for (E) only saline and (F) IHV-2.

5B.2.6 *In-vivo* activity (Subcutaneous model of MRSA infection)

Since the gel without any antibiotic was also able to prevent the sepsis, the superior antibacterial efficacy of the antibiotic loaded gels was established in another model via subcutaneous injection and infection.[15] First, IHV-2 (100 µL) was injected subcutaneously in mice that were already rendered neutropenic. In one group (n = 5) bacteria (40 µL of 10^7 CFU/mL MRSA) were then directly injected into the gel. In another group bacteria were injected at a distal site in order to study the efficacy of the gel to deliver antibiotic locally and also to evaluate efficacy in clearing infection far from the implantation site. Bacteria were

injected subcutaneously without the gel and gel without any antibiotic (IHV-0) and were used as controls. Once the infection was clinically evident in the control mice (after 72 h), both the control and experimental mice were killed and infection sites were imaged. While significant amount of pus formation was noticed when MRSA was injected in mice, no pus formation was observed when bacteria were injected into the gel. Interestingly, no pus formation was observed even when the bacteria were injected at a distal site from the gel thereby suggesting that the antibiotic got released from the gel and reduced the viable bacterial.

To quantify the ability of the vancomycin-loaded gel in eradicating infections both at the site of implantation as well as far from the injection site, we evaluated the bacterial count at the surrounding tissues. First, the infected tissue were collected and subsequently homogenised. Finally, the tissue lysate was then plated on suitable agar plate and enumerated for bacterial count. Notably, skin tissue surrounding the IHV-2 gel showed 6.1 log CFU less MRSA as compared to the non-treated tissue sample when the bacteria were injected directly onto the gel (while the non-treated tissue showed ~9.9 log CFU/g of MRSA, the gel treated tissue sample showed 3.8 log CFU/g of MRSA) (Figure 5B.8D). Most importantly, 5.8 log reduction of MRSA was observed for IHV-2 gel when bacteria were injected at a distal site from the gel (Figure 5B.8D). This is possible due to the gradual release of the antibiotic in the surroundings over time thus leading to the inhibition of bacterial growth even when the bacteria were injected far from the gel. To establish that it is the released antibiotics which reduced MRSA count, we also injected bacteria far from the gel that contain no antibiotic (IHV-0), almost same amount of MRSA like the control case (~9.6 log CFU/g) was observed. The above results therefore suggested that the antibiotic loaded gels not only showed higher antibacterial efficacy but also capable of delivering antibiotic into the target area locally. The efficacy of the gel was further established by histopathology examination of both treated and untreated tissue samples. While the control tissue samples showed severe infiltration of inflammatory cells mostly neutrophils and mononuclear cells in the subcutaneous tissues (arrow) with congestion of blood vessels (inset) (Figure 5B.8E), tissue surrounding the antibiotic loaded gel showed normal morphology with minimal inflammation at the epidermis, dermis and skin tissue (Figure 5B.8F). Collectively, the above results indicated that the vancomycin containing gel was able to reduce infection in the surrounding tissues and prevent the spreading of infections.

5B.3 Conclusion

In this chapter vancomycin was loaded into an inherently antibacterial injectable hydrogel thereby not only delivering the antibiotic locally but also enhancing the antibacterial efficacy of the system. The syringe deliverable hydrogel was prepared by mixing the aqueous solution of PDA containing the antibiotics and a cationic antibacterial polymer HTCC. The antibiotic was loaded via both non-covalently and covalently and was shown to get released over an extended period of time at different pH. The gels showed much higher activity than the gel alone against bacteria. Further, the gels were shown to be completely active till the tested period of time (till day 14). The gels were also shown to be highly active under *in-vivo* conditions against MRSA when the bacteria were directly injected into the gel. Moreover, when MRSA was injected at a distal site far from the gel, the vancomycin loaded gel was shown to be effective in clearing the surrounding MRSA infections. One of the most active formulations (PDA 2.5 wt%, HTCC 2.0% with 0.3 wt% vancomycin) showed no toxicity towards human red blood cells and to the surrounding tissue when injected subcutaneously in mice. Thus hydrogels developed herein thus might hold promise to be used in combating infections in less vascular and avascular tissue level.

5B.4 Experimental section

5B.4.1 Materials and instrumentation

Dextran from *Leuconostic* spp. (M_r ~40 kDa), glycidyltrimethylammonium chloride (GTMAC), acetic acid, sodium periodate ($NaIO_4$), hydroxyl amine, methyl orange were purchased from Sigma-Aldrich, USA as used as received. Low molecular chitosan with a degree of acetylation (DA) ~85% (molecular weight = 15 kDa) was purchased from Polysciences, USA. Acetone, ethanol and other organic solvents were of analytical grade and purchased from Spectrochem, India. The water used in all experiments was Millipore water with a resistivity of 18.6 MΩ cm. *Staphylococcus aureus* (MTCC 737) was purchased from MTCC (Chandigarh, India). Methicilin-resistant *Staphylococcus aureus* (MRSA) (ATCC 33591) was obtained from ATCC (Rockvillei, Md). Bacterial growth media and agar were supplied by HIMEDIA, India. Nuclear magnetic resonance spectra (^{1}H NMR and ^{13}C NMR) were recorded on a Bruker AMX-400 instrument (400 MHz) in deuterated solvents. Solid state NMR (^{13}C cross polarization magic angle spinning, ^{13}C CP-MAS), was performed in Bruker Avance III spectrometer. FT-IR spectra of the solid compounds were recorded on Bruker IFS66 V/s spectrometer using KBr pellets. Electron microscopy images were captured

in using field emission scanning electron microscope (Quanta 3D FEG, FEI). Oscillatory rheology experiments were performed on preformed adhesive gels using a TA Instrument AR-G2 rheometer, using a 25 mm diameter stainless steel parallel plate tool. Adhesive strength of the gels was performed using Q800 dynamic mechanical analyser (DMA) (TA, Instruments). Eppendorf 5810R centrifuge was used for centrifugation. TECAN (Infinite series, M200 pro) Plate Reader was used to measure optical density. Studies on animal subjects were performed following the protocols approved by Institutional Bio-safety Committee (IBSC) of Jawaharlal Nehru Centre for Advanced Scientific Research (JNCASR). Studies with the animals were performed following protocols approved by the Institutional Animal Ethics Committee (IAEC) in the institute (Jawaharlal Nehru Centre for Advanced Scientific Research).

5B.4.2 Synthesis of HTCC

The antibacterial polymer **HTCC 3** having 46% quaternary ammonium group, 39% primary amine group and 15% of *N*-acetyl group was synthesized from chitosan (degree of acetylation 15%) according to the protocol described in the section 5A.4.2.1 of chapter 5A.

5B.4.3 Synthesis of PDA

The bioadhesive polymer PDA with ~51% degree of functionality was synthesized from dextran according to the protocol described in the section 5A.4.2.3 of chapter 5A.

5B.4.4 Synthesis of vancomycin loaded hydrogels

First vancomycin was dissolved in phosphate buffer (23.5 mM NaH_2PO_4, 80.5 mM Na_2HPO_4) at required amount (1 mg/mL, 6 mg/mL and 12 mg/mL). To this PDA (50 mg) was added to obtain PDA solution containing vancomycin in the above mentioned concentration (5 wt% PDA, 0.1 wt%, 0.6 wt% and 1.2 wt% vancomycin respectively). After 1 h, an equal volume of 40 mg/mL **HTCC 3** (4.0 wt%) dissolved in water was added to the PDA solution containing vancomycin. The mixture was then kept in an incubator for 15 min at 37 ˚C to allow hydrogel formation. This resulted in various gel formulations (IHV-1: 2.5 wt% PDA with 0.05 wt% vancomycin and 2.0 wt% HTCC; IHV-2: 2.5 wt% PDA with 0.3 wt% vancomycin and 2.0 wt% HTCC; IHV-3: 2.5 wt% PDA with 0.6 wt% vancomycin and 2.0 wt% HTCC). Thus three different gel compositions were obtained where the wt% of vancomycin was varied keeping the amount of HTCC and PDA constant. Hydrogel without

any vancomycin (IHV-0) was prepared by adding 5 wt% PDA solution to 4 wt% **HTCC 3** solution. The gels were prepared directly in the wells of a 96-well plate or in a sample vial or in petri dish either by simple mixing of the solutions or by mixing via dual barrel syringe.

5B.4.5 Characterization of the hydrogels

5B.4.5.1 Gelation time

The gelation time, i.e., the time required to form the gel upon mixing the components together, was determined according to the protocol described in the section 5A.4.4.1 of chapter 5A.

5B.4.5.2 Morphologies (Scanning electron microscopy)

Morphologies of the hydrogels were characterized by field emission scanning electron microscopy (FESEM) with the preformed hydrogel following the same protocol as described in the section 5A.4.4.2 of chapter 5A.

5B.4.5.3 Fourier transformed infrared (FT-IR)

Fourier transformed infrared (FTIR) spectra of PDA, HTCC and hydrogel were recorded following the same protocol as described in the section 5A.4.4.3 of chapter 5A.

5B.4.5.4 Viscoelastic properties

Viscoelastic properties were measured using an oscillatory rheometer on preformed hydrogels following the same protocol as described in the section 5A.4.4.4 of chapter 5A.

5B.4.6 Determination of adhesive stress

The adhesive strength of the gel was measured by fixing the gel between two sections of porcine skin following the same protocol as described in the section 5A.4.5 of chapter 5A.

5B.4.7 Determination of PDA-conjugated vancomycin (% of covalent encapsulation of antibiotic)

The extent of covalent conjugation of vancomycin to PDA and hence in the gel was determined as follows: PDA (50 mg) and vancomycin (1 mg or 6 mg or 12 mg) were dissolved in phosphate buffer and kept at 37 ˚C for 1 h in the dark. The solution was then dialyzed using membranes (molecular cut off 3500) at 4 ˚C in deionized water in the dark by

changing water quickly for 6-8 h on a regular interval with 0.5 h between each water change. The solution was then freeze dried and stored at 4 ˚C in the dark for characterization. ^{1}H-NMR and FT-IR spectra of the freeze dried sample was then recorded. Also the freeze dried sample was first fully dried in a vacuum over at 55 ˚C and then used for elemental analyses.

5B.4.8 *In-vitro* antibacterial activity

First the hydrogels with or without antibiotic were prepared in the wells of a 96-well plate (50 μL 50 mg/mL of PDA containing 1 mg/mL or 6 mg/mL or 12 mg/mL of vancomycin and 50 μL 40 mg/mL of **HTCC 3**). The plate was then kept for 10-15 min in an incubator to allow the gel formation. To the wells containing the gel bacteria (150 μL of ~10^5 CFU/mL or 10^7 CFU/mL of *S. aureus* and MRSA) were added. The plates containing bacteria were then incubated at 37 ˚C for about 6 h under constant shaking. After incubation, 50 μL of bacterial suspension was either directly plated or diluted following 10-fold serial dilution and then plated on suitable agar plate. The agar plates were then incubated for about 24 h at 37 ˚C. Finally bacterial colonies were counted to evaluate the reduction in viable cells. The presence of viable bacterial count in each case was then expressed as log CFU/mL. A similar experiment was performed with the blank wells without any gels and hydrogel without any vancomycin as controls.

5B.4.9 Determination of dual mechanism of action

5B.4.9.1 Determination of released-based activity (Zone of inhibition)

Nutrient agar gels were prepared in petri dishes (90 mm) according to the manufacturer's protocols. Briefly, 2.5 g of nutrient agar was dissolved in 100 mL of Millipore water and then autoclaved for 15-18 min at 121 ˚C. After cooling to 50 ˚C, a volume of 12-15 mL of the agar solution was added to the petri dishes and allowed to cool to room temperature, resulting in solid agar gel. A circular piece (6 mm in diameter) of the agar gel was removed by incision to reveal the underlying polystyrene. A 50 μL of IHV-0, IHV-1, IHV-6 and IHV-12 gel was then prepared in the cavity of agar plates following the method as mentioned previously. The hydrogel was incubated at 37 ˚C for 15 min, after which the gel surfaces were washed three times with 5 mL of PBS to remove any non-cross-linked **HTCC 3** and to ensure that the pH was equilibrated. A volume of 1 mL ml of 10^8 CFU/mL of *S. aureus* and MRSA was added to each dish and gently rocked to provide the full surface coverage. The plates were then incubated for 24 h imaged by Cell biosciences gel documentation instrument.

5B.4.9.2 Determination of contact-based activity

The contact based and release based mode of action of the vancomycin loaded hydrogel was determined following the same protocol as described in the section 5A.4.7 of chapter 5A by preparing the gel into the inserts of of a trans-well cell culture plate (24-well).

5B.4.10 Long lasting antibacterial activity

Hydrogel (IHV-2) was prepared in eppendorf tube (2 mL) by mixing the components (200 μL of 50 mg/mL PDA with 6 mg/mL vancomycin and 200 μL of 40 mg/mL **HTCC 3**). After the preparation, 1 mL of PBS buffer or nutrient media was added on top of the gel. Then the gel with the added liquid was kept for constant shaking at 37 °C for 24 h. After 24 h, the buffer or media was collected and replaced with the fresh buffer. The process was repeated for next 14 days. Finally, the antibacterial activity of the released vancomycin was determined by taking 450 μL of the buffer or media with 50 μL of ~10^7 CFU/mL MRSA. The bacterial mixture was kept for 24 h and then OD value was recorded. Also, the released media-bacterial solution was directly spot plated on agar plate to determine the bactericidal effect of the released vancomycin.

5B.4.11 *In-vitro* release kinetics of vancomycin from the gels

Hydrogel (IHV-2) was prepared in eppendorf tube (2 mL) by mixing the components in a similar way as described in previously (200 μL of 50 mg/mL PDA with 6 mg/mL vancomycin and 200 μL of 40 mg/mL **HTCC 3**). After the preparation, 1 mL of phosphate buffer of varying pH (5.5, 6.2 and 7.2) was added on top of the gel. Then the gel with the added buffer was kept for constant shaking at 37 °C for 24 h. After 24 h, the buffer was collected and replaced with the fresh buffer. The process was repeated for next 14 days. Finally, the amount of released vancomycin was determined by UV-visible absorption spectroscopy. A standard calibration curve of absorption intensity *vs* concentration was generated for vancomycin (absorbance at 281 nm). The concentration of the released vancomycin was then determined after measuring the absorbance and fixing the value in the absorption intensity *vs* concentration curve.

5B.4.12 Biocompatibility

5B.4.12.1 Systemic toxicity with HTCC

Systemic toxicity of the HTCC polymers was determined following the same protocol as described in the section of 4A.4.14.3 in Chapter 4A.

5B.4.12.2 Sub-chronic toxicity with HTCC

BALB/c mice were used for the sub-chronic toxicity studies (four groups of mice, 10 mice in each group).[24] Polymer solution in sterilized saline (200 μL) was given via i.p. injection of **HTCC 3** at a dosage of 55 mg/kg in two groups and the remaining two groups were used as control. After 2 days, blood was collected from both control and treated mice (10 mice for HTCC, 10 mice for control), and analyzed for different parameters like ALT (alanine transaminase), AST (aspartate transaminase), creatinine, blood urea nitrogen, and electrolytes like sodium ion, potassium ion and chloride ion. Also after 14 days, blood was collected similarly from the remaining 20 mice (10 mice for **HTCC 3**, 10 mice for control) and analyzed for the above mentioned parameters. The data are presented as mean ± standard deviation, based on the values obtained from 10 mice (n = 10 for the data from this report). Student's t-test was used for statistical analysis. Differences are considered statistically significant with probability (p) < 0.05.

5B.4.12.3 *In-vitro* toxicity of hydrogel (Hemolytic assay)

Hemolytic activity of the antibiotic loaded hydrogels was evaluated following same protocol as described in the section 5A.4.9 in Chapter 5A.

5B.4.12.4 *In-vivo* toxicity of hydrogel (Subcutaneous injection)

In-vivo toxicity of the antibiotic loaded hydrogels was evaluated by subcutaneous injection of the gels in mice following same protocol as described in the section 5A.4.10.3 in Chapter 5A.

5B.4.13 *In-vivo* activity of hydrogel

5B.4.13.1 Cecal ligation and puncture (CLP) model of sepsis

Cecam ligation and puncture model of sepsis for the antibiotic loaded hydrogels was evaluated following same protocol as described in the section 5A.4.13 in Chapter 5A.

5B.4.13.2 Subcutaneous infection model

Subcutaneous infection model to evaluate the *in-vivo* efficacy of the antibiotic loaded hydrogels was evaluated following same protocol as described in the section 5A.4.14 in Chapter 5A.

BIBLIOGRAPHY

1. Sauermann, R.; Karch, R.; Langenberger, H.; Kettenbach, J.; Mayer-Helm, B.; Petsch, M.; Wagner, C.; Sautner, T.; Gattringer, R.; Karanikas, G.; Joukhadar, C. Antibiotic abscess penetration: fosfomycin levels measured in pus and simulated concentration-time profiles. *Antimicrob. Agents Chemother.* **2005**, *49*, 4448-4454.
2. Nandi, S. K.; Mukherjee, P.; Roy, S.; Kundu, B.; De, D. K.; Basu, D. Local antibiotic delivery systems for the treatment of osteomyelitis - a review. *Mater. Sci.Eng. C Mater. Biol. Appl.* **2009**, *29*, 2478-2485.
3. Han, G.; Martinez, L. R.; Mihu, M. R.; Friedman, A. J.; Friedman, J. M.; Nosanchuk, J. D. Nitric oxide releasing nanoparticles are therapeutic for Staphylococcus aureus abscesses in a murine model of infection. *PLoS One* **2009**, *4*, e7804
4. Kojic, N.; Pritchard, E. M.; Tao, H.; Brenckle, M. A.; Mondia, J. P.; Panilaitis, B.; Omenetto, F.; Kaplan, D. L. Focal infection treatment using laser-mediated heating of injectable silk hydrogels with gold nanoparticles. *Adv. Funct. Mater.* **2012**, *22*, 3793-3798.
5. Darouiche, R. O. Device-associated infections: A macroproblem that starts with microadherence. *Clin. Infect. Dis.* **2001**, *33*, 1567-1572.
6. Donlan, R. M. Biofilms and device-associated infections. *Emerg. Infect. Diseases* **2001**, *7*, 277-281.
7. Hempel, S.; Newberry, S. J.; Maher, A. R.; Wang, Z.; Miles, J. N. V.; Shanman, R.; Johnsen, B.; Shekelle, P. G. Probiotics for the prevention and treatment of antibiotic-associated diarrhea a systematic review and meta-analysis. *JAMA* **2012**, *307*, 1959-1969.
8. Marx, R. E.; Sawatari, Y.; Fortin, M.; Broumand, V. Bisphosphonate-induced exposed bone (osteonecrosis/osteopetrosis) of the jaws: risk factors, recognition, prevention, and treatment. *J. Oral Maxillofac. Surg.* **2005**, *63*, 1567-1575.
9. Fitzgerald, R. H., Jr. Experimental osteomyelitis: description of a canine model and the role of depot administration of antibiotics in the prevention and treatment of sepsis. *J. Bone Joint Surg. Am.* **1983**, *65*, 371-380.
10. Drillich, M.; Beetz, O.; Pfutzner, A.; Sabin, M.; Sabin, H. J.; Kutzer, P.; Nattermann, H.; Heuwieser, W. Evaluation of a systemic antibiotic treatment of toxic puerperal metritis in dairy cows. *J. Dairy Sci.* **2001**, *84*, 2010-2017.
11. Blair, J. M. A.; Webber, M. A.; Baylay, A. J.; Ogbolu, D. O.; Piddock, L. J. V. Molecular mechanisms of antibiotic resistance. *Nature Rev.Microbiol.* **2015**, *13*, 42-51.
12. Stewart, P. S.; Costerton, J. W. Antibiotic resistance of bacteria in biofilms. *Lancet* **2001**, *358*, 135-138.
13. Mehdizadeh, M.; Yang, J. Design strategies and applications of tissue bioadhesives. *Macromol. Biosci.* **2013**, *13*, 271-288.
14. Guo, J. S.; Wang, W.; Hu, J. Q.; Xie, D. H.; Gerhard, E.; Nisic, M.; Shan, D. Y.; Qian, G. Y.; Zheng, S. Y.; Yang, J. Synthesis and characterization of anti-bacterial and anti-fungal citrate-based mussel-inspired bioadhesives. *Biomaterials* **2016**, *85*, 204-217.
15. Giano, M. C.; Ibrahim, Z.; Medina, S. H.; Sarhane, K. A.; Christensen, J. M.; Yamada, Y.; Brandacher, G.; Schneider, J. P. Injectable bioadhesive hydrogels with innate antibacterial properties. *Nat. Commun.* **2014**, *5*.
16. Zhao, X.; Li, P.; Guo, B. L.; Ma, P. X. Antibacterial and conductive injectable hydrogels based on quaternized chitosan-graft-polyaniline/oxidized dextran for tissue engineering. *Acta Biomater.* **2015**, *26*, 236-248.
17. Hudson, S. P.; Langer, R.; Fink, G. R.; Kohane, D. S. Injectable in situ cross-linking hydrogels for local antifungal therapy. *Biomaterials* **2010**, *31*, 1444-1452.

18. Zhang, Y.; Zhang, J. H.; Chen, M. G.; Gong, H.; Tharnphiwatana, S.; Eckmann, L.; Gao, W. W.; Zhang, L. F. A bioadhesive nanoparticle-hydrogel hybrid system for localized antimicrobial drug delivery. *ACS Appl. Mater. Interfaces* **2016**, *8*, 18367-18374.
19. Hamada, Y.; Kuti, J. L.; Nicolau, D. P. Vancomycin serum concentrations do not adequately predict tissue exposure in diabetic patients with mild to moderate limb infections. *J. Antimicrob. Chemother.* **2015**, *70*, 2064-2067.
20. Fish, R.; Nipah, R.; Jones, C.; Finney, H.; Fan, S. L. S. Intraperitoneal vancomycin concentrations during peritoneal dialysis-associated peritonitis: correlation with serum levels. *Perit. Dial. Int.* **2012**, *32*, 332-338.
21. Sharpe, J. N.; Shively, E. H.; Polk, H. C., Jr. Clinical and economic outcomes of oral linezolid versus intravenous vancomycin in the treatment of MRSA-complicated, lower-extremity skin and soft-tissue infections caused by methicillin-resistant Staphylococcus aureus. *Am. J. Surg.* **2005**, *189*, 425-428.
22. Pritchard, E. M.; Valentin, T.; Panilaitis, B.; Omenetto, F.; Kaplan, D. L. Antibiotic-releasing silk biomaterials for infection prevention and treatment. *Adv. Funct. Mater.* **2013**, *23*, 854-861.
23. Gustafson, C. T.; Boakye-Agyeman, F.; Brinkman, C. L.; Reid, J. M.; Patel, R.; Bajzer, Z.; Dadsetan, M.; Yaszemski, M. J. Controlled delivery of vancomycin via charged hydrogels. *PLoS One* **2016**, *11*, e0146401.
24. Uppu, D. S.; Manjunath, G. B.; Yarlagadda, V.; Kaviyil, J. E.; Ravikumar, R.; Paramanandham, K.; Shome, B. R.; Haldar, J. Membrane-active macromolecules resensitize NDM-1 gram-negative clinical isolates to tetracycline antibiotics. *PLoS One* **2015**, *10*, e0119422.

List of publications

PhD Thesis Publications

1. **J. Hoque**, P. Akkapeddi, V. Yadav, G. B. Manjunath, D. S. S. M. Uppu, M. M. Konai, V. Yarlagadda, K. Sanyal and J. Haldar. Broad spectrum antibacterial and antifungal polymeric paint materials: synthesis, structure-activity relationship and membrane-active mode of action**.** *ACS Appl. Mater. Interfaces* **2015**, *7*, 1804-1815.

2. **J. Hoque**, M. M. Konai, S. Gonuguntla, G. B. Manjunath, S. Samaddar, V. Yarlagadda and J. Haldar. Membrane active small molecules show selective broad spectrum antibacterial activity with no detectable resistance and eradicate biofilms. *J. Med. Chem.* **2015**, *58*, 5486-5500.

3. J. Hoque, M. M. Konai, S. Samaddar, S. Gonuguntla, G. B. Manjunath, C. Ghosh and J. Haldar. Selective and broad spectrum amphiphilic small molecules to combat bacterial resistance and eradicate biofilm. *Chem. Commun.* **2015**, 51, 13670-13673.

4. **J. Hoque**, U. Adhikary, V. Yadav, S. Samaddar, M. M. Konai, R. G. Prakash, K. Sanyal and J. Haldar. Chitosan derivatives active against multi-drug-resistant bacteria and pathogenic fungi: *in vivo* evaluation as topical antimicrobials. *Mol. Pharmacutics* **2016**, *13*, 3578-3589.

5. **J. Hoque**, P. Akkapeddi, C. Ghosh, D. S. S. M. Uppu and J. Haldar. A biodegradable polycationic paint that kills bacteria *in-vitro* and *in-vivo*. *ACS Appl. Mater Interface* **2016**, 8, 29298-29309.

6. **J. Hoque**, M. M. Konai, S. S. Sequeira, S. Samaddar and J. Haldar. Spatial control of hydrophobicity for governing selective antibacterial activity of biofilm eradicating small molecules. *J. Med. Chem.* **2016**, *59*, 10750-10762.

7. **J. Hoque**, Sandip Samaddar, Relekar G. Prakash, Krishnamoorthy Paramanandham, Bibek R. Shome and Jayanta Haldar. A polycationic injectable sealant with potent wound healing and antibacterial properties. *Mol. Pharmaceutics* **2016**, Under revision.

8. **J. Hoque** and J. Haldar. Dual action injectable bioadhesive hydrogel for extended release of antibiotics and effective killing of bacteria. Manuscript to be communicated.

9. **J. Hoque**, S. Samaddar and J. Haldar. Direct synthesis of dextran-based antibacterial hydrogels for extended release of biocides and eradication of biofilms. Manuscript to be communicated.

10. **J. Hoque** and J. Haldar; "Charge Switchable Polymeric Coatings: Tuning Antibacterial and Cytotoxic Activities of Side Chain Degradable Polyethylenimine Derivatives." Manuscript to be communicated.

11. **J. Hoque**, V. Yadav, C. Ghosh, S. Samaddar, R. G. Prakash, K. Paramanandham, B. R. Shome, K. Sanyal and J. Haldar. Broad-spectrum polycationic paint kills multi-drug-resistant

bacteria and pathogenic fungi and inhibits biofilm formation: an *in vitro* and *in vivo* evaluation. Manuscript to be communicated.

12. **J. Hoque**, S. Samaddar, R. G. Prakash and J. Haldar. *In-situ* synthesis of dual action polymer-silver nanocomposites that effectively kill microbes and inhibit biofilm formation. Manuscript under preparation.

13. **J. Hoque**, M. M. Konai, S. S. Sequeira, S. Samaddar and J. Haldar. Cationic small molecules active against clinical isolates of bacteria: structure-activity relationship, mechanism of action and *in-vitro* and *in-vivo* Evaluation. Manuscript under preparation.

Miscellaneous Publications

1. **J. Hoque**, P. Kumar, V. K. Aswal and J. Haldar. Aggregation properties of amide bearing cleavable gemini surfactants by small angle neutron scattering and conductivity studies. *J. Phys. Chem. B*, **2012**, *116*, 9718-9726.

2. **J. Ho**que, P. Akkapeddi, V. Yarlagadda, D. S. S. M. Uppu, P. Kumar, and J. Haldar; Cleavable cationic antibacterial amphiphiles: synthesis, mechanism of action, and cytotoxicities. *Langmuir*, **2012**, *28*, 12225-12234.

3. **J. Hoque**, S. Gonuguntla, V. Yarlagadda, V. K. Aswal and J. Haldar. Effect of amide bonds on the self-assembly of gemini surfactants. *Phys. Chem. Chem. Phys.* **2014**, *16*, 11279-11288.

4. D. S. S. M. Uppu, P. Akkapeddi, G. B. Manjunath, V. Yarlagadda, **J. Hoque** and J. Haldar. Polymers with tunable side-chain amphiphilicity as non-hemolytic antibacterial agents. *Chem. Commun.* **2013**, 49, 9389-9391.

5. C. Ghosh, G. B. Manjunath, P. Akkapeddi, V. Yarlagadda, **J. Hoque**, D. S. S. M. Uppu, M. M. Konai, and J. Haldar. Small molecular antibacterial peptoid mimics: the simpler the better**!** *J. Med. Chem.* **2014**, *57*, 1428-1436.

6. C. Ghosh, G. B. Manjunath, M. M. Konai, D. S. S. M. Uppu, **J. Hoque**, K. Paramanandham, B. R. Shome and J. Haldar. Aryl-alkyl-lysines: agents that kill planktonic cells, persister cells, biofilms of MRSA and protect mice from skin-infection. *PLoS One* **2015**, *10*, e0144094.

7. D. S. S. M. Uppu, S. Samaddar, **J. Hoque**, M. M. Konai, K. Paramanandham, B. R. Shome and J. Haldar. Side chain degradable cationic-amphiphilic polymers with tunable hydrophobicity show *in-vivo* activity. *Biomacromolecules* **2016**, *17*, 3094-3102.

Patents

1. **J. Hoque**, P. Akkapeddi, G. B. Manjunath and J. Haldar. Chitin derivatives, method for production and uses thereof. WO 2015 092520A1. National Phase Applications have been filed in USA (15105153) and India.

2. **J. Hoqu**e and J. Haldar. A polymer network method for production, and uses thereof. Provisional application number 2016 41026116.

Miscellaneous Highlights of PhD Work

1. **Gandhian Young Technological Innovation (GYTI) Award**, **2016** under Technological-Edge category (BIRAC-GYTI) by Society for Research and Initiatives for Sustainable Technologies and Institutions (SRISTI) and National Innovation Foundation (NIF), New Delhi, 2016.

2. **Best Poster award** in "The first International Conference on Emerging Technologies for Clean Water" at Indian Institute of Technology Madras (IITM), Chennai, India, 2012.

3. Part of the work has been highlighted in **Science Journal** "*Toward substitution with no regrets*" on 13th March, 2015.

4. **The Economic Times** highlighted part of the research work as "*Three weapons to slow down bacteria spread in hospital"* on 4th April, 2015.

5. Part of the work has been highlighted in **Indian Express** as "*Scientist invents biodegradable detergent*" on 5th May, 2015.

6. Part of the work has been highlighted in the National News Paper **The Hindu** as "*A cleaner way to clean up*" on 13th May, 2015.